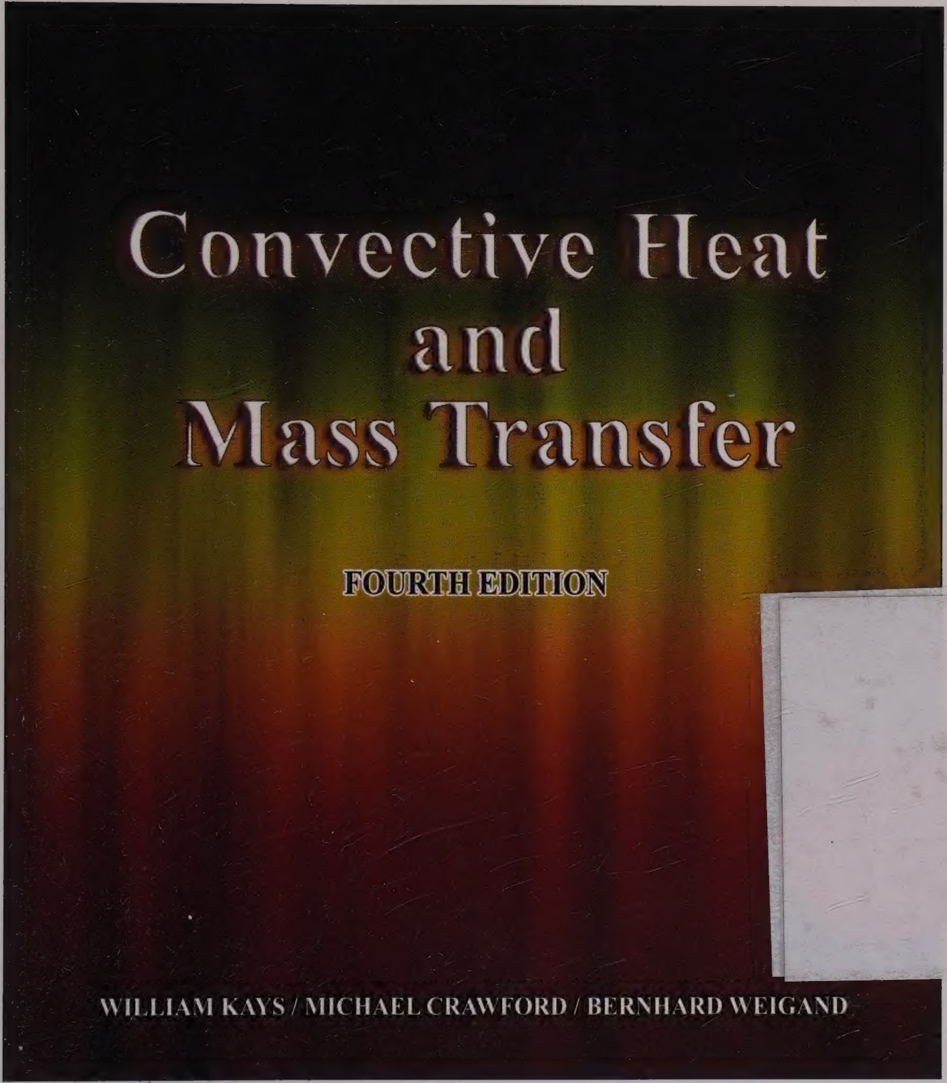

Convective Heat and Mass Transfer

FOURTH EDITION

WILLIAM KAYS / MICHAEL CRAWFORD / BERNHARD WEIGAND

INDIAN EDITION

Mc Graw Hill Education

Convective Heat and Mass Transfer

McGraw-Hill Series in Mechanical Engineering

Alciatore and Histand
Introduction to Mechatronics and Measurement Systems

Anderson
Computational Fluid Dynamics: The Basics with Applications

Anderson
Fundamentals of Aerodynamics

Anderson
Introduction to Flight

Anderson
Modern Compressible Flow

Barber
Intermediate Mechanics of Materials

Beer/Johnston
Vector Mechanics for Engineers

Beer/Johnston/DeWolf
Mechanics of Materials

Borman and Ragland
Combustion Engineering

Budynas
Advanced Strength and Applied Stress Analysis

Cengel and Boles
Thermodynamics: An Engineering Approach

Cengel and Turner
Fundamentals of Thermal-Fluid Sciences

Cengel
Heat Transfer: A Practical Approach

Cengel
Introduction to Thermodynamics & Heat Transfer

Crespo da Silva
Intermediate Dynamics

Dunn
Measurement & Data Analysis for Engineering & Science

Dieter
Engineering Design: A Materials & Processing Approach

Dieter
Mechanical Metallurgy

Doebelin
Measurement Systems: Application & Design

EDS, Inc.
I-DEAS Student Guide

Hamrock/Jacobson/Schmid
Fundamentals of Machine Elements

Henkel and Pense
Structure and Properties of Engineering Material

Heywood
Internal Combustion Engine Fundamentals

Holman
Experimental Methods for Engineers

Holman
Heat Transfer

Hsu
MEMS & Microsystems: Manufacture & Design

Hutton
Fundamentals of Finite Element Analysis

Kays/Crawford/Weigand
Convective Heat and Mass Transfer

Kelly
Fundamentals of Mechanical Vibrations

Kreider/Rabl/Curtiss
The Heating and Cooling of Buildings

Mattingly
Elements of Gas Turbine Propulsion

Meirovitch
Fundamentals of Vibrations

Norton
Design of Machinery

Palm
System Dynamics

Reddy
An Introduction to Finite Element Method

Ribando
Heat Transfer Tools

Schaffer et al.
The Science and Design of Engineering Materials

Schey
Introduction to Manufacturing Processes

Schlichting
Boundary-Layer Theory

Shames
Mechanics of Fluids

Shigley/Mischke/Budynas
Mechanical Engineering Design

Smith
Foundations of Materials Science and Engineering

Stoecker
Design of Thermal Systems

Suryanarayana and Arici
Design and Simulation of Thermal Systems

Turns
An Introduction to Combustion: Concepts and Applications

Ugural
Stresses in Plates and Shells

Ugural
Mechanical Design: An Integrated Approach

Ullman
The Mechanical Design Process

Wark and Richards
Thermodynamics

White
Fluid Mechanics

White
Viscous Fluid Flow

Zeid
Mastering CAD/CAM

Convective Heat and Mass Transfer

Fourth Edition

W. M. Kays
Professor of Mechanical Engineering, Emeritus
Stanford University

M. E. Crawford
Professor of Mechanical Engineering
The University of Texas at Austin

Bernhard Weigand
Professor of Aerospace Thermodynamics
Universitat Stuttgart

McGraw Hill Education (India) Private Limited
CHENNAI

McGraw Hill Education Offices
Chennai New York St Louis San Francisco Auckland Bogotá Caracas
Kuala Lumpur Lisbon London Madrid Mexico City Milan Montreal
San Juan Santiago Singapore Sydney Tokyo Toronto

McGraw Hill Education (India) Private Limited

CONVECTIVE HEAT AND MASS TRANSFER, FOURTH EDITION

Copyright © 2005, 1993, 1980, 1966 by The McGraw Hill Companies, Inc. All rights reserved.

Fifth reprint 2018
RDQLCRDEDLYZR

No part of this publication may be reproduced or distributed in any form or by any means, electronic, mechanical, photocopying, recording, or otherwise or stored in a database or retrieval system without the prior written consent of The McGraw-Hill Companies, Inc., including, but not limited to, in any network or other electronic storage or transmission, or broadcast for distance learning.

Some ancillaries, including electronic and print components, may not be available to customers outside the United States

McGraw Hill Education (India) Edition 2012

Reprinted in India by arrangement with McGraw-Hill Global Education Holdings, LLC, New York

Sales territories: India, Pakistan, Nepal, Bangladesh, Sri Lanka and Bhutan

Library of Congress Cataloging-in-Publication Data

Kays, W.M. (William Morrow)
Convective heat and mass transfer. —4th ed. / William M. Kays, Michael Crawford, Bernhard Weigand.
p. cm.—(McGraw-Hill series in mechanical engineering)
Includes index.
ISBN 0-07-246876-9 (acid-free paper)
1. Convection. 2. Mass transfer. I. Crawford, M.E. (Michael E.) II. Weigand, Bernhard, 1962–. III. Title. IV. Series.
QC327.K37 2005
621.402'2—dc22 2004040215
CIP

ISBN-13: 978-1-25-902562-4
ISBN-10: 1-25-902562-4

05 06 07 08 09 SAI 22 21 20 19 18

Published by McGraw Hill Education (India) Private Limited
444/1, Sri Ekambara Naicker Industrial Estate, Alapakkam, Porur, Chennai 600 116, Tamil Nadu, India

Printed and bound in India at Sai Printo Pack Pvt. Ltd., Delhi 110 020

Visit us at: www.mheducation.co.in

ABOUT THE AUTHORS

William M. Kays is Emeritus Professor of Mechanical Engineering at Stanford University. He received his Ph.D. degree in mechanical engineering at Stanford University in 1951 and has spent all of his professional life at Stanford, serving as Head of the Mechanical Engineering Department from 1961 to 1972 and Dean of Engineering from 1972 to 1984. He is a Member of the National Academy of Engineering and a Fellow of the American Society of Mechanical Engineering. Professor Kays has done extensive research on compact heat exchanger surfaces and on heat transfer from the turbulent boundary layer. He is also a coauthor of *Compact Heat Exchangers*.

Michael E. Crawford is Professor of Mechanical Engineering at The University of Texas at Austin. He received his doctoral degree in mechanical engineering at Stanford University in 1976, and he received his earlier degrees from Arizona State University. He joined the faculty of The University of Texas in 1980, and he served the department in various associate chair positions from 1995–2001. His teaching focuses primarily on heat transfer and thermodynamics at the undergraduate level, and convective heat transfer at the graduate level. Dr. Crawford's research programs have included liquid-metal magnetohydrodynamics, binary solution solidification, gas turbine film cooling, turbulence modeling for simulation of bypass-level transition, and modeling of wake-induced transition. He is the author of the boundary layer numerical simulation code STAN5 and its successor TEXSTAN. He is a Fellow of the American Society of Mechanical Engineers, and he is a registered professional engineer in the State of Texas. Dr. Crawford is currently working in the area of engineering multicultural team dynamics.

Bernhard Weigand is Professor and Head of the Institute of Aerospace Thermodynamics at Stuttgart University in Germany. He received his doctoral degree in 1992 at Darmstadt University, and he received his habilitation degree from Darmstadt University in 1997. From 1992 to 1999 he was employed at ABB Power Generation in Switzerland, where his positions included basic development in heat transfer and cooling for gas turbine blades, as well as the heat transfer and cooling design for next-generation blading. In 1999 he joined Stuttgart University and since 2002, he has been Dean of the faculty of Aerospace Engineering at Stuttgart University. Dr. Weigand's teaching focuses primarily on thermodynamics and heat transfer. His current research programs include numerical and experimental studies of gas turbine heat transfer, phase-change problems, and droplet dynamics.

To our children

BRIEF CONTENTS

Preface to the Fourth Edition xiv
Preface to the Third Edition xvii
Preface to the Second Edition xix
Preface to the First Edition xxi
List of Symbols xxiii

Chapters

1 Introduction 1
2 Conservation Principles 5
3 Fluid Stresses and Flux Laws 9
4 Differential Equations for the Laminar Boundary Layer 17
5 Integral Equations for the Boundary Layer 40
6 Differential Equations for the Turbulent Boundary Layer 52
7 Laminar Internal Flows: Momentum Transfer 67
8 Laminar Internal Flows: Heat Transfer 80
9 Laminar External Boundary Layers: Momentum Transfer 130
10 Laminar External Boundary Layers: Heat Transfer 148
11 Turbulent External Boundary Layers: Momentum Transfer 178
12 Turbulent External Boundary Layers: Heat Transfer 229
13 Turbulent Internal Flows: Momentum Transfer 282
14 Turbulent Internal Flows: Heat Transfer 292
15 Influence of Temperature-Dependent Fluid Properties 330
16 Convective Heat Transfer at High Velocities 344
17 Convective Heat Transfer with Body Forces 367
18 Convective Mass Transfer: Basic Definitions and Formulation of a Simplified Theory 399
19 Convective Mass Transfer: Evaluation of the Mass-Transfer Conductance from the Conserved-Property ($\mathcal{P}$) Equation 413
20 Convective Mass Transfer: Examples for Application of the Simplified Method 429

Appendixes

A Property Values 457
B Dimensions and Conversion to SI 471
C Some Tables of Functions Useful in Boundary-Layer Analysis 475
D Operations Implied by the ∇ Operator 477
E Detailed Derivation of the Simplified Mass-Diffusion and Energy Equation ($\mathcal{P}$ Equation) for Convective Mass Transfer Problems and the Corresponding Boundary Conditions 481
F The TEXSTAN Boundary-Layer Code 496
G Blasius Flow—A Sample Data Set for TEXSTAN 510
H TEXSTAN Data Sets 522
Index 531

CONTENTS

Preface to the Fourth Edition xiv
Preface to the Third Edition xvii
Preface to the Second Edition xix
Preface to the First Edition xxi
List of Symbols xxiii

Chapter **1**
Introduction 1

Chapter **2**
Conservation Principles 5

The Control Volume 5
Principle of Conservation of Mass 5
The Momentum Theorem 6
Principle of Conservation of Energy 7

Chapter **3**
Fluid Stresses and Flux Laws 9

Viscous Fluid Stresses 9
Fourier's Law of Heat Conduction 11
Fick's Law of Diffusion 13
Dimensionless Groups of Transport Properties 15
Turbulent-Flow Transport Coefficients 15
References 16

Chapter **4**
Differential Equations for the Laminar Boundary Layer 17

The Concept of the Boundary Layer 17
The Continuity Equations 19
The Momentum Equations 22
The Mass-Diffusion Equations 25
The Energy Equations 29
Problems 38
References 39

Chapter **5**
Integral Equations for the Boundary Layer 40

The Momentum Integral Equation 40
The Displacement and Momentum Thicknesses 43
Alternative Forms of the Momentum Integral Equation 45
The Energy Integral Equation 46
The Enthalpy and Conduction Thicknesses 48
Alternative Forms of the Energy Integral Equation 49
Problems 51
Reference 51

Chapter **6**
Differential Equations for the Turbulent Boundary Layer 52

Momentum and Thermodynamic Variables 52
Newtonian Stress and Fourier Heat-Flux Models 53
Instantaneous Equations of Turbulence 54
Reynolds Decomposition 55
Time-Averaging and Turbulence Statistics 57
Reynolds-Averaged Transport Equations of Turbulence 58
Problems 66
References 66

Chapter 7

Laminar Internal Flows: Momentum Transfer 67

Fully Developed Laminar Flow in Circular Tubes 67
Fully Developed Laminar Flow in Other Cross-Sectional Shape Tubes 71
The Laminar Hydrodynamic Entry Length 74
Problems 76
TEXSTAN Problems 78
References 79

Chapter 8

Laminar Internal Flows: Heat Transfer 80

The Energy Differential Equations for Flow through a Circular Tube 81
The Circular Tube with Fully Developed Velocity and Temperature Profiles 82
The Concentric Circular-Tube Annulus with Fully Developed Velocity and Temperature Profiles, Asymmetric Heating 92
Solutions for Tubes of Noncircular Cross Section with Fully Developed Velocity and Temperature Profiles 95
Circular-Tube Thermal-Entry-Length Solutions 97
Thermal-Entry-Length Solutions for the Rectangular Tube and Annulus 105
The Effect of Axial Variation of the Surface Temperature with Hydrodynamically Fully Developed Flow 109
The Effect of Axial Variation of Heat Flux 115
Combined Hydrodynamic and Thermal Entry Length 117
Problems 120
TEXSTAN Problems 125
References 128

Chapter 9

Laminar External Boundary Layers: Momentum Transfer 130

Similarity Solutions: The Laminar Incompressible Boundary Layer with Constant Properties and Constant Free-Stream Velocity 131
Similarity Solutions for the Laminar Incompressible Boundary Layer for $u_\infty = Cx^m$ 137
Similarity Solutions for the Laminar Incompressible Boundary Layer for $v_s \neq 0$ 139
Nonsimilar Momentum Boundary Layers 141
An Approximate Laminar Boundary-Layer Solution for Constant Free-Stream Velocity Developed from the Momentum Integral Equation 141
An Approximate Laminar Boundary-Layer Solution for Arbitrarily Varying Free-Stream Velocity over a Body of Revolution 143
Problems 145
TEXSTAN Problems 146
References 147

Chapter 10

Laminar External Boundary Layers: Heat Transfer 148

Constant Free-Stream Velocity Flow along a Constant-Temperature Semi-Infinite Plate 149
Flow with $u_\infty = Cx^m$ along a Constant-Temperature Semi-Infinite Plate 154
Flow along a Constant-Temperature Semi-Infinite Plate with Injection or Suction 157
Nonsimilar Thermal Boundary Layers 159
Constant Free-Stream Velocity Flow along a Semi-Infinite Plate with Unheated Starting Length 159
Constant Free-Stream Velocity Flow along a Semi-Infinite Plate with Arbitrarily Specified Surface Temperature 162

Constant Free-Stream Velocity Flow along a Semi-Infinite Plate with Arbitrarily Specified Surface Heat Flux 165
Flow Over a Constant-Temperature Body of Arbitrary Shape 166
Flow Over a Body of Arbitrary Shape and Arbitrarily Specified Surface Temperature 170
Flow Over Bodies with Boundary-Layer Separation 171
Problems 172
TEXSTAN Problems 176
References 177

Chapter 11

Turbulent External Boundary Layers: Momentum Transfer 178

Transition of a Laminar Boundary Layer to a Turbulent Boundary Layer 178
The Qualitative Structure of the Turbulent Boundary Layer 180
The Concepts of Eddy Diffusivity and Eddy Viscosity 182
The Prandtl Mixing-Length Theory 183
Wall Coordinates 186
The Law of the Wall for the Case of $p^+ = 0.0$ and $v_s^+ = 0.0$ 187
An Approximate Solution for the Turbulent Momentum Boundary Layer 191
A Continuous Law of the Wall: The Van Driest Model 194
Summary of a Complete Mixing-Length Theory 196
A Model Based on the Turbulence Kinetic Energy Equation 201
The k–ε Model 206
Equilibrium Turbulent Boundary Layers 208
The Transpired Turbulent Boundary Layer 212
The Effects of Surface Roughness 215
The Effects of Axial Curvature 219
The Effects of Free-Stream Turbulence 221
Problems 223
TEXSTAN Problems 226
References 227

Chapter 12

Turbulent External Boundary Layers: Heat Transfer 229

The Concepts of Eddy Diffusivity for Heat Transfer, Eddy Conductivity, and Turbulent Prandtl Number 229
The Reynolds Analogy 231
Turbulent Prandtl Number 233
A Conduction Model for Turbulent Prandtl Number 239
Complete Solution of the Energy Equation 242
A Law of the Wall for the Thermal Boundary Layer 242
Effect of Pressure Gradient on Temperature Profiles 247
A Heat-Transfer Solution for Constant Free-Stream Velocity and Surface Temperature 248
Constant Free-Stream Velocity Flow along a Semi-Infinite Plate with Unheated Starting Length 251
Constant Free-Stream Velocity Flow along a Semi-Infinite Plate with Arbitrarily Specified Surface Temperature 254
Constant Free-Stream Velocity Flow along a Semi-Infinite Plate with Arbitrarily Specified Heat Flux 255
An Approximate Solution for Varying Free-Stream Velocity 256
Strongly Accelerated Boundary Layers 259
The Transpired Turbulent Boundary Layer 260
Full-Coverage Film Cooling 265
Film Cooling 267

The Effects of Surface Roughness 268
The Effects of Axial Curvature 271
The Effects of Free-Stream Turbulence 273
Problems 275
TEXSTAN Problems 279
References 280

Chapter 13
Turbulent Internal Flows: Momentum Transfer 282

Fully Developed Flow in a Circular Tube 282
Tubes of Noncircular Cross Section 287
Effects of Surface Roughness 287
Problems 289
TEXSTAN Problems 290
References 290

Chapter 14
Turbulent Internal Flows: Heat Transfer 292

Circular Tube with Fully Developed Velocity and Temperature Profiles, Constant Heat Rate, Prandtl Numbers 0.6–6.0 294
Circular Tube with Fully Developed Flow, Higher Prandtl Numbers 297
Very Low-Prandtl-Number Heat Transfer, Liquid Metals 299
Circular Tube, Fully Developed Profiles, Constant Surface Temperature 302
Effect of Peripheral Heat-Flux Variation 304
Fully Developed Turbulent Flow between Parallel Planes and in Concentric Circular-Tube Annuli 305
Fully Developed Turbulent Flow in Other Tube Geometries 309
Experimental Correlations for Flow in Tubes 311
Thermal-Entry Length for Turbulent Flow in a Circular Tube 312
Thermal-Entry Length for Turbulent Flow between Parallel Planes 317
The Effects of Axial Variations of Surface Temperature and Heat Flux 319
Combined Hydrodynamic- and Thermal-Entry Length 319
The Influence of Surface Roughness 322
Problems 323
TEXSTAN Problems 326
References 328

Chapter 15
Influence of Temperature-Dependent Fluid Properties 330

Laminar Flow in Tubes: Liquids 332
Laminar Flow in Tubes: Gases 334
Turbulent Flow in Tubes: Liquids 334
Turbulent Flow in Tubes: Gases 335
The Laminar External Boundary Layer: Gases 336
The Laminar External Boundary Layer: Liquids 340
The Turbulent External Boundary Layer: Liquids 340
The Turbulent External Boundary Layer: Gases 341
Problems 342
References 342

Chapter 16
Convective Heat Transfer at High Velocities 344

The Stagnation Enthalpy Equation 346
The High-Velocity Thermal Boundary Layer for a Fluid with $\Pr = 1$ 349
The Laminar Constant-Property Boundary Layer for $\Pr \neq 1$ 351
The Laminar Boundary Layer for a Gas with Variable Properties 355

The Use of Reference Properties for High-Velocity Laminar Boundary-Layer Calculations 358
The Turbulent Boundary Layer for a Gas with Variable Properties 360
Reference Properties for High-Velocity Turbulent Boundary-Layer Calculations 363
Mach Number and Large-Temperature-Difference Corrections for Variable Free-Stream Velocity and Variable Temperature Differences 363
Problems 364
References 366

Chapter **17**
Convective Heat Transfer with Body Forces 367

Boundary-Layer Equations for Free Convection 368
Scaling and Flow Regimes in Free Convection 370
Similarity Solutions: Laminar Flow on a Constant-Temperature, Vertical, and Semi-Infinite Flat Plate 374
Similarity Solutions with Variable Surface Temperature 378
Similarity Solutions with Wall Suction or Blowing 380
Approximate Integral Solution: Laminar Flow on a Constant-Temperature, Vertical, and Semi-Infinite Flat Plate 381
The Effect of Variable Properties 382
Turbulent Flow on a Vertical and Semi-Infinite Flat Plate 383
Heat-Transfer Solutions for Other Geometries 386
Mixed Free and Forced Convection 389
Natural Convection in Enclosures 390
Problems 394
References 396

Chapter **18**
Convective Mass Transfer: Basic Definitions and Formulation of a Simplified Theory 399

Definitions 400
The Differential Equations of the Concentration Boundary Layer 401
Simplified Equations for the Concentration Boundary Layer 404
Boundary Conditions 406
Definition of the Mass-Transfer Conductance and Driving Force 409
Problems 411
References 412

Chapter **19**
Convective Mass Transfer: Evaluation of the Mass-Transfer Conductance from the Conserved-Property ($\mathscr{P}$) Equation 413

The Prediction of the Mass-Transfer Conductance g^* for Low Mass-Transfer Rates 414
The Laminar Constant-Property Boundary Layer for Low Mass-Transfer Rates 414
The Turbulent Constant-Property Boundary Layer for Low Mass-Transfer Rates 416
The Prediction of the Mass-Transfer Conductance g for High Mass-Transfer Rates 418
High Mass-Transfer-Rate Convection in a Laminar Couette Flow 418
The Laminar Constant-Property Boundary Layer, Similarity Solutions for High Mass-Transfer Rates 420
The Laminar Boundary Layer for High Mass-Transfer Rates: Some Variable-Property Solutions 424
The Laminar Constant-Property Boundary Layer with Arbitrary Varying Free-Stream Velocity and High Mass-Transfer Rates 425

The Turbulent Constant-Property Boundary Layer with Constant Free-Stream Velocity and High Mass-Transfer Rates 426

The Turbulent Boundary Layer: Some Variable-Property Solutions 427

Problems 427

References 428

Chapter 20

Convective Mass Transfer: Examples for Application of the Simplified Method 429

General Problem Solution Procedure 429

Thermodynamics of the Air–Water-Vapor System 430

Analysis of the Wet-Bulb Psychrometer 433

Drying 437

Evaporative Cooling 438

Naphthalene Sublimation from a Flat Plate 439

Burning of a Volatile Fuel in Air 442

Simple Graphite Burning in Air 444

Graphite Ablation with More than One Reaction 446

The High-Temperature Boundary Layer with Dissociation 448

Transpiration Cooling by Gas Injection 449

Problems 452

References 456

Appendix A Property Values 457

Appendix B Dimensions and Conversion to SI 471

Appendix C Some Tables of Functions Useful in Boundary-Layer Analysis 475

Appendix D Operations Implied by the ∇ Operator 477

Appendix E Detailed Derivation of the Simplified Mass-Diffusion and Energy Equation ($\mathcal{P}$ Equation) for Convective Mass Transfer Problems and the Corresponding Boundary Conditions 481

Appendix F The TEXSTAN Boundary-Layer Code 496

Appendix G Blasius Flow—A Sample Data Set for TEXSTAN 510

Appendix H TEXSTAN Data Sets 522

Index 531

PREFACE TO THE FOURTH EDITION

A decade has passed since our last edition and with it has come both change and constancy in the world of graduate-level convective heat and mass transfer. One important change is our new coauthor, Bernhard Weigand, educated at Darmstadt University in Germany, and currently Professor and Director of the Institute for Aerospace Thermodynamics at Stuttgart University.

As we have always done in the classroom, we assign a certain number of problems that promote the ideas of approximate analytical solutions to convection. One example is the classic unheated starting-length problem, which has an integral solution that can be easily solved by incorporating gamma and beta functions, once the integrals are properly transformed. The resulting answers are quite compact and somewhat intuitive. So how does this relate to change? Beginning around the early to mid-1990s, graduate students began submitting solutions that were strictly numerical, as if the thought of analytical integration had never occurred to them. Had they done both, their transformed integrals would have been much easier to numerically integrate. This seems to coincide with the gradual departure of graduate-level engineering education away from higher-level mathematics per se. In fact, numerical solutions can be economical and are often easy to produce, yielding valuable but sometimes unintended consequences.

Students entering graduate-level convection courses have already been introduced to the world of convective heat and mass transfer through correlations for the heat-transfer coefficient, and their educational focus is mostly about how to make judicious choices for the correlations. This "handbook approach" permits an order-of-magnitude estimation for a large class of engineering problems, but it falls far short in understanding the relationship between the surface friction, heat, and mass transfer and the corresponding flow fields for momentum, thermal energy, and mass concentration. And turbulent flow further complicates the understanding.

In the classroom, as we strive to merge academic convection with "real-world" heat and mass transfer problems, we find that we usually need to focus on complex thermal boundary conditions and variable-property effects because of large temperature differences or high-speed flow. These issues, along with three-dimensional effects, are usually well beyond handbook analysis techniques. No matter what approach we take to solving these real-world problems, the solution format is similar: we develop a model for the problem based on assumptions, we solve the modeled problem, and then we compare the model performance to the real-world performance. To create a convective solution we utilize convective tools of various kinds, including approximate and/or exact analytical analysis, numerical analysis via computer codes, physical experiments and data analysis, and the powerful concept embodied in the heat-mass-momentum analogy.

There are several challenges facing heat-transfer engineers if they choose a numerical computer code as the tool appropriate to a given problem. They need to understand how the code works and what assumptions are embodied in the code. To some degree they need to know the trend of the answer before they begin to search for it. And as they choose a numerical code for solution they have to keep in mind the time and monetary cost of the choice. Often a simple time- and money-cost choice leads to an answer that is nearly the same as a more time- or money-cost-intensive solution (the 10-minute analysis versus the 10-hour analysis).

There exists a strong analogy between numerical experimentation and physical experimentation, and the study of one enhances the effectiveness of performing the other. With either class of experimentation there are two essential requirements: the numerical/physical tool must be calibrated and the user of the tool must be "calibrated." And with either class, the answers must be checked for plausibility, and an uncertainty analysis must be carried out to accompany the acquired data. *Calibrating the user* can usually be carried out by having him or her perform benchmark experiments that yield data which can be compared against benchmark results. Ideally the class of benchmark results will be drawn from approximate or analytical methods as well as "accepted" numerical or experimental data. Convective examples might include reproducing fully developed heat transfer data or Blasius/Falkner-Skan data, or their turbulent counterparts. The end result is that the user learns how to not misuse the tool. *Calibrating the tool* requires the user to understand the limitations of the tool, and in the case of a numerical tool, to understand what physics are incorporated into the code containing the numerics. This is an especially important check because, for commercial codes, experience shows that what is advertised is not a guarantee of what has been correctly implemented into the code. The end result is that the user gains confidence about how the limits of the tool match the assumptions that underlie the model.

One of the grand masters of experimentation is Professor Peter K. Stein,[1] a highly regarded expert on mechanical instrumentation. During his long career, he developed a unified approach to the engineering of measurement systems, and his belief is that one can and one must develop the knowledge to obtain "valid data on purpose." We extend his philosophy to apply to the world of numerical convective heat and mass transfer, and it is in alignment with the ideas of calibration of the tool and the user (of the tool) before the tool is applied to convective problems. To this extent, the analogy between numerical experimentation and physical experimentation converges.

New to this edition of the textbook is an increased emphasis on using numerical tools, and we have specifically focused on TEXSTAN. a boundary-layer teaching code for solving two-dimensional convective heat- and mass-transfer problems. The compiled code (together with extensive test data sets and an input manual) is freely available to the worldwide academic and research community. We hope that by incorporating numerical solutions in your study of convective heat and mass transfer you will enhance your understanding of the relationship between the surface friction, heat, and mass transfer and their respective flow fields.

---

[1] Professor Peter K. Stein can be located via his website at http://home.globalcrossing.net/~meas-sys/index.html

Also new to this edition, in response to reviewers, is an enlarged chapter on convective heat transfer with body forces. And this edition presents a completely rewritten set of mass-transfer chapters, including more engineering examples for both low and high transfer rates. By rewriting these chapters, we hope to provide the reader with more insight into a seemingly difficult subject.

We note that the two chapters on heat exchangers have been removed from this current edition, because extensive material can be found in a republished form of the classic text on the subject by Professors Kays and London.[2]

We would like to thank the following reviewers for their feedback regarding the fourth edition: Sumanta Acharya, Louisiana State University; Srinath Ekkad, Louisiana State University; Pei-feng Hsu, Florida Institute of Technology; James R. Leith, The University of New Mexico; Ramendra P. Roy, Arizona State University; Brian Vick, Virginia Tech; and Donald Wroblewski, Boston University.

One of us (B. Weigand) gratefully acknowledges the many helpful discussions with Prof. J. von Wolfersdorf from Stuttgart University about the new edition of the present book.

W. M. Kays
M. E. Crawford
B. Weigand

---

[2] Kays, W. M., and A. L. London: *Compact Heat Exchangers*, 3rd ed., Krieger Publishing Company, Melbourne, Florida, 1984.

PREFACE TO THE THIRD EDITION

The trends in the development of the science of convective heat transfer, as described in the Preface to the Second Edition, 1980, have continued unabated. The influence of the digital computer has become even more pervasive since the personal computer came upon the scene, and today students and engineers can carry out computations at home or at their desk that 20 years ago would would have required a large mainframe computer and a well-staffed computer center.

One must pose the same question as in the previous edition. Where does this leave the older analytic approach with its classical solutions for particular boundary conditions and its many approximate procedures for more general boundary conditions? And the answer to this question is the same: the classical approach has become *less* important, but it has still not lost its importance.

This new edition has been prepared in response to this answer, but also in recognition of the continually growing importance of computer-based finite-difference solutions and new mathematical models, especially in the calculation of turbulent boundary layers. However, this is not a book on numerical methods, but rather, as before, an introduction to boundary-layer theory, recognizing the increasing importance of computer-based solutions.

The old Chapter 4 on the differential equations of the boundary layer has been subdivided into two chapters, with all of the material on the turbulent boundary layer equations now in a new Chapter 5, and with a considerable expansion of that material.

The four chapters on the turbulent boundary layer and turbulent flow in tubes have been completely rewritten to reflect new methods and new experimental data. Most of the other chapters have been revised only moderately.

A major change has been the inclusion of two new chapters on heat-exchanger analysis and design (Chapter 18) and on compact heat-exchanger surfaces (Chapter 19). The rationale for this addition is that heat-exchanger analysis and design provides one of the most important applications of convective heat-transfer theory, and this is particularly true for heat exchangers involving gases. An introductory course in convective heat transfer *should* include a section on heat exchangers, and it is inconvenient to require students to have two textbooks.

McGraw-Hill and the authors would like to thank the following reviewers for their many helpful comments and suggestions: Ralph Grief, University of California–Berkeley; John Lienhard, Massachusetts Institute of Technology; Jack Lloyd, Michigan State University; Terry Simon, University of Minnesota;

Brent Webb, Brigham Young University; and Ralph Webb, Pennsylvania State University.

The authors would like to express their thanks to Kiran Kimbell for her editorial assistance in preparing the third edition.

W. M. Kays
M. E. Crawford

PREFACE TO THE SECOND EDITION

When the first edition of this book was being prepared in the early 1960s, the art and science of convective heat transfer were well into what might be called the second phase. The first phase was the period of almost exclusive reliance on experimental correlations of overall heat-transfer behavior, with the pertinent variables reduced to the nondimensional groupings so familiar to all heat-transfer engineers. In the second phase the effort was increasingly to develop mathematical models of the basic phenomena and then to deduce system behavior through mathematical reasoning, an effort which greatly expanded the ability of the analyst or designer to handle new and complex applications and which also enhanced understanding of the phenomena involved. The primary objective of the first edition was to bring together some of these analytic methods and results, to encourage their routine use by heat-transfer engineers, and perhaps also to encourage the development of a new breed of heat-transfer engineer with a somewhat different point of view.

Since publication of the first edition in 1966, two closely related developments in convective heat transfer are having a profound influence. The large-capacity digital computer, together with new and better finite-difference techniques, has largely removed the mathematical difficulties of handling boundary-layer flows, and this has been especially significant in the case of turbulent flows. When it was no longer necessary to make mathematical compromises, it became possible to focus attention on the basic transport mechanisms, and thus our knowledge and our ability to model the basic mechanisms have greatly improved. It is now possible and practicable to routinely calculate both laminar and turbulent boundary layers, and tube flows, with high precision for a very wide variety of conditions.

The question now is: Where does this leave the older analytic approach with its classical solutions for particular boundary conditions and its many approximate procedures for more general boundary conditions? The authors have two answers to this question. Intelligent use of computer-based methods requires an understanding of both the basic processes and, in at least a general way, the consequences of particular sets of conditions. This understanding is difficult to obtain when the computer is relied on exclusively. Equally important is the fact that a very high percentage of engineering heat-transfer problems do not require the high precision and detail generally available from a computer solution, but they are problems for which quick, low-cost answers are essential. For such problems the computer-based finite-difference solution is elegant, but overkill. The point at which overkill occurs is moving inexorably away from the classical methods, but in the authors' view the distance to go is still large, and in any case is going to vary greatly with local conditions. It is a question of engineering judgment; an engineer must optimize not only the system being designed but also his or her own expenditure of time.

In this second edition the authors have retained the basic objectives of the first edition, while at the same time modernizing it and shifting emphasis where appropriate, but they have also tried to provide a theoretical framework for finite-difference methods. The relevant differential equations are developed, and simple turbulent transport models applicable to finite-difference procedures are discussed. Since the literature abounds with references to computer programs and model developments, the authors have tried mainly to refer to survey articles in the discussions.

As before, not everything can be covered. The topics chosen and the depth of coverage represents a personal judgment as to what is of first importance for a mechanical, aerospace, or nuclear engineering student at about the fifth-year level. A chapter on free convection has been added, and the discussion of the effects of surface roughness has been greatly expanded. Several chapters have been reorganized to completely separate laminar and turbulent flows, and the approach to turbulent transport processes has been drastically modified. Because of their continuing evolution, though, higher-order turbulence closure models are not discussed. Finally, it should be emphasized that only two-dimensional boundary-layer flows are treated, and only single-phase systems are considered.

Finally, the second author would like to express his gratitude to Professor Kays for the honor and privilege of being asked to coauthor the second edition. Professor Kays' style of teaching, both in the classroom and otherwise, and his approach to the subject of heat transfer will be forever with me. I would also like to express my indebtedness to Professor R. J. Moffat at Stanford, who taught me all I profess to know about experimental heat transfer and the art of written and oral communication. Lastly, I would like to express appreciation to two more colleagues, Professor A. L. London at Stanford and Professor J. L. Smith, Jr, at M.I.T., who have taught me the closely allied field of thermodynamics and the general methodology behind engineering problem solving.

W. M. Kays
M. E. Crawford

PREFACE TO THE FIRST EDITION

Prior to World War II, convective heat and mass transfer were largely empirical sciences, and engineering design was accomplished almost exclusively by the use of experimental data, generalized to some degree by dimensional analysis. During the past two decades great strides have been made in developing analytical methods of convection analysis, to the point where today experiment is assuming more its classical role of testing the validity of theoretical models. This is not to say that direct experimental data are not still of vital importance in engineering design, but there is no question that the area of complete dependence on direct experimental data has been greatly diminished. With this change our understanding of convection phenomena has been greatly enhanced, and we find ourselves in a position to handle, with confidence, problems for which experiment would be time-consuming and expensive. This book has been prepared as a response to this trend.

It is axiomatic that the engineering student must learn to reason from first principles so that she or he is not at a loss when faced by new problems. But time spent solving a complex problem from first principles is time wasted if the solution already exists. By their very nature analytic convection solutions often tend to be lengthy and difficult. Thus familiarity with, and an understanding of, some of the more important of the available analytic convective solutions should be an important part of the background of the heat-transfer engineer. One of the objectives of this book is to bring together in an easily usable form some of the many solutions to the boundary-layer equations. Although these are available in the heat-transfer literature, they are not always readily accessible to the practicing engineer, for whom time is an important consideration.

The author feels that a study of these solutions, in a logical sequence, also provides the best way for a student to develop an understanding of convective heat and mass transfer. Thus it is hoped that this book will serve both as a classroom text and as a useful reference book for the engineer.

This book is the outgrowth of a set of notes which the author has developed over the past ten years to supplement lectures in the "convection" portion of a one-year course in heat transfer for first-year graduate students. The students in the course have been largely mechanical, nuclear, and aeronautical engineers, interested in problems associated with thermal power systems and thermal environmental control.

It is assumed that the student has a typical undergraduate background in applied thermodynamics, fluid mechanics, and heat transfer. Heat transfer, although not mandatory, is usually of considerable help in orienting the student's thinking and establishing a sense of need for a deeper study of the subject. In particular, some familiarity with the commonly employed empirical methods of calculating convection heat-transfer rates is assumed, but only so that the student has an appreciation for the usefulness of a heat-transfer coefficient and some grasp of the basic physics of the convection process.

The choice of subject matter reflects quite frankly the author's own interests, and the depth to which each topic is pursued represents a compromise made necessary by what can be practicably accomplished in approximately one semester (or perhaps two quarters). It will be found that the momentum boundary layer is heavily compressed, with only sufficient material presented to support the heat- and mass-transfer sections. The student desiring to concentrate heavily in boundary-layer theory will undoubtedly want to take a separate course on viscous fluid mechanics, for which adequate texts exist. And, for that matter, there is certainly a great deal more to convective heat and mass transfer than is presented here, not only in the topics considered but also in those not even mentioned. In the latter category the reader may miss such topics as natural convection, heat-exchanger theory, rotating surfaces, nonsteady flows, two-phase flows, boiling and condensation, non-Newtonian fluids, internally radiating gases, rarefied gases, magnetohydrodynamic flows, and coupling between heat and mass transfer. But this only suggests why second editions are usually bigger than first editions.

Finally, I would like to acknowledge my indebtedness to some of my colleagues, without whose assistance, conscious or otherwise, this book could never have been written. First, Professor A. L. London taught me all that I profess to know about teaching, introduced me to heat transfer, and has been a constant source of help and inspiration. Professor W. C. Reynolds has worked with me on some of the research that is summarized in the book, and substantial parts of it are the result of his work alone. Several months spent with Professor D. B. Spalding at Imperial College in London were a rare privilege, and his influence will be found throughout the book. But most specifically, Spalding's generalization of the convective mass-transfer problem forms the entire basis for the last three chapters. Although available in Spalding's many papers, it is hoped that its inclusion here will encourage its more extensive use. Lastly I would like to express appreciation to Mr. R. J. Moffat, who read the manuscript and made many helpful suggestions.

W. M. Kays

LIST OF SYMBOLS

English letter symbols

A^+	Van Driest constant
A_c	flow cross-sectional area, m^2
A_s	surface area, m^2
B	mass transfer driving force
B_f	transpiration parameter
B_h	heat transfer transpiration parameter
Bo	Boussinesq number, Gr Pr^2
Br$'$	Brinkman number, $V^2/(q_s''D)$
b_f	transpiration parameter
b_h	transpiration parameter
C	surface curvature in flow direction, $1/R$, 1/m
C_D	drag coefficient
Cr	$\nu/u_\infty R$, a curvature parameter
c	specific heat at constant pressure, J/(kg · K)
c	molar concentration
c_f	local friction coefficient
c_{f_m}	mean friction coefficient with respect to length
$\bar{c}_{f_{\mathrm{app}}}$	apparent mean friction coefficient
c_{f0}	value of local friction coefficient with vanishingly small mass-transfer rate
c_v	specific heat at constant volume, J/(kg · K)
c_j	specific heat at constant pressure for component j of a mixture, J/(kg · K)
D	inside diameter of a circular tube, m
D_h	hydraulic diameter, $D_h = 4r_h = 4A_cL/A$, m
D_j	mass diffusion coefficient for component j in a multi-component mixture, m^2/s
d	outside diameter of a circular tube, m
$\mathcal{D}_{ij}$	mass diffusion coefficient for a binary (two-component) mixture, m^2/s; note that $\mathcal{D}_{ij} = \mathcal{D}_{ji}$
$\dot{E}$	rate of energy transfer by convection across a control surface, J/s, W
e	internal thermal and chemical energy, J/kg
F	mass flux ratio, $\dot{m}''/G_\infty$
$\mathbf{F}$	resultant of all external forces acting on a control volume, N
G	mass flux, or mass velocity, ρu, $\mathrm{kg/(m^2 \cdot s)}$
G	Clauser shape factor

G_∞	mass velocity in the free-stream, ρu_∞, kg/(m$^2 \cdot$ s)
$\mathbf{G}$	mass flux, or mass velocity vector, $\rho \mathbf{V}$, at any point in the stream, kg/(m$^2 \cdot$ s)
G_x, G_y, G_z	components of the mass flux vector, kg/(m$^2 \cdot$ s)
$\mathbf{G}_{\mathrm{diff},j}$	mass flux of component j transported by diffusion, kg/m^2
Gr_x	local Grashof number, $g\beta(T_s - T_\infty)\psi_x^3/\nu^2$
Gr_x^*	modified Grashof number, $g\beta q_s'' x^4/k\nu^2$
Gr_D	Grashof number based on diameter
Gr_L	Grashof number based on $L =$ surface area/surface perimeter
g	mass transfer conductance, kg/(s $\cdot$ m^2)
g_i	enthalpy conductance, kg/(s $\cdot$ m^2)
g	acceleration due to gravity, m/s^2
g^*	value of mass-transfer conductance for vanishingly small mass-transfer rate, kg/(s $\cdot$ m^2)
H	boundary layer shape factor
H_0	heat of combustion, per unit of fuel mass, at a reference temperature T_0, J/kg
h	heat-transfer coefficient, or convection conductance, W/(m$^2 \cdot$ K)
h_k	roughness heat-transfer coefficient, W/(m$^2 \cdot$ K)
i	static enthalpy, and enthalpy of a mixture, $e + P/\rho$, J/kg
i'	fluctuating component of static enthalpy, J/kg
$\bar{i}$	time-mean static enthalpy, J/kg
i_j	partial enthalpy of component j of a mixture, J/kg
i^*	stagnation enthalpy, $i + \frac{1}{2}u^2$, J/kg
$\overline{i^*}$	time-mean stagnation enthalpy, J/kg
i_R	reference enthalpy for evaluation of fluid properties, J/kg
K	acceleration parameter
K_p	equilibrium constant
k	instantaneous value of turbulence kinetic energy, $\frac{1}{2}u_i'u_i'$, m^2/s^2
k'	fluctuating component of k, $k' = k - \bar{k}$, m^2/s^2
$\bar{k}$	time-mean value of k, $\frac{1}{2}\overline{u_i'u_i'}$, m^2/s^2
k	thermal conductivity, W/(m $\cdot$ K)
k_{eff}	$k + k_t$
k_s	equivalent "sand grain" roughness, m
k_t	eddy or turbulent conductivity, W/(m $\cdot$ K)
k_T	thermal diffusion ratio
L	flow length of a tube, m
L^*	characteristic length
Le_j	Lewis number, γ_j/Γ, $\mathrm{Pr}/\mathrm{Sc}_j$ (sometimes defined as the inverse of this)
l	mixing length, m
l_t	turbulence length scale, m
M	blowing-rate parameter
M	Mach number
m	mass, kg

m	exponent
m_j	mass concentration (mass fraction) of substance j in a mixture
$\dot{m}$	mass flow rate, kg/s
$\dot{m}''$	total mass flux (mass-flow rate per unit area) at surface or phase interface, kg/(m$^2 \cdot$ s)
$\dot{m}_j''$	mass flux of substance j at surface or phase interface, kg/(m$^2 \cdot$ s)
$\dot{m}_j'''$	rate of creation of substance j, per unit volume, by chemical reaction, kg/(m$^3 \cdot$ s)
$\mathfrak{M}$	molecular weight, kg/kmol
n_α	mass fraction of element α in a mixture of compounds
$n_{\alpha,j}$	mass fraction of element α in a compound substance j
Nu	Nusselt number, hD/k, $4r_h h/k$, hD_h/k, xh/k
P	pressure, Pa, N/m^2
P_a	partial pressure of substance a in a gas mixture, Pa, N/m^2
P'	fluctuating component of pressure, Pa, N/m^2
$\bar{P}$	local time-mean value of pressure, Pa, N/m^2
p	tube perimeter, m
p^+	nondimensional pressure gradient (wall coordinates)
$\mathcal{P}$	conserved property of the second kind
Pe	Péclet number, Re Pr
Pe$_t$	turbulent Péclet number, ε_M/ν
Pr	Prandtl number, $\mu c/k$, μ/Γ, ν/α
Pr$_{\text{eff}}$	$\mu_{\text{eff}}/(k_{\text{eff}}/c)$
Pr$_t$	turbulent Prandtl number
q	heat, energy in transit by virtue of a temperature gradient, J
$\dot{q}$	heat transfer rate, W
$\dot{\mathbf{q}}''$	heat flux vector, heat-transfer rate per unit area, W/m^2
$\dot{q}_s''$	heat flux, heat-transfer rate per unit area, at surface or phase interface, W/m^2
R	universal gas constant, J/(kg $\cdot$ K)
R	radius of a body of revolution, radius of a cylinder or sphere, m
R	radius of curvature in flow direction, m
$\mathcal{R}$	universal gas constant, J/(kmol-kg)
Ra	Rayleigh number, Gr Pr
Ri	Richardson number, $(u/R)/(du/dR)$
r	radial distance in cylindrical or spherical coordinates, m
r	boundary layer thickness ratio, Δ/δ
r	mass ratio of oxidant to fuel in a simple chemical reaction
r_c	recovery factor
r_h	hydraulic radius, $A_c L/A$, m
r_i	inner radius of annulus, m
r_o	outer radius of annulus, m
r_s	radius of a circular tube, m
r^+	nondimensional radial coordinate, r/r_s
r^*	r_o/r_i, radius ratio for annulus

Re	Reynolds number, $4r_hG/\mu$, DG/μ, $xu_\infty\rho/\mu$, xu_∞/ν, δ_2u_∞/ν, Δ_2u_∞/ν, etc.
Re_k	roughness Reynolds number, k_su_τ/μ
Re_t	Reynolds number of turbulence
S	energy source in control volume, J
S	source function, thermal energy created per unit volume, W/m^3
S_{ij}	strain rate tensor, 1/s
Sc_j	Schmidt number, μ/γ_j, $m/\rho D_h$
Sc_k	Schmidt number for diffusion of turbulence kinetic energy
Sc_ε	Schmidt number for diffusion of turbulence dissipation
Sh	Sherwood number, gx/γ
St	Stanton number, h/Gc, $h/(u_\infty\rho c)$
St*	value of local Stanton number with vanishingly small mass-transfer rate
St_k	roughness Stanton number
s	entropy, J/(kg · K)
T	temperature, °C or K
T	boundary layer shape factor
T_R	reference temperature for evaluation of fluid properties, K
Tu	turbulence intensity
t	time, s
T'	fluctuating component of temperature, °C or K
$\bar{T}$	time-mean value of temperature
$\overline{T'v'}$	apparent turbulent heat flux, (K · m)/s
T_{aw}	adiabatic wall temperature, °C or K
T_e	fluid temperature at entrance to a tube, °C or K
T_m	mixed mean fluid temperature, °C or K
T_s	fluid temperature at surface or phase interface, °C or K
T_∞	temperature in the free stream at the outer edge of the boundary layer, °C or K
T^*	stagnation temperature, K
T_{db}	dry-bulb temperature, °C
T_{wb}	wet-bulb temperature, °C
T^+	nondimensional temperature in wall coordinates
u	velocity component in the x direction, m/s
u'	fluctuating component of velocity in the x direction, m/s
$\bar{u}$	time-mean velocity in the x direction, m/s
u_c	velocity at centerline of tube, m/s
$\rho\overline{u'v'}$	turbulent shear stress in a two-dimensional boundary layer, N/m^2
$\overline{u'X'}$	turbulent velocity–body force correlation, N/(s · m^2)
u_i, u_j	generalized velocity in tensor notation, m/s
$\rho\overline{u'_ju'_i}$	turbulent stress tensor or Reynolds stress tensor, N/m^2
$\rho\overline{u'_ji'}$	enthalpy flux vector, J/(s · m^2)
u^+	nondimensional velocity in wall coordinates; also nondimensional velocity in a tube, u/V

u_τ	"shear velocity" or "friction velocity," m/s
u_∞	velocity in the free stream at the outer edge of the boundary layer, m/s
V	volume, m^3
V	mean fluid velocity in a tube, m/s; also uniform velocity upstream of a blunt body, m/s
$\mathbf{V}$	velocity vector, m/s
$\mathbf{V}'$	fluctuating component of the velocity vector in a turbulent flow, m/s
$\bar{\mathbf{V}}$	local mean value of the velocity vector, m/s
v	velocity component in the y direction, m/s
v'	fluctuating component of velocity in the y direction, m/s
$\bar{v}$	local time-mean velocity in the y direction, m/s
$\rho c \overline{v'T'}$	turbulent heat flux in a two-dimensional boundary layer, $J/(s \cdot m^2)$
v	fluid specific volume, m^3/kg
v_s	normal fluid velocity at a surface, m/s
v_s^+	nondimensional form of v_s in wall coordinates
v_r	velocity component in the r direction, m/s
W	mechanical or electrical work, J, $N \cdot m$
$\dot{W}$	rate of doing mechanical work, J/s, W
w	velocity component in the z direction, m/s
w'	fluctuating component of velocity in the z direction, m/s
$\bar{w}$	local time-mean velocity in the z direction, m/s
X	body force acting on a fluid in the x direction per unit of volume, N/m^3
X'	fluctuating component of body force in the x direction, N/m^3
X_i	body force acting in the x_i direction, N/m^3
x	a spatial coordinate in Cartesian and cylindrical systems; also flow length in a tube, or distance measured along the surface of a body, m
x_j	mole fraction, c_j/c
$\mathbf{x}$	vector location (x, y, z) or (x_1, x_2, x_3)
x^+	nondimensional axial distance inside a tube, $(x/r_s)/(\text{Re}\,\text{Pr})$; also nondimensional form of x in wall coordinates
x_i, x_j	generalized coordinates in tensor notation, m
Y	upper-bound value of spatial coordinate y in integral-equation control volume analysis, m
y	a spatial coordinate in a Cartesian system, distance normal to the surface in a boundary layer, m
y^+	nondimensional distance from wall in wall coordinates
z	a spatial coordinate in a Cartesian system; also elevation with respect to a given datum in a gravity field, m

Greek letter symbols

α	molecular thermal diffusivity, $k/\rho c$, m^2/s
β	a pressure-gradient parameter
β	wedge angle
β	volumetric coefficient of thermal expansion, K^{-1}

Γ	thermal diffusion coefficient, k/c, kg/(m · s)
Γ	gamma function
γ	ratio of specific heats, c/c_v
γ_j	mass-diffusion coefficient for substance j in a mixture, ρD_j, kg/(m · s)
Δ	designates a difference when used as a prefix
Δ	thickness of a thermal boundary layer, m
Δ_2	enthalpy thickness of a thermal boundary layer, m
Δ_4	conduction thickness of a thermal boundary layer, k/h, m
δ	thickness of a momentum boundary layer, m
$\delta(\,)$	differential displacement of the variable ( )
δ_1	displacement thickness of a momentum boundary layer, m
δ_2	momentum thickness of a boundary layer, m
δ_3	Clauser boundary-layer thickness, m
δ_4	shear thickness of a boundary layer, m
δ_{99}	99 percent boundary-layer thickness, m
δ_{ij}	Kronecker delta function
δy_s	roughness displacement in mixing length
ε	turbulence dissipation rate, N/(s · m^2)
ε_H	eddy diffusivity for heat transfer, m^2/s
ε_M	eddy diffusivity for momentum transfer, m^2/s
ε_k	eddy diffusivity for the diffusion of turbulence kinetic energy, m^2/s
ε_ε	eddy diffusivity for the diffusion of turbulence energy dissipation, m^2/s
ζ	dependent variable in Blasius equation, $u/u_\infty = \zeta'(\eta)$
η	similarity parameter: independent variable in Blasius and other similarity solution equations
η	film-cooling effectiveness
θ	$(T_s - T)/(T_s - T_c)$, nondimensional fluid temperature in a tube
θ	nondimensional temperature used in full-coverage film cooling
θ	$(T_s - T)/(T_s - T_\infty)$, nondimensional fluid temperature in an external boundary layer, for the case of a step change in surface temperature
θ	temperature difference, °C or K
θ	angular coordinate in a spherical system
κ	mixing-length constant
γ	inclination angle of a flat plate
λ	nondimensional boundary-layer parameter
λ	mixing length constant
μ	dynamic viscosity coefficient, Pa · s, N · s/m^2
μ_t	eddy or turbulent viscosity, Pa · s, N · s/m^2
μ_{eff}	$\mu + \mu_t$
ν	kinematic viscosity, μ/ρ, m^2/s

ξ	distance from beginning of tube or plate to point where heat transfer starts; also a dummy length variable; may be dimensional or nondimensional, according to context
ρ	fluid density, mass per unit volume, kg/m^3
σ	Stefan–Boltzmann constant, W/(m$^2 \cdot$ K^4)
σ	normal stress on an element of fluid, Pa, N/m^2
σ_{ij}	fluid stress tensor, Pa, N/m^2
τ	shear stress, Pa, N/m^2
τ_{ij}	viscous stress tensor, Pa, N/m^2
τ_s	shear stress evaluated at wall surface, Pa, N/m^2
ϕ	angular coordinate in cylindrical and spherical coordinate systems
ϕ	dissipation function
φ	relative humidity
Φ	diffusion coefficient, Γ, γ_j
ψ	stream function, m^2/s
ω	absolute humidity, kg (vapor)/kg (dry air)
Ω_{ij}	rotation tensor

Superscripts

*	value at vanishingly small mass-transfer rate

Subscripts

c	evaluated at centerline of tube
s	evaluated within the boundary layer or considered phase but at the surface or wall
o	refers to the outer surface of an annulus
oo	outer surface of an annulus when outer surface alone is heated
∞	evaluated at the free stream
D	evaluated based on diameter
e	evaluated at the tube entrance
m	evaluated at the mixed mean state; also denotes other mean values
R	refers to reference temperature, or properties evaluated at reference temperature; radius of cylinder
x	evaluated at a particular point along the surface
aw	evaluated at "adiabatic" wall state
L	evaluated at the surface but within the neighboring phase
T	evaluated at the transferred-substance state
j	refers to a substance j that is a component of a mixture
α	refers to a particular chemical element α in a compound and/or mixture
i	refers to the inner surface of an annulus
ii	inner surface of an annulus when inner surface alone is heated

CP	refers to constant-property solution with all fluid properties introduced at either mixed-mean or free-stream state
Ⓗ	refers to solution for constant heat rate per unit of tube length
Ⓣ	refers to solution for constant surface temperature

(The meanings of other subscripts should be apparent from the context of their use.)

Note

The dimensions of all quantities listed are given in standard SI base or derived units, or both. Some quantities are customarily expressed in decimal multiples or submultiples of these units, and care should be taken to note this fact in making arithmetic calculations. Typical examples are pressure, usually expressed in kilopascals, kPa, specific heat capacity, kJ/(kg · K), and enthalpy, MJ/kg or kJ/kg.

CHAPTER 1

Introduction

Among the tasks facing the engineer is the calculation of energy-transfer rates and mass-transfer rates at the interface between phases in a fluid system. Most often we are concerned with transfer at a solid–fluid interface where the fluid may be visualized as moving relative to a stationary solid surface, but there are also important applications where the interface is between a liquid and a gas.

If the fluids are everywhere at rest, the problem becomes one of either simple heat conduction where there are temperature gradients normal to the interface (which will be subsequently referred to as the *surface*) or simple mass diffusion where there are mass concentration gradients normal to the surface. However, if there is fluid motion, energy and mass are transported both by potential gradients (as in simple conduction) and by movement of the fluid itself. This complex of transport processes is usually referred to as *convection.* Thus the essential feature of a convective heat-transfer or a convective mass-transfer process is the transport of energy or mass to or from a surface by both molecular conduction processes and bulk fluid movement.

Popular usage forces us to use the term *convection* somewhat loosely. We will speak of the *convective* terms in our differential equations, as opposed to diffusive terms; here we refer to that *part* of the transport process attributable to the bulk fluid motion alone.

If the fluid motion involved in the process is induced by some external means (pump, blower, wind, vehicle motion, etc.), the process is generally called *forced convection.* If the fluid motion arises from external force fields, such as gravity, acting on density gradients induced by the transport process itself, we usually call the process *natural convection.*

Engineering applications of convective heat and mass transfer are extremely varied. In a multifluid heat exchanger we are concerned solely with heat-transfer rates between the fluids and the solid surfaces of the heat exchanger separating the fluids. Calculation of the temperature of a cooled turbine blade or the throat of a rocket nozzle involves convective heat transfer alone, but if a fluid is injected through the surface (transpiration cooling), the problem is also a mass-transfer one. If the surface material is allowed to vaporize and/or burn to protect it from a high-temperature gas (ablation), we have another combination convective heat- and mass-transfer problem. The aerodynamic heating of high-speed aircraft is a convective heat-transfer process, but it also becomes a mass-transfer process when temperatures are so high that the gas dissociates, forming mass concentration gradients. The sling psychrometer presents a combination heat- and mass-transfer process. Combustion of a volatile fluid in air involves heat and mass transfer as well as chemical reaction within the transfer region.

Obviously the combination heat-transfer, mass-transfer, and chemical reaction problem is the most challenging of the convection problems. Nevertheless, the bulk of this book is devoted to convective heat transfer, for it will be shown that for many applications the mass-transfer and the combination problems lead (after suitable simplifying assumptions) to the same differential equations as simple heat transfer. Thus much of convective heat-transfer theory can be used directly in mass transfer, and it is perhaps simpler to develop the solutions on the heat-transfer framework than to employ a more general approach.

In simple convective heat transfer, it is convenient in most cases to define a convection *heat-transfer conductance*, or *coefficient*, such that the heat flux at the surface is the product of the conductance and a temperature potential difference. Thus

$$\dot{q}_s'' = h(T_1 - T_2) \tag{1-1}$$

The conductance h is essentially a fluid mechanic property of the system, whereas the temperature difference is, of course, a thermodynamic quantity. The usefulness of Eq. (1-1) lies largely in the fact that in a great many technical applications $\dot{q}_s''$ is close to being directly proportional to $T_1 - T_2$, as the linearity of the applicable differential equation reveals. Nevertheless, numerous nonlinear problems are encountered where h itself is a function of the temperature difference. It is important to note that this does not destroy the validity of Eq. (1-1) as a definition of h, although it may well reduce the usefulness of the conductance concept.

In convective mass transfer we find it convenient to define a convective *mass-transfer conductance* such that the total mass flux at the surface is the product of the conductance g and a driving force B. Thus

$$\dot{m}'' = gB \tag{1-2}$$

The conductance g is again essentially a fluid mechanic property of the system, whereas the driving force B is a thermodynamic property.[†] However, it is a somewhat more subtle property than the simple temperature difference of Eq. (1-1), and it has quite a different meaning depending on the nature of the problem. As a matter of fact, Eq. (1-1) can be *extracted* as a special case of Eq. (1-2), but consideration of the rather general nature of Eq. (1-2) is deferred until after simple convective heat-transfer theory is developed. The mass-transfer problem can also be nonlinear, which simply means that g becomes a function of B as well as the fluid mechanics of the system, but this again does not destroy the validity of Eq. (1-2).

[†] The mass-transfer development here is based largely on the work of D. B. Spalding while at the Imperial College of Science and Technology, London.

In relatively simple mass-transfer applications where there are no chemical reactions, and where the mass concentrations of the transferred substance are small relative to 1, Eq. (1-2) will be shown to reduce to

$$\dot{m}'' = g\left(m_{j_1} - m_{j_2}\right) \tag{1-3}$$

where the m_j are mass concentrations. Equation (1-3) has the same form as Eq. (1-1), and this fact has given rise to heat- and mass-transfer *analogies*. However, it is important to realize that Eq. (1-3) is but a special case of the more general Eq. (1-2).

Stated in the simplest possible way, the primary objective of this book is to develop methods to evaluate the functions h and g for a variety of engineering applications. Knowing h, we can evaluate $\dot{q}_s''$ given the temperature difference, or vice versa. For the mass-transfer, or combination, problem we also have to learn how to evaluate B, since B is not quite so simple as the temperature difference of the heat-transfer problem.

Almost all of the applications considered in this book are those for which the so-called *boundary-layer* approximations are valid. That is, consideration will be restricted to a thin region near a phase boundary where most of the resistance to momentum, heat, and mass transfer resides. The vast majority of heat- and mass-transfer problems of engineering interest are subsumed under this restriction, but certainly by no means all. However, the solution of convection problems, usually three-dimensional, for which the boundary-layer approximations are not valid is beyond the scope of this book, although the basic differential equations for such problems are indeed developed.

In the solution of practically all heat- and mass-transfer convection problems, the corresponding fluid dynamic problem must first be solved, provided it is not completely coupled to the heat- and mass-transfer problems. Although this is not intended to be a book on viscous fluid dynamics, it will prove convenient to develop a considerable portion of viscous momentum boundary-layer theory to provide the foundation on which convection theory can be built. The criterion for selection of topics is simply that only those parts of momentum boundary-layer theory are developed that contribute directly to convection solutions to follow.

A final introductory note should be added about the manner of development of the various partial differential equations. In their most general form the equations are large and cumbersome, and the basic physics going into their development is often obscured by algebraic complexity. To provide a simple and clear development, we derive all differential equations in two dimensions and at the same time introduce the conventional boundary-layer approximations. Following this, in each case we extend the equations to three dimensions, dropping the boundary-layer approximations, and finally we render the equations in vector notation, and in some cases Cartesian tensor notation. Nothing is really lost by this procedure, for the extensions will be perfectly clear and obvious, and much is gained in algebraic simplicity. And, of course, it is generally the boundary-layer equations that we solve later, although we have the more general equations at our disposal when we need them.

CHAPTER 2

Conservation Principles

The solution of a convection problem starts with the combination of an appropriate conservation principle and one or more flux laws. In this chapter we set down the ground rules that we will employ for application of the conservation principles and then introduce these principles and a suitable system of nomenclature.

THE CONTROL VOLUME

Consider a defined region in space across the boundaries of which mass, energy, and momentum may flow, within which changes of mass, energy, and momentum storage may take place, and on which external forces may act. Such a region is termed a *control volume*, and the boundary surfaces are called the *control surface*. The control volume comprises our region of interest in application of the various conservation principles discussed below. The volume may be finite in extent, or all its dimensions may be infinitesimal.

The complete definition of a control volume must include at least the implicit definition of some kind of coordinate system, for the control volume may be moving or stationary, and the coordinate system may be fixed on the control volume or elsewhere.

A control volume across whose surface no matter passes during the process in question is sometimes referred to as a *fixed-mass system*, or a *simple thermodynamic system.*

PRINCIPLE OF CONSERVATION OF MASS

Let the term *creation* have the connotation of *outflow* minus *inflow* plus *increase of storage*: then the principle of conservation of mass, when applied to a control volume (Fig. 2-1), may be expressed as

$$\text{Rate of creation of mass} = 0 \tag{2-1}$$

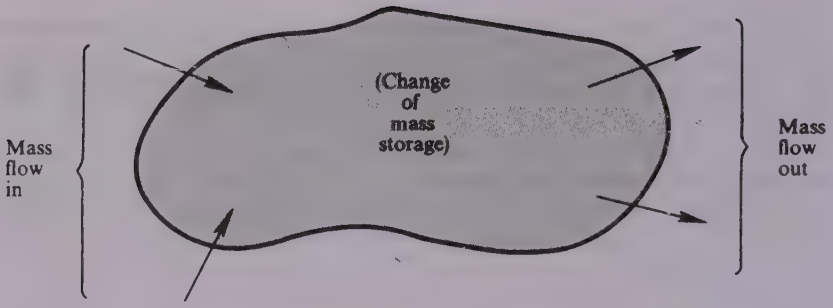

Figure 2-1 Control volume for application of conservation-of-mass principle.

If, in a flow system, the relative velocity normal to the control surface is designated as V, m/s, the total mass flux crossing the surface is

$$G = \rho V, \quad \text{kg/(s} \cdot \text{m}^2) \tag{2-2}$$

where ρ is the fluid density.

If G is constant over a cross-sectional area A, the total rate of mass flow across A is then

$$\dot{m} = GA = \rho VA, \quad \text{kg/s} \tag{2-3}$$

THE MOMENTUM THEOREM

The *momentum* of an element of matter may be defined as a quantity equal to the product of the mass of that element and its velocity. Since velocity is a vector quantity, momentum is also a vector quantity. The momentum theorem may be expressed either in vector form or, using a Cartesian coordinate system, as separate equations for the x, y, and z directions, employing the components of momentum and external forces in each of these respective directions. The momentum theorem, when applied to a control volume, as in Fig. 2-2, may be

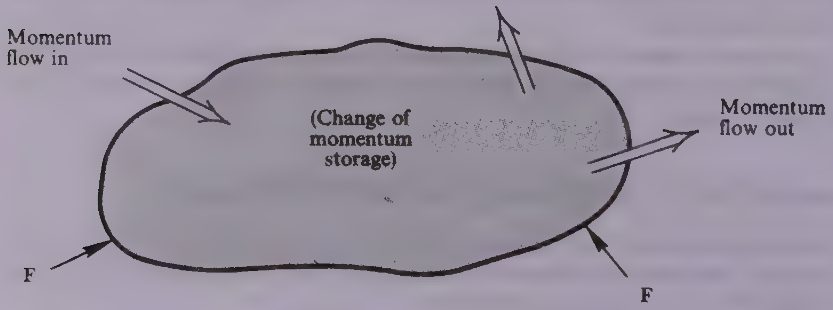

Figure 2-2 Control volume for application of momentum theorem.

expressed vectorially as

$$\text{Rate of creation of momentum} = \mathbf{F} \qquad (2\text{-}4)$$

with the following notation:

$m\mathbf{V}$	Momentum
m	mass, kg
$\mathbf{V}$	velocity, referred to an inertial or nonaccelerating coordinate system, m/s
$\dot{m}\mathbf{V}$	momentum rate across control surface
$\dot{m}$	rate of mass flow across control surface, kg/s
$\mathbf{F}$	resultant of all external forces acting on control surface or volume, N

Again the term *creation* has the same connotation as for Eq. (2-1), that is, *outflow minus inflow plus increase of storage.*

Application of Eq. (2-4) involves a summation of the momentum flux terms over the entire control surface to evaluate the outflow and inflow terms, a summation of rates of changes of momentum over the control volume to evaluate the increase-of-storage term, and a summation of the external forces over the surface and/or volume to evaluate the resultant external force.

Note that the velocities associated with the outflow and inflow terms are, in general, different from the velocities involved in the storage terms, and all must be referred to a nonaccelerating coordinate system.

PRINCIPLE OF CONSERVATION OF ENERGY

The principle of conservation of energy is a general expression of the first law of thermodynamics as applied to a control volume. Consider the energy that might cross the control surface and the changes of energy storage that might take place in the control volume shown in Fig. 2-3. The principle of conservation of energy

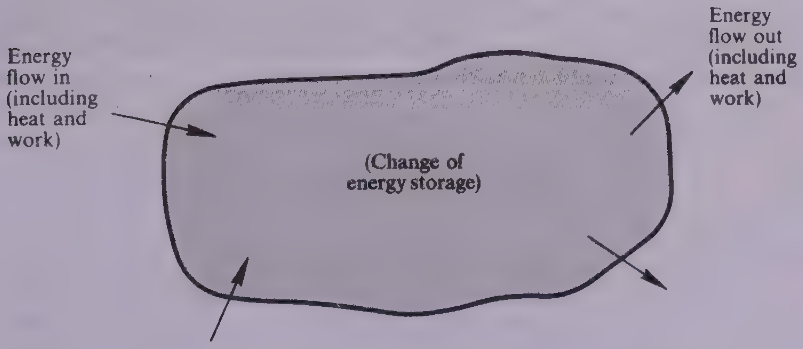
Energy flow in (including heat and work)
Energy flow out (including heat and work)
(Change of energy storage)

Figure 2-3 Control volume for application of conservation-of-energy principle.

can then be stated as

$$\text{Rate of creation of energy} = S \tag{2-5}$$

where S is the energy source within the control volume, in joules.

Application of Eq. (2-5) involves the same kind of summation as required for Eqs. (2-1) and (2-4). Energy can cross the surface in the form of work or heat transfer, or it can cross as energy stored in any mass that flows across the surface. Some of the forms of energy frequently encountered in flow systems are as follows:

Energy that can cross a control surface

Mechanical (or electrical) work	W
Flow work	Work done by each unit mass of flowing fluid on the control volume, or by the control volume, as it flows across the control surface. In general, the flow work done by a unit mass is equal to the product of the normal fluid stress and the fluid specific volume, both evaluated at the control surface. If velocity gradients are not large, the normal stress is essentially the simple thermodynamic pressure, and the unit flow work becomes merely Pv, where v is the specific volume of the fluid.
Heat	q, energy transferred by virtue of a temperature gradient

Energy stored per unit mass as it crosses the control surface

Internal thermal energy	e (including stored chemical energy)
Kinetic energy	$\frac{1}{2}V^2$
Potential energy	gz, where z is elevation with respect to some datum in a gravity field of constant strength g
Enthalpy	i, a thermodynamic property, the sum $e + Pv$

CHAPTER 3

Fluid Stresses and Flux Laws

In this chapter we set forth the equations we will use to evaluate the normal stresses and the shear stresses in a viscous fluid as well as the basic flux laws we will use to evaluate local heat flux and local mass diffusion flux. In Chapter 4 we combine these relations with the conservation principles of the previous chapter to develop a set of differential equations that must be satisfied in the region of interest.

VISCOUS FLUID STRESSES

Let us draw a rectangular box around a point in a viscous fluid flow field, as illustrated in the Cartesian coordinate representation in Fig. 3-1. This two-dimensional box defines the stress nomenclature to be employed. Normal stresses are designated by σ and shear stresses by τ. The subscript convention follows that of elastic body mechanics. Notation is shown for the xy plane, with a similar scheme employed for the xz and yz planes.

For a Newtonian fluid (and only Newtonian fluids are considered here), the shear stresses are postulated to be directly proportional to the time rate of deformation of a fluid element, the proportionality factor being the dynamic viscosity coefficient μ. In Cartesian coordinates, with u, v, w representing the components of velocity in the x, y, z directions, again as shown in Fig. 3-1, the shear stresses then become

$$\tau_{xy} = \tau_{yx} = \mu\left(\frac{\partial v}{\partial x} + \frac{\partial u}{\partial y}\right) \tag{3-1}$$

$$\tau_{yz} = \tau_{zy} = \mu\left(\frac{\partial w}{\partial y} + \frac{\partial v}{\partial z}\right) \tag{3-2}$$

$$\tau_{zx} = \tau_{xz} = \mu\left(\frac{\partial u}{\partial z} + \frac{\partial w}{\partial x}\right) \tag{3-3}$$

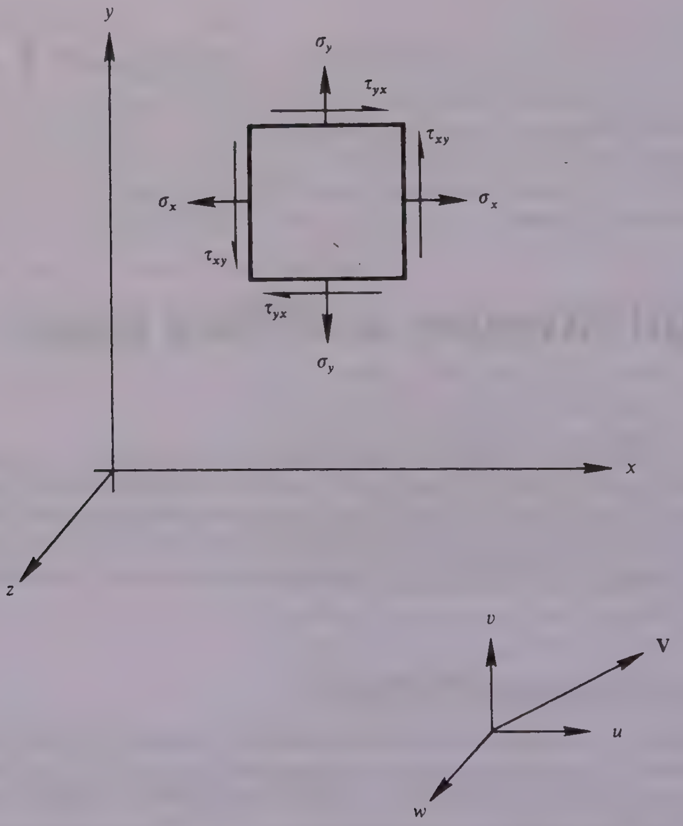

Figure 3-1 Stresses acting on element of fluid; components of fluid velocity.

The equations for the normal stresses in a viscous fluid are simply postulated here without development or further argument. They can be derived for a simple gas by the kinetic theory of gases, but require certain critical assumptions for a more general development. In particular, the use of $-\frac{2}{3}\mu$ as the coefficient of the second term appears to be strictly limited to the low-density gas regime.[1]

$$\sigma_x = -P + 2\mu\frac{\partial u}{\partial x} - \frac{2}{3}\mu\left(\frac{\partial u}{\partial x} + \frac{\partial v}{\partial y} + \frac{\partial w}{\partial z}\right) \tag{3-4}$$

$$\sigma_y = -P + 2\mu\frac{\partial v}{\partial y} - \frac{2}{3}\mu\left(\frac{\partial u}{\partial x} + \frac{\partial v}{\partial y} + \frac{\partial w}{\partial z}\right) \tag{3-5}$$

$$\sigma_z = -P + 2\mu\frac{\partial w}{\partial z} - \frac{2}{3}\mu\left(\frac{\partial u}{\partial x} + \frac{\partial v}{\partial y} + \frac{\partial w}{\partial z}\right) \tag{3-6}$$

P is the simple thermodynamic pressure under these assumptions and, for the majority of applications, is the only term of real significance. For a *constant-density fluid* it is seen later that the second term in each equation is always zero and that only when there are very large velocity gradients in the direction of the stress (last term) does σ differ appreciably from P. Analysis of a normal shock wave is an example where all the terms are of significance.

Equations (3-1)–(3-6) can be compactly written using Cartesian tensor notation[†] as

$$\sigma_{ij} = -P\delta_{ij} + \mu\left(\frac{\partial u_i}{\partial x_j} + \frac{\partial u_j}{\partial x_i}\right) - \frac{2}{3}\mu\frac{\partial u_k}{\partial x_k}\delta_{ij} \tag{3-7}$$

Some representative data on viscosity coefficients of fluids are given in App. A. The viscosity coefficient varies somewhat with the temperature of a fluid. Generally for a liquid it is a decreasing function of temperature, whereas for a gas it is an increasing function. μ has the dimensions Pa · s, or kg/(m · s).

FOURIER'S LAW OF HEAT CONDUCTION

Fourier's law of heat conduction states that heat transfer by molecular interactions at any point in a solid or fluid is proportional in magnitude and coincident with the direction of the negative gradient of the temperature field. Conduction heat transfer is thus a vector quantity, and the basic Fourier equation for the heat flux vector is

$$\dot{\mathbf{q}}'' = -k\nabla T \tag{3-8}$$

where k is the thermal conductivity of the conducting media and has the dimensions W/(m · K).

Fourier's law is the simplest form of a general energy flux law and is strictly applicable only when the system is uniform in all respects except for the temperature gradient; that is, there are no mass concentration gradients or gradients in other intensive properties.

Given a system with gradients of temperature, pressure, mass concentration, magnetic field strength, and so on, there is no a priori justification for ignoring the possibility that each of these gradients might contribute to the energy flux. The simplest expression that could describe this relationship would be a linear combination of terms, one for each of the existing potential gradients. Experience shows that there are, in fact, measurable "coupled" effects, such as energy fluxes due to mass concentration gradients, and that this more general form of the linear rate equation is necessary under certain conditions.

[†] In using tensor notation the indices in the subscripts can have the values 1, 2, 3, and they have the following meaning: $x_1 = x$, $x_2 = y$, $x_3 = z$, and $u_1 = u$, $u_2 = v$, $u_3 = w$. Repeated indices in a term of an equation imply summation of the term over the three values of k (*summation convention*). The Kronecker delta is $\delta_{ij} = 0, i \neq j$, and $\delta_{ij} = 1, i = j$. In the symbol σ_{ij} the subscript i is the direction of the outward normal to the surface on which the stress acts, and the subscript j indicates the direction of the stress itself. By symmetry of the stress tensor, $\sigma_{12} = \sigma_{21} = \tau_{xy}$, $\sigma_{23} = \sigma_{32} = \tau_{yz}$, $\sigma_{31} = \sigma_{13} = \tau_{zx}$, $\sigma_{11} = \sigma_x$, $\sigma_{22} = \sigma_y$, $\sigma_{33} = \sigma_z$.

The relationships among the coefficients of this equation have been the subject of several investigations[2–4] in irreversible thermodynamics. These relationships fall into the domain of irreversible thermodynamics by the very nature of the diffusive transport process. One of the principal contributions of irreversible thermodynamics has been to show that, for example, if energy is transported because of a concentration gradient then mass will be transported because of a temperature gradient, and the coefficients of these two coupled interactions will be the same, provided that the driving potentials are appropriately chosen as a thermodynamically consistent set.

Since we are primarily concerned here with temperature gradients and mass concentration gradients, only the coupling between these effects is discussed. An explicit relation for the energy flux can be derived for a low-density gas from kinetic theory. The following equation for the thermal flux in a binary gas mixture (two components of the gas only) is given by Baron[5] and follows from the development by Chapman and Cowling[6]:

$$\dot{\mathbf{q}}'' = -k\nabla T + \left(i_1 + i_2 + \frac{RTk_T}{m_1 m_2 \mathfrak{M}}\right)(\mathbf{G}_{\mathrm{diff},1}) \tag{3-9}$$

where 1 and 2 refer to the two components of the mixture, i is the enthalpy, m is the mass concentration, $\mathfrak{M}$ is the mean molecular weight of the mixture, R is the universal gas constant, $\mathbf{G}_{\mathrm{diff},1}$ is the mass diffusion flux of component 1, and k_T is a "thermal diffusion ratio." The effect incorporated in the last term is frequently known as the *diffusion-thermo*, or *Dufour*, effect.

Information on k_T is rather meager and largely derived from kinetic theory for gases, but calculations to establish the importance of this effect in typical boundary-layer flows have been made.[5,7,9] In this book, however, we assume that this effect is negligible in all the applications considered, although the transport of enthalpy by mass diffusion (first term in the first set of parentheses) is included where appropriate. With this exception, then, Fourier's law of heat conduction is assumed to represent the heat flux in all cases.

Some representative data on the thermal conductivity k of fluids are given in App. A. The thermal conductivity of liquids is relatively independent of temperature, but for gases it is an increasing function of temperature similar to the viscosity coefficient.

In some applications the thermal conductivity occurs naturally in combination with specific heat. In these cases it becomes convenient to define

$$\Gamma = k/c, \quad \mathrm{kg/(s \cdot m)} \tag{3-10}$$

where c is the specific heat of the fluid, $J/(\mathrm{kg} \cdot \mathrm{K})$. (For gases c will be understood to be the specific heat at constant pressure c_p.) Thus if Γ is employed, Eq. (3-8) becomes

$$\dot{\mathbf{q}}'' = -\Gamma c \nabla T \tag{3-11}$$

FICK'S LAW OF DIFFUSION

Before introducing Fick's law, it is useful to discuss some definitions, and to make a distinction between mass transfer by *convection*, or bulk fluid movement, and mass transfer by *diffusion*, which is primarily caused by concentration gradients. We will define

$$\begin{aligned} \mathbf{G} &= \text{total mass flux vector, kg/(s}\cdot\text{m}^2) \\ \mathbf{V} &= \mathbf{G}/\rho \\ &= \text{total velocity vector, m/s} \end{aligned}$$

where ρ is the mixture density, kg/m^3.

These terms have the same meaning whether the fluid has one component, multiple components, or multiple components with concentration gradients.

If there are multiple components in the fluid, we will define the *total* mass flux vector for some component j as

$$\mathbf{G}_{\text{tot},j}, \quad \text{kg/(s}\cdot\text{m}^2)$$

We will then define the *convected* mass flux of component j as the flux of j attributable to bulk fluid movement, i.e.,

$$\mathbf{G}_{\text{conv},j} = m_j\mathbf{G}$$

where m_j is the mass concentration of component j, kilogram of j per kilogram of mixture. Also $m_j = \rho_j/\rho$.

Finally we will define the *diffusion* mass flux of component j as the difference, if any, between the total and convected fluxes:

$$\mathbf{G}_{\text{diff},j} = \mathbf{G}_{\text{tot},j} - \mathbf{G}_{\text{conv},j}$$

It follows from these definitions that

$$\sum_j m_j = 1$$

$$\sum_j \mathbf{G}_{\text{tot},j} = \mathbf{G}$$

$$\sum_j \mathbf{G}_{\text{conv},j} = \mathbf{G}\sum_j m_j = \mathbf{G}$$

and thus

$$\sum_j \mathbf{G}_{\text{diff},j} = 0$$

Note then that even if there is no bulk movement of the fluid, it is still possible to have diffusion taking place, but the vector sum of the diffusion of the various components of the mixture will be zero.

It is found that the rate of *diffusion* of any single component of a mixture of fluids, $\mathbf{G}_{\text{diff},j}$, is a function of the concentration gradient of that component, and is also a function of certain other potential gradients acting on the system, such as temperature and pressure gradients, and the concentration gradients of each of the other components. An exact equation can be developed from kinetic theory for the mass flux of one component in a multicomponent mixture of low-density, simple gases,[8] although it is a rather complex expression.

A more restricted relation, which is exact for mass-diffusion in a binary mixture in the absence of other potential gradients, is Fick's law:

$$\mathbf{G}_{\text{diff},j} = -\rho D_j \nabla m_j \tag{3-12}$$

where D_j is a mass diffusion coefficient, m^2/s.

The corresponding energy relation, Fourier's law, was restricted to cases in which the system was completely described by the specification of one gradient, the temperature gradient. Similarly, the description of the mass-diffusion system must be fixed by ∇m_j alone before Fick's law is strictly applicable.

Most of the specific applications considered in this book involve only *binary* mixtures, so that Fick's law is applicable (in the absence of the Soret effect discussed later). However, we would like to develop the differential equations somewhat more generally, and we would like to consider at least some applications of diffusion in multicomponent systems. Knuth[10] shows that Fick's law describes accurately the diffusion of one component in a multicomponent mixture provided that the *binary* diffusion coefficients for each pair of components in the mixture are all the same and equal to D_j, that is,

$$D_j = \mathcal{D}_{12} = \ldots = \mathcal{D}_{ij}$$

where the $\mathcal{D}_{ij} = \mathcal{D}_{ji}$ are the diffusion coefficients for a *binary* mixture of i and j alone.

We use Fick's law exclusively, and the degree of approximation introduced in multicomponent applications then depends on the actual differences present in the $\mathcal{D}_{ij}$. Generally, binary diffusion coefficients are rather strongly dependent on relative molecular weight, and thus the molecular weight differences provide an approximate measure of the applicability of Fick's law to multicomponent systems. It should also be added that in a *turbulent* flow the simple transport model that we use also leads to approximate equality of the diffusion coefficients.

We find it convenient to write the coefficient in Fick's law in combination with the fluid density as follows:

$$\gamma_j = \rho D_j \tag{3-13}$$

Thus Eq. (3-12) becomes

$$\mathbf{G}_{\text{diff},j} = -\gamma_j \nabla m_j \tag{3-14}$$

Then γ_j is dimensionally similar to μ and Γ. Some representative data on γ_j for binary mixtures are given in App. A.

As discussed earlier, mass diffusion is a function not only of concentration gradients but also of the other potential gradients acting on the system. Here we are primarily concerned with the coupling effects of mass concentration and temperature gradients. Although pressure gradients and body forces, among others, can also induce mass diffusion, they are not generally important in the types of applications considered. For a gas, explicit relations can be derived from kinetic theory. The following equation for the diffusion of component 1 in the binary mixture under the influence of both a concentration gradient and a temperature gradient is given by Baron[5] and follows from a development by Chapman and Cowling[6]:

$$\mathbf{G}_{\mathrm{diff},j} = -\rho\mathcal{D}_{12}\left(\nabla m_j + \frac{\mathfrak{M}_1\mathfrak{M}_2}{\mathfrak{M}^2}k_T\nabla \ln T\right) \tag{3-15}$$

The effect incorporated in the last term is frequently known as the *thermodiffusion*, or *Soret*, effect. Again, in this book we assume that this effect is negligible in the applications considered.

DIMENSIONLESS GROUPS OF TRANSPORT PROPERTIES

The shear-stress equations and the two flux laws can each be written in terms of one coefficient; and each coefficient is dimensionally the same as the viscosity. Thus we can form three dimensionless groups by simple ratios, which appear later as parameters in our differential equations.

Prandtl number

$$\mathrm{Pr} = \frac{\mu}{\Gamma} = \frac{\mu c}{k} \tag{3-16}$$

Schmidt number

$$\mathrm{Sc}_j = \frac{\mu}{\gamma_j} = \frac{\mu}{\rho D_j} \tag{3-17}$$

Lewis number[†]

$$\mathrm{Le}_j = \frac{\gamma_j}{\Gamma} = \frac{\mathrm{Pr}}{\mathrm{Sc}_j} \tag{3-18}$$

TURBULENT-FLOW TRANSPORT COEFFICIENTS

The three transport coefficients defined above are all associated with molecular transport processes. In a turbulent flow these definitions are still valid, but they are involved in time-dependent terms in the differential equations. It proves mathematically convenient to postulate a model of the turbulent transport process that will lead to shear and flux laws similar in form to the molecular laws given. These, in turn, give rise to *turbulent* transport coefficients, which are dimensionally similar to the molecular coefficients but are functions of the dynamics of the flow field rather than being simple fluid properties. Consideration of the turbulent transport mechanism is deferred until later.

[†] The inverse, Γ/γ_j, is also frequently defined as the Lewis number.

REFERENCES

1. Rosenhead, L.: *Proc. Roy Soc. (London)*, ser. A, vol. 226, p. 1, 1954.
2. DeGroot, S. R.: *Thermodynamics of Irreversible Processes*, Interscience, New York, 1952.
3. Keenan, J. H.: *Appl. Mech. Rev.*, vol. 49, 1955.
4. Onsager, L.: (I) *Phys. Rev.*, vol. 37, p. 405, 1931; (II) *Phys. Rev.*, vol. 38, p. 2265, 1931.
5. Baron, J. R.: *ARS J.*, vol. 32, pp. 1053–1059, 1962.
6. Chapman, S., and T. G. Cowling: *The Mathematical Theory of Non-Uniform Gases*, Cambridge University Press, London, 1961.
7. Tewfik, O. E.: *Int. J. Heat Mass Transfer*, vol. 7, pp. 409–421, 1964.
8. See, for example, Hirschfelder, J. O., C. F. Curtiss, and R. B. Bird: *Molecular Theory of Gases and Liquids*, Wiley, New York, 1954.
9. Rosner, D. E.: *PCH Physicochemical Hydrodynamics*, vol. 1, pp. 91–123, 1980.
10. Knuth, E. L.: *Phys. Fluids*, vol. 2, p. 340, 1959.

CHAPTER 4

Differential Equations for the Laminar Boundary Layer

In this chapter we develop the differential equations that must be satisfied in the flow field about a body when there is heat transfer and mass transfer between the fluid and the body. From the conservation-of-mass principle we develop two equations: the continuity equation and the mass-diffusion equation. From the momentum theorem we develop the momentum equation of the laminar boundary layer and the Navier–Stokes equations. From the conservation-of-energy principle we develop various forms of the energy equation of the laminar boundary layer and the general viscous energy equation.

THE CONCEPT OF THE BOUNDARY LAYER

A complete viscous fluid solution for flow about a body poses considerable mathematical difficulty for all but the most simple flow geometries. A great practical breakthrough was made when Prandtl discovered that for most applications the influence of viscosity is confined to an extremely thin region very close to the body and that the remainder of the flow field could to a good approximation be treated as inviscid, that is, it could be calculated by the methods of potential flow theory.

The thin region near the body surface, which is known as the boundary layer, lends itself to relatively simple analysis by the very fact of its thinness relative to the dimensions of the body. A fundamental assumption of the boundary-layer approximation is that the fluid immediately adjacent to the body surface is at rest relative to the body, an assumption that appears to be valid except for very low-pressure gases when the mean free path of the gas molecules is large relative to the body. Thus the hydrodynamic or *momentum boundary layer* may be defined as the region in which the fluid velocity changes from its free-stream, or potential flow, value to zero at the body surface (Fig. 4-1).

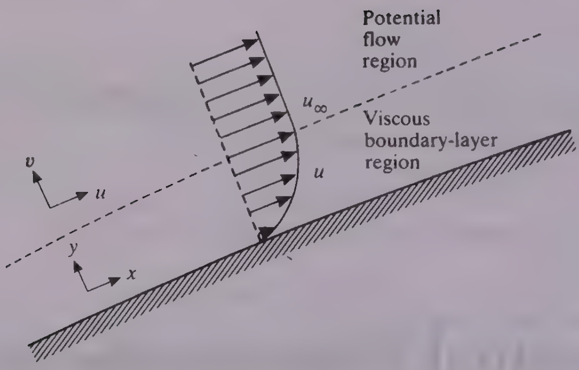

Figure 4-1 Momentum or viscous boundary layer on an external surface.

In reality there is no precise "thickness" to the boundary layer defined in this manner; and until we have developed a precise definition for boundary-layer thickness, we simply imply that the boundary-layer thickness is the distance in which *most* of the velocity change takes place.

If the boundary-layer thickness is very small relative to all other flow dimensions, it is apparent that, for the two-dimensional boundary-layer representation shown in Fig. 4-1, the following conditions must prevail within the boundary layer:

$$u \gg v$$

$$\frac{\partial u}{\partial y} \gg \frac{\partial u}{\partial x}, \quad \frac{\partial v}{\partial x}, \quad \frac{\partial v}{\partial y}$$

These conditions in turn simplify the application of Eq. (3-1) to the momentum theorem, and, although not so readily obvious, they also lead to a simplification of Eq. (3-4), namely,

$$\sigma_x \approx -P$$

and

$$\frac{\partial P}{\partial y} \approx 0, \qquad \frac{\partial P}{\partial x} \approx \frac{dP}{dx}$$

We develop the momentum equation of the boundary layer on this basis; then, after solving the equation for a particular case, we can show the conditions under which the boundary layer is truly "thin." We refer to the above conditions as the *boundary-layer approximations*.

Flow inside a tube is a form of boundary-layer problem in which, near the tube entrance, the boundary layer grows in much the same manner as over an external surface until its growth is stopped by symmetry at the centerline of the tube (Fig. 4-2). Thus the tube radius becomes the ultimate boundary-layer thickness.

When there is heat transfer or mass transfer between the fluid and the surface, it is also found that in most practical applications the major temperature and

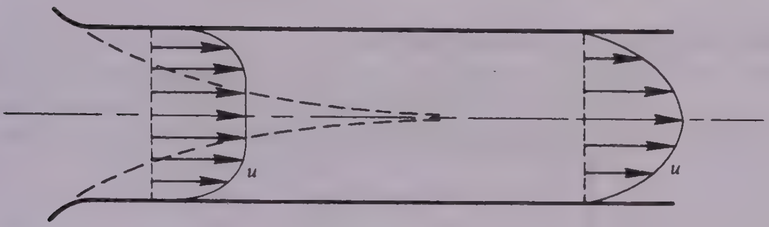

Figure 4-2 Development of a momentum boundary layer in the hydrodynamic entry region of a tube.

concentration changes occur in a region very close to the surface. This gives rise to the concept of the *thermal boundary layer* and the *concentration boundary layer*, and again the relative thinness of these boundary layers permits the introduction of boundary-layer approximations similar to those introduced for the momentum boundary layer; for example,

$$\frac{\partial T}{\partial y} \gg \frac{\partial T}{\partial x}$$

$$\frac{\partial m_j}{\partial y} \gg \frac{\partial m_j}{\partial x}$$

The thermal and concentration boundary layers are not necessarily the same thickness as the momentum boundary layer, and the conditions under which the boundary-layer approximations are valid are consequently different.

THE CONTINUITY EQUATIONS

Consider a two-dimensional flow in the xy plane, and cut out a control volume of infinitesimal dimensions (Fig. 4-3). Consider the total mass rate of flow across the control surface, and the rate of change of mass storage within, for a unit depth normal to the plane of the figure.

Let **G** represent mass flux (mass flow rate per unit of normal area), where G_x and G_y are the x and y components, respectively. The development of the principle of conservation of mass in Chapter 2 requires formulation of the outflow, inflow, and increase in storage terms,

$$\text{Outflow} = \left(G_y + \frac{\partial G_y}{\partial y}\delta y\right)\delta x + \left(G_x + \frac{\partial G_x}{\partial x}\delta x\right)\delta y$$

$$\text{Inflow} = G_x\,\delta y + G_y\,\delta x$$

$$\text{Increase of storage} = \frac{\partial \rho}{\partial t}\delta x\,\delta y$$

where t is *time*. Application of the principle of conservation of mass, Eq. (2-1), yields

$$\frac{\partial G_x}{\partial x} + \frac{\partial G_y}{\partial y} + \frac{\partial \rho}{\partial t} = 0$$

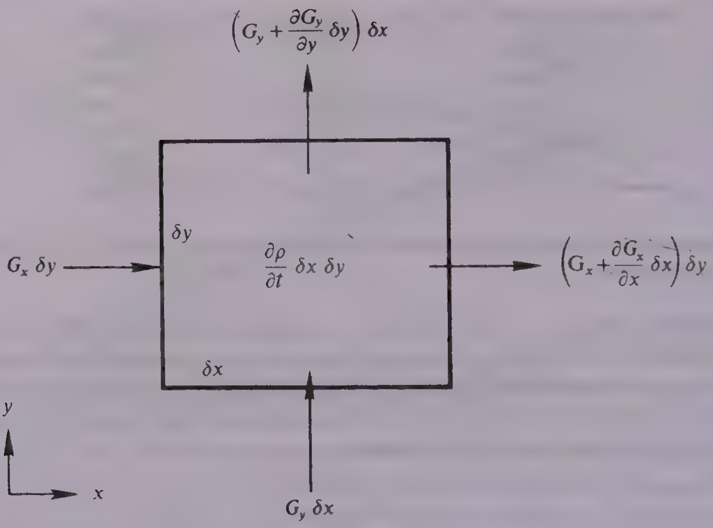
$\left(G_y + \frac{\partial G_y}{\partial y}\delta y\right)\delta x$
δy
$G_x\,\delta y$
$\frac{\partial \rho}{\partial t}\,\delta x\,\delta y$
$\left(G_x + \frac{\partial G_x}{\partial x}\delta x\right)\delta y$
δx
y
x
$G_y\,\delta x$

Figure 4-3 Control volume for development of the continuity equation.

The appearance of time in the equation suggests that, in general, density can vary with both space and time. There are two conditions for which the time term disappears. The first is based on the assumption that the fluid is *incompressible*, typically for a liquid such as water or oil, and the second is based on the assumption that the fluid is *constant density*, typically for gases with small changes in pressure or temperature within the flow field.

The assumption of *steady flow* requires both the density and velocity components not to vary with time, applicable to both liquids and gases, but the density can have spatial variation due to changes in the temperature or pressure fields. The usual condition for steady flow is to have the pressure field be independent of time. With the energy equation we will introduce the assumption of *steady state*, which will require the temperature field to be independent of time.

With the assumption of steady flow, or the assumption of incompressible flow, or the assumption of constant-density flow, the continuity equation for two-dimensional flow in Cartesian coordinates becomes

$$\frac{\partial G_x}{\partial x} + \frac{\partial G_y}{\partial y} = 0 \tag{4-1}$$

The corresponding three-dimensional continuity equation must then be

$$\frac{\partial G_x}{\partial x} + \frac{\partial G_y}{\partial y} + \frac{\partial G_z}{\partial z} = 0 \tag{4-2}$$

or, in vector notation,

$$\nabla \cdot \mathbf{G} = 0 \tag{4-3}$$

The vector notation allows the coordinate system to remain unspecified. Appendix D summarizes the vector and scalar operations implied by the ∇ operator for Cartesian, cylindrical, and spherical coordinate systems.

In Cartesian tensor notation the continuity equation (4-2) or (4-3) becomes

$$\frac{\partial}{\partial x_j}(\rho u_j) = 0 \tag{4-4}$$

For a constant-density flow Eq. (4-3) reduces to

$$\nabla \cdot \mathbf{V} = 0 \tag{4-5}$$

and Eq. (4-4) becomes

$$\frac{\partial u_j}{\partial x_j} = \frac{\partial u}{\partial x} + \frac{\partial v}{\partial y} + \frac{\partial w}{\partial z} = 0 \tag{4-6}$$

For constant-density flow in a *two-dimensional boundary layer* the continuity equation becomes simply

$$\frac{\partial u}{\partial x} + \frac{\partial v}{\partial y} = 0 \tag{4-7}$$

For flow in a *circular tube* with axial symmetry it is convenient to employ a cylindrical coordinate system with nomenclature as defined in Fig. 4-4. Then Eq. (4-3) reduces to

$$\frac{\partial(\rho u)}{\partial x} + \frac{1}{r}\frac{\partial}{\partial r}(r\rho v_r) = 0 \tag{4-8}$$

and, for constant-density flow, to

$$\frac{\partial u}{\partial x} + \frac{1}{r}\frac{\partial}{\partial r}(r v_r) = 0 \tag{4-9}$$

Note that the continuity equation does not involve any boundary-layer assumptions and thus is generally applicable.

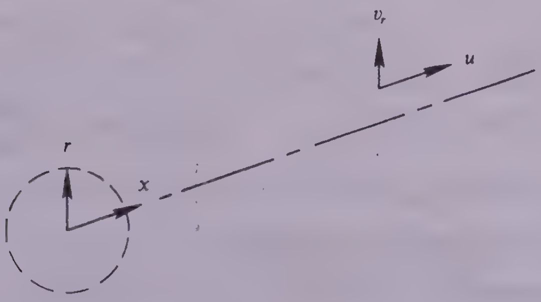

Figure 4-4 Coordinate system and velocity components for axisymmetric flow in a circular tube.

THE MOMENTUM EQUATIONS

The Steady-Flow Momentum Equation of the Boundary Layer

Consider steady flow along a semi-infinite two-dimensional surface of small curvature with a free-stream velocity u_∞. Let x be measured along the surface and y normal to the surface. The requirement of zero tangential velocity at the surface results in the development of a *momentum boundary layer*, defined as the region in which u changes from 0 to u_∞ (Fig. 4-5).

Cut out an infinitesimal stationary control volume of unit depth within the boundary layer, and consider the external forces acting on this control volume in the x direction and the x momentum fluxes crossing the control surface (Fig. 4-6).

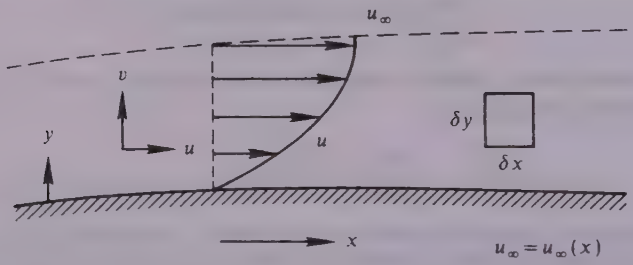

Figure 4-5 Coordinate system, velocity components, and control volume for development of the momentum differential equation of the boundary layer.

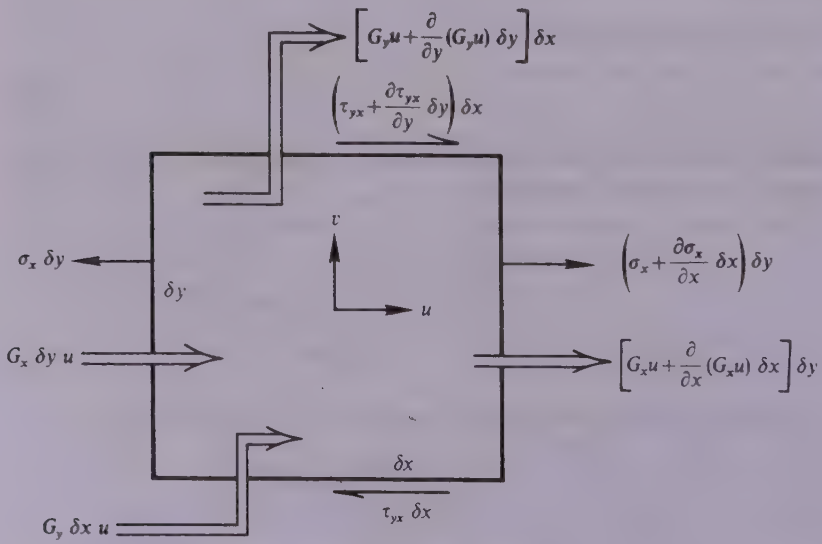
$\left[G_y u + \frac{\partial}{\partial y}(G_y u)\,\delta y\right]\delta x$
$\left(\tau_{yx} + \frac{\partial \tau_{yx}}{\partial y}\,\delta y\right)\delta x$
v
$\sigma_x\,\delta y$
δy
u
$\left(\sigma_x + \frac{\partial \sigma_x}{\partial x}\,\delta x\right)\delta y$
$G_x\,\delta y\,u$
$\left[G_x u + \frac{\partial}{\partial x}(G_x u)\,\delta x\right]\delta y$
δx
$\tau_{yx}\,\delta x$
$G_y\,\delta x\,u$

Figure 4-6 Control volume, momentum fluxes, and external forces for development of the steady-flow momentum differential equation of the boundary layer.

(For brevity let us omit body forces such as gravity, although these can simply be added if desired.)

Note that the stipulation of steady flow implies a laminar flow, since a turbulent flow is by its nature unsteady.

The development of the momentum theorem in Chapter 2 requires formulation of the outflow, inflow, and increase-in-storage terms, along with the various external forces on the control volume. For x-direction momentum,

$$\text{Outflow of momentum} = \left[G_x u + \frac{\partial}{\partial x}(G_x u)\,\delta x\right]\delta y + \left[G_y u + \frac{\partial}{\partial y}(G_y u)\,\delta y\right]\delta x$$

$$\text{Inflow of momentum} = (G_x\,\delta y)u + (G_y\,\delta x)u$$

$$\text{Increase of momentum storage} = 0 \text{ (steady flow)}$$

$$\text{External forces} = -\sigma_x\,\delta y - \tau_{yx}\,\delta x + \left(\sigma_x + \frac{\partial \sigma_x}{\partial x}\delta x\right)\delta y + \left(\tau_{yx} + \frac{\partial \tau_{yx}}{\partial y}\delta y\right)\delta x$$

Applying the momentum theorem, Eq. (2-4), with the assumption of steady flow, and simplifying, yields

$$\frac{\partial}{\partial x}(G_x u) + \frac{\partial}{\partial y}(G_y u) = \frac{\partial \sigma_x}{\partial x} + \frac{\partial \tau_{yx}}{\partial y}$$

This form is often referred to as the conservative form of the x-momentum equation. Expanding the left-hand terms gives

$$G_x\frac{\partial u}{\partial x} + u\frac{\partial G_x}{\partial x} + G_y\frac{\partial u}{\partial y} + u\frac{\partial G_y}{\partial y} = \frac{\partial \sigma_x}{\partial x} + \frac{\partial \tau_{yx}}{\partial y}$$

and applying continuity equation (4-1) using the assumption of a steady flow yields

$$G_x\frac{\partial u}{\partial x} + G_y\frac{\partial u}{\partial y} = \frac{\partial \sigma_x}{\partial x} + \frac{\partial \tau_{yx}}{\partial y}$$

Next, applying the boundary-layer approximations to the shear stress term, Eq. (3-1), and the normal stress term, Eq. (3-4), gives us

$$\frac{\partial \sigma_x}{\partial x} = -\frac{dP}{dx}$$

$$\frac{\partial \tau_{yx}}{\partial y} = \frac{\partial}{\partial y}\left(\mu\frac{\partial u}{\partial y}\right)$$

Also note that

$$G_x = \rho u, \qquad G_y = \rho v$$

With these substitutions, we have the *momentum equation of the boundary layer*:

$$\rho u\frac{\partial u}{\partial x} + \rho v\frac{\partial u}{\partial y} = -\frac{dP}{dx} + \frac{\partial}{\partial y}\left(\mu\frac{\partial u}{\partial y}\right) \tag{4-10}$$

Note that this equation is valid for variable properties ρ and μ.

For *axisymmetric flow in a circular tube* we can develop a similar boundary-layer equation in cylindrical coordinates by identical methods:

$$\rho u \frac{\partial u}{\partial x} + \rho v_r \frac{\partial u}{\partial r} = -\frac{dP}{dx} + \frac{1}{r}\frac{\partial}{\partial r}\left(r\mu \frac{\partial u}{\partial r}\right) \tag{4-11}$$

The Navier–Stokes Equations

Now, suppose we apply the momentum theorem in precisely the same manner to a three-dimensional flow, without the simplifying assumptions of the boundary layer but including changes with time and including external body forces. Employing a Cartesian coordinate system and applying the momentum theorem in the x direction, we obtain

$$\begin{aligned}\rho\left(\frac{\partial u}{\partial t} + u\frac{\partial u}{\partial x} + v\frac{\partial u}{\partial y} + w\frac{\partial u}{\partial z}\right)\\ = -\frac{\partial P}{\partial x} + \frac{\partial}{\partial x}\left\{\mu\left[2\frac{\partial u}{\partial x} - \frac{2}{3}\left(\frac{\partial u}{\partial x} + \frac{\partial v}{\partial y} + \frac{\partial w}{\partial z}\right)\right]\right\}\\ + \frac{\partial}{\partial y}\left[\mu\left(\frac{\partial u}{\partial y} + \frac{\partial v}{\partial x}\right)\right] + \frac{\partial}{\partial z}\left[\mu\left(\frac{\partial w}{\partial x} + \frac{\partial u}{\partial z}\right)\right] + X\end{aligned} \tag{4-12}$$

Similar equations are obtained for the y and z directions.

The origin of the various terms in (4-12) can readily be seen by comparison with (4-10) and the stress equations (3-1)–(3-6). X is the body force in the x direction, N/m^3.

These three equations can be written more compactly in Cartesian tensor notation[1]:

$$\rho\left(\frac{\partial u_i}{\partial t} + u_j\frac{\partial u_i}{\partial x_j}\right) = \frac{\partial \sigma_{ji}}{\partial x_j} + X_i \tag{4-13}$$

where the stress tensor σ_{ij} is defined in Eq. (3-7).

For *constant-property flow* a considerably simpler formulation can be obtained:

$$\rho\left(\frac{\partial u}{\partial t} + u\frac{\partial u}{\partial x} + v\frac{\partial u}{\partial y} + w\frac{\partial u}{\partial z}\right) = -\frac{\partial P}{\partial x} + \mu\left(\frac{\partial^2 u}{\partial x^2} + \frac{\partial^2 u}{\partial y^2} + \frac{\partial^2 u}{\partial z^2}\right) + X \tag{4-14}$$

or, more briefly,

$$\rho\frac{Du}{Dt} = -\frac{\partial P}{\partial x} + \mu\,\nabla^2 u + X \tag{4-15}$$

where D represents the *substantial derivative*, defined as indicated.

Again, analogous equations can be written for the y and z directions; or, abandoning a coordinate system, the constant-properties equations can be put in vector notation as

$$\rho \frac{D\mathbf{V}}{Dt} = -\nabla P + \mu \nabla^2 \mathbf{V} + \mathbf{F} \tag{4-16}$$

In tensor notation the constant-properties equations become

$$\rho \left(\frac{\partial u_i}{\partial t} + u_j \frac{\partial u_i}{\partial x_j} \right) = -\frac{\partial P}{\partial x_i} + \mu \frac{\partial^2 u_i}{\partial x_j \partial x_j} + X_i \tag{4-17}$$

It should be noted here that the momentum equation of the two-dimensional boundary layer, Eq. (4-10), can readily be derived from the Navier–Stokes equations, and indeed this is the procedure preferred by many authors rather than deriving the boundary-layer equation directly after making the boundary-layer assumptions. This procedure involves an assumption that the boundary layer is "thin," after which an order-of-magnitude analysis of the various terms in the Navier–Stokes equations is made. This analysis leads to a conclusion that the criterion for a "thin" boundary layer on a flat plate with constant free-stream velocity is that the Reynolds number based on distance from the leading edge x, $\rho u_\infty x/\mu = \mathrm{Re}_x$, must be large relative to unity. Further details on the order-of-magnitude analysis may be found in, for example, Schlichting[2] or Streeter.[3]

THE MASS-DIFFUSION EQUATIONS

Steady-Flow Mass-Diffusion Equation of the Boundary Layer

Consider steady flow along the surface of a body, and let there be a transfer of mass to or from the fluid at the surface. If the transferred substance contains different chemical species than the free-stream fluid, concentration gradients will be established. In general, there may be any number of chemical components in the resulting mixture, and, as suggested by Fick's law, Eq. (3-14), each will tend to diffuse in the direction of the negative of its own concentration gradient (but see comments on the applicability of Fick's law to multicomponent diffusion in Chap. 3). Additionally, various components may combine chemically to form new species, so that creation and destruction of various components of the mixture may occur at any point, resulting in concentration gradients. Thus, if there is chemical reaction, mass diffusion can occur even with no mass transfer at the body surface. The principle of conservation of mass requires a continuity equation for each species: and the mass-diffusion equation is the species continuity equation.

Let us consider some particular component of the mixture, to be designated by a subscript j. At the body surface this component has a particular concentration, possibly determined by the conditions of thermodynamic equilibrium at the surface. In the free stream the concentration of j is presumably some known value, frequently zero. Then the region in which the concentration of j changes from its body-surface value to its free-stream value is defined as the *concentration*

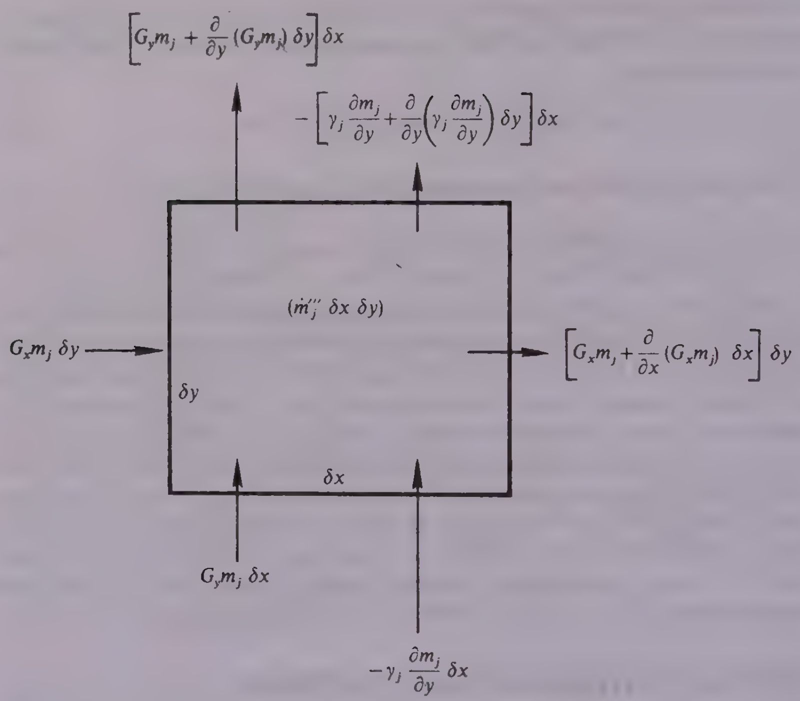
$\left[G_y m_j + \frac{\partial}{\partial y}(G_y m_j)\,\delta y\right]\delta x$
$-\left[\gamma_j \frac{\partial m_j}{\partial y} + \frac{\partial}{\partial y}\left(\gamma_j \frac{\partial m_j}{\partial y}\right)\delta y\right]\delta x$
$(\dot{m}_j''' \,\delta x\,\delta y)$
$G_x m_j\,\delta y$
$\left[G_x m_j + \frac{\partial}{\partial x}(G_x m_j)\,\delta x\right]\delta y$
δy
δx
$G_y m_j\,\delta x$
$-\gamma_j \frac{\partial m_j}{\partial y}\,\delta x$

Figure 4-7 Control volume and mass-transfer terms for development of the steady-flow mass-diffusion differential equation of the boundary layer.

boundary layer and may be represented as in Fig. 4-5, but with m_j replacing u and with m_j having a finite value at the surface, rather than zero as for u.

Let us cut out a stationary infinitesimal control volume of unit depth within this boundary layer and examine the ways in which component j can cross the control surface (Fig. 4-7) in steady flow.

Across each side, component j is carried by the movement of the entire stream (convected transfer), and these terms are then the product of the total mass flow rate and the concentration of component j, m_j, kg of component j per kg of total mixture. Transport of component j also takes place quite independently by diffusion. We assume that Fick's law of diffusion holds. However, here we invoke the boundary-layer approximations, assuming that the only concentration gradient of significance is in the y direction, normal to the surface.

To combine the terms on Fig. 4-7, we need to modify our conservation-of-mass principle, Eq. (2-1), to account for the creation term. Within the control volume, component j may be created (or destroyed) by chemical reaction. We designate the rate of creation of j per unit volume by $\dot{m}_j'''$, kg of j per m^3. Note that

$$\sum_j \dot{m}_j''' = 0$$

Thus

$$\text{Rate of creation of component } j = \dot{m}_j'''$$

The development of the mass-diffusion equation follows the development in Chap. 2 for the principle of conservation of mass, requiring formulation of the outflow, inflow, and increase in storage terms, along with the source term for the control volume,

$$\text{Outflow of } j = \left[G_x m_j + \frac{\partial}{\partial x}(G_x m_j)\,\delta x\right]\delta y + \left[G_y m_j + \frac{\partial}{\partial y}(G_y m_j)\,\delta y\right]\delta x$$
$$- \left[\gamma_j \frac{\partial m_j}{\partial y} + \frac{\partial}{\partial y}\left(\gamma_j \frac{\partial m_j}{\partial y}\right)\delta y\right]\delta x$$

$$\text{Inflow of } j = G_x m_j\,\delta y + G_y m_j\,\delta x - \gamma_j \frac{\partial m_j}{\partial y}\delta x$$

$$\text{Increase of storage of } j = 0 \quad \text{(steady flow)}$$

Applying the conservation principle, along with the assumption of steady flow, and simplifying, yields

$$\frac{\partial}{\partial x}(G_x m_j) + \frac{\partial}{\partial y}(G_y m_j) - \frac{\partial}{\partial y}\left(\gamma_j \frac{\partial m_j}{\partial y}\right) = \dot{m}_j'''$$

Expanding the left-hand terms, we have

$$G_x \frac{\partial m_j}{\partial x} + m_j \frac{\partial G_x}{\partial x} + G_y \frac{\partial m_j}{\partial y} + m_j \frac{\partial G_y}{\partial y} - \frac{\partial}{\partial y}\left(\gamma_j \frac{\partial m_j}{\partial y}\right) = \dot{m}_j'''$$

and applying continuity equation (4-1) using the assumption of a steady flow yields

$$G_x \frac{\partial m_j}{\partial x} + G_y \frac{\partial m_j}{\partial y} - \frac{\partial}{\partial y}\left(\gamma_j \frac{\partial m_j}{\partial y}\right) = \dot{m}_j''' \tag{4-18}$$

or

$$\rho u \frac{\partial m_j}{\partial x} + \rho v \frac{\partial m_j}{\partial y} - \frac{\partial}{\partial y}\left(\gamma_j \frac{\partial m_j}{\partial y}\right) = \dot{m}_j''' \tag{4-19}$$

If component j is *chemically inert* in the system, that is, there is *no chemical reaction,* then $\dot{m}_j''' = 0$, and (4-18) becomes

$$G_x \frac{\partial m_j}{\partial x} + G_y \frac{\partial m_j}{\partial y} - \frac{\partial}{\partial y}\left(\gamma_j \frac{\partial m_j}{\partial y}\right) = 0 \tag{4-20}$$

For *axisymmetric flow in a circular tube with axisymmetric diffusion*, an identical method leads to

$$\rho u \frac{\partial m_j}{\partial x} + \rho v_r \frac{\partial m_j}{\partial r} - \frac{1}{r}\frac{\partial}{\partial r}\left(r\gamma_j \frac{\partial m_j}{\partial r}\right) = 0 \tag{4-21}$$

General Equation for Steady-Flow Diffusion

If we discard the boundary-layer approximations and consider the complete steady-flow convection–diffusion problem in three dimensions, we need only add one more convection term and two additional diffusion terms. However, in this case the Cartesian coordinate representation becomes cumbersome. A neater formulation of the equations can be obtained by using vector notation. Thus the more general counterparts of Eqs. (4-18) and (4-20) become, respectively,

$$\mathbf{G} \cdot \nabla m_j - \nabla \cdot \gamma_j \nabla m_j = \dot{m}_j''' \tag{4-22}$$

$$\mathbf{G} \cdot \nabla m_j - \nabla \cdot \gamma_j \nabla m_j = 0 \tag{4-23}$$

Diffusion of Chemical Element α

It is sometimes more convenient, in considering diffusion with chemical reaction, to follow a particular chemical element rather than a compound. The advantage obviously lies in the fact that whereas a compound may be created or destroyed at any point in the flow field, an element is considered indestructible.

Define the mass concentration of an element α as follows. Let

n_α = kg of element α per kg of total mixture
$n_{\alpha,j}$ = kg of element α per kg of substance j

Note that $n_{\alpha,j}$ is not a variable but is simply fixed by the composition of substance j. For example, let α be carbon, then if the j-substance is CO, $n_{\mathrm{C,CO}} = 12/30$.

It then follows from the definitions that

$$n_\alpha = \sum_j n_{\alpha,j} m_j$$

$$\sum_\alpha n_\alpha = 1$$

Conservation of element α requires that

$$\sum_j n_{\alpha,j} \dot{m}_j''' = 0$$

We now use this expression, together with Eq. (4-18), to develop a boundary-layer diffusion equation for α. Multiply Eq. (4-18) through by $n_{\alpha,j}$:

$$n_{\alpha,j} G_x \frac{\partial m_j}{\partial x} + n_{\alpha,j} G_y \frac{\partial m_j}{\partial y} - n_{\alpha,j} \frac{\partial}{\partial y}\left(\gamma_j \frac{\partial m_j}{\partial y}\right) = n_{\alpha,j} \dot{m}_j'''$$

Summing over j yields

$$G_x \sum_j n_{\alpha,j} \frac{\partial m_j}{\partial x} + G_y \sum_j n_{\alpha,j} \frac{\partial m_j}{\partial y} - \sum_j n_{\alpha,j} \frac{\partial}{\partial y}\left(\gamma_j \frac{\partial m_j}{\partial y}\right) = \sum_j n_{\alpha,j} \dot{m}_j''' = 0$$

But since $n_{\alpha,j}$ is not a function of x or y, we can write

$$G_x \frac{\partial}{\partial x}\sum_j n_{\alpha,j}m_j + G_y \frac{\partial}{\partial y}\sum_j n_{\alpha,j}m_j - \frac{\partial}{\partial y}\sum_j \gamma_j \frac{\partial}{\partial y}(n_{\alpha,j}m_j) = 0$$

We now substitute the result that

$$\sum_j n_{\alpha,j}m_j = n_\alpha$$

and obtain the final form

$$G_x \frac{\partial n_\alpha}{\partial x} + G_y \frac{\partial n_\alpha}{\partial y} - \frac{\partial}{\partial y}\sum_j \gamma_j \frac{\partial}{\partial y}(n_{\alpha,j}m_j) = 0 \qquad \text{(4-24)}$$

Note that Eq. (4-24) is very similar to (4-20); and, in fact, if the γ_j are all the same, it will become identical, which is in anticipation of a simplification to be introduced later.

If we now discard the boundary-layer approximations and consider the complete steady-flow diffusion problem in three dimensions, it follows directly that

$$\mathbf{G} \cdot \nabla n_\alpha - \nabla \cdot \left(\sum_j \gamma_j n_{\alpha,j} \nabla m_j\right) = 0 \qquad \text{(4-25)}$$

which is comparable to Eq. (4-23).

THE ENERGY EQUATIONS

The Steady-Flow Energy Equation of the Boundary Layer

Consider steady flow along a semi-infinite surface with a free-stream velocity u_∞ and a free-stream temperature T_∞. Let the surface temperature be T_s, which may vary along the surface. There may or may not be mass transfer from the surface, and there may or may not be concentration gradients throughout the flow field. Chemical reaction may be taking place in the flow field.

In general, there will be heat exchange between the surface and the fluid. Thermodynamic equilibrium requires that the fluid just adjacent to the surface be at T_s, and the region in which the temperature changes from T_s to T_∞ is called the *thermal boundary layer* (Fig. 4-8).

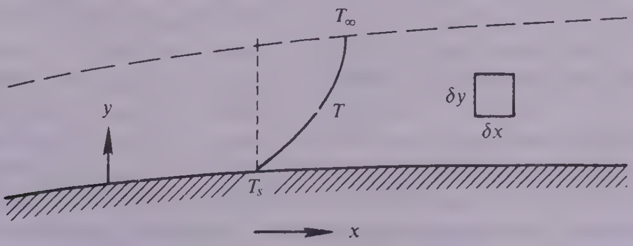

Figure 4-8 The thermal boundary layer.

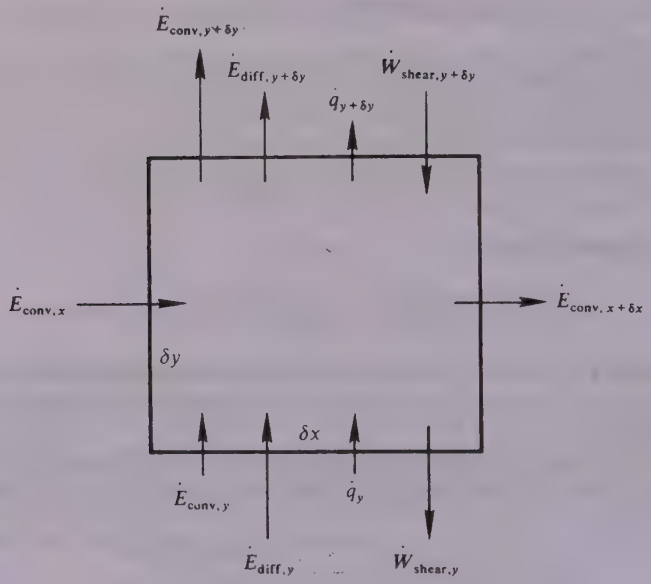
$\dot{E}_{\text{conv},y+\delta y}$
$\dot{E}_{\text{diff},y+\delta y}$
$\dot{W}_{\text{shear},y+\delta y}$
$\dot{q}_{y+\delta y}$
$\dot{E}_{\text{conv},x}$
$\dot{E}_{\text{conv},x+\delta x}$
δy
δx
$\dot{E}_{\text{conv},y}$
$\dot{q}_y$
$\dot{E}_{\text{diff},y}$
$\dot{W}_{\text{shear},y}$

Figure 4-9 Control volume and energy-transfer terms for development of the steady-flow energy differential equation of the boundary layer.

Let us cut out an infinitesimal stationary control volume of unit depth and examine the various rates of energy transfer across the control surface (Fig. 4-9). Several forms of energy transfer are present. Fluid crossing the boundary will carry its own internal thermal and chemical energy, as well as its kinetic energy and potential energy with respect to external force fields, and will do flow work on the control volume. Heat will be transferred as a result of the temperature gradients at the surface. If there are concentration gradients, there will be mass diffusion, and each component of the fluid mixture will carry its own energy. Work will be done on the control volume, and its surfaces, by shear forces.

These various energy-transfer streams are indicated symbolically on Fig. 4-9. Note that the boundary-layer approximation has been invoked so that velocity, temperature, and concentration gradients in the y direction only are considered.

Before evaluating the various energy-transfer terms on Fig. 4-9, let us examine in a little more detail the enthalpy i that will appear in all the convection terms and in the mass-diffusion terms. As a part of the boundary-layer approximation, it is assumed that the gradient of the normal stress is simply the gradient of the thermodynamic pressure. Thus the flow work done by each element of fluid as it crosses the control surface is merely Pv or P/ρ. The mixture enthalpy $i = e + P/\rho$ is then the sum of the internal energy and the flow work of the fluid, per unit mass. For substances that can react chemically, the internal energy includes the stored chemical energy. This point is developed in detail later. The distinction between i and i_j should next be noted: i without subscript refers to the entire mixture, J/kg, of mixture; i_j is the *partial enthalpy* of component j, J/kg of component j. Thus

$$\sum_j m_j i_j = i$$

The partial enthalpy i_j is a function of chemical composition, temperature, and pressure, although frequently we assume perfect gas behavior and hence neglect the pressure dependence. We have more to say later about the evaluation of i for particular fluid systems.

Making the assumptions (in addition to the boundary-layer approximations) of *steady flow and steady state, no internal heat generation, and no work done by external fields*, the energy-transfer terms become

$$\dot{E}_{\text{conv},\,x} = G_x\,\delta y\left(i + \tfrac{1}{2}u^2\right) \quad \text{(enthalpy plus kinetic energy, assuming } u^2 \gg v^2\text{)}$$

$$\dot{E}_{\text{conv},\,x+\delta x} = \delta y\left\{G_x\left(i + \frac{1}{2}u^2\right) + \frac{\partial}{\partial x}\left[G_x\left(i + \frac{1}{2}u^2\right)\right]\delta x\right\}$$

$$\dot{E}_{\text{conv},\,y} = G_y\,\delta x\left(i + \frac{1}{2}u^2\right)$$

$$\dot{E}_{\text{conv},\,y+\delta y} = \delta x\left\{G_y\left(i + \frac{1}{2}u^2\right) + \frac{\partial}{\partial y}\left[G_y\left(i + \frac{1}{2}u^2\right)\right]\delta y\right\}$$

$$\dot{E}_{\text{diff},\,y} = -\left(\sum_j \gamma_j \frac{\partial m_j}{\partial y} i_j\right)\delta x$$

(sum of diffusion rate of each component times enthalpy of that component, neglecting Soret effect)

$$\dot{E}_{\text{diff},\,y+\delta y} = -\left[\sum_j \gamma_j \frac{\partial m_j}{\partial y} i_j + \frac{\partial}{\partial y}\left(\sum_j \gamma_j \frac{\partial m_j}{\partial y} i_j\right)\delta y\right]\delta x$$

$$\dot{q}_y = -k\left(\frac{\partial T}{\partial y}\right)\delta x \qquad \text{(conduction heat transfer, neglecting Dufour effect)}$$

$$\dot{q}_{y+\delta y} = -\left[k\frac{\partial T}{\partial y} + \frac{\partial}{\partial y}\left(k\frac{\partial T}{\partial y}\right)\delta y\right]\delta x$$

$$\dot{W}_{\text{shear},\,y} = (\tau_{yx}u)\,\delta x \qquad \text{(shear force times velocity)}$$

$$\dot{W}_{\text{shear},\,y+\delta y} = \left[\tau_{yx}u + \frac{\partial}{\partial y}(\tau_{yx}u)\,\delta y\right]\delta x$$

Combining the above by the principle of conservation of energy, Eq. (2-5), and simplifying, we obtain

$$\frac{\partial}{\partial x}\left[G_x\left(i + \frac{1}{2}u^2\right)\right] + \frac{\partial}{\partial y}\left[G_y\left(i + \frac{1}{2}u^2\right)\right] - \frac{\partial}{\partial y}\left(k\frac{\partial T}{\partial y}\right)$$
$$- \frac{\partial}{\partial y}\left(\sum_j \gamma_j \frac{\partial m_j}{\partial y} i_j\right) - \frac{\partial}{\partial y}(\tau_{yx}u) = 0$$

Now expand the first two terms in this equation:

$$G_x\frac{\partial}{\partial x}\left(i+\frac{1}{2}u^2\right)+\left(i+\frac{1}{2}u^2\right)\frac{\partial G_x}{\partial x}+G_y\frac{\partial}{\partial y}\left(i+\frac{1}{2}u^2\right)+\left(i+\frac{1}{2}u^2\right)\frac{\partial G_y}{\partial y}$$
$$-\frac{\partial}{\partial y}\left(k\frac{\partial T}{\partial y}\right)-\frac{\partial}{\partial y}\left(\sum_j \gamma_j\frac{\partial m_j}{\partial y}i_j\right)-\frac{\partial}{\partial y}(\tau_{yx}u)=0$$

But, since by the continuity equation for a steady flow $\partial G_x/\partial x+\partial G_y/\partial y=0$, the second and fourth terms drop out. We then have

$$G_x\frac{\partial}{\partial x}\left(i+\frac{1}{2}u^2\right)+G_y\frac{\partial}{\partial y}\left(i+\frac{1}{2}u^2\right)-\frac{\partial}{\partial y}\left(k\frac{\partial T}{\partial y}\right)$$
$$-\frac{\partial}{\partial y}\left(\sum_j \gamma_j\frac{\partial m_j}{\partial y}i_j\right)-\frac{\partial}{\partial y}(\tau_{yx}u)=0 \tag{4-26}$$

Equation (4-26) is useful in its own right, and we use it in a later chapter. However, at present we combine it with the momentum equation to get a different form.

First take the term containing τ_{yx} and expand it:

$$\frac{\partial}{\partial y}(\tau_{yx}u)=\tau_{yx}\frac{\partial u}{\partial y}+u\frac{\partial \tau_{yx}}{\partial y}$$

From Eq. (3-1), under the boundary-layer approximations,

$$\tau_{yx}=\mu\frac{\partial u}{\partial y}$$

Substituting, we get

$$\frac{\partial}{\partial y}(\tau_{yx}u)=\mu\left(\frac{\partial u}{\partial y}\right)^2+u\frac{\partial}{\partial y}\left(\mu\frac{\partial u}{\partial y}\right)$$

To obtain an expression for the last term on the right-hand side, transpose the momentum equation, Eq. (4-10), and multiply through by u:

$$u\frac{\partial}{\partial y}\left(\mu\frac{\partial u}{\partial y}\right)=\rho u^2\frac{\partial u}{\partial x}+\rho uv\frac{\partial u}{\partial y}+u\frac{dP}{dx}$$

Now, combine the last two equations, substitute the result into Eq. (4-26), carry out the differentiation of the first two terms of Eq. (4-26), substitute $\rho u=G_x$ and $\rho v=G_y$, and the result can readily be simplified to

$$\rho u\frac{\partial i}{\partial x}+\rho v\frac{\partial i}{\partial y}-\frac{\partial}{\partial y}\left(k\frac{\partial T}{\partial y}\right)-\frac{\partial}{\partial y}\left(\sum_j \gamma_j\frac{\partial m_j}{\partial y}i_j\right)-\mu\left(\frac{\partial u}{\partial y}\right)^2-u\frac{dP}{dx}=0 \tag{4-27}$$

This is the steady flow energy equation of the boundary layer, including variable fluid properties, mass diffusion and chemical reaction, and viscous energy dissipation.

Both Eqs. (4-26) and (4-27) are perfectly valid energy equations of the boundary layer. The distinction is that the terms in Eq. (4-26) represent conservation of the sum of both mechanical and thermal energy (the First Law of Thermodynamics), while Eq. (4-27) is a statement of conservation of thermal energy alone and thus includes a thermal energy *creation* term (the term involving viscosity). The fact that Eq. (4-27) is in reality a *thermal* energy equation is obscured by the use of the enthalpy i, which contains a mechanical energy component. However, this component, the flow work, is actually offset by the pressure-gradient term.

It should be noted that in developing the equation we neglected *potential energy* due to *external fields* for the sake of brevity. However, had we included a force field in the x direction and then included the corresponding body force in the momentum equation that we combined with the energy equation, we would have found that the effects of the external fields cancel. Thus Eq. (4-27) is valid in the presence of external force fields. On the other hand, a body force X (which might be a gravity force) would result in an additional term, $-uX$, on the left-hand side of Eq. (4-26).

Note that we have also neglected any internal heat sources, such as might be produced by the resistance offered to an electric current. Such effects, which are lumped into a source function S, W/m^3, in the more general energy equation given below, can be subtracted from the left-hand sides of Eqs. (4-26) and (4-27) if desired. Note, however, that conversion of chemical energy to thermal energy has already been included in the enthalpy terms by the definition of the internal energy.

The corresponding equation for *axisymmetric flow in a circular tube with axisymmetric heating* can be developed in an identical manner to yield

$$\rho u \frac{\partial i}{\partial x} + \rho v_r \frac{\partial i}{\partial r} - \frac{1}{r}\frac{\partial}{\partial r}\left(rk\frac{\partial T}{\partial r}\right) - \frac{1}{r}\frac{\partial}{\partial r}\left(r\sum_j \gamma_j \frac{\partial m_j}{\partial r} i_j\right)$$

$$-\mu\left(\frac{\partial u}{\partial r}\right)^2 - u\frac{dP}{dx} = 0 \qquad (4\text{-}28)$$

A little more insight into the significance of the mass-diffusion term in the energy equation and the net mass flux G can be gained if we reexamine the mass crossing the lower surface of the control volume shown in Fig. 4-7. It should be borne in mind here that we are discussing mixtures of fluids rather than single-component fluids; hence when we speak of the velocity of the mixture, the term *velocity* is ambiguous. There is no velocity that is entirely appropriate; what is meant by mixture velocity is the mass-weighted average of the velocities of the various components. Some of the components are moving faster, and some slower, than this average.

According to Fig. 4-7, the total flow of component j crossing the lower surface is

$$G_y m_j \,\delta x - \gamma_j \frac{\partial m_j}{\partial y}\,\delta x$$

The total flow of *all* components crossing this surface must be the summation of this quantity over j; *but, by definition of* G_y, this is also $G_y\,\delta x$. Thus

$$G_y\,\delta x = G_y\,\delta x \sum_j m_j - \delta x \sum_j \gamma_j \frac{\partial m_j}{\partial y}$$

But

$$\sum_j m_j = 1$$

Therefore

$$G_y = G_y - \sum_j \gamma_j \frac{\partial m_j}{\partial y}$$

or

$$\sum_j \gamma_j \frac{\partial m_j}{\partial y} = 0 \tag{4-29}$$

This result simply means that diffusion of a certain mass of one or more components in the positive y direction is always accompanied by diffusion of an equal mass of other components in the negative y direction. This obviously must be the case, for it is not possible to have a concentration gradient of one component without corresponding opposite concentration gradients of the other components. Note again that G is the net mass flux, regardless of whether diffusion is taking place.

If one now examines the mass-diffusion term in Eq. (4-26) in the light of conclusion (4-29), it is apparent that this term is of importance only when the enthalpy of the various components differs; if each component has the same enthalpy then the i_j factors out and the summation goes to zero. This fact permits some later simplifications to the energy equation.

The General Viscous Energy Equation

Now let us consider the general three-dimensional problem in Cartesian coordinates, including nonsteady flow with a source function. In so doing, let us use the complete expressions for the normal stresses, Eqs. (3-4)–(3-6), when evaluating the work done on the control volume as each unit of mass crosses the surface, rather than merely the thermodynamic pressure as before. Let us also use the complete shear-stress equations, Eqs. (3-1)–(3-3). This complicates the problem algebraically to a considerable degree, but in principle the procedure is no different from that used to develop Eq. (4-26), and from there to develop Eq. (4-27). In the final step, analogous to the development of Eq. (4-27), the Navier–Stokes equations are combined with the energy equation. The resulting equation can be simplified to a form in which the various terms are arranged in the same order as in Eq. (4-27), so that the origin of each term can be readily appreciated.

$$\left(\rho u\frac{\partial i}{\partial x}+\rho v\frac{\partial i}{\partial y}+\rho w\frac{\partial i}{\partial z}+\rho\frac{\partial i}{\partial t}\right)$$
$$-\left[\frac{\partial}{\partial x}\left(k\frac{\partial T}{\partial x}\right)+\frac{\partial}{\partial y}\left(k\frac{\partial T}{\partial y}\right)+\frac{\partial}{\partial z}\left(k\frac{\partial T}{\partial z}\right)\right]$$
$$-\left[\frac{\partial}{\partial x}\left(\sum_j \gamma_j\frac{\partial m_j}{\partial x}i_j\right)+\frac{\partial}{\partial y}\left(\sum_j \gamma_j\frac{\partial m_j}{\partial y}i_j\right)+\frac{\partial}{\partial z}\left(\sum_j \gamma_j\frac{\partial m_j}{\partial z}i_j\right)\right]$$
$$-\mu\phi-\left(u\frac{\partial P}{\partial x}+v\frac{\partial P}{\partial y}+w\frac{\partial P}{\partial z}+\frac{\partial P}{\partial t}\right)=S \qquad (4\text{-}30)$$

where ϕ is the *dissipation function*:

$$\phi=2\left[\left(\frac{\partial u}{\partial x}\right)^2+\left(\frac{\partial v}{\partial y}\right)^2+\left(\frac{\partial w}{\partial z}\right)^2\right]+\left[\left(\frac{\partial u}{\partial y}+\frac{\partial v}{\partial x}\right)^2+\left(\frac{\partial v}{\partial z}+\frac{\partial w}{\partial y}\right)^2\right.$$
$$\left.+\left(\frac{\partial w}{\partial x}+\frac{\partial u}{\partial z}\right)^2\right]-\frac{2}{3}\left[\frac{\partial u}{\partial x}+\frac{\partial v}{\partial y}+\frac{\partial w}{\partial z}\right]^2$$

The terms in the first and last brackets of the dissipation function come from the viscous part of the normal stresses, whereas the second bracketed terms come from the shear stresses. Note that in the boundary-layer approximation only 1 of these 12 terms is retained.

Equation (4-30) can be written more compactly by using vector notation and the substantial derivative, thus avoiding reference to any coordinate system:

$$\rho\frac{Di}{Dt}-\nabla\cdot k\,\nabla T-\nabla\cdot\left(\sum_j \gamma_j i_j\,\nabla m_j\right)-\mu\phi-\frac{DP}{Dt}=S \qquad (4\text{-}31)$$

In Cartesian tensor notation the general viscous energy equation becomes

$$\rho\frac{Di}{Dt}-\frac{\partial}{\partial x_l}\left(k\frac{\partial T}{\partial x_l}\right)-\frac{\partial}{\partial x_l}\left(\sum_j \gamma_j i_j\frac{\partial m_j}{\partial x_l}\right)-\mu\phi-\frac{DP}{Dt}=S \qquad (4\text{-}32)$$

where

$$\phi=\left(\frac{\partial u_i}{\partial x_j}+\frac{\partial u_j}{\partial x_i}-\frac{2}{3}\frac{\partial u_l}{\partial x_l}\delta_{ij}\right)\frac{\partial u_i}{\partial x_j}$$

The most general coordinate system for the continuity, Navier–Stokes, and viscous energy equations is that of curvilinear orthogonal coordinates; see Back.[4]

Various Particularizations of the Energy Equation

We have actually already considered some particular forms of the energy equation, having directly derived Eq. (4-27) for steady flow in a two-dimensional

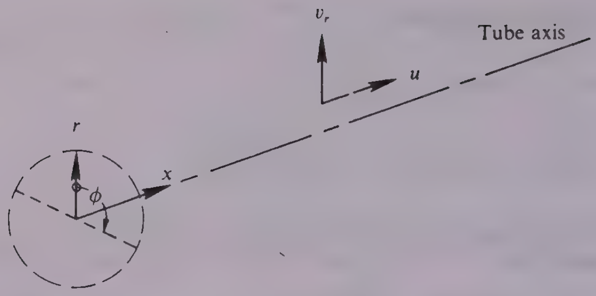

Figure 4-10 Coordinate system for flow in a circular tube.

boundary layer and, by implication, Eq. (4-28) for steady axisymmetric flow and heating in a circular tube. Since we are going to be concerned with the energy equation throughout this book, it is worthwhile at this time to assemble some of the other forms of this equation that are employed later.

If we restrict consideration for the moment to *steady flow*, the time dependence of Eq. (4-31) can be dropped, and the $\rho(Di/Dt)$ term can then be expressed in terms of the mass-flux vector. If we further limit consideration to *no source function* and to *low velocities* such that the dissipation function may be neglected (and this approximation is discussed further later) and then *neglect the pressure-gradient term* (which is often justifiable), we obtain

$$\mathbf{G} \cdot \nabla i - \nabla \cdot k\,\nabla T - \nabla \cdot \left(\sum_j \gamma_j i_j \nabla m_j \right) = 0 \tag{4-33}$$

and for the case of no mass concentration gradients

$$\mathbf{G} \cdot \nabla i - \nabla \cdot k\,\nabla T = 0 \tag{4-34}$$

which is similar in form to (4-23) and (4-25).

For flow in a *circular tube*, or a circular tube annulus, we are concerned with problems where the flow is hydrodynamically axisymmetric but where the heat transfer may not be axisymmetric. By employing the cylindrical coordinate system shown on Fig. 4-10, Eq. (4-34) becomes

$$u\rho\frac{\partial i}{\partial x} + v_r\rho\frac{\partial i}{\partial r} - \left[\frac{1}{r}\frac{\partial}{\partial r}\left(rk\frac{\partial T}{\partial r}\right) + \frac{1}{r^2}\frac{\partial}{\partial \phi}\left(k\frac{\partial T}{\partial \phi}\right) + \frac{\partial}{\partial x}\left(k\frac{\partial T}{\partial x}\right)\right] = 0 \tag{4-35}$$

Note that this equation contains a conduction term in the x direction, which was neglected under the boundary-layer assumption in the development of Eq. (4-28).

For flow in *rectangular* or *triangular tubes* a Cartesian coordinate system becomes convenient (Fig. 4-11), and the corresponding equation is then

$$u\rho\frac{\partial i}{\partial x} + v\rho\frac{\partial i}{\partial y} + w\rho\frac{\partial i}{\partial z} - \left[\frac{\partial}{\partial x}\left(k\frac{\partial T}{\partial x}\right) + \frac{\partial}{\partial y}\left(k\frac{\partial T}{\partial y}\right) + \frac{\partial}{\partial z}\left(k\frac{\partial T}{\partial z}\right)\right] = 0 \tag{4-36}$$

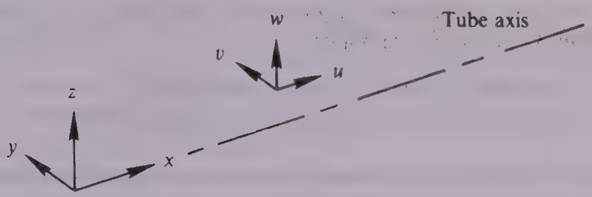

Figure 4-11 Coordinate system and corresponding velocity components for flow in a rectangular tube.

Obviously there are a great variety of particular forms of the energy equation, depending on the idealizations that can be made in particular applications. Equations (4-30)–(4-32) provide the basic relations from which these forms can be developed.

In addition to the system geometry and the idealizations, one other factor affects the form of the energy equation: the fluid. The applicable *thermodynamic equation of state* has a rather considerable influence on the form that the energy equation ultimately takes, for the enthalpy i must be related to the other fluid properties. For example, let us go back to the boundary-layer energy equation (4-27) and consider the case of a perfect gas. Then

$$di = c\,dT$$

where c is understood to represent the constant-pressure specific heat.

Let us omit mass diffusion for brevity and note that for a gas the $(u\,dP/dx)$ term can generally be shown to be negligible for cases where the stagnation enthalpy equation does not have to be used. Then Eq. (4-27) becomes

$$u\rho c\frac{\partial T}{\partial x} + v\rho c\frac{\partial T}{\partial y} - \frac{\partial}{\partial y}\left(k\frac{\partial T}{\partial y}\right) - \mu\left(\frac{\partial u}{\partial y}\right)^2 = 0 \qquad (4\text{-}37)$$

On the other hand, for a liquid with *constant density*

$$di = d\left(e + \frac{P}{\rho}\right) = c\,dT + \frac{1}{\rho}dP$$

Substituting in Eq. (4-27) and again omitting mass diffusion but *not* the pressure-gradient term, we obtain

$$\rho u\left(c\frac{\partial T}{\partial x} + \frac{1}{\rho}\frac{dP}{dx}\right) + \rho v\left(c\frac{\partial T}{\partial y} + 0\right) - \frac{\partial}{\partial y}\left(k\frac{\partial T}{\partial y}\right) - \mu\left(\frac{\partial u}{\partial y}\right)^2 - u\frac{dP}{dx} = 0$$

This time the pressure-gradient term cancels without any assumptions about its influence, and we again obtain Eq. (4-37).

If the thermal conductivity k can be treated as constant, which is a quite good assumption for liquids and a reasonable assumption for a gas with small temperature gradients, Eq. (4-37) becomes

$$u\frac{\partial T}{\partial x} + v\frac{\partial T}{\partial y} - \frac{k}{\rho c}\frac{\partial^2 T}{\partial y^2} - \frac{\mu}{\rho c}\left(\frac{\partial u}{\partial y}\right)^2 = 0$$

Defining $\alpha = k/\rho c$, the *thermal diffusivity* of the fluid, and introducing the Prandtl number, $\mathrm{Pr} = \mu c/k$, we obtain

$$u\frac{\partial T}{\partial x} + v\frac{\partial T}{\partial y} - \alpha\left[\frac{\partial^2 T}{\partial y^2} + \frac{\mathrm{Pr}}{c}\left(\frac{\partial u}{\partial y}\right)^2\right] = 0 \qquad (4\text{-}38)$$

Here we see the dissipation function (the last term) depends not only on the velocity but also on the Prandtl number. Viscous energy dissipation can be important for high-Prandtl-number fluids (oils, for example), even for rather moderate velocities and velocity gradients. For gases, on the other hand, where the Prandtl number is near 1, we shall see later that the velocity must approach the speed of sound before this term is significant.

Under conditions where viscous energy dissipation can be neglected, Eq. (4-38) finally becomes

$$u\frac{\partial T}{\partial x} + v\frac{\partial T}{\partial y} - \alpha\frac{\partial^2 T}{\partial y^2} = 0 \qquad (4\text{-}39)$$

and integration of this equation, or its equivalent in other coordinate systems, for various boundary conditions constitutes a substantial part of some of the later chapters.

PROBLEMS

4-1. Consider steady flow of a constant-property fluid in a long duct formed by two parallel planes. Consider a point sufficiently far removed from the duct entrance that the y component of velocity is zero and the flow is entirely in the x direction. Write the Navier–Stokes equations for both the x and y directions. What can you deduce about the pressure gradients?

4-2. Consider flow in the eccentric annulus of a journal bearing in which there is no axial flow. Deduce the applicable laminar boundary-layer equations (continuity, momentum, energy) for a constant-density fluid, with uniform composition, in an appropriate coordinate system.

4-3. Deduce a set of boundary-layer differential equations (continuity, momentum, energy) for steady flow of a constant-property fluid without body forces, and with negligible viscous dissipation, in a coordinate system suitable for analysis of the boundary layer on the surface of a rotating disk.

4-4. Starting with the general viscous energy equation, show by a succession of steps how and why it reduces to the classic heat-conduction equation for a solid, and finally to the Laplace equation.

4-5. Derive Eq. (4-18) using Eq. (4-1) and the definitions from the Fick's law section of Chap. 3.

4-6. Derive the conservation laws for axisymmetric flow in a pipe using control volume principles similar to that developed in the text for Cartesian coordinate flow. Assume steady flow, steady state, and constant properties. For the momentum equation neglect body forces. For the energy equation neglect body force work and the energy source. Also, for the energy equation use the thermal equation of state for ideal gases or incompressible liquids, and assume the Mach number is small for the case of the ideal gas, but do not neglect viscous dissipation. Assume boundary-layer flow, but do not neglect axial conduction.

4-7. Derive the constant-property energy equation (4-39) starting with Eq. (4-26). Be sure to state all assumptions made.

REFERENCES

1. Deissler, R. G.: *Am. J. Phys.*, vol. 44, pp. 1128–1130, 1976.
2. Schlichting, H.: *Boundary Layer Theory*, 6th ed., pp. 117–121, McGraw-Hill, New York, 1968.
3. Streeter, V. L.: *Fluid Dynamics*, pp. 242–243, McGraw-Hill, New York, 1948.
4. Back, L. H.: TR 32-1332, Jet Propulsion Laboratory, California Institute of Technology, Pasadena, September 15, 1968. (See also *Handbook of Tables for Applied Engineering Science*, 2d ed., pp. 496–501, Chemical Rubber Company Press, Cleveland, Ohio, 1973.)

5 CHAPTER

Integral Equations for the Boundary Layer

Particular solutions to the boundary-layer differential equations can be obtained, at least for a laminar flow, for almost any boundary condition. Exact analytic solutions have been obtained only for certain classes of problems, however, and numerical methods are frequently necessary for the more general problem. When the calculation procedure becomes tedious, it is often worthwhile to look for approximate methods of solution, such as integral methods. The integral equations of the boundary layer provide the basis for a number of approximate procedures, but are, in themselves, exact, at least within the boundary-layer approximation. The approximate nature of the integral solutions arises from the manner in which they are generally employed.

First we develop the momentum integral equation of the boundary layer in a fairly general manner, so that it can be employed for flow inside and over axisymmetric bodies as well as along plane surfaces. Then we use a similar procedure to develop an energy integral equation. In so doing, we also take the opportunity to introduce and define some useful integral parameters: the displacement thickness, the momentum thickness, and the enthalpy thickness.

THE MOMENTUM INTEGRAL EQUATION

Consider a body of revolution over which there is axisymmetric flow. Assume that a thin momentum boundary layer is developing on this surface, with the various dimensions and parameters defined as in Fig. 5-1.

Let us consider a stationary control volume fixed to the body surface. Take the length of the control volume in the x direction (along the surface) to be infinitesimal, δx, but let the height (normal to the surface) be a finite distance Y.

The distance Y may extend to a point within the boundary layer, or it may extend effectively beyond the boundary layer; in either case the assumption of a "thin" boundary layer allows the stipulation that $Y \ll R$, where R is the radius

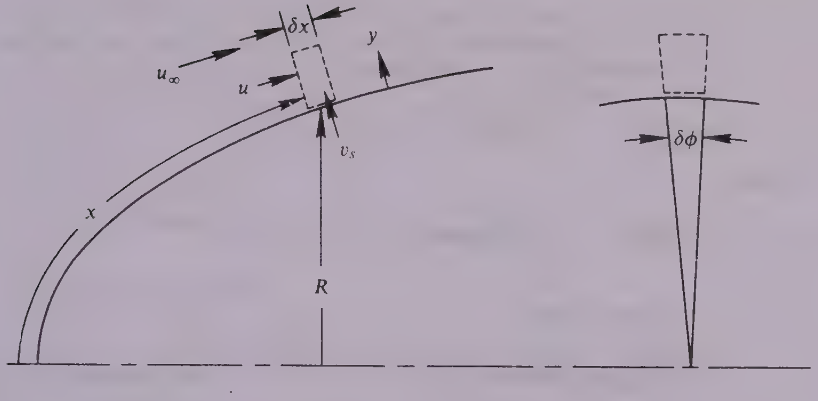

(a) (b)

Figure 5-1 Coordinate system and location of the control volume for development of the momentum integral equation of the boundary layer on a body of revolution.

of revolution (transverse radius of curvature) of the body. Thus the surface could also be the inside of a circular-section nozzle, with R measured from a centerline in the main fluid stream. In either case, as R is made indefinitely large, we approach a two-dimensional surface, that is, a plane. Presumably we can express $R = R(x)$.

Let u_∞ designate the free-stream velocity in the x direction just *outside* the boundary layer. If the boundary layer is "thin," u_∞ will be approximately equal to the velocity at the surface, as computed by a potential flow analysis for the body. Presumably $u_\infty = u_\infty(x)$.

We assume that there is fluid flow through the body surface by injection, suction, or other forms of mass transfer. Using a subscript s to designate fluid conditions at the interface, the velocity of the injected fluid is v_s in the y direction.

By employing a control volume that is infinitesimal in the x direction but finite in the y direction, we intend to develop a differential equation that has, in effect, already been integrated in the y direction. We do so by simply applying the principles of conservation of mass and momentum to the control volume shown in Fig. 5-2 for steady flow. Note that $R \gg Y$.

Applying Eq. (2-1), we have

$$\left[R\,\delta\phi\,\delta x\,v_Y\rho_Y + R\,\delta\phi\int_0^Y u\rho\,dy + \delta\phi\frac{d}{dx}\left(R\int_0^Y u\rho\,dy\right)\delta x\right]$$
$$-\left(R\,\delta\phi\,\delta x\;v_s\rho_s + R\,\delta\phi\int_0^Y u\rho\,dy\right) = 0$$

from which

$$v_Y\rho_Y = v_s\rho_s - \frac{1}{R}\frac{d}{dx}\left(R\int_0^Y u\rho\,dy\right) \tag{5-1}$$

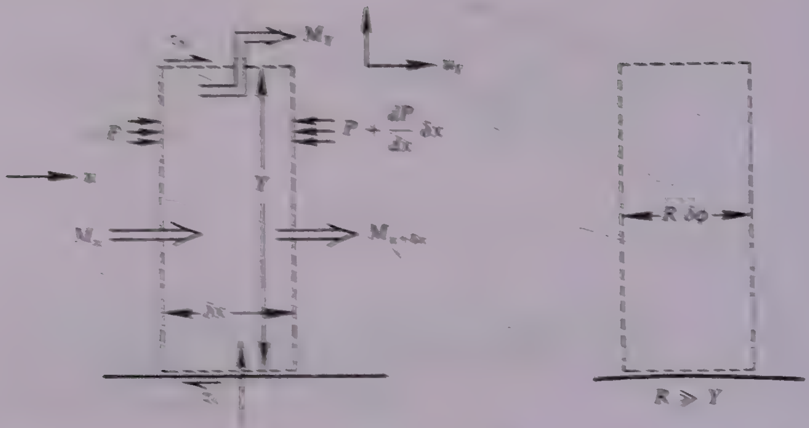

Figure 5-2 Control volume for development of the momentum integral equation of the boundary layer.

We then apply Eq. (2-4) to the control volume in the same manner, considering momentum flux and forces in the x direction only. Thus

$$M_x = R\,\delta\phi \int_0^Y \rho u^2\, dy$$

$$M_{x+\delta x} = R\,\delta\phi \int_0^Y \rho u^2\, dy + \delta\phi \frac{d}{dx}\left(R \int_0^Y \rho u^2\, dy\right)\delta x$$

$$M_Y = R\,\delta\phi\,\delta x\, v_Y \rho_Y u_Y$$

(Note that M_Y is the product of the mass flow across the top of the control volume and the x component of velocity of that flow.)

Combining these momentum terms with the pressure and shear force terms in Fig. 5-2, and simplifying, we obtain

$$\tau_Y - \tau_s - Y\frac{dP}{dx} = \frac{1}{R}\frac{d}{dx}\left(R \int_0^Y \rho u^2\, dy\right) + \rho_Y v_Y u_Y$$

Now combine with Eq. (5-1), and at the same time let Y become sufficiently large that $u_Y = u_\infty$ and $\tau_Y = 0$; in other words, let Y be larger than the effective boundary-layer thickness:

$$-\tau_s = \frac{1}{R}\frac{d}{dx}\left(R \int_0^Y \rho u^2\, dy\right) - \frac{u_\infty}{R}\frac{d}{dx}\left(R \int_0^Y \rho u\, dy\right) + \rho_s v_s u_\infty + \int_0^Y \frac{dP}{dx}\, dy \tag{5-2}$$

Since Y extends past the boundary layer, the velocity u_∞ is related to the pressure P by inviscid flow behavior. Accordingly, we can take advantage of the

Bernoulli equation for inviscid flow along a streamline to relate the pressure-gradient term to the free-stream velocity gradient:

$$\frac{dP}{\rho_\infty} = -d\left(\frac{u_\infty^2}{2}\right)$$

from which

$$\frac{dP}{dx} = -\rho_\infty u_\infty \frac{du_\infty}{dx} \tag{5-3}$$

Then Eq. (5-2) becomes

$$-\tau_s = \frac{1}{R}\frac{d}{dx}\left(R\int_0^Y \rho u^2\,dy\right) - \frac{u_\infty}{R}\frac{d}{dx}\left(R\int_0^Y \rho u\,dy\right) + \rho_s v_s u_\infty + \int_0^Y\left(-\rho_\infty u_\infty \frac{du_\infty}{dx}\right)dy \tag{5-4}$$

Equation (5-4) is the momentum integral equation of the boundary layer, developed under conditions where the fluid density may be variable, and applicable for flow over or inside an axisymmetric body where the boundary-layer thickness is much less than the local radius of curvature. For a two-dimensional body the radius R obviously drops out.

After defining and developing the boundary-layer thickness parameters below, we will be able to write more compact forms of the momentum integral equation.

THE DISPLACEMENT AND MOMENTUM THICKNESSES

Mathematically the boundary layer extends indefinitely in the y direction, although practically speaking the major velocity change takes place, in the usual case, very close to the body surface. Nevertheless, there is generally some ambiguity in speaking of the boundary-layer "thickness" if what is meant is the region in which velocity changes from u_∞ to 0. We find it both convenient and far more useful to define some boundary-layer thickness parameters that are completely unambiguous. These are called the *displacement thickness* δ_1 and the *momentum thickness* δ_2.

Consider a two-dimensional flow along a flat surface (Fig. 5-3) such that a boundary layer grows, starting at $x = 0$.

Take a control surface $ABCD$ and consider the following integral statements:

$$\text{Mass flow across } AB = \int_0^Y u_\infty \rho_\infty\,dy$$

$$\text{Mass flow across } CD = \int_0^Y u\rho\,dy$$

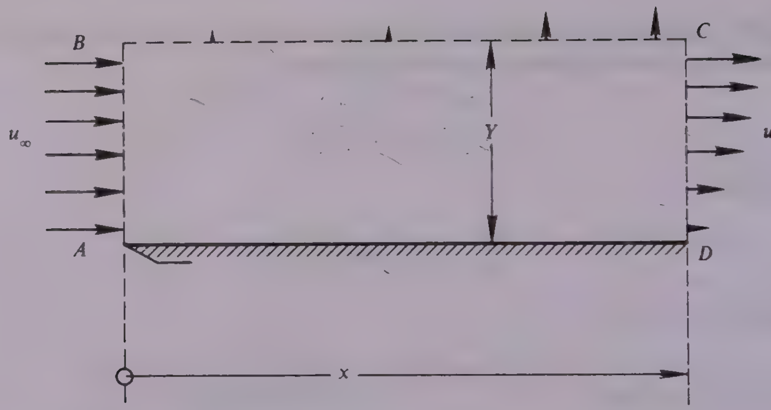

Figure 5-3 Control volume for development of the concept of displacement thickness and momentum thickness of the boundary layer.

Thus, by conservation of mass,

$$\text{Mass flow across } BC = \int_0^Y u_\infty \rho_\infty \, dy - \int_0^Y u\rho \, dy$$
$$= u_\infty \rho_\infty \int_0^Y \left(1 - \frac{u\rho}{u_\infty \rho_\infty}\right) dy$$

Now let $Y \to \infty$ so that the entire boundary layer is enclosed; let us *define* δ_1 such that

$$\delta_1 u_\infty \rho_\infty = u_\infty \rho_\infty \int_0^\infty \left(1 - \frac{u\rho}{u_\infty \rho_\infty}\right) dy$$
$$\delta_1 = \int_0^\infty \left(1 - \frac{u\rho}{u_\infty \rho_\infty}\right) dy \tag{5-5}$$

Thus δ_1 is a measure of the *displacement* of the main stream resulting from the presence of the flat plate and its boundary layer. Similarly,

$$x\text{-momentum flux across } AB = \int_0^Y \rho_\infty u_\infty^2 \, dy$$

$$x\text{-momentum flux across } CD = \int_0^Y \rho u^2 \, dy$$

If Y is sufficiently large that u is essentially u_∞ at Y then

$$x\text{-momentum flux across } BC = u_\infty \left[u_\infty \rho_\infty \int_0^Y \left(1 - \frac{u\rho}{u_\infty \rho_\infty}\right) dy \right]$$

Then the net rate of loss of momentum in the control volume is

$$\int_0^Y \rho_\infty u_\infty^2\,dy - \int_0^Y \rho u^2\,dy - u_\infty^2\rho_\infty \int_0^Y \left(1 - \frac{u\rho}{u_\infty\rho_\infty}\right) dy = \int_0^Y \rho u(u_\infty - u)\,dy$$

Again let $Y \to \infty$ and then define δ_2 such that

$$\delta_2 u_\infty^2 \rho_\infty = \int_0^\infty \rho u(u_\infty - u)\,dy$$

$$\delta_2 = \int_0^\infty \frac{\rho u}{\rho_\infty u_\infty}\left(1 - \frac{u}{u_\infty}\right) dy \tag{5-6}$$

Thus the *momentum thickness* is a measure of the momentum flux decrement caused by the boundary layer, which, according to the momentum theorem, is proportional to the drag of the plate.[†]

ALTERNATIVE FORMS OF THE MOMENTUM INTEGRAL EQUATION

Examination of Eq. (5-4) reveals that the integrals are essentially the same as appear in the definitions of δ_1 and δ_2, provided we change the upper limit in Eqs. (5-5) and (5-6) from ∞ to Y. This is valid since we have already assumed in the development of Eq. (5-4) that Y is sufficiently large that $u_Y = u_\infty$. Thus we can evidently replace the integrals in Eq. (5-4) and express the momentum integral equation in terms of the boundary-layer thickness parameters. After rearranging and simplifying, we obtain

$$\frac{\tau_s}{\rho_\infty u_\infty^2} + \frac{\rho_s v_s}{\rho_\infty u_\infty} = \frac{d\delta_2}{dx} + \delta_2\left[\left(2 + \frac{\delta_1}{\delta_2}\right)\frac{1}{u_\infty}\frac{du_\infty}{dx} + \frac{1}{\rho_\infty}\frac{d\rho_\infty}{dx} + \frac{1}{R}\frac{dR}{dx}\right] \tag{5-7}$$

Equation (5-7) is simply an ordinary differential equation for δ_2 as a function of x, and this equation, although in a sense exact, also forms the basis for many approximate boundary-layer solutions. The approximations generally arise as the result of some assumptions about the relationship between τ_s and δ_2, the thickness ratio δ_1/δ_2 (frequently called the *shape factor*), or an assumed function for the velocity profile u/u_∞.

Various particularizations of Eq. (5-7) can be obtained by dropping suitable terms. For example, for constant-density flow along a two-dimensional surface

---

[†] Note that if $v_s \neq 0$, or if R varies with x, then δ_1 and δ_2 no longer have the simple physical meaning implied in this development. Nevertheless, the defining equations (5-5) and (5-6) remain valid and unambiguous. The reader is referred to Hokenson[1] for boundary-layer thickness parameter definitions that are more general.

$(R \to \infty)$ with no suction or blowing $(v_s = 0)$, we obtain the simpler form

$$\frac{\tau_s}{\rho_\infty u_\infty^2} = \frac{d\delta_2}{dx} + \delta_2 \left[\left(2 + \frac{\delta_1}{\delta_2} \right) \frac{1}{u_\infty} \frac{du_\infty}{dx} \right] \tag{5-8}$$

A still more restricted form results if there is no pressure gradient, so that u_∞ is a constant:

$$\frac{\tau_s}{\rho_\infty u_\infty^2} = \frac{d\delta_2}{dx} \tag{5-9}$$

Later we will find it convenient to define a local friction coefficient c_f that is dimensionless and given by

$$c_f = \frac{\tau_s}{\frac{1}{2}\rho_\infty u_\infty^2} \tag{5-10}$$

Substituting in Eq. (5-9),

$$\frac{c_f}{2} = \frac{d\delta_2}{dx} \tag{5-11}$$

THE ENERGY INTEGRAL EQUATION

Integral methods for solution of the thermal boundary layer can be used to obtain approximate solutions in much the same manner as for the momentum boundary layer. The energy integral equation of the boundary layer is developed in a rather general manner applicable to a compressible, high-velocity fluid, with or without suction or injection, including viscous heat generation and chemical reaction, and for a body of revolution as well as a flat plate.

Consider a body of revolution over which there is steady axial fluid flow (Fig. 5-4). Let the surface temperature of the body vary in the direction of flow in any arbitrary manner, and let there be fluid flow through the body surface at a

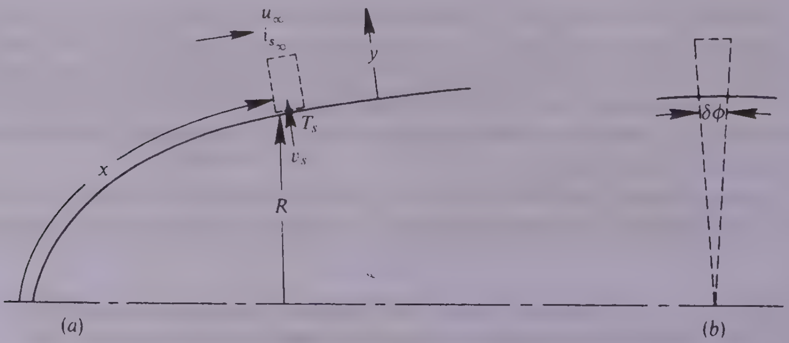

Figure 5-4 Coordinate system and location of the control volume for development of the energy integral equation of the boundary layer.

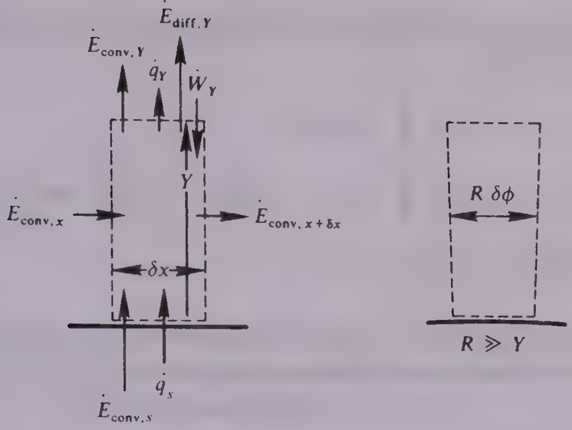
$\dot{E}_{\text{diff},Y}$
$\dot{E}_{\text{conv},Y}$
$\dot{q}_Y$
$\dot{W}_Y$
Y
$\dot{E}_{\text{conv},x}$
$\dot{E}_{\text{conv},x+\delta x}$
δx
$\dot{q}_s$
$\dot{E}_{\text{conv},s}$
$R\,\delta\phi$
$R \gg Y$

Figure 5-5 Control volume for development of the energy integral equation of the boundary layer.

velocity (normal to the free-stream direction) that can vary in an arbitrary manner along the surface. The fluid flowing through the wall can, in general, be the same as or different from the free-stream fluid. There are no variations of any kind in the ϕ direction, and the *stagnation enthalpy* of the free-stream fluid is everywhere constant.

Consider the steady-state energy-transfer rates across the surfaces of a control volume in the boundary layer (Fig. 5-5). Let the control volume be of infinitesimal extent in the flow direction, but of finite height Y in the direction normal to the surface; and let it be fixed to the surface at $y = 0$. Assume that velocity and temperature gradients in the x direction are negligible relative to the corresponding gradients in the y direction (the boundary-layer approximation), and ignore the work done on the control volume by the normal *viscous* stresses. Convection will be the only energy transport mechanism in the x direction, while in the y direction there will be heat transfer and shear-work transfer as well as convection.

Application of the conservation-of-energy principle, Eq. (2-5), to the control volume for steady flow yields

$$(\dot{E}_{\text{conv},x+\delta x} + \dot{E}_{\text{conv},Y} + \dot{E}_{\text{diff},Y} + \dot{q}_Y) - (\dot{E}_{\text{conv},x} + \dot{E}_{\text{conv},s} + \dot{q}_s + \dot{W}_Y) = 0 \tag{5-12}$$

Each of the convection terms is the product of the mass flow and of the stagnation enthalpy (thermal and chemical enthalpy plus kinetic energy). For the enthalpy terms, we can simplify the algebra if we shift the reference or datum for enthalpy by letting the *enthalpy datum* be the *free-stream stagnation state*, which has already been designated as a constant. Thus

$$i^*_{\text{ref}} = \left(i + \tfrac{1}{2}u^2\right) - \left(i_\infty + \tfrac{1}{2}u^2_\infty\right)$$

and

$$i^*_{\text{ref},\infty} = 0$$

We now write expressions for each of the terms in Eq. (5-12), based on the appropriate flux laws:

$$\dot{E}_{\text{conv},x} = R\,\delta\phi \int_0^Y \rho u i^*_{\text{ref}}\,dy$$

$$\dot{E}_{\text{conv},x+\delta x} = R\,\delta\phi \int_0^Y \rho u i^*_{\text{ref}}\,dy + \delta\phi \frac{d}{dx}\left(R \int_0^Y \rho u i^*_{\text{ref}}\,dy\right) dx$$

$$\dot{E}_{\text{conv},s} = R\,\delta\phi\,\delta x\;\rho_s v_s i^*_{\text{ref},s}$$

$$\dot{q}_s = R\,\delta\phi\,\delta x\;\dot{q}''_s$$

Now let Y be sufficiently large that all properties at Y are free-stream properties; that is, Y is larger than the boundary-layer thickness. Under these conditions,

$$\dot{E}_{\text{conv},Y} = R\,\delta\phi\,\delta x\;\rho_Y v_Y i^*_{\text{ref},Y} = 0$$

$$\dot{E}_{\text{diff},Y} = 0$$

$$\dot{q}_Y = 0, \qquad \dot{W}_Y = 0$$

Substituting in Eq. (5-12) and rearranging, we have

$$\dot{q}''_s = \frac{1}{R}\frac{d}{dx}\left(R \int_0^Y \rho u i^*_{\text{ref}}\,dy\right) - \rho_s v_s i^*_{\text{ref},s} \tag{5-13}$$

Equation (5-13) is the energy integral equation of the boundary layer. After developing the thermal boundary-layer thickness parameters below, we will be able to write more compact forms of the energy integral equation.

THE ENTHALPY AND CONDUCTION THICKNESSES

The problem of defining a thickness of the thermal boundary layer is similar to that posed by the momentum boundary layer. Again we can define integral thickness parameters in an unambiguous way, and we make use of two—the *enthalpy thickness* and the *conduction thickness*. The physical significance of these parameters should be apparent merely from their definitions. The enthalpy thickness is defined as

$$\Delta_2 = \int_0^\infty \frac{\rho u i^*_{\text{ref}}}{\rho_\infty u_\infty i^*_{\text{ref},s}}\,dy \tag{5-14}$$

For a low-velocity *constant-property flow* of a perfect gas with no chemical reaction, Δ_2 can be expressed in terms of temperature as follows:

$$i^*_{\text{ref}} = c(T - T_\infty)$$

$$\Delta_2 = \int_0^\infty \frac{u}{u_\infty}\left(\frac{T - T_\infty}{T_s - T_\infty}\right) dy \tag{5-15}$$

Equation (5-15) is also applicable to a constant-property liquid to a good approximation.

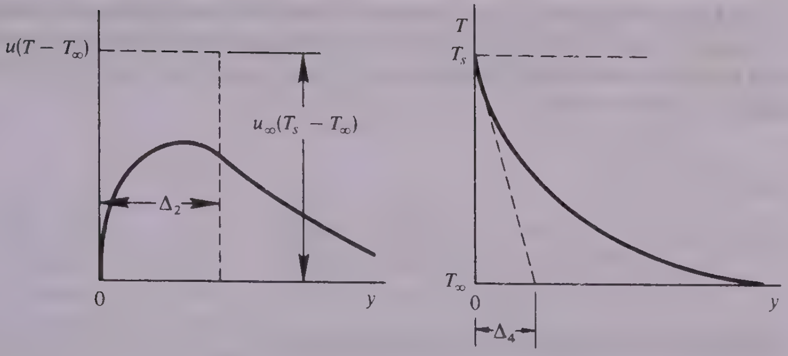

Figure 5-6 Graphical illustrations of the meaning of the enthalpy thickness and the conduction thickness of the boundary layer.

A *conduction thickness* Δ_4 may be defined as

$$\Delta_4 = \frac{k(T_s - T_\infty)}{\dot{q}_s''}$$

where k is the thermal conductivity of the fluid.

Later we will want to define a *convection conductance*, or *heat-transfer coefficient*, as

$$h = \frac{\dot{q}_s''}{T_s - T_\infty}$$

Thus

$$\Delta_4 = k/h \tag{5-16}$$

The physical significance of both the enthalpy thickness and the conduction thickness may be appreciated by reference to Fig. 5-6.

ALTERNATIVE FORMS OF THE ENERGY INTEGRAL EQUATION

Making use of the definition of the enthalpy thickness of the boundary layer, we can now replace the integral in Eq. (5-13), provided only that we let $Y \to \infty$. Substituting, and then expanding the derivative and rearranging, we obtain

$$\frac{\dot{q}_s''}{\rho_\infty u_\infty i^*_{\text{ref},s}} + \frac{\rho_s v_s}{\rho_\infty u_\infty}$$
$$= \frac{d\Delta_2}{dx} + \Delta_2 \left(\frac{1}{u_\infty}\frac{du_\infty}{dx} + \frac{1}{\rho_\infty}\frac{d\rho_\infty}{dx} + \frac{1}{R}\frac{dR}{dx} + \frac{1}{i^*_{\text{ref},s}}\frac{di^*_{\text{ref},s}}{dx} \right) \tag{5-17}$$

Note the similarity in form to Eq. (5-7). When it is expressed in this manner, the significance of the various terms is apparent.

Let us now examine a more restricted form of the energy integral equation, for example, low-velocity gas flow, no chemical reaction, $v_s = 0$, and constant fluid properties across the boundary layer. Then Δ_2 takes on the form given by Eq. (5-15), and we obtain

$$\frac{\dot{q}_s''}{\rho_\infty u_\infty c(T_s - T_\infty)} = \frac{d\Delta_2}{dx} + \Delta_2\left[\frac{1}{u_\infty}\frac{du_\infty}{dx} + \frac{1}{\rho_\infty}\frac{d\rho_\infty}{dx} + \frac{1}{R}\frac{dR}{dx} + \frac{1}{(T_s - T_\infty)}\frac{d(T_s - T_\infty)}{dx}\right] \tag{5-18}$$

A more compact expression of the same equation is

$$\frac{\dot{q}_s''}{c} = \frac{1}{R}\frac{d}{dx}[\Delta_2 R\rho_\infty u_\infty(T_s - T_\infty)] \tag{5-19}$$

Note that in each of these equations the product $\rho_\infty u_\infty$ always appears, rather than ρ_∞ and u_∞ independently. Thus we frequently find it convenient to employ the mass velocity or mass flux, $G_\infty = \rho_\infty u_\infty$; Eq. (5-19) then becomes

$$\frac{\dot{q}_s''}{c} = \frac{1}{R}\frac{d}{dx}[\Delta_2 RG_\infty(T_s - T_\infty)] \tag{5-20}$$

and Eqs. (5-17) and (5-18) can be similarly simplified. In internal flows, such as flows through nozzles, G_∞ is an especially convenient parameter, for it is merely the mass flow rate divided by the flow cross-sectional area [see Eq. (2-3)]. In such problems it is then unnecessary to evaluate separately the density and velocity. Note that this simplification is not available to us for the *momentum* integral equation (5-7), which means that to solve momentum problems we must separately evaluate free-stream velocity and density at all points along the surface.

Let us now see to what form the energy integral equation reduces for the simplest conceivable boundary-layer problem. Consider flow over a flat plate, $R \to \infty$, with constant pressure and free-stream velocity $du_\infty/dx = 0$, constant properties $d\rho_\infty/dx = 0$, and constant fluid-to-surface temperature difference $d(T_s - T_\infty)/dx = 0$. Equation (5-18) then becomes

$$\frac{\dot{q}_s''}{\rho u_\infty c(T_s - T_\infty)} = \frac{d\Delta_2}{dx} \tag{5-21}$$

If we now define a local heat-transfer coefficient

$$h = \frac{\dot{q}_s''}{T_s - T_\infty} \tag{5-22}$$

then

$$\frac{h}{\rho u_\infty c} = \frac{d\Delta_2}{dx}$$

The group of variables on the left-hand side is nondimensional and is called the *local Stanton number* St. Thus

$$\mathrm{St} = \frac{h}{\rho u_\infty c} = \frac{h}{G_\infty c} \tag{5-23}$$

and

$$\mathrm{St} = \frac{d\Delta_2}{dx} \tag{5-24}$$

Note the analogous relation from the momentum integral equation (5-11).

It should also be apparent that an integral boundary-layer equation for the diffusion of some component j in a fluid mixture can be developed in the same manner.

PROBLEMS

5-1. Develop a momentum integral equation for steady flow without blowing or suction for use in the entry region of a circular tube. Note that Eq. (5-4) is not applicable for this case because it has been assumed that the boundary-layer thickness is small relative to the body radius R; in the present case the boundary layer ultimately grows to the centerline of the tube.

5-2. Develop the corresponding energy integral equation for Prob. 5-1.

5-3. Develop a boundary-layer integral equation for the diffusion of component j in a multicomponent mixture.

5-4. Derive the momentum integral equation (5-8) and the energy integral equation (5-21).

REFERENCE

1. Hokenson, G. L.: *AIAA J.*, vol. 15, pp. 597–600, 1977.

6

CHAPTER

Differential Equations for the Turbulent Boundary Layer

In this chapter we develop the differential equations applicable to turbulent boundary-layer flows, often called the *Reynolds-averaged equations*. These evolve from the same basic equations developed for laminar flows, namely the conservation-of-mass equation, the Navier–Stokes equations, and the conservation-of-energy equation. However, they differ in basic form by the addition of the time-dependent term, reflecting the fact that turbulent flows are inherently unsteady. For a large class of turbulent flows the unsteady equations can be greatly simplified through a time-averaging process to yield equations similar to those for steady laminar flows. The consequence of this reformulation is the introduction of new unknowns within the equations, called the *turbulent* or *Reynolds stresses* for momentum and the *turbulent heat fluxes* for energy.

The chapter begins by presenting the variables and differential equations applicable to a time-dependent turbulent flow. The concepts of Reynolds decomposition and time-averaging are then developed, followed by formulation of the variable-property time-averaged turbulent flow equations, along with their two-dimensional boundary-layer forms. Kinetic energy equations for the mean flow and turbulence field are then developed, along with discussion of the dissipation transport equation. The turbulence kinetic energy and dissipation transport equations form the basis for the k–ε two-equation turbulence model as an alternative to the conventional Prandtl mixing-length model of turbulence.

MOMENTUM AND THERMODYNAMIC VARIABLES

The momentum variables in the turbulent equations are identical in typestyle to their laminar counterparts, but are considered to represent instantaneous quantities as a function of position (x, y, z) and time (t). When the same variables appear with overbars they represent mean values as a function of position only, and when the variables appear primed they represent time-dependent fluctuations about their respective mean values. The momentum variables are generalized using index notation, since development of the equations for turbulent flow is more easily carried out in this way, and the vector concepts likewise are generalized using tensors. Most of the thermodynamic variables remain simple because of their scalar nature.

The Cartesian coordinate directions (x, y, z) in index notation become (x_1, x_2, x_3), and the associated velocity components (u, v, w) become (u_1, u_2, u_3). Commonly used momentum variables include the x_i-direction mass flux, ρu_i, the x_i-direction momentum per unit mass u_i, and the body force per unit volume X_i. Thermodynamic and energy variables associated with the turbulent flow equations include the pressure P, temperature T, enthalpy i, internal energy e, density ρ, and specific heat c. Molecular transport coefficients include the dynamic viscosity μ and the thermal conductivity k. The kinetic energy per unit mass is $\frac{1}{2}u_i u_i$, and S is a volumetric energy source term.

NEWTONIAN STRESS AND FOURIER HEAT-FLUX MODELS

The Newtonian stress model for turbulent flow is of the same form as Eq. (3-7) for laminar flow, but the terms are functions of both space and time. It is a second-order tensor of the form

$$\sigma_{ij} = -P\delta_{ij} + \tau_{ij} \tag{6-1}$$

where δ_{ij} is the Kronecker delta, a unit second-order tensor, and the viscous stress tensor τ_{ij} reflects the deformations caused by spatial velocity gradients $\partial u_i/\partial x_j$. These gradients are a form of second-order tensor, which can be decomposed into the sum of a symmetric tensor S_{ij} and an antisymmetric tensor Ω_{ij}:

$$\frac{\partial u_i}{\partial x_j} = S_{ij} + \Omega_{ij} \tag{6-2}$$

Here S_{ij} is the strain-rate tensor, related to the deformation of the fluid, while the tensor Ω_{ij} relates to the rotation of the fluid. They are defined as

$$S_{ij} = \frac{1}{2}\left(\frac{\partial u_i}{\partial x_j} + \frac{\partial u_j}{\partial x_i}\right) \tag{6-3}$$

and

$$\Omega_{ij} = \frac{1}{2}\left(\frac{\partial u_i}{\partial x_j} - \frac{\partial u_j}{\partial x_i}\right) \tag{6-4}$$

On the basis of the assumptions that the viscous stress field is linearly proportional to the strain-rate field, that it is symmetric, and that it obeys the Stokes hypothesis, the viscous stress tensor becomes

$$\tau_{ij} = 2\mu S_{ij} - \tfrac{2}{3}\mu S_{kk}\delta_{ij} \tag{6-5}$$

and Eq. (6-1) becomes

$$\sigma_{ij} = -P\delta_{ij} + 2\mu S_{ij} - \tfrac{2}{3}\mu S_{kk}\delta_{ij} \tag{6-6}$$

The Fourier heat-flux model is of a form similar to the vector equation (3-8), but $\dot{q}''$ is temporarily replaced by $\dot{q}/A$ to avoid confusion with the primed quantities. For heat flux in the x_i direction

$$\left(\frac{\dot{q}}{A}\right)_i = -k\frac{\partial T}{\partial x_i} \tag{6-7}$$

INSTANTANEOUS EQUATIONS OF TURBULENCE

The turbulence equations are similar to the laminar flow equations of Chap. 4, and in some instances they are identical, although perhaps rearranged. The time-derivative term in each equation reflects the unsteady nature of the turbulent flow.

Conservation of mass is similar to Eq. (4-4), with the addition of the time (unsteady) term:

$$\frac{\partial \rho}{\partial t} + \frac{\partial}{\partial x_j}(\rho u_j) = 0 \tag{6-8}$$

The x_i-*momentum equation* follows Eq. (4-13), and becomes

$$\frac{\partial}{\partial t}(\rho u_i) + \frac{\partial}{\partial x_j}(\rho u_j u_i) = \frac{\partial \sigma_{ji}}{\partial x_j} + X_i \tag{6-9}$$

or, with the stress model (6-1),

$$\frac{\partial}{\partial t}(\rho u_i) + \frac{\partial}{\partial x_j}(\rho u_j u_i) = \frac{\partial}{\partial x_j}(-P\delta_{ij} + \tau_{ij}) + X_i \tag{6-10}$$

The *conservation of energy* for a single species can be written using either stagnation enthalpy or total energy, i.e., internal energy plus kinetic energy. The former is typically used in convective heat transfer. The latter allows insight into the various forms of energy transfer between the mean flow field and the turbulence field, as well as transfer between mechanical and thermal energy forms, which eventually leads to an increase in entropy. Both forms of the equation evolve from each other by separation of the pressure part of the stress tensor to form a flow work term. The *stagnation enthalpy equation* form is similar to that developed in Eq. (4-26):

$$\frac{\partial}{\partial t}\left[\rho\left(i^* - \frac{P}{\rho}\right)\right] + \frac{\partial}{\partial x_j}(\rho u_j i^*) = \frac{\partial}{\partial x_j}\left(-\frac{\dot{q}}{A}\right)_j + \frac{\partial}{\partial x_j}(u_i \tau_{ji}) + u_i X_i + S \tag{6-11}$$

where

$$i^* = e + \frac{P}{\rho} + \frac{1}{2}u_i u_i = i + \frac{1}{2}u_i u_i$$

Development of a *mechanical energy equation* is carried out by multiplying the x_i-momentum equation by the velocity component u_i and invoking the conservation of mass on the convective terms to yield

$$\frac{\partial}{\partial t}\left(\rho\frac{u_i u_i}{2}\right)+\frac{\partial}{\partial x_j}\left(\rho u_j\frac{u_i u_i}{2}\right)=u_i\frac{\partial}{\partial x_j}(\sigma_{ji})+u_i X_i \qquad (6\text{-}12)$$

A *thermal energy equation* is developed in a manner similar to that carried out to develop the static enthalpy equation (4-27). It is a split equation, whereby the kinetic energy component is removed from the total energy equation by subtracting the mechanical energy equation (6-12).

REYNOLDS DECOMPOSITION

The time dependence of a turbulent flow is the result of relatively small-scale vorticity in the flow; virtually every fluid particle is a part of a so-called turbulent eddy or structure, of which there are a very large number in a typical flow. A mechanical or optical experimental measurement at a point within a turbulent flow reveals a velocity that fluctuates in a random manner around a steady time-independent velocity. Any attempt to completely describe the velocity field, either through measurements or numerical simulations, as a function of time is difficult to impossible, except for simple flows at relatively low Reynolds numbers. On the other hand, because the fluctuating velocity components for a majority of turbulent flows tend to be small relative to the mean velocity, it appears practicable to adopt a statistical approach to describe the effects of the time-dependent components of the flow, and thereby treat the flow as if it were steady.

Figure 6-1 shows a way of describing the velocity in a turbulent flow, reduced for clarity to a two-dimensional flow. $\overline{\mathbf{V}}$ is a vector representing the steady velocity component, and $\mathbf{V}'$ is the fluctuating component, which varies with time but which must be zero when averaged over time, in keeping with the statistical approach. The total instantaneous velocity is $\mathbf{V}$. The figure shows a Cartesian decomposition of the instantaneous velocity into components in the x direction,

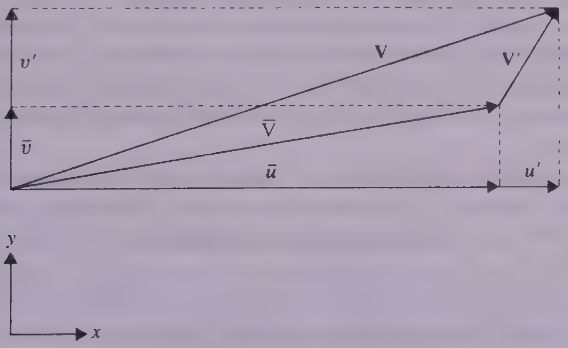

Figure 6-1 Velocity components for a turbulent flow (shown in two dimensions only).

or x_1 direction, and in the y direction, or x_2 direction. The x component is composed of the steady quantity $\bar{u}$ and its fluctuation quantity u', and the y component is composed of the steady quantity $\bar{v}$ and its fluctuation quantity v'. For two-dimensional turbulent flows experiments show that there exists a fluctuation quantity w' in the z direction, or x_3 direction, although $\bar{w}$ is zero. The instantaneous velocity components u_i for $i = 1, 2, 3$ can be expressed as

$$u = \bar{u} + u', \qquad v = \bar{v} + v', \qquad w = \bar{w} + w' \tag{6-13}$$

These are referred to as the (Osborne) Reynolds decompositions. Likewise, scalar quantities such as pressure and temperature also fluctuate, and they are expressed in terms of decompositions as

$$P = \bar{P} + P', \qquad T = \bar{T} + T' \tag{6-14}$$

The enthalpy terms need special consideration. Both the stagnation enthalpy and the static enthalpy have Reynolds decompositions similar to that for temperature:

$$i^* = \overline{i^*} + i^{*\prime}, \qquad i = \bar{i} + i' \tag{6-15}$$

Substituting decompositions for i and u_i into the definition $i^* = i + \frac{1}{2}u_i u_i$ and comparing with the decomposition for $\overline{i^*}$ leads to the following definitions for mean and fluctuating components:

$$\overline{i^*} = \bar{i} + \tfrac{1}{2}\bar{u}_i\bar{u}_i, \qquad i^{*\prime} = i' + \bar{u}_i u_i' + \tfrac{1}{2}u_i' u_i' \tag{6-16}$$

If the definition of $\overline{i^*}$ is to include the component $\frac{1}{2}\overline{u_i' u_i'}$, which is the mean value of the turbulence kinetic energy, then this component must appear in the definition of $i^{*\prime}$ with opposite sign.

Thermodynamic and thermophysical properties such as density, dynamic viscosity, specific heat, and thermal conductivity can also fluctuate in response to the pressure and temperature fields. Arguments for neglecting the density fluctuations are based primarily on arguments related to the Mach number of the turbulence, as discussed in Hinze[2] or Cebeci and Bradshaw.[3] For buoyancy-driven flows, or flows with large absolute temperature differences, the fluctuating density field cannot be ignored. For the treatment of turbulence in this book, however, we will assume that fluctuations of all properties are small, and thus all properties will appear without an overbar to signify the lack of consideration of their fluctuations.

Decompositions involving velocity gradients and temperature gradients are straightforward. However, it becomes convenient to define the strain rate tensor, stress tensor, and viscous stress tensor decompositions

$$S_{ij} = \bar{S}_{ij} + s_{ij}', \qquad \sigma_{ij} = \bar{\sigma}_{ij} + \sigma_{ij}', \qquad \tau_{ij} = \bar{\tau}_{ij} + \tau_{ij}' \tag{6-17}$$

Body force and source terms have the decompositions

$$X_i = \bar{X}_i + X_i', \qquad S = \bar{S} + S' \tag{6-18}$$

TIME-AVERAGING AND TURBULENCE STATISTICS

If we assume that the flow has a measurable continuous time history, we can define a *time-averaging operator* to create statistics of the flow. Consider some variable or property of the flow, $f(\mathbf{x}, t)$. The statistical mean value of that variable or property at $\mathbf{x}$, where $\mathbf{x}$ is the vector location (x_1, x_2, x_3), is

$$\bar{f}(\mathbf{x}) = \lim_{t\to\infty} \frac{1}{t} \int_{t_0}^{t_0+t} f(\mathbf{x}, t)\, dt \tag{6-19}$$

The variable $\bar{f}(\mathbf{x})$ exists if the limit converges, and it is stationary if it does not depend on the start time of the averaging process, t_0. An alternative to Eq. (6-19) would be to consider ensemble-averaging, whereby a large number of measurements or samples of $f(\mathbf{x}, t)$ are collected and averaged.

Working with the velocity component u, we can form its mean value at a location $\mathbf{x}$ by averaging its instantaneous variation over a long time:

$$\bar{u} = \frac{1}{t} \int_{t_0}^{t_0+t} u(\mathbf{x}, t)\, dt \tag{6-20}$$

From the definition of the Reynolds decomposition we require that the fluctuations about the mean be zero, i.e.,

$$\overline{u'} = \frac{1}{t} \int_{t_0}^{t_0+t} [u(\mathbf{x}, t) - \bar{u}]\, dt = \frac{1}{t} \int_{t_0}^{t_0+t} u'\, dt$$

and

$$\overline{u'} = 0$$

The variance, or second moment, of u' at a location $\mathbf{x}$ is obtained by changing the integrand in Eq. (6-19) to $[u(\mathbf{x}, t) - \bar{u}]^2$ and carrying out the time-averaging process:

$$\overline{u'u'} = \overline{u'^2} = \overline{u_1'u_1'} = \frac{1}{t} \int_{t_0}^{t_0+t} [u(\mathbf{x}, t) - \bar{u}]^2\, dt$$

The double-velocity correlation of the components u and v at a single point $\mathbf{x}$ in the flow is similar in concept to the covariance in statistics. It is obtained by carrying out the time-averaging process:

$$\overline{u'v'} = \overline{u_1'u_2'} = \frac{1}{t} \int_{t_0}^{t_0+t} [u(\mathbf{x}, t) - \bar{u}][v(\mathbf{x}, t) - \bar{v}]\, dt$$

The variance for any of the velocity components u_i at a point will be a second-order tensor. Likewise, the double-velocity correlation between velocity components u_i and u_j at a point will also be a second-order tensor. Triple single-point correlations are formed using any of the three components, yielding a third-order tensor. Similarly, double- and triple-correlation statistics involving one or more velocity components and a thermodynamic variable can also be formed.

With these operations defined, we can state some simple averaging rules, which are readily developed by simple substitution:

$$\bar{\bar{u}} = \bar{u} \text{ (mean rule)}, \quad \overline{u+v} = \bar{u} + \bar{v} \text{ (sum rule)}, \quad \overline{u'} = 0, \quad \overline{\bar{u}u'} = 0$$

$$\overline{uv} = \overline{(\bar{u}+u')(\bar{v}+v')} = \overline{\bar{u}\bar{v} + \bar{u}v + \bar{v}u' + u'v'} = \overline{\bar{u}\bar{v}} + \overline{u'v'} = \bar{u}\bar{v} + \overline{u'v'}$$

$$\overline{u^2} = \overline{(\bar{u}+u')(\bar{u}+u')} = \overline{\bar{u}\bar{u} + \bar{u}u' + \bar{u}u' + u'u'} = \overline{\bar{u}\bar{u}} + \overline{u'u'} = \bar{u}\bar{u} + \overline{u'u'}$$

Assuming that the turbulence field is such that mean quantities are independent of the start of the averaging process, integration and differentiation can be interchanged:

$$\overline{\frac{\partial u}{\partial x}} = \frac{\partial \bar{u}}{\partial x} \quad \text{(derivative rule)}$$

These examples and rules for averaging are extended in a straightforward way to the variables written using indices.

REYNOLDS-AVERAGED TRANSPORT EQUATIONS OF TURBULENCE

Development of the Reynolds-averaged equations to describe turbulent flows that have a statistically steady mean is achieved by substituting the various velocity and scalar Reynolds decompositions into the instantaneous equations and operating on the equations with the time-averaging operator, Eq. (6-19). Equations for the fluctuating components can then be developed by subtracting the mean equations from their instantaneous forms. Transport equations for the various turbulence statistics are obtained by manipulation of the fluctuating component equations and then time-averaging the residual equations. These become the transport equations for various turbulence quantities such as turbulence kinetic energy, dissipation, Reynolds stresses, and turbulent heat-flux components.

Conservation of Mass

This equation is obtained by first substituting the Reynolds decomposition velocity terms into the instantaneous conservation-of-mass equation (6-8):

$$\frac{\partial \rho}{\partial t} + \frac{\partial}{\partial x}[\rho(\bar{u}+u')] + \frac{\partial}{\partial y}[\rho(\bar{v}+v')] + \frac{\partial}{\partial z}[\rho(\bar{w}+w')] = 0$$

which, upon separating components, becomes

$$\frac{\partial \rho}{\partial t} + \frac{\partial}{\partial x}(\rho\bar{u}) + \frac{\partial}{\partial x}(\rho u') + \frac{\partial}{\partial y}(\rho\bar{v}) + \frac{\partial}{\partial y}(\rho v') + \frac{\partial}{\partial z}(\rho\bar{w}) + \frac{\partial}{\partial z}(\rho w') = 0$$

Now, the entire equation is averaged over time using Eq. (6-19), the sum rule is applied to break up the averaging into individual terms, the derivative rule is applied to each term, and, on dropping the time term, the resulting equation becomes

$$\frac{\partial}{\partial x}(\overline{\rho\bar{u}}) + \frac{\partial}{\partial x}(\overline{\rho u'}) + \frac{\partial}{\partial y}(\overline{\rho\bar{v}}) + \frac{\partial}{\partial y}(\overline{\rho v'}) + \frac{\partial}{\partial z}(\overline{\rho\bar{w}}) + \frac{\partial}{\partial z}(\overline{\rho w'}) = 0$$

Applying the mean rule for time-averages of mean quantities, and noting that the time-average of the product of a mean quantity and a fluctuating quantity is zero, the resulting Reynolds-averaged conservation-of-mass equation is

$$\frac{\partial}{\partial x}(\rho \bar{u}) + \frac{\partial}{\partial y}(\rho \bar{v}) + \frac{\partial}{\partial z}(\rho \bar{w}) = 0 \tag{6-21}$$

or, in index notation,

$$\frac{\partial}{\partial x_j}(\rho \bar{u}_j) = 0 \tag{6-22}$$

Note that for constant-density turbulent flow the density term can be removed from the spatial-derivative term, with the resulting equation being the same as Eq. (4-4). Also, for constant-density flow, an equation for the fluctuating velocity components is obtained by substracting the Reynolds-averaged form from the instantaneous form, ignoring the time variation of density, to yield

$$\frac{\partial}{\partial x_j}(\rho u'_j) = 0 \tag{6-23}$$

Conservation of Mass for the Turbulent Boundary Layer

If we now restrict consideration to the simple two-dimensional turbulent boundary layer with constant density, the conservation-of-mass equation becomes

$$\frac{\partial \bar{u}}{\partial x} + \frac{\partial \bar{v}}{\partial y} = 0 \tag{6-24}$$

Momentum Transport Equation in the x_i Direction

Development of this equation proceeds by first substituting the Reynolds decompositions into the instantaneous x_i-direction momentum equation (6-9), time-averaging, and then applying the derivative rule:

$$\frac{\partial}{\partial x_j}\overline{[\rho(\bar{u}_j + u'_j)(\bar{u}_i + u'_i)]} = \frac{\partial}{\partial x_j}\overline{(\bar{\sigma}_{ji} + \sigma'_{ji})} + \overline{\bar{X}_i + X'_i}$$

Again, recall that density does not carry an overbar, reminding us that we are not considering a density decomposition. Should fluctuations in density need to be considered, we would have to mass- or Favre-average rather than time-average.[1] Application of the time-averaging rules leads to the following form of the x_i-momentum equation:

$$\frac{\partial}{\partial x_j}(\rho \bar{u}_j \bar{u}_i + \rho \overline{u'_j u'_i}) = \frac{\partial}{\partial x_j}(\bar{\sigma}_{ji}) + \bar{X}_i \tag{6-25}$$

Several variations of the x_i-momentum equation must be developed to assist in formation of other turbulence equations and in turbulent transport models. The first variation follows from decomposition of the stress tensor into the pressure term and the viscous stress tensor, coupled with movement of the new convective term to the right-hand side of the equation:

$$\frac{\partial}{\partial x_j}(\rho \bar{u}_j \bar{u}_i) = -\frac{\partial \bar{P}}{\partial x_i} + \frac{\partial}{\partial x_j}(\bar{\tau}_{ji} - \rho \overline{u'_j u'_i}) + \bar{X}_i \tag{6-26}$$

where the pressure term has been converted using the relationship $\partial(-\bar{P}\delta_{ij})/\partial x_j = -\partial \bar{P}/\partial x_i$.

This form of the momentum equation gives rise to an analogy between the viscous stress tensor and the term $-\rho\overline{u'_j u'_i}$, *a turbulent stress tensor*, although in the turbulence literature this tensor often appears without the minus sign. It is a set of nine terms: $j = 1, 2, 3$ for each of the $i = 1, 2, 3$, or x-, y-, z-direction momentum equations, although symmetry arguments will reduce this to a set of six terms. While the $\rho\overline{u'_i u'_j}$ are derived mathematically as a consequence of time-averaging the x_i-momentum transport equation for turbulence, they are easily quantified by experimental techniques. They are highly nonlinear and important, reflecting the inherently time-dependent character of the turbulent flow. With the minus sign dropped, the term $\rho\overline{u'_j u'_i}$ is called the *Reynolds stress tensor*, and often given the second-order tensor symbol R_{ij}.

Momentum Equation for the Turbulent Boundary Layer

If we now restrict Eq. (6-26) to the x direction, the turbulent stress term for $i = 1$ becomes

$$\begin{aligned}\frac{\partial}{\partial x_j}(-\rho\overline{u'_j u'_{i=1}}) &= \frac{\partial}{\partial x_1}(-\rho\overline{u'_1 u'_1}) + \frac{\partial}{\partial x_2}(-\rho\overline{u'_2 u'_1}) + \frac{\partial}{\partial x_3}(-\rho\overline{u'_3 u'_1}) \\ &= \frac{\partial}{\partial x}(-\rho\overline{u'u'}) + \frac{\partial}{\partial y}(-\rho\overline{v'u'}) + \frac{\partial}{\partial z}(-\rho\overline{w'u'})\end{aligned}$$

In the two-dimensional boundary layer the $\overline{w'u'}$ term is found from experimental evidence to be essentially zero, although w' exists for all turbulent flows because of the nature of the fluctuating vorticity. The variance $\overline{w'^2}$ is an important quantity, and is part of the turbulence kinetic energy of the flow. The term $\overline{u'u'} = \overline{u'^2}$ is likewise an important quantity and part of the turbulence kinetic energy of the flow, although for two-dimensional boundary-layer flows its streamwise gradient is found to be negligible except in the vicinity of the stagnation point or near boundary-layer separation. It is eliminated in keeping with the boundary-layer approximations. Likewise, the $\bar{\tau}_{ji}$ tensor for $i = 1$ is reduced to a single component τ_{yx}, reflecting the requirement to only consider y-direction gradients in the boundary-layer approximations.

For two-dimensional "steady" turbulent boundary-layer flows, the x_i-momentum equation (6-26) for $i = 1$ is reduced using the boundary-layer approximations, and combined with the conservation-of-mass equation (6-22) to form the standard variable-property form

$$\rho\bar{u}\frac{\partial \bar{u}}{\partial x} + \rho\bar{v}\frac{\partial \bar{u}}{\partial y} = -\frac{d\bar{P}}{dx} + \frac{\partial}{\partial y}(\tau_{yx} - \rho\overline{u'v'}) + \bar{X} \tag{6-27}$$

For constant-density flow with negligible body forces, the boundary-layer momentum equation is recast using Newton's law of viscosity to become

$$\bar{u}\frac{\partial\bar{u}}{\partial x}+\bar{v}\frac{\partial\bar{u}}{\partial y}=-\frac{1}{\rho}\frac{d\bar{P}}{dx}+\frac{\partial}{\partial y}\left(\nu\frac{\partial\bar{u}}{\partial y}-\overline{u'v'}\right) \tag{6-28}$$

Stagnation Enthalpy Transport Equation

Development of this equation proceeds by first substituting the various Reynolds decompositions into the instantaneous stagnation enthalpy equation (6-11), time-averaging, and then applying the derivative rule:

$$\begin{aligned}\frac{\partial}{\partial x_j}\overline{[\rho(\bar{u}_j+u'_j)(\bar{i}^*+i^{*\prime})]}&=\frac{\partial}{\partial x_j}\overline{\left[\overline{\left(-\frac{\dot{q}}{A}\right)}_j+\left(-\frac{\dot{q}}{A}\right)'_j\right]}\\&\quad+\frac{\partial}{\partial x_j}\overline{[(\bar{u}_i+u'_i)(\bar{\tau}_{ji}+\tau'_{ji})]}\\&\quad+\overline{(\bar{u}_i+u'_i)(\bar{X}_i+X')}+\overline{(\bar{S}+S')}\end{aligned}$$

Application of the time-averaging rules leads to the following form of the stagnation enthalpy equation:

$$\begin{aligned}\frac{\partial}{\partial x_j}(\rho\bar{u}_j\bar{i}^*+\rho\overline{u'_ji^{*\prime}})&=\frac{\partial}{\partial x_j}\overline{\left(-\frac{\dot{q}}{A}\right)}_j+\frac{\partial}{\partial x_j}(\bar{u}_i\bar{\tau}_{ji}+\overline{u'_i\tau'_{ji}})\\&\quad+\bar{u}_i\bar{X}_i+\overline{u'_iX'}+\bar{S}\end{aligned} \tag{6-29}$$

The new convective transport term as a result of the time-averaging can be expanded using the definition of $i^{*\prime}$ to yield

$$\rho\overline{u'_ji^{*\prime}}=\rho\overline{u'_ji'}+\rho\bar{u}_i\overline{u'_ju'_i}+\rho u'_j\frac{\overline{u'_iu'_i}}{2} \tag{6-30}$$

Substitution of the expanded convective term into the time-averaged equation and rearrangement leads to the general form of the stagnation enthalpy equation:

$$\begin{aligned}\frac{\partial}{\partial x_j}(\rho\bar{u}_j\bar{i}^*)&=\frac{\partial}{\partial x_j}\left[\overline{\left(-\frac{\dot{q}}{A}\right)}_j-\rho\overline{u'_ji'}\right]+\frac{\partial}{\partial x_j}[\bar{u}_i(\bar{\tau}_{ji}-\rho\overline{u'_ju'_i})]\\&\quad+\frac{\partial}{\partial x_j}\overline{\left[u'_i\left(\tau'_{ji}-\rho\frac{u'_ju'_i}{2}\right)\right]}+\bar{u}_i\bar{X}_i+\overline{u'_iX'}+\bar{S}\end{aligned} \tag{6-31}$$

This form of the stagnation enthalpy equation gives rise to an analogy between the molecular heat-flux vector and the term $-\rho\overline{u'_ji'}$, with the latter being considered as a turbulent *enthalpy flux vector*. Like its counterpart $-\rho\overline{u'_iu'_j}$, it is mathematically derived as a consequence of making the stagnation enthalpy transport equation for turbulence a time-independent equation. The other new terms include the various work and dissipation terms, along with the $\overline{u'_iX'}$ body force term and volumetric source term.

Energy Equations for the Turbulent Boundary Layer

This equation is developed in a manner similar to the boundary-layer momentum equation. We first consider the turbulent enthalpy-flux term. As with the momentum equation, the z-component term is found from experimental evidence to be negligible, principally because there are no gradients in mean value of energy in the z-direction. The x-direction gradient is neglected primarily because of the boundary-layer approximations, although it may be important for low-Pr turbulent flows with significant surface temperature gradients in the flow direction. The stagnation enthalpy equation (6-31) is reduced by applying the boundary-layer approximations, combined with the conservation of mass equation (6-22), and neglecting the higher-order fluctuation correlation, to yield

$$\rho\bar{u}\frac{\partial\overline{i^*}}{\partial x}+\rho\bar{v}\frac{\partial\overline{i^*}}{\partial y}=\frac{\partial}{\partial y}(-\dot{q}''-\rho\overline{v'i'})+\frac{\partial}{\partial y}[\bar{u}(\tau_{yx}-\rho\overline{u'v'})]+\bar{u}\bar{X}+\overline{u'X'}+\bar{S} \tag{6-32}$$

where the molecular heat-flux term symbol has been replaced with the conventional double-prime notation to indicate a flux (per unit area).

For two-dimensional boundary-layer flow with low velocities, no fluctuating or mean work terms, no body forces or sources, and with $de = c\,dT$, Eq. (6-32) reduces to

$$\rho c\bar{u}\frac{\partial\bar{T}}{\partial x}+\rho c\bar{v}\frac{\partial\bar{T}}{\partial y}=\frac{\partial}{\partial y}(-\dot{q}''-\rho c\overline{v'T'}) \tag{6-33}$$

and for constant-density flow with constant specific heat the two-dimensional boundary-layer energy equation for turbulent flow with Fourier's law for molecular heat flux becomes

$$\bar{u}\frac{\partial\bar{T}}{\partial x}+\bar{v}\frac{\partial\bar{T}}{\partial y}=\frac{\partial}{\partial y}\left(\alpha\frac{\partial\bar{T}}{\partial y}-\overline{v'T'}\right) \tag{6-34}$$

Mechanical Energy Transport Equation

This equation considers the transport of the mean kinetic energy per unit mass of the flow, and it is derived by multiplying the time-averaged x_i-direction momentum-transport equation (6-26) by $\bar{u}_i$ and applying the conservation-of-mass equation (6-22) to the convective term to yield

$$\frac{\partial}{\partial x_j}\left(\rho\bar{u}_j\frac{\bar{u}_i\bar{u}_i}{2}\right)=\bar{u}_i\frac{\partial\bar{P}}{\partial x_i}+\bar{u}_i\frac{\partial}{\partial x_j}(\bar{\tau}_{ji}-\rho\overline{u_j'u_i'})+\bar{u}_i\bar{X}_i$$

Application of the chain rule to the stress terms leads to the final form of the mean mechanical energy equation:

$$\frac{\partial}{\partial x_j}\left(\rho\bar{u}_j\frac{\bar{u}_i\bar{u}_i}{2}\right)=\frac{\partial(\bar{u}_i\bar{P})}{\partial x_i}-\bar{P}\frac{\partial\bar{u}_i}{\partial x_i}+\frac{\partial}{\partial x_j}(\bar{u}_i\bar{\tau}_{ji})-\bar{\tau}_{ji}\frac{\partial\bar{u}_i}{\partial x_j}$$
$$+\frac{\partial}{\partial x_j}[\bar{u}_i(-\rho\overline{u_j'u_i'})]-(-\rho\overline{u_j'u_i'})\frac{\partial\bar{u}_i}{\partial x_j}+\bar{u}_i\bar{X}_i \tag{6-35}$$

The major significance of this rearranged form (6-35) is that we can identify stress--velocity gradient products, which usually represent source or sink terms in conversion or energy from one form to another, and velocity–stress products, which represent work rate or power terms.

Turbulence Kinetic Energy Transport Equation

This equation considers the turbulence kinetic energy per unit mass of the flow, and it is derived as follows. First a *transport equation for the fluctuating velocity* is created by inserting the various Reynolds decompositions into the instantaneous x_i-direction momentum equation (6-9) and then subtracting from it the time-averaged momentum equation (6-25) and ignoring the time term:

$$\frac{\partial}{\partial x_j}(\rho\bar{u}_j u'_i + \rho u'_j \bar{u}_i + \rho u'_j u'_i) = \frac{\partial}{\partial x_j}(\sigma'_{ji}) - \frac{\partial}{\partial x_j}(-\overline{\rho u'_j u'_i}) + X'_i \qquad \text{(6-36)}$$

Second, the transport equation for the fluctuating velocity is multiplied by u'_i:

$$u'_i\frac{\partial}{\partial x_j}(\rho\bar{u}_j u'_i + \rho u'_j \bar{u}_i + \rho u'_j u'_i) = u'_i\frac{\partial}{\partial x_j}(\sigma'_{ji}) - u'_i\frac{\partial}{\partial x_j} - (\overline{\rho u'_j u'_i}) + u'_i X'_i$$

and the resulting three convective terms are manipulated via chain-rule operations and the conservation-of-mass equations (6-22) and (6-23):

$$u'_i\frac{\partial}{\partial x_j}(\rho\bar{u}_j u'_i) = \frac{\partial}{\partial x_j}\left(\rho\bar{u}_j\frac{u'_i u'_i}{2}\right), \qquad u'_i\frac{\partial}{\partial x_j}(\rho u'_j \bar{u}_i) = u'_i \rho u'_j \frac{\partial \bar{u}_i}{\partial x_j}$$

$$u'_i\frac{\partial}{\partial x_j}(\rho u'_j u'_i) = \frac{\partial}{\partial x_j}\left(\rho u'_j\frac{u'_i u'_i}{2}\right)$$

Substitution of these rearranged terms and time-averaging leads to the following form of the turbulence kinetic energy equation:

$$\frac{\partial}{\partial x_j}\left(\rho\bar{u}_j\frac{\overline{u'_i u'_i}}{2} + \overline{\rho u'_j\frac{u'_i u'_i}{2}}\right) + \overline{\rho u'_j u'_i}\frac{\partial \bar{u}_i}{\partial x_j} = \overline{u'_i\frac{\partial}{\partial x_j}(\sigma'_{ji})} + \overline{u'_i X'_i}$$

The chain rule is applied to the fluctuating velocity–fluctuating stress-gradient correlation, and it is expanded using the Reynolds decomposition for the fluctuating stress tensor. Then applying the fluctuating velocity conservation-of-mass equation (6-23) with constant density to eliminate the fluctuating pressure–fluctuating velocity-gradient term yields

$$\overline{u'_i\frac{\partial}{\partial x_j}(\sigma'_{ji})} = \frac{\partial}{\partial x_j}(\overline{u'_i\sigma'_{ji}}) - \overline{\sigma'_{ji}\frac{\partial u'_i}{\partial x_j}} = \frac{\partial}{\partial x_j}(-\overline{u'_i P'}\delta_{ji} + \overline{u'_i\tau'_{ji}}) - \overline{\tau'_{ji}\frac{\partial u'_i}{\partial x_j}}$$

Substitution of this expansion into the turbulence kinetic energy equation leads to the following form:

$$\frac{\partial}{\partial x_j}\left(\rho\bar{u}_j\frac{\overline{u'_i u'_i}}{2}\right) = \frac{\partial}{\partial x_j}\left(-\rho\overline{u'_j\frac{u'_i u'_i}{2}} - \overline{u'_j P'} + \overline{u'_i\tau'_{ji}}\right)$$

$$+ (-\rho\overline{u'_j u'_i})\frac{\partial \bar{u}_i}{\partial x_j} - \overline{\tau'_{ji}\frac{\partial u'_i}{\partial x_j}} + \overline{u'_i X'_i} \qquad \text{(6-37)}$$

In this equation the fluctuating viscous stress tensor–fluctuating velocity-gradient correlation can be rewritten in terms of the fluctuating strain-rate tensor s'_{ij} (recall that τ'_{ij} is symmetric) for the case where the compressibility term is neglected. To convert the correlation to its positive-definite form, note that the stress–velocity gradient correlation is the same with interchange of the i and j indices, allowing it to be added and divided by 2, to create the second fluctuating stress tensor. The following equation results:

$$\overline{\tau'_{ij}\frac{\partial u'_i}{\partial x_j}} = 2\mu\overline{s'_{ij}\frac{\partial u'_i}{\partial x_j}} = 2\mu\frac{1}{2}\left(\overline{s'_{ij}\frac{\partial u'_i}{\partial x_j}} + \overline{s'_{ji}\frac{\partial u'_j}{\partial x_i}}\right) = 2\mu\overline{s'_{ij}s'_{ij}}$$

This form shows that the fluctuating viscous stress tensor–fluctuating velocity–gradient correlation is positive-definite preceded by a minus sign, signifying a negative source or a sink term for the turbulence kinetic energy. It represents the rate at which the viscous stress performs deformation work against the fluctuating strain rate, and is dissipative in nature.

A common manipulation of the transport equation for turbulence kinetic energy is carried out by combining the gradient of the fluctuating velocity–fluctuating viscous stress correlation, which represents the rate of work by the fluctuating viscous stresses of the turbulent flow, with the fluctuating viscous stress tensor–fluctuating velocity-gradient correlation. Manipulation of these two terms leads to

$$\frac{\partial}{\partial x_j}(\overline{u'_i\tau'_{ji}}) - \overline{\tau'_{ji}\frac{\partial u'_i}{\partial x_j}} = \rho\left\{\frac{\partial}{\partial x_j}\mu\left[\frac{\partial}{\partial x_j}\left(\frac{\overline{u'_iu'_i}}{2}\right)\right] - \rho\nu\overline{\frac{\partial u'_i}{\partial x_j}\frac{\partial u'_i}{\partial x_j}}\right\}$$

where the second tensor is called the turbulence dissipation rate ε:

$$\varepsilon = \nu\overline{\frac{\partial u'_i}{\partial x_j}\frac{\partial u'_i}{\partial x_j}}$$

With this manipulation, Eq. (6-37) becomes

$$\frac{\partial}{\partial x_j}\left(\rho\bar{u}_j\frac{\overline{u'_iu'_i}}{2}\right) = \frac{\partial}{\partial x_j}\left[-\rho\overline{u'_j\frac{u'_iu'_i}{2}} - \overline{u'_jP'} + \mu\frac{\partial}{\partial x_j}\left(\frac{\overline{u'_iu'_i}}{2}\right)\right]$$
$$+(-\rho\overline{u'_ju'_i})\frac{\partial\bar{u}_i}{\partial x_j} - \rho\varepsilon + \overline{u'_iX'_i} \qquad (6\text{-}38)$$

The turbulence kinetic energy is commonly defined as one of the following quantities:

$$\bar{k} = \tfrac{1}{2}\overline{u'_iu'_i} = \tfrac{1}{2}(\overline{u'_1u'_1} + \overline{u'_2u'_2} + \overline{u'_3u'_3}) = \tfrac{1}{2}(\overline{u'u'} + \overline{v'v'} + \overline{w'w'})$$

This definition is consistent in notation with the other Reynolds decompositions, in that a decomposition represents a mean value (with overbar symbol) and a fluctuating value (with prime symbol). As such, we define the instantaneous quantity $k = \frac{1}{2}u'_iu'_i$ and the mean value of that quantity as $\bar{k} = \frac{1}{2}\overline{u'_iu'_i}$. With these definitions, k' is the difference between the instantaneous and fluctuating quantities.

The structure of the $\bar{k}$-transport equation (6-38) takes a form similar to the other transport equations:

$$\text{convection } (\bar{k}) = \text{diffusion } (\bar{k}) \pm \text{source } (\bar{k}) \tag{6-39}$$

Comparison of this with Eq. (6-38) suggests that the $\partial/\partial x_j$ term to the right of the equal sign is composed of three diffusional quantities, although the first two terms are really energy-transfer terms representing diffusion of $\bar{k}$ by the turbulence itself and turbulent flow work (multiply and divide by ρ), while the third term represents viscous self-diffusion of $\bar{k}$. The last three terms of (6-38) represent sources and/or sinks of $\bar{k}$. The Reynolds stress–mean velocity-gradient product $(-\rho\overline{u_j'u_i'})\,\partial\bar{u}_i/\partial x_j$ is a source for $\bar{k}$, and it is generally positive, especially for boundary-layer flows. This term appears in the mean mechanical energy equation (6-35) with a negative sign, indicating that it is a transfer of energy from the mean field to the turbulence field. As indicated above, $\rho\varepsilon$ represents a dissipation of $\bar{k}$, being positive-definite with a minus sign. It will appear in a thermal energy equation with a positive sign, showing it to be a source of thermal energy in the energy-transfer process. The $\overline{u_i'X_i'}$ velocity–body force correlation is likewise a source of $\bar{k}$.

$\bar{k}$ Equation for the Turbulent Boundary Layer

Development of this equation primarily requires elimination of the x-direction gradient by applying the boundary-layer approximations and elimination of the z-direction components and gradients by restriction to two-dimensional flow. The $\bar{k}$-transport equation (6-38), combined with the conservation-of-mass equation (6-22), becomes, neglecting body forces,

$$\rho\bar{u}\frac{\partial\bar{k}}{\partial x}+\rho\bar{v}\frac{\partial\bar{k}}{\partial y}=\frac{\partial}{\partial y}\left[-\rho\overline{v'k'}-\overline{v'P'}+\mu\left(\frac{\partial\bar{k}}{\partial y}\right)\right]+(-\rho\overline{u'v'})\frac{\partial\bar{u}}{\partial y}-\rho\varepsilon \tag{6-40}$$

Dissipation Transport Equation

The derivation of the dissipation rate equation is quite tedious, involving differentiation of the instantaneous transport equation for the velocity fluctuation (6-36) with respect to x_l, multiplication of the resulting equation by the term $\nu(\partial u_i'/\partial x_l)$, then time-averaging. Implicit in the derivation is that the kinematic viscosity does not have spatial variations. The resulting transport equation contains a multitude of new fluctuation correlations, none of which explicitly appear in any other transport equation, and whose values are practically impossible to experimentally quantify. The general form of the resulting equation[4] is

$$\frac{\partial}{\partial x_j}(\rho\bar{u}_j\varepsilon)=\frac{\partial}{\partial x_j}[\rho(T_\varepsilon+\Pi_\varepsilon+D_\varepsilon)]+\rho(P_\varepsilon-\varepsilon_\varepsilon) \tag{6-41}$$

This form is adapted from Mansour, Kim, and Moin,[4] except that the three diffusion-like terms are written explicitly to reflect their diffusive nature.

This equation is quite similar in form to Eq. (6-38) for the turbulence energy. In Eq. (6-38) the three-part diffusion term is equivalent to the $T_\varepsilon + \Pi_\varepsilon + D_\varepsilon$ term, where T_ε represents transfer of ε due to the turbulence itself, Π_ε represents transfer by pressure fluctuations, and D_ε represents viscous diffusion of ε. The P_ε term is a collection of four terms representing production of ε by the mean and the turbulence fields, and ε_ε represents the viscous dissipation of ε.

ε Equation for the Turbulent Boundary Layer

This equation evolves by elimination of the x-direction gradient because of the boundary-layer approximations and elimination of the z-direction components and gradients by the restriction of two-dimensional flow. The ε-transport equation (6-41), combined with the conservation-of-mass equation (6-22), becomes

$$\rho\bar{u}\frac{\partial\varepsilon}{\partial x} + \rho\bar{v}\frac{\partial\varepsilon}{\partial y} = \frac{\partial}{\partial y}[\rho(T_\varepsilon + \Pi_\varepsilon + D_\varepsilon)] + \rho(P_\varepsilon - \varepsilon_\varepsilon) \qquad (6\text{-}42)$$

PROBLEMS

6-1. Using appropriate assumptions, reduce Eq. (6-9) to compare it with Eq. (4-17).

6-2. Convert Eq. (6-11) to Eq. (4-32) using the definition of the substantial (or total) derivative.

6-3. Carry out the necessary algebra to show that Eqs. (6-16) represent the appropriate decompositions for the stagnation enthalpy.

6-4. Using the averaging rules, develop the conservation-of-mass equation (6-21), including all the intermediate steps.

6-5. Reduce Eq. (6-26) to the boundary-layer equation (6-28) using appropriate assumptions.

6-6. Derive the stagnation enthalpy equation (6-31), and reduce it to its low-velocity, constant-property boundary-layer form given by Eq. (6-34).

6-7. Carry out the derivation of the turbulence kinetic energy equation (6-38).

6-8. The construction of the boundary-layer equations for momentum and energy can be considered using the formulation of Eq. (6-39). Recast the laminar boundary-layer equations for momentum, Eq. (4-10), and energy Eq. (4-39), and their turbulent counterparts. Eqs. (6-28) and (6-34), into the form given by Eq. (6-39) to identify the convection, diffusion, and source terms for each equation.

REFERENCES

1. Rubesin, M. W., and W. C. Rose: NASA TM X-62248, Ames Research Center, Moffett Field, California, 1973.
2. Hinze, J. O.: *Turbulence*, 2d ed., p. 22, McGraw-Hill, New York, 1975.
3. Cebeci, T., and P. Bradshaw: *Physical and Computational Aspects of Convective Heat Transfer*, pp. 48–53, Springer-Verlag, New York, 1984.
4. Mansour, N. N., J. Kim, and P. Moin: *AIAA J.*, vol. 27, pp. 1068–1073, 1989.

CHAPTER 7

Laminar Internal Flows: Momentum Transfer

In this chapter we develop some of the very simplest solutions for the velocity distribution for steady laminar flow inside smooth tubes. Our primary concern is circular tubes, although some additional cross-sectional shapes are also considered.

FULLY DEVELOPED LAMINAR FLOW IN CIRCULAR TUBES

Consider the steady laminar flow of a viscous fluid inside a circular tube, as shown in Fig. 7-1. Let the fluid enter with a uniform velocity over the flow cross section. As the fluid moves down the tube a boundary layer of low-velocity fluid forms and grows on the surface because the fluid immediately adjacent to the surface must have zero velocity.

A particular and simplifying feature of viscous flow inside cylindrical tubes is the fact that the boundary layer must meet itself at the tube centerline, and the velocity distribution then establishes a fixed pattern that is invariant thereafter. We refer to the *hydrodynamic entry length* as that part of the tube in which the momentum boundary layer grows and the velocity distribution changes with length. We speak of the *fully* developed velocity profile as the fixed velocity distribution in the fully developed region. It should be added that we are assuming in this discussion that the fluid properties, including density, are not changing along the length of the tube.

Without yet worrying about how long the hydrodynamic entry length must be in order for a fully developed velocity profile to obtain, let us evaluate the fully developed velocity distribution for a laminar flow with constant viscosity. The applicable equation of motion must evidently be the momentum equation for axisymmetric flow in a circular tube, Eq. (4-11). However, by definition of a fully developed velocity profile, it is apparent that $v_r = 0$ and $\partial u/\partial x = 0$, and u

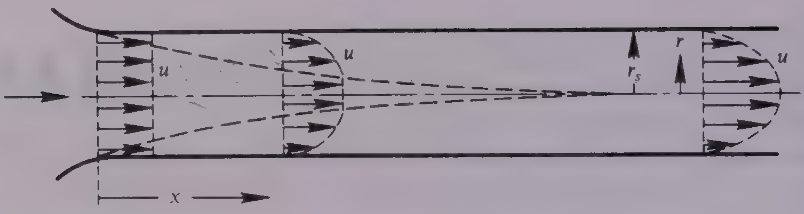

Figure 7-1 Development of the velocity profile in the hydrodynamic entry region of a pipe.

is a function of r alone. Thus Eq. (4-11) becomes

$$0 = -\frac{dP}{dx} + \frac{1}{r}\frac{\partial}{\partial r}\left(r\mu\frac{\partial u}{\partial r}\right) \tag{7-1}$$

Since the pressure is independent of r, Eq. (7-1) can be integrated directly twice with respect to r to yield the desired velocity function. Applying the boundary conditions

$$\frac{du}{dr} = 0 \quad \text{at } r = 0$$
$$u = 0 \quad \text{at } r = r_s$$

we readily obtain

$$u = \frac{r_s^2}{4\mu}\left(-\frac{dP}{dx}\right)\left(1 - \frac{r^2}{r_s^2}\right) \tag{7-2}$$

Equation (7-2) is the familiar parabolic law. However, it proves more useful to express the velocity in terms of a *mean velocity* V rather than the pressure gradient. If we designate the flow cross-sectional area of a tube as A_c, the mass rate of flow across an elemental segment of that area dA_c is, by Eq. (2-3),

$$d\dot{m} = \rho u\, dA_c$$

Then the total mass flow rate through the tube is

$$\dot{m} = \int_{A_c} \rho u\, dA_c$$

Let us define a mean velocity V such that

$$\dot{m} = \rho V A_c, \qquad V = \frac{\dot{m}}{\rho A_c} \tag{7-3}$$

Then

$$V = \frac{1}{\rho A_c}\int_{A_c} \rho u\, dA_c \tag{7-4}$$

or, since the density is constant,

$$V = \frac{1}{A_c}\int_{A_c} u\,dA_c \tag{7-5}$$

For axisymmetric flow in a circular tube $dA_c = 2\pi r\,dr$ and $A_c = \pi r_s^2$. Thus

$$V = \frac{2}{r_s^2}\int_0^{r_s} ur\,dr \tag{7-6}$$

If we now substitute Eq. (7-2) into Eq. (7-6) and integrate, we obtain

$$V = \frac{r_s^2}{8\mu}\left(-\frac{dP}{dx}\right) \tag{7-7}$$

Equation (7-7), together with (7-3), can be used directly to calculate pressure drop. We can also combine (7-7) with (7-2) to obtain a simpler expression for the local velocity:

$$u = 2V\left(1 - \frac{r^2}{r_s^2}\right) \tag{7-8}$$

The shear stress at the surface can be evaluated from the gradient of the velocity profile at the surface. From Eq. (3-1),

$$\tau_s = \mu\left(\frac{\partial u}{\partial r}\right)_{r=r_s} = \mu\left[2V\left(-\frac{2r_s}{r_s^2}\right)\right] = -\frac{4V\mu}{r_s} \tag{7-9}$$

To provide consistency with procedures to be used later, it is worth noting an alternative procedure to evaluate shear stress. Consider a stationary control volume as shown in Fig. 7-2. Let us apply the momentum theorem, Eq. (2-4), in the x direction, noting that, because of the fully developed nature of the flow, there is no net change in momentum flux. Thus

$$0 = P\pi r^2 - \left(P + \frac{dP}{dx}\delta x\right)\pi r^2 - \tau 2\pi r\,\delta x\,.$$

$$\tau = \frac{r}{2}\left(-\frac{dP}{dx}\right) \tag{7-10}$$

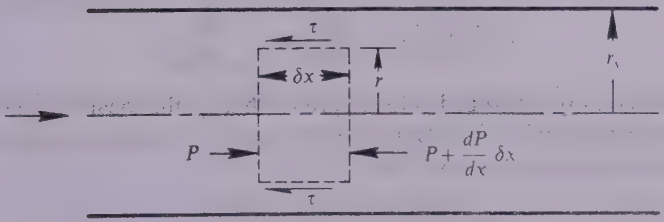

Figure 7-2 Control volume for analyzing fully developed flow in a pipe.

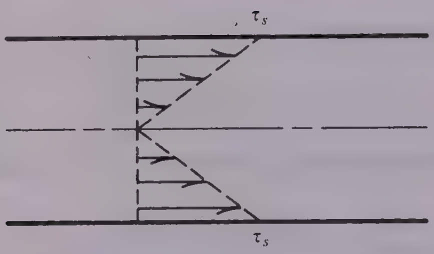

Figure 7-3 Shear-stress distribution for fully developed flow in a pipe.

and

$$\tau_s = \frac{r_s}{2}\left(-\frac{dP}{dx}\right) \tag{7-11}$$

Equations (7-10) and (7-11) are equally applicable to a fully developed *turbulent* flow, as long as it is understood that τ refers to an apparent shear stress that is the linear combination of the viscous stress and the apparent turbulent shear stress.

Also,

$$\frac{\tau}{\tau_s} = \frac{r}{r_s} \tag{7-12}$$

Note, then, that in a fully developed pipe flow, whether laminar or turbulent, the apparent shear stress varies *linearly* from a maximum at the surface to zero at the pipe or tube centerline (Fig. 7-3).

Finally, Eq. (7-11) can be combined with Eq. (7-7), and we again obtain Eq. (7-9).

We can express the surface shear stress in terms of a nondimensional friction coefficient c_f defined as in Eq. (5-10). Let us base the definition arbitrarily on the mean velocity. Thus

$$\tau_s = c_f \frac{\rho V^2}{2} \tag{7-13}$$

Then, employing (7-9) and considering the absolute value of the shear stress, to preserve the fact that surface shear is always opposite to the flow, we get

$$c_f = \frac{4V\mu/r_s}{\rho V^2/2} = \frac{8\mu}{r_s \rho V} = \frac{16}{2r_s\rho V/\mu}$$

We note for the fully developed velocity profile that c_f, the local friction coefficient, is independent of x. The nondimensional group of variables in the denominator is the *Reynolds number* Re. Thus

$$\text{Re} = \frac{2r_s\rho V}{\mu} = \frac{D\rho V}{\mu} = \frac{DG}{\mu} \tag{7-14}$$

where $D = 2r_s$, the pipe diameter, and $G = \dot{m}/A_c$, the mean mass velocity. Thus

$$c_f = \frac{16}{\text{Re}} \tag{7-15†}$$

We have dealt with this most elementary of internal flow problems in excessive detail perhaps, but it has provided us with an opportunity to define a number of terms that we use later.

FULLY DEVELOPED LAMINAR FLOW IN OTHER CROSS-SECTIONAL SHAPE TUBES

Laminar velocity profile solutions have been obtained for the fully developed flow case for a large variety of flow cross-sectional shapes. The applicable equation of motion for steady, constant-property, fully developed flow with no body forces, and with x the flow direction coordinate, can be readily deduced from the Navier–Stokes equation (4-15). Thus

$$0 = -\frac{dP}{dx} + \mu\nabla^2 u \tag{7-16}$$

By assuming dP/dx to be constant over the flow cross section, this equation has been solved by various procedures, including numerically, for various shapes of tube. In most cases the shear stress will vary around the periphery of the tube; but if a mean shear stress with respect to peripheral area is defined (and this is the stress needed to calculate pressure drop), a friction coefficient can be defined in terms of Eq. (7-13).

On Fig. 7-4 the fully developed friction coefficients for the family of rectangular tubes,[1] extending from the square tube to flow between parallel planes, are plotted. Figure 7-5 gives similar results for flow between concentric annuli,[2] where the definition of c_f for the annulus is given by the area-weighted average based on the inner surface, A_i, and the outer surface, A_o, as

$$c_f = \frac{\tau_i A_i + \tau_o A_o}{A_i + A_o}\Big/(\rho V^2/2)$$

Individual surface shear stress values for the inner and outer radius can be found in Shaw and London.[3]

For flow through an *equilateral triangular tube*

$$c_f \,\text{Re} = 13.33$$

The Reynolds number in all these results is defined as

$$\text{Re}_{D_h} = \frac{4r_h G}{\mu} = \frac{D_h G}{\mu} \tag{7-17}$$

[†] Integration of Eq. (7-11) and substitution of the friction coefficient definition results in the pressure-drop equation $\Delta P = 4c_f(L/D)(\rho V^2/2)$. The product $4c_f$ is f, the conventional friction factor used in fluid mechanics in conjunction with the Moody diagram. Then Eq. (7-15) becomes $f = 64/\text{Re}$.

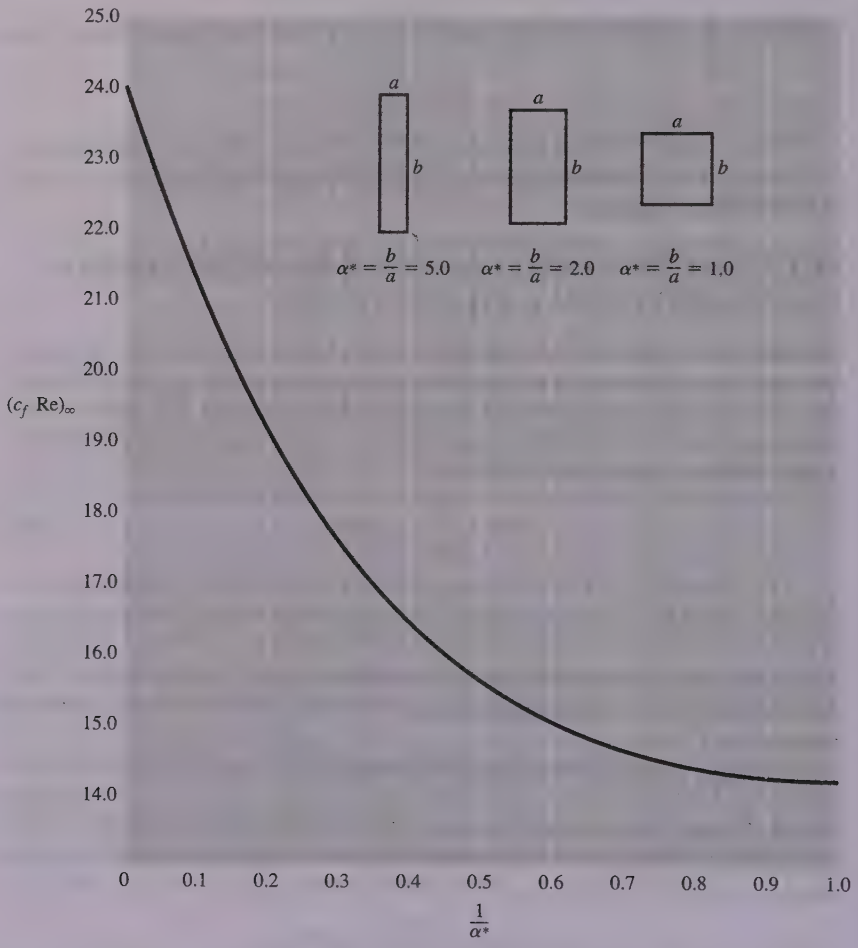

Figure 7-4 Friction coefficients for fully developed laminar flow in rectangular tubes.

where the "hydraulic radius"[†] and hydraulic diameter are defined by

$$r_h = \frac{A_c L}{A} = \frac{\text{cross-sectional area}}{\text{wetted perimeter}}$$

$$D_h = 4r_h$$

[†] The choice of the hydraulic radius as the length dimension in the Reynolds number is actually a purely arbitrary one, since any length that characterizes the size of the flow passage would suffice as long as it is defined. However, we find that for a turbulent flow the hydraulic radius does lead to approximate correlation between the behavior of tubes of various cross-sectional shape, and we use the hydraulic radius for both laminar and turbulent flow to provide a consistent treatment and to avoid confusion. Note that $4r_h = D_h$, the hydraulic diameter; for circular tubes the tube diameter and hydraulic diameter are equivalent.

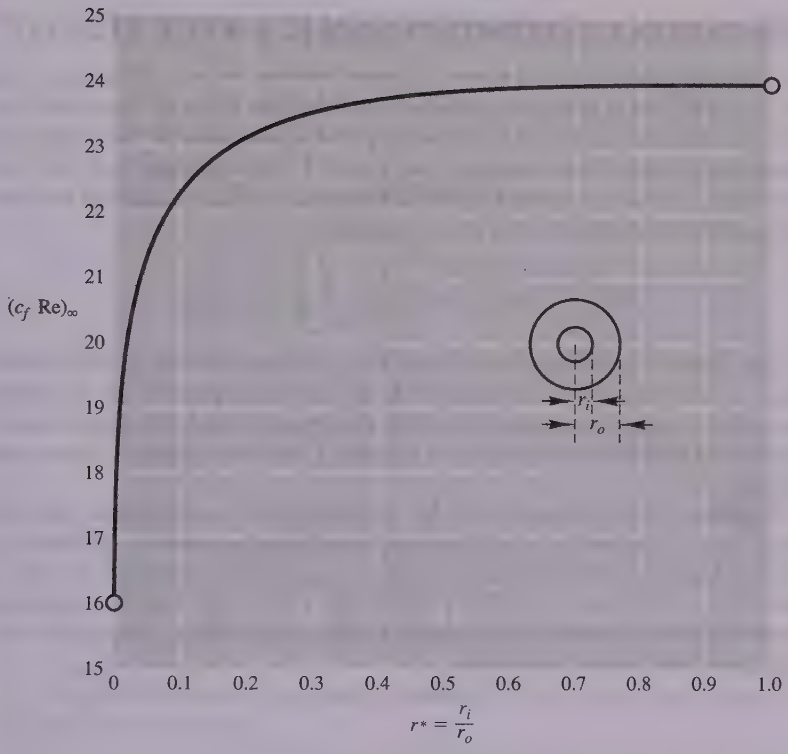

Figure 7-5 Friction coefficients for fully developed laminar flow in circular-tube annuli.

and where A_c = cross-sectional area
L = tube length
A = total tube surface area in length L
G = mean mass flux, $\dot{m}/A_c$

It has been found by experiment that if Eq. (7-17) is used for the Reynolds number, laminar flow is obtained for flow inside a round tube as long as the Reynolds number is less than about 2300, and this criterion appears to be a good approximation for smooth tubes regardless of tube cross-sectional shape. Above this Reynolds number, the flow becomes unstable to small disturbances, and a transition to a turbulent type of flow generally occurs, although a fully established turbulent flow may not occur until the Reynolds number reaches about 10,000.

Fully developed flow solutions for a great many other tube shapes may be found in Shah and London[3] and in Kakac, Shah, and Aung.[4] All can be presented in precisely the same way as used here.

THE LAMINAR HYDRODYNAMIC ENTRY LENGTH

The preceding discussion has been concerned with the velocity distribution and friction coefficient at points far removed from the tube entrance where fully developed conditions obtain. The complete hydrodynamic solution for a tube must include some kind of entry length, as in Fig. 7-1. For a *circular tube* with axisymmetric, constant-property flow the differential equation of motion becomes the momentum equation (4-11), with μ constant:

$$\rho u \frac{\partial u}{\partial x} + \rho v_r \frac{\partial u}{\partial r} = -\frac{dP}{dx} + \frac{1}{r}\frac{\partial}{\partial r}\left(r\mu \frac{\partial u}{\partial r}\right) \tag{7-18}$$

The simplest entry condition would be a uniform velocity at the tube entrance, $x = 0$, as shown in Fig. 7-1. Even for a sharp-cornered or abrupt-contraction entrance, the velocity profile develops in much the same manner, although the behavior for the first few diameters from the entrance is somewhat different.

Equation (7-18) incorporates the boundary-layer assumptions and thus would not be expected to be valid very close to the tube entrance. According to Shah and London, if the full Navier–Stokes equations are employed, it is found that for $\mathrm{Re} < 400$ and $(x/D)/\mathrm{Re} < 0.005$, Eq. (7-18) will lead to error in the computed velocity profiles. The solutions discussed below are thus only accurately applicable beyond this region.

The entry-length initial and boundary conditions of interest, then, are

$$\left.\begin{aligned} u &= V \\ v_r &= 0 \end{aligned}\right\} \quad \text{at } x = 0$$

$$\left.\begin{aligned} u &= 0 \\ v_r &= 0 \end{aligned}\right\} \quad \text{at } r = r_s$$

$$\frac{\partial u}{\partial r} = 0 \qquad \text{at } r = 0$$

Hornbeck[10] has solved this problem *numerically* without any simplifying assumptions (other than the boundary layer assumptions). Figure 7-6 shows some of Hornbeck's results for the axial velocity profiles, and here it can be seen how the velocity profile develops and approaches the fully developed condition. Approximate solutions to this problem can be obtained by solving the linearized momentum equation, such as described by Langhaar[5] or Sparrow, Lin, and Lundgren.[6]

Pressure-drop calculations in a tube must consider the entry region because of the variation in momentum flux due to flow acceleration, as well as the effects of increased surface shear forces. A calculating equation for the total pressure drop from entrance to a point beyond the hydrodynamically fully developed location can be obtained either by integration of Eq. (4-11) in the flow direction or by using a control volume procedure. For the case of constant properties, the resulting total

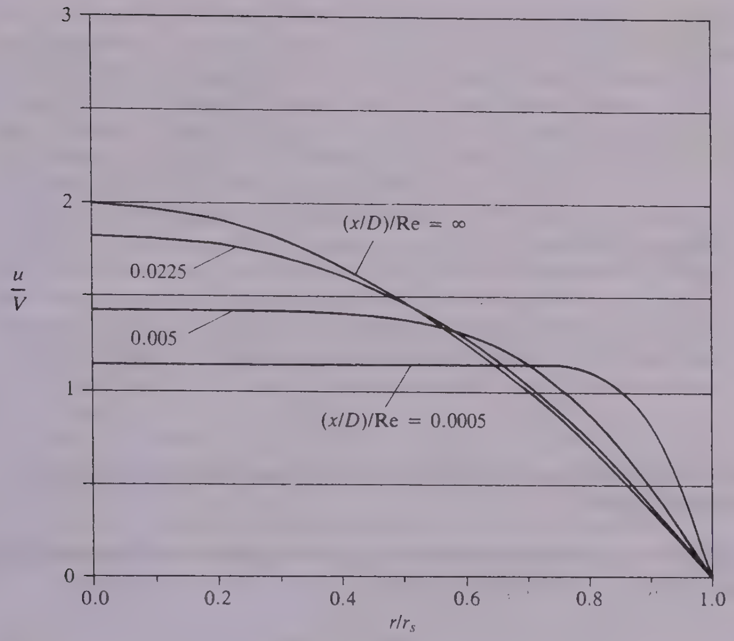

Figure 7-6 Axial velocity distribution in the hydrodynamic entrance region of a circular tube.

pressure drop becomes

$$\frac{\Delta P}{\frac{1}{2}\rho V^2} = c_{f,m}\frac{x}{(D_h/4)} + \frac{2}{A_c}\int_{A_c}\left(\frac{u}{V}\right)^2 dA_c - 2 \tag{7-19}$$

where the first term contains the surface friction contribution to the pressure drop and c_{f_m} is the *mean friction coefficient* from $x = 0$ to x,

$$c_{f_m} = \frac{\frac{1}{x}\int_0^x \tau_s\, dx}{\frac{1}{2}\rho V^2} \tag{7-20}$$

and the second and third terms contain the flow acceleration effects on the pressure drop. These combined effects of surface shear and flow acceleration can be incorporated into a single *apparent* mean friction coefficient $\bar{c}_{f_{\text{app}}}$. The pressure drop from 0 to x can then be evaluated from the following nondimensional pressure drop equation

$$\Delta P^* = \frac{\Delta P}{\frac{1}{2}\rho V^2} = 4\bar{c}_{f_{\text{app}}}\frac{x}{D} \tag{7-21}$$

Friction coefficients based on Langhaar's solution are plotted on Fig. 7-7, in the form $c_f\text{Re} = f[\text{Re}/(x/D)]$. Three friction coefficients are indicated: c_f, c_{f_m}, and $\bar{c}_{f_{\text{app}}}$.

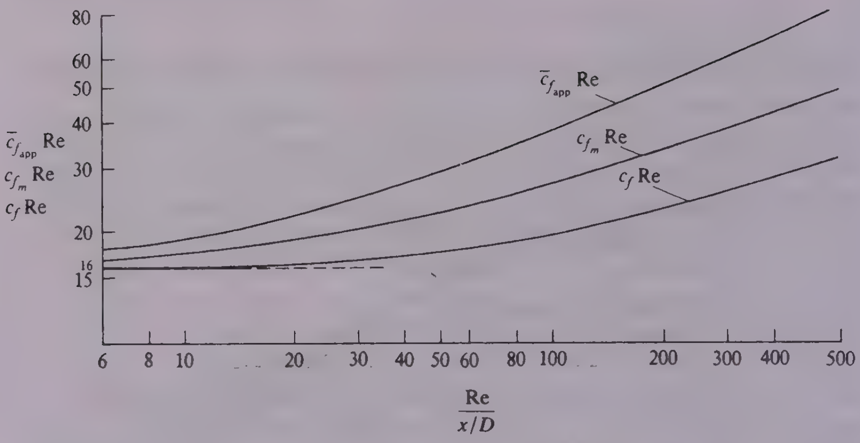

Figure 7-7 Friction coefficients for laminar flow in the hydrodynamic entry length of a circular tube (Langhaar[5]).

In Fig. 7-7, c_f is the *local friction coefficient*, based on the actual local surface shear stress at x by rearranging Eq. (7-13),

$$c_f = \frac{\tau_s}{\frac{1}{2}\rho V^2} \tag{7-22}$$

The approach of c_f toward 16/Re in Fig. 7-7 is a measure of the development of the velocity profile toward a fully developed profile. Note that c_f has reached within about 2 percent of its ultimate magnitude at $\text{Re}/(x/D) = 20$. Thus, a good approximate figure for the length of tube necessary for the development of the laminar velocity profile is

$$\frac{x}{D} = \frac{\text{Re}}{20} \tag{7-23}$$

Solutions based on the same procedure as that used by Langhaar, but for flow in concentric-tube annuli—including flow between parallel planes—have been obtained by Heaton, Reynolds, and Kays.[7] A general method for computing velocity profiles and pressure drop in the entrance region of ducts of arbitrary cross section is given by Fleming and Sparrow.[8]

A considerable number of additional solutions for both fully developed flow and entry-length flow are presented in Shah and London,[3] and a correlation for entry-length flow is given in Shah.[9]

PROBLEMS

7-1. Consider steady, laminar, constant-property flow in a duct formed by two parallel planes. Let the velocity be uniform at the duct entrance. Calculate the development of the velocity profile in the entry length, using the momentum integral equation (5-4), and an assumption that the velocity profile may be approximated by a constant-velocity segment across the center portion of the duct and by simple parabolas in the growing boundary layer adjacent to the surfaces. Note that the mean velocity, Eq. (7-3), must be a constant, and thus Eq. (7-4) must be satisfied. [Some help in this problem may be obtained from an examination of the development of the momentum integral equation, Eq. (5-8).] Evaluate the hydrodynamic entry length and compare with Eq. (7-23).

7-2. Starting with the momentum theorem, develop Eq. (7-19) for the pressure drop in steady flow of a constant-property fluid in a tube of constant cross-sectional shape as a function of the friction coefficient, mean velocity, and tube length. Start with a control volume that is of infinitesimal dimension in the flow direction but that extends across the entire flow section. Then reconsider the problem when fluid density varies in some known manner along the tube but can be considered as effectively constant over the flow cross section. Discuss the implications of the latter assumption.

7-3. Consider fully developed laminar flow of a constant-property fluid in a circular tube. At a particular flow cross section, calculate the total axial momentum flux by integration over the entire cross section. Compare this with the momentum flux evaluated by multiplying the mass flow rate times the mean velocity. Explain the difference, then discuss the implications for the last part of Prob. 7-2.

7-4. Two air tanks are connected by two parallel circular tubes, one having an inside diameter of 1 cm and the other an inside diameter of 0.5 cm. The tubes are 2 m long. One of the tanks has a higher pressure than the other, and air flows through the two tubes at a combined rate of 0.00013 kg/s. The air is initially at 1 atm pressure and 16°C. Assuming that fluid properties remain constant and that the entrance and exit pressure losses are negligible, calculate the pressure differences between the two tanks.

7-5. A particular heat exchanger is built of parallel plates, which serve to separate the two fluids, and parallel continuous fins, which extend between the plates so as to form rectangular flow passages. For one of the fluids the plate separation is 1 cm and the nominal fin separation is 2 mm. However, manufacturing tolerance uncertainties lead to the possibility of a 10 percent variation in the fin separation. Consider the extreme case where a 10 percent oversize passage is adjacent to a 10 percent undersize passage. Let the flow be laminar and the passages sufficiently long that an assumption of fully developed flow throughout is reasonable. For a fixed pressure drop, how does the flow rate differ for these two passages and how does it compare to what it would be if the tolerance were zero?

7-6. Develop the analysis that leads to the linear shear stress distribution described by Eq. (7-12).

7-7. Using the methodology developed in the text for a circular pipe, develop the fully developed mean velocity profile and fully developed friction coefficient for the flow between parallel planes. Compare your friction result with Fig. 7-4 and Fig. 7-5.

7-8. Repeat Prob. 7-7 for an annulus with radius ratio r^*. Compare your velocity-profile result with Eq. (8-26) and your friction result with Fig. 7-5 and Shah and London.[3]

TEXSTAN PROBLEMS

7-9. TEXSTAN *analysis of laminar entry flow in a circular pipe*: Let the Reynolds number be 1000, and pick fluid properties that are appropriate to the Prandtl number of air or water. You can choose how to set up the TEXSTAN problem in terms of values for the geometrical dimensions and mean velocity for the pipe to provide the required Reynolds number and a pipe length equivalent to $x^+ = (x/D)/\text{Re} = 0.3$. Note that the x^+ variable is the inverse of the Langhaar variable, used in Fig. 7-7. Use constant fluid properties, and note that the energy equation does not have to be solved. For initial conditions let the velocity profile be flat at a value equal to the mean velocity.

Use Eq. (7-20) to obtain the mean friction coefficient and use Eq. (7-21) along with the pressure drop data to obtain the apparent friction coefficient, then plot the local, mean, and apparent friction coefficient versus x^+ to show how the data approach the hydrodynamic fully developed values that are shown on Fig. 7-7 and in Shaw and London.[3] Confirm the hydrodynamic entrance length, and compare to Eq. (7-23). Plot the nondimensional velocity profiles at various x^+ locations and compare to Fig. 7-6 to demonstrate the concept of how the profiles evolve from a flat profile into hydrodynamically fully developed profile. Plot the absolute value of the pressure gradient versus x^+ to show how the gradient becomes constant beyond the hydrodynamic entrance region. Evaluate the ratio of centerline velocity to mean velocity and plot it versus x^+ to show how the ratio becomes a constant (= 2.0) beyond the hydrodynamic entrance region.

7-10. TEXSTAN *analysis of laminar entry flow between parallel planes*: Follow the instructions for Prob. 7-9 to set up TEXSTAN, but use the geometry option that permits the centerline of the parallel planes channel to be a symmetry line. Use Eq. (7-20) to obtain the mean friction coefficient and use Eq. (7-21) along with the pressure drop data to obtain the apparent friction coefficient, then plot the local, mean, and apparent friction coefficient versus x^+ to show how the data approach the hydrodynamic fully developed values that are given in Shaw and London.[3] Confirm the hydrodynamic entrance length using data in Shaw and London.[3] Plot the nondimensional velocity profiles at various x^+ locations, using the ideas in Fig. 7-6 to demonstrate the concept of how the profiles evolve from a flat profile into hydrodynamically fully developed profile, and compare the fully developed profile with that given in Shaw and London.[3] Plot the absolute value of the pressure gradient versus x^+ to show how the gradient becomes constant beyond the hydrodynamic entrance region. Evaluate the centerline velocity to mean velocity ratio and plot it versus x^+ to show how the ratio becomes a constant (= 1.5) beyond the hydrodynamic entrance region.

7-11. TEXSTAN *analysis of laminar entry flow in a circular-tube annulus with* $r^* = 0.5$: Follow the instructions for Prob. 7-9 to set up TEXSTAN, but use the geometry option that permits the annulus. Use Eq. (7-20) to obtain the mean friction coefficient and use Eq. (7-21) along with the pressure drop data to obtain the apparent friction coefficient, then plot the local, mean, and apparent friction coefficient versus x^+ to show how the data approach the hydrodynamic fully-developed values that are given in Shaw and London.[3] Confirm the hydrodynamic entrance length using data in Shaw and London.[3] Plot the nondimensional velocity profiles at various x^+ locations using the ideas in Fig. 7-6 to demonstrate the concept of how the profiles evolve from a flat profile into hydrodynamically fully developed profile, and compare the fully developed profile with that given in Eq. (8-26). Plot the absolute value of the pressure gradient versus x^+ to show how the gradient becomes constant beyond the hydrodynamic entrance region. Evaluate the ratio of centerline velocity to mean velocity and plot it versus x^+ to show how the ratio becomes a constant beyond the hydrodynamic entrance region.

REFERENCES

1. Kays, W. M., and S. H. Clark: TR no. 17, Department of Mechanical Engineering, Stanford University, Stanford, California, August 15, 1953.
2. Lundberg, R. E., W. C. Reynolds, and W. M. Kays: NASA TN D-1972, Washington, August 1963.
3. Shah, R. K., and A. L. London: "Laminar Flow Forced Convection in Ducts," *Advances in Heat Transfer*, Academic Press, New York, 1978.
4. Kakac, S., R. K. Shah, and W. Aung: *Handbook of Single-Phase Convective Heat Transfer*, John Wiley, New York, 1987.
5. Langhaar, H. L.: *J. Appl. Mech.*, vol. 9, 1942.
6. Sparrow, E. M., S. H. Lin, and T. S. Lundgren: *Phys. Fluids*, vol. 7, pp. 338–347, 1964.
7. Heaton, H. S., W. C. Reynolds, and W. M. Kays: *Int. J. Heat Mass Transfer*, vol. 7, p. 763, 1964.
8. Fleming, D. P., and E. M. Sparrow: *J. Heat Transfer*, vol. 91, pp. 345–354, 1969.
9. Shah, R. K.: *J. Fluids Engng*, vol. 100, pp. 177–179, 1978.
10. Hornbeck, R. W.: *Appl. Sci. Res., Ser. A*, vol. 13, pp. 224–232, 1964.

8

CHAPTER

Laminar Internal Flows: Heat Transfer

In this chapter we consider heat exchange between a fluid and a solid surface, when the fluid is flowing steadily with laminar motion inside a smooth tube. We assume that all body forces are negligible and that the fluid is forced through the tube by some external means, unrelated to the temperature field in the fluid. All the laminar flow solutions considered in this chapter are based on the idealization of constant fluid properties. The influence of temperature-dependent properties is discussed in Chap. 15.

Since the major technical applications of these results are in the analysis and design of heat exchangers, it would be well at this point to discuss the distinction between heat-exchanger theory and the convection theory with which we are concerned here. Heat-exchanger theory concerns the total heat-transfer rates and terminal fluid temperatures in multifluid heat exchangers, the influence of the flow arrangement of the two or more fluids, and the effect of total surface area on these heat-transfer rates and temperatures. The application of heat-exchanger theory depends upon prior knowledge of the local heat-transfer conductance between the fluid and the tube surface, Eq. (1-1), for the particular flow situation existing within the heat-exchanger tubes. This conductance, or heat-transfer coefficient, may be obtained experimentally or numerically, or in some cases it may be deduced by analytic means. In this study we are concerned primarily with the analytic evaluation of the conductance under various conditions. The results of the evaluation can then be used, together with heat-exchanger theory, for the analysis of complete heat exchangers. Some of our results have significant application outside the realm of heat-exchanger theory, and we will also discover situations where the conductance concept loses its useful significance. In these cases it is more convenient to work directly with temperatures and heat-transfer rates than to employ a conductance.

We start with a consideration of the region far removed from the entrance to the tube, where both a fully developed velocity profile and a fully developed temperature profile obtain. Here we consider tubes of various flow cross-section shapes: a circular tube, circular-tube annuli, rectangular tubes, and triangular tubes. We consider heating (or cooling) from the two surfaces of an annulus and the effects of a peripheral heat-flux variation around a tube.

Next we consider a class of problems in which the velocity profile is fully developed and remains fixed while the temperature profile develops. The fluid temperature upstream of some point is assumed to be uniform and equal to the surface temperature, there being no heat transfer in this region. Following this point, heat transfer takes place; then we are concerned with the development of the temperature profile. These *thermal-entry-length* or *unheated-starting-length* solutions are considered in some detail for the circular tube, and results are also presented for rectangular tubes and concentric circular-tube annuli. A method is then developed whereby the thermal-entry-length solutions for constant surface temperature and constant heat flux can be used to solve for the temperature distribution resulting from any arbitrary axial distribution of surface temperature or heat flux. Finally, some results are presented for the *combined hydrodynamic- and thermal-entry length*, that is, where both the velocity and fluid temperatures are uniform at the tube entrance.

Beginning with this chapter we recast the various forms of the energy equation that were developed in Chap. 4. Recall, they were developed following the principle of conservation of energy, Eq. (2-5), whereby all terms involving convection by the mass flux terms, heat and mass transfer by diffusion, and either shear work or viscous dissipation were retained on the left-hand side of the equal sign, and these terms were collectively set equal to a source term for energy. A more traditional form has the convective terms retained on the left-hand side of the equal sign, and all remaining terms moved to the right-hand side. The generalized form becomes

$$\text{convection}(\ ) = \text{diffusion}(\ ) \pm \text{source}(\ )$$

Note that this form can be used to describe the various terms of the momentum equation as well, where the viscous stress term becomes the diffusion term, and the source terms include the pressure gradient and body force.

THE ENERGY DIFFERENTIAL EQUATIONS FOR FLOW THROUGH A CIRCULAR TUBE

We have already developed the applicable differential energy equation (4-35) for flow in a circular tube under conditions of steady laminar flow with negligible viscous dissipation and flow-direction velocity–pressure gradient terms, no mass-concentration gradients, and no source functions. Let us restrict the problem to constant properties and introduce, for an ideal gas, the enthalpy relation

$$di = c\,dT$$

Equation (4-35), rewritten into the form of convection = diffusion ± source, becomes

$$\rho c u \frac{\partial T}{\partial x} + \rho c v_r \frac{\partial T}{\partial r} = \left[\frac{k}{r} \frac{\partial}{\partial r} \left(r \frac{\partial T}{\partial r} \right) + \frac{k}{r^2} \frac{\partial^2 T}{\partial \phi^2} + k \frac{\partial^2 T}{\partial x^2} \right] \tag{8-1}$$

[As noted in the discussion following Eq. (4-37), this equation is also valid for an incompressible liquid with no assumption regarding the pressure-gradient term such as was necessary in the development of Eq. (4-35).]

Let us now further restrict the problem to symmetric heat transfer ($\partial^2 T/\partial \phi^2 = 0$) and hydrodynamically fully developed flow ($v_r = 0$). Equation (8-1) then becomes

$$u \frac{\partial T}{\partial x} = \left(\frac{k}{\rho c} \right) \left[\frac{1}{r} \frac{\partial}{\partial r} \left(r \frac{\partial T}{\partial r} \right) + \frac{\partial^2 T}{\partial x^2} \right] \tag{8-2}$$

Let $\alpha = k/\rho c$, the *molecular thermal diffusivity* of the fluid. Thus

$$u \frac{\partial T}{\partial x} = \alpha \left[\frac{1}{r} \frac{\partial}{\partial r} \left(r \frac{\partial T}{\partial r} \right) + \frac{\partial^2 T}{\partial x^2} \right] \tag{8-3}$$

If we can neglect axial conduction relative to radial conduction (and we investigate the conditions under which this is permissible later) then $\partial^2 T/\partial x^2 = 0$, and we finally obtain the energy equation for laminar flow in a circular tube, solutions to which constitute the major part of this chapter:

$$u \frac{\partial T}{\partial x} = \alpha \frac{1}{r} \frac{\partial}{\partial r} \left(r \frac{\partial T}{\partial r} \right) \tag{8-4}$$

THE CIRCULAR TUBE WITH FULLY DEVELOPED VELOCITY AND TEMPERATURE PROFILES

The existence of a fully developed temperature profile at points far removed from the entrance to the tube is a little more difficult to visualize than the fully established velocity profile of Chap. 7. However, under a few possible heating conditions we can visualize the possibility of there existing a nondimensional temperature profile that is invariant with tube length, and under these conditions a solution to the energy equation can be effected very easily.

Criterion for a Fully Developed Temperature Profile

The term *fully developed temperature profile* implies that there exists, under certain conditions, a generalized temperature profile that is invariant with tube length, as in Fig. 8-1.

For convenience T_m is defined as the *mass-averaged fluid temperature*. This temperature is also sometimes referred to as the mixed mean temperature, bulk fluid temperature, or mixing-cup temperature: it is the temperature that

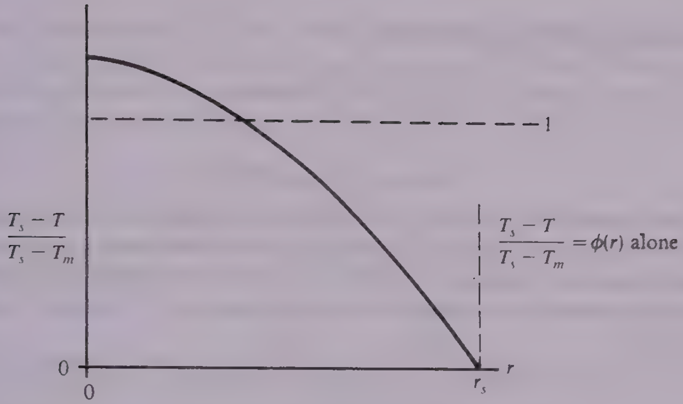

Figure 8-1 A fully developed temperature profile.

characterizes the average thermal energy state of the fluid. We have

$$\text{Axial convected thermal energy rate} = \dot{m}cT_m = (\rho V A_c)cT_m = \int_{A_c} \rho c u T \, dA_c$$

Then

$$T_m = \frac{1}{V A_c} \int_{A_c} u T \, dA_c \tag{8-5}$$

[Compare with the definition of the mean velocity, Eq. (7-5).]

If the nondimensional temperature is defined in terms of T_m, the mixed mean temperature, and T_s, the surface temperature, and if the nondimensional temperature profile is invariant in the flow direction, we can write the following for the conditions at the surface:

$$\left[\frac{\partial}{\partial r}\left(\frac{T_s - T}{T_s - T_m}\right)\right]_{r=r_s} = \text{const} = -\frac{(\partial T/\partial r)_{r=r_s}}{T_s - T_m}$$

Let us now introduce a *convection conductance*, or *heat-transfer coefficient h*, defined as in Eq. (1-1), with T_1 becoming the surface temperature T_s and T_2 becoming the mass-averaged or mixed-mean temperature T_m; then

$$\dot{q}_s'' = h(T_s - T_m) \tag{8-6}$$

Note that this conductance is defined with reference to the mixed mean temperature; this is quite arbitrary, but convenient.

From the definition of thermal conductivity, the following must apply at the surface (and this must be the case whether the flow is laminar or turbulent):

$$\dot{q}_s'' = -k\left(\frac{\partial T}{\partial r}\right)_{r=r_s}$$

Combining these three equations yields

$$\frac{\dot{q}_s''/k}{\dot{q}_s''/h} = \frac{h}{k} = \text{const}$$

Thus

$$h = \text{const}, \quad \text{invariant with } x$$

Experimentally this is often noted to be at least approximately true at points removed from the tube entrance for certain particular boundary conditions. Thus the nondimensional temperature profile is commonly observed to be invariant with tube length; in fact, most heat-exchanger analysis is based on a constant conductance h.

The statement that this profile is invariant with x can be expressed as

$$\frac{\partial}{\partial x}\left(\frac{T_s - T}{T_s - T_m}\right) = 0$$

Differentiating and solving for $\partial T/\partial x$ gives

$$\frac{\partial T}{\partial x} = \frac{dT_s}{dx} - \frac{T_s - T}{T_s - T_m}\frac{dT_s}{dx} + \frac{T_s - T}{T_s - T_m}\frac{dT_m}{dx} \tag{8-7}$$

This expression can now be substituted into the left-hand-side convective term of the energy differential equation (8-4). If we do so, we see that there are at least two boundary conditions (and these are special cases of a more general boundary condition, which we shall examine later) for which it will be possible to integrate the energy equation directly with respect to r, that is, treat it as an ordinary differential equation. Let us first examine some possible conditions.

Consider the case of *constant heat rate* Ⓗ per unit of tube length. Technically, constant-heat-rate problems arise in a number of situations: electric resistance heating, radiant heating, nuclear heating, and in counterflow heat exchangers when the fluid capacity rates[†] are the same. This is, then, a rather important boundary condition. The convection rate equation is

$$\dot{q}_s'' = h(T_s - T_m) = \text{const}$$

If h is a constant then

$$T_s - T_m = \text{const}$$

from which

$$\frac{dT_s}{dx} - \frac{dT_m}{dx} = 0, \qquad \frac{dT_s}{dx} = \frac{dT_m}{dx}$$

Thus, substituting in Eq. (8-7) gives

$$\frac{\partial T}{\partial x} = \frac{dT_s}{dx} = \frac{dT_m}{dx} \tag{8-8}$$

It also follows that dT_m/dx is a constant, as a simple energy balance reveals.

[†] Product of mass flow rate and specific heat of fluid.

Next consider the case where the *surface temperature* Ⓣ is *constant*. This is another very common convection application, and it occurs in such heat exchangers as evaporators, condensers, and, in fact, any heat exchanger where one fluid has a very much higher capacity rate than the other. For constant surface temperature,

$$\frac{dT_s}{dx} = 0$$

and Eq. (8-7) reduces to

$$\frac{\partial T}{\partial x} = \frac{T_s - T}{T_s - T_m}\frac{dT_m}{dx} \tag{8-9}$$

For these two conditions, *constant heat rate* and *constant surface temperature*, Eqs. (8-8) and (8-9) can be substituted into the energy equation (8-4) to yield the following two differential equations:

Constant heat rate Ⓗ

$$u\left(\frac{dT_m}{dx}\right) = \alpha\frac{1}{r}\frac{\partial}{\partial r}\left(r\frac{\partial T}{\partial r}\right)$$

Constant surface temperature Ⓣ

$$u\left(\frac{T_s - T}{T_s - T_m}\frac{dT_m}{dx}\right) = \alpha\frac{1}{r}\frac{\partial}{\partial r}\left(r\frac{\partial T}{\partial r}\right)$$

The corresponding temperature variations with tube length for these two conditions are shown in Fig. 8-2.

In both cases the independent variables (x, r) have been separated so that we can hold x constant and integrate directly with respect to r and determine the temperature profile.

The fundamental boundary conditions of constant-surface-temperature and constant-heat-rate are shown by Sparrow and Patankar[1] to be special cases of a more general exponential heat-flux boundary condition. But these two fundamental boundary conditions do cover the usual extremes met in heat-exchanger

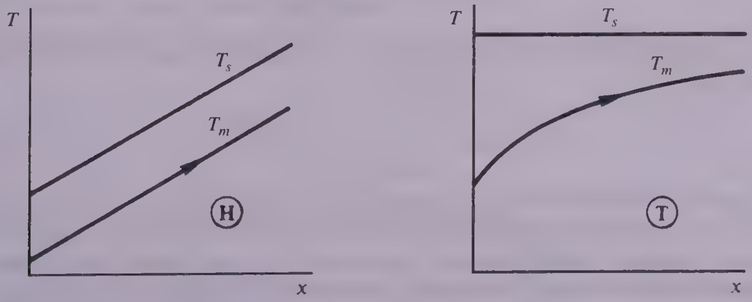

Figure 8-2

design, and are thus of great technical importance. It must be remembered, however, that we are still restricted to a long tube; near the tube entrance a fully developed temperature profile will not exist.

Constant-Heat-Rate Solution Ⓗ

The equation to be solved is

$$u\left(\frac{dT_m}{dx}\right)=\alpha\frac{1}{r}\frac{\partial}{\partial r}\left(r\frac{\partial T}{\partial r}\right) \tag{8-10}$$

The applicable boundary conditions are

$$T = T_s \qquad \text{at } r = r_s$$

$$\frac{\partial T}{\partial r} = 0 \qquad \text{at } r = 0$$

Substituting the parabolic velocity profile, Eq. (7-8), for u yields

$$\left[\frac{2V}{\alpha}\left(1-\frac{r^2}{r_s^2}\right)\right]\left(\frac{dT_m}{dx}\right)=\alpha\frac{1}{r}\frac{\partial}{\partial r}\left(r\frac{\partial T}{\partial r}\right)$$

This equation can now be directly integrated twice with respect to r, and the two constants of integration can be evaluated from the boundary conditions:

$$T = T_s - \frac{2V}{\alpha}\frac{dT_m}{dx}\left(\frac{3r_s^2}{16}+\frac{r^4}{16r_s^2}-\frac{r^2}{4}\right) \tag{8-11}$$

Equation (8-11) is then the desired temperature profile. With the temperature profile established, the mixed mean temperature can be evaluated next. From Eq. (8-5),

$$T_m = \frac{2}{Vr_s^2}\int_0^{r_s} uTr\,dr \tag{8-12}$$

If Eq. (7-8) and (8-11) are substituted for u and T, this equation can be readily integrated to yield

$$T_m = T_s - \frac{11}{96}\frac{2V}{\alpha}\frac{dT_m}{dx}r_s^2 \tag{8-13}$$

At this point the conductance h can be evaluated by use of its defining equation (8-6):

$$\dot{q}_s'' = h(T_s - T_m) = h\frac{11}{96}\frac{2V}{\alpha}\frac{dT_m}{dx}r_s^2 \tag{8-14}$$

The surface heat flux must yet be evaluated, and this can be done in one of two ways. The temperature profile, Eq. (8-11), can be differentiated to give the temperature gradient at the surface, from which $\dot{q}_s''$ can be evaluated from the conduction rate equation. A still simpler method is to make an energy balance on a differential control volume, as shown in Fig. 8-3.

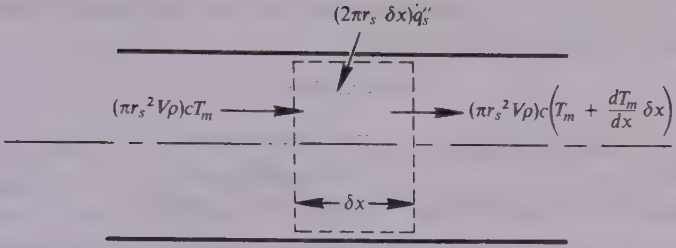
$(2\pi r_s\,\delta x)\dot{q}_s''$
$(\pi r_s^2 V\rho)cT_m$
$(\pi r_s^2 V\rho)c\left(T_m + \frac{dT_m}{dx}\delta x\right)$
δx

Figure 8-3 Control volume for an energy flow in a circular tube.

Applying the conservation-of-energy principle,[†] Eq. (2-5), and solving for the surface heat flux, we have

$$\dot{q}_s'' = \frac{r_s V\rho c}{2}\frac{dT_m}{dx} \tag{8-15}$$

Combining (8-14) and (8-15), and solving for h,

$$h = \frac{48}{11}\frac{k}{D} = 4.364\frac{k}{D} \tag{8-16}$$

where $D = 2r_s$.

Note the simple form of the solution as soon as we introduce the conductance. Since all temperatures cancel, we see that $\dot{q}_s''$ is in this case truly proportional to the temperature difference, which is the reason for introducing the convection rate equation and defining a conductance. The rate equation and the conductance are purely conveniences that are extremely useful in presenting the solution in a compact form and in using the solution to calculate heat-transfer rates. Later we run into situations where the conductance does not introduce any simplification and therefore loses its useful significance, and in those cases we dispense with it.

Note that the conductance h depends only on k and D, and is independent of V, ρ, c, and so on. This is true only for laminar flow, however, and only for the special case of fully developed velocity and temperature profiles. This independence results from the fact that the energy transport is a purely molecular conduction problem under these conditions.

Equation (8-16) is most often expressed in nondimensional form as follows:

$$hD/k = 4.364$$

or

$$\mathrm{Nu} = 4.364 \tag{8-17}$$

where $\mathrm{Nu} = hD/k$ is called the *Nusselt number.*

[†] Note in this case that any conversion of mechanical to thermal energy is neglected, so that conservation of thermal energy only is considered.

This solution can be represented in a different way that allows an interesting comparison. By dimensional reasoning,

$$\mathrm{Nu} = \mathrm{St}\,\mathrm{Pr}\,\mathrm{Re}$$

where $\mathrm{St} = h/\rho Vc$ or h/Gc, the Stanton number
$\mathrm{Pr} = \mu c/k$, the Prandtl number
$\mathrm{Re} = D\rho VD/\mu$ or GD/μ, the Reynolds number

Note that the Nusselt number and the Stanton number are simply two different nondimensional versions of the heat-transfer coefficient. Both are extensively used, but the choice is usually a personal one; one can always be evaluated from the other. The Prandtl number was previously defined in Chap. 3.

Thus

$$\mathrm{St}\,\mathrm{Pr}\,\mathrm{Re} = 4.364$$

$$\mathrm{St}\,\mathrm{Pr} = \frac{4.364}{\mathrm{Re}} \tag{8-18}$$

Note the similarity in form to the corresponding friction coefficient, Eq. (7-15). The Prandtl number is merely a fluid property parameter, so it is evident that a fixed relation exists between the Stanton number and the friction factor. It is found later in fully developed (turbulent flow that the Stanton number is again proportional (approximately) to the friction coefficient.

Constant-Surface-Temperature Solution Ⓣ

The equation to be solved is

$$u\left(\frac{T_s - T}{T_s - T_m}\frac{dT_m}{dx}\right) = \alpha\frac{1}{r}\frac{\partial}{\partial r}\left(r\frac{\partial T}{\partial r}\right) \tag{8-19}$$

The applicable boundary conditions are

$$T = T_s \quad \text{at } r = r_s$$

$$\frac{\partial T}{\partial r} = 0 \quad \text{at } r = 0$$

The parabolic velocity profile, Eq. (7-8), is substituted for u, as before, yielding

$$\left[\frac{2V}{\alpha}\left(1 - \frac{r^2}{r_s^2}\right)\right]\left(\frac{T_s - T}{T_s - T_m}\frac{dT_m}{dx}\right) = \alpha\frac{1}{r}\frac{\partial}{\partial r}\left(r\frac{\partial T}{\partial r}\right)$$

This problem has been solved by Bhatti,[7] as reported by Kakac, Shah, and Aung.[8] The solution is in the form of an infinite series:

$$\frac{T_s - T}{T_s - T_{\text{centerline}}} = \sum_{n=0}^{\infty} C_{2n}\left(\frac{r}{r_s}\right)^{2n} \tag{8-20}$$

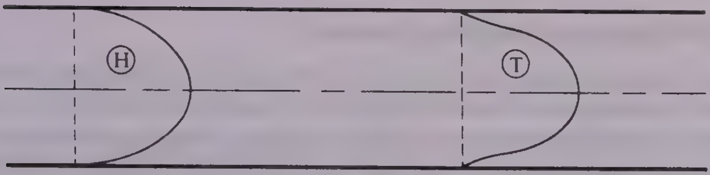

Figure 8-4 Fully developed temperature profiles for constant heat rate and constant surface temperature.

where the coefficients C_{2n} are given by

$$C_0 = 1, \qquad C_2 = -\tfrac{1}{4}\lambda_0^2 = -1.828397$$

$$C_{2n} = \frac{\lambda_0^2}{(2n)^2}(C_{2n-4} - C_{2n-2})$$

$$\lambda_0 = 2.704364$$

and $(T_{\text{centerline}} - T_s)/(T_m - T_s) = 1.803$.

The Nusselt number corresponding to the temperature distribution of Eq. (8-20) can be shown to be

$$\text{Nu} = \tfrac{1}{2}\lambda_0^2 = 3.657 \qquad \text{(8-21)}$$

This result is 16 percent less than the solution for constant heat rate. The difference in conductance can be explained simply by the slightly different shape of the generalized temperature profile, Fig. 8-4.

It is thus seen that the convection conductance depends to some degree on the type of the surface temperature variation. More is seen of this effect later.

Exponentially Varying Heat-Flux Solution

The two cases just considered, where a fully developed temperature profile is physically possible at some distance from the tube entrance, are special cases of a more general boundary condition where the heat flux varies *exponentially* along the tube:

$$q_s''(x^+) = q_s''(x^+ = 0)\ \exp\left(\tfrac{1}{2}nx^+\right)$$

where n is a constant exponent that can assume positive or negative values and $x^+ = x/(2r_s \text{ Re Pr})$. The case $n = 0$ corresponds to the constant-heat-rate case, and $n = -2\lambda_0^2 = -14.63$ corresponds to the constant-surface-temperature case. Shah and London[5] have developed the following correlation equation, which fits the exact solution within 3 percent over the range:

$$-51.36 < n < 100$$

$$\begin{aligned}\text{Nu} = 4.3573 + 0.0424n - 2.8368 \times 10^{-4}n^2 + 3.6250 \times 10^{-6}n^3 \\ - 7.6497 \times 10^{-8}n^4 + 9.1222 \times 10^{-10}n^5 - 3.8446 \times 10^{-12}n^6 \qquad \text{(8-22)}\end{aligned}$$

Effect of Peripheral Heat-Flux Variation

In the two examples already considered, both the heat flux and the surface temperature were uniform around the tube periphery. Frequently the heat flux is unevenly distributed around the tube (a bank of tubes radiantly heated on one side, for example), which leads to hot spots on the tube surface. If the tube surface material is thick and has a sufficiently high conductivity, peripheral conduction in the surface may alleviate this problem, but for thin-walled tubes the difficulty can be acute.

The problem of laminar flow in a circular tube with fully developed, constant-heat-rate conditions axially, but with any arbitrary peripheral variation of heat flux, has been treated by Reynolds.[2,3]

For the applicable differential energy equation, we go back to Eq. (8-1) but again set $v_r = 0$ and $\partial^2 T/\partial x^2 = 0$. This yields the equation for fully developed, constant heat rate:

$$u\frac{\partial T}{\partial x} = u\left(\frac{dT_m}{dx}\right) = \alpha\left[\frac{1}{r}\frac{\partial}{\partial r}\left(r\frac{\partial T}{\partial r}\right) + \frac{1}{r^2}\frac{\partial^2 T}{\partial \phi^2}\right]$$

Of particular interest is the rather simple result obtained for a cosine heat-flux variation, since many nonuniform heating problems can be at least approximated by a cosine variation (Fig. 8-5). For this case $\dot{q}_s''(\phi) = \dot{q}_a''(1 + b\cos\phi)$, and the local Nusselt number turns out to be

$$\mathrm{Nu}(\phi) = \frac{1 + b\cos\phi}{\frac{11}{48} + \frac{1}{2}b\cos\phi} \tag{8-23}$$

If $b = 0$, the Nusselt number becomes independent of ϕ and equal to 4.364, as would be expected.

Depending on the magnitude of b, the Nusselt number can vary in very strange ways. For example, if $b = 0.458$, it goes to infinity at $\phi = \pi$. This is a result of the definition of the Nusselt number, which is constructed from a conductance based on the difference between the local surface temperature and the mixed mean fluid temperature; that is,

$$\mathrm{Nu} = hD/k$$
$$\dot{q}_s'' = h(T_s - T_m)$$

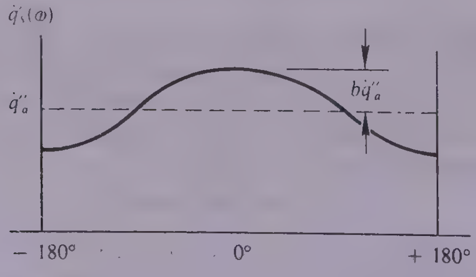

Figure 8-5

or

$$T_s - T_m = \dot{q}_s''/h$$

An infinite conductance merely means that the surface temperature is the same as the mixed mean temperature, and does not imply an infinite heat flux. In constant-heat-rate problems (constant heat rate per unit of length) the mixed mean temperature of the fluid can always be determined at any point along the tube, by an energy balance; the heat-transfer problem is merely to determine the difference between the mean fluid temperature and the surface temperature.

The Effect of Fluid Axial Conduction

In the development of Eq. (8-4), the axial fluid conduction term $\partial^2 T/\partial x^2$ was neglected. For the fully developed *constant-heat-rate* case this term is always 0, so the Nusselt number is not affected by axial conduction. But for the *constant-surface-temperature* case axial conduction can be of significance at low values of Re and/or Pr. In fact, the significant parameter is the *Péclet number* Pe = Re Pr. This problem has been investigated by Michelsen and Villadsen,[9] and the following equations are recommended:

$$\mathrm{Nu} = \begin{cases} 4.180654 - 0.183460\,\mathrm{Pe} & \text{for Pe} < 1.5 \\ 3.656794 + 4.487/\mathrm{Pe}^2 & \text{for Pe} > 5 \end{cases} \tag{8-24}$$

As can be seen, the effect of axial fluid conduction is totally negligible for Pe = 100, and is quite small even for Pe = 10. In practical applications axial conduction is frequently of considerable significance for laminar flow of liquid metals, which have very low Prandtl numbers. For gases axial conduction is mostly important at extremely low Reynolds numbers, and for most liquids it is seldom of significance. There is an exception to this rule for short heated sections. Weigand et al.[19] have analytically investigated this case for a piecewise constant heat flux at the surface and found that axial heat conduction effects can also be important for larger Peclet numbers, especially near the entrance and near the exit of the heated section.

Effects of Viscous Dissipation and Internal Heat Sources

In the development of Eq. (8-10) for fully developed, constant heat rate, the influences of both viscous energy dissipation and any internal sources of heat were neglected. The two terms that are introduced by these effects can be seen in Eq. (4-31), namely $\mu\phi$ for viscous dissipation and S for a volumetric heat source. These terms can be carried through in the development and will then appear in Eq. (8-10) as simply additive on the right-hand side. For fully developed conditions $\mu\phi$ becomes $\mu(\partial\mu/\partial r)^2$ and is thus independent of x. If S is held constant, it too is then also independent of x. In either case the temperature profile can still be fully developed and independent of x in a nondimensional sense. Equation (8-10) can be integrated directly as before, with a closed-form algebraic result, and a simple algebraic equation results for the Nusselt number. Kakac, Shah, and Aung[8] present the following results:

$$\mathrm{Nu} = 192/(44 + 3\lambda) \tag{8-25}$$

where

$$\lambda = \mathrm{SD}/q_s'' + 64\ \mathrm{Br}'$$

and

$$\mathrm{Br}' = V^2\mu/q_s''D$$

Br′ is known as the *Brinkman number* and is the characteristic nondimensional parameter for viscous dissipation for heat-flux-specified problems.

Note that Eq. (8-25) reduces to Eq. (8-17) in the absence of both viscous dissipation and internal heat sources.

Viscous dissipation is generally negligible for low-Prandtl-number fluids unless velocity is extremely high, but can become very important for high-Prandtl-number fluids such as oils, even at very moderate velocities.

THE CONCENTRIC CIRCULAR-TUBE ANNULUS WITH FULLY DEVELOPED VELOCITY AND TEMPERATURE PROFILES, ASYMMETRIC HEATING

Heat transfer to a fluid flowing in a circular-tube annulus is a particularly interesting problem, and one of considerable technical importance because either or both of the surfaces can be heated independently. If we restrict consideration, for the moment, to points far removed from the entrance to the tube (as in the previously discussed circular-tube problems), there are again heating conditions of technical interest for which a fully developed temperature profile is possible—constant heat rate per unit of length but with the heat flux on each surface independently specified, and constant but independently specified temperatures on each surface. This problem in all its variations has been completely solved[4] (including the thermal-entry-length problem), but we consider here only the constant-heat-rate case. In principle, the case of exponentially varying heat flux will lead to fully developed temperature profiles, but this more general case has apparently not been solved.)

The annulus system and the nomenclature to be employed are shown in Fig. 8-6.

The energy differential equation that is applicable to the constant-axial-heat-rate case is exactly the same as for the circular-tube, constant-heat-rate problem, that is, Eq. (8-10). The velocity profile must first be determined, and this can be done by integration of Eq. (7-1):

$$\frac{u}{V} = \frac{2}{M}\left[1 - \left(\frac{r}{r_o}\right)^2 + B\ln\frac{r}{r_o}\right] \tag{8-26}$$

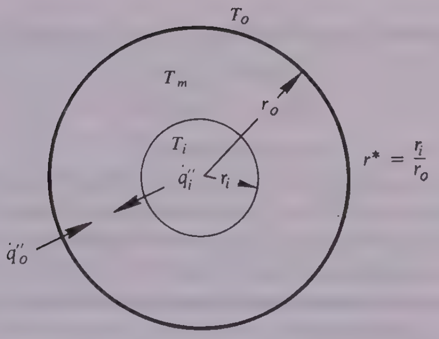

Figure 8-6 Nomenclature for flow in a circular-tube annulus.

where

$$B = \frac{r^{*2} - 1}{\ln r^*}$$
$$M = 1 + r^{*2} - B$$

and $r^* = r_i/r_o$ as shown in Fig. 8-6. Then the energy equation becomes

$$\left[\frac{2V}{M}\left[1 - \left(\frac{r}{r_o}\right)^2 + B \ln \frac{r}{r_o}\right]\right]\left(\frac{dT_m}{dx}\right) = \alpha\left[\frac{1}{r}\frac{\partial}{\partial r}\left(r\frac{\partial T}{\partial r}\right)\right] \tag{8-27}$$

As was the case for the circular tube, this equation may be directly integrated without difficulty. The heat flux at each of the two surfaces specifies the temperature gradient at the surfaces, which provides the necessary boundary conditions. However, it is not necessary to solve the equation for each particular application; the linearity of the energy equation suggests that superposition methods may be employed to build solutions for asymmetric heating by merely adding other solutions. Superposition methods are based on the fact that any number of solutions to a homogeneous and linear differential equation may be added and the result will still satisfy the differential equation. It remains only to add solutions in such a way as to satisfy the desired boundary conditions. In this problem only two fundamental solutions are needed: (1) the outer surface heated with the inner insulated and (2) the inner surface heated with the outer insulated. The algebra of this development is lengthy and is not repeated here; only the final form is given.

Denote the heat fluxes on the inner and outer tubes by $\dot{q}_i''$ and $\dot{q}_o''$, respectively, positive when heat flows *into* the fluid. The heat-transfer coefficients on the inner and outer tubes are defined as follows:

$$\dot{q}_i'' = h_i(T_i - T_m)$$
$$\dot{q}_o'' = h_o(T_o - T_m)$$

We define the inner- and outer-surface Nusselt numbers as

$$\mathrm{Nu}_i = h_i D_h / k$$

$$\mathrm{Nu}_o = h_o D_h / k$$

where $D_h = 4r_h = 2(r_o - r_i)$ for an annulus.

Next, let Nu_{ii} be defined as the inner-tube Nusselt number when the inner tube alone is heated, and let Nu_{oo} be the outer-tube Nusselt number when the outer tube alone is heated; that is, these are the fundamental solutions. Define θ_i^* and θ_o^* as influence coefficients, which may be evaluated from the fundamental solutions. The Nusselt numbers on the inner and outer tubes for any heat-flux ratio can then be evaluated from

$$\mathrm{Nu}_i = \frac{\mathrm{Nu}_{ii}}{1 - (\dot{q}_o''/\dot{q}_i'')\theta_i^*} \tag{8-28}$$

$$\mathrm{Nu}_o = \frac{\mathrm{Nu}_{oo}}{1 - (\dot{q}_i''/\dot{q}_o'')\theta_o^*} \tag{8-29}$$

The complete set of functions for the annulus for fully developed laminar flow is given in Table 8-1.

It is of interest to examine how the Nusselt number can vary with asymmetric heating. Take, for example, the case of flow between parallel planes, which is one of the limiting cases of the annulus: $r^* = 1$. Equations (8-28) and (8-29) become identical in this case, so let us refer to sides 1 and 2 rather than the inner and outer surfaces. Then

$$\mathrm{Nu}_1 = \frac{5.385}{1 - 0.346\dot{q}_2''/\dot{q}_1''}$$

If $\dot{q}_2'' = 0$, $\mathrm{Nu}_1 = 5.385$, which is, of course, the solution for only one side heated. If both sides are heated equally, $\dot{q}_2''/\dot{q}_1'' = 1$, and then $\mathrm{Nu}_1 = \mathrm{Nu}_2 = 8.23$. Now note what happens if

$$0.346\dot{q}_2''/\dot{q}_1'' = 1$$

In this case

$$\mathrm{Nu}_1 = \infty$$

Table 8-1 Circular-tube annulus solutions for constant heat rate and fully developed velocity and temperature profiles

r^*	Nu_{ii}	Nu_{oo}	θ_i^*	θ_o^*
0	∞	4.364	∞	0
0.05	17.81	4.792	2.18	0.0294
0.10	11.91	4.834	1.383	0.0562
0.20	8.499	4.883	0.905	0.1041
0.40	6.583	4.979	0.603	0.1823
0.60	5.912	5.099	0.473	0.2455
0.80	5.58	5.24	0.401	0.299
1.00	5.385	5.385	0.346	0.346

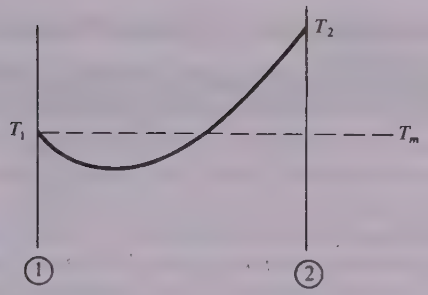

Figure 8-7 Temperature distribution resulting from unequal heating on the two sides of a flat duct.

and

$$\dot{q}_2''/\dot{q}_1'' = 2.9$$

This does not imply an infinite heat-transfer rate but merely that $T_1 - T_m = 0$ because of the temperature profile shown in Fig. 8-7.

If $\dot{q}_2''/\dot{q}_1'' > 2.9$, the Nusselt number, and thus the conductance, becomes negative. This fact does not destroy either the validity or the usefulness of the Nusselt number, as long as we understand the physical reason.

SOLUTIONS FOR TUBES OF NONCIRCULAR CROSS SECTION WITH FULLY DEVELOPED VELOCITY AND TEMPERATURE PROFILES

Rectangular and Triangular Tubes

Solutions have been obtained for rectangular and triangular tubes in much the same manner as for the circular tubes. The applicable energy differential equation may be deduced from Eq. (4-36):

$$u\frac{\partial T}{\partial x} = \alpha \nabla^2 T = \alpha\left(\frac{\partial^2 T}{\partial y^2} + \frac{\partial^2 T}{\partial z^2}\right)$$

The velocity u is obtained from solutions of the corresponding momentum equation (7-16).

Some of these results, obtained by numerical integration,[5] are listed in Table 8-2. For both the constant-heat-rate case and the constant-surface-temperature case the temperature is assumed to be constant around the tube periphery, and the conductance used in calculating Nu is an average with respect to peripheral area. For tube walls that have finite conductivity in the peripheral and or axial direction Nu is different from those given in Table 8-2. These Nusselt

Table 8-2 Nusselt numbers for fully developed velocity and temperature profiles in tubes of various cross sections

Cross-sectional shape	b/a	$\mathrm{Nu}_{\textcircled{\scriptsize H}}$[†]	$\mathrm{Nu}_{\textcircled{\scriptsize T}}$
		4.364	3.66
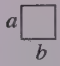	1.0	3.61	2.98
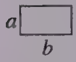	1.43	3.73	3.08
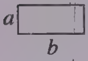	2.0	4.12	3.39
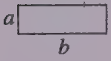	3.0	4.79	3.96
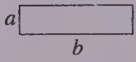	4.0	5.33	4.44
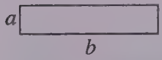	8.0	6.49	5.60
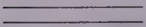	∞	8.235	7.54
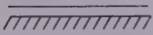		5.385	4.86
		3.11	2.49

[†] The constant-heat-rate solutions are based on constant *axial* heat rate, but with constant *temperature* around the tube periphery. Nusselt numbers are averages with respect to tube periphery.

number variations and those for various other boundary conditions are discussed in detail in Shah and London[5] and summarized by the same authors in Ref. 6 (see also Ref. 8).

In all cases the Nusselt number is defined as hD_h/k, where

$$D_h = 4 \times (\text{flow area}/\text{wetted perimeter})$$

This definition of hydraulic diameter is used consistently throughout this book.

An interesting feature of the solutions for shapes with sharp corners, like the square, is the fact that the local heat-transfer conductance varies around the periphery and approaches zero at the corners; this means that the heat flux goes to zero at the corners.

Other Tube Cross-Sectional Shapes

The number of possibly interesting shapes of tubes for technical applications is virtually infinite. For each of these there are a considerable number of possible heating boundary conditions that will lead to fully developed temperature profiles, and thereby to constant Nusselt numbers. A large number of solutions of one type or another have been developed for various of these cases. No attempt will be made here to consider all of these possibilities. Shah and London[5] tabulate a number of these solutions, and also the *Handbook of Single-Phase Convective Heat Transfer*[8] is a useful source of data.

CIRCULAR-TUBE THERMAL-ENTRY-LENGTH SOLUTIONS

So far we have considered only problems where we have fully established velocity and temperature profiles and in which the conductance h is constant with length. Next we consider some cases where the temperature of the fluid is uniform over the flow cross section at the point where heat transfer begins, but the velocity profile is already fully established and invariant. Under these conditions we find that the conductance varies along the length of the tube. We restrict consideration to laminar, incompressible, low-velocity flow.

Strictly speaking, these solutions apply rigorously only when a hydrodynamic starting length is provided so that the velocity profile is fully developed before heat transfer starts, a condition rarely encountered in technical applications. Such solutions are, however, excellent approximations for fluids whose Prandtl numbers are high relative to 1. It is well, therefore, to discuss briefly the significance of the Prandtl number in such problems.

The Prandtl number is a nondimensional group of fluid transport properties:

$$\mathrm{Pr} = \frac{\mu c}{k}$$

If the numerator and denominator are multiplied by density, the Prandtl number can be written as

$$\mathrm{Pr} = \frac{v}{\alpha} = \frac{\text{kinematic viscosity}}{\text{thermal diffusivity}}$$

The kinematic viscosity is a diffusivity for momentum, or for velocity, in the same sense that the thermal diffusivity is a diffusivity for heat, or for temperature. (*Diffusivity* is defined as the rate at which a particular effect is diffused through the medium.) If the Prandtl number is 1 then heat and momentum are diffused through the fluid at the same rates: if the velocity and temperature are both uniform at the entrance to a tube, then the velocity and temperature profiles develop together. Later, in consideration of external boundary layers, it is seen that $\mathrm{Pr} = 1$ leads to great simplifications for this reason. If the Prandtl number is greater than 1, it must follow that the velocity profile develops more rapidly than the temperature profile. Actually if the Prandtl number is greater than about 5, the velocity profile leads the temperature profile sufficiently that a solution based on an already fully developed velocity profile will apply quite accurately even though there is no hydrodynamic starting length.

Of course, the opposite also holds: and for a fluid with a Prandtl number less than 1 the temperature profile develops more rapidly than the velocity profile.

The Prandtl number for any particular fluid generally varies somewhat with temperature, but only over a limited range. Figure 8-8 shows the Prandtl number spectrum. Note that the area of applicability of the solutions we are about to consider is limited to $\mathrm{Pr} \geq 5$. Of course, if a hydrodynamic starting length is actually provided, the solutions are applicable for any fluid. The necessary length

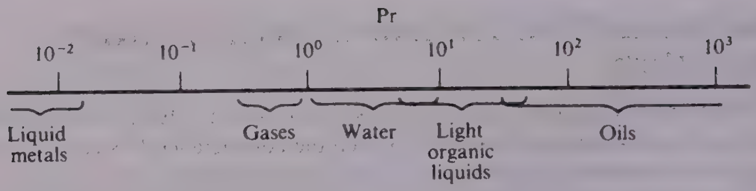

Figure 8-8 Prandtl number spectrum of fluids.

of tube for development of the laminar velocity profile is discussed in connection with Eq. (7-20).

Uniform Surface Temperature

The applicable differential energy equation is again Eq. (8-3):

$$u\frac{\partial T}{\partial x} = \alpha\left[\frac{1}{r}\frac{\partial}{\partial r}\left(r\frac{\partial T}{\partial r}\right) + \frac{\partial^2 T}{\partial x^2}\right] \tag{8-30}$$

It is convenient to put this equation in nondimensional form before discussing its solution. The form of the solution and the pertinent nondimensional parameters can be deduced from the differential equation itself. Let us introduce the following dimensionless variables:

$$\theta = \frac{T_s - T}{T_s - T_e}$$

where T_s is the constant surface temperature and T_e is the uniform entering fluid temperature;

$$r^+ = \frac{r}{r_s}, \qquad u^+ = \frac{u}{V}, \qquad x^+ = \frac{2(x/D)}{\mathrm{Re}\,\mathrm{Pr}}$$

where x is the axial distance from the point where heat transfer starts.

The particular form of x^+ is chosen so that the parameters will be absorbed within the variables (at least after axial conduction is neglected). At first it may not be apparent that such a choice for x^+ will accomplish this, but if x/r_s alone had been chosen for the nondimensional length, Re Pr would appear in the normalized equation and it would be easily seen that this group can be absorbed within the definition of the nondimensional length.

If we now form the indicated derivatives and substitute into Eq. (8-30), we obtain

$$\frac{u^+}{2}\frac{\partial \theta}{\partial x^+} = \frac{\partial^2 \theta}{\partial r^{+2}} + \frac{1}{r^+}\frac{\partial \theta}{\partial r^+} + \frac{1}{(\mathrm{Re}\,\mathrm{Pr})^2}\frac{\partial^2 \theta}{\partial x^{+2}} \tag{8-31}$$

The last term in this equation takes into account heat conduction in the axial direction. Whether this term can be neglected apparently depends on the magnitude of Re Pr, large values of this parameter suppressing the term. The differential equation alone is insufficient to tell how large this parameter must be in order to neglect axial conduction, but it was seen in connection with the fully developed temperature profile problem that the effect of axial conduction is quite small for $\text{Re}\,\text{Pr} > 10$, and completely negligible for $\text{Re}\,\text{Pr} > 100$. For present purposes this term will be neglected.

For hydrodynamically fully developed laminar flow the parabolic velocity profile, Eq. (7-8), is applicable:

$$u = 2V\left(1 - \frac{r^2}{r_s^2}\right), \qquad u^+ = 2(1 - r^{+2})$$

By substituting these into Eq. (8-31), the final form of the differential equation is obtained:

$$(1 - r^{+2})\frac{\partial \theta}{\partial x^+} = \frac{\partial^2 \theta}{\partial r^{+2}} + \frac{1}{r^+}\frac{\partial \theta}{\partial r^+} \tag{8-32}$$

The solution sought is then

$$\theta = \theta(x^+, r^+)$$

for the boundary conditions

$$\theta(0, r^+) = 1, \qquad \theta(x^+, 1) = 0, \qquad \left(\frac{\partial \theta}{\partial r^+}\right)_{x^+, r^+=0} = 0$$

Graphically the thermal-entry-length solution at constant surface temperature will appear as in Fig. 8-9. Once we have obtained this solution, we can calculate

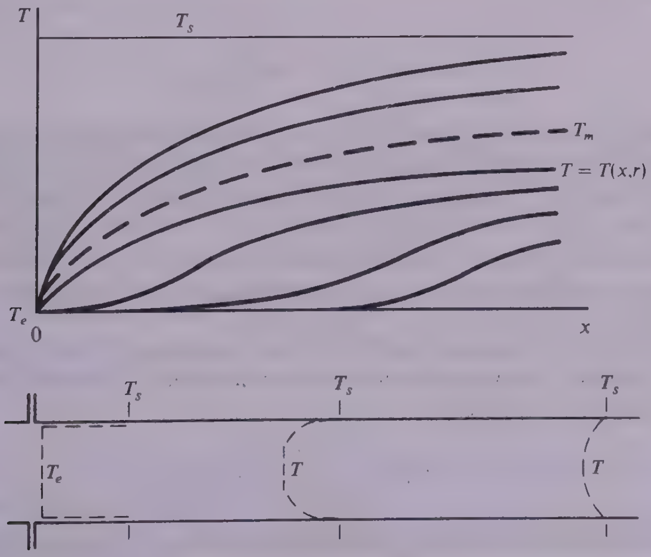

Figure 8-9 Development of the temperature profile in the thermal-entry region of a pipe.

the heat flux at any x^+ from the slope of the temperature profile at the surface:

$$\dot{q}_s''(x^+) = -k\left(\frac{\partial T}{\partial r}\right)_{r=r_s} = k\frac{T_s - T_e}{r_s}\left(\frac{\partial \theta}{\partial r^+}\right)_{r^+=1}$$

Next, we can determine the local mixed mean temperature of the fluid as a function of x^+ by either of two methods: (1) by integrating over the flow cross section, employing Eq. (8-12), or (2) by integrating $\dot{q}_s''(x^+)$ from $x^+ = 0$ to x^+ and applying an energy balance to define the mass-averaged or mixed-mean temperature

$$\theta_m(x^+) = \frac{T_s - T_m}{T_s - T_e}$$

Then we can define and evaluate a local convection conductance, or heat-transfer coefficient, h_x and a local Nusselt number, which is simply a nondimensional conductance:

$$\begin{aligned}
\dot{q}_s''(x^+) &= h_x(T_m - T_s) = -h_x(T_s - T_e)\theta_m(x^+) \\
h_x &= \frac{-\dot{q}_s''(x^+)}{(T_s - T_e)\theta_m(x^+)} \\
\mathrm{Nu}_x &= \frac{2r_s h_x}{k} = -\frac{2r_s\dot{q}_s''(x^+)}{k(T_s - T_e)\theta_m(x^+)} = \frac{-2}{\theta_m}\left(\frac{\partial \theta}{\partial r^+}\right)_{r^+=1}
\end{aligned} \tag{8-33}$$

Thus we see that

$$\mathrm{Nu}_x = f(x^+) = f\left(\frac{2(x/D)}{\mathrm{Re\,Pr}}\right)$$

Note that, by normalizing the differential equation, the dimensionless parameters necessary to describe the solution are derived before the latter is obtained.

The boundary conditions are such that the temperature gradient at the surface is infinite at $x^+ = 0$; therefore $\mathrm{Nu}_x = \infty$ at $x^+ = 0$. At points far down the tube we would expect the Nusselt number to approach the fully established condition previously discussed. The complete solution could be expected to appear as in Fig. 8-10.

Often in heat-exchanger analysis a mean conductance with respect to tube length, and thus a mean Nusselt number, is of more utility than the local conductance and Nusselt number:

$$\mathrm{Nu}_m = \frac{1}{x^+}\int_0^{x^+} \mathrm{Nu}_x\, dx^+ \tag{8-34}$$

It is generally simpler to employ heat-exchanger theory and work directly with the mixed mean temperature than to integrate Eq. (8-34). The solution for a

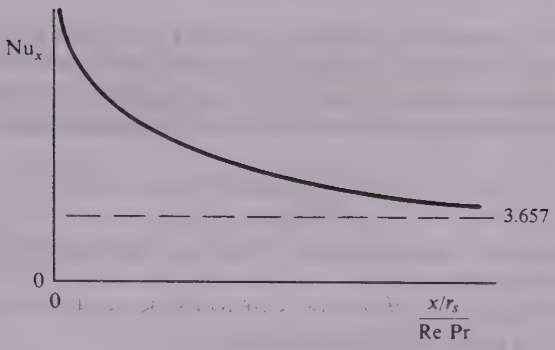

Figure 8-10 Variation of local Nusselt number in the thermal-entry region of a tube with constant surface temperature.

simple heat exchanger with constant surface temperature can be expressed as

$$\frac{T_m - T_e}{T_s - T_e} = 1 - \exp\left(-\frac{2\pi r_s}{\dot{m}c}\int_0^x h_x\,dx\right)$$
$$= 1 - \exp\left(-2\int_0^{x^+} \text{Nu}_x\,dx^+\right) = 1 - \theta_m$$

Combining and solving for Nu_m, we get

$$\text{Nu}_m = \frac{1}{2x^+}\ln\frac{1}{\theta_m} \tag{8-35}$$

Let us now examine the final solution to Eq. (8-32) for the indicated boundary conditions. This equation is linear and homogeneous, and such a partial differential equation can always be solved by the method of separation of variables. Let us assume that the solution to (8-32) can be represented by the product

$$\theta = R(r^+)\cdot X(x^+)$$

Then substitution into Eq. (8-32) results in two ordinary differential equations:

$$X' + \lambda^2 X = 0$$

$$R'' + \frac{1}{r^+}R' + \lambda^2 R(1 - r^{+2}) = 0$$

We use $-\lambda^2$ as the separation constant, and the primes refer to differentiation with respect to the independent variables.

The first of these equations is satisfied by a simple exponential function

$$X = C\exp(-\lambda^2 x^+)$$

Solutions to the second that satisfy the boundary conditions can be found for an infinite number of suitable values of λ, and they have been obtained by both numerical and approximate means.[10] This is an equation of the Sturm–Liouville type, and it has been studied extensively. The final solution takes the form

$$\theta(x^+, r^+) = \sum_{n=0}^{\infty} C_n R_n(r^+) \exp\left(-\lambda_n^2 x^+\right) \tag{8-36}$$

where the λ_n are the eigenvalues, the R_n are the corresponding eigenfunctions, and the C_n are constants.

From (8-36), the heat flux at the surface can be readily evaluated from the derivative at the surface, as indicated previously:

$$\dot{q}_s''(x^+) = -\frac{2k}{r_s}(T_s - T_e)\sum_{n=0}^{\infty} G_n \exp\left(-\lambda_n^2 x^+\right) \tag{8-37}$$

where $G_n = -\frac{1}{2}C_n R_n'(1)$ for brevity. Next, the mixed mean temperature θ_m can be evaluated after integration of Eq. (8-37) from $x = 0$ to x^+:

$$\theta_m = 8\sum_{n=0}^{\infty} \frac{G_n}{\lambda_n^2} \exp\left(-\lambda_n^2 x^+\right) \tag{8-38}$$

The local and mean Nusselt numbers are then readily evaluated from Eqs. (8-33) and (8-35):

$$\mathrm{Nu}_x = \frac{\sum_{n=0}^{\infty} G_n \exp\left(-\lambda_n^2 x^+\right)}{2\sum_{n=0}^{\infty} \left(G_n/\lambda_n^2\right) \exp\left(-\lambda_n^2 x^+\right)} \tag{8-39}$$

$$\mathrm{Nu}_m = \frac{1}{2x^+} \ln\left[\frac{1}{8\sum_{n=0}^{\infty} \left(G_n/\lambda_n^2\right) \exp\left(-\lambda_n^2 x^+\right)}\right] \tag{8-40}$$

The constants and eigenvalues for these infinite series, as presented by Sellers, Tribus, and Klein,[10] are given in Table 8-3. The complete results of the constant-surface-temperature solution are presented in Table 8-4.

Table 8-3 Infinite-series-solution functions for thermal-entry length in the circular tube; constant surface temperature

N	λ_n^2	G_n
0	7.313	0.749
1	44.61	0.544
2	113.9	0.463
3	215.2	0.415
4	348.6	0.383

For $n > 2$, $\lambda_n = 4n + \frac{8}{3}$; $G_n = 1.01276\lambda_n^{-1/3}$.

Table 8-4 Nusselt numbers and mean temperature for thermal-entry length in the circular tube; constant surface temperature

x^+	Nu_x	Nu_m	θ_m
0	∞	∞	1.000
0.001	12.80	19.29	0.962
0.004	8.03	12.09	0.908
0.01	6.00	8.92	0.837
0.04	4.17	5.81	0.628
0.08	3.77	4.86	0.459
0.10	3.71	4.64	0.396
0.20	3.66	4.15	0.190
∞	3.66	3.66	0.0

For large x^+ the series become increasingly more convergent, until finally, for $x^+ > 0.1$, only the first term is of significance. Then Eq. (8-39) becomes

$$\mathrm{Nu}_x = \frac{G_0 \exp\left(-\lambda_0^2 x^+\right)}{2(G_0/\lambda_0^2)\exp\left(-\lambda_0^2 x^+\right)} = \frac{1}{2}\lambda_0^2 = 3.657 \tag{8-41}$$

This is, of course, the Nusselt number for a fully developed temperature profile, as discussed earlier. Thus the thermal-entry length must be approximately $x^+ = 0.1$

$$x^+ = 0.1 = \frac{2(x/D)}{\mathrm{Re}\,\mathrm{Pr}}$$

Thus

$$(x/D)_{\text{fully dev}} \approx 0.05\,\mathrm{Re}\,\mathrm{Pr}$$

For example, for air with $\mathrm{Pr} = 0.7$, flowing with $\mathrm{Re} = 500$,

$$(x/D)_{\text{fully dev}} \approx 17.5$$

On the other hand, for an oil with $\mathrm{Pr} = 100$, flowing with $\mathrm{Re} = 500$,

$$(x/D)_{\text{fully dev}} \approx 2500$$

In an oil heat exchanger it is very rare indeed that anything approaching a fully developed temperature profile is attained; the fully developed profile solutions previously discussed are of very little utility in high-Prandtl-number applications.

Let us consider application of this solution to an oil heat exchanger for which the Prandtl number is 100, the Reynolds number is 500, and each of the tubes in the heat exchanger is 100 diameters long (there may be several passes, but the fluid completely mixes between passes and a new thermal-entry length must develop in each). If the oil is being heated or cooled by an essentially constant-temperature fluid, this solution should provide the proper conductance for the oil side of the heat exchanger. In a problem of this sort the mean conductance is required for use in the heat-exchanger analysis. Under these conditions,

$$x^+ = \frac{2(100)}{500 \times 100} = 0.004$$

Thus, from Table 8-4, $\mathrm{Nu}_m = 12.09$. Note the very large error that would have been obtained if the fully developed solution had been used.

One note of caution should be mentioned here. All the laminar flow solutions considered so far have been based on constant fluid properties. For liquids where the viscosity varies markedly with temperature (and oils are the worst offenders in this regard) considerable error may be introduced unless a correction is made for the variation of viscosity over the flow cross section. This subject is discussed in more detail in Chap. 15.

Uniform Heat Flux

The thermal-entry-length problem for laminar flow at uniform heat flux in a circular tube is very similar to the same problem at constant surface temperature. The same energy equation (8-32), must be solved, with the difference being that the constant-surface-temperature boundary condition is replaced by a constant temperature gradient at the surface. Also, the definition of θ is replaced by

$$\theta = \frac{T_e - T}{\dot{q}_s'' D / k}$$

The method of separation of variables and Sturm–Liouville theory have been employed[11] to obtain an eigenvalue solution, which is presented here only in terms of the local Nusselt number:

$$\mathrm{Nu}_x = \left[\frac{1}{\mathrm{Nu}_\infty} - \frac{1}{2} \sum_{m=1}^{\infty} \frac{\exp\left(-\gamma_m^2 x^+\right)}{A_m \gamma_m^4} \right]^{-1} \tag{8-42}$$

The necessary eigenvalues and constants are given in Table 8-5.

$\mathrm{Nu}_\infty = \frac{48}{11}$ or 4.364, as previously evaluated, and a complete tabulation of Nu_x is given in Table 8-6.

In a constant-heat-flux problem the mixed mean temperature of the fluid varies linearly with x^+ and can be established by simple energy balance methods.

Table 8-5 Infinite-series-solution functions for thermal-entry length in the circular tube; constant heat rate

m	γ_m^2	A_m
1	25.68	7.630×10^{-3}
2	83.86	2.053×10^{-3}
3	174.2	0.903×10^{-3}
4	296.5	0.491×10^{-3}
5	450.9	0.307×10^{-3}

For larger m, $\gamma_m \doteq 4m + \frac{4}{3}$; $A_m = 0.4165\gamma_m^{-7/3}$.

Table 8-6 Nusselt numbers for thermal-entry length in the circular tube; constant heat rate

x^+	Nu_x
0	∞
0.002	12.00
0.004	9.93
0.010	7.49
0.020	6.14
0.040	5.19
0.100	4.51
∞	4.36

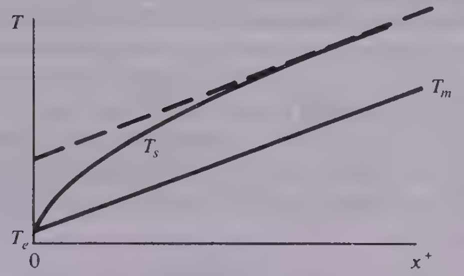

Figure 8-11 Temperature variations in the thermal-entry region of a tube with constant heat rate per unit of tube length.

The purpose of the heat-transfer solution is to relate the surface temperature to the mean fluid temperature through the definition of the conductance, that is,

$$T_s - T_m = \frac{\dot{q}_s''}{h_x} = \frac{\dot{q}_s'' D}{\mathrm{Nu}_x k}$$

Thus the mean fluid and the surface temperatures plotted as functions of distance along the tube appear as in Fig. 8-11.

THERMAL-ENTRY-LENGTH SOLUTIONS FOR THE RECTANGULAR TUBE AND ANNULUS

Laminar-flow thermal-entry-length solutions will be presented for two families of tube cross-sectional geometries. Entry-length solutions for other geometries and boundary conditions, as well as further discussion, can be found in Shah and London,[5] and in Kakac, Shah, and Aung.[8]

For the rectangular tube and annulus a fully developed laminar velocity profile, with all its implications, is assumed and the fluid properties are treated as constant. The problem is basically an extension of the circular-tube problem, but it is more difficult because of the more complex geometry. In the case of the annulus the differential equation to be solved is identical to the equation for the circular tube; only the boundary conditions differ. The entire family of circular-tube annuli from the single circular tube to the case of two parallel planes has been solved in a very general way for every possible heat-flux and surface-temperature combination on the two surfaces involved. For the rectangular tube there are three independent space variables in place of two; otherwise, essentially the same energy equation must be solved.

Only the final results of these analyses are presented. In the case of the annulus there are so many boundary condition possibilities that space permits presentation of only the most important.

The Rectangular Tube

The only member of the rectangle family that has been handled in a complete way is the case of flow between parallel planes,[4,10,12] for the obvious reason that this is geometrically a simpler case than even the circular tube. Only the case of both surfaces at the same constant temperature is presented here: some other boundary conditions are considered in the next section, where the parallel-planes geometry forms one of the limits of the circular-tube annulus problem.

Any constant-surface-temperature solution can be presented in the form of Eqs. (8-38)–(8-40) if we define x^+ in some consistent manner. For the solutions to be presented here let

$$x^+ = \frac{2(x/D_h)}{\text{Re Pr}}$$

where D_h is the hydraulic diameter defined as

$$D_h = \frac{4 \times \text{cross-sectional area}}{\text{wetted perimeter}}$$

(For the flow between parallel planes D_h becomes twice the plate spacing.) The eigenvalues and constants for the parallel-plane system are given in Table 8-7. (These have been modified from the original references to make them usable directly in Eqs. (8-38)–(8-40).)

The square tube has been studied,[13] and only the first three eigenvalues and constants are available. However, even this truncated part of the series is quite sufficient for $x^+ > 0.01$. These functions are given in Table 8-8.

Thermal-entry-length solutions for the entire family of rectangular tubes have been obtained by numerical integration[14] for uniform surface temperature. An abstract of these results is given in Table 8-9. Here b/a is the ratio of the long

Table 8-7 Infinite-series-solution functions for thermal-entry length in the parallel-plane system; both surfaces at constant temperature

n	λ_n^2	G_n
0	15.09	1.717
1	171.3	1.139
2	498	0.952

For higher n, $\lambda_n = 16\sqrt{\frac{1}{3}}n + \frac{20}{3}\sqrt{\frac{1}{3}}$; $G_n = 2.68\,\lambda_n^{-1/3}$.

Table 8-8 Infinite-series-solution functions for thermal-entry length in the square tube; constant surface temperature

n	λ_n^2	G_n
0	5.96	0.598
1	35.64	0.462
2	78.9	0.138

Table 8-9 Nusselt numbers for thermal-entry length in the rectangular-tube family; constant surface temperature

	Nu_x					Nu_m				
	b/a					b/a				
x^+	1	2	4	6	∞	1	2	4	6	∞
0	∞	∞	∞	∞	∞	∞	∞	∞	∞	∞
0.01	4.55	5.72	6.57	7.02	8.52	8.63	8.58	9.47	10.01	11.63
0.02	4.12	4.72	5.55	6.07	7.75	6.48	6.84	7.71	8.17	9.83
0.05	3.46	3.85	4.87	5.48	7.55	4.83	5.24	6.16	6.70	8.48
0.10	3.10	3.54	4.65	5.34	7.55	4.04	4.46	5.44	6.04	8.02
0.20	2.99	3.43	4.53	5.24	7.55	3.53	3.95	5.00	5.66	7.78
∞	2.98	3.39	4.51	5.22	7.55	2.98	3.39	4.51	5.22	7.55

Table 8-10 Nusselt numbers for thermal-entry length in the rectangular-tube family; constant-heat-rate axially, constant surface temperature peripherally

	Nu_x				
	b/a				
x^+	1	2	0.333	4	∞
0	∞	∞	∞	∞	∞
0.01	7.10	7.46	8.02	8.44	
0.02	5.69	6.05	6.57	7.00	8.80
0.05	4.45	4.84	5.39	5.87	
0.10	3.91	4.38	5.00	5.62	8.25
0.20	3.71	4.22	4.85	5.45	
∞	3.60	4.11	4.77	5.35	8.235

side of the rectangle to the short side, as in Table 8-2. (The results given for the square, $b/a = 1.0$, have been calculated from the eigenvalues and constants given in Table 8-8, while those for $b/a = \infty$ have been calculated from the eigenvalues and constants given in Table 8-7.) The accuracy of the numerical calculations is difficult to determine, but some inconsistencies are noted in Table 8-9.

The thermal-entry-length Nusselt numbers for the rectangular tube family for constant-heat-rate have been computed numerically[14] and are presented in Table 8-10.

The Concentric Circular-Tube Annulus

The concentric circular-tube annulus presents the possibility of a large variety of combinations of surface temperature and heat flux. This problem in all its

Table 8-11 Nusselt numbers and influence coefficients for thermal-entry length in the circular-tube-annulus family; constant heat rate

$r^* = r_i/r_o$	x^+	Nu_{ii}	Nu_{oo}	θ_i^*	θ_o^*
0.05	0.002	33.2	13.4	0.1265	0.00255
	0.01	24.2	7.99	0.460	0.00760
	0.02	21.5	6.58	0.817	0.0125
	0.10	18.1	4.92	2.13	0.0278
	0.20	17.8	4.80	2.17	0.0293
	∞	17.8	4.79	2.18	0.0294
0.10	0.002	25.1	13.5	0.0914	0.00491
	0.01	17.1	8.08	0.311	0.0147
	0.02	14.9	6.65	0.540	0.241
	0.10	12.1	4.96	1.296	0.0531
	0.20	11.9	4.84	1.38	0.0560
	∞	11.9	4.83	1.38	0.0562
0.25	0.002	18.9	13.8	0.0605	0.01104
	0.01	12.1	8.28	0.194	0.0328
	0.02	10.2	6.80	0.325	0.0540
	0.10	7.94	5.04	0.746	0.118
	0.20	7.76	4.91	0.789	0.125
	∞	7.75	4.90	0.793	0.125
0.50	0.002	16.4	14.2	0.0437	0.0189
	0.01	10.1	8.55	0.1347	0.0570
	0.02	8.43	7.03	0.224	0.0934
	0.10	6.35	5.19	0.498	0.204
	0.20	6.19	5.05	0.526	0.215
	∞	6.18	5.04	0.528	0.216
1.00 (parallel planes)	0.0005	23.5	23.5	0.01175	0.01175
	0.005	11.2	11.2	0.0560	0.0560
	0.02	7.49	7.49	0.1491	0.1491
	0.10	5.55	5.55	0.327	0.327
	0.25	5.39	5.39	0.346	0.346
	∞	5.385	5.385	0.346	0.346

possible variations has been solved exactly.[4] The most interesting as well as the most common problems that arise in annulus heat transfer are generally those where the heat fluxes on the two surfaces are specified. To save space, the eigenvalues and functions are omitted and only the Nusselt numbers and influence coefficients are presented as functions x^+ (see Table 8-11).

For these solutions x^+ is defined[†] as

$$x^+ = \frac{2(x/D_h)}{\mathrm{Re}\,\mathrm{Pr}}$$

and

$$D_h = 2(r_o - r_i)$$

[†] x^+ as defined here is twice the $\bar{x}$ employed in Ref. 4.

Where the heat flux on each surface is constant along the length of the tube (invariant with x^+), these results are directly applicable to Eqs. (8-28) and (8-29). The use of these results for the case where the heat flux varies with length, as in a nuclear reactor, for example, is discussed in the next section.

THE EFFECT OF AXIAL VARIATION OF THE SURFACE TEMPERATURE WITH HYDRODYNAMICALLY FULLY DEVELOPED FLOW

All the convection solutions considered so far have been based on either a constant surface temperature or a constant heat flux (axially). It was noted in connection with the fully developed temperature profile solutions that the conductance for constant heat flux is considerably higher than the conductance for a constant surface temperature. Under fully developed temperature profile conditions with a constant heat flux, the surface temperature varies linearly along the length of the tube (as does the mean fluid temperature). It thus appears that the convection conductance is, at least to some degree, dependent on how the surface temperature varies along the tube. Engineers should understand fully under what conditions the conductance varies markedly with tube length and under what conditions it can be treated as at least approximately a constant, since the simpler methods of heat-exchanger analysis are based on a conductance constant with length, or at least a mean overall conductance with respect to length. It is the purpose of this section to investigate this effect.

Because of the linear nature of the energy equation (8-4), a sum of solutions is again a solution. It is thus possible to construct a solution for any kind of arbitrary surface temperature variation with length by merely breaking up the surface temperature into a number of constant-temperature steps and summing, or superposing, the thermal-entry-length solutions at constant surface temperature for each step. This superposition technique can be employed for turbulent flow as well as laminar flow, and for flow over external surfaces as well as flow inside tubes. All that is needed as a starting point is a "step-function" solution, that is, a solution for the case where the fluid and surface are initially at the same temperature and then, at some point $x = 0$, the surface temperature steps to some different temperature and remains constant thereafter. Equation (8-36) is such a solution for a circular tube: it is based on a fully developed velocity profile, and $x = 0$ is taken as the point where heat transfer starts, not at the entrance to the tube.

The method of superposition can best be understood by reference to the diagram in Fig. 8-12. Let the fluid enter the tube at a uniform temperature T_e, and let the velocity profile be fully developed at the point $x^+ = 0$. Let the surface temperature vary in any arbitrary manner, starting at $x^+ = 0$, and let it be represented by a series of infinitesimal steps, or finite steps, or both. The fluid temperature at x^+ and any r^+ can then be determined by summing the contribution of each of the steps, either infinitesimal or finite. For the summation to be considered, x^+ is the point at which it is desired to determine the fluid temperature,

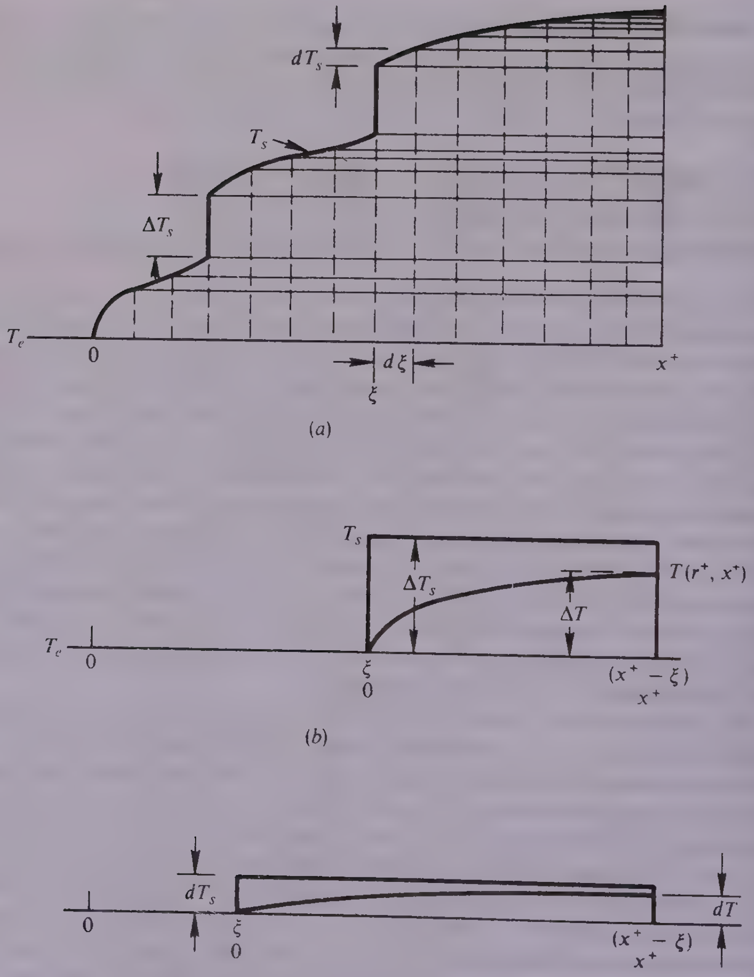

Figure 8-12

and thus x^+ is treated as a constant. A dummy length variable ξ is used to designate the location of each step; ξ thus varies from 0 to x^+.

Consider now the solution for the temperature of the fluid at x^+ resulting from a single, finite step in surface temperature at $x^+ = 0$. This is Eq. (8-36), where

$$\theta(x^+, r^+) = \frac{T_s - T}{T_s - T_e}$$

Now if the surface temperature step occurs at ξ, as in Fig. 8-12*b*, the same solution applies, but the temperature at x^+ becomes

$$\theta(x^+ - \xi, r^+) = \frac{T_s - T}{T_s - T_e}$$

Suppose we consider next the temperature at x^+ resulting from an infinitesimal step in surface temperature at ξ (Fig. 8-12*c*). The same solution θ applies, and the infinitesimal increase in fluid temperature at x^+ can be calculated as follows:

$$\frac{dT_s - dT}{dT_s} = \theta(x^+ - \xi, r^+)$$

from which

$$dT = [1 - \theta(x^+ - \xi, r^+)]\,dT_s$$

Similarly, the finite temperature rise at x^+ resulting from a finite step in surface temperature ΔT_s is

$$\Delta T = [1 - \theta(x^+ - \xi, r^+)]\,\Delta T_s$$

The complete solution for the fluid temperature at x^+ is simply a summation of the contributions of all the infinitesimal and finite surface-temperature steps from $\xi = 0$ to $\xi = x^+$. The linearity and homogeneity of the energy equation (8-4) ensure that such a sum of solutions still satisfies the differential equation. Examination of the result demonstrates that the boundary conditions are truly satisfied; that is, the fluid temperature is a uniform T_e at $x^+ = 0$, and at $r^+ = 1$, and follows the specified surface temperature T_s.

This summation can be represented by an ordinary Riemann integral wherever T_s is continuous, plus a summation of the contribution of the discontinuities, if any. (The combination of the Riemann integral and the summation may be represented by what is known as a Stieltjes integral.) Thus the fluid temperature at any x^+ and r^+ is

$$T - T_e = \int_{\xi=0}^{\xi=x^+} [1 - \theta(x^+ - \xi, r^+)]\,dT_s + \sum_{i=1}^{k} [1 - \theta(x^+ - \xi_i, r^+)]\,\Delta T_{s,i}$$

where $\Delta T_{s,i}$ is the temperature difference across the discontinuity at ξ_i. For example, with two steps, $\Delta T_{s,1} = T_1 - T_e$ and $\Delta T_{s,2} = T_2 - T_1$.

The integral may be evaluated by substituting $(dT_s/d\xi)\,d\xi$ for dT_s. The derivative is presumably a known function of ξ, and θ is a known step-function solution such as Eq. (8-36). Then[†]

$$T - T_e = \int_0^{x^+} [1 - \theta(x^+ - \xi, r^+)]\frac{dT_s}{d\xi}\,d\xi + \sum_{i=1}^{k} [1 - \theta(x^+ - \xi_i, r^+)]\,\Delta T_{s,i} \tag{8-43}$$

[†] This problem can also be approached by direct application of Duhamel's theorem, developed for transient boundary conditions for solid conduction problems, an analogous situation: see Ref. 15.

The final step is the evaluation of the local surface heat-transfer rate at x^+. A heat-transfer conductance and a Nusselt number can then be evaluated, or not, as desired. Often the heat-transfer rate alone is what is really desired. From Fourier's law,

$$\dot{q}''_s(x^+) = k\left(\frac{\partial T}{\partial r}\right)_{r=r_s} = \frac{k}{r_s}\left(\frac{\partial T}{\partial r^+}\right)_{r^+=1}$$

Differentiating Eq. (8-43) with respect to r^+ at $r^+ = 1$ and substituting gives

$$\dot{q}''_s(x^+) = -\frac{k}{r_s}\left[\int_0^{x^+} \theta_{r^+}(x^+ - \xi, 1)\frac{dT_s}{d\xi}\,d\xi + \sum_{i=1}^{k} \theta_{r^+}(x^+ - \xi_i, 1)\,\Delta T_{s,i}\right] \tag{8-44}$$

The derivative θ_{r^+} may be obtained by differentiation of Eq. (8-36) with respect to r^+:

$$\theta_{r^+}(x^+, 1) = \sum_{n=0}^{\infty} C_n R'_n(1)\exp\left(-\lambda_n^2 x^+\right)$$

$$= -2\sum_{n=0}^{\infty} G_n \exp\left(-\lambda_n^2 x^+\right)$$

Then

$$\theta_{r^+}(x^+ - \xi, 1) = -2\sum_{n=0}^{\infty} G_n \exp\left[-\lambda_n^2(x^+ - \xi)\right] \tag{8-45}$$

For any given application the integral and summation of Eq. (8-44) must be evaluated. This can always be done numerically, but for certain elementary surface-temperature distributions an analytic expression for the heat flux can be readily obtained. As an example of an application of the method, a solution is developed for the case of a step in surface temperature at $x^+ = 0$ followed by a linear variation in surface temperature either increasing or decreasing. Thus the surface temperature is as shown in Fig. 8-13.

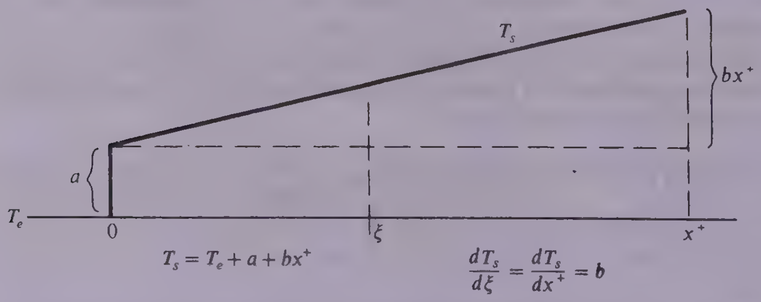

Figure 8-13 Example of a step–ramp surface temperature.

Substituting Eq. (8-45) into Eq. (8-44), with b for $dT_s/d\xi$, and including the one step at $x^+ = 0$ with $\Delta T_s = a$, we obtain

$$\dot{q}_s''(x^+) = -\frac{k}{r_s}\left\{\int_0^{x^+}\left[-2\sum_{n=0}^{\infty} G_n \exp\left[-\lambda_n^2(x^+ - \xi)\right]\right] b\, d\xi \right.$$
$$\left. - 2a\sum_{n=0}^{\infty} G_n \exp\left(-\lambda_n^2 x^+\right)\right\}$$

By performing the integration, taking limits, and noting that $\Sigma_{n=0}^{\infty}(G_n/\lambda_n^2) = \frac{1}{8}$ [see Eq. (8-38)], we reduce the result to

$$\dot{q}_s''(x^+) = \frac{2k}{r_s}\left[\frac{b}{8} - b\sum_{n=0}^{\infty}\frac{G_n}{\lambda_n^2}\exp\left(-\lambda_n^2 x^+\right) + a\sum_{n=0}^{\infty} G_n \exp\left(-\lambda_n^2 x^+\right)\right] \qquad \text{(8-46)}$$

A local Nusselt number may now be evaluated by first integrating Eq. (8-46) from 0 to x^+, to determine the total heat transfer to this point, and then applying an energy balance to evaluate the mixed mean fluid temperature at x^+:

$$\dot{q} = \frac{4\pi r_s^3 V\rho c}{k}\int_0^{x^+}\dot{q}_s''\, dx^+ = \pi r_s^2 V\rho c(T_m - T_e)$$

When we combine these equations and evaluate the integral, the mixed mean temperature becomes

$$T_m - T_e = bx^+ + a - 8b\sum_{n=0}^{\infty}\frac{G_n}{\lambda_n^4} + 8b\sum_{n=0}^{\infty}\frac{G_n}{\lambda_n^4}\exp\left(-\lambda_n^2 x^+\right)$$
$$- 8a\sum_{n=0}^{\infty}\frac{G_n}{\lambda_n^2}\exp\left(-\lambda_n^2 x^+\right) \qquad \text{(8-47)}$$

Next a local conductance h_x can be defined and a local Nusselt number evaluated:

$$q_s''(x^+) = h_x(T_s - T_m)$$

and

$$\mathrm{Nu}_x = \frac{b - 8b\sum_{n=0}^{\infty}\frac{G_n}{\lambda_n^2}\exp\left(-\lambda_n^2 x^+\right) + 8a\sum_{n=0}^{\infty} G_n\exp\left(-\lambda_n^2 x^+\right)}{16b\sum_{n=0}^{\infty}\frac{G_n}{\lambda_n^4} - 16b\sum_{n=0}^{\infty}\frac{G_n}{\lambda_n^4}\exp\left(-\lambda_n^2 x^+\right) + 16a\sum_{n=0}^{\infty}\frac{G_n}{\lambda_n^2}\exp\left(-\lambda_n^2 x^+\right)}$$
$$\text{(8-48)}$$

A number of interesting features of this result are worth noting. First note that for large x^+, all summations containing the exponential go to zero, and then the constant b cancels, which results in

$$\mathrm{Nu}_x = \frac{1}{16\sum_{n=0}^{\infty}\left(G_n/\lambda_n^4\right)} \qquad \text{(8-49)}$$

If Table 8-3 is employed to evaluate the series, the sum is 0.01433 and the result is then

$$\mathrm{Nu}_x = \frac{1}{16 \times 0.01433} = 4.364$$

This is immediately recognized as the previously derived Nusselt number for constant heat rate for a fully developed velocity and temperature profile; it is precisely the situation far downstream, when the surface temperature varies linearly.

Note also that for $b = 0$, Eq. (8-48) reduces again to the constant-surface-temperature case.

Equation (8-48) is useful to demonstrate the rather strange things that can happen to the heat-transfer coefficient, and thus the Nusselt number, under variable-surface-temperature conditions. Consider the following unheated starting length problem where the flow is hydrodynamically fully developed and the fluid temperature is equal to the entrance temperature T_e, which is also the surface temperature T_s. At a location arbitrarily assigned $x^+ = 0$, the surface temperature is elevated to some arbitrary value $T_{s,e}$ and then allowed to linearly decrease back to a value equal to the fluid entering temperature T_e over the distance $0 \leq x^+ \leq 0.2$. Thus

$$T_s = T_e + (1 - 5x^+)(T_{s,e} - T_e)$$

Equations (8-46)–(8-48) are then directly applicable if b is set equal to $-5a$. Surface temperature, mixed mean fluid temperature, heat flux, and local Nusselt number are then readily evaluated as functions of x^+. The results are illustrated in Fig. 8-14. Quite obviously the convection conductance (in the Nusselt number) loses its useful significance when it behaves in such a manner as this.

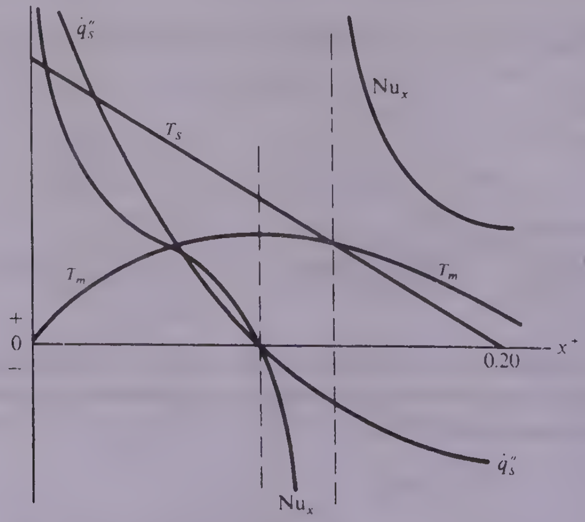

Figure 8-14 The effects of a positive value of a and a negative value of b in Fig. 8-12.

THE EFFECT OF AXIAL VARIATION OF HEAT FLUX

Just as the constant-surface-temperature solution was used as the basic building block for any arbitrary axial variation in surface temperature, so also can the constant-heat-flux solutions be used to build up solutions for any arbitrary axial variation in surface heat flux. We do not develop this in detail but indicate only the results and the calculating procedures (see, for example, Ref. 10).

Let $\dot{q}_s''(x^+) = \dot{q}_s''(\xi)$ be any arbitrary axial heat-flux function that may be specified. Then the surface temperature can be calculated from

$$T_s(x^+) - T_e = \frac{r_s}{k}\int_0^{x^+} g(x^+ - \xi)\dot{q}_s''(\xi)\,d\xi \tag{8-50}$$

where

$$g(x^+) = 4 + \sum_m \frac{\exp\left(-\gamma_m^2 x^+\right)}{\gamma_m^2 A_m} \tag{8-51}$$

The eigenvalues and constants for the circular tube in laminar flow are given in Table 8-5.

As before, we can easily evaluate the mixed mean fluid temperature by considering the total heat transferred up to x^+:

$$T_m(x^+) - T_e = \frac{4r_s}{k}\int_0^{x^+} \dot{q}_s''(\xi)\,d\xi \tag{8-52}$$

and then, if desired, a conductance and Nusselt number can be readily defined and evaluated.

An interesting and important example of an application where the heat flux varies in a specified manner along the tube is a nuclear reactor, in which the heat flux can vary sinusoidally along the cooling tubes:

$$\frac{\dot{q}_s''}{\dot{q}_{s,\max}''} = \sin\frac{\pi x}{L} \tag{8-53}$$

where L is the total tube length. By substituting (8-53) and (8-52), we find the mean fluid temperature becomes

$$T_m - T_e = \frac{4\dot{q}_{s,\max}'' r_s}{k\beta}(1 - \cos\beta x^+) \tag{8-54}$$

where $\beta = r_s \operatorname{Re}\operatorname{Pr}\pi/L$. Substituting into Eq. (8-50) yields the surface temperature:

$$T_s - T_e = \frac{\dot{q}_{s,\max}'' r_s}{k}\left[\frac{4}{\beta}(1 - \cos\beta x^+) + \sin\beta x^+ \sum_m \frac{1}{A_m\left(\gamma_m^4 + \beta^2\right)} - \beta\cos\beta x^+ \sum_m \frac{1}{\gamma_m^2 A_m\left(\gamma_m^4 + \beta^2\right)} + \beta\sum_m \frac{\exp\left(-\gamma_m^2 x^+\right)}{\gamma_m^2 A_m\left(\gamma_m^4 + \beta^2\right)}\right] \tag{8-55}$$

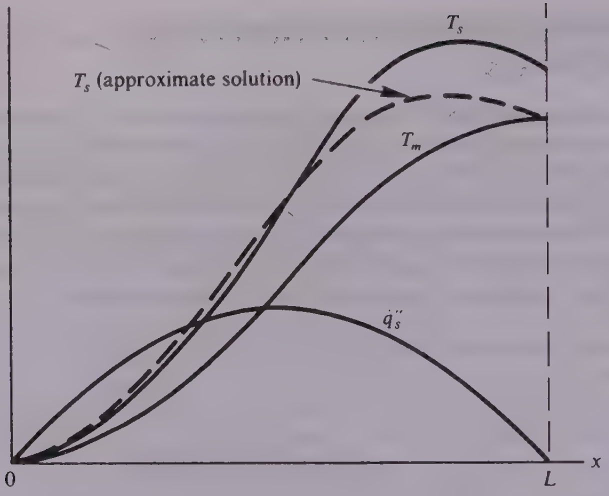

Figure 8-15 The effects of heat flux varying sinusoidally with tube length.

Figure 8-15 shows a typical plot of these results. Also shown by the dashed line is the surface temperature that would be predicted by employing the given heat flux and fluid temperature but using a constant conductance based on the constant-heat-flux solutions. Note that the "exact" solution yields a higher peak surface temperature and that the peak occurs at a different place. How much these differences amount to depends, of course, on all the various system parameters. Although it is certainly simple, in applications of this type, to make use of a constant conductance, it is important to know the kind of error that is introduced by this simplification.

An analysis of these examples of surface temperature and heat flux varying in the axial direction yields the following conclusions:

1. An increasing $T_s - T_m$ and/or $\dot{q}_s''$ in the flow direction tends to yield a high heat-transfer coefficient h.
2. A decreasing $T_s - T_m$ and/or $\dot{q}_s''$ in the flow direction tends to yield a low heat-transfer coefficient h.

These conclusions apply only for continuous tubes, but the effects can be fairly important for laminar flow; the same conclusions apply for turbulent flow, but the effects are much less pronounced except for very low-Prandtl-number fluids for reasons that will be apparent later.

The constant-heat-rate annulus solutions given in Table 8-11 can also be used as a basis for calculating variable-heat-flux problems. The following equations for the inner and outer surface temperatures result directly from superposition:

$$T_i(x^+) - T_m = \frac{D_h}{k}\left[\int_0^{x^+} \frac{1}{\text{Nu}_{ii}(x^+ - \xi)}\,d\dot{q}_i''(\xi) - \int_0^{x^+} \frac{\theta_i^*(x^+ - \xi)}{\text{Nu}_{ii}(x^+ - \xi)}\,d\dot{q}_o''(\xi)\right] \tag{8-56}$$

$$T_o(x^+) - T_m = \frac{D_h}{k}\left[\int_0^{x^+} \frac{1}{\text{Nu}_{oo}(x^+ - \xi)}\,d\dot{q}_o''(\xi) - \int_0^{x^+} \frac{\theta_o^*(x^+ - \xi)}{\text{Nu}_{oo}(x^+ - \xi)}\,d\dot{q}_i''(\xi)\right] \tag{8-57}$$

The fluid mixed mean temperature T_m is determined by integrating the prescribed heat flux from $\xi = 0$ to $\xi = x^+$, as in Eq. (8-52).

These integrals are Stieltjes integrals, and for computational purposes can each be split into a Riemann integral plus a summation, as in Eq. (8-43). For example,

$$\int_0^{x^+} \frac{1}{\text{Nu}_{ii}(x^+ - \xi)}\,d\dot{q}_i''(\xi)$$

$$= \int_0^{x^+} \frac{1}{\text{Nu}_{ii}(x^+ - \xi)}\,\frac{d\dot{q}_i''}{d\xi}\,d\xi + \sum_{j=1}^{k} \frac{1}{\text{Nu}_{ii}(x^+ - \xi_j)}(\Delta\dot{q}_i'')_j$$

where $(\Delta\dot{q}_i'')_j$ is the heat-flux difference across the discontinuity at ξ_j. The integral is then used for continuously varying heat flux, and all discontinuities in heat flux are contained in the summation. The problem collapses back to the constant-heat-flux problem if $d\dot{q}_i''/d\xi = 0$, $\xi_j = 0$, and $k = 1$.

Note that the first term of Eq. (8-57) can also be used for the *circular-tube* variable-heat-flux problem, employing Table 8-6 with x^+ replaced by $x^+ - \xi_j$, and this is then an alternative to Eq. (8-50).

COMBINED HYDRODYNAMIC AND THERMAL ENTRY LENGTH

All the laminar-flow solutions considered so far have been based on the idealization that the velocity profile is fully developed, which, according to Eq. (7-20) for a circular tube, occurs when x/D is greater than approximately $\frac{1}{20}$Re. On the other hand, it was shown in connection with Eq. (8-41) that for a Prandtl number greater than about 5, the velocity profile develops so much faster than the temperature profile that even if both temperature and velocity are uniform at the tube entrance, the fully developed velocity idealization introduces little error. At low Prandtl numbers, however, the temperature profile develops more rapidly than the velocity profile, and the fully developed velocity idealization is no longer valid for a thermal-entry-length solution. If x/D is greater than $\frac{1}{20}$Re, a fully developed velocity profile exists regardless of Prandtl number; but for applications where a *mean* conductance with respect to length is required, as in heat-exchanger analysis, the effects of the undeveloped velocity profile near the entrance can be substantial even for tubes much longer than $x/D = \frac{1}{20}\mathrm{Re}$.

The development of the velocity profile in a circular tube was considered in Chap. 7, where the solution by Langhaar was discussed. The applicable energy differential equation for calculation of the temperature field under conditions of a developing velocity field, axisymmetric heating, and negligible axial conduction must be Eq. (8-1), with the appropriate terms omitted:

$$\rho c u \frac{\partial T}{\partial x} + \rho c v_r \frac{\partial T}{\partial r} = \frac{k}{r}\frac{\partial}{\partial r}\left(r\frac{\partial T}{\partial r}\right) \tag{8-58}$$

The Prandtl number becomes a parameter in the solution for the combined hydrodynamic and thermal-entry-length problem because, while the velocity development is independent of Prandtl number, the temperature profile is Prandtl-number-dependent. Recall that when the velocity profile was assumed to be fully developed, the Prandtl number did not explicitly appear in the solution.

Several workers have solved Eq. (8-58) numerically, either using Langhaar's entry-region velocity profiles or generating the velocity solution numerically; and various degrees of approximation have been employed, resulting in considerable discrepancy among different solutions. Some results for a *constant surface temperature* for three different values of Prandtl number are given in Table 8-12. These come from Ref. 5 and are based on the numerical solutions of Hornbeck.[16,17] It is instructive to compare the results for Pr = 5 with the fully developed velocity-profile solution of Table 8-4. It is apparent that for Pr > 5 the eigenfunction solution for the thermal-entry length is a good approximation even if the velocity profile is developing simultaneously. For lower Prandtl numbers the Nusselt number for the combined entry length is always higher than for the thermal-entry length alone.

A rather different procedure was employed by Heaton, Reynolds, and Kays,[18] who linearized Eq. (8-58) by an approximation first introduced by

Table 8-12 Nusselt numbers for combined thermal- and hydrodynamic-entry length in the circular tube; constant surface temperature

	Nu_x			Nu_m		
x^+	Pr = 0.7	Pr = 2	Pr = 5	Pr = 0.7	Pr = 2	Pr = 5
0.001	16.8	14.8	13.5	30.6	25.2	22.1
0.002	12.6	11.4	10.6	22.1	19.1	16.8
0.004	9.6	8.8	8.2	16.7	14.4	12.9
0.006	8.25	7.5	7.1	14.1	12.4	11.0
0.01	6.8	6.2	5.9	11.3	10.2	9.2
0.02	5.3	5.0	4.7	8.7	7.8	7.1
0.05	4.2	4.1	3.9	6.1	5.6	5.1
∞	3.66	3.66	3.66	3.66	3.66	3.66

Table 8-13 Nusselt numbers and influence coefficients for combined thermal- and hydrodynamic-entry length in the circular-tube annulus family; constant heat rate

	Circular tube		Parallel planes		Circular-tube annulus $r^* = 0.50$[†]			
Pr	x^+	**Nu**	Nu_{11}	θ_1^*	Nu_{ii}	Nu_{oo}	θ_i^*	θ_i^*
0.01	0.002	24.2	24.2	0.048	—	24.2	—	0.0322
	0.010	12.0	11.7	0.117	—	11.8	—	0.0786
	0.020	9.10	8.80	0.176	9.43	8.90	0.252	0.118
	0.10	6.08	5.77	0.378	6.40	5.88	0.525	0.231
	0.20	5.73	5.53	0.376	6.22	5.60	0.532	0.238
	∞	4.36	5.39	0.346	6.18	5.04	0.528	0.216
0.70	0.002	17.8	18.5	0.037	19.22	18.30	0.0513	0.0243
	0.010	9.12	9.62	0.096	10.47	9.45	0.139	0.0630
	0.020	7.14	7.68	0.154	8.52	7.50	0.228	0.0998
	0.10	4.72	5.55	0.327	6.35	5.27	0.498	0.207
	0.20	4.41	5.40	0.345	6.19	5.06	0.527	0.215
	∞	4.36	5.39	0.346	6.18	5.04	0.528	0.216
10.0	0.002	14.3	15.6	0.0311	16.86	15.14	0.045	0.0201
	0.010	7.87	9.20	0.092	10.20	8.75	0.136	0.0583
	0.020	6.32	7.49	0.149	8.43	7.09	0.224	0.0943
	0.10	4.51	5.55	0.327	6.35	5.20	0.498	0.204
	0.20	4.38	5.40	0.345	6.19	5.05	0.527	0.215
	∞	4.36	5.39	0.346	6.18	5.04	0.528	0.216

[†] For other radius ratios see Ref. 18.

Langhaar in connection with the velocity problem, and who were then able to obtain a generalized entry-region temperature profile that could be used in the energy integral equation. They obtained solutions for the entire family of circular-tube annuli for *constant heat rate* and various Prandtl numbers. An abstract of the results of Heaton, Reynolds, and Kays is presented in Table 8-13.

The annulus and parallel-planes results are applicable to Eqs. (8-28) and (8-29), and therefore different rates of heating from the two surfaces may be calculated. (See Table 8-13.) These results are *not* applicable to problems where the heat flux varies axially. Such problems can be solved by superposition only if a family of step-function solutions is available for surface heat-flux steps at all points in the hydrodynamic-entry length.

It should finally be added that any of these variable-surface-temperature and variable-heat-flux problems can also be readily solved by direct numerical solution of the appropriate differential equations. This is today a very practicable alternative, even in engineering applications, especially for the simpler geometries such as circular tubes, circular-tube annuli, and flat ducts. It is the preferred procedure when the specified surface temperature and/or heat flux is a complex function. There is no particular advantage to be gained using superposition techniques if numerical calculations must be used to evaluate the functions. Direct numerical procedures also have the virtue that such further complications as variable fluid properties can be readily introduced.

PROBLEMS

8-1. Starting from the appropriate momentum and energy differential equations, evaluate the Nusselt number for both surfaces of a parallel-plane channel in which there is fully developed laminar flow (both velocity and temperature developed) and in which there is heating from both surfaces but the heat flux from one surface is twice the flux from the other surface, and again when the heat flux from one surface is 5 times the flux from the other surface. The heat-transfer rate per unit of duct length is constant. Compare your results with those given in the text (Table 8-1).

TEXSTAN can be used to confirm the results of this problem. Let the Reynolds number be 1000, select a Prandtl number for either air or water, and pick fluid properties that are appropriate to the Prandtl number. You can choose channel geometrical dimensions and a mass flow rate for the channel to provide the required Reynolds number and a channel length of 20–40 hydraulic diameters. Use constant fluid properties and do not consider viscous dissipation. The thermal boundary condition is constant heat flux, and you can choose an arbitrary value for one surface and the required ratio for the other surface, to represent the asymmetrical heating. This is a thermally fully developed problem, so the initial conditions will be a velocity profile that is hydrodynamically fully developed and a temperature profile that is thermally fully developed. Because this problem has asymmetrical thermal boundary conditions, choose the option in TEXSTAN that permits calculation from surface to surface.

8-2. With a low-Prandtl-number fluid, the temperature profile in a tube develops more rapidly than the velocity profile. Thus, as the Prandtl number approaches zero, the temperature profile can approach a fully developed form before the velocity profile has even started to develop (although this is a situation of purely academic interest). Convection solutions based on a uniform velocity over the cross section, as described, are called *slug-flow* solutions. Develop an expression for the slug-flow, fully developed temperature-profile Nusselt number for constant heat rate per unit of tube length for a concentric circular-tube annulus with a radius ratio of 0.60 for the case where the inner tube is heated and the outer tube is insulated. Compare with the results in Table 8-1 and discuss.

8-3. Consider a 0.6-cm (inside-diameter) circular tube that is of sufficient length that the flow is hydrodynamically fully developed. At some point beyond the fully developed location, a 1.2-m length of the tube is wound by an electric resistance heating element to heat the fluid, an organic fuel, from its entrance temperature of 10°C to a final value of 65°C. Let the mass flow rate of the fuel be 1.26×10^{-3} kg/s. The following average properties may be treated as constant:

$$\begin{aligned} \mathrm{Pr} &= 10 \\ \rho &= 753\ \mathrm{kg/m^3} \\ c &= 2.092\ \mathrm{kJ/(kg \cdot K)} \\ k &= 0.137\ \mathrm{W/(m \cdot K)} \\ \mu &= 0.00065\ \mathrm{Pa \cdot s} \end{aligned}$$

Calculate and plot both tube surface temperature and fluid mean temperature as functions of tube length. What is the highest temperature experienced by any of the fluid?

TEXSTAN can be used to confirm the results of this problem. Use constant fluid properties and do not consider viscous dissipation. The thermal boundary condition is constant heat flux; use the value calculated from the problem analysis. This is an unheated starting length problem, so the initial conditions are a velocity profile that is hydrodynamically fully developed and a temperature profile that is flat at a value equal to the entry temperature.

8-4. Consider fully developed, constant-property laminar flow between parallel planes with constant heat rate per unit of length and a fully developed temperature profile. Suppose heat is transferred to the fluid on one side and *out* of the fluid on the other at the *same rate*. What is the Nusselt number on each side of the passage? Sketch the temperature profile. Suppose the fluid is an oil for which the viscosity varies greatly with temperature, but all the other properties are relatively unaffected by temperature. Is the velocity profile affected? Is the temperature profile affected? Is the Nusselt number affected? Explain.

TEXSTAN can be used to confirm the Nusselt number result of this problem. Let the Reynolds number be 1000, select a Prandtl number, and pick fluid properties that are appropriate to the Prandtl number. You can choose geometrical dimensions and a mass flow rate for the channel to provide the required Reynolds number and a channel length of 20–40 hydraulic diameters. Use constant fluid properties and do not consider viscous dissipation for this part of the problem. The thermal boundary condition is constant heat flux, and you can choose an arbitrary value for one surface and the value for the other surface will be the same magnitude with opposite sign. This is a thermally fully developed problem, so the initial conditions will be a velocity profile that is hydrodynamically fully developed and a temperature profile that is thermally fully developed. Because this problem has asymmetrical thermal boundary conditions, choose the option in TEXSTAN that permits calculation from surface to surface.

8-5. Consider a concentric circular-tube annulus, with outer diameter 2.5 cm and inner diameter 1.25 cm, in which air is flowing under fully developed, constant-heat-rate conditions. Heat is supplied to the inner tube, and the outer tube is externally insulated. The radiation emissivity of both tube surfaces is 0.8. The mixed mean temperature of the air at a particular point in question is 260°C. The inner-tube surface temperature at this point is 300°C. What is *total* heat flux from the inner-tube surface at this point? What is the outer-tube surface temperature at this point? What percentage of the heat supplied to the inner tube is transferred directly to the air, and what percentage indirectly from the outer surface? Assume that the Reynolds number is sufficiently low that the flow is laminar. Assume that the air is transparent to the thermal radiation. Make use of any of the material in the text as needed.

8-6. The heat flux along a flat cooling tube in a typical nuclear power reactor may often be approximated by

$$\dot{q}_s'' = a + b \sin \frac{\pi x}{L}$$

where L is the length of the flat tube and x is the distance along the flat tube.

A particular air-cooled reactor is to be constructed of a stack of fuel plates with a 3-mm air space between them. The length of the flow passage will be 1.22 m, and the heat flux at the plate surfaces will vary according to the above equation with $a = 900\ \text{W/m}^2$ and $b = 2500\ \text{W/m}^2$. The air mass velocity is to be 7.5 kg/(s · m²). The air enters the reactor at 700 kPa and 100°C. The properties of air at 250°C may be used in the analysis and treated as constant.

Prepare a scale plot of heat flux, air mean temperature, and plate surface temperature as a function of distance along the flow passage. Although the heat flux is not constant along the passage, the passage length-to-gap ratio is sufficiently large that the constant-heat-rate heat-transfer solution for the conductance h is not a bad approximation. Therefore assume h is a constant. We are most interested here in the peak surface temperature; if this occurs in a region where the heat flux is varying only slowly, the approximation is still better. This is a point for discussion.

TEXSTAN can be used to help understand the results of this problem. Let the Reynolds number be 1000, and pick fluid properties that are appropriate to the air Prandtl number at 250°C. Use constant fluid properties and do not consider viscous dissipation. The geometry for this problem is modeled as a combined entry problem in a parallel planes channel, and for initial conditions let the velocity profile be flat at a value equal to the mean velocity and the temperature profile be flat at some value T_e. Because this problem has symmetrical thermal boundary conditions, choose the option in TEXSTAN that permits the centerline of the parallel planes channel to be a symmetry line. For the surface heat flux profile, break up the length of the channel into 10 to 20 segments and evaluate the heat flux function at these x locations. These values then become the variable heat flux boundary. Note that the smaller the segments the more closely the sine function is modeled.

8-7. A lubricating oil flows through a long 0.6-cm (inner-diameter) tube at a mean velocity of 6 m/s. If the tube is effectively insulated, calculate and plot the temperature distribution, resulting from *frictional* heating, in terms of the pertinent parameters. Let the fluid properties be those of a typical engine oil at 100°C. Start with Eq. (4-28).

8-8. Consider a journal bearing using the oil of Prob. 8-7. Let the journal diameter be 7.6 cm, the clearance be 0.025 cm, and the rpm be 3600. Neglecting end effects, and assuming no flow of oil into or out of the system, calculate the temperature distribution in the oil film on the assumption that there is no heat transfer into the journal (the inner surface) but that the bearing (the outer surface) is maintained at 80°C. Calculate the rate of heat transfer per square meter of bearing surface. Assume no eccentricity, that is, no load on the bearing. How much power is needed to rotate the journal if the bearing is 10 cm long?

8-9. Consider uniform-temperature laminar flow in a circular tube with a fully developed velocity profile. At some point $x^+ = 0$ the surface temperature is raised above the fluid temperature by an amount a. It remains constant at this value until a point $x^+ = x_1^+$ is reached, where the surface temperature is again raised an amount b, remaining constant thereafter. Develop a general expression for the surface heat flux, and for the mean fluid temperature θ_m, in the part of the tube following the second step in surface temperature. Use variable-surface-temperature theory.

8-10. Consider laminar flow in a circular tube with a fully developed velocity profile. Let heat be added at a constant rate along the tube from $x^+ = 0$ to $x^+ = 0.10$. Thereafter let the tube surface be adiabatic. Calculate and plot the tube surface temperature as a function of x^+.

TEXSTAN can be used to confirm this analysis. Let the Reynolds number be 1000, choose air or water as the Prandtl number, and pick fluid properties that are appropriate to the chosen Prandtl number. Use constant fluid properties and do not consider viscous dissipation. You can choose how to set up the TEXSTAN problem in terms of values for the thermal boundary and initial conditions, and for geometrical dimensions and mass flow rate for the pipe to provide the required Reynolds number and a pipe length equivalent to about $x^+ = 0.3$ (long enough for the boundary condition effect to decay). The geometry for this problem is modeled as an unheated starting length problem, and for initial conditions let the velocity profile be hydrodynamically fully developed and the temperature profile be flat at some value T_e. The thermal boundary condition will be a constant value of heat flux from start of calculation until the x-location corresponding to $x^+ = 0.10$ and then a value of zero heat flux to the x location corresponding to $x^+ = 0.30$.

8-11. Consider laminar flow in a circular tube with a fully developed velocity profile. Let the tube surface be alternately heated at a constant rate per unit of length and adiabatic, with each change taking place after intervals of x^+ of 0.020. How large must x^+ be for the effects of the original entry length to damp out? How does the Nusselt number vary along the heated segments after the effects of the original entry length have damped out?

TEXSTAN can be used to confirm this analysis. Let the Reynolds number be 1000, choose air or water as the Prandtl number, and pick fluid properties that are appropriate to the chosen Prandtl number. Use constant fluid properties and do not consider viscous dissipation. You can choose how to set up the TEXSTAN problem in terms of values for the thermal boundary and initial conditions, and for geometrical dimensions and mass flow rate for the pipe to provide the required Reynolds number and a pipe length equivalent to about $x^+ = 0.3$ (long enough for the boundary condition effect to decay). The geometry for this problem is modeled as an unheated starting length problem, and for initial conditions let the velocity profile be hydrodynamically fully developed and the temperature profile be flat at some value T_e. The thermal boundary condition will be a constant value of heat flux from start of calculation until the x location corresponding to $x^+ = 0.020$ and then a value of zero heat flux to the x location corresponding to $x^+ = 0.040$, and then periodically repeated out to $x^+ = 0.3$.

8-12. Evaluate and plot both local and mean Nusselt numbers for fully developed laminar flow in a square tube. At what value of x^+ does the local Nusselt number come within two percent of the asymptotic value?

8-13. Consider the problem posed by Eq. (8-53). Let $\beta = 6$ and let the tube be circular. Evaluate and plot the local Nusselt number as a function of x/L. Explain physically the reasons for the behavior noted.

8-14. Consider fully developed laminar flow in a circular tube in which the heat flux varies axially according to the relation

$$\dot{q}_s'' = a + b \sin \frac{\pi x}{L}$$

where L is the total length of the tube, and a and b are constants (this is an approximation for a nuclear reactor cooling tube). Derive a general expression for the mean fluid temperature T_m as a function of x_1 and the tube surface temperature T_s as a function of x, using variable-heat-flux theory [that is, an expression corresponding to Eq. (8-55) for the simple sinusoidal variation of heat flux].

8-15. Consider fully developed laminar flow in a circular-tube annulus with $r^* = 0.50$. Let there be heat transfer from the inner tube only (outer tube insulated), and let the heat flux on the inner tube vary as in Prob. 8-14. Describe in detail a computing procedure for evaluating both the inner- and outer-tube surface temperatures as functions of length along the tube.

8-16. Helium flows through a thin-walled 1.25-cm-diameter circular tube at a mean velocity of 6 m/s under the following conditions at a particular point along the tube:

$$P = 345 \text{ kPa}, \qquad T_m = 200^\circ\text{C}$$

The tube is exposed on one side to an infinite *plane* that emits black-body radiation at 1100°C, while the remainder of the surrounding space is effectively nonradiating. Assuming that (1) the tube wall is sufficiently thin that peripheral conduction in the wall is negligible and (2) the outer surface is a black body and evaluating radiation *from* the tube as if the entire tube were at a uniform temperature of 300°C (re-radiation will be relatively small and an exact solution would require iteration), calculate the net heat flux to the tube and estimate the temperature distribution in the wall around the tube. Assume that the heat-transfer resistance of the wall is negligible in the radial direction and that fluid properties are constant.

8-17. Consider steady flow in a tube with a fully developed velocity profile at the tube entrance. Let the fluid temperature at the tube entrance be uniform at T_e. Then let the tube surface temperature vary axially according to the relation

$$T_s - T_e = \frac{a}{b}[\exp(bx^+) - 1]$$

where a and b are arbitrary constants. Derive an expression for the local Nusselt number as a function of x^+. Show that all members of this family of solutions lead to Nusselt numbers that are independent of x^+ at sufficiently large values of x^+. What are the implications of this result? Discuss how the constant b affects the asymptotic Nusselt number.

8-18. Consider fully developed laminar flow with constant properties in a circular tube. Let there be heat transfer to or from the fluid at a constant rate per unit of tube length. Determine the Nusselt number if the effect of frictional heating (viscous mechanical energy dissipation) is included in the analysis. How does frictional heating affect the Nusselt number? What are the significant new parameters? Consider some numerical examples and discuss the results.

8-19. Consider fully developed laminar flow with constant properties in a circular tube. Let there be heat transfer to or from the fluid at a constant rate per unit of tube length. Additionally, let there be heat generation within the fluid (perhaps by nuclear reaction) at a rate S, W/m^3, that is everywhere the same. Determine an expression for the Nusselt number as a function of the pertinent parameters. (What are they?) Evaluate the convection conductance in the usual manner, on the basis of heat flux through the surface, surface temperature, and fluid mixed mean temperature.

8-20. Consider fully developed laminar flow with constant properties in a circular tube. Let the surface be insulated, but let there be heat generation within the fluid at a rate S, W/m^3, that is everywhere the same. From an examination of the applicable energy differential equation alone, deduce the approximate shape of the temperature profile within the fluid, and determine whether the highest temperature of the fluid at any axial position occurs at the tube surface or at the tube centerline. Explain the reasons for the result.

TEXSTAN PROBLEMS

8-21. TEXSTAN *analysis of laminar thermal entry flow in a circular pipe with constant surface temperature*: Calculate the flow and construct a plot similar to Fig. 8-10 to show development of the Nusselt number with $x^+ = 2(x/D_h)/\text{Re Pr}$ over the range $x^+ = 0\text{–}0.3$. Let the Prandtl number be 0.7. Compare the results with Table 8-4. Feel free to evaluate the nondimensional temperature profiles at various x^+ locations to demonstrate the concept of how the profiles evolve from a flat profile into thermally fully developed profile, and to investigate any other attribute of the entry region or thermally fully developed region of the flow.

Let the Reynolds number be 1000, and pick fluid properties that are appropriate to the chosen Prandtl number. You can choose how to set up the TEXSTAN problem in terms of values for the thermal boundary and initial conditions, and for geometrical dimensions and mass flow rate for the pipe to provide the required Reynolds number and a pipe length equivalent to $x^+ = 0.3$. Use constant fluid properties and do not consider viscous dissipation. For initial conditions let the velocity profile be hydrodynamically fully developed and the temperature profile be flat at some value T_e.

8-22. TEXSTAN *analysis of the effects of Prandtl number on laminar thermal entry flow in a circular pipe with constant surface temperature*: This is a variation of Prob. 8-21 to show the independence of Pr as the thermally fully developed flow condition is met. For this problem, choose Pr values of 0.01, 1.0, and 10, and compare the results to Table 8-4. Follow the TEXSTAN setup described in Prob. 8-21, but adjust the pipe length such that a thermally fully developed Nusselt number is achieved for the selected Pr.

8-23. TEXSTAN *analysis of laminar thermal entry flow in a circular pipe with constant surface heat flux, heating case*: Calculate the flow and construct a plot to show development of the Nusselt number with $x^+ = 2(x/D_h)/\text{Re Pr}$ over the range $x^+ = 0\text{–}0.3$. Let the Prandtl number be 0.7. Compare the results with Table 8-6. Follow the TEXSTAN setup described in Prob. 8-21.

8-24. TEXSTAN *analysis of laminar thermal entry flow in a parallel planes channel with constant surface temperature for both planes*: Calculate the flow and construct a plot to show development of the Nusselt number with $x^+ = 2(x/D_h)/\text{Re Pr}$ over the range $x^+ = 0\text{–}0.3$. Let the Prandtl number be 0.7. Compare the results with the entries for $b/a = \infty$ in Table 8-9. Feel free to evaluate the nondimensional temperature profiles at various x^+ locations to demonstrate the concept of how the profiles evolve from a flat profile into a thermally fully developed profile, and to investigate any other attribute of the entry region or thermally fully developed region of the flow.

Let the Reynolds number be 1000, and pick fluid properties that are appropriate to the chosen Prandtl number. You can choose how to set up the TEXSTAN problem in terms of values for the thermal boundary and initial conditions, and for geometrical dimensions and mass flow rate for the channel to provide the required Reynolds number and a channel length equivalent to $x^+ = 0.3$. Use constant fluid properties and do not consider viscous dissipation. For initial conditions let the velocity profile be hydrodynamically fully developed and the temperature profile be flat at some value T_e. Because this problem has symmetrical thermal boundary conditions, choose the option in TEXSTAN that permits the centerline of the parallel planes channel to be a symmetry line.

8-25. TEXSTAN *analysis of laminar thermal entry flow in a parallel planes channel with constant surface heat flux, heating case, for both planes*: Calculate the flow and construct a plot to show development of the Nusselt number with $x^+ = 2(x/D_h)/\text{Re Pr}$ over the range $x^+ = 0$–0.3. Let the Prandtl number be 0.7. Compare the results with the entries for $b/a = \infty$ in Table 8-10. Feel free to evaluate the nondimensional temperature profiles at various x^+ locations to demonstrate the concept of how the profiles evolve from a flat profile into thermally fully developed profile, and to investigate any other attribute of the entry region or thermally fully developed region of the flow. Follow the TEXSTAN setup described in Prob. 8-24.

8-26. TEXSTAN *analysis of laminar thermal entry flow in a parallel-plane channel with asymmetrical heat flux in which one plane has a constant surface heat flux, heating case, and the other plane has an adiabatic surface*: Calculate the flow and construct a plot to show development of the Nusselt number with $x^+ = 2(x/D_h)/\text{Re Pr}$ over the range $x^+ = 0$–0.3. Let the Prandtl number be 0.7. Compare the results with the $\text{Nu}_{ii} = \text{Nu}_{oo}$ values for $r^* = 1.00$ in Table 8-11 (note the influence coefficients are not used for this problem). Feel free to evaluate the nondimensional temperature profiles at various x^+ locations to demonstrate the concept of how the profiles evolve from a flat profile into thermally fully developed profile, and to investigate any other attribute of the entry region or thermally fully developed region of the flow.

Let the Reynolds number be 1000, and pick fluid properties that are appropriate to the chosen Prandtl number. You can choose how to set up the TEXSTAN problem in terms of values for the thermal boundary and initial conditions, and for geometrical dimensions and mass flow rate for the channel to provide the required Reynolds number and a channel length equivalent to $x^+ = 0.3$. Use constant fluid properties and do not consider viscous dissipation. For initial conditions let the velocity profile be hydrodynamically fully developed and the temperature profile be flat at some value T_e. Because this problem has asymmetrical thermal boundary conditions, choose the option in TEXSTAN that permits the calculation from surface to surface of the parallel-plane channel.

8-27. TEXSTAN *analysis of laminar combined entry flow in a circular pipe with constant surface temperature*: Calculate the flow and construct a plot similar to Fig. 8-10 to show development of the Nusselt number with $x^+ = 2(x/D_h)/\text{Re Pr}$ over the range $x^+ = 0$–0.3. Let the Prandtl number be 0.7. Compare the results with Table 8-12. Feel free to evaluate the nondimensional temperature profiles at various x^+ locations to demonstrate the concept of how the profiles evolve from a flat profile into thermally fully developed profile, and to investigate any other attribute of the entry region or thermally fully developed region of the flow.

Let the Reynolds number be 1000, and pick fluid properties that are appropriate to the chosen Prandtl number. You can choose how to set up the TEXSTAN problem in terms of values for the thermal boundary and initial conditions, and for geometrical dimensions and mean velocity for the pipe to provide the required Reynolds number and a pipe length equivalent to $x^+ = 0.3$. Use constant fluid properties and do not consider viscous dissipation. For initial conditions let the velocity profile be flat at a value equal to the mean velocity and the temperature profile be flat at some value T_e.

8-28. TEXSTAN *analysis of laminar combined entry flow in a parallel planes channel with asymmetrical heat flux in which one plane has a constant surface heat flux, heating case, and the other plane has an adiabatic surface*: Calculate the flow and construct a plot to show development of the Nusselt number with $x^+ = 2(x/D_h)/\text{Re Pr}$ over the range $x^+ = 0$–0.3. Let the Prandtl number be 0.7. Compare the results with the Nu_{11} values for parallel planes in Table 8-13 (note the influence coefficient is not used for this problem). Feel free to evaluate the nondimensional temperature profiles at various x^+ locations to demonstrate the concept of how the profiles evolve from a flat profile into thermally fully developed profile, and to investigate any other attribute of the entry region or thermally fully developed region of the flow.

Let the Reynolds number be 1000, and pick fluid properties that are appropriate to the chosen Prandtl number. You can choose how to set up the TEXSTAN problem in terms of values for the thermal boundary and initial conditions, and for geometrical dimensions and mass flow rate for the channel to provide the required Reynolds number and a channel length equivalent to $x^+ = 0.3$. Use constant fluid properties and do not consider viscous dissipation. For initial conditions let the velocity profile be flat at a value equal to the mean velocity and the temperature profile be flat at some value T_e. Because this problem has asymmetrical thermal boundary conditions, choose the option in TEXSTAN that permits the calculation from surface to surface.

8-29. TEXSTAN *analysis of laminar combined entry flow in a circular-tube annulus with $r^* = 0.5$* and *asymmetrical surface heat flux in which one surface has a constant heat flux, heating case, and the other surface is adiabatic*: Calculate the flow and construct a plot to show development of the Nusselt number with $x^+ = 2(x/D_h)/\text{Re Pr}$ over the range $x^+ = 0$–0.3. Let the Prandtl number be 0.7. Test two cases: constant heat flux on the inside surface and the outside surface adiabatic, and then the opposite case. Compare the results with the Nu_{ii} and Nu_{oo} entries for $r^* = 0.5$ in Table 8-13 (note the influence coefficients are not used for this problem). Feel free to evaluate the nondimensional temperature profiles at various x^+ locations to demonstrate the concept of how the profiles evolve from a flat profile into thermally fully developed profile, and to investigate any other attribute of the entry region or thermally fully developed region of the flow.

Let the Reynolds number be 1000, and pick fluid properties that are appropriate to the chosen Prandtl number. You can choose how to set up the TEXSTAN problem in terms of values for the thermal boundary and initial conditions, and for geometrical dimensions and mass flow rate for the channel to provide the required Reynolds number, a value of $r^* = 0.5$, and a channel length equivalent to $x^+ = 0.3$. Use constant fluid properties and do not consider viscous dissipation. For initial conditions let the velocity profile be flat at a value equal to the mean velocity and the temperature profile be flat at some value T_e. Because this problem has asymmetrical thermal boundary conditions, choose the option in TEXSTAN that permits the calculation from surface to surface.

8-30. TEXSTAN *analysis of laminar thermal-entry flow in a circular pipe with the effect of axial variation of surface temperature,* $T_s = f(x)$ *from Fig. 8-14 over the distance* $0.0 \leq x^+ \leq 0.2$: Let the Reynolds number be 1000, and pick fluid properties that are appropriate to an air Prandtl number of 0.7. You can choose how to set up the TEXSTAN problem in terms of values for the thermal boundary and initial conditions, and for geometrical dimensions and mass flow rate for the pipe to provide the required Reynolds number and a pipe length equivalent to $x^+ = 0.2$. Use constant fluid properties and do not consider viscous dissipation. For initial conditions let the velocity profile be hydrodynamically fully developed and the temperature profile be flat at some value T_e. Calculate the flow and compare the results with Fig. 8-14. Discuss the behavior of the various variables in terms of the temperature profiles obtained as a part of the computer analysis.

REFERENCES

1. Sparrow, E. M., and S. V. Patankar: *J. Heat Transfer*, vol. 99, pp. 483–485, 1977.
2. Reynolds, W. C.: *Trans. ASME*, ser. C, vol. 82, p. 108, 1960.
3. Reynolds, W. C.: *Int. J. Heat Mass Transfer*, vol. 6, pp. 445–454, 1963.
4. Lundberg, R. E., W. C. Reynolds, and W. M. Kays: NASA TN D-1972, Washington, August 1963.
5. Shah, R. K., and A. L. London: "Laminar Flow Forced Convention in Ducts," *Advances in Heat Transfer*, Academic Press, New York, 1978.
6. Shah, R. K., and A. L. London: *J. Heat Transfer*, vol. 96, pp. 159–165, 1974.
7. Bhatti, M. S.: "Fully Developed Temperature Distribution in a Circular Tube With Uniform Wall Temperature," Unpublished paper, Owens–Corning Fiberglass Corporation, Granville, Ohio, 1985 (cited in Ref. 8).
8. Kakac, S., R. K. Shah, and W. Aung: *Handbook of Single-Phase Convective Heat Transfer*, John Wiley, New York, 1987.
9. Michelsen, M. L., and J. Villadsen, *Int. J. Heat Mass Transfer*, vol. 17, pp. 1391–1402, 1974.
10. Sellars, J. R., M. Tribus, and J. S. Klein: *Trans. ASME*, vol. 78, pp. 441–448, 1956.
11. Seigel, R., E. M. Sparrow, and T. M. Hallman: *Appl. Sci. Res.*, ser. A, vol. 7, pp. 386–392, 1958.
12. Cess, R. D., and E. C. Shaffer: *J. Aero-Space Sci.*, p. 538, 1959.
13. Dennis, S. C. R., A. McD. Mercer, and G. Poots: *Q. Appl. Math.*, vol. 17, pp. 285–297, 1959.

14. Wibulswas, P.: Ph.D. thesis, London University, 1966.
15. Carslaw, H. S., and J. C. Jaeger: *Conduction of Heat in Solids*, 2d ed., Oxford University Press, London, 1959.
16. Hornbeck, R. W.: ASME Paper no. 65-WA HT-36, 1965.
17. Hornbeck, R. W.: NASA SP-297, Washington, 1973.
18. Heaton, H. S., W. C. Reynolds, and W. M. Kays: *Int. J. Heat Mass Transfer*, vol. 7, pp. 763–781, 1964.
19. Weigand, B., M. Kanzamar, and H. Beer: *Int. J. Heat Mass Transfer*, vol. 44, pp. 3941–3952, 2001.

9 CHAPTER

Laminar External Boundary Layers: Momentum Transfer

The development of the laminar momentum boundary layer for a constant-property fluid flowing over an external surface is considered in this chapter. We use the term *external flow*, as opposed to *internal flow*, to characterize flow along a surface on which the boundary-layer thickness is small relative to the distance to any other surface. Thus the viscous flow region is bounded by a solid surface on one side only, and is bounded on the other side by an inviscid potential flow. In an internal flow (flow in a pipe) we are usually concerned with the viscous effects on the entire region between boundary surfaces, although the hydrodynamic entry region of a pipe has the characteristics of an external flow.

First we consider the family of *similarity* solutions to the momentum equation of the boundary layer for a steady laminar flow. We treat the concept of similarity solutions to a partial differential equation in some detail, since this forms the basis for the majority of useful laminar boundary-layer solutions, including the thermal and concentration boundary layers. Nonsimilar boundary layers are then discussed, and *local similarity* and *local nonsimilarity* solutions are described.

Then we develop two approximate laminar boundary-layer solutions, employing the momentum integral equation, including a relatively simple procedure for handling a flow in a pressure gradient.

The momentum boundary-layer theory presented only outlines and highlights this large area of study, and the reader is referred to the more comprehensive treatises on the subject, such as Schlichting[1] or Moore,[2] for further details.

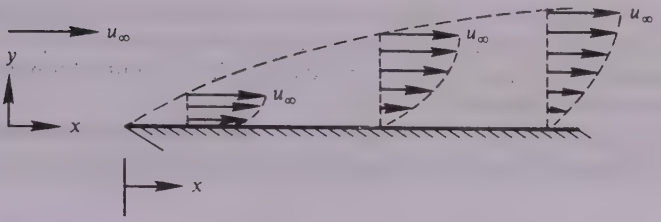

Figure 9-1 Development of a laminar boundary layer on a flat plate with constant free-strain velocity.

SIMILARITY SOLUTIONS: THE LAMINAR INCOMPRESSIBLE BOUNDARY LAYER WITH CONSTANT PROPERTIES AND CONSTANT FREE-STREAM VELOCITY

Consider steady flow without turbulence over a semi-infinite flat plate aligned with the flow (Fig. 9-1). Let the free-stream velocity u_∞ be constant, and let all fluid properties be constant. The physical requirement of zero velocity at the surface must result in the development of a momentum boundary layer, starting at the leading edge of the plate, as shown in Fig. 9-1. The applicable equations of motion must be the momentum equation[†] (4-10), together with the continuity equation (4-7). Since u_∞ is stipulated as constant, dP/dx must be zero according to Eq. (5-3). With viscosity constant, and $\nu = \mu/\rho$ introduced, our equations then become

$$u\frac{\partial u}{\partial x} + v\frac{\partial u}{\partial y} = \nu\frac{\partial^2 u}{\partial y^2} \tag{9-1}$$

$$\frac{\partial u}{\partial x} + \frac{\partial v}{\partial y} = 0 \tag{9-2}$$

The boundary conditions are

$$\left.\begin{aligned} u &= 0 \\ v &= 0 \end{aligned}\right\} \quad \text{at } y = 0$$

$$u \to u_\infty \quad \text{at } y \to \infty$$

$$u = u_\infty \quad \text{at } x = 0$$

The shapes that the velocity profiles (Fig. 9-1) must take in order to satisfy the boundary conditions suggest that they may possibly be geometrically similar, differing only by a stretching factor on the y coordinate, such a factor being some function of the distance x along the plate. It frequently occurs that partial differential equations have solutions that involve this kind of similarity; if a differential equation has a family of similar solutions, these are usually much easier to obtain than other solutions.

[†] Many authors prefer to develop the boundary-layer momentum equation from the more general Navier–Stokes equation (4-14), employing an order-of-magnitude argument, which, in turn, shows that Eq. (9-1) is valid only for $\text{Re}_x = (u_\infty \rho x/\mu) \gg 1$.

The statement that the velocity profiles at all the x positions are geometrically similar, differing only by a multiplying factor, is equivalent to the statement that

$$u = f[y \cdot g(x)] \tag{9-3}$$

Let us now see if an assumption that the solution can be expressed in this form truly leads to such a solution. Let

$$\eta = y \cdot g(x) \tag{9-4}$$

Then

$$u = f(\eta) \tag{9-5}$$

With the nomenclature $f' = df/d\eta$ and $g' = dg/dx$, Eq. (9-3) can be substituted into the boundary-layer equations (9-1) and (9-2) as follows:

$$\frac{\partial u}{\partial x} = \frac{\partial f}{\partial x} = \frac{\partial f}{\partial \eta}\frac{\partial \eta}{\partial x} = f' y g'$$

$$\frac{\partial u}{\partial y} = \frac{\partial f}{\partial y} = \frac{\partial f}{\partial \eta}\frac{\partial \eta}{\partial y} = f' g$$

$$\frac{\partial^2 u}{\partial y^2} = \frac{\partial^2 f}{\partial y^2} = \frac{\partial}{\partial y}\left(\frac{\partial f}{\partial y}\right) = \frac{\partial}{\partial \eta}\left(\frac{\partial f}{\partial y}\right)\frac{\partial \eta}{\partial y} = f'' g^2$$

Substituting these derivatives into Eqs. (9-1) and (9-2) yields

$$f f' y g' + v f' g = \nu f'' g^2$$

$$f' y g' + \frac{\partial v}{\partial y} = 0$$

Combining these equations to eliminate v, and then rearranging to separate variables, we obtain

$$\frac{1}{f}\frac{d}{d\eta}\left(\frac{f''}{f'}\right) = \frac{1}{\nu}\frac{g'}{g^3} \tag{9-6}$$

Since one side is a function of η only and the other side is a function of x only, and since x and η are independent, then each side must be a constant; that is, we have successfully separated variables and reduced the problem to the solution of two ordinary differential equations. This result immediately suggests that a similarity solution does indeed exist.

Consider first the right-hand side, and set it equal to an arbitrary constant, $-k$:

$$\frac{1}{\nu}\frac{g'}{g^3} = -k$$

Solving gives

$$\frac{dg}{g^3} = -k\nu\, dx, \qquad -\frac{1}{2g^2} = -k\nu x + C$$

At $y = \infty$, $u = u_\infty$; but at $x = 0$ a boundary condition is that $u = u_\infty$ even at $y = 0$. Thus $g(0)$ must be infinite. It thus follows that $C = 0$. Then

$$g = \frac{1}{\sqrt{2k\nu x}}, \qquad \eta = yg = \frac{y}{\sqrt{2k\nu x}} \tag{9-7}$$

Note the implications of this result. Evidently the velocity function is of the form

$$u = f\left(\frac{y}{\sqrt{x}}\right)$$

This always turns out to be the case for those solutions of the boundary-layer equations where similar velocity profiles are obtained, and $y/\sqrt{x}$ is sometimes referred to as a *similarity parameter.*

Let us now consider the left-hand side of Eq. (9-6):

$$\frac{1}{f}\frac{d}{d\eta}\left(\frac{f''}{f'}\right) = -k$$

$$d\left(\frac{f''}{f'}\right) = -kf\, d\eta$$

$$\frac{f''}{f'} = -k\int f\, d\eta + C$$

To evaluate the constant of integration, note that

$$\left.\begin{aligned} \eta &= 0 \\ u &= 0 \\ v &= 0 \\ f &= 0 \end{aligned}\right\} \quad \text{at } y = 0$$

and, from Eq. (9-1),

$$\frac{\partial^2 u}{\partial y^2} = 0 = \frac{\partial^2 f}{\partial \eta^2} = f'' \quad (\text{if } v_s = 0)$$

Thus $C = 0$, and

$$\frac{f''}{f'} = -k\int_0^\eta f\, d\eta$$

Let us now define a *nondimensional* velocity in terms of a *derivative* of a function of η, the derivative being for the purpose of eliminating the integral.

Let

$$\zeta'(\eta) = \frac{u}{u_\infty} = \frac{f}{u_\infty}$$

Then

$$\begin{aligned} f &= u_\infty \zeta' \\ f' &= u_\infty \zeta'' \\ f'' &= u_\infty \zeta''' \end{aligned}$$

and

$$\frac{f''}{f'} = \frac{\zeta'''}{\zeta''}$$

Substituting gives

$$\frac{\zeta'''}{\zeta''} = -k \int_0^\eta u_\infty \frac{d\zeta}{d\eta}\, d\eta = -k u_\infty \zeta$$

$$\zeta''' + k u_\infty \zeta \zeta'' = 0$$

Since k is an arbitrary constant but $k u_\infty$ must be nondimensional, let

$$k u_\infty = \tfrac{1}{2}$$

Thus

$$\zeta''' + \tfrac{1}{2}\zeta\zeta'' = 0 \tag{9-8}$$

where

$$\eta = \frac{y}{\sqrt{\nu x / u_\infty}} \qquad \zeta'(\eta) = \frac{u}{u_\infty}$$

Equation (9-8) is the Blasius equation, an ordinary differential equation for which the boundary conditions must be

$$\begin{aligned} u &= 0 \quad \text{at } y = 0 \\ v &= 0 \quad \text{at } y = 0 \\ u &\to u_\infty \quad \text{at } y \to \infty \end{aligned}$$

Then

$$\zeta'(0) = 0, \qquad \zeta'(\infty) = 1$$

Since

$$f''(0) = 0, \qquad \zeta'''(0) = 0 \quad (\text{provided that } v_s = 0)$$

Then, from Eq. (9-8),

$$\zeta(0)\zeta''(0) = 0$$

It is not possible that all the derivatives are zero at the surface [in fact, $\zeta''(0) = 0$ would correspond to zero shear stress at the surface], so we conclude that

$$\zeta(0) = 0$$

Equation (9-8) can also be developed by introducing a stream function ψ, although this is not necessary. The stream function is simply a device for replacing the u and v components of velocity by a single function. If we define $\psi(x, y)$ by

$$u = \frac{\partial\psi}{\partial y}, \qquad v = -\frac{\partial\psi}{\partial x} \tag{9-9}$$

we find that such a definition satisfies the continuity equation (9-2). It can readily be shown that ψ is directly related to ζ; in fact,

$$\psi = \sqrt{\nu x u_\infty}\,\zeta \tag{9-10}$$

As before, $\zeta = \zeta(\eta)$, and

$$\eta = \frac{y}{\sqrt{\nu x/u_\infty}} \tag{9-11}$$

Note that by combining these equations we obtain $u = u_\infty \zeta'(\eta)$.

With these definitions, the Blasius equation is readily developed by just substituting Eq. (9-9) into Eq. (9-1) and then replacing ψ by ζ through Eq. (9-10).

Equation (9-8) was first solved numerically (and undoubtedly by hand) by Blasius,[3] but it can be readily solved now by standard computer-based numerical procedures. A brief summary of typical results is given in Table 9-1.

The velocity profiles are given by $\zeta' = u/u_\infty$. We can also evaluate a friction coefficient based on free-stream velocity, using the defining equation (5-10):

$$c_f = \frac{\tau_s}{\frac{1}{2}\rho u_\infty^2} \tag{9-12}$$

The surface shear stress τ_s can then be evaluated from (3-1) by invoking the boundary-layer approximations:

$$\tau_s = \mu\left(\frac{\partial u}{\partial y}\right)_s = \mu\left[f'\left(\frac{\partial \eta}{\partial y}\right)\right]_s = \mu\sqrt{u_\infty^3/\nu x}\,\zeta''(0)$$

The value for $\zeta''(0) = 0.332$ and thus

$$c_f = \frac{0.664}{\sqrt{u_\infty x/\nu}} = \frac{0.664}{\mathrm{Re}_x^{1/2}} \tag{9-13}$$

where we define

$$\mathrm{Re}_x = \frac{u_\infty x}{\nu} = \frac{u_\infty \rho x}{\mu} = \frac{G_\infty x}{\mu} \tag{9-14}$$

We term c_f the *local* friction coefficient since it is used to evaluate the *local* surface shear stress. We may also be interested in the total shear force from 0 to x, in which case we would like to know the *mean* shear stress from 0 to x. We

Table 9-1 Solutions to the laminar constant-property boundary layer with an impermeable surface and u_∞ = constant

η	ζ	ζ'	ζ''
0	0	0	0.3321
0.2	0.00664	0.06641	0.3320
0.4	0.02656	0.13277	0.3315
0.6	0.05974	0.19894	
0.8	0.10611	0.26471	
1.0	0.16557	0.32979	
1.2	0.23795	0.39378	
1.4	0.32298	0.45627	
1.6	0.42032	0.51676	
1.8	0.52952	0.57477	
2.0	0.65003	0.62977	
2.2	0.78120	0.68132	
2.4	0.92230	0.72899	
2.6	1.07252	0.77246	
2.8	1.23099	0.81152	
3.0	1.39682	0.84605	
3.2	1.56911	0.87609	
3.4	1.74696	0.90177	
3.6	1.92954	0.92333	
3.8	2.11605	0.94112	
4.0	2.30576	0.95552	
4.2	2.49806	0.96696	
4.4	2.69238	0.97587	
4.6	2.88826	0.98269	
4.8	3.08534	0.98779	
5.0	3.28329	0.99155	

For higher values of η, $\zeta = \eta - 1.72$

can define a mean friction coefficient on this basis; it is easy to show that this is simply the average of c_f with respect to x. Performing the integration, we find the mean friction coefficient c_{f_m} becomes

$$c_{f_m} = \frac{1.328}{\mathrm{Re}_x^{1/2}} \tag{9-15}$$

By use of Eq. (5-11), c_f can also be expressed in terms of the *momentum thickness* Reynolds number

$$c_f/2 = 0.2204/\mathrm{Re}_{\delta_2} \tag{9-16}$$

The previously defined boundary-layer thickness parameters δ_1 and δ_2, Eqs. (5-5) and (5-6), can now be readily evaluated from the data of Table 9-1 (note that in the integrations $dy = \sqrt{\nu x/u_\infty}\, d\eta$). Thus

$$\delta_1 = 1.72\sqrt{\nu x/u_\infty} \qquad \text{(displacement thickness)} \tag{9-17}$$

$$\delta_2 = 0.664\sqrt{\nu x/u_\infty} \qquad \text{(momentum thickness)} \tag{9-18}$$

Note also that δ_2 can be perhaps more easily evaluated by integration of Eq. (5-11), obtained from the momentum integral equation.

Our original simplifying assumption in developing the boundary-layer equations was that the boundary layer remains "thin," so that $\partial u/\partial y$ is always very much greater than any other velocity gradient. This assumption would seem to be valid as long as $\delta_1 \ll x$. From Eq. (9-17)

$$\frac{\delta_1}{x} = \frac{1.72\sqrt{\nu x/u_\infty}}{x} = \frac{1.72}{\mathrm{Re}_x^{1/2}} \tag{9-19}$$

Thus the boundary-layer approximation would appear to be valid as long as $\mathrm{Re}_x \gg 1$. Thus, for example, our boundary-layer approximation would not be valid in the region very close to the leading edge of the plate.

SIMILARITY SOLUTIONS FOR THE LAMINAR INCOMPRESSIBLE BOUNDARY LAYER FOR $u_\infty = Cx^m$

Similar solutions to the boundary-layer equations can be obtained if the free-stream velocity varies as

$$u_\infty = Cx^m \tag{9-20}$$

Before examining this family of solutions, let us consider what physical problems are approximated by such a velocity variation. Note the family of two-dimensional potential flows shown in Fig. 9-2.

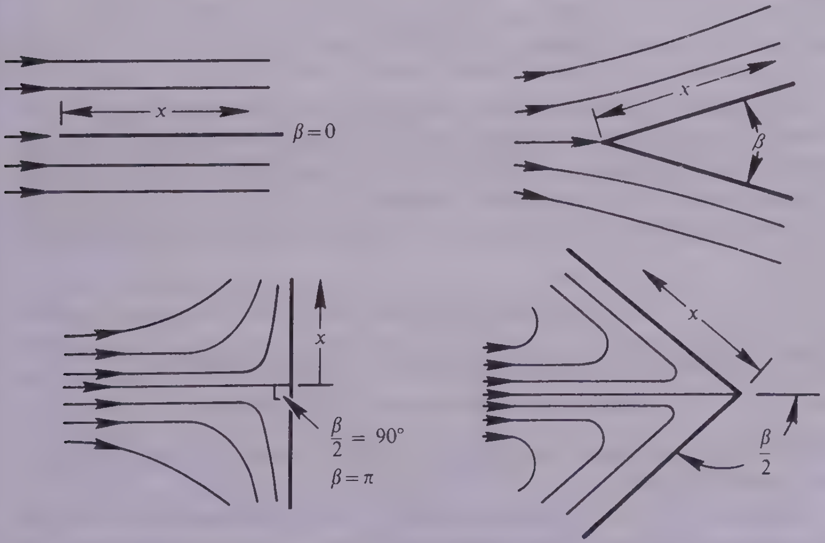

Figure 9-2 The family of "wedge" flows.

These flows are very easily solved by potential flow theory, and it is found that the velocity along the surface varies according to Eq. (9-20) in each case; in fact, it is found that

$$m = \frac{\beta/\pi}{2-\beta/\pi} = \frac{x}{u_\infty}\frac{du_\infty}{dx} \tag{9-21}$$

The boundary-layer solutions corresponding to these potential flows are frequently called *wedge-flow* solutions for obvious reasons. They are also frequently called the Falkner and Skan flows after the authors who first published their boundary-layer solutions.[4] The previously obtained solution for constant free-stream velocity is a special case of these flows, $\beta = 0$, and the family includes the two-dimensional stagnation point $\beta = \pi$.

For constant-property, two-dimensional flow the boundary-layer *momentum equation* (4-10) becomes

$$u\frac{\partial u}{\partial x} + v\frac{\partial u}{\partial y} = -\frac{1}{\rho}\frac{dP}{dx} + \nu\frac{\partial^2 u}{\partial y^2} \tag{9-22}$$

The pressure-gradient term can be expressed in terms of the velocity via the Bernoulli equation, as was done in Eq. (5-3), which is valid in the free stream where a potential flow presumably exists. Combining Eq. (9-20) with Eq. (5-3), we get

$$\frac{dP}{dx} = -\rho C x^m C m x^{m-1} = -\frac{\rho u_\infty^2 m}{x}$$

Thus

$$u\frac{\partial u}{\partial x} + v\frac{\partial u}{\partial y} = \frac{u_\infty^2 m}{x} + \nu\frac{\partial^2 u}{\partial y^2} \tag{9-23}$$

In addition to Eq. (9-23), the continuity equation (9-2) is still applicable.

We now seek similarity solutions in the same manner as before. Actually the same similarity parameter is applicable; the simplest procedure is to substitute Eq. (9-9) into Eq. (9-23) and then transform to (ζ, η) using Eqs. (9-10) and (9-11). An ordinary differential equation results, so that similarity solutions must exist:

$$\zeta''' + \tfrac{1}{2}(m+1)\zeta\zeta'' + m(1-\zeta'^2) = 0 \tag{9-24}$$

The boundary conditions are the same as for the previous problem:

$$\zeta(0) = 0, \qquad \zeta'(0) = 0, \qquad \zeta'(\infty) = 1$$

[Note that the constant-u_∞ problem, Eq. (9-8), is merely a special case of this more general problem.]

Equation (9-24) can be solved numerically for the indicated boundary conditions. For $m > 0$, the solutions are unique. For $m < 0$, two families of solutions exist for a limited range of negative β, corresponding either to a decelerating

Table 9-2 Solutions to the laminar constant-property boundary layer with an impermeable surface and $u_\infty = Cx^m$

β	m	$\zeta''(0)$
2π	∞	∞
π	1.0	1.233 Stagnation
1.57	0.333	0.759
0.627	0.111	0.510
0	0	0.332 Flat plate
−0.314	−0.0476	0.220
−0.625	−0.0904	0 Separation

mainstream to the point of incipient separation or to flows in a laminar boundary layer after separation. A partial summary[4] of the results for $m > 0$ and for the $m < 0$ decelerating flows is given in Table 9-2. A friction coefficient can be evaluated as before:

$$c_f = \frac{2\zeta''(0)}{\mathrm{Re}_x^{1/2}} \tag{9-25}$$

We make more use of the wedge solutions later when we consider heat transfer.

SIMILARITY SOLUTIONS FOR THE LAMINAR INCOMPRESSIBLE BOUNDARY LAYER FOR $v_s \neq 0$

A boundary condition employed in the examples considered so far has been that the velocity normal to the surface at the surface is zero; that is, $v_s = 0$. A number of interesting applications occur in which there is mass transfer, and hence a normal velocity component, at the surface. Evaporation from or condensation onto a surface is one example. Another is that of a porous surface through which a fluid (possibly the same fluid as the main stream) is being forced in order to protect the surface from an extremely high-temperature main stream. Another might be the case of a porous surface through which part of the main stream is being sucked, possibly to prevent boundary-layer separation because of an adverse pressure gradient.

The applicable differential equation is still Eq. (9-22), and we are merely changing a boundary condition. The general problem where v_s varies in any arbitrary manner along the surface can probably be solved only by direct numerical integration of Eq. (9-22). However, let us examine the conditions under which similarity solutions exist. This merely involves examination of the possible boundary conditions for Eq. (9-23) to see if a change of boundary conditions allows v_s to be nonzero, and, if so, how v_s must vary along the surface.

From Eqs. (9-9), (9-10), and (9-20),

$$v = -\frac{\partial \psi}{\partial x}, \qquad \psi = \sqrt{\nu x u_\infty}\,\zeta(\eta) \qquad u_\infty = Cx^m$$

Combining these gives

$$v = -\zeta(\eta)\frac{m+1}{2}x^{(m-1)/2}\sqrt{C\nu} - Cy\frac{m-1}{2}\zeta'(\eta)x^{m-1}$$

But $\eta = 0$ and $v = v_s$ at $y = 0$. Thus

$$v_s = -\zeta(0)\frac{m+1}{2}x^{(m-1)/2}\sqrt{C\nu} \tag{9-26}$$

We now let $C = u_\infty/x^m$ and obtain

$$v_s = -\frac{m+1}{2}\zeta(0)\frac{u_\infty}{\sqrt{u_\infty x/\nu}} \tag{9-27}$$

and

$$\zeta(0) = -\frac{2}{m+1}\frac{v_s}{u_\infty}\sqrt{\frac{u_\infty x}{\nu}} = -\frac{2}{m+1}\frac{v_s}{u_\infty}\mathrm{Re}_x^{1/2} \tag{9-28}$$

Thus $\zeta(0) =$ constant, as a boundary condition to Eq. (9-24), gives us a family of similarity solutions for $v_s \neq 0$. However, for $\zeta(0)$ to be a constant, v_s must vary along the surface in the particular manner prescribed in Eq. (9-26); that is

$$v_s \propto x^{(m-1)/2} \tag{9-29}$$

Note that only for the stagnation point $m = 1$ can v_s be a constant, for $u_\infty =$ constant, $m = 0$ and v_s must vary as $1/\sqrt{x}$ in order for similar velocity profiles to obtain.

The group of variables

$$\frac{v_s}{u_\infty}\mathrm{Re}_x^{1/2} \tag{9-30}$$

is frequently referred to as the "blowing" (or "suction") parameter. Equation (9-24) has been solved numerically for various values of this parameter, as well as various values of m. Some of the results for $m = 0$ are given in Table 9-3, from which the local friction coefficient may be evaluated from Eq. (9-25). Further results may

Table 9-3 Solutions to the laminar constant-property boundary layer with blowing or suction at the surface and $u_\infty =$ constant

$\frac{v_s}{u_\infty}\mathrm{Re}_x^{1/2}$	$\zeta''(0)$	
−2.500	2.590	Suction
−0.750	0.945	
−0.250	0.523	
0	0.332	
+0.250	0.165	Blowing (Separation)
+0.375	0.094	
+0.500	0.036	
+0.585	0	

be found in Ref. 5. However, the major area of usefulness of these solutions arises in connection with heat- and mass-transfer solutions to be considered later, where the complete $\zeta(\eta)$ is required for each case.

NONSIMILAR MOMENTUM BOUNDARY LAYERS

In the preceding sections we transformed the momentum equation and boundary conditions using η, a similarity variable, to eliminate the x dependence from the equation and boundary conditions. We found that the transformation was successful, provided that u_∞ was constant or u_∞ and/or v_s had power-law variations with x. For arbitrary u_∞, v_s constant, or arbitrary transverse surface curvature, the boundary-layer flow will be nonsimilar.

Several classes of solution methods exist for solving the nonsimilar laminar boundary-layer problem. Perhaps the most exact solution is a numerical solution to the governing partial differential equations by finite-difference or finite-element methods. A second class comprises the approximate boundary-layer solutions employing the momentum integral equation. This class is discussed in the sections following this one.

The third class of approximate solutions employs the concept of local similarity and local nonsimilarity. Consider the general transformation of the independent variables in the momentum equation and boundary conditions from (x, y) to (ξ, η). If either ξ or derivatives with respect to ξ remain after transformation, similarity solutions will not exist.[†] However, *local similarity* solutions can be obtained by dropping the ξ derivatives from the transformed momentum equation and boundary conditions and retaining ξ as a parameter. The resulting solution is generally valid if ξ or the discarded derivatives are small. *Local* nonsimilarity solutions carry the essence of the local similarity solution a step further by retaining the ξ derivatives in the solution procedure. Sparrow, Quack, and Boerner[7] develop a procedure to generate an additional equation and boundary conditions for $\partial\zeta/\partial\xi$ and solve it and the momentum equation simultaneously. A solution procedure using asymptotic expansions is described by Dewey and Gross.[8] With both the local similar and local nonsimilar methods, the solutions are independent of the upstream history of the flow.

AN APPROXIMATE LAMINAR BOUNDARY-LAYER SOLUTION FOR CONSTANT FREE-STREAM VELOCITY DEVELOPED FROM THE MOMENTUM INTEGRAL EQUATION

To illustrate the power and simplicity of the momentum integral equations as a device for approximate solution of the boundary layer, let us again consider the laminar constant-property boundary layer with constant free-stream velocity.

[†] It is possible that another set of similarity variables will result in similarity. The free-parameter method described by Hansen[6] is a useful method for searching for similarity variables.

The applicable form of the momentum integral equation is Eq. (5-9). The surface shear stress can be expressed in terms of the velocity gradient at the surface, and thus Eq. (5-9) becomes

$$\frac{d\delta_2}{dx} = \frac{\nu}{u_\infty^2}\left(\frac{\partial u}{\partial y}\right)_s \tag{9-31}$$

We now must propose some kind of velocity profile in the boundary layer so that we can develop an expression for the momentum thickness δ_2. The power of the method lies in the fact that the solution is not highly dependent on the shape of the velocity profile. Previous experience with laminar flow in a tube might suggest that a simple parabola would be satisfactory; and, as a matter of fact, a quite good solution can be obtained with a simple parabola. A better solution is obtained, however, if the boundary-layer differential equation (9-1) is examined and it is noted that the second derivative of u with respect to y must go to zero at the surface. A simple parabola does not have this property, but a cubic parabola does. Consider the cubic parabola

$$u = ay + by^3$$

A parabolic velocity profile implies that the boundary layer has a definite, finite thickness, rather than extending indefinitely in the y direction as in the exact solution, and this artificiality must be accepted in the integral methods. Suppose we let this distance be a boundary-layer thickness δ. Then we can introduce the boundary conditions that $\partial u/\partial y = 0$ and $u = u_\infty$ when $y = \delta$. The constants a and b can then be evaluated, yielding

$$\frac{u}{u_\infty} = \frac{3}{2}\frac{y}{\delta} - \frac{1}{2}\left(\frac{y}{\delta}\right)^3 \tag{9-32}$$

Substitution of (9-32) into the integral definition of δ_2, Eq. (5-6), yields an expression for δ_2. This expression is, in turn, differentiated with respect to x and substituted in place of the right-hand side of Eq. (9-31). The left-hand side is obtained directly from Eq. (9-32), with the final result

$$\delta\, d\delta = \frac{140}{13}\frac{\nu}{u_\infty}\, dx$$

This equation is readily integrated for the boundary condition $\delta = 0$ at $x = 0$ (for example, the boundary layer originates at the beginning of the plate), yielding

$$\delta = 4.64\sqrt{\nu x/u_\infty} \tag{9-33}$$

Equation (9-33) gives the boundary-layer thickness (artificial though it may be) as a function of x. The surface shear stress can next be evaluated by substituting Eq. (9-33) into Eq. (9-32), which gives the complete velocity field, and then evaluating the gradient at the surface. Next the friction coefficient, Eq. (5-10), is introduced, and the final result for the local friction coefficient is

$$c_f = \frac{0.646}{\mathrm{Re}_x^{1/2}} \tag{9-34}$$

This result is within 3 percent of the exact Blasius solution, Eq. (9-13), and is illustrative of the power of the method. We use this result later in connection with a heat-transfer solution, where it proves more convenient than the exact solution.

AN APPROXIMATE LAMINAR BOUNDARY-LAYER SOLUTION FOR ARBITRARILY VARYING FREE-STREAM VELOCITY OVER A BODY OF REVOLUTION

A somewhat different use of the momentum integral equation in an approximate solution is illustrated by the following simple and powerful procedure.

Consider Eq. (5-7) with density constant and no injection or suction:

$$\frac{\tau_s}{\rho u_\infty^2} = \frac{d\delta_2}{dx} + \delta_2 \left(2 + \frac{\delta_1}{\delta_2}\right) \frac{1}{u_\infty} \frac{du_\infty}{dx} + \frac{\delta_2}{R} \frac{dR}{dx} \tag{9-35}$$

To simplify the algebra, let us introduce still another boundary-layer thickness: the *shear thickness*

$$\delta_4 = \frac{\mu u_\infty}{\tau_s} = \frac{u_\infty}{(\partial u/\partial y)_s} \tag{9-36}$$

As a further simplification, let

$$T = \frac{\delta_2}{\delta_4}, \qquad H = \frac{\delta_1}{\delta_2} \tag{9-37}$$

Substituting these definitions into Eq. (9-35) and then rearranging, we get

$$\frac{u_\infty}{\nu} \frac{d\delta_2^2}{dx} + \frac{2\delta_2^2}{\nu} \frac{u_\infty}{R} \frac{dR}{dx} = 2\left[T - (2 + H)\frac{\delta_2^2}{\nu} \frac{du_\infty}{dx}\right] \tag{9-38}$$

Let us define a local parameter:

$$\lambda = \frac{\delta_2^2}{\nu} \frac{du}{dx} \tag{9-39}$$

Let us now make the *assumption* that the boundary-layer velocity profile depends only on local conditions and, specifically, that

$$T = T(\lambda), \qquad H = H(\lambda)$$

A dimensional analysis of the variables on which the momentum thickness must depend would also suggest that the λ group is a significant parameter. The right-hand side of (9-38) is, then, entirely a function of λ; that is,

$$\frac{u_\infty}{\nu} \frac{d\delta_2^2}{dx} + \frac{2\delta_2^2}{\nu} \frac{u_\infty}{R} \frac{dR}{dx} = F(\lambda) \tag{9-40}$$

where

$$F(\lambda) = 2[T - (2 + H)\lambda]$$

Attempts to find a satisfactory form for $F(\lambda)$ have followed various courses. Examination of various *exact* solutions indicates that the fundamental assumption is valid to a good degree of approximation; for example, a plot of F versus λ from the wedge solutions and from various other particular solutions yields curves that are quite close together, especially for accelerating flows. Thwaites[9] made such a comparison and further showed that the function could be quite well approximated by a linear relation, which greatly simplifies the algebra:

$$F = a - b\lambda = 0.44 - 5.68\lambda \tag{9-41}$$

A more exact but somewhat less convenient procedure is suggested by Spalding.[10]

Substituting Eq. (9-41) into Eq. (9-40), rearranging, and combining the derivatives, we get

$$d\left(R^2\delta_2^2 u_\infty^b\right) = a\nu u_\infty^{b-1} R^2\,dx$$

Integrating between 0 and x yields

$$R^2\delta_2^2 u_\infty^b - R_0^2\delta_{2,0}^2 u_{\infty,0}^b = a\nu \int_0^x u_\infty^{b-1} R^2\,dx$$

Take $x = 0$ as the leading edge of the body; one of the following is also zero there: R_0, $\delta_{2,0}$, or $u_{\infty,0}$. Thus

$$R^2\delta_2^2 u_\infty^b = a\nu \int_0^x u_\infty^{b-1} R^2\,dx$$

Taking the given values of a and b and solving for δ_2, we find

$$\delta_2 = \frac{0.664\nu^{0.5}}{R u_\infty^{2.84}} \left(\int_0^x u_\infty^{4.68} R^2\,dx\right)^{0.5} \tag{9-42}$$

Solution of (9-42) then involves only a simple integration procedure that depends on the given variation of u_∞ and R with x. Once we have the momentum thickness δ_2, the shear thickness and the local surface shear stress can be evaluated from Table 9-4 on the basis of the wedge solutions.

Table 9-4 Functions for use with Eq. (9-42)

$\lambda = \dfrac{\delta_2^2}{\nu}\dfrac{du_\infty}{dx}$	$T = \dfrac{\delta_2}{\delta_4} = \dfrac{\delta_2\tau_s}{\mu u_\infty}$	$H = \dfrac{\delta_1}{\delta_2}$
−0.082	0	3.70 Separation
−0.080	0.039	3.58
−0.070	0.089	3.17
−0.060	0.113	2.99
−0.040	0.153	2.81
−0.024	0.182	2.71
0	0.220	2.60 Flat plate
0.016	0.244	2.55
0.048	0.291	2.44
0.080	0.333	2.34 Stagnation (approx.)
0.12	0.382	2.23
0.25	0.500	2.00

More exact procedures for calculating the laminar boundary layer may be found in many places in the literature, and the appropriate one should be used where precise results are required. Most, however, require tedious numerical calculations, and for many engineering purposes Eq. (9-42) will suffice.

PROBLEMS

9-1. Air at 26°C and 1 atm pressure flows normally to a 5-cm-diameter circular cylinder at a velocity of 9 m/s. It can be shown from potential flow theory that in the vicinity of the forward stagnation point for flow normal to a cylinder the velocity along the surface, u_∞ (which is the velocity just outside of any boundary layer), is given by

$$u_\infty = \frac{4Vx}{D}$$

where V is the oncoming normal velocity, x is the distance along the surface measured from the stagnation point, and D is the diameter of cylinder. Calculate the displacement thickness of the boundary layer at the stagnation point, and discuss the significance of the result.

9-2. Derive Eq. (9-21) from potential flow theory.

9-3. Solve the laminar boundary layer for constant free-stream velocity, using the momentum integral equation and an assumption that the velocity profile may be approximated by

$$\frac{u}{u_\infty} = \sin \frac{\pi y}{2\delta}$$

Evaluate the momentum thickness, displacement thickness, and friction coefficient, and compare with the exact solution.

9-4. Redevelop Eq. (9-42) for the case where density and dynamic viscosity are functions of x.

9-5. Air emerges from the axisymmetric nozzle shown in Fig. 9-3 at a centerline velocity of 10 m/s at 1 atm pressure and 21°C. Assuming an essentially constant-density and constant-temperature process (and this is ensured by the low velocity), calculate the displacement thickness of the boundary layer at the nozzle throat, assuming that the free-stream velocity along the inner surface of the nozzle varies linearly with distance, starting with $u_\infty = 0$ at the sharp corner. Calculate the air mass flow rate through the nozzle and the overall pressure drop through the nozzle. On the basis of these results, discuss the concept of a nozzle "discharge coefficient." What would be the discharge coefficient of this nozzle? If you were to define a Reynolds number based on throat diameter and mean velocity, how would the discharge coefficient vary with Reynolds number?

9-6. Derive Eq. (9-24) in a manner similar to that used in the development of Eq. (9-8) for zero pressure gradient.

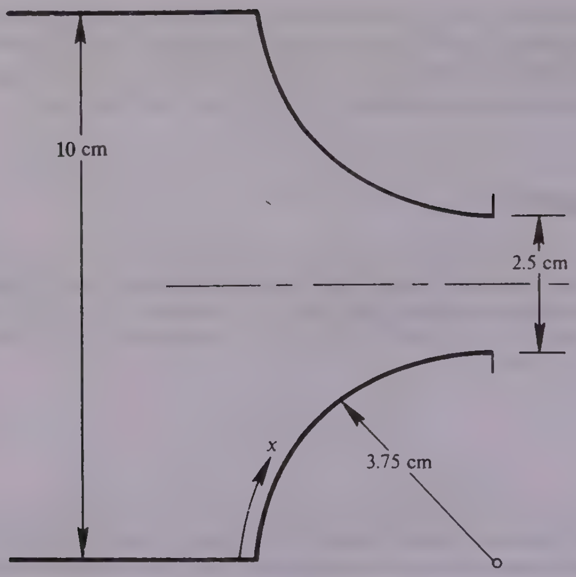

Figure 9-3

TEXSTAN PROBLEMS

9-7. TEXSTAN *analysis of the laminar momentum boundary layer over a flat plate with zero pressure gradient*: Choose a starting x-Reynolds number of about 1000 and pick fluid properties that are appropriate to air, evaluated at a free stream temperature of 300 K. Use constant fluid properties, and note that the energy equation does not have to be solved. The geometrical dimensions of the plate are 1 m wide (a unit width) by 0.2 m long in the flow direction, corresponding to an ending Re_x of about 2×10^5. Let the velocity boundary condition at the free stream be 15 m/s. The initial velocity profile appropriate to the starting x-Reynolds number (a Blasius profile) can be supplied by using the *kstart*=4 choice in TEXSTAN.

Calculate the boundary layer flow and compare the results with the similarity solution for development in the streamwise direction of such quantities as the boundary-layer thickness (see Table 9-1), displacement thickness (see Eq. 9-17), and momentum thickness (see Eq. 9-18). Evaluate the concept of boundary-layer similarity by comparing nondimensional velocity profiles at several x-locations to themselves and to Table 9-1. Compare the friction coefficient results based on x-Reynolds number with Eq. (9-13) and momentum-thickness Reynolds number with Eq. (9-16). Calculate the friction coefficient distribution using momentum integral Eq. (5-11) and compare with the TEXSTAN calculations. Feel free to investigate any other attribute of the boundary-layer flow.

9-8. TEXSTAN *analysis of the laminar momentum boundary layer stagnation flow (the Falkner-Skan $m = 1$ case):* Choose a starting x-Reynolds number of about 200 and pick fluid properties that are appropriate to air, evaluated at a free-stream temperature of 300 K. Use constant fluid properties, and note that the energy equation does not have to be solved. The geometrical dimensions of the plate are 1 m wide (a unit width) by 0.12 m long in the flow direction, corresponding to an ending Re_x of about 4×10^5. The initial velocity profile appropriate to the starting x-Reynolds number (a Falkner-Skan $m = 1$ profile) can be supplied by using the *kstart*=5 choice in TEXSTAN. Note that the profile comes from solving Eq. (9-24). Because this is a variable free-stream-velocity flow, there are two choices within TEXSTAN: either the user provides a table of u_∞ versus x, computed from the function $u_\infty(x) \propto x^m$, or the user lets TEXSTAN supply the distribution for $m = 1$ by using the $k4 = 4$. With the latter choice, TEXSTAN builds the table using

$$u_\infty(x) \propto x^m = A\left(\frac{x - C}{B - C}\right)^m$$

The user will supply the values for A, B, C (called *axx*, *bxx*, and *cxx* in TEXSTAN), where C is a virtual origin for the flow, which for stagnation flow corresponds to $C = 0$, and A and B are linked to make sure that whatever starting x value is chosen gives a free-stream velocity such that the starting x-Reynolds number is correct. Typically we can set $B = 1$, and then for a given choice of starting Re_x, the corresponding u_∞ value permits calculation of A.

Calculate the boundary layer flow and compare the friction coefficient results based on x-Reynolds number with the results in the text. Evaluate the concept of boundary-layer similarity by comparing nondimensional velocity profiles at several x locations with each other. Calculate the friction coefficient distribution using momentum integral Eq. (5-8) and compare with the TEXSTAN calculations. Feel free to investigate any other attribute of the boundary-layer flow and to compare your results with other open-literature solutions.

REFERENCES

1. Schlichting, H.: *Boundary Layer Theory*, 6th ed., McGraw-Hill, New York, 1968.
2. Moore, F. K. (ed.): *Theory of Laminar Flows*, vol. 13: *High Speed Aerodynamics and Jet Propulsion*, Princeton University Press, Princeton, NJ 1964.
3. Blasius, H.: *Z. (Angew) Math. Phys.*, vol. 56, 1908.
4. Falkner, V. M., and S. W. Skan: *Phil. Mag.*, vol. 12, p. 865, 1931.
5. NASA TN 3151, Washington, September 1954.
6. Hansen, A. G.: *Similarity Analysis of Boundary Value Problems in Engineering*, Prentice-Hall, Englewood Cliffs, NJ, 1964.
7. Sparrow, E. M., H. Quack, and C. J. Boerner, *AIAA J.*, vol. 8, pp. 1936–1942, 1970.
8. Dewey, C. F., Jr, and J. F. Gross: *Advances in Heat Transfer*, vol. 4, pp. 317–446. Academic Press, New York, 1964.
9. Thwaites, H.: *Aero. Q.*, vol. 1, p. 245, 1949.
10. Spalding, D. B.: *J. Fluid Mech.*, vol. 4, p. 22, 1958.

10 CHAPTER

Laminar External Boundary Layers: Heat Transfer

Heat transfer between a body and a fluid flowing with steady laminar motion over that body is considered in this chapter. It is assumed that the thermal and momentum boundary layers that develop along the surface of the body are not influenced by the development of boundary layers on any adjacent surfaces; this is the distinguishing feature of the problems considered in this chapter as compared with the internal flow problems of Chap. 8. This chapter covers a very broad range of applications, including flow over airfoils, turbine blades, flow inside nozzles, and flow at the stagnation points of cylinders and spheres.

We assume that all body forces are negligible, so that the fluid is forced over the body by some external means unrelated to the temperature field in the fluid. All the laminar flow solutions considered in this chapter are based on an idealization of constant fluid properties, unaffected by temperature. The influence of temperature-dependent properties is discussed later in Chap. 15. Constant properties also imply no concentration gradients, so mass diffusion is neglected here but taken up later in Chap. 18. Consideration is also restricted to velocity sufficiently low that the viscous dissipation term in the energy equation can be neglected; the high-velocity boundary layer is considered in Chap. 16.

We consider first constant free-stream velocity flow along a flat, constant-temperature surface, then the same problem with $u_\infty = Cx^m$ and with injection or suction of fluid at the surface. For all these problems the applicable energy differential equation of the boundary layer is Eq. (4-39). These problems have in common the fact that similarity solutions are obtainable in much the same fashion as for the laminar momentum boundary layer in Chap. 8. In fact, the velocity solutions from Chap. 8 are employed in solving the energy equation.

Next a solution is developed for the thermal boundary layer on a flat plate with constant free-stream velocity but with an unheated starting length. In this case the energy integral equation (5-20) is employed to obtain an approximate solution. Then, by employing superposition, the unheated starting-length solution is used to develop solutions for any arbitrarily specified surface temperature or heat flux. These solutions are restricted to the case of constant free-stream velocity.

Finally, an approximate solution is developed for variable free-stream velocity flow over a body of arbitrary shape.

CONSTANT FREE-STREAM VELOCITY FLOW ALONG A CONSTANT-TEMPERATURE SEMI-INFINITE PLATE

This is perhaps the most elementary of the laminar-boundary-layer heat-transfer solutions. Specification of a constant-temperature surface means that a thermal boundary layer will originate together with the momentum boundary layer at the leading edge of the plate. The system to be analyzed, the coordinate system, the development of the thermal boundary layer, and the expected temperature profiles are indicated in Fig. 10-1.

The applicable energy differential equation of the boundary layer is Eq. (4-39). Let us first define a nondimensional temperature θ:

$$\theta = \frac{T_s - T}{T_s - T_\infty} \tag{10-1}$$

Then Eq. (4-39) becomes

$$u\frac{\partial \theta}{\partial x} + v\frac{\partial \theta}{\partial y} = \alpha \frac{\partial^2 \theta}{\partial y^2} \tag{10-2}$$

We seek a solution to Eq. (10-2) subject to the boundary conditions

$$\theta = 0 \quad \text{at } y = 0$$
$$\theta = 1 \quad \text{at } y \to \infty$$
$$\theta = 1 \quad \text{at } x = 0$$

We already have a solution for the hydrodynamic counterpart of this problem, Eqs. (9-1) and (9-2), and associated boundary conditions; this solution is given in Eq. (9-15) and Table 9-1.

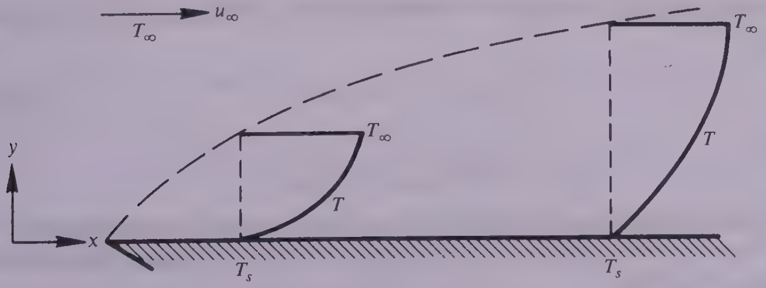

Figure 10-1 Temperature profiles in the thermal boundary layer.

Before discussing a general solution to Eq. (10-2) for the specific boundary conditions, it is worth noting one particular solution that can be readily obtained, simply by analogy. Note that Eq. (10-2) is very similar to the corresponding momentum equation of the boundary layer, Eq. (9-1). In fact, the same function will satisfy both equations and boundary conditions if $\alpha = \nu$. But $\alpha = \nu$ corresponds to $\Pr = 1$. Thus for a fluid with $\Pr = 1$ the nondimensional velocity and temperature profiles are similar and grow along the plate at the same rate.

Similar velocity and temperature profiles can be easily shown to lead to a simple relation between the Stanton number and the friction coefficient:

$$\mathrm{St} = c_f/2 \tag{10-3}$$

We already know c_f for this case from Eq. (9-15). Thus, purely by inspection, we already have one heat-transfer solution to the laminar boundary layer. Let us now proceed to a more general solution to Eq. (10-2).

The shape of the nondimensional temperature profiles and the fact that at $\Pr = 1$ the temperature profiles are identical to the velocity profiles suggest that similarity solutions may be obtainable for this problem. We could go through the identical procedure that we used for the velocity part of this problem, but it seems rather likely that we will obtain the same similarity parameter as before. Let us assume that this is so; the validity of this assumption will depend on whether we are successful in obtaining a solution.

Let us assume that

$$\theta = \theta(\eta)$$

where

$$\eta = \frac{y}{\sqrt{\nu x / u_\infty}}$$

To introduce the velocities u and v, which have already been evaluated in Chap. 9, let us use the stream function ψ and the relation between ψ and ζ as given in Eqs. (9-9) and (9-10):

$$u = \frac{\partial \psi}{\partial y}, \qquad v = -\frac{\partial \psi}{\partial x}, \qquad \psi = \sqrt{\nu x u_\infty}\,\zeta$$

Performing the indicated differentiation and substituting in Eq. (10-2), we obtain

$$\theta'' + \frac{\Pr}{2}\zeta\theta' = 0 \tag{10-4}$$

where

$$\theta = \theta(\eta), \qquad \zeta = \zeta(\eta)$$

The ζ function was found in Chap. 9 from solutions to the Blasius equation.

We thus seek solutions to this ordinary differential equation subject to the boundary conditions

$$\theta(0) = 0, \qquad \theta(\infty) = 1$$

The fact that we were successful in reducing the partial differential equation (10-2) to an ordinary differential equation (10-4) indicates that similarity solutions do indeed exist for the constant-surface-temperature boundary condition.

Equation (10-4) may be directly integrated as follows:

$$\frac{d\theta'}{d\eta} + \frac{\Pr}{2}\zeta\theta' = 0, \qquad \frac{d\theta'}{\theta'} + \frac{\Pr}{2}\zeta\, d\eta = 0$$

$$\tau' = C_1 \exp\left(-\frac{\Pr}{2}\int_0^\eta \zeta\, d\eta\right) \tag{10-5}$$

$$\theta = C_1 \int_0^\eta \left[\exp\left(-\frac{\Pr}{2}\int_0^\eta \zeta\, d\eta\right)\right] d\eta + C_2 \tag{10-6}$$

In applying the boundary condition $\theta = 0$ at $\eta = 0$ it is apparent that

$$C_2 = 0$$

For the boundary condition $\theta = 1$ at $\eta = \infty$,

$$C_1 = \frac{1}{\displaystyle\int_0^\infty \left[\exp\left(-\frac{\Pr}{2}\int_0^\eta \zeta\, d\eta\right)\right] d\eta} \tag{10-7}$$

Therefore

$$\theta(\eta) = \frac{\displaystyle\int_0^\eta \left[\exp\left(-\frac{\Pr}{2}\int_0^\eta \zeta\, d\eta\right)\right] d\eta}{\displaystyle\int_0^\infty \left[\exp\left(-\frac{\Pr}{2}\int_0^\eta \zeta\, d\eta\right)\right] d\eta} \tag{10-8}$$

Equation (10-8) can now be readily solved for any particular Prandtl number, since we already have a tabulation of $\zeta(\eta)$, Table 9-1. We can also define a local conductance, or heat-transfer coefficient, h_x as follows:

$$h_x = \frac{\dot{q}_s''}{T_s - T_\infty} \qquad \text{(positive } \dot{q}'' \text{ in the positive } y \text{ direction)}$$

$$\dot{q}_s'' = -k\left(\frac{\partial T}{\partial y}\right)_s = -k(T_\infty - T_s)\left(\frac{\partial \theta}{\partial y}\right)_s$$

$$= k(T_s - T_\infty)\left(\frac{d\theta'}{d\eta}\frac{\partial \eta}{\partial y}\right)_s = \frac{k(T_s - T_\infty)}{\sqrt{\nu x/u_\infty}}\theta'(0)$$

To put the conductance in nondimensional form, a local Nusselt number Nu_x can then be defined:

$$\mathrm{Nu}_x = \frac{h_x x}{k} = \frac{x}{\sqrt{\nu x/u_\infty}}\theta'(0) = \frac{\theta'(0)}{\sqrt{\nu/x u_\infty}} = \mathrm{Re}_x^{1/2}\theta'(0)$$

From Eq. (10-5) it is apparent that

$$\theta'(0) = C_1$$

and

$$\mathrm{Nu}_x = \frac{\mathrm{Re}_x^{1/2}}{\displaystyle\int_0^\infty \left[\exp\left(-\frac{\mathrm{Pr}}{2}\int_0^\eta \zeta\, d\eta\right)\right] d\eta} \tag{10-9}$$

Again, since we already know $\zeta(\eta)$, we can readily evaluate the integrals for any particular Prandtl number.

The results of such calculations, based in part on the calculations of Elzy and Sisson,[23] are given in Table 10-1.

Over the Prandtl number range 0.5–15 these results are very well approximated by the equation

$$\mathrm{Nu}_x = 0.332\,\mathrm{Pr}^{1/3}\,\mathrm{Re}_x^{1/2} \tag{10-10}$$

We could have anticipated the result for $\mathrm{Pr} = 1$ from Eq. (10-3).

Temperature profiles for this solution are shown on Fig. 10-2. The curve for $\mathrm{Pr} = 1.00$ is identical to the velocity profile. Note in particular the strong dependence of the thermal boundary-layer thickness on Prandtl number. Low values of

Table 10-1 Values of $\mathrm{Nu}_x\,\mathrm{Re}_x^{-1/2}$ for various Prandtl numbers; heat transfer to the laminar constant-property boundary layer (u_∞, T_∞, T_s = const)

Pr	0.001	0.01	0.1	0.5	0.7	1.0	7.0	10.0	15.0	50	100	1000
$\mathrm{Nu}_x\,\mathrm{Re}_x^{-1/2}$	0.0173	0.0516	0.140	0.259	0.292	0.332	0.645	0.730	0.835	1.247	1.572	3.387

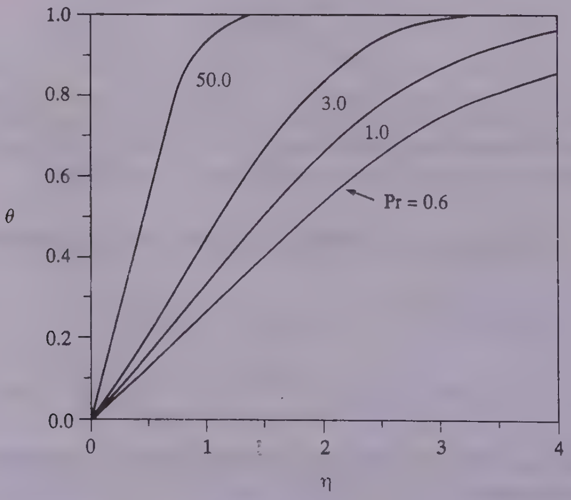

Figure 10-2 Temperature profiles for the laminar constant-property boundary layer, with constant free-stream velocity and constant surface temperature.

the Prandtl number result in a thermal boundary thickness greater than the momentum boundary-layer thickness, while high values of the Prandtl number result in thermal boundary-layer thickness smaller than the momentum boundary-layer thickness.

Simple closed-form solutions can easily be obtained for fluids whose Prandtl number is either very high or very low.

For very low Prandtl numbers the thermal boundary layer will develop very much faster than the velocity boundary layer, and little error will be introduced if the velocity everywhere in the thermal boundary layer is assumed to be the free-stream velocity u_∞. If we transpose Eq. (10-4) and differentiate with respect to η, we obtain

$$\frac{d(\theta/\theta')''}{d\eta} + \frac{\Pr}{2}\zeta' = 0$$

But $\zeta' = u/u_\infty$. If u is everywhere equal to u_∞ then $\zeta' = 1$. Thus

$$\frac{d(\tau''/\tau')}{d\eta} + \frac{\Pr}{2} = 0$$

This equation can now be integrated three times with respect to η. An additional necessary boundary condition is that $\theta''(0) = 0$, which can be obtained from the original partial differential equation (10-2), noting that at the surface $v = 0$ and $\partial\theta/\partial x = 0$. Carrying through as before, we obtain the following for the local Nusselt number:

$$\text{Nu}_x = 0.565\,\Pr^{1/2}\,\text{Re}_x^{1/2} \quad \text{for } \Pr \ll 1 \tag{10-11}$$

When the Prandtl number is very high, the velocity boundary layer will be very much thicker than the thermal boundary layer. If we assume that the thermal boundary layer is entirely within the part of the velocity boundary layer in which the velocity profile is approximately linear, we can get a simple solution to Eq. (10-4). From Table 9-1 we note that

$$\zeta''(0) = 0.3321$$

Then letting $\zeta'' = \zeta''(0)$ in the region of interest and integrating twice with respect to η, we get

$$\zeta = \frac{0.3321}{2}\eta^2$$

Substituting in Eq. (10-4) and completing the integration, we obtain

$$\text{Nu}_x = 0.339\,\Pr^{1/3}\,\text{Re}_x^{1/2} \quad \text{for } \Pr \gg 1 \tag{10-12}$$

Equation (10-12) corresponds closely to the exact solution for $\Pr \geq 10$.

Note that these solutions can also be expressed in terms of a Stanton number, since Nu = St Pr Re. Thus Eq. (10-10) becomes

$$\text{St}\,\Pr^{2/3} = 0.332\,\text{Re}_x^{-1/2} \tag{10-13}$$

The heat-transfer coefficient h decreases in the flow direction as the boundary layer becomes thicker. As $x \to 0$, on the other hand, h becomes indefinitely large, since the temperature gradient at the surface is infinite at $x = 0$.

Equation (10-10), or Eq. (10-13), can be used to evaluate the local heat-transfer rate at any point along the plate, but often we are interested in the total heat transfer. From each of the previous solutions we note that

$$h = Cx^{-1/2}$$

To calculate total heat-transfer rates, we would like a mean conductance with respect to x. Thus

$$h_m = \frac{1}{x}\int_0^x h\,dx = \frac{C}{x}\int_0^x x^{-1/2}\,dx = 2h \tag{10-14}$$

Then the complete result for the mean conductance is

$$\mathrm{Nu}_m = 0.664\,\mathrm{Pr}^{1/3}\,\mathrm{Re}_x^{1/2} \tag{10-15}$$

or

$$\mathrm{St}_m\,\mathrm{Pr}^{2/3} = 0.664\,\mathrm{Re}_x^{-1/2}$$

Equations (10-13) and (10-15) are frequently referred to as the *Pohlhausen solutions.*

It is sometimes convenient to be able to express the Stanton number as a function of a Reynolds number based on *enthalpy thickness* rather than distance x along the surface. The *energy integral equation* (5-24) is applicable to this particular case. If Eq. (10-13) is substituted into Eq. (5-24), and the equation is then integrated, a relation between enthalpy thickness and distance is obtained. Substituting this result back into Eq. (10-13) yields

$$\mathrm{St}\,\mathrm{Pr}^{4/3} = 0.2204/\mathrm{Re}_{\Delta_2} \tag{10-16}$$

FLOW WITH $u_\infty = Cx^m$ ALONG A CONSTANT-TEMPERATURE SEMI-INFINITE PLATE

For this problem Eq. (4-39) is again applicable, and since the temperature boundary conditions are the same, Eq. (10-2) with the indicated boundary conditions is again applicable. Since similarity solutions were obtained for the momentum equation, it might be expected that similarity solutions would be obtained for the energy equation. Using the same substitution of variables as above, the energy equation is transformed to an ordinary differential equation similar to Eq. (10-4), but with Pr replaced by Pr $(m + 1)$. The solution becomes Eq. (10-8) with Pr replaced by Pr $(m + 1)$. The solution for ζ is obtained from the appropriate wedge solution of Chap. 8, and a few of the results of this calculation by Eckert[1] are given in Table 10-2.

It is of interest to evaluate the mean conductance along the plate and compare it with the local conductance as tabulated above. For any value of m and Pr

Table 10-2 Values of $\mathrm{Nu}_x\,\mathrm{Re}_x^{-1/2}$ for various Prandtl numbers; heat transfer to the laminar constant-property boundary layer (T_∞, $T_s = \text{const}$; $u_\infty = Cx^m$)

	Pr				
m	0.7	0.8	1.0	5.0	10.0
−0.0753	0.242	0.253	0.272	0.457	0.570
0	0.292	0.307	0.332	0.585	0.730
0.111	0.331	0.348	0.378	0.669	0.851
0.333	0.384	0.403	0.440	0.792	1.013
1.0	0.496	0.523	0.570	1.043	1.344
4.0	0.813	0.858	0.938	1.736	2.236

the results for the local Nusselt number are given in Table 10-2 in the form

$$\mathrm{Nu}_x\,\mathrm{Re}_x^{-1/2} = \text{const}$$

from which

$$\frac{hx}{k}\left(\frac{xu_\infty}{\nu}\right)^{-1/2} = \text{const}, \qquad h = \frac{(\text{const})kx^{-1/2}u_\infty^{1/2}}{\nu^{1/2}}$$

But for the wedge problem $u_\infty = Cx^m$. Then

$$h = \frac{(\text{const})k}{\nu^{1/2}}x^{(m-1)/2}$$

Note that for $m = 1$, the two-dimensional stagnation point, h is a constant and does not vary with x. Since all temperature profiles are similar, a constant h can only mean that the thermal boundary layer is of constant thickness for $m = 1$. Note that for $m < 1$ (including negative m and $m = 0$, the flat-plate case), h starts indefinitely large at $x = 0$ and decreases along the plate. For $m > 1$, h starts at zero and increases with x.

The mean conductance h_m from $x = 0$ to x is defined as

$$h_m = \frac{1}{x}\int_0^x h\,dx$$

Then

$$h_m = \frac{1}{x}\int_0^x \frac{Ck}{\nu^{1/2}}x^{(m-1)/2}\,dx = \frac{2}{m+1}\frac{Ck}{\nu^{1/2}}x^{(m-1)/2}$$

Thus

$$\frac{h_m}{h} = \frac{2}{m+1} \tag{10-17}$$

For $m = 1$ and a Prandtl number not too far removed from 1 the Nusselt number varies as about the 0.4 power of the Prandtl number, so that to a good approximation the solution for $m = 1$ may be expressed as

$$\mathrm{Nu}_x = 0.57\,\mathrm{Re}_x^{1/2}\,\mathrm{Pr}^{0.4} \tag{10-18}$$

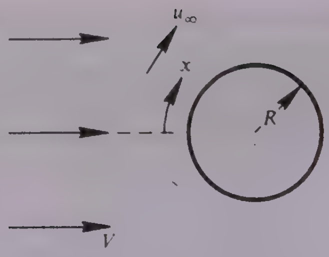

Figure 10-3 Nomenclature for flow normal to a cylinder or sphere.

By a transformation[†] of the coordinate system it is possible to obtain a similar solution for a three-dimensional axisymmetric stagnation point such as occurs as the nose of a blunt-nosed axisymmetric body[3]:

$$\mathrm{Nu}_x = 0.76\,\mathrm{Re}_x^{1/2}\,\mathrm{Pr}^{0.4} \tag{10-19}$$

In order to make use of either Eq. (10-18) or Eq. (10-19), it is necessary to know the variation of free-stream velocity in the vicinity of the stagnation point. In the general case this must be evaluated from the applicable potential flow solution for the region outside the boundary layer. However, a good approximation for the stagnation point for any rounded-nosed two-dimensional or axisymmetric body may be obtained from the potential flow solutions for flow normal to a cylinder and a sphere, respectively. For a cylinder the velocity, referring to Fig. 10-3, is

$$u_\infty = \frac{2Vx}{R} \quad \text{for small } \frac{x}{R} \tag{10-20}$$

Similarly, for the sphere

$$u_\infty = \frac{3Vx}{2R} \quad \text{for small } \frac{x}{R} \tag{10-21}$$

Substituting Eq. (10-20) into Eq. (10-18), and Eq. (10-21) into Eq. (10-19), it is found that in both cases x cancels (indicating, as we have already seen, that the conductance is constant in the stagnation region), and we can re-form the Nusselt numbers and Reynolds numbers with R as the length dimension and V the velocity, yielding

$$\mathrm{Nu}_R = 0.81\,\mathrm{Re}_R^{1/2}\,\mathrm{Pr}^{0.4} \tag{10-22}$$

for the two-dimensional stagnation point and

$$\mathrm{Nu}_R = 0.93\,\mathrm{Re}_R^{1/2}\,\mathrm{Pr}^{0.4} \tag{10-23}$$

for the axisymmetric stagnation point.

[†] Mangler transformation; see Ref. 2, p. 235.

Equations (10-22) and (10-23) can now be used as an approximation for the stagnation-point heat transfer for any rounded-nose blunt body by simply using the radius of curvature at the nose for R and the oncoming velocity for V.

Making use of the energy integral equation, Eq. (10-19) for the axisymmetric stagnation point can also be expressed in terms of the local *enthalpy thickness* Reynolds number:

$$\mathrm{St} = 0.45/\mathrm{Re}_{\Delta_2} \quad (\text{for } \mathrm{Pr} = 0.7) \tag{10-24}$$

FLOW ALONG A CONSTANT-TEMPERATURE SEMI-INFINITE PLATE WITH INJECTION OR SUCTION

It was seen in Chap. 8 that similar solutions to the momentum equation of the boundary layer are obtainable for v_s nonzero (normal velocity at the surface) for $u_\infty = Cx^m$ provided that v_s varies in the following manner along the surface:

$$v_s \propto x^{(m-1)/2}$$

The differential equation is unchanged; only the boundary conditions are different. The same is true of the energy differential equation, except that the boundary conditions are also unchanged; that is, Eq. (10-4) is again applicable, as well as its symbolic solution, Eqs. (10-8) and (10-9). However, for $m \neq 0$, Pr must be replaced by $\mathrm{Pr}(m+1)$ as discussed previously in connection with the wedge solutions. It is only necessary to employ the appropriate values of $\zeta(\eta)$ from the solutions to the momentum equation for various values of the blowing parameter $v_s \mathrm{Re}_x^{1/2}/u_\infty$.

Some of the available results are given in Tables 10-3 and 10-4.[4, 8.23]

Solutions of the axisymmetric stagnation point can be deduced again by employing the Mangler transformation. Some results are given in Table 10-5.[9]

Examination of the Nusselt numbers tabulated in Tables 10-3 to 10-5 shows that injection causes a decrease in the heat-transfer rate while suction increases

Table 10-3 Values of $\mathrm{Nu}_x \mathrm{Re}_x^{-1/2}$ for various Prandtl numbers and rates of blowing or suction; heat transfer to the laminar constant-property boundary layer ($T_\infty, T_s, u_\infty = \text{const}$)

$\frac{v_s}{u_\infty}\mathrm{Re}_x^{1/2}\left(\frac{2}{m+1}\right)^{1/2}$	**Pr = 0.7**	**Pr = 0.8**	**Pr = 1.0**
−2.50	1.850	2.097	2.59
−0.750	0.772	0.797	0.945
−0.250	0.429	0.461	0.523
0	0.292	0.307	0.332
0.250	0.166	0.166	0.165
0.375	0.107	0.103	0.0937
0.500	0.0517	0.0458	0.0356
0.619			0

Table 10-4 Values of $\mathrm{Nu}_x \mathrm{Re}_x^{-1/2}$ for various rates of blowing or suction and various values of m; heat transfer to the laminar constant-property boundary layer (T_∞, $T_s = \text{const}$; $\mathrm{Pr} = 0.7$)

	m							
$\dfrac{v_s}{u_\infty}\mathrm{Re}_x^{1/2}\left(\dfrac{2}{m+1}\right)^{1/2}$	**−0.0476**	**−0.0244**	**0**	**0.0256**	**0.0526**	**0.111**	**0.333**	**1**
−5	2.489	2.489	2.551	2.583	2.617	2.689	2.946	3.61
−2	1.108	1.108	1.136	1.151	1.167	1.2	1.319	1.622
−1	0.674	0.676	0.695	0.706	0.717	0.74	0.819	1.016
−0.5	0.468	0.472	0.487	0.497	0.506	0.526	0.59	0.741
0	0.267	0.278	0.293	0.303	0.313	0.331	0.384	0.496
0.1	0.226	0.24	0.256	0.267	0.277	0.296	0.347	0.452
0.2	0.182	0.202	0.22	0.231	0.243	0.261	0.311	0.409
0.3		0.164	0.185	0.198	0.209	0.228	0.277	0.368
0.4		0.124	0 15	0.166	0.178	0.197	0.245	0.33
0.5		0.0687	0.117	0.135	0.148	0.168	0.214	0.293
0.6			0.0849	0.106	0.12	0.141	0.186	0.259
0.8			0.024	0.0569	0.0727	0.0938	0.135	0.198
1				0.023	0.0376	0.057	0.0937	0.146

Table 10-5 Values of $\mathrm{Nu}_x \mathrm{Re}_x^{-1/2}$ for various rates of blowing for the axisymmetric stagnation point; heat transfer to the laminar constant-property boundary layer (T_∞, $T_s = \text{const}$; $\mathrm{Pr} = 0.7$)

$\dfrac{v_s}{u_\infty}\sqrt{\dfrac{\rho u_\infty x}{\mu}}$	0	0.567	1.154
$\mathrm{Nu}\,\mathrm{Re}_x^{-1/2}$	0.664	0.419	0.227

heat transfer. Thus, injection can be used as a means for cooling surfaces exposed to extremely hot gases such as rocket nozzles or rocket vehicle nose cones. Note that these solutions contain the condition that the fluid being injected is the same as the free-stream fluid, and that the temperature of the injected fluid is at the surface temperature. For suction the same is also true, because a boundary condition is that the fluid immediately adjacent to the surface is at surface temperature. As injection is increased, the Nusselt number ultimately become zero, which simply means that the boundary layer is completely blown off so that the fluid temperature gradient at the surface is zero. If the suction rate is increased indefinitely, the heat-transfer rate ultimately becomes equal to the change of enthalpy of the fluid sucked in, since it is changed to surface temperature right at the surface. The problem of injection of a fluid *different* from the free-stream fluid becomes one of mass diffusion in addition to heat transfer. The solution to the mass-diffusion problem is based on the same basic similarity solutions as presented here, but the whole problem must be cast in a somewhat different form.

In Chap. 19 this same problem is formulated in a different manner, with the results presented in Eq. (19-7) and Table 19-2 actually including all of Tables 10-3 to 10-5 as well as other interpolated values of the parameters.

NONSIMILAR THERMAL BOUNDARY LAYERS

The previous solutions have all been based on the energy and momentum differential equations of the boundary layer, but only those particular boundary conditions leading to similarity solutions have been considered. A comprehensive set of solutions to the laminar boundary-layer similarity equations for a perfect gas is given by Dewey and Gross.[10] As with the momentum boundary layer, several classes of solution methods exist for solving the nonsimilar thermal boundary-layer problem. The *first* class is a numerical solution whereby the momentum and energy differential equations are finite-differenced and then integrated. With this method, any number of other boundary conditions can be handled. The *second* class comprises the approximate boundary-layer solutions employing the energy integral equation. The *third* class of solutions employs the concept of local similarity and local nonsimilarity. This method is described by Sparrow and Yu.[11] The *fourth* class of solutions employs the concept of linear superposition similar to that developed for heat transfer in tube flow. In the following sections methods belonging to the second and fourth classes will be developed.

CONSTANT FREE-STREAM VELOCITY FLOW ALONG A SEMI-INFINITE PLATE WITH UNHEATED STARTING LENGTH

As an example of the use of the energy integral equation of the boundary layer, the laminar incompressible boundary layer on a flat plate with no pressure gradient is solved for the case where heating starts at a point $x = \xi$ on the plate, rather than $x = 0$ where the hydrodynamic boundary layer starts. A quite satisfactory approximate solution may be obtained using integral methods.[12] Later the result is used to solve the laminar boundary layer on a flat plate with no pressure gradient for the case where the surface temperature varies in an arbitrary manner along the surface.

The hydrodynamic and thermal boundary layers will build up on the plate as shown in Fig. 10-4. It is assumed that the thermal boundary layer is always

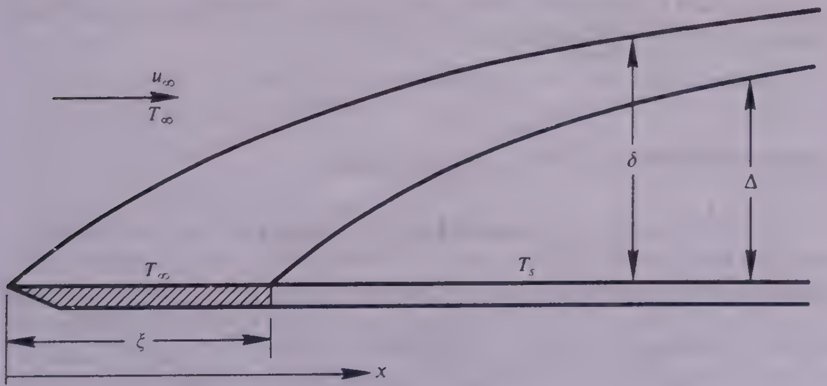

Figure 10-4 Boundary-layer development on a plate with an unheated starting length.

thinner than the hydrodynamic boundary layer (the implications of this assumption will become apparent later).

In Chap. 8 a reasonably good solution to the hydrodynamic boundary layer under these conditions was obtained using a cubic parabola to approximate the velocity profile:

$$\frac{u}{u_\infty} = \frac{3}{2}\frac{y}{\delta} - \frac{1}{2}\left(\frac{y}{\delta}\right)^3$$

A reason for choosing the cubic parabola was that it yields a zero second derivative at the surface, a condition demanded by the boundary-layer differential equation. The same condition obtains for the energy differential equation (10-2), suggesting that a cubic parabola might also be satisfactory for the thermal boundary layer. On this basis, let

$$\theta = T_s - T, \qquad \theta_s = T_s - T_\infty$$

and let

$$\frac{\theta}{\theta_s} = \frac{3}{2}\frac{y}{\Delta} - \frac{1}{2}\left(\frac{y}{\Delta}\right)^3 \tag{10-25}$$

As is characteristic of the integral methods, the thermal boundary layer is treated as if it had a finite thickness Δ, whereas in reality it is recognized that this is not the case. The assumption of a finite thickness is one of the idealizations of the method.

Equations (9-32) and (10-25) can now be used to develop an expression for the enthalpy thickness of the thermal boundary layer Δ_2 by simply substituting into Eq. (5-15) and integrating. The integration need be carried through only the thermal boundary layer, because the integrand is zero for $y > \Delta$. Thus

$$\Delta_2 = \frac{3}{20}\frac{\Delta^2}{\delta} - \frac{3}{280}\frac{\Delta^4}{\delta^3}$$

The ratio of the thermal and hydrodynamic boundary-layer thicknesses at any point x is now defined as

$$r = \frac{\Delta}{\delta}, \qquad \Delta = r\delta$$

Making this substitution for Δ and simplifying,

$$\Delta_2 = 3\delta\left(\frac{1}{20}r^2 - \frac{1}{280}r^4\right)$$

from which we obtain the following for $d\Delta_2/dx$:

$$\frac{d\Delta_2}{dx} = 3\delta\left(\frac{1}{10}r - \frac{1}{70}r^3\right)\frac{dr}{dx} + 3\left(\frac{1}{20}r^2 - \frac{1}{280}r^4\right)\frac{d\delta}{dx}$$

If $r < 1$, the second term in each parenthetical expression is small, and we obtain, approximately,

$$\frac{d\Delta_2}{dx} = \frac{3\delta r}{10}\frac{dr}{dx} + \frac{3r^2}{20}\frac{d\delta}{dx}$$

The applicable form of the energy integral equation is Eq. (5-21), and the heat-flux term $\dot{q}_s''$ can be expressed in terms of the temperature gradient at the surface. Thus

$$\frac{d\Delta_2}{dx} = \frac{\dot{q}_s''}{\rho u_\infty c(T_s - T_\infty)} = \frac{-k(\partial T/\partial y)_s}{\rho u_\infty c(T_s - T_\infty)}$$

Substituting these expressions for $d\Delta_2/dx$ and evaluating the gradient at the surface from Eq. (10-25), we finally obtain the following ordinary differential equation:

$$2r^2\delta^2\frac{dr}{dx} + r^3\delta\frac{d\delta}{dx} = \frac{10\alpha}{u_\infty}, \qquad \alpha = \frac{k}{\rho c}$$

Note that δ and $\delta\, d\delta/dx$ are already available from the earlier solution of the hydrodynamic boundary layer in Chap. 9, Eq. (9-33). Substituting for these terms, we obtain the following ordinary differential equation for r, noting that $\nu/\alpha = \text{Pr}$:

$$r^3 + 4r^2x\frac{dr}{dx} = \frac{13}{14}\frac{1}{\text{Pr}}$$

This differential equation can readily be solved to yield

$$r^3 = Cx^{-3/4} + \frac{13}{14}\frac{1}{\text{Pr}}$$

The constant is evaluated from the boundary conditions, $r = 0$ at $x = \xi$. The final result for r is

$$r = \frac{\text{Pr}^{-1/3}}{1.026}\left[1 - \left(\frac{\xi}{x}\right)^{3/4}\right]^{1/3} \tag{10-26}$$

Note that for no unheated starting length ($\xi = 0$), the ratio of boundary-layer thicknesses becomes

$$r = \frac{1}{1.026\,\text{Pr}^{1/3}} \tag{10-27}$$

At $\text{Pr} = 1$ the two boundary layers have close to the same thickness; at high Prandtl numbers the hydrodynamic boundary layer is thicker than the thermal boundary layer; at low Prandtl numbers the thermal boundary layer is evidently the thicker, but the solution is not applicable for this situation because Δ was assumed to be always less than δ. Thus care must be exercised in using this solution for Prandtl numbers below 1, although in the gas Prandtl number range

(0.5–1.0) it is applicable over a reasonable range. For example, for $\mathrm{Pr} = 0.7$, $r \le 1$ for $0.2 < \xi/x < 1$. As is seen below, even for $\xi/x = 0$ the final solution for the Nusselt number is very close to the known exact solution in the gas range, so that it would appear that the entire solution is a very good approximation in this Prandtl number range.

The heat-transfer rate at the surface and a heat-transfer coefficient can now be evaluated from the assumed temperature profile, since δ and r are now known:

$$\dot{q}_s'' = -k\left(\frac{\partial T}{\partial y}\right)_s = h\theta_s$$

Substituting Eq. (10-25) for θ, Eq. (9-33) for δ, and Eq. (10-26) for r, and solving for h, we get

$$h = \frac{0.332k\,\mathrm{Pr}^{1/3}}{\sqrt{\nu x/u_\infty}[1 - (\xi/x)^{3/4}]^{1/3}}$$

A local Nusselt number can then be formed, and the final result is

$$\mathrm{Nu}_x = \frac{0.332\,\mathrm{Pr}^{1/3}\,\mathrm{Re}_x^{1/2}}{[1 - (\xi/x)^{3/4}]^{1/3}} \tag{10-28}$$

For the case of no unheated starting length ($\xi = 0$), Eq. (10-28) becomes

$$\mathrm{Nu}_x = 0.332\,\mathrm{Pr}^{1/3}\,\mathrm{Re}_x^{1/2} \tag{10-29}$$

The result is seen to be identical to the exact solution, Eq. (10-10).

This development provides a striking example of the power of the integral methods to yield quite adequate solutions for a problem where an exact solution might be considerably more difficult. Equation (10-28) is used later to build up flat-plate laminar-boundary-layer solutions for any type of surface-temperature variation rather than just the constant surface temperature that had to be assumed in the above analysis.

CONSTANT FREE-STREAM VELOCITY FLOW ALONG A SEMI-INFINITE PLATE WITH ARBITRARILY SPECIFIED SURFACE TEMPERATURE

All the boundary-layer solutions considered so far have been for either a constant surface temperature or an unheated starting length followed by a step in surface temperature to a constant surface temperature. The method of superposition can be used in the same manner as for tube flow to develop heat-transfer solutions for the boundary layer for an arbitrary surface-temperature variation because of the linearity of the energy differential equation of the boundary layer, Eq. (10-2).

Let $\theta(\xi, x, y)$ be a solution to Eq. (10-2) for constant-property, constant free-stream velocity flow along a flat plate for the step-function boundary condition

$T_s = T_\infty$ for $x < \xi$, $T_s =$ constant (different from T_∞) for $x > \xi$. Then θ will be defined such that

$$\frac{T_s - T}{T_s - T_\infty} = \theta(\xi, x, y)$$

Then, by following the same line of reasoning as in the tube flow problem, a solution to Eq. (4-39) for any arbitrary variation in surface temperature T_s, but with free-stream temperature constant, is

$$T - T_\infty = \int_0^x [1 - \theta(\xi, x, y)] \frac{dT_s}{d\xi}\, d\xi + \sum_{i=1}^{k} [1 - \theta(\xi_i, x, y)]\, \Delta T_{s,i} \tag{10-30}$$

The heat flux from the surface is determined from

$$\dot{q}_s'' = -k \left(\frac{\partial T}{\partial y}\right)_s$$

Differentiating Eq. (10-30) with respect to y at $y = 0$, and substituting,

$$\dot{q}_s'' = k \left[\int_0^x \theta_y(\xi, x, 0) \frac{dT_s}{d\xi}\, d\xi + \sum_{i=1}^{k} \theta_y(\xi_i, x, 0)\, \Delta T_{s,i} \right]$$

For the single-step-function solution,

$$\dot{q}_s'' = -k \left(\frac{\partial T}{\partial y}\right)_{y=0} = k\theta_y(\xi, x, 0)(T_s - T_\infty) = h(T_s - T_\infty)$$

$$h(T_s - T_\infty) = k\theta_y(\xi, x, 0)(T_s - T_\infty)$$

$$\theta_y(\xi, x, 0) = \frac{h(\xi, x)}{k}$$

Thus for arbitrary surface-temperature variation,

$$\dot{q}_s'' = \int_0^x h(\xi, x) \frac{dT_s}{d\xi}\, d\xi + \sum_{i=1}^{k} h(\xi_i, x)\, \Delta T_{s,i} \tag{10-31}$$

where $h(\xi, x)$ is the local unit conductance from the single-step-function solution.

The previously derived step-function solution for the laminar boundary layer, Eq. (10-28), can be rewritten as

$$h(\xi, x) = \frac{0.332k}{x} \mathrm{Pr}^{1/3} \mathrm{Re}_x^{1/2} \left[1 - \left(\frac{\xi}{x}\right)^{3/4} \right]^{-1/3} \tag{10-32}$$

Equation (10-32) substituted into Eq. (10-31) then provides the method for the calculation of heat-transfer rates from a flat plate with a laminar boundary layer and any axial surface-temperature distribution. It is necessary to insert only the desired $dT_s/d\xi$ as a function of ξ in the integral and any abrupt changes in surface temperature in the summation.

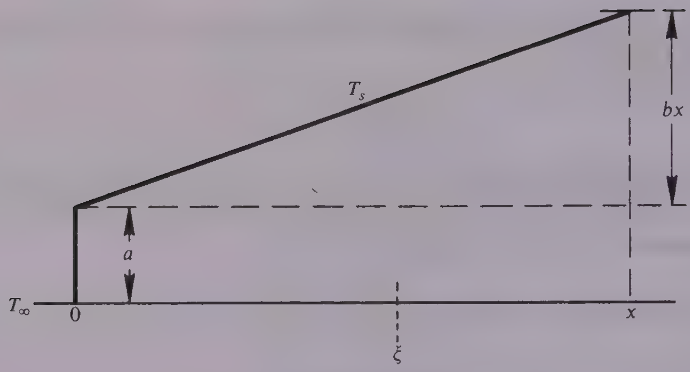

Figure 10-5 Example of a step–ramp surface temperature.

As an example of the method, consider a plate with a step in surface temperature at the leading edge, followed by a linear surface-temperature variation (Fig. 10-5). Then

$$T_s = T_\infty + a + bx$$

$$\frac{dT_s}{dx} = b = \frac{dT_s}{d\xi}$$

Equation (10-31) can now be evaluated. There is only one step in surface temperature, at $\xi = 0$, so there is only one term in the summation. Thus

$$\dot{q}_s'' = \frac{0.332k}{x}\mathrm{Pr}^{1/3}\,\mathrm{Re}_x^{1/2}\left\{\int_0^x \left[1-\left(\frac{\xi}{x}\right)^{3/4}\right]^{-1/3} b\,d\xi + a\right\} \tag{10-33}$$

Problems of this sort lead typically to integrals of the type

$$\int_0^1 Z^{m-1}(1-Z)^{n-1}\,dZ = \beta(m,n) \tag{10-34}$$

where the beta function

$$\beta(m,n) = \frac{\Gamma(m)\Gamma(n)}{\Gamma(m+n)} \tag{10-35}$$

for $m > 0$ and $n < \infty$.

The following change of variable in the integral of Eq. (10-33) transforms the integral into the form of the beta function, Eq. (10-34):

$$u = 1 - \left(\frac{\xi}{x}\right)^{3/4}$$

The integral is then readily evaluated by use of beta function tables (see App. C), giving

$$\dot{q}_s'' = 0.332\frac{k}{x}\mathrm{Pr}^{1/3}\,\mathrm{Re}_x^{1/2}(1.612bx + a)$$

A local heat-transfer coefficient and a local Nusselt number are then defined, leading to the final result

$$\mathrm{Nu}_x = \frac{0.332\,\mathrm{Pr}^{1/3}\,\mathrm{Re}_x^{1/2}(1.61bx + a)}{a + bx} \tag{10-36}$$

For $b = 0$ this equation reduces to the constant-surface-temperature solution. Note that for $a = 0$ the solution reduces to a similar expression, but the Nusselt number is always 61 percent greater than for a constant surface temperature.[†] The importance of taking into consideration any variation of surface temperature is then apparent.

A solution for the case where the surface temperature can be expressed as a power series is also readily obtainable by the same methods. If the surface temperature is expressed by

$$T_s = T_\infty + A + \sum_{n=1}^{\infty} B_n x^n$$

the heat flux at any point on the plate may be expressed by

$$\dot{q}_s'' = 0.332\frac{k}{x}\mathrm{Pr}^{1/3}\,\mathrm{Re}_x^{1/2}\left(\sum_{n=1}^{\infty} nB_n\frac{4}{3}x^n\beta_n + A\right) \tag{10-37}$$

where

$$\beta_n = \frac{\Gamma\left(\frac{4}{3}n\right)\Gamma\left(\frac{2}{3}\right)}{\Gamma\left(\frac{4}{3}n + \frac{2}{3}\right)}$$

A heat-transfer coefficient and a Nusselt number could be easily evaluated, but the Nusselt number begins to lose its usefulness when the surface temperature varies markedly.

CONSTANT FREE-STREAM VELOCITY FLOW ALONG A SEMI-INFINITE PLATE WITH ARBITRARILY SPECIFIED SURFACE HEAT FLUX

In many cases of practical interest the heat-flux distribution is given and the surface-temperature distribution is to be found. For certain special cases the heat-transfer coefficient resulting from a step-function solution can be put in the form

$$h(\xi, x) = f(x)(x^\gamma - \xi^\gamma)^{-\alpha}$$

For these cases the solution for heat transfer can be modified to yield the surface temperature as a function of heat input.[13] The result is in the form

$$T_s(x) - T_\infty = \int_0^x \dot{q}_s''(\xi)g(\xi, x)\,d\xi \tag{10-38}$$

[†] For $\mathrm{Pr} = 0.7$ this case leads to $\mathrm{Nu}_x = 0.475\,\mathrm{Re}_x^{1/2}$. An exact similarity solution can be obtained for this case, leading to $\mathrm{Nu}_x = 0.4803\,\mathrm{Re}_x^{1/2}$, differing by only 1.1 percent. This provides some indication of the accuracy of this approximate procedure.

where $\dot{q}_s''(\xi) = \dot{q}_s''(x)$ is the arbitrarily prescribed surface heat flux and $g(\xi, x)$ is a modification of the function $h(\xi, x)$ found by the relation

$$g(\xi, x) = \frac{(x^\gamma - \xi^\gamma)^{\alpha-1}\gamma\xi^{\gamma-1}}{f(\xi)(-\alpha)!\,(\alpha-1)!} \tag{10-39}$$

For a laminar boundary layer on a flat plate the step-function solution previously obtained is of the requisite form, and thus $g(\xi, x)$ can be readily evaluated from Eq. (10-28). The result is

$$g(\xi, x) = \frac{\mathrm{Pr}^{-1/3}\,\mathrm{Re}_x^{-1/2}}{6\Gamma\left(\frac{4}{3}\right)\Gamma\left(\frac{5}{3}\right)(0.332)\,k}\left[1 - \left(\frac{\xi}{x}\right)^{3/4}\right]^{-2/3} \tag{10-40}$$

Substituting Eq. (10-40) into Eq. (10-38) yields an expression that describes the surface temperature of a plate with any arbitrary flux variation:

$$T_s(x) - T_\infty = \frac{0.623}{k}\mathrm{Pr}^{-1/3}\,\mathrm{Re}_x^{-1/2}\int_0^x \left[1 - \left(\frac{\xi}{x}\right)^{3/4}\right]^{-2/3} \dot{q}_s''(\xi)\,d\xi \tag{10-41}$$

An obvious illustrative example is the case of constant heat rate per unit area. If $\dot{q}_s''$ = constant in Eq. (10-41), the integral is easily converted to the form of the beta function and can then be evaluated. The surface temperature is then evaluated, and a convection conductance and a Nusselt number can be defined. The result is

$$\mathrm{Nu}_x = 0.453\,\mathrm{Pr}^{1/3}\,\mathrm{Re}_x^{1/2} \tag{10-42}$$

This result indicates a heat-transfer coefficient about 36 percent higher than at the comparable point on a plate with constant surface temperature, Eq. (10-10). Recall that the constant-surface-temperature solution was obtained using similarity analysis. For the constant-heat-flux boundary condition, no similarity solutions exist.

It is now of interest to employ the *energy integral equation* to determine the enthalpy thickness Δ_2 for this case, and then express the Stanton number as a function of *enthalpy thickness* Reynolds number. The following result is obtained:

$$\mathrm{St}\,\mathrm{Pr}^{4/3} = 0.205/\mathrm{Re}_{\Delta_2} \tag{10-43}$$

Note that there is very little difference from the comparable result obtained for the case of a *constant surface temperature*, Eq. (10-16). In other words, when a *local* length parameter Δ_2 is used, the past history of the thermal boundary layer is of less importance. This is going to provide the key to an approximate procedure, employing the energy integral equation, that will be used later.

FLOW OVER A CONSTANT-TEMPERATURE BODY OF ARBITRARY SHAPE

A rigorous calculation of heat transfer through a laminar boundary layer on a body of arbitrary shape involves first solving the momentum equation to establish the velocity field and then solving the energy equation. This can be done to any degree of precision desired by using numerical finite-difference procedures,[14] or approximate solutions can be obtained based on the momentum and energy integral equations developed in Chap. 5.

A still simpler approach, but one introducing a greater degree of approximation, involves a solution to *either* the momentum or the energy integral equation, but not both. The most successful of the procedures, for a constant surface temperature but with free-stream velocity arbitrarily variable, is based on the energy integral equation.

Eckert[1] proposed a scheme, later modified by others, wherein it is assumed that the rate of growth of any of the thermal boundary-layer thicknesses Δ is a function of local parameters alone, that is,

$$\frac{d\Delta}{dx} = f\left(\Delta, u_\infty, \frac{du_\infty}{dx}, \nu, \mathrm{Pr}\right)$$

Actually, any of the thermal boundary-layer thicknesses might be used, but for convenience let us use the conduction thickness: $\Delta_4 = k/h_x$. By dimensional analysis, the variation of Δ_4 can be expressed in nondimensional form as

$$\frac{u_\infty}{\nu}\frac{d\Delta_4^2}{dx} = f\left(\frac{\Delta_4^2}{\nu}\frac{du_\infty}{dx}, \mathrm{Pr}\right) \tag{10-44}$$

The essence of the method lies in the assumption that the function f for an arbitrary variation of free-stream velocity is the same as for the family of wedge flows, since the latter can be readily evaluated via the similarity solutions.

In Table 10-2 there is tabulated, for each particular value of m and Prandtl number,

$$\mathrm{Nu}_x \, \mathrm{Re}_x^{-1/2} = c_1$$

from which

$$h \propto u_\infty^{1/2} x^{-1/2}$$

Employing

$$u_\infty = Cx^m \quad \text{(the wedge condition)}$$

and

$$\Delta_4 = k/h$$

the following expressions can be easily developed for the wedge solutions:

$$\frac{u_\infty}{\nu}\frac{d\Delta_4^2}{dx} = \frac{1-m}{c_1^2} \tag{10-45}$$

$$\frac{\Delta_4^2}{\nu}\frac{du_\infty}{dx} = \frac{m}{c_1^2} \tag{10-46}$$

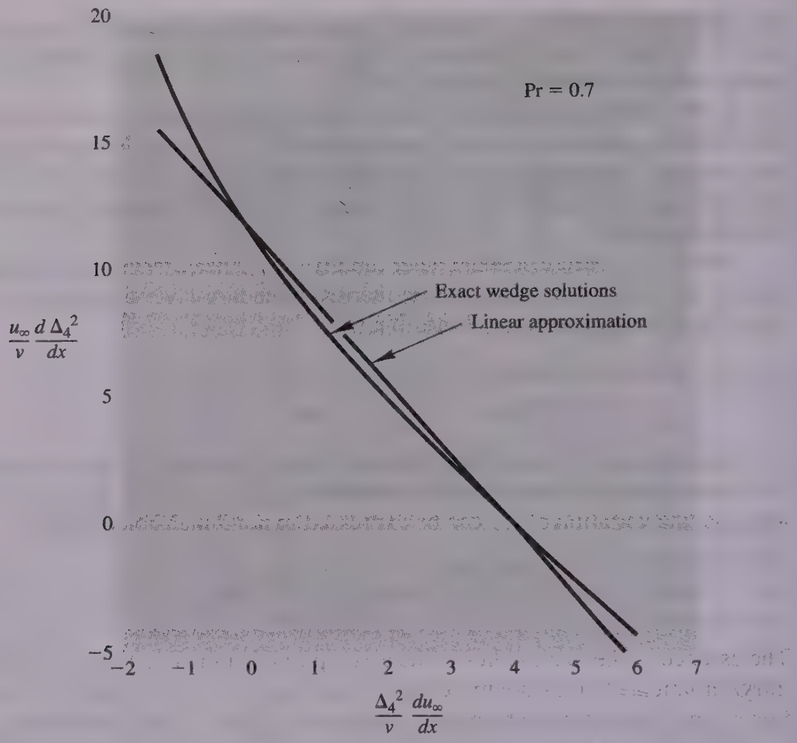

Figure 10-6

For each Prandtl number a plot of Eq. (10-44) can then be prepared from the data in Table 10-2. Such a plot is shown in Fig. 10-6 for Pr = 0.7.

Eckert proposes to solve Eq. (10-44) numerically for any arbitrary free-stream velocity variation employing such a plot of the wedge solutions for the function f; and, of course, this can be readily done. Smith and Spalding[15] propose a further simplification, albeit a grosser approximation, by replacing the curve with a straight line, which leads to a simpler integration procedure. For Pr = 0.7 the following linear relation fits the wedge data exactly for the stagnation point and for the flat plate; it is a fair fit in-between, but begins to depart markedly for strongly decelerating flows, although boundary-layer separation limits the curve in this direction:

$$\frac{u_\infty}{\nu}\frac{d\Delta_4^2}{dx} = 11.68 - 2.87\frac{\Delta_4^2}{\nu}\frac{du_\infty}{dx} \tag{10-47}$$

Equation (10-47) then integrates and reduces to

$$\Delta_4^2 = \frac{11.68\nu\int_0^x u_\infty^{1.87}\,dx}{u_\infty^{2.87}} \tag{10-48}$$

Equation (10-48) can now easily be evaluated for any desired variation of u_∞ with x, so the conduction thickness, and thus the local heat-transfer rate, can be readily calculated. However, before converting Eq. (10-48) to an explicit solution for the local conductance, we can transform the problem from the two-dimensional case to the *axisymmetric* case and thus have a much more useful solution. This is essentially the Mangler transformation.

The integral energy equation (5-18), with $T_s - T_\infty$ and density constant, and with Δ_4 introduced, may be rewritten as

$$\frac{k}{(R\Delta_4)\rho u_\infty c} = \frac{1}{R^2}\frac{d(R\Delta_2)}{dx} - \frac{R\Delta_2}{u_\infty}\frac{1}{R^2}\frac{du_\infty}{dx} \tag{10-49}$$

Now if R is constant, the problem reduces to the two-dimensional problem, and Eq. (10-49) becomes

$$\frac{k}{\Delta_4 \rho u_\infty c} = \frac{d\Delta_2}{dx} + \frac{\Delta_2}{u_\infty}\frac{du_\infty}{dx} \tag{10-50}$$

However, suppose that in Eq. (10-49) we make the following change of variables, where L is some arbitrary reference length:

$$\Delta_4' = \frac{R}{L}\Delta_4, \qquad \Delta_2' = \frac{R}{L}\Delta_2, \qquad dx' = \frac{R^2}{L^2}\,dx$$

Substituting, and noting that L cancels, we obtain

$$\frac{k}{\Delta_4' \rho u_\infty c} = \frac{d\Delta_2'}{dx'} + \frac{\Delta_2'}{u_\infty}\frac{du_\infty}{dx'} \tag{10-51}$$

With this transformation, Eq. (10-51) is identical to the two-dimensional equation (10-50). A solution of the two-dimensional problem can be transformed into a solution to the axisymmetric problem by the same change of variables. In the present case Eq. (10-48) can be considered a solution to Eq. (10-51), and with the indicated change of variables becomes (note that L cancels)

$$R^2\Delta_4^2 = \frac{11.68\nu \int_0^x u_\infty^{1.87} R^2\,dx}{u_\infty^{2.87}}$$

Noting that $\Delta_4 = k/h$. transposing to form a Stanton number, and inserting $\mathrm{Pr} = 0.7$, we obtain

$$\mathrm{St} = 0.418\frac{\nu^{1/2} R u_\infty^{0.435}}{\left(\int_0^x u_\infty^{1.87} R^2\,dx\right)^{0.5}} \tag{10-52}$$

Equation (10-52) has been derived for constant fluid properties. In many applications the fluid density varies markedly in the direction of flow. Examination of the manner in which u_∞ and ρ appear together in the integral energy equation suggests that the following form of Eq. (10-52) should be reasonably accurate for

Table 10-6 Constants in Eq. (10-54) for various Prandtl numbers; heat transfer to the laminar, constant-property boundary layer ($T_\infty, T_s = \text{const}$)

Pr	C_1	C_2	C_3
0.7	0.418	0.435	1.87
0.8	0.384	0.450	1.90
1.0	0.332	0.475	1.95
5.0	0.117	0.595	2.19
10.0	0.073	0.685	2.37

variable-density flow:

$$\text{St} = 0.418 \frac{\mu^{1/2} R G_\infty^{0.435}}{\left(\int_0^x G_\infty^{1.87} R^2\, dx\right)^{0.5}} \tag{10-53}$$

where $G_\infty = \rho u_\infty$.

Equation (10-53) provides a very powerful and simple method for calculating the convection conductance for a laminar boundary layer on a constant-surface-temperature body of revolution with any variation of u_∞ along its surface. For the two-dimensional case R simply cancels. It is found that Eq. (10-53) reduces to the flat-plate solution, Eq. (10-13), and likewise reduces to both the two-dimensional and the axisymmetric stagnation-point solutions, Eqs. (10-18) and (10-19). Thus, as indicated in Fig. 10-6, the method is exact for the flat plate and the stagnation points and is a reasonable approximation for any other case.

This development has been entirely confined to a fluid with a Prandtl number of 0.7, but it should be quite apparent how a similar solution can be obtained for any Prandtl number for which the wedge solutions are available (Table 10-2). The results for the other Prandtl numbers can be expressed in the form

$$\text{St}_x = \frac{C_1 \mu^{1/2} R G_\infty^{C_2}}{\left(\int_0^x G_\infty^{C_3} R^2\, dx\right)^{1/2}} \tag{10-54}$$

where the constants for various Prandtl numbers are given in Table 10-6.

In Chap. 19 this scheme is extended to the blowing and suction problem.

FLOW OVER A BODY OF ARBITRARY SHAPE AND ARBITRARILY SPECIFIED SURFACE TEMPERATURE

The variable-surface-temperature problem for a body over which the free-stream velocity varies must be handled by solving first the momentum equation for the specified free-stream velocity and then the energy equation for the varying surface temperature; thus, it is more difficult than the constant-surface-temperature problem where the free-stream velocity varies. A number of methods are presented in the literature, of which perhaps the most complete is that given by Spalding.[16] But in most applications of this type direct numerical solution of the differential equations of the boundary layer proves to be the more practicable approach; and if fluid properties are not constant, this is even more true. A point is ultimately reached where approximate methods become so complex that it is simpler to seek close-to-exact solutions by numerical integration.

FLOW OVER BODIES WITH BOUNDARY-LAYER SEPARATION

In the presence of a positive pressure gradient in the flow direction (decelerating free-stream velocity) the velocity in the boundary layer decreases in such a way that the velocity gradient at the surface can go to zero. In such cases the entire boundary layer separates from the surface, leaving a region of reversed flow or stall near the surface. Separation can and does frequently occur on smooth, continuous surfaces, and virtually always occurs where there is an abrupt step in the surface.

Detailed flow-field and heat-transfer studies of separated flows have followed the advent of large-memory computers and boundary-layer diagnostic tools such as the laser–Doppler anemometer. Some of the flows of interest are laminar separation bubbles on airfoils, shock-induced separation in supersonic flow, and flow over bluff bodies. Reviews of laminar separated flows are given by Brown and Stewartson[17] and Williams.[18] Two simple bluff-body flows are considered here.

For flow normal to a circular cylinder or flow normal to a sphere, a laminar boundary layer forms on the upstream surface (at least for Reynolds numbers sufficiently small that transition to a turbulent boundary layer does not occur). Calculation of local heat-transfer rates at the stagnation point and over the entire upstream surface can be accomplished by methods already discussed. However, at a point just before the maximum diameter, boundary-layer separation occurs (it occurs somewhat later for a turbulent boundary layer), and over the remainder of the cylinder or sphere the local heat-transfer rate fluctuates as vortices are shed into the wake.

The average conductance over the entire surface (front and rear) has been measured by numerous experimenters. An extensive summary of available data for cylinders in cross flow is given by Morgan.[19] These results can be presented in terms of a Nusselt number based on the cylinder diameter and a Reynolds number based on cylinder diameter and the upstream normal velocity. If the following form of the relation is used, the constants C_1 and C_2 recommended by Morgan for air are as given in Table 10-7:

$$\mathrm{Nu}_D = C_1 \,\mathrm{Re}_D^{C_2} \tag{10-55}$$

Heat transfer with flow past spheres in the Reynolds number range 3600–52,000 has been studied by Raithby and Eckert.[20] They recommend the use of Eq. (10-55) with $C_1 = 0.257$ and $C_2 = 0.588$ if the sphere is supported from behind. For cross-supported spheres the C_1 coefficient increases by 13 percent.

Table 10-7 Constants in Eq. (10-55) for various Reynolds numbers; flow normal to a circular cylinder; air

Re_D	C_1	C_2
10^{-4}–4×10^{-3}	0.437	0.0895
4×10^{-3}–9×10^{-2}	0.565	0.136
9×10^{-2}–1	0.800	0.280
1–35	0.795	0.384
35–5×10^3	0.583	0.471
5×10^3–5×10^4	0.148	0.633
5×10^4–2×10^5	0.0208	0.814

It has been previously noted that for a laminar boundary layer the Nusselt number (for a fixed Reynolds number) varies approximately as $\mathrm{Pr}^{1/3}$, except at very low Pr. Since the boundary layers on the cylinders and spheres under consideration are essentially laminar, Eq. (10-55) for air can be extended to high-Prandtl-number fluids on the basis of this approximation.

There is evidence that the cylinder and sphere behavior is rather sensitive to the turbulence intensity in the upstream flow, and this effect apparently is due to a disturbance of the boundary layer in the vicinity of the upstream stagnation point.[19,20]

Flow normal to *banks* of circular tubes is a configuration extensively used in the construction of heat exchangers. The effect of adjacent and preceding tubes on the behavior of any one tube in the bank is substantial and varies greatly with tube spacing. Extensive data are available, and the reader is referred to Kays and London[21] and to an extensive review by Zukauskas.[22]

The flow passages in high-performance heat exchangers are frequently constructed with extended surface, or fins, and the flow is interrupted in such a way that a laminar boundary layer forms on each fin segment, only to separate and begin again on the next fin. The flow pattern and the heat-transfer mechanism around each fin are very complex and do not lend themselves readily to boundary-layer analysis. Thus the heat-exchanger designer relies on overall experimental data. Data on a few such heat-exchanger surfaces may be found for a large variety in Ref. 21.

PROBLEMS

10-1. Derive Eqs. (10-11), and (10-12) in the text. (See App. C for tables of error and gamma functions.)

10-2. For flow along a plate with constant free-stream velocity and constant fluid properties develop a similarity solution for a constant-temperature plate for a fluid with $\mathrm{Pr} = 0.01$. Compare with the approximate results of Prob. 10-1. Note that numerical integration is required.

10-3. Develop an approximate solution of the energy equation for flow at a two-dimensional stagnation point for a fluid with very low Prandtl number, using the assumption that the thermal boundary layer is very much thicker than the momentum boundary layer. From this, develop an equation for heat transfer at the stagnation point of a circular cylinder in cross flow, in terms of the oncoming velocity and the diameter of the tube.

10-4. Repeat Prob. 10-2 for a two-dimensional stagnation point and compare with the results of Prob. 10-3. The following results from the momentum equation solution for the stagnation point are needed:

η	$\zeta(\eta)$
0	0
0.5	0.12
1.0	0.46
1.5	0.87
2.0	1.36
3.0	2.35
$\eta > 3.0$	$\zeta = \eta - 0.65$

10-5. Consider constant-property flow along a surface with constant free-stream velocity. Let the temperature difference between the surface and the fluid, $T_s - T_\infty$, vary as x^m, where m is a constant. Show that a similarity solution to the energy equation is obtainable under these conditions. Carry out the necessary calculations to obtain the Nusselt number as a function of Reynolds number for $\text{Pr} = 0.7$ and $m = 1$.

10-6. Using the approximate solution developed in the text for a laminar boundary layer with constant free-stream velocity and a simple step in surface temperature at some arbitrary point, develop a solution for $\text{Pr} = 0.7$ and $T_s - T_\infty$ varying directly with x, using superposition theory. Compare with the exact result from Prob. 10-5.

10-7. Consider liquid sodium at 200°C flowing normal to a 2.5-cm-diameter tube at a velocity of 0.6 m/s. Using the results of Prob. 10-3, calculate the "conduction" thickness of the thermal boundary layer at the stagnation point. Calculate the corresponding "shear" thickness of the momentum boundary layer at the stagnation point and discuss the significance of the results.

10-8. Let air at 540°C and 1 atm pressure flow at a velocity of 6 m/s normal to a 2.5-cm-diameter cylinder. Let the cylinder be of a thin-walled porous material so that air can be pumped inside the cylinder and out through the pores in order to cool the walls. Let the cooling air be at 40°C where it actually enters the porous material.

The objective of the problem is to calculate the cylinder surface temperature in the region of the stagnation point for various cooling-air flow rates, expressed as the mass rate of cooling air per square meter of cylinder surface. The problem is to be worked first for no radiation and then assuming that the cylinder surface is a black body radiating to a large surrounding (say a large duct) at 540°C.

The same cooling air could be used to cool the surface internally by convection without passing through the surface out into the main stream. Assuming that the cooling air is again available at 40°C and is ducted away from the surface at surface temperature, calculate the surface temperature as a function of cooling-air rate per square meter of cylinder surface area for this case and compare with the results above.

10-9. Let air at a constant velocity of 7.6 m/s, a temperature of 90°C, and 1 atm pressure flow along a smooth, flat surface. Let the plate be divided into three sections, each 10 cm in flow length. The first 10 cm section is maintained at 40°C, the second at 80°C, and the third at 40°C. Evaluate and plot the heat flux at all points along the 30 cm of plate length, and find the local heat-transfer coefficient.

TEXSTAN can be used to confirm the results of this variable surface-temperature problem. Choose a starting x-location near the leading edge, say 0.1 cm, and pick fluid properties that are appropriate to air, evaluated at the free stream temperature. Use constant fluid properties and do not consider viscous dissipation. The piecewise surface temperature boundary condition is modeled easily in TEXSTAN by providing temperatures at two x locations for each segment, e.g., at $x = 0$, $x = 0.10$, $x = 0.101$, $x = 0.2$, $x = 0.201$, and $x = 0.3$ m. Because TEXSTAN linearly interpolates the surface thermal boundary condition between consecutive x locations, a total of six boundary condition locations is sufficient to describe the surface temperature variation. The initial velocity and temperature profiles (Blasius similarity profiles) can be supplied by using the *kstart*=4 choice in TEXSTAN.

10-10. Repeat Prob. 10-9 but let the surface temperature vary sinusoidally from 40°C at the leading and trailing edges to 80°C at the centerline.

TEXSTAN can be used to confirm the results of this variable surface-temperature problem. For the surface temperature distribution, break up the length of the plate into 10 to 20 segments and evaluate the surface temperature at these x locations. These values then become the variable surface temperature boundary condition. Note that a larger number of points will more closely model the sine function.

10-11. The potential flow solution for the velocity along the surface of a cylinder with flow normal at a velocity V is

$$u_\infty = 2V \sin \theta$$

where θ is measured from the stagnation point. Assuming that this is a reasonable approximation for a real flow on the upstream side of the cylinder, calculate the local Nusselt number as a function of θ for $0 < \theta < \frac{1}{2}\pi$ for a fluid with $\mathrm{Pr} = 0.7$ and prepare a plot. Compare these results with the experimental data for the average Nusselt number around a cylinder. What can you conclude about the heat-transfer behavior in the wake region on the rear surface of the cylinder?

TEXSTAN can be used to confirm the results of this variable free-stream velocity problem. For the velocity distribution, break up the surface length of the cylinder over which the boundary layer flows into at least 20 segments and evaluate the velocity at these x locations. These values then become the variable velocity boundary condition. A larger number of points will more closely model the distribution, which is especially important because this distribution is differentiated to formulate the pressure gradient, as described by Eq. (5-3). Note that TEXSTAN spline-fits these velocity boundary condition values to try to provide a smooth velocity gradient in construction of the pressure gradient, but it is the user's responsibility to have the velocity distribution as smooth as possible. The initial velocity and temperature profiles (Falkner-Skan $m = 1$ similarity profiles, applicable to a cylinder in crossflow) can be supplied by using the *kstart*=6 choice in TEXSTAN.

10-12. The potential flow solution for the velocity along the surface of a sphere with flow normal at a velocity V is

$$u_\infty = \tfrac{3}{2} V \sin \theta$$

Do the same problem as the preceding one for the sphere.

10-13. Let air at a constant velocity of 7.6 m/s, a temperature of −7°C, and 1 atm pressure flow along a smooth, flat surface. The plate is 15 cm long (in the flow direction). The entire surface of the plate is adiabatic except for a 2.5 cm wide strip, located between 5 and 7.5 cm from the leading edge, which is electrically heated so that the heat-transfer rate per unit of area on this strip is uniform. What must be the heat flux from this strip such that the temperature of the surface at the trailing edge of the plate is above 0°C? Plot the temperature distribution along the entire plate surface. Discuss the significance of this problem with respect to wing deicing. (A tabulation of incomplete beta functions, necessary for this solution, is found in App. C)

TEXSTAN can be used to confirm the results of this variable surface heat flux problem. Choose a starting x location near the leading edge, say 0.1 cm, and pick fluid properties that are appropriate to air, evaluated at the free stream temperature. Use constant fluid properties and do not consider viscous dissipation. The piecewise surface heat flux boundary condition is modeled easily in TEXSTAN by providing heat flux values at two x-locations for each segment, e.g., at $x = 0$, $x = 0.05$, $x = 0.0501$, $x = 0.075$, $x = 0.0751$, and $x = 0.15$ m. Because TEXSTAN linearly interpolates the surface thermal boundary condition between consecutive x locations, a total of six boundary condition locations is sufficient to describe the surface heat flux variation. The initial velocity and temperature profiles (Blasius similarity profiles) can be supplied by using the *kstart*=4 choice in TEXSTAN.

10-14. Let air at a constant velocity of 15 m/s, a temperature of 300°C, and 1 atm pressure flow along a smooth, flat surface. Let the first 15 cm of the surface be cooled by some internal means to a uniform temperature of 90°C. How does the surface temperature vary for the next 45 cm?

Hint: Note that the first 15 cm must be treated as a surface-temperature-specified problem, while the last 45 cm must be treated as a surface-heat-flux-specified problem. Because this problem requires two different types of thermal boundary conditions, TEXSTAN is not suitable for this problem.

10-15. Water at 10°C flows from a reservoir through the convergent nozzle shown in Fig. 10-7 into a circular tube. The mass flow rate of the water is 9 g/s. Making

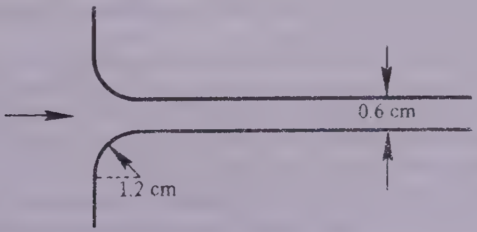

Figure 10-7

a plausible assumption as to the origin of the boundary layer in the nozzle and assuming that the nozzle surface is at a uniform temperature different from 10°C, calculate the heat-transfer coefficient at the throat of the nozzle. How does this compare with the coefficient far downstream in the tube if the tube surface is at a uniform temperature?

TEXSTAN PROBLEMS

10-16. TEXSTAN *analysis of the laminar thermal boundary layer over a flat plate with constant surface temperature and zero pressure gradient*: Choose a starting x-Reynolds number of about 1000 (a momentum Re of about 20) and pick fluid properties that are appropriate to fluids with a Prandtl number = 0.7, 1.0, and 5.0, evaluated at the free stream temperature. Use constant fluid properties and do not consider viscous dissipation. The geometrical dimensions of the plate are 1 m wide (a unit width) by 0.2 m long in the flow direction, corresponding to an ending Re_x of about 2×10^5 (a momentum Re of about 300). Let the velocity boundary condition at the free stream be 15 m/s and let the energy boundary conditions be a free stream temperature of 300 K and a constant surface temperature of 295 K. The initial velocity and temperature profiles appropriate to the starting x-Reynolds number (Blasius similarity profiles) can be supplied by using the *kstart*=4 choice in TEXSTAN.

For each Prandtl number calculate the boundary-layer flow and evaluate the concept of boundary-layer similarity by comparing nondimensional temperature profiles at several x locations to themselves for independence of x. Compare the Nusselt number results based on x-Reynolds number with Eq. (10-10). Convert the Nusselt number to Stanton number and compare the Stanton number results based on x-Reynolds number with Eq. (10-13) and based on enthalpy-thickness Reynolds number with Eq. (10-16). Calculate the Stanton number distribution using energy integral Eq. (5-24) and compare with the TEXSTAN calculations. Feel free to investigate any other attribute of the boundary-layer flow.

10-17. TEXSTAN *analysis of the laminar thermal boundary layer stagnation flow (the Falkner-Skan $m = 1$ case) and constant surface temperature*: Refer to Prob. 9-8 for the plate geometry and the setup of the velocity boundary condition. Pick fluid properties that are appropriate to fluids with a Prandtl number = 0.7, 1.0, and 5.0, evaluated at the free stream temperature. Use constant fluid properties and do not consider viscous dissipation. The energy boundary conditions are a free stream temperature of 300 K and a constant surface temperature of 295 K.

For each Prandtl number calculate the boundary layer flow and evaluate the concept of boundary-layer similarity by comparing nondimensional temperature profiles at several x locations to themselves for independence of x. Compare the Nusselt number results based on x-Reynolds number with Table 10-2. Evaluate the concepts of thermal and velocity profile similarity for $\mathrm{Pr} = 1.0$, examine the development of the momentum and thermal boundary layers, and discuss the validity of $h = \text{const}$ for this case. Convert the Nusselt number to Stanton number, calculate the Stanton number distribution using energy integral

Eq. (5-24) and compare with the TEXSTAN calculations. Also, evaluate the validity of the approximate integral solution, Eq. (10-52). Feel free to investigate any other attribute of the boundary-layer flow.

REFERENCES

1. Eckert, E. R. G.: *VDI-Forschungsh.*, vol. 416, pp. 1–24, 1942.
2. Schlichting, H.: *Boundary Layer Theory*, 6th ed., McGraw-Hill, New York, 1968.
3. Reshotko, E., and C. B. Cohen: NACA (now NASA) TN 3513, Washington, July 1955.
4. Mickley, H. S., R. C. Ross, A. L. Squyers, and W. E. Stewart: NACA TN 3208, Washington, 1954.
5. Emmons, H. W., and D. Leigh: Combustion Aerodynamics Laboratory Report 9, Harvard University, Cambridge, Mass., 1953.
6. Brown, W. B., and P. L. Donoughe: NACA TN 2489, Washington, 1951.
7. Donoughe, P. L., and J. N. B. Livingood: NACA TN 3151, Washington, 1954.
8. Livingood, J. N. B., and P. L. Donoughe: NACA TN 3588, Washington, 1955.
9. Howe, J. T., and W. A. Mersman: NASA TN-D-12, Washington, D.C., 1959.
10. Dewey, C. F., Jr, and J. F. Gross: *Advances in Heat Transfer*, vol. 4, pp. 317–446, Academic Press, New York, 1967.
11. Sparrow, E. M., and H. S. Yu: *J. Heat Transfer*, vol. 93, pp. 328–334, 1971.
12. Eckert, E. R. G., and R. M. Drake, Jr: *Heat and Mass Transfer*, pp. 173–176, McGraw-Hill, New York, 1959.
13. Klein, J., and M. Tribus: ASME Paper 53-SA-46, ASME Semiannual Meeting, 1953; also *Symposium on Heat Transfer*, University of Michigan Press, 1953, and *Trans. ASME*, February 1956 and May 1957.
14. Blottner, F. G.: AGARD-LS-73 (NTIS AD-A013 269), von Kármán Institute, Brussels, February 1975.
15. Smith, A. G., and D. B. Spalding: *J. Roy. Aero. Soc.*, vol. 62, p. 60, 1958.
16. Spalding, D. G.: *J. Fluid Mech.*, vol. 4, p. 22, 1958.
17. Brown, S. N., and K. Stewartson: *Annual Review of Fluid Mechanics*, vol. 1, pp. 45–72, 1969.
18. Williams, J. C., III: *Annual Review of Fluid Mechanics*, vol. 9, pp. 113–144, 1977.
19. Morgan, V. T.: *Advances in Heat Transfer*, vol. 11, pp. 199–264, Academic Press, New York, 1975.
20. Raithby, G. D., and E. R. G. Eckert: *Int. J. Heat Mass Transfer*, vol. 11, pp. 1133–1152, 1968.
21. Kays, W. M., and A. L. London: *Compact Heat Exchangers*, 2d ed., McGraw-Hill, New York, 1964.
22. Zukauskas, A.: *Advances in Heat Transfer*, vol. 8, pp. 93–160, 1972.
23. Elzy, E., and R. M. Sisson: "Tables of Similar Solutions to the Equations of Momentum, Heat and Mass Transfer in Laminar Boundary Layer Flow," Bulletin no. 40, Engineering Experiment Station, Oregon State University, Corvalis, Oregon, February 1967.

11 CHAPTER

Turbulent External Boundary Layers: Momentum Transfer

In this chapter the stability of the laminar boundary layer is discussed, and a transition to a turbulent type of boundary layer is described. The characteristics of the turbulent boundary layer are first discussed in general terms. Following this, the Prandtl mixing-length theory is introduced as one method for solving the boundary-layer equations. This leads to the concept of a viscous sublayer and the development of the *law of the wall* for the near-wall region using a two-layer mixing-length model.

At this point an *approximate* solution to the momentum equation of the boundary layer is developed, leading to algebraic equations for the momentum thickness and friction coefficient. Next the Van Driest model for the sublayer is introduced, leading to a continuous *law of the wall.* The mixing-length theory is then extended over the entire boundary layer, and a method for solving the complete boundary-layer equations using finite-difference methods is described.

A turbulence model employing the *turbulence kinetic energy* equation is next described, and this leads to a so-called two-equation model based on the turbulence energy equation and another equation based on the turbulence dissipation rate, the k–ε model of turbulence.

There then follows a discussion of the concept of "equilibrium" turbulent boundary layers, the effects of transpiration, surface roughness, axial surface curvature, and free-stream turbulence.

TRANSITION OF A LAMINAR BOUNDARY LAYER TO A TURBULENT BOUNDARY LAYER

An important characteristic of a laminar boundary layer, and of a laminar flow in a pipe or duct, is that under certain conditions the flow is unstable in the presence of small disturbances, and a transition to a fundamentally different kind of flow, a turbulent flow, can occur. The viscous forces, largely responsible for the characteristics of a laminar flow, have the effect of restoring the flow to its previous state when it is subjected to an external disturbance; on the other hand, inertia forces associated with the velocity changes caused by a disturbance have quite the opposite effect. Inertia forces tend to be destabilizing and thus to amplify local disturbances. The Reynolds number is a ratio of inertia to viscous forces, and thus one might well expect that the stability of a laminar flow is in considerable part associated with the value of the Reynolds number, stable laminar flows being associated with low Reynolds numbers.

For a simple laminar boundary layer on a flat, smooth surface with no pressure gradient, it is found in typical laboratory wind tunnel experiments that a transition to a turbulent type of boundary layer tends to occur when the length Reynolds number Re_x reaches the range 300,000–500,000. But this particular range of critical Reynolds numbers seems to be associated with the surface roughness and free-stream disturbances characteristic of typical laboratory wind tunnels for low-speed flows. Laminar boundary layers have been observed to persist to Reynolds numbers several orders or magnitude higher if the free stream is devoid of disturbances and the surface is very smooth. Such conditions frequently occur during the reentry of space vehicles into the Earth's atmosphere.

At low Reynolds numbers it is found experimentally that a laminar boundary layer under a zero pressure gradient is stable to even very large disturbances if the length Reynolds number is less than about 60,000. Similarly, it is found that fully developed laminar flow in a pipe or duct is stable to large disturbances if the Reynolds number based on hydraulic diameter is less than about 2300.

There exists a theory of *viscous stability*—for that is what we are discussing here—and, for small disturbances (which permit a linearized theory), it is found that the laminar external boundary layer for zero pressure gradient is stable for Re_x less than about 60,000. It can also be shown that a "favorable" pressure gradient (accelerating flow) leads to higher critical Reynolds numbers, and an "unfavorable" pressure gradient (decelerating flow) leads to lower critical Reynolds numbers. Suction or blowing at the surface might be expected to have similar effects, with suction being stabilizing and blowing destabilizing.

The length Reynolds number Re_x is not a particularly convenient parameter to use as a transition criterion, since it has useful significance only for flows of constant free-stream velocity (no pressure gradient). If it is assumed that the phenomenon is primarily a local one, then a local Reynolds number criterion might be more generally useful. Either the displacement or momentum thickness Reynolds numbers might be used, but since the momentum thickness Reynolds number must generally be evaluated in any case in most applications, its use is suggested here.

Let us evaluate the momentum thickness Reynolds number Re_{δ_2} for the laminar, zero-pressure-gradient boundary layer as it reaches its lower critical Reynolds number, $\mathrm{Re}_x = 60{,}000$. From Eq. (9-20)

$$\delta_2 = 0.664\sqrt{\nu x / u_\infty}$$

Then

$$\mathrm{Re}_{x,\mathrm{crit}} = 60{,}000 = \frac{u_\infty x}{\nu}$$

Combining, and eliminating x,

$$60{,}000 = \frac{(u_\infty \delta_2/\nu)^2}{0.442}$$

But

$$u_\infty \delta_2/\nu = \mathrm{Re}_{\delta_2}$$

Thus

$$\mathrm{Re}_{\delta_2,\mathrm{crit}} = 162 \tag{11-1}$$

This value of Re_{δ_2} is now proposed as a general criterion for transition whenever substantial free-stream disturbances are present, regardless of pressure gradient or mass transfer at the surface, and this seems to correspond reasonably well with the experimental facts. The laminar boundary layer can, of course, persist to higher values of Re_{δ_2} under undisturbed conditions. A strongly accelerated laminar boundary layer may have a somewhat higher critical Reynolds number, but such an acceleration inhibits the growth of Re_{δ_2} (it can actually decrease), so the point is usually moot.

It is interesting to note that if the equivalent of the momentum thickness Reynolds number is evaluated for fully developed laminar flow in a *flat duct* at a value of the hydraulic diameter Reynolds number equal to 2300, almost the same value of Re_{δ_2} is found as for the simple external boundary layer. This further suggests the general applicability of Eq. (11-1).

THE QUALITATIVE STRUCTURE OF THE TURBULENT BOUNDARY LAYER

The breakdown of the laminar boundary layer discussed in the preceding section does not occur everywhere across the flow at the same distance x. It occurs at certain favorable "spots" and then spreads laterally and downstream until the entire boundary layer is engulfed. There is thus a three-dimensional aspect to transition, and there is a definable "transition region," which can be as long or longer than the preceding laminar region. Ultimately however, a fully developed turbulent boundary layer is established, and this new boundary layer is again, on the average, two-dimensional to the same order as the preceding laminar boundary layer.

We are not going to attempt here to develop a theory for the *transition region*, other than to suggest that in engineering design the extent of this region can usually be assumed to be about the same length as the laminar region, and that the friction, heat-transfer, and mass-transfer coefficients can usually be assumed to (on average) vary continuously from the laminar to the fully developed turbulent region. With this said, we are going to skip forward to the fully developed turbulent region. Let us first see what it looks like and what seems to be happening.

The important characteristics of a turbulent flow adjacent to a solid surface differ little whether we are speaking of a turbulent boundary layer on an external surface or fully developed turbulent flow in a pipe or duct. Experimentally, at least two regions are observed: (1) a predominantly viscous region immediately adjacent to the wall surface where the momentum and heat transfer can be largely accounted for by the simple mechanisms of viscous shear and molecular conduction; and (2) a fully turbulent region, comprising most of the boundary layer, where velocity is nowhere independent of time, where "eddy" motion is observed, and where momentum and heat are transported normally to the flow direction at rates that are generally very much greater than can be accounted for by viscous shear and molecular conduction alone.

Examination of the fully turbulent region reveals that the velocity at any point seems to consist of a relatively large time-averaged velocity, upon which is superimposed a smaller fluctuating velocity with instantaneous components in all directions. The existence of velocity components normal to the mean velocity vector means that fluid is moving, at least momentarily, in the normal direction; this fluid carries momentum with it, and it may carry thermal energy, or any other property for which there is a mean gradient in the normal direction; and, in fact, this is the primary mechanism whereby such effects are transported in the normal direction.

Further examination of the fully turbulent region reveals that the velocity fluctuations are the result of *vorticity* in the fluid. In fact, virtually every particle is a part of fluid eddies that are turning over in various directions, and this is what we mean by a turbulent flow.

The thin, viscous region close to the wall, which we call the *viscous sublayer*, is in some ways of more importance than the fully turbulent region. It is in this sublayer that events leading to the production of turbulence occur. A simple description of the sublayer is that it is essentially like a continually developing laminar boundary layer, which grows until its local Reynolds number becomes supercritical, at which point it becomes locally unstable and suffers a local breakdown. This breakdown is identified with a "burst" of turbulence from the wall region. The bursts are sufficiently frequent in both space and time to cause the sublayer to maintain, on the average, a constant *thickness* Reynolds number.

A "burst" resulting from local instability is a three-dimensional event that results in the ejection from the wall region of a relatively large element of slow-moving fluid, which moves out into the fully turbulent region, and its replacement by a similar element of higher-velocity fluid. Although there is some momentum (and heat) transfer within the sublayer associated with these events, viscous shear (and molecular conduction) remains the predominant transport mechanism in the inner part of the sublayer, especially immediately adjacent to the wall, simply because of the relative infrequency of the event.

These elements colliding with the higher-velocity fluid in the fully turbulent region outside of the sublayer provide the primary source of the turbulence kinetic energy in that region, i.e., the kinetic energy of the eddies. As we move out through the turbulent region, more turbulence kinetic energy is then generated through the interaction of the turbulent eddies with the mean velocity gradient. While this production of turbulence kinetic energy is taking place, the viscosity of the fluid is acting to decay the eddies and transform the turbulence energy into thermal energy. A *new state of stability* is established in which the production of turbulence energy is equal to the dissipation of that energy, plus a certain part that is convected and diffused outwards.

In a sense, then, the turbulent boundary layer is a stable region possessing the property of diffusing momentum, and other properties, very much more rapidly than by simple molecular processes. Although an instability in the sublayer is an essential feature, the overall structure is completely stable, self-adjusting, and experimentally repeatable.

As we move along the surface in the downstream direction, the turbulent boundary layer grows, much like the laminar boundary layer but more rapidly, and its momentum thickness Reynolds number grows. But the sublayer maintains essentially the same *thickness* Reynolds number (obviously a *critical* Reynolds number having to do with its viscous stability), and thus becomes a smaller and smaller fraction of the overall boundary layer.

THE CONCEPTS OF EDDY DIFFUSIVITY AND EDDY VISCOSITY

A useful, though not totally necessary, concept is now introduced. To perform turbulent boundary-layer calculations, we need either information or a theory to evaluate the term $-\overline{u'v'}$ in Eq. (6-28). This is frequently referred to in the literature as the turbulence "closure" problem, and it is usually solved by solving an algebraic equation, or a differential equation, for $-\overline{u'v'}$. In Chap. 6, $-\overline{u'v'}$ is defined as an apparent turbulent shear stress, and it seems plausible that it should go to zero if there is no gradient in the mean velocity profile, just as the viscous shear stress goes to zero. In actual fact, this is not precisely so, but it is close enough for many practical applications. Thus it seems reasonable to state that

$$-\overline{u'v'} \propto \frac{\partial \bar{u}}{\partial y}$$

For the proportionality factor, we define the eddy diffusivity for momentum ε_M:

$$-\overline{u'v'} = \varepsilon_M \frac{\partial \bar{u}}{\partial y} \tag{11-2}$$

This is nothing more than a definition; we still have the problem of evaluating ε_M.

Let us now examine the implications of this definition. When Eq. (11-2) is substituted into Eq. (6-28), the momentum differential equation for the constant-property turbulent boundary layer becomes

$$\bar{u}\frac{\partial \bar{u}}{\partial x} + \bar{v}\frac{\partial \bar{u}}{\partial y} = -\frac{1}{\rho}\frac{d\bar{P}}{dx} + \frac{\partial}{\partial y}\left[(\nu + \varepsilon_M)\frac{\partial \bar{u}}{\partial y}\right] \tag{11-3}$$

ε_M is dimensionally the same as the kinematic viscosity ν, and the turbulent contribution to diffusion in the y direction can be readily compared with the molecular contribution. In most cases it is found that $\varepsilon_M \gg \nu$ in the fully turbulent region, while $\nu \gg \varepsilon_M$ in the viscous sublayer close to the wall.

It is sometimes convenient to define an eddy viscosity μ_t. By analogy with the corresponding molecular quantities,

$$\mu_t = \rho\varepsilon_M \tag{11-4}$$

THE PRANDTL MIXING-LENGTH THEORY

The Prandtl mixing-length theory is by all odds the simplest, as well as the oldest, of the turbulence closure models. Despite its simplicity, it provides a remarkably adequate basis for many engineering applications. We will carry the mixing-length theory as far as seems practicable, and then develop a more sophisticated model based on the turbulence kinetic energy equation and an equation for the turbulence dissipation rate (the k–ε model). The differences between these two models will then be demonstrated by some actual comparisons with experimental data.

The defining equation for the mixing length, by itself, provides an adequate starting hypothesis for development of the mixing-length theory. However, the following development is given not as a *proof* of anything, but rather as a plausible argument for the *form* of the mixing-length equation.

Let us idealize the turbulent fluctuating-velocity components u' and v' as simple harmonic functions having the same period t_1 but differing amplitudes and phase angles. That is,

$$u' = u'_{\max} \sin \frac{2\pi t}{t_1}$$

$$v' = v'_{\max} \sin \frac{2\pi(t + \alpha_1)}{t_1}$$

Next, form the time average of the product of u' and v':

$$-\overline{u'v'} = \frac{1}{t_1}\int_0^{t_1} u'v'\,dt = \frac{u'_{\max}v'_{\max}}{2}\cos\frac{2\pi\alpha_1}{t_1}$$

From this result we see that if u' and v' are in phase, or nearly in phase, the "turbulent shear stress" $-\overline{u'v'}$ is a finite quantity, although it is also possible for $-\overline{u'v'}$ to be zero (if $\alpha_1/t_1 = \frac{1}{4}$). The first condition evidently does obtain when there is a *gradient* in the mean velocity profile, because we do observe substantial turbulent shear stresses in such situations.

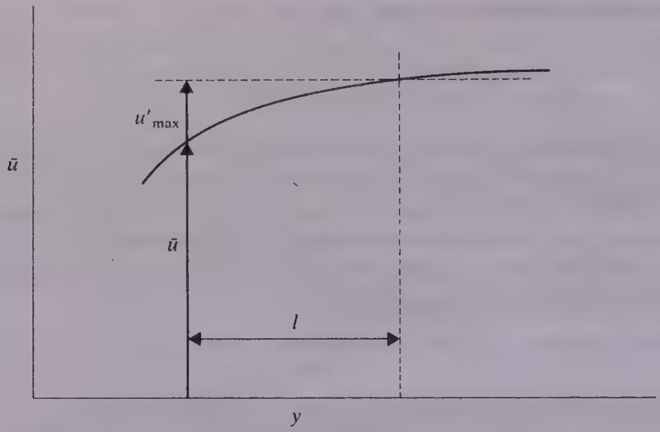

Figure 11-1 Graphical definition of the mixing length.

Now let us define a "mixing length" l in the manner illustrated in Fig. 11-1. If l is small relative to the other dimensions of the system then, approximately,

$$u'_{\max} = l\left|\frac{\partial \bar{u}}{\partial y}\right|$$

Next let us assume that

$$v'_{\max} = ku'_{\max} = Cl\left|\frac{\partial \bar{u}}{\partial y}\right|$$

where C is simply a local constant. Then, for the case $\alpha_1 = 0$, we obtain

$$-\overline{u'v'} = \frac{1}{2}u'_{\max}v'_{\max} = \frac{1}{2}Cl^2\left(\frac{\partial \bar{u}}{\partial y}\right)^2$$

Next, we absorb $\frac{1}{2}C$ into l, which has yet to be determined anyway, and we obtain the defining equation for the mixing length:

$$-\overline{u'v'} = l^2\left(\frac{\partial \bar{u}}{\partial y}\right)^2 \tag{11-5}$$

If we prefer to express the mixing length in terms of ε_M and/or μ_t, we can then use Eqs. (11-2) and (11-4) to obtain

$$\mu_t = \rho l^2\left|\frac{\partial \bar{u}}{\partial y}\right|, \qquad \varepsilon_M = l^2\left|\frac{\partial \bar{u}}{\partial y}\right| \tag{11-6}$$

We are still faced with the proposition of assigning a value to l, but here simple dimensional reasoning can be useful. One can ask the question, on what system dimension would the mixing length be expected to scale? In the region not

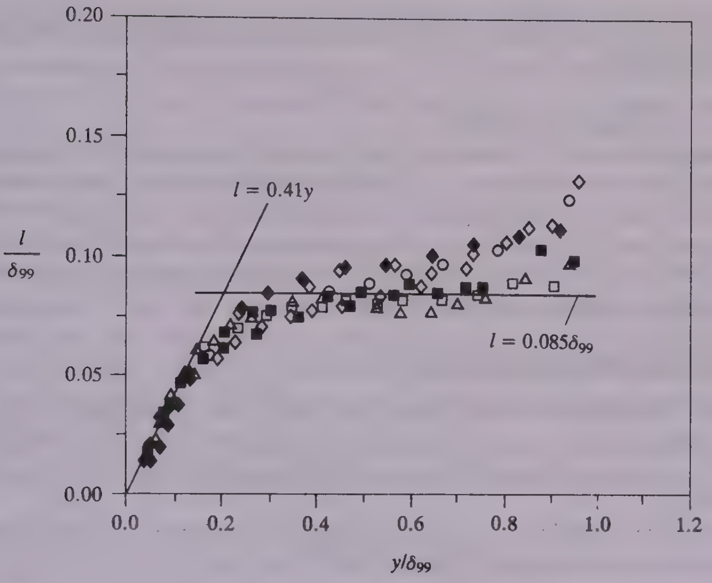

Figure 11-2 Mixing-length measurements of Andersen[1] for no pressure gradient, adverse pressure gradient, blowing, and suction.

too distant from the wall the only significant length dimension is the *distance* from the wall, and thus it is reasonable to assume that the mixing length might scale on that distance. If we let the proportionality factor be κ, we can then obtain

$$l = \kappa y \tag{11-7}$$

The validity of all these assumptions rests on whether κ does, in fact, turn out to be a constant when measured at various points in the boundary layer. Figure 11-2 shows some typical experimental measurements of l at five different stations along a surface (δ_{99} is the boundary-layer thickness at the point where $\bar{u}/u_\infty = 0.99$). In the region near the wall the data do indeed appear to be well represented by Eq. (11-7), with κ taking a value of about 0.41 (κ is usually called the *von Kármán constant*).

It should be added that the mixing length is not a quantity that can be "measured" directly. It is actually determined from measurements of the turbulent shear stress and the velocity gradient, employing Eq. (11-5).

There remains a region still closer to the wall, the *viscous sublayer*, where Eq. (11-7) is no longer valid, but the measurements shown on Fig. 11-2 do not go this close to the wall. We will discuss this region later.

In the outer part of the boundary layer it is apparent from Fig. 11-2 that the mixing length is proportional to total boundary-layer thickness rather than the distance from the wall. For y/δ_{99} greater than about 0.7, the value of the mixing length becomes relatively unimportant, so the outer region can be adequately approximated by

$$l = \lambda \delta_{99} \tag{11-8}$$

where λ is typically about 0.085.

Similar behavior is noted for adverse pressure gradients, favorable pressure gradients, blowing and suction, and the observed values for κ and λ seem little affected by these differing boundary conditions. Strictly speaking, these observations are valid for so-called *equilibrium* boundary layers, a subject that is discussed later, but the turbulent boundary layer tends to approach equilibrium, at least in the inner region, remarkably quickly.

WALL COORDINATES

Before discussing the viscous sublayer, we will find it convenient to introduce a new coordinate system that is meaningful in the region close to the wall. But first we will develop an expression for the distribution of the *total shear stress* near the wall.

From the definition of ε_M and the viscosity coefficient, the total apparent shear stress, molecular plus turbulent, can be expressed as

$$\frac{\tau}{\rho} = (\nu + \varepsilon_M)\frac{\partial \bar{u}}{\partial y} \tag{11-9}$$

Substituting this into Eq. (11-3), we obtain

$$\rho\bar{u}\frac{\partial \bar{u}}{\partial x} + \rho\bar{v}\frac{\partial \bar{u}}{\partial y} = -\frac{d\bar{P}}{dx} + \frac{\partial \tau}{\partial y} \tag{11-10}$$

[Note that Eq. (11-10) does not include any assumption about the shear mechanism; in fact, it is also valid for a steady laminar boundary layer.]

Let us now confine our attention to a region relatively close to the wall such that $\rho\bar{u}\,\partial\bar{u}/\partial x$ is sufficiently smaller than the other terms that it can be neglected. We are talking about a region that generally extends outside the viscous sublayer, and in some cases can include as much as one-third of the entire boundary layer. We call this a *Couette flow* assumption and speak of a *Couette flow* region.

Under this assumption, $\rho\bar{u}\,\partial\bar{u}/\partial x = 0, \bar{u} = \bar{u}(y)$ alone, Eq. (11-10) becomes an ordinary differential equation, and $\bar{v} = v_s$, the value of the normal velocity component at the wall surface (which would be 0 unless there is blowing or suction at the surface):

$$\rho v_s \frac{d\bar{u}}{dy} = -\frac{d\bar{P}}{dx} + \frac{d\tau}{dy} \tag{11-11}$$

This equation can now be integrated with respect to y between the limits $\tau = \tau_s$ and $\bar{u} = 0$ at $y = 0$, and corresponding values at any distance y, resulting in an equation for the shear stress ratio:

$$\frac{\tau}{\tau_s} = 1 + \frac{\rho v_s \bar{u}}{\tau_s} + \frac{d\bar{P}}{dx}\frac{y}{\tau_s} \tag{11-12}$$

Next we will introduce a set of nondimensional variables that are based on quantities that are significant in the near-wall region; these are what are referred to as *wall coordinates*. First, from the definition of the friction coefficient we define a *shear velocity*, or *friction velocity*, u_τ for the constant-property boundary layer:

$$\frac{\tau_s}{\rho} = \frac{c_f u_\infty^2}{2} = u_\tau^2$$

Thus

$$u_\tau = \sqrt{\tau_s/\rho}$$

Note that u_τ has the dimensions of velocity. Employing u_τ as a characteristic velocity, the following nondimensional variables can be formed (although these nondimensional variables can also be expressed in terms of the free-stream velocity and the friction coefficient, they are fundamentally independent of the former):

$$u^+ = \frac{\bar{u}}{u_\tau} = \frac{\bar{u}/u_\infty}{\sqrt{c_f/2}}$$

$$y^+ = \frac{y u_\tau}{\nu} = \frac{y\sqrt{\tau_s/\rho}}{\nu} = \frac{y u_\infty \sqrt{c_f/2}}{\nu}$$

$$v_s^+ = \frac{v_s}{u_\tau} = \frac{v_s}{\sqrt{\tau_s/\rho}} = \frac{v_s/u_\infty}{\sqrt{c_f/2}}$$

$$p^+ = \frac{\mu\, d\bar{P}/dx}{\rho^{1/2}\tau_s^{3/2}}$$

When these are substituted into Eq. (11-12), we obtain

$$\frac{\tau}{\tau_s} = \tau^+ = 1 + v_s^+ u^+ + p^+ y^+ \tag{11-13}$$

Note that Eq. (11-13) is valid only in the region where the Couette flow assumption is valid; at the outer edge of the boundary layer τ/τ_s must go to 0.

THE LAW OF THE WALL FOR THE CASE OF $p^+ = 0.0$ AND $v_s^+ = 0.0$

This is the simplest possible boundary layer, with constant free-stream velocity, no transpiration, and an aerodynamically smooth surface. If we consider only the Couette flow region, i.e., that near the wall, Eq. (11-13) reduces to

$$\frac{\tau}{\tau_s} = 1$$

To obtain the law of the wall, we integrate Eq. (11-9) under this condition. Thus,

$$\frac{\tau_s}{\rho} = (\nu + \varepsilon_M)\frac{d\bar{u}}{dy} \tag{11-14}$$

Now we will propose a model of the turbulent boundary layer consisting of two distinct regions, a *viscous sublayer* for which we will assume $\nu \gg \varepsilon_M$, and a *fully turbulent* region for which $\varepsilon_M \gg \nu$. For the latter we will employ the Prandtl mixing-length model of turbulence. Later we will examine a considerably better model of the near-wall region, but we will still employ the mixing-length theory.

For the *viscous sublayer*, Eq. (11-14) reduces to

$$d\bar{u} = \frac{\tau_s}{\rho\nu}dy = \frac{\tau_s}{\mu}dy$$

Integrating from the wall,

$$\int_0^{\bar{u}} d\bar{u} = \frac{\tau_s}{\mu}\int_0^y dy$$

$$\bar{u} = \frac{\tau_s}{\mu}y$$

We now introduce the wall coordinate definitions for u^+ and y^+, and obtain

$$u^+ = y^+ \tag{11-15}$$

This can also be arrived at by recasting Eq. (11-14) in terms of the wall coordinate variables,

$$\tau^+ = \left(1 + \frac{\varepsilon_M}{\nu}\right)\frac{du^+}{dy^+}$$

Then with the use of Eq. (11-13), and $\nu \gg \varepsilon_M$,

$$\tau^+ = 1.0 = \frac{du^+}{dy^+}$$

and thus we obtain Eq. (11-15) upon integration.

Next we must face the question of the *effective thickness* of the sublayer. Experimentally we find that the sublayer thickness can be expressed in terms of a critical value of y^+, and this value remains unchanged regardless of the total thickness of the boundary layer. The reason is that y^+ is simply a local thickness Reynolds number, and the stability of the viscous sublayer is such that this Reynolds number always remains a constant at the outer edge of the sublayer. It is a completely self-adjusting process related to the local collapses and "bursting" phenomena discussed earlier. If the effective value of y^+ at the outer edge of the sublayer exceeds this critical value, the sublayer becomes unstable and a "burst" ejects low-momentum fluid, replacing it with higher-momentum fluid from outside the sublayer, thereby momentarily decreasing the sublayer thickness.

For the fundamental case of $p^+ = 0$ and $v_s^+ = 0$, it is found that the critical value of y^+ for this *two-layer model* is 10.8. But note that this is an *effective* thickness that is obtained when using the rather artificial two-layer model. In actual fact, the viscous-flow-dominated region can be much thicker, although locally and momentarily it can be thinner. The artificiality of the thickness will be seen shortly when we compare the results of this model with experimental data.

If we introduce a pressure gradient in the direction of flow, or introduce blowing or suction, or consider a rough surface, then the critical value of y^+ changes. We will discuss these effects later in connection with a better sublayer model.

For the *fully turbulent* region, where we intend to neglect ν relative to ε_M, Eq. (11-14) becomes

$$\frac{\tau_s}{\rho} = \varepsilon_M \frac{d\bar{u}}{dy}$$

Now let us introduce the Prandtl mixing-length theory, Eqs. (11-6) and (11-7). Note that we are still confining attention to the region for which Eq. (11-7) is valid:

$$\frac{\tau_s}{\rho} = l^2 \left(\frac{d\bar{u}}{dy}\right)^2 = \kappa^2 y^2 \left(\frac{d\bar{u}}{dy}\right)^2$$

Next, we introduce the definitions of u^+ and y^+; after taking the root of the resulting equation, we obtain

$$\frac{du^+}{dy^+} = \frac{1}{\kappa y^+}$$

We then integrate from the outer edge of the viscous sublayer:

$$\int_{10.8}^{u^+} du^+ = \frac{1}{\kappa} \int_{10.8}^{y^+} \frac{dy^+}{y^+}$$

$$u^+ - 10.8 = \frac{1}{\kappa} \ln \frac{y^+}{10.8}$$

Setting $\kappa = 0.41$ and rearranging, we obtain the logarithmic equation that is generally called the *law of the wall*:

$$u^+ = 2.44 \ln y^+ + 5.0 \qquad (11\text{-}16)$$

A comparison with experiment is shown on Fig. 11-3. Data from two different investigators, one using water and the other air, at widely differing momentum thickness Reynolds numbers are plotted, along with Eqs. (11-15) and (11-16), plotted on semi-logarithmic coordinates. Note that the data for these two velocity profiles depart in the outer part of the boundary layer, but they collapse together in the inner region and are well represented by Eq. (11-16) down to about $y^+ = 40$, where the effects of the sublayer begin to be seen (although the data of Wieghardt do not extend into the sublayer region). Numerous other experiments at widely differing values of velocity, fluid properties, and Reynolds number yield essentially the same results.

Note that very close to the wall, i.e., for $y^+ < 5$, the data do approach Eq. (11-15). However, the artificiality represented in the two-layer model is apparent, and what is meant by an *effective sublayer thickness* should be evident.

Note the use of semi-logarithmic coordinates to represent these data. This coordinate system results in a straight line for the region where the law of the wall is valid, but it also has the effect of expanding the region near the wall and

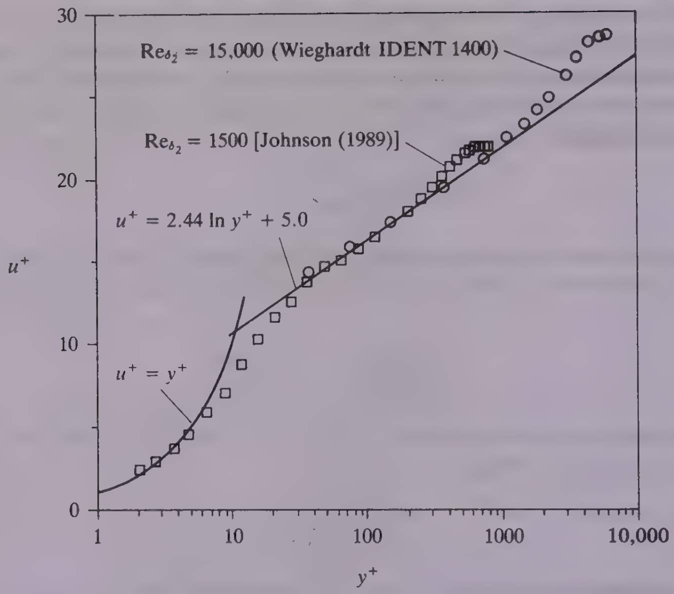

Figure 11-3 The law of the wall (constant free-stream velocity): turbulent boundary-layer profiles in wall coordinates.[†]

[†]The term IDENT refers to the data sets used at the 1968 Stanford University AFOSR Conference, as well as to data sets tabulated in App. E.

compressing the outer region. Since most of the velocity change takes place in the inner region, the logarithmic scale provides a convenient way to critically examine the most important region, and for that reason it is extensively employed in presenting experimental data.

In the outer part of the boundary layer the departure of the two profiles from one another, and from Eq. (11-16), results from both Eqs. (11-7) and (11-13) no longer being valid—facts that were of course anticipated. As we go to higher and higher Reynolds numbers, the outer edge of the boundary layer goes to higher and higher values of y^+, and the range of y^+ for which Eq. (11-16) is applicable increases. At the outer edge there is yet another interesting feature. For the case of no pressure gradient and no blowing or suction, the value of u^+ at the outer edge of the boundary layer is always approximately 2.3 above Eq. (11-16), a fact that is observed experimentally, and is also predictable if l in the outer region is evaluated from Eq. (11-8) and the full partial differential equation (11-3) is solved. The outer region in which there is a departure from the logarithmic law of the wall is frequently called the *wake region.*

Figure 11-4 shows the effects of streamwise pressure gradients, both positive and negative, on the velocity profile. Note that the *wake* is very different. For an accelerating flow (a favorable pressure gradient) the wake is diminished and

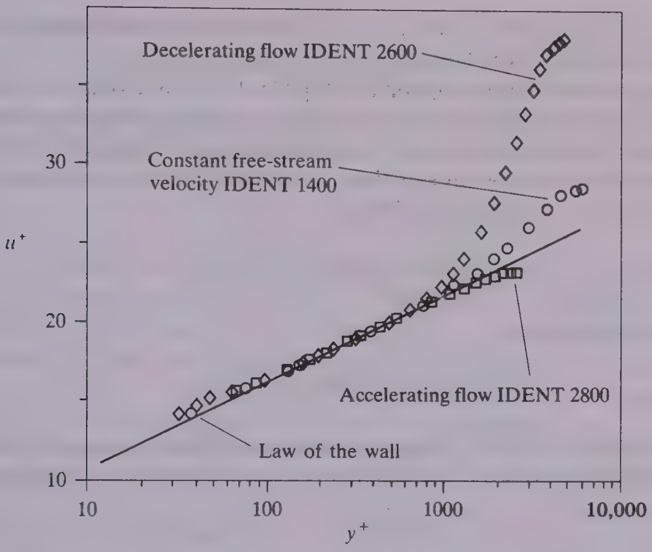

Figure 11-4 The effect of pressure gradient on the turbulent velocity profile.

can even be negative, i.e., u^+ can fall *below* the law of the wall, while a decelerating flow (adverse pressure) leads to a much larger wake. But notice that Eq. (11-16) is again approached in the inner region of the boundary layer. This is the reason why Eq. (11-16) is usually called the *law of the wall*, because it appears to be somewhat more general than the simple case of no pressure gradient for which it was derived.

Although a logarithmic form of the law of the wall generally fits the data better, a *power law* is sometimes more convenient. A *power law* that fits the logarithmic form fairly well out to at least $y^+ = 1500$ is

$$u^+ = 8.75 y^{+1/7} \tag{11-17}$$

We will use this equation to develop an approximate solution for the friction coefficient.

AN APPROXIMATE SOLUTION FOR THE TURBULENT MOMENTUM BOUNDARY LAYER

Equation (11-17), together with the momentum integral equation, can be used to obtain a relatively simple algebraic equation for the friction coefficient for a simple turbulent boundary layer. Since Eq. (11-17) was developed for the case of constant free-stream velocity, i.e., no pressure gradient, this result is likewise so restricted. However, it turns out to be a quite good approximation for rather strongly accelerated flows and a fair approximation for very mild decelerations. But it is not at all useful when there is blowing or suction.

First we make the assumption that Eq. (11-17) is valid over the entire boundary layer, i.e., we ignore the wake. Let the total boundary layer thickness be designated as δ, the location at which the velocity is u_∞. We are thus assuming that the boundary layer has a finite thickness, but since the thickness cancels out later, this is not a critical assumption. Then

$$\frac{u_\infty}{\sqrt{\tau_s/\rho}} = 8.75\left(\frac{\delta\sqrt{\tau_s/\rho}}{\nu}\right)^{1/7}$$

Solving for τ_s gives

$$\tau_s = 0.0225\rho u_\infty^2\left(\frac{\delta u_\infty}{\nu}\right)^{-1/4} \tag{11-18}$$

Next, δ_1 and δ_2 the displacement and momentum thicknesses, respectively, can be evaluated substituting Eq. (11-17) into Eqs. (5-5) and (5-6), with the results

$$\frac{\delta_1}{\delta} = 0.125, \qquad \frac{\delta_2}{\delta} = 0.097$$

From these we get the following ratio, the *shape factor*, which is used later:

$$\delta_1/\delta_2 = 1.29 = H$$

Next, Eq. (11-18) can be expressed in terms of the *momentum thickness*:

$$\tau_s = 0.0125\rho u_\infty^2\left(\frac{\delta_2 u_\infty}{\nu}\right)^{-1/4} \tag{11-19}$$

Now introducing the definition of the friction coefficient, we obtain an expression for the friction coefficient as a function of a Reynolds number based on the local momentum thickness, i.e.,

$$c_f/2 = 0.0125\,\mathrm{Re}_{\delta_2}^{-1/4} \tag{11-20}$$

Next we would like to develop a way to evaluate δ_2 as a function of x along the surface. Let us assume that Eq. (11-19) is a reasonable approximation for the surface shear stress even when the free-stream velocity is increasing or decreasing in the direction of flow. This is a reasonable assumption for an accelerating flow, but for a decelerating flow (adverse pressure gradient) it is adequate only for very mild decelerations. The momentum integral equation, Eq. (5-7), for the case of $v_s = 0$ and constant density is

$$\frac{\tau_s}{\rho u_\infty^2} = \frac{d\delta_2}{dx} + \delta_2\left[\left(2 + \frac{\delta_1}{\delta_2}\right)\frac{1}{u_\infty}\frac{du_\infty}{dx} + \frac{1}{R}\frac{dR}{dx}\right]$$

Substituting Eq. (11-19) for the shear stress and taking a value of 1.29 for the shape factor H yields

$$0.0125\left(\frac{u_\infty\delta_2}{\nu}\right)^{-1/4} = \frac{d\delta_2}{dx} + 3.29\frac{\delta_2}{u_\infty}\frac{du_\infty}{dx} + \frac{\delta_2}{R}\frac{dR}{dx}$$

This can be rearranged to

$$d\left(\delta_2^{5/4} R^{5/4} u_\infty^{4.11}\right) = 0.0156 R^{5/4} u_\infty^{3.86} \nu^{1/4}\, dx$$

For integration with the initial condition that at $x = 0$, at least one of δ_2, R, or u_∞ will be zero, and solving for δ_2, we obtain

$$\delta_2 = \frac{0.036\nu^{0.2}}{R u_\infty^{3.29}} \left(\int_0^x R^{5/4} u_\infty^{3.86}\, dx \right)^{0.8} \tag{11-21}$$

Like its laminar flow counterpart, Eq. (9-42), this equation then involves a simple procedure that depends upon a given variation of u_∞ and R with x. With δ_2 established as a function of x, the shear stress, or the friction coefficient, is then determined from Eq. (11-19). However, it should again be emphasized that Eq. (11-21) should not be used for any but very mild adverse pressure gradients, although it is quite reasonable for favorable pressure gradients.

This equation implies that the turbulent boundary layer originates at $x = 0$, without a preceding laminar boundary layer and transition region. In such a case, and in Eqs. (11-22)–(11-24) to follow, the point $x = 0$ is a fictitious *virtual origin* of the turbulent boundary layer—the point where the turbulent boundary layer would have originated were it not preceded by a laminar boundary and a transition region, provided that the same turbulent transport mechanisms were applicable down to zero Reynolds number.

Note that if a laminar boundary layer precedes the turbulent boundary layer, and if sufficient information is available to solve the laminar boundary layer and to determine the "point" of transition, then the value of δ_2 at transition as determined from the laminar boundary-layer solution would provide the necessary lower limit on δ_2 at transition in the equation preceding Eq. (11-21). Without this information, we will simply use Eq. (11-21) with the understanding that x is the distance from the *virtual origin* of the turbulent boundary layer. Practically speaking, if x is sufficiently large, the difference between the real and virtual origins is often sufficiently small that little error is introduced if the preceding laminar boundary layer is ignored, and that is the course we will follow for the moment. If such an assumption is not warranted, it is a relatively simple matter to start back at the equation preceding Eq. (11-21).

Let us now reduce Eq. (11-21) to the elementary case of constant u_∞ and constant (or very large) R:

$$\delta_2 = \frac{0.036\nu^{0.2}}{u_\infty^{3.29}} \left(u_\infty^{3.86} x\right)^{0.8}$$

or

$$\frac{\delta_2}{x} = \frac{0.036\nu^{0.2}}{u_\infty^{0.2} x^{0.2}} = 0.036\,\mathrm{Re}_x^{-0.2} \tag{11-22}$$

This result can now be substituted into Eq. (11-19), and, after introduction of the definition of the local friction coefficient, we obtain

$$c_f/2 = 0.0287\,\mathrm{Re}_x^{-0.2} \tag{11-23}$$

Equation (11-23) is in quite good agreement with experiments for Reynolds numbers up to several million, but then becomes increasingly lower than the experimental data for higher Reynolds numbers. The reason is that Eq. (11-17) is no longer a good approximation to the law of the wall at higher Reynolds numbers. Equation (11-17) could be modified for higher Reynolds numbers by using a smaller exponent, but this hardly seems worthwhile, since empirical equations based on experimental data are available, and also since a solution to the full partial differential momentum equation (11-3) can be readily obtained using numerical methods and the same mixing-length theory. Probably the most definitive experimental correlation is that of Schultz-Grunow,[3] which is valid from $\mathrm{Re}_x = 5 \times 10^5$ to very high Reynolds numbers:

$$c_f/2 = 0.185(\log_{10} \mathrm{Re}_x)^{-2.584} \tag{11-24}$$

A CONTINUOUS LAW OF THE WALL: THE VAN DRIEST MODEL

It is quite possible to improve upon the two-layer model of the turbulent boundary layer in a number of ways, but any model that involves a totally viscous sublayer ($\varepsilon_M = 0$), while perhaps satisfactory for solution of the momentum equation, can lead to substantial underprediction of heat transfer, especially at high Prandtl numbers. The reason is that a very small eddy diffusivity in the region $y^+ < 5.0$ can contribute greatly to the heat-transfer rate while having a negligible effect on momentum transfer.

The concept of a sublayer in which relatively large elements of fluid lift off the surface, to be replaced immediately by other fluid from the fully turbulent region—the "bursting" phenomenon that was discussed earlier—demands a sublayer model for which the eddy diffusivity retains a finite magnitude throughout the sublayer and goes to zero only at the wall itself. The idea that ε_M is nonzero, though very small, very near the wall does not mean that we are talking about small turbulent eddies. ε_M is a statistical quantity averaged over time and space, and very small ε_M in the sublayer merely implies a relatively infrequent event.

The Van Driest hypothesis[4] is a sublayer scheme that provides for an eddy diffusivity that is only 0 at $y = 0$, and that also has the virtue that it allows a continuous calculation through the sublayer and into the fully turbulent region with no discontinuities. It does a reasonable job of predicting the various flow parameters throughout the entire sublayer region. There are other schemes that will do much the same thing, so the particular function used in the Van Driest hypothesis should not be regarded as having any theoretical basis.

With this scheme, we use the Prandtl mixing length all the way to the wall instead of truncating it to zero at an assumed effective outer edge of the sublayer, but we simulate the sublayer by introducing a damping function into the mixing-length equation (11-7). An exponential function has the desired characteristics, so Van Driest proposed that

$$l = \kappa y(1 - e^{-y/A})$$

The constant A is an empirically determined effective sublayer thickness, but since it is a dimensional quantity, and we have previously argued that the sublayer thickness should be expressed as a local thickness Reynolds number, we should multiply the numerator and denominator of the exponent by u_τ/ν so as to obtain y^+/A^+. Then

$$l = \kappa y(1 - e^{-y^+/A^+}) \qquad (11\text{-}25)$$

We now propose to evaluate the total shear stress using Eqs. (11-6) and (11-9) throughout the entire boundary layer, without neglecting either ε_M or ν anywhere. If we confine attention to the region relatively near the wall, we can still make the Couette flow assumption if desired, but we are forced to make computer calculations using finite-difference methods, and simple algebraic solutions are no longer feasible.

There remains the problem of determining A^+. This is done by assuming various values of A^+ and carrying out calculations until the calculated values of u^+ outside of the sublayer correspond to the law of the wall, Eq. (11-16). The results of such calculations for $A^+ = 25.0$ are shown on Fig. 11-5.

$A^+ = 25.0$ is determined for a boundary layer with no axial pressure gradient and no blowing or suction; it is found that both pressure gradient and transpiration (as well as surface roughness and perhaps other effects) have a pronounced effect upon A^+. Since the latter is an effective sublayer thickness, these other parameters apparently influence the sublayer thickness. A favorable

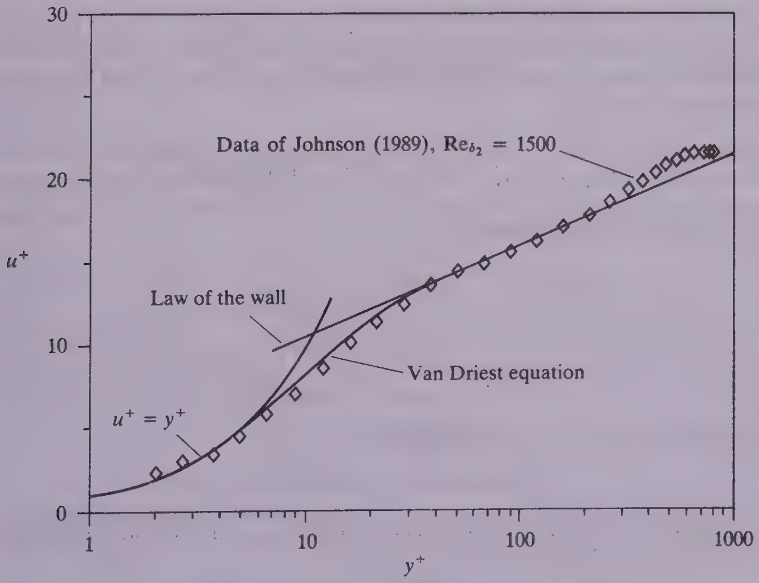

Figure 11-5 The Van Driest sublayer (constant free-stream velocity): the sublayer as calculated using the Van Driest equation with $A^+ = 25.0$.

pressure gradient (accelerating flow) induces a thicker sublayer; an adverse pressure gradient has the opposite effect. Blowing decreases A^+, while suction increases it. Roughness, discussed later, decreases A^+. These results are not surprising when one contemplates the probable influence of these various effects on the stability of the viscous sublayer.

An empirical equation for A^+ as a function of the pressure gradient parameter p^+ and the transpiration parameter v_s^+ (both in wall coordinates) is presented by Kays and Moffat.[5]

$$A^+ = \frac{25.0}{a\{v_s^+ + b[p^+/(1+cv_s^+)]\}+1} \tag{11-26}$$

where

$$a = 7.1, \qquad b = 4.25, \qquad c = 10.0$$

If $p^+ > 0$, then $b = 2.9$ and $c = 0.0$.

SUMMARY OF A COMPLETE MIXING-LENGTH THEORY

In the preceding sections we have discussed the elements of a complete mixing-length theory, and then approximate procedures that lead to simple algebraic solutions. For the sake of clarity it is now worthwhile to summarize the complete mixing-length theory, which does, however, require a finite-difference procedure and a digital computer for implementation.

The momentum boundary-layer equation to be solved, together with the appropriate version of the continuity equation and any desired initial and boundary conditions, is Eq. (11-3).

$$\bar{u}\frac{\partial \bar{u}}{\partial x} + \bar{v}\frac{\partial \bar{u}}{\partial y} = -\frac{1}{\rho}\frac{d\bar{P}}{dx} + \frac{\partial}{\partial y}\left[(\nu+\varepsilon_M)\frac{\partial \bar{u}}{\partial y}\right]$$

or, for variable property behavior,

$$\begin{aligned}\bar{u}\frac{\partial \bar{u}}{\partial x} + \bar{v}\frac{\partial \bar{u}}{\partial y} &= -\frac{1}{\rho}\frac{d\bar{P}}{dx} + \frac{1}{\rho}\frac{\partial}{\partial y}\left[(\mu+\mu_t)\frac{\partial \bar{u}}{\partial y}\right]\\ &= -\frac{1}{\rho}\frac{d\bar{P}}{dx} + \frac{1}{\rho}\frac{\partial}{\partial y}\left[\mu_{\text{eff}}\frac{\partial \bar{u}}{\partial y}\right]\end{aligned}$$

where the effective viscosity is defined as

$$\mu_{\text{eff}} = \mu + \mu_t = \rho(\nu + \varepsilon_M)$$

and the model for either the turbulent diffusivity μ_t or the eddy diffusivity ε_M comes from Eq. (11-6),

$$\mu_t = \rho l^2 \left|\frac{\partial \bar{u}}{\partial y}\right|, \qquad \varepsilon_M = l^2 \left|\frac{\partial \bar{u}}{\partial y}\right|$$

In the outer part of the boundary layer, the mixing length l is evaluated from Eq. (11-8), while in the inner part it is evaluated from Eq. (11-25), and the effective sublayer thickness A^+ in the Van Driest damping function evaluated from Eq. (11-26). In summary,

$$l(y) = \begin{cases} \kappa y D \\ \lambda \delta_{99} \end{cases}$$

$$D = (1 - e^{-y^+/A^+})$$

$$l(y) = \min(\kappa y D, \lambda \delta_{99})$$

On the basis of results from Figs. 11-2, 11-5, and 11-6 the model constants of $\kappa = 0.41$ and $\lambda = 0.085$, coupled with $A^+ = 25$ work for flat plate (zero pressure gradient) turbulent boundary layers at moderate Re_{δ_2}. For lower values of Re_{δ_2}, λ increases, and a function that more accurately represents the λ behavior is

$$\lambda = \min\left[\lambda_\infty, \frac{2.9345758\,\lambda_\infty}{(\mathrm{Re}_{\delta_2})^{0.125}}\left(1 - 67.5\frac{v_s}{U_\infty}\right)\right]$$

where $\lambda_\infty = 0.085$.

One difficulty that arises in using Eq. (11-26) is that the sublayer thickness does not instantaneously change when p^+ and/or v_s^+ are abruptly changed. A new state of sublayer equilibrium may not obtain for some distance along the surface, and the following lag equation provides a convenient and reasonably practicable way to handle this problem:

$$\frac{dA^+_{\mathrm{eff}}}{dx^+} = \frac{(A^+ - A^+_{\mathrm{eff}})}{C} \tag{11-27}$$

where A^+ is the value determined from Eq. (11-26), $x^+ = x\sqrt{\tau_s/\rho}/\nu$, and C is an empirical constant. Since $A^+ = A^+(p^+, v_s^+)$, a more accurate way to reflect the change of the sublayer thickness is to reformulate Eq. (11-26) to become

$$A^+ = \frac{25.0}{a\{v^+_{s,\mathrm{eff}} + b[p^+_{\mathrm{eff}}/(1 + c v^+_{s,\mathrm{eff}})]\} + 1}$$

and compute the effective value of p^+ using the following scheme based on a form of lag Eq. (11-27)

$$\frac{dp^+_{\mathrm{eff}}}{dx^+} = \frac{(p^+ - p^+_{\mathrm{eff}})}{C}$$

which upon integration becomes

$$p^+_{\mathrm{eff}}\Big|_{x+dx} = p^+\Big|_{x+dx} - \left(p^+\Big|_{x+dx} - p^+_{\mathrm{eff}}\Big|_x\right)\exp\left(\frac{dx^+}{C}\right)$$

$$dx^+ = dx\sqrt{\tau_s/\rho}/\nu$$

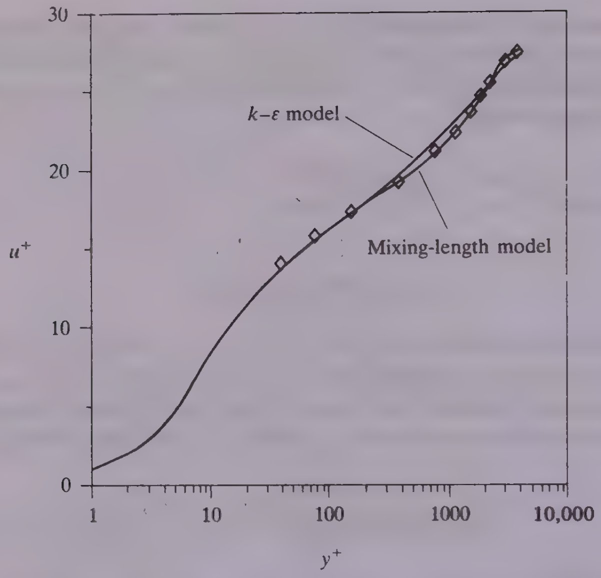

Figure 11-6 Prediction of a constant free-stream velocity profile (data of Wieghardt IDENT 1400, $\mathrm{Re}_{\delta_2} = 10{,}600$).

For the pressure gradient lag equation, $C = 4000$, and this value is reduced to $C = 1200$ if the equilibrium value exceeds the effective value. With acceleration and blowing, the effective value of p^+ cannot be more negative than -0.032. A similar equation is used for v_s^+.

Figure 11-6 shows an example of a complete velocity profile calculated by the mixing-length procedure just described. (Also included is a velocity profile calculated by using the k–ε model, which will be discussed later.) This is a case of constant free-stream velocity, which is easy for most models to handle, but it is worth noting that the "wake" is quite well reproduced by this very simple version of a mixing-length model.

Figure 11-7 shows the friction coefficient plotted as a function of Re_{δ_2} for this model, together with experimental data, and also Eq. (11-23). Note that the mixing-length model (and also the k–ε model) predicts this case very well, but that Eq. (11-23) tends to underpredict $c_f/2$ at the higher Reynolds numbers. The reasons for this were discussed earlier.

Figure 11-8 shows a prediction of $c_f/2$ for an accelerating flow. Here again the mixing-length model fares rather well, and it is likewise quite adequate for blowing and suction, and strong acceleration. Where it fares less well is for adverse pressure gradients (as shown in Fig. 11-9) and for strongly nonequilibrium boundary layers, a topic that will be discussed later (as shown in Fig. 11-10).

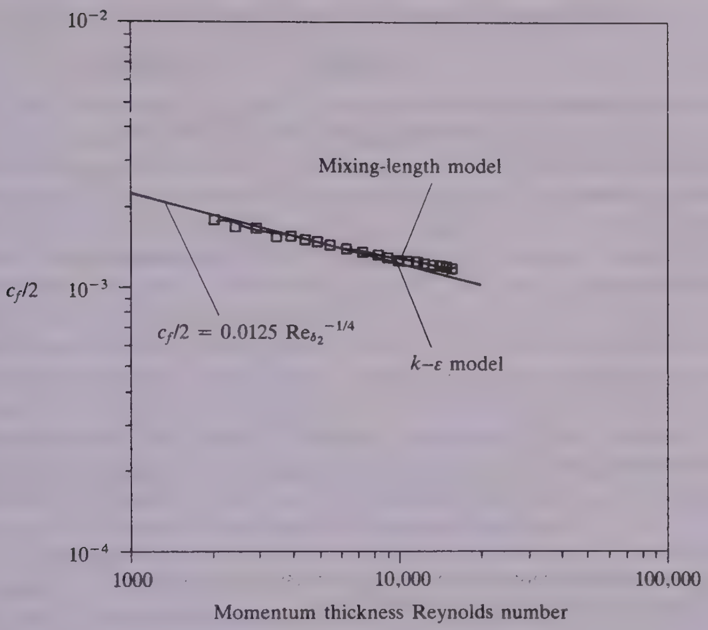

Figure 11-7 Friction coefficient for constant free-stream velocity (data of Wieghardt IDENT 1400).

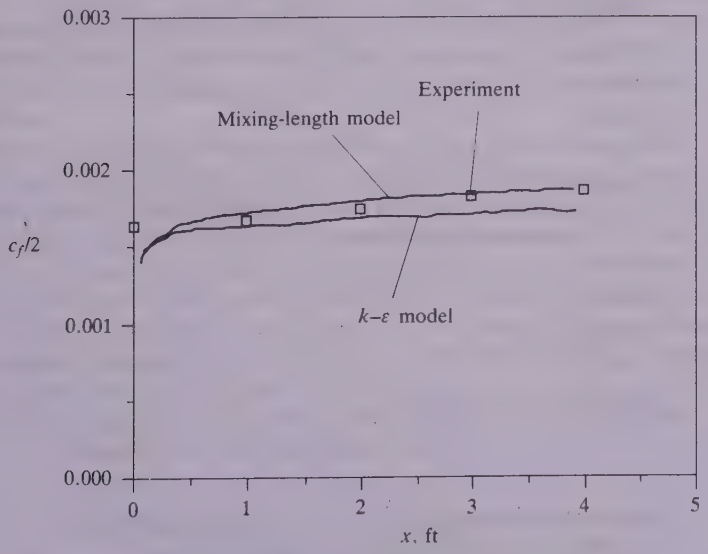

Figure 11-8 Friction coefficient for an accelerating flow. Accelerating flow IDENT 2800.

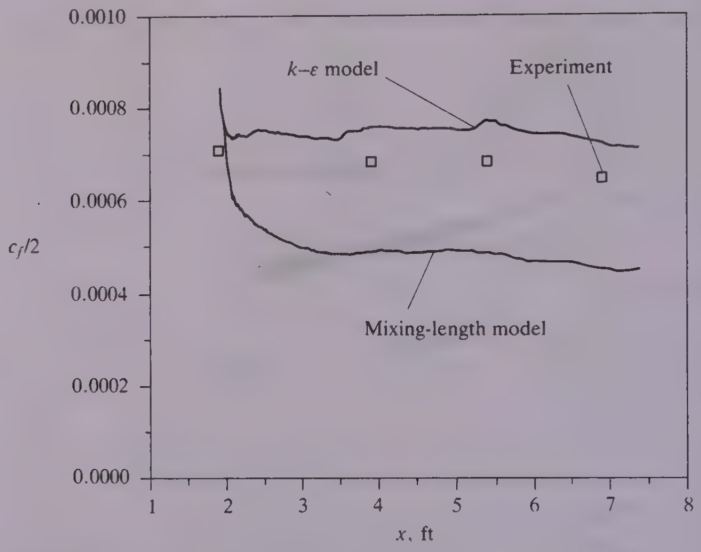

Figure 11-9 Friction coefficient for an adverse pressure gradient. Equilibrium decelerating flow IDENT 2600.

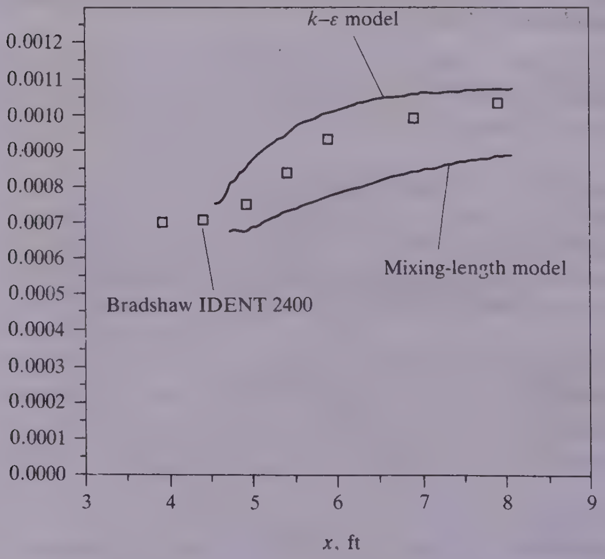

Figure 11-10 Friction coefficient for a strongly nonequilibrium boundary layer (constant free-stream velocity following an adverse pressure gradient). Bradshaw relaxing flow IDENT 2400.

A MODEL BASED ON THE TURBULENCE KINETIC ENERGY EQUATION

Some of the limitations of the mixing-length model of turbulence were noted in the last section. Although the mixing-length model seems quite adequate for accelerating flows, and it also seems adequate for blowing and suction (although this has not yet been examined), its limitations begin to show up when decelerating flows (adverse pressure gradients) are considered, and it becomes quite evident that it has serious limitations in nonequilibrium situations. An example of a nonequilibrium flow was shown in Fig. 11-10. In that case an adverse-pressure-gradient flow, where the velocity profile has a large wake, is followed by constant free-stream velocity. The level of turbulence in the outer part of the boundary layer is very much greater than it would be for a constant free-stream velocity, and the boundary layer in the constant free-stream section is rather slow to respond to this change of boundary conditions; the mixing-length model provides no provision for this possibility. The result is a considerable underprediction of the friction coefficient. The mixing-length model also contains no simple way to account for the effects of free-stream turbulence.

When heat and mass transfer are considered, situations may be encountered where there is a substantial level of turbulence but no gradient in the mean velocity profile. The mixing-length model would predict zero eddy diffusivity, which is obviously incorrect. An example of this possibility would be the region near the centerline of a duct where the velocity gradient is zero or near zero. The eddy diffusivity in this region can be quite substantial, which would have little effect on velocity-profile calculations, but could have very substantial effects on heat-transfer calculations if the duct were heated asymmetrically.

The difficulty is that it is only for a few relatively simple cases that the mixing length is a function of distance from the wall and/or boundary-layer thickness.

However, a model based on the *kinetic energy of turbulence* offers a possibility for predicting the eddy diffusivity under conditions such as those described, because it seems plausible that there is a relationship between eddy diffusivity and turbulence kinetic energy. Furthermore, Eq. (6-40), developed in Chap. 6, shows that the turbulence kinetic energy is a quantity that is produced and decays in the boundary layer, but that also diffuses across the boundary layer in much the same manner as heat. And, in fact, it seems to have some of the very characteristics that would be necessary to account for the apparent behavior of the eddy diffusivity in the examples cited above.

If the fluid density is treated as constant, the turbulence kinetic energy equation for the boundary layer, Eq. (6-40), becomes

$$\bar{u}\frac{\partial \bar{k}}{\partial x} + v\frac{\partial \bar{k}}{\partial y} = \frac{\partial}{\partial y}\left[\nu\frac{\partial \bar{k}}{\partial y} - \overline{(k' + P'/\rho)v'}\right] + (-\overline{u'v'})\frac{\partial \bar{u}}{\partial y} - \varepsilon \qquad (11\text{-}28)$$

The terms on the left-hand side are analogous to similar terms found in the momentum equation and the energy equation in that they represent convection of turbulence kinetic energy. The first term on the right-hand side is diffusional in nature, because of both molecular and turbulent motion. The second term on the right-hand side accounts for the *production* of turbulence kinetic energy, while the third represents the *dissipation* of that energy into thermal energy through the action of viscosity.

Note that the equation tells us that it requires turbulence to produce turbulence, and that turbulence is produced only when there is a gradient in the mean velocity. The equation further implies that viscosity continually acts to decay the turbulent motion regardless of whether turbulence is being produced. The convection and diffusion terms act to transport the turbulence into regions where it is not being produced.

Equation (11-28) is valid only in the region where turbulence is fully developed. It is not applicable in the sublayer region, where viscous forces predominate.

We will now introduce some simplifications into Eq. (11-28). First the definition of eddy diffusivity, Eq. (11-2), provides a way of evaluating $\overline{u'v'}$. Next the similarity of the term $\overline{(k' + P'/\rho)v'}$ to the molecular term suggests that an eddy diffusivity for the turbulent transport of turbulent kinetic energy be defined:

$$\overline{\left(k' + \frac{P'}{\rho}\right)v'} = -\varepsilon_k \frac{\partial \bar{k}}{\partial y} \tag{11-29}$$

With these substitutions, Eq. (11-28) becomes

$$\bar{u}\frac{\partial \bar{k}}{\partial x} + \bar{v}\frac{\partial \bar{k}}{\partial y} = \frac{\partial}{\partial y}\left[(\nu + \varepsilon_k)\frac{\partial \bar{k}}{\partial y}\right] + \varepsilon_M\left(\frac{\partial \bar{u}}{\partial y}\right)^2 - \varepsilon \tag{11-30}$$

To help develop a relationship between eddy diffusivity and the turbulence kinetic energy, we consider dimensional analysis of the model for mixing length, Eq. (11-6)

$$\varepsilon_M = l^2\left|\frac{\partial \bar{u}}{\partial y}\right| = l_{m-l}\cdot\left(l_{m-l}\left|\frac{\partial \bar{u}}{\partial y}\right|\right)$$

For this choice for the decomposition we can observe that the eddy diffusivity for momentum is the product of a length scale and a velocity scale. On the basis of this idea, the following model is proposed:

$$\varepsilon_M = a l_k \sqrt{\bar{k}} \tag{11-31}$$

Here the length scale l_k can be interpreted as a scale associated with the size of the turbulent eddies. Information on this scale will have to be supplied, as with the mixing length, and the constant a will have to be interpreted. Note that in the mixing-length model the constant is absorbed in the definition of l_{m-l}. The velocity scale $\sqrt{\bar{k}}$ will be computed directly from the turbulence kinetic energy equation.

To use Eq. (11-30) we observe that we will also need models for ε_k and ε. First we consider the dissipation ε because it reflects the behavior of $\bar{k}$ both within the boundary layer and in the free stream. If we consider first the free stream, the form of Eq. (11-30) reduces to

$$u_\infty \frac{\partial \bar{k}_\infty}{\partial x} = -\varepsilon_\infty$$

Using this equation, we again invoke dimensional analysis, and we observe that ε can be formed purely from velocity and length scales. Thus we propose a model for the dissipation:

$$\varepsilon = C_D \frac{\left(\sqrt{\bar{k}}\right)^3}{l_\varepsilon} = C_D \frac{\bar{k}^{3/2}}{l_\varepsilon} \tag{11-32}$$

Once again, the velocity scale is chosen to be $\sqrt{\bar{k}}$, and the corresponding length scale is a dissipation length scale, l_ε. From turbulence measurements in the free stream, we know that $\bar{k}$ decays in the flow direction and the corresponding length scale of the turbulent eddies in the free stream becomes larger. The constant of proportionality for the model is C_D.

Recall that a primary reason for selecting a turbulence kinetic energy equation model over the Prandtl mixing-length model is to account for the effects of free-stream turbulence on the eddy diffusivity for momentum within the boundary layer. Within the boundary layer, especially near the wall, we will expect both models to have similar behavior, because within this region the production of turbulence will be expected to dominate. Now let us examine the region near the wall, but outside of the sublayer, where the law of the wall, Eq. (11-16), is applicable. For a flat-plate (zero pressure gradient) turbulent boundary layer in this region, experimental results show that the wall shear stress is constant, $\tau = \tau_s$; the effects of the laminar shear stress is negligible such that $\nu \ll \varepsilon_m$; and $\bar{u}$ is a function of y alone. Measurements of $\bar{k}$ in this region show it to be somewhat constant, and the ratio of turbulence kinetic energy to turbulent shear stress, $\bar{k}/\overline{u'v'}$, is also nearly constant. With this information, Eq. (11-30) reduces to

$$0 = \varepsilon_M \left(\frac{\partial \bar{u}}{\partial y}\right)^2 - \varepsilon \tag{11-33}$$

This reduced form of the turbulence kinetic energy equation is often interpreted as stating that in the region where the law of the wall is valid (the log region) a local equilibrium exists such that the production of $\bar{k}$ is balanced by the dissipation of $\bar{k}$. We can now work with this reduced form (production = dissipation) to gain further insight into the model constant C_D. To do so, we first need an expression for the velocity gradient in the law of the wall region using ideas similar to what was needed to develop Eq. (11-16).

In the fully turbulent region, Eq. (11-9), converted to wall coordinates, and with $\nu \ll \varepsilon_m$, becomes

$$\tau^+ = \left(1 + \frac{\varepsilon_M}{\nu}\right)\frac{du^+}{dy^+} \approx \frac{\varepsilon_M}{\nu}\frac{du^+}{dy^+}$$

Equation (11-13) for the flat-plate turbulent boundary layer is reduced to

$$\frac{\tau}{\tau_s} = \tau^+ = 1$$

These two equations combine to give

$$\frac{du^+}{dy^+} = \frac{\tau^+}{\varepsilon_M/\nu} = \frac{1}{\varepsilon_M/\nu}$$

or, in terms of physical coordinates

$$\frac{du}{dy} = \frac{u_\tau^2}{\varepsilon_M}$$

Using this expression for the velocity gradient and using Eq. (11-32) for the dissipation, Eq. (11-33) becomes

$$\frac{u_\tau^4}{\varepsilon_M} = C_D \frac{\bar{k}^{3/2}}{l_\varepsilon}$$

If we convert k to the inner-layer wall-coordinate form

$$k^+ = \frac{\bar{k}}{u_\tau^2}$$

and use Eq. (11-31) for the eddy diffusivity for momentum, we find the relationship between a and C_D:

$$C_D = \frac{1}{a}\frac{l_\varepsilon}{l_k}\left(\frac{1}{k^+}\right)^2$$

It is generally assumed that in the log region the length scales for production (relating to l_k) and dissipation (relating to l_ε) are similar, and the expression for C_D reduces to

$$C_D = \frac{1}{a}\left(\frac{1}{k^+}\right)^2 \tag{11-34}$$

Turbulent boundary layer experimental data for zero-pressure-gradient flows show k^+ to be in the range of about 3–5 in the region where production balances dissipation. If we absorb the constant a into l_k as is done in the mixing-length model, $a = 1$, and let k^+ be 3.33 we obtain $C_D = 0.09$.

We now need to relate l_k to l_{m-l}, the traditional mixing length. Once again we examine the relationship between production and dissipation of turbulence kinetic energy, Eq. (11-33), and we substitute the dissipation model for the dissipation term (Eq. 11-32), obtaining

$$\varepsilon_M\left(\frac{\partial \bar{u}}{\partial y}\right)^2 = C_D \frac{\bar{k}^{3/2}}{l_\varepsilon}$$

For the log region, the velocity gradient is replaced by that derived from the law of the wall,

$$\varepsilon_M\left(\frac{u_\tau^2}{\varepsilon_M}\right)^2 = C_D\frac{\bar{k}^{3/2}}{l_\varepsilon}$$

Now we substitute the mixing-length model for the eddy diffusivity for momentum (Eq. 11-6), and we obtain

$$(l_{m-l})^2\left(\frac{u_\tau}{l_{m-l}}\right)^3 = C_D\frac{\bar{k}^{3/2}}{l_\varepsilon}$$

Rearranging, we obtain,

$$\frac{l_\varepsilon}{l_{m-l}} = C_D\left(\frac{\sqrt{\bar{k}}}{u_\tau}\right)^3 = C_D\left(\sqrt{k^+}\right)^3$$

Inserting Eq. (11-34) for C_D, along with $a = 1$ and the approximation of $l_k = l_\varepsilon$, yields the relationship between l_k and l_{m-l},

$$\frac{l_k}{l_{m-l}} = C_D^{1/4} \tag{11-35}$$

The final form of Eq. (11-31) for the turbulence kinetic energy model of eddy diffusivity for momentum is now complete. The eddy diffusivity model becomes

$$\varepsilon_M = C_D^{1/4} l_{m-l}\sqrt{\bar{k}} = 0.548 l_{m-l}\sqrt{\bar{k}} \tag{11-36}$$

and the dissipation model becomes

$$\varepsilon = C_D\frac{\left(\sqrt{\bar{k}}\right)^3}{l_{m-l}C_D^{1/4}} = C_D^{3/4}\frac{\bar{k}^{3/2}}{l_{m-l}} = 0.164\frac{\bar{k}^{3/2}}{l_{m-l}} \tag{11-37}$$

Any adjustment to this model to further establish the validity of the model will focus on C_D, relating to the value of k^+ in the log region and the balance between production and dissipation.

To complete the model, we need to be able to evaluate ε_k, the eddy diffusivity for turbulence kinetic energy transport. If we assume that a direct relationship probably exists between ε_k and ε_M, we can define a turbulence Schmidt number Sc_k, and treat it as an experimental constant; i.e.,

$$\mathrm{Sc}_k = \varepsilon_M/\varepsilon_k \tag{11-38}$$

To use this model, it is necessary to solve Eq. (11-30) simultaneously with the momentum equation, so there is an additional partial differential equation to deal with; however, this is not difficult to do on a computer when performing numerical calculations, because the two equations have similar structures.

It is also necessary to provide some kind of independent solution for the sublayer region, where this model is not valid. We assume that the sublayer is not affected by variations in $\bar{k}$ in the outer region; i.e., the sublayer comes to equilibrium with the imposed boundary conditions more quickly than does the outer region. The mixing-length model can then be used to solve the momentum equation through the sublayer and for some predetermined distance into the logarithmic region. At this point, which can be arbitrarily chosen, ε_M is established from the mixing-length solution, and then Eq. (11-36) can be used to determine $\bar{k}$ at this point. Equation (11-30) is then solved from this point outwards using the calculated value of $\bar{k}$ as its inner boundary condition. This procedure is called a *two-layer model procedure.*

The boundary condition on $\bar{k}$ at the outer edge of the boundary layer is either 0 or whatever is specified as the free-stream value of $\bar{k}$. Traditionally this value comes from measurement of the flow-direction fluctuation in u_∞, which is normalized and called *flow-direction turbulence intensity,*

$$\mathrm{Tu} = \frac{\sqrt{\overline{u'^2_\infty}}}{\bar{u}_\infty}$$

and then converted to turbulence kinetic energy with the assumption that the fluctuations are isotropic, namely the same in the two coordinate directions perpendicular to the flow direction. Thus the free-stream turbulence kinetic energy becomes

$$\bar{k}_\infty = \frac{3}{2}\left(\mathrm{Tu}\cdot\bar{u}_\infty\right)^2$$

Values for Tu are traditionally reported in percentage, and they can range from so-called low values near 1 percent, associated with "quiet" experimental wind-tunnel facilities, and upward to 20 percent or more, associated with products of combustion. Tu either is treated as frozen, that is, unchanging, or is permitted to change in the flow direction, following the physics of the turbulence decay process.

The unsatisfactory aspect of this model is the necessity to provide an empirical algebraic equation for the length scale, since one would expect the length scale to be affected by the very same influences that cause $\bar{k}$ to depart from its equilibrium values. It is feasible to develop a differential equation for the length scale (actually the product $\bar{k}l_k$) similar in form to the equation for $\bar{k}$ (see, for example, Ref. 6), and the solution of such an equation simultaneously with Eq. (11-30) would in principle provide a more satisfactory model. However, a differential equation for the dissipation rate ε can also be developed (see Chap. 6), and the dissipation rate equation, together with Eq. (11-30), has been found to provide a more satisfactory model. This two-equation model, which is usually referred to as the k–ε model, was apparently first proposed by Harlow and Nakayama,[7] and first popularized by Jones and Launder.[8] This model is the subject of the next section.

THE k–ε MODEL

A transport equation for the dissipation rate ε was introduced in Chap. 6. Although this equation is significantly more complex than the k equation, its modeling proceeds in an almost identical manner. Two modeling issues must be addressed, namely the diffusion terms and the source and sink terms, i.e., the production and dissipation of ε. In the set of diffusion terms $T_\varepsilon + \Pi_\varepsilon + D_\varepsilon$, the pair $T_\varepsilon + \Pi_\varepsilon$ are modeled by using the same eddy diffusivity concept as that leading to Eq. (11-29), and D_ε is modeled as a molecular-gradient diffusion term. The set $P_\varepsilon - \varepsilon_\varepsilon$ is modeled by using dimensional analysis and the requirements that it reflect production of ε proportional to the production of k, and dissipation of ε that follows the trend of the decay of grid-generated turbulence as observed experimentally. With these models, the boundary-layer form of the dissipation equation (5-42) becomes, for the case of constant fluid properties,

$$\bar{u}\frac{\partial \varepsilon}{\partial x} + \bar{v}\frac{\partial \varepsilon}{\partial y} = \frac{\partial}{\partial y}\left[(\nu + \varepsilon_\varepsilon)\frac{\partial \varepsilon}{\partial y}\right] + C_1\frac{\varepsilon}{\bar{k}}\left[\varepsilon_m\left(\frac{\partial u}{\partial y}\right)^2\right] - C_2\frac{\varepsilon^2}{\bar{k}} \qquad (11\text{-}39)$$

The eddy diffusivity for the turbulent transport of ε, ε_ε, can be assumed to be related to the eddy diffusivity for momentum, ε_M, so we will define a turbulent Schmidt number for the transport of dissipation rate:

$$\mathrm{Sc}_\varepsilon = \varepsilon_M / \varepsilon_\varepsilon \qquad (11\text{-}40)$$

The hope here, of course, is that Sc_ε can be treated as an experimentally determined constant.

To use this model, let us return to Eqs. (11-31) and (11-37). If these are each solved for l_t and then combined to eliminate l_t, we obtain an equation for ε_M in terms of $\bar{k}$ and ε (the constants have been combined into a new constant C_μ):

$$\varepsilon_M = C_\mu \bar{k}^2 / \varepsilon \qquad (11\text{-}41)$$

Thus if we have a solution to both the $\bar{k}$ equation (11-30) and the ε equation (11-39), we can determine ε_M. A set of constants recommended by Jones and Launder[8] after examination of a considerable body of experimental data is

$$C_\mu = 0.09, \qquad C_1 = 1.44, \qquad C_2 = 1.92$$
$$\mathrm{Sc}_k = 1.0, \qquad \mathrm{Sc}_\varepsilon = 1.3$$

Once more, this equation is valid only *outside* of the sublayer. The sublayer region can be calculated using mixing-length theory, and then the value of ε at the point at which it is desired to patch the inner and outer regions together can be determined from Eq. (11-41). In other words, the wall region is handled in the same manner as described for the $\bar{k}$ equation. The boundary condition on ε at the outer edge of the boundary layer is determined by using a value specified from what is known about the free stream, or, if the free-stream turbulence is specified as zero, an adequate procedure is to assume that the gradient of ε with respect to y is zero. Note that if the free-stream turbulence kinetic energy and the length scale for the free-stream turbulence are known, a boundary value for ε can be evaluated from Eq. (11-37).

The k–ε model thus involves simultaneous solution of the momentum equation, continuity equation, $\bar{k}$ equation, and ε equation. Since these equations all have the same general structure, their simultaneous solution by numerical methods does not add greatly to the complexity and time required for solution.

Numerous proposals have been made to extend the $\bar{k}$ and ε equations all the way to the wall. This has generally involved adding additional terms to the right-hand sides of Eqs. (11-30) and (11-39), together with additional experimental constants. However, it is not at present clear which proposal is definitive. In the meantime, using mixing-length theory for the sublayer, or simply using an algebraic equation such as the law of the wall, is adequate for many applications. The use of an algebraic equation is often referred to as "using a wall function."

Some examples of use of the k–ε model are shown in Figs. 11-6 to 11-10. Figure 11-6 shows a comparison of a velocity profile, as predicted by the k–ε model, with experiment for the case of constant free-stream velocity. Note that the model does predict a wake, although it does not fit the experimental data quite as well as the mixing-length model. The prediction for the friction coefficient, Fig. 11-7, for the same case is virtually identical to the results from the mixing-length model. Figure 11-8 shows friction-coefficient results for an accelerating flow. The mixing-length model appears to give slightly better results than the k–ε model, but the differences are small. Where the k–ε model appears to be an improvement is shown in Figs. 11-9 and 11-10. Figure 11-9 shows the case of an adverse pressure gradient (decelerating flow), while Fig. 11-9 shows a non-equilibrium case produced by following an adverse pressure gradient with a constant free-stream velocity section. In both cases the mixing-length model underpredicts the friction coefficient while the k–ε model comes considerably closer to the data.

EQUILIBRIUM TURBULENT BOUNDARY LAYERS

In the preceding sections reference has been made to *equilibrium* boundary layers without precisely defining what the term implies. In the study of laminar boundary layers it was found that significant simplifications occurred when attention was confined to certain classes of flows, in particular to those flows that led to *similarity* solutions and geometrically similar velocity profiles.

In the study of *turbulent* boundary layers it would be convenient to be able to define some kind of similarity that would lead to a classifiable group of flows. The problem is not quite so straightforward as for laminar boundary layers. In our discussion of the law of the wall we observed a type of similarity in the *inner region* in (u^+, y^+) coordinates, but in that coordinate system the outer region is not self-similar, as can be seen when the two velocity profiles shown in Fig. 11-3 are compared. We are now going to seek a family of flows having *outer-region similarity*, even if we have to sacrifice inner-region similarity in order to define such flows.

Clauser[9] proposed that turbulent boundary layers having outer-region similarity be called *equilibrium boundary layers*, and that an equilibrium boundary layer be one for which the velocity profiles plotted in *velocity defect coordinates* be universal, i.e.,

$$\frac{\bar{u} - u_\infty}{u_\tau} = f\left(\frac{y}{\delta_3}\right)$$

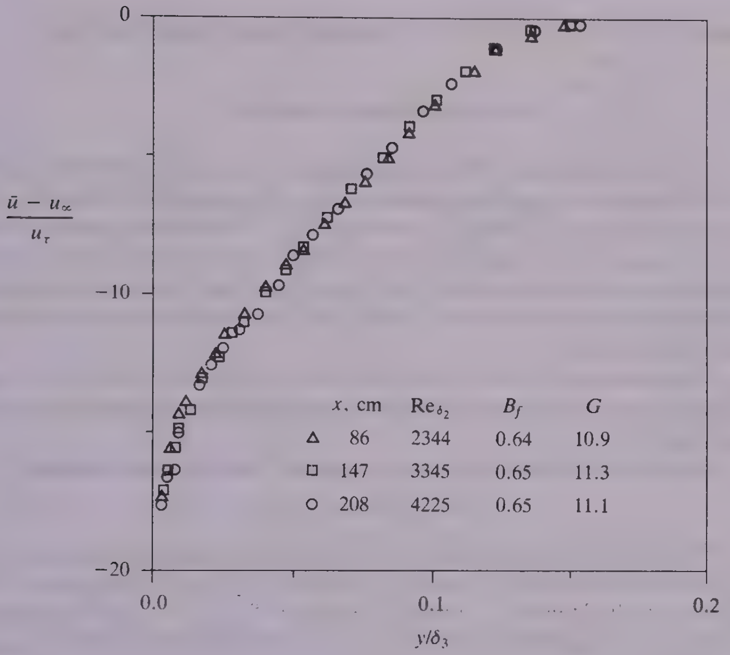

Figure 11-11 Defect profiles for an adverse pressure gradient, transpired turbulent boundary layer (data of Andersen *et al.*[1]).

where this function is independent of position along the surface, and where

$$\delta_3 = -\int_0^\infty \frac{\bar{u} - u_\infty}{u_\tau}\, dy \tag{11-42}$$

Figure 11-11 shows a plot of three velocity profiles for a typical equilibrium boundary layer. (Actually, this one is an adverse-pressure-gradient boundary layer with blowing.)

Clauser also proposed a *shape factor* that would be a constant, independent of x, under these conditions:

$$G = \int_0^\infty \left(\frac{\bar{u} - u_\infty}{u_\tau}\right)^2 d\left(\frac{y}{\delta_3}\right) \tag{11-43}$$

It is now instructive to examine the *momentum integral equation*, which can be put in the following form (for ρ constant):

$$\frac{d(u_\infty^2 \delta_2)}{dx} = \frac{\tau_s}{\rho}(1 + B_f + \beta) \tag{11-44}$$

where $B_f = \dfrac{v_s/u_\infty}{c_f/2} = \dfrac{\rho v_s u_\infty}{\tau_s}$, a blowing or transpiration parameter

$\beta = \dfrac{\delta_1}{\tau_s}\dfrac{dP}{dx}$, a pressure-gradient parameter

B_f is really the same "blowing parameter" that we encountered in connection with the laminar similarity solutions, i.e., the parameter that had to be maintained constant (recall that $c_f/2$ varies as $\mathrm{Re}_x^{-1/2}$ for laminar boundary layers). But its *physical* interpretation can be seen in the second term. It is the ratio of the *transpired momentum flux* to the *wall shear force*, and thus it is this ratio that is being maintained constant when the laminar similarity solutions for blowing or suction are obtained.

β is another force ratio, of *axial pressure force* to *wall shear force*. Note that the overall equation expresses the rate of growth of the momentum deficit of the boundary layer.

β is related to some of the other parameters that we have discussed:

$$\beta = p^+ H \,\mathrm{Re}_{\delta_2} (c_f/2)^{1/2}$$

We find experimentally that if for a turbulent boundary layer B_f or β or both are constant, we also observe outer-region similarity and G is constant. As a matter of fact, we find that G is a unique function of $B_f + \beta$, as can be seen from the experimental data plotted on Fig. 11-12—data that include a variety of combinations of B_f and β.

Finally, the question remains as to how free-stream velocity or axial pressure-gradient must vary in order to maintain constant β. For a *laminar* boundary layer it was found that similarity solutions were obtained if

$$u_\infty = Cx^m$$

Not too surprisingly, the same free-stream velocity variation for a turbulent boundary layer leads to constant G, that is, to equilibrium boundary layers having outer region similarity.

Another rather special case of equilibrium boundary layers occurs in accelerating flows if an acceleration parameter K is maintained constant along the surface:

$$K = \frac{\nu}{u_\infty^2}\frac{du_\infty}{dx} \tag{11-45}$$

Note that K is related to the inner-region pressure-gradient parameter p^+ by

$$p^+ = \frac{-K}{(c_f/2)^{3/2}}$$

Using this parameter K, the momentum integral equation (for plane flows and constant density) may be written as

$$\frac{1}{u_\infty/\nu}\frac{d\,\mathrm{Re}_{\delta_2}}{dx} = \frac{c_f}{2} + \frac{v_s}{u_\infty} - K(1+H)\,\mathrm{Re}_{\delta_2} \tag{11-46}$$

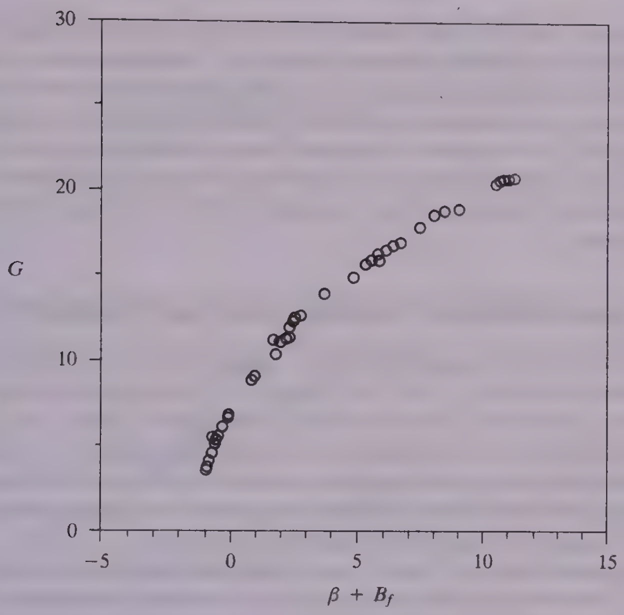

Figure 11-12 Clauser shape factor for a variety of equilibrium turbulent boundary layers, no pressure gradient with and without transpiration, and various adverse pressure gradients with and without transpiration (data of Andersen *et al.*[1]).

If K and v_s/u_∞ are maintained constant with respect to x, if K is positive, and if the last two terms sum to a negative number, then the boundary layer inevitably approaches an equilibrium condition for which Re_{δ_2} is constant. We speak of this as an *asymptotic accelerating flow* (it is also called a *sink flow*). Actually, it is a boundary layer that has both *inner* and *outer* similarity; not only is Re_{δ_2} constant, but so also are $c_f/2$, H, G, and β.

Note that for $K = 0$ an asymptotic layer will be reached for *negative* values of v_s/u_∞, that is, constant suction. This is spoken of as an *asymptotic suction layer.*

If $v_s/u_\infty = 0$, the value of Re_{δ_2} at the point of equilibrium depends on K, large values of K leading to low Re_{δ_2}. Note that Re_{δ_2} can decrease in the flow direction if K is large. If K is sufficiently large, the equilibrium value of Re_{δ_2} can be below the critical Reynolds number for transition from a laminar to a turbulent boundary layer, in which case turbulence production ceases, the turbulence decays, and a laminar boundary layer reemerges. Experimentally, this phenomenon, which is often called *laminarization*, occurs when K exceeds about 3×10^{-6}, although "*laminar-like*" heat-transfer behavior is observed at considerably lower values of K. This phenomenon is frequently seen in highly accelerated flows in nozzles.

As can be seen from the relation following Eq. (11-45), a large value of K is accompanied by a large negative value of p^+. Referring now to Eq. (11-26) for the effective sublayer thickness A^+, a large negative value of p^+ causes A^+ to increase; i.e., the viscous sublayer becomes thicker. At approximately $K = 3 \times 10^{-6}$, A^+ becomes indefinitely large, which means that the viscous sublayer overwhelms the entire boundary layer, all turbulence production ceases, and the boundary layer becomes laminar. So this is another way to explain laminarization.

THE TRANSPIRED TURBULENT BOUNDARY LAYER

So far we have discussed only turbulent boundary layers for which the normal component of velocity v_s is zero, i.e., the case of the impermeable wall. Nonzero values of v_s can occur if the wall is porous and fluid is "blown" or injected into the boundary layer, or is withdrawn or "sucked." Evaporation or condensation or mass transfer in general lead to nonzero values of v_s. We use the term *transpiration*, or the *transpired boundary layer*, as a general description interchangeably with blowing, suction, mass transfer at the surface, etc.

For laminar boundary layers it was found that *similarity solutions* exist for nonzero values of v_s provided that a blowing parameter, essentially B_f, is maintained constant. We have already noted that constant B_f results in an *equilibrium* turbulent boundary layer.

Transpiration alters the structure of the turbulent boundary layer rather considerably, affecting the shear-stress distribution [see Eq. (11-13)], and also strongly affecting the sublayer thickness A^+ [see Eq. (11-26)]. The transpired boundary layer can be calculated quite adequately by finite-difference techniques using the mixing-length model discussed earlier. It is found that both κ and λ are essentially unchanged, so one only need account for the effect of transpiration on A^+. Alternatively, the k–ε model can be used, but since the primary effect of transpiration is in the sublayer, and the k–ε model described here is valid only in the outer region, it is still A^+ that provides the critical information. It is also quite possible to develop a transpiration *law of the wall* comparable to Eq. (11-16) but with an additional log-squared term.

Figure 11-13 shows two typical velocity profiles, in wall coordinates, for a turbulent boundary layer with strong blowing and one with strong suction. Two things are worthy of note. First, in both cases there is definitely a "logarithmic" region close to the wall (a region that yields a straight line on semi-logarithmic coordinates), but it departs significantly from the law of the wall, Eq. (11-16). Second, the *wake* is very large for the blowing case and resembles the wake for an adverse pressure gradient; see Fig. 11-4. Suction has the opposite effects, and the wake completely disappears under strong suction conditions, like the wake for a favorable pressure gradient.

As an alternative to complete solution to the momentum partial differential equation, approximate closed-form algebraic solutions can be developed that are extremely useful and provide quick and easy ways to obtain engineering answers

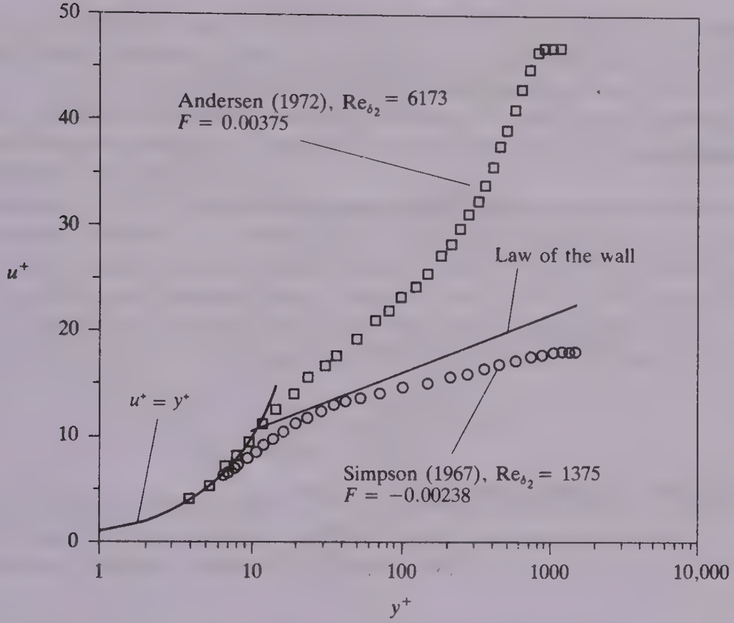

Figure 11-13 The effect of transpiration on velocity profiles, constant free-stream velocity (data of Andersen[10] and Simpson[11]).

that are frequently quite adequate. The following Couette flow solution is rather crude theoretically, but has the virtue of fitting the experimental data surprisingly well.

Consider Eq. (11-3) under the conditions of no pressure gradient, and apply the Couette flow approximation:

$$v_s \frac{d\bar{u}}{dy} = \frac{d}{dy}\left[(\nu + \varepsilon_M)\frac{d\bar{u}}{dy}\right]$$

Let the boundary conditions be

$$\bar{u} = 0, \quad \frac{\tau_s}{\rho} = \nu\left(\frac{d\bar{u}}{dy}\right)_s \qquad \text{at } y = 0$$

$$\bar{u} = u_\infty \qquad \text{at } y = \delta$$

Integrating once and applying the first boundary condition, we get

$$v_s \bar{u} = (\nu + \varepsilon_M)\frac{d\bar{u}}{dy} - \frac{\tau_s}{\rho}$$

Rearranging, and integrating across the boundary layer gives

$$\int_0^{u_\infty} \frac{d\bar{u}}{v_s \bar{u} + \tau_s/\rho} = \int_0^{\delta} \frac{dy}{\nu + \varepsilon_M}$$

that is,

$$\frac{1}{v_s}\ln\left(1+\frac{v_s u_\infty \rho}{\tau_s}\right)=\int_0^\delta \frac{dy}{\nu+\varepsilon_M}$$

But note that

$$\frac{v_s u_\infty \rho}{\tau_s}=B_f=\frac{v_s/u_\infty}{c_f/2}$$

Then

$$\ln(1+B_f)=\frac{c_f}{2}B_f u_\infty \int_0^\delta \frac{dy}{\nu+\varepsilon_M}$$

$$\frac{c_f}{2}=\frac{\ln(1+B_f)}{B_f}\frac{1}{u_\infty}\left(\int_0^\delta \frac{dy}{\nu+\varepsilon_M}\right)^{-1}$$

This equation is indeterminate for $B_f=0$, but

$$\lim_{B_f\to 0}\frac{\ln(1+B_f)}{B_f}=1.0$$

So,

$$\left(\frac{c_f}{2}\right)_0=\frac{1}{u_\infty}\left(\int_0^\delta \frac{dy}{\nu+\varepsilon_M}\right)^{-1}$$

where subscript 0 refers to the $B_f=0$ case.

Then if we make the assumption (obviously not proved) that the two integrals are independent of B_f, dividing the two equations yields

$$\frac{c_f/2}{(c_f/2)_0}=\frac{\ln(1+B_f)}{B_f} \qquad (11\text{-}47)$$

We find that this is an excellent representation of the available experimental data for the no-pressure-gradient case if $(c_f/2)_0$ is evaluated at the *same x-Reynolds number.* Thus we can use Eq. (11-23) to obtain

$$\frac{c_f}{2}=0.0287\frac{\ln(1+B_f)}{B_f}\text{Re}_x^{-0.2} \qquad (11\text{-}48)$$

By use of the momentum integral equation, this result can also be expressed as a function of the *momentum thickness Reynolds number*:

$$\frac{c_f}{2}=0.0125\left[\frac{\ln(1+B_f)}{B_f}\right]^{1.25}(1+B_f)^{0.25}\,\text{Re}_{\delta_2}^{-0.25} \qquad (11\text{-}49)$$

Experimental data indicate that the function $(c_f/2)/(c_f/2)_0$ implied by Eq. (11-49) applies equally well in pressure gradients if the comparison is made at the same value of Re_{δ_2}. (Experimental data supporting this point will be presented later in connection with the corresponding heat-transfer problem.)

Furthermore, although the experiments for which these relations have been established were generally carried out at constant B_f (i.e., equilibrium boundary layers), it is found that they hold quite well if B_f varies along the surface, as, for example, when v_s/u_∞ is held constant rather than B_f. This is simply because the viscous sublayer and the inner region of the turbulent boundary layer come into "equilibrium" very quickly.

Because we have specified a constant-density fluid throughout this discussion, density canceled out of the defining equation for B_f, leaving a velocity ratio v_s/u_∞. If the numerator and denominator are multiplied by ρ, this becomes a mass-flux ratio, and it is really mass flux rather than velocity that is responsible for the phenomena observed. Since many applications, especially to gases, involve significant density differences across the boundary layer, a preferred definition for B_f is

$$B_f = \frac{\dot{m}''/G_\infty}{c_f/2}$$

where $\dot{m}''$ is the mass flux at the wall surface and G_∞ is the free-stream mass flux; that is $G_\infty = u_\infty \rho_\infty$. (Note that $\dot{m}''/G_\infty$ is also denoted by F.)

Another "blowing parameter" frequently used is

$$b_f = \frac{\dot{m}''/G_\infty}{(c_f/2)_0}$$

From Eq. (11-47) we then find that $b_f = \ln(1 + B_f)$, and then

$$\frac{(c_f/2)}{(c_f/2)_0} = \frac{b_f}{e^{b_f} - 1} \tag{11-50}$$

It is frequently more convenient to use b_f than B_f in the evaluation of c_f because of the implicit nature of such an equation as Eq. (11-48). However, Eq. (11-50) is valid only when u_∞ is a constant.

Two limits to the transpired boundary layer should be pointed out. One, the *asymptotic suction layer*, was described in the discussion of equilibrium boundary layers. From Eq. (11-46), for $K = 0$, a constant negative value of v_s/u_∞ (or $\dot{m}''/G_\infty$) leads to constant Re_{δ_2}, and then

$$c_f/2 = -\dot{m}''/G_\infty$$

The second limit occurs at large values of blowing, where the friction coefficient tends to *zero* and the boundary layer is literally blown off the wall surface, an occurrence similar to the separation of a boundary layer in an adverse pressure gradient. Two commonly used rules of thumb for "blow-off" are $\dot{m}''/G_\infty = 0.01$ and $b_f = 4.0$.

THE EFFECTS OF SURFACE ROUGHNESS

In all of the preceding discussion of the turbulent boundary layer, it has been assumed that the surface is aerodynamically smooth, without defining what that term implies. At this point it is appropriate to discuss a rational definition of roughness, so as to establish the limits of the theory already presented, and then to describe some of the effects of roughness.

Surface roughness can take on many shapes. The name of Nikuradse[12] is indelibly associated with the rational analysis of rough surfaces as a result of his experiments with turbulent flow in pipes that were artificially roughened with uniform grains of sand. Schlichting[13] introduced the concept of equivalent sand-grain roughness as a means of characterizing other types of roughness elements by referring to the equivalent net effect produced by Nikuradse's experiments. We will use the symbol k_s, a length dimension, to describe roughness element size, k_s being actually the size of sieve used by Nikuradse to sift the sand.

The effect of roughness on a turbulent boundary layer is primarily right at the wall, and thus a nondimensional expression of a roughness size is logically based on the shear velocity u_τ. This leads to a roughness Reynolds number Re_k as a nondimensional measure of surface roughness:

$$\mathrm{Re}_k = u_\tau k_s/\nu$$

Three regimes can be identified from the experimental data in terms of values of Re_k. For $\mathrm{Re}_k < 5.0$ the surface behaves as perfectly *smooth* (aerodynamically smooth). For $5.0 < \mathrm{Re}_k < 70.0$ there is an increasing effect of roughness, but some of the smooth-surface characteristics persist, and this is called the range of *transitional roughness.* The range $\mathrm{Re}_k > 70.0$ is the regime of a *fully rough* surface. A basic characteristic of the latter is that the friction coefficient c_f becomes independent of Reynolds number, which essentially means that viscosity is no longer a significant variable.

A mixing-length model can be readily developed for the fully rough region. The first effect of roughness is to destabilize the viscous sublayer, which results in an effectively thinner sublayer. At about $\mathrm{Re}_k = 70$ the sublayer disappears entirely, which accounts for the fact that viscosity is no longer a significant variable. But this also means that the shear stress must be transmitted to the wall by some mechanism other than viscous shear. This different mechanism is quite obviously pressure drag directly on the roughness elements, i.e., a result of impact or dynamic pressure on the upstream side of each element.

If the Prandtl mixing-length scheme is used, it is apparent that Eq. (11-7) is no longer valid at the wall surface, because l, and thus ε_M, cannot go to zero at the wall, for otherwise there is no mechanism for transferring the shear stress to the wall. The eddy diffusivity and mixing length must apparently be finite at $y = 0$ for a fully rough surface. This fact can be readily modeled by a near-wall mixing-length equation

$$l = \kappa(y + \delta y_s) \qquad (11\text{-}51)$$

where δy_s might be expected to be proportional to k_s (actually, δy_s turns out to be considerably smaller than k_s).

If we use wall coordinates, the nondimensional form of δy_s is then

$$(\delta y_s)^+ = \frac{\delta y_s\, u_\tau}{\nu} \qquad (11\text{-}52)$$

Experimentally it is found that, approximately,

$$(\delta y_s)^+ = 0.031\,\mathrm{Re}_k \tag{11-53}$$

To develop a law of the wall for the fully rough region, we go back to the development leading to Eq. (11-16) and simply replace $l = \kappa y$ with Eq. (11-51). This then leads to

$$\frac{du^+}{dy^+} = \frac{1}{\kappa[y^+ + (\delta y_s)^+]}$$

Since there is no sublayer in the fully rough region, the lower limit of integration for this differential equation is at $y^+ = 0$:

$$\int_0^{u^+} du^+ = \frac{1}{\kappa}\int_0^{y^+} \frac{dy^+}{y^+ + (\delta y_s)^+}$$

that is,

$$u^+ = \frac{1}{\kappa}\ln\left[\frac{y^+}{(\delta y_s)^+} + 1\right] \tag{11-54}$$

We then substitute Eq. (11-53):

$$u^+ = \frac{1}{\kappa}\ln\left(\frac{32.6y^+}{\mathrm{Re}_k} + 1\right) \tag{11-55}$$

For $y^+ \geq \mathrm{Re}_k$ the last term in the parentheses can be neglected and a simpler form results:

$$u^+ = \frac{1}{\kappa}\ln y^+ + \frac{1}{\kappa}\ln\frac{32.6}{\mathrm{Re}_k} \tag{11-56}$$

This equation fits the available experimental data in the fully rough region for zero pressure gradient and no transpiration quite well, using $\kappa = 0.41$.[14]

An approximate expression for the friction coefficient under the same conditions can be readily developed from Eq. (11-56). Recall that it was noted in connection with Eq. (11-16) that at the outer edge of the boundary layer, for the case of zero pressure gradient and no transpiration, u^+ is always greater than the law of the wall by an additive 2.3. Assuming that the same wake effect obtains for a rough-surface boundary layer, Eq. (11-56) can be modified to yield the value of u^+ at the outer edge of the boundary layer:

$$u_\infty^+ = \frac{1}{\kappa}\ln\frac{\delta u_\tau}{\nu} + \frac{1}{\kappa}\ln\frac{32.6}{\mathrm{Re}_k} + 2.3$$

Then noting that

$$u_\infty^+ = \frac{u_\infty}{u_\tau} = \frac{1}{\sqrt{c_f/2}}$$

we obtain

$$\frac{1}{\sqrt{c_f/2}} = \frac{1}{\kappa}\ln\frac{84\delta}{k_s}$$

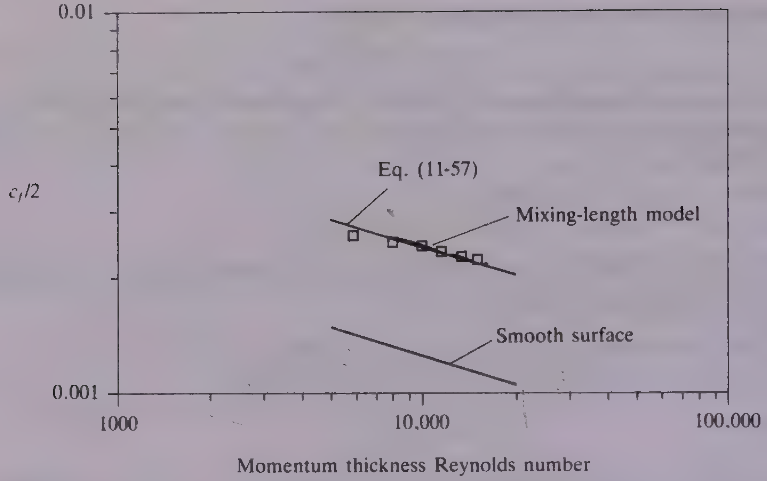

Figure 11-14 Comparison of Eq. (11-57), and the mixing-length model, with experimental data of Pimenta[14] for a rough surface composed of packed balls at constant free-stream velocity (IDENT 71374 fully rough surface, 1.27 mm spheres, $k_s = 0.787$ mm.)

Then if $\delta_2/\delta = 0.097$ still applies, which is a reasonable assumption,

$$\frac{c_f}{2} = \frac{0.168}{[\ln(864\delta_2/k_s)]^2} \tag{11-57}$$

Note that c_f depends only on boundary-layer thickness and the roughness size, and is independent of viscosity and velocity. Figure 11-14 shows a comparison of Eq. (11-57) with experiment. To express $c_f/2$ as a function of distance x along a surface, the momentum integral equation can be used.

Of course the comparison with theory in Fig. 11-14 demonstrates only that k_s is a constant, since the value of k_s used was in fact determined to fit the data. A more convincing demonstration is shown in Fig. 11-15 where a complete velocity profile is shown and compared with Eq. (11-56). Note that the effect of roughness is to move the $u^+ - y^+$ curve downward, although it retains its original slope.

This model can be readily adapted to complete solution of the momentum differential equation of the boundary layer using finite-difference techniques. Referring to the earlier section of this chapter entitled "Summary of a Complete Mixing-Length Theory" it is only necessary to include Eqs. (11-51) and (11-53), and then modify the A^+ function, Eq. (11-26), to account for the reduction of A^+ caused by surface roughness.[†] Examples of such calculations are shown on both Figs. 11-14 and 11-15. The results are virtually identical to those provided by the more approximate theory, except that now the *wake* is reproduced, and of course other boundary conditions can be easily introduced.

[†] For this type of calculation Eq. (11-53) is better approximated by $(\delta y_s)^+ = 0.031(\text{Re}_k - 43)$

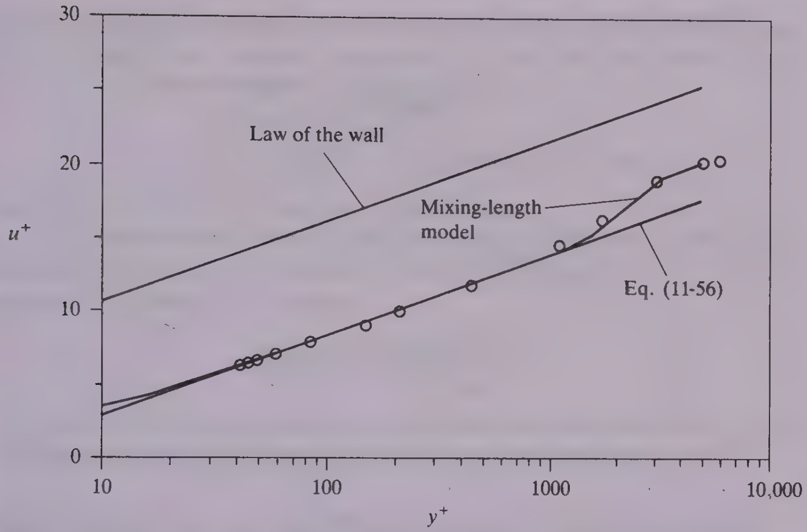

Figure 11-15 Comparison of theory with experiment for a velocity profile for a fully rough surface (data from IDENT 71374, packed spheres, 1.27 mm diameter, $k_s = 0.787$; air, constant $u = 39.82$ m/s, $\mathrm{Re}_{\delta_2} = 11{,}509$, $\mathrm{Re}_k = 101$).

A reasonably adequate procedure for the transitional roughness regime is to let A^+ vary from its smooth-surface value at $\mathrm{Re}_k = 5$ to zero at $\mathrm{Re}_k = 70$. In the absence of other information, a linear variation will usually suffice.

Blowing and suction also affect the way in which a surface responds to roughness. The effective value of Re_k is increased by blowing, and it is found that the following modification of the definition of Re_k provides a reasonable way to account for this fact:

$$\mathrm{Re}_k = k_s(\rho u_\tau + 14\dot{m}'')/\mu$$

THE EFFECTS OF AXIAL CURVATURE

All of the boundary layers considered to this point have been on a flat surface. If, in the direction of flow, the surface is either convex or concave, substantial changes in the structure of the boundary layer can occur. Figure 11-16 shows some examples of the measured friction coefficients for concave and convex surfaces having in both cases a constant radius of curvature of 2.44 m. Convex curvature causes the friction coefficient to decrease, while concave curvature has the opposite effect.

Convex curvature has a *stabilizing* effect on the boundary layer, while concave curvature is *destabilizing*. One would expect then that the sublayer would thicken with convex curvature and thin with concave curvature. While there is some evidence that this may be true, the effect is small. What happens to the

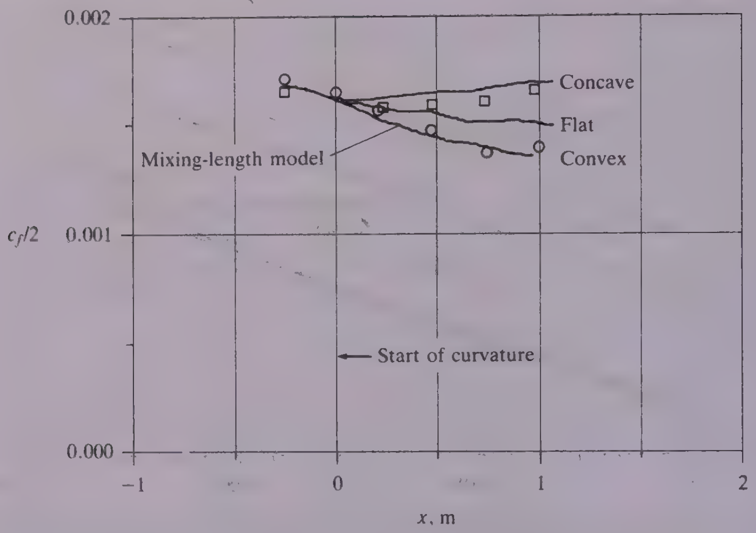

Figure 11-16 The effect of axial surface curvature on the friction coefficient (data of Gibson IDENT 8000/8100; curvature 0.41/m, $u = 23$ m/s).

outer part of the boundary layer is much more dramatic. Convex curvature can cause a substantial *reduction* in the eddy diffusivity over the entire outer region. Concave curvature causes just the reverse, i.e., an *increase* in eddy diffusivity over the entire outer region. A local nondimensional variable that can be used to describe this effect is the *curvature Richardson number* Ri, defined as follows:

$$\mathrm{Ri} = \frac{\bar{u}}{R} \Big/ \frac{d\bar{u}}{dy}$$

where R is the radius of curvature in the flow direction, taken *positive* for convex curvature.

A fairly good mixing-length model for weak curvature ($\delta/R < 0.05$) can be constructed by assuming that the *effective* mixing length at any point in the boundary layer can be determined from the following linear function of Ri:

$$l_{\text{eff}} = l(1 - 10\,\mathrm{Ri})$$

Thus convex curvature has the effect of reducing mixing length, and concave curvature of increasing it.

The rather small effect on sublayer thickness can be modeled by the following modification of the A^+ equation:

$$A^+_{\text{eff}} = \left(1 + \frac{1000\nu}{Ru_\tau}\right) A^+$$

It is found that upon entering a curved region there is a substantial lag in the reduction or augmentation of the mixing length. The following rate equation has been found to provide a reasonable way to approximate this lag, introducing an effective value for the radius of curvature. Let $C = 1/R$, the curvature, and let C_{eff} be the *effective* value of the curvature. Then

$$\frac{dC_{\text{eff}}}{dx} = \frac{0.1(C - C_{\text{eff}})}{\delta_{99}}$$

where δ_{99} is the 99 percent boundary-layer thickness.

If a convex-curved region is followed by a region with no curvature, the boundary layer returns to equilibrium rather slowly. Again this effect can be modeled by a similar rate equation:

$$\frac{dC_{\text{eff}}}{dx} = \frac{800(C - C_{\text{eff}})}{\text{Re}_{\delta_2}\,\delta_{99}}$$

Figure 11-16 shows examples of friction-coefficient predictions for both convex and concave curvature using this mixing-length model.

THE EFFECTS OF FREE-STREAM TURBULENCE

It has been assumed in all of the preceding that turbulence in the free stream outside of the boundary layer is negligible. It is customary to describe the intensity of turbulence in terms of the root mean square of the velocity fluctuation in the flow direction. If the turbulence were *isotropic*, the velocity components in the other directions would be the same, but of course this is not always the case. The turbulence intensity can be expressed nondimensionally by normalizing with respect to other velocities. If the free-stream mean velocity is used for normalization, the turbulence intensity is then defined as

$$\text{Tu} = \frac{\sqrt{\overline{u'^2_\infty}}}{u_\infty} \tag{11-58}$$

The main effect of free-stream turbulence has been found to occur in the outer part of the boundary layer, the wake, where free-stream turbulence increases the eddy diffusivity. The sublayer and the inner part of the logarithmic region are generally unaffected, although it seems likely that sufficiently high free-stream turbulence would affect the entire boundary layer.

Figure 11-17 shows three examples of velocity profiles with free-stream turbulence 0.0, 0.05, and 0.075. There it can be seen rather clearly how the wake is depressed at increasingly higher values of Tu, and nearly all of the available experimental data show similar behavior. Note that the inner region seems virtually unaffected.

The value of u^+ at the outer edge of a turbulent boundary layer is always equal to $1/\sqrt{c_f/2}$, so it is apparent that free-stream turbulence has the effect of *increasing* the friction coefficient.

At the present time there seems to be no generally agreed correlation for the effect of Tu on c_f. Some researchers (see, for example, Hancock and

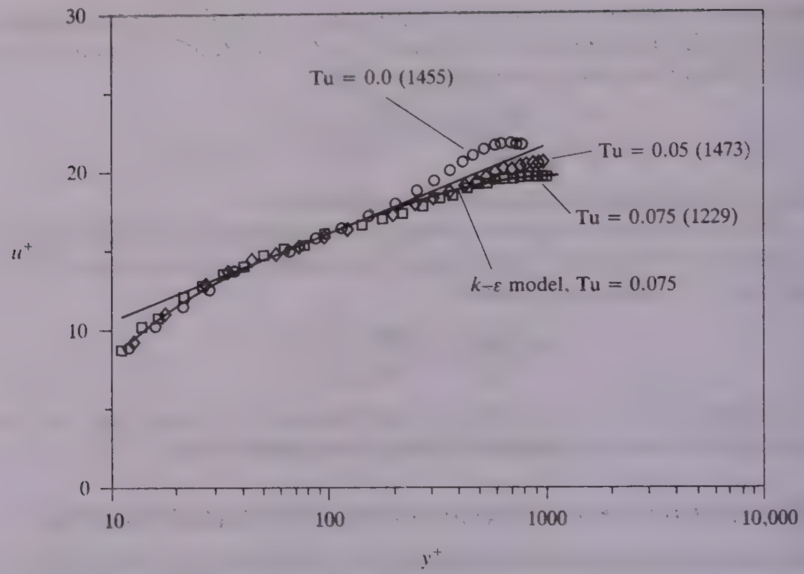

Figure 11-17 The effect of free-stream turbulence on velocity profiles; Re_{δ_2} in parentheses (data of Johnson and Johnston[2]).

Bradshaw[15]) feel that the enhancement of the friction coefficient is a function of both Tu and the *scale* of the free-stream turbulence. The problem is further complicated by the fact that free-stream turbulence decays in the flow direction at a rate that itself depends upon the scale. This decay can be calculated using the turbulence energy equation (11-30) and the dissipation equation (11-39). In both equations it need only be noted that there are no gradients in the y direction in the free stream, so from these we obtain a pair of ordinary differential equations for $\bar{k}$ and ε. Then Eq. (11-37) can be used to evaluate a length scale, and in fact a similar procedure is often used to determine a length scale from the measurements of the decay of $\sqrt{u'^2_\infty}$.

The idea that free-stream turbulence effects are a function of both the turbulence intensity and a length scale suggests that the k–ε model might provide a useful tool for calculating such effects.

Figure 11-17 shows an example of a k–ε calculation. It was assumed that the free-stream turbulence was isotropic, so that the turbulent kinetic energy could be evaluated from Tu. The value of free-stream ε used was based on the experimental value of a length scale and Eq. (11-37). However, the results were relatively insensitive to free-stream length scale. If this were generally true, it would be fortunate, because estimating the free-stream dissipation rate is a vexing problem in design applications. On the other hand, there remains the apparent experimental evidence that this is indeed an important parameter. Although it appears that the k–ε model yields reasonable results for Tu ≤ 0.075, it remains to be seen whether it is adequate at higher turbulence levels.

PROBLEMS

11-1. Using the Van Driest equation for the mixing length in the sublayer, determine u^+ as a function of y^+ for $p^+ = 0$ and $v_s^+ = 0$ by numerical integration of the momentum equation in the region where the Couette flow approximation is valid, for $A^+ = 22, 25$, and 27, and compare with the experimental data in Fig. 11-3. (It is presumed that a programmable computer is used for this problem.)

11-2. Develop a law of the wall for a transpired turbulent boundary layer (that is, $v_s^+ \neq 0$) based on the Prandtl mixing-length theory and a two-layer model of the Couette flow region near the wall. Note that you need to develop a new relation for both the viscous sublayer and the fully turbulent region, and the apparent thickness of the sublayer will be a constant to be determined from experiments.

The table below shows two sets of experimental points for turbulent velocity profiles for $p^+ = 0$ but $v_s^+ \neq 0$. Plot these profiles on semi-logarithmic paper and superimpose the equation you have derived for the fully turbulent region, determining the apparent sublayer thickness from the best fit to the data. Note that there is a "wake," or outer region, for which your analysis does not apply. Finally, plot the apparent sublayer thickness y_{crit}^+ as a function of v_s^+ and discuss the significance of the results.

$v_s^+ = 0.1773$		$v_s^+ = -0.065$	
y^+	u^+	y^+	u^+
30.6	16.84	35.6	12.33
50.3	19.37	48.7	13.02
99.6	23.41	81.7	13.59
148.9	25.72	150.8	14.24
247.6	29.99	249.6	14.80
362.6	34.11	364.8	15.34
510.6	39.36	496.5	15.87
724.3	45.13	628.2	16.20
921.5	47.29	792.8	16.31
1053.0	47.32	990.4	16.31

11-3. Repeat Prob. 11-2 using the Van Driest equation for the sublayer mixing length and numerical integration of the momentum equation. Determine the values of A^+ that best fit the experimental data, and plot these as a function of v_s^+. (It is presumed that a programmable computer is used for this problem.)

11-4. Consider constant-property flow along a flat plate with constant u_∞. Let the boundary layer starting at the origin of the plate be laminar, but assume that a transition to a turbulent boundary layer takes place abruptly at some prescribed critical Reynolds number. Assuming that at the point of transition the momentum thickness of the turbulent boundary layer is the same as the laminar boundary layer (and this is a point for discussion), calculate the development of the turbulent boundary layer and the friction coefficient for the turbulent boundary layer. Plot the friction coefficient as a function of Reynolds number on log–log paper for transition Reynolds numbers (based on distance from the leading edge) of 300,000 and 1,000,000, and compare with the turbulent flow

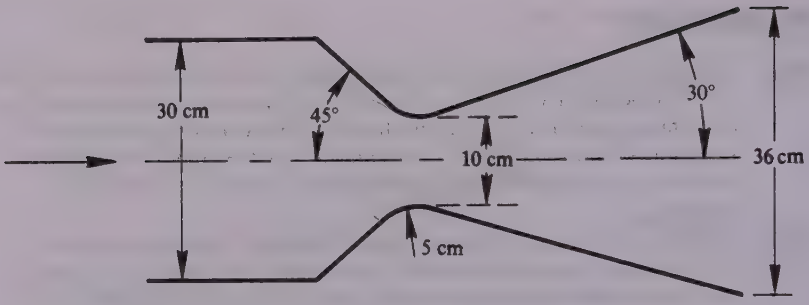

Figure 11-18

friction coefficient that would obtain were the boundary layer turbulent from the plate origin. On the basis of these results, determine a "virtual origin" of a turbulent boundary layer preceded by a laminar boundary layer; that is, the turbulent boundary layer will behave as if the boundary layer had been entirely a turbulent one starting at the virtual origin.

11-5. Redevelop Eq. (11-21) for the case where density and viscosity are functions of x.

11-6. A nuclear rocket nozzle of circular cross section has the geometry shown in Fig. 11-18. The working fluid is helium, and the stagnation pressure and temperature are 2100 kPa and 2475 K, respectively. Assuming one-dimensional isentropic flow, constant specific heats, and a specific heat ratio of 1.67, calculate the mass flow rate and the gas pressure, temperature, and density as functions of distance along the axis. Then, assuming that a laminar boundary layer originates at the corner where the convergence starts, calculate the momentum thickness of the boundary layer and the momentum thickness Reynolds number as functions of distance along the surface. Assume that a transition to a turbulent boundary layer takes place if and when the momentum thickness Reynolds number exceeds 162.

An approximate analysis may be carried out on the assumption of constant fluid properties, in which case let the properties be those obtaining at the throat. Alternatively, a better approximation can be based on the results of Prob. 11-5. In either case it may be assumed that the viscosity varies approximately linearly from $\mu = 5.9 \times 10^{-5}$ N · s/m^2 at 1400 K to $\mu = 8.3 \times 10^{-5}$ N · s/m^2 at 2500 K.

11-7. Work Prob. 11-6 but let the fluid be air and the stagnation pressure and temperature be 2100 kPa and 1275 K, respectively. Calculate the displacement thickness of the boundary layer at the throat of the nozzle. Is any correction to the mass flow rate warranted on the basis of this latter calculation?

11-8. A gas turbine blade, as illustrated in Fig. 11-19, has the following operating conditions:

Fluid: air

Stagnation conditions:

$$P^* = 515.7 \text{ kPa}, \qquad T^* = 1139 \text{ K}$$

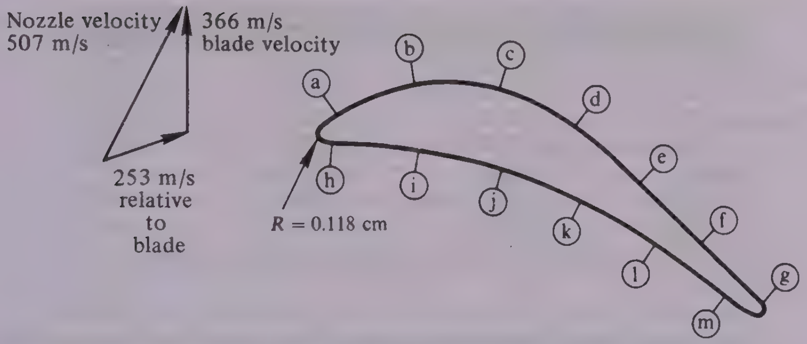

Figure 11-19

Conditions just upstream of the blade:

$$P = 473.7\ \text{kPa}, \qquad T = 1111\ \text{K}$$
$$V = 253\ \text{m/s}, \qquad G = 376\ \text{kg/(s} \cdot \text{m}^2)$$

Free-stream conditions along blade surface:

Point	Distance from leading edge, cm	G, kg/(s · m²)	ρ, kg/m³	T, K
a	0.38	537	1.36	1072
b	1.40	586	1.31	1052
c	2.41	635	1.10	988
d	3.18	620	1.23	1031
e	4.19	576	1.31	1056
f	5.21	547	1.34	1068
g	6.22	537	1.36	1972
h	0.25	293	1.52	1122
i	1.27	317	1.51	1121
j	2.29	327	1.51	1118
k	3.30	352	1.50	1116
l	4.32	430	1.45	1100
m	5.33	537	1.36	1072

Calculate the momentum thickness and the momentum thickness Reynolds number along both surfaces of the blade. Assume that a transition to a turbulent boundary layer takes place when the momentum thickness Reynolds number exceeds 162. Describe how the forces acting on the blade could be analyzed from the given data.

11-9. The following table is an actual velocity profile measured through a turbulent boundary layer on a rough surface made up of 1.27-mm balls packed in a dense, regular pattern. There is no pressure gradient or transpiration. The fluid is air at 1 atm and 19°C; and $u_\infty = 39.7$ m/s, $\delta_2 = 0.376$ cm, $\text{Re}_{\delta_2} = 9974$, $c_f/2 = 0.00243$. The distance y is measured from the plane of the tops of the balls. The objective of this problem is to analyze these data in the framework

y, cm	u, m/s	y, cm	u, m/s
0.020	12.94	0.660	27.38
0.030	14.08	1.10	31.10
0.051	15.67	1.61	34.15
0.081	17.31	2.12	37.21
0.127	19.24	2.82	39.37
0.191	20.87	3.58	39.68
0.279	22.68		
0.406	24.54		

of the rough-surface theory developed in the text. What is the apparent value of k_s? Of Re_k? What is the roughness regime? What is the apparent value of κ? How does the wake compare with that of a smooth surface? Do the data support the theory?

The use of the plane of the tops of the balls as the origin for y is purely arbitrary. Feel free to move the origin if this will provide a more coherent theory.

TEXSTAN PROBLEMS

11-10. TEXSTAN *analysis of the turbulent momentum boundary layer over a flat plate with zero pressure gradient*: Choose a starting x-Reynolds number of about 2×10^5 (corresponding to a momentum Reynolds number of about 700) and pick fluid properties that are appropriate to air, evaluated at a free-stream temperature of 300 K. Use constant fluid properties, and note that the energy equation does not have to be solved. The geometrical dimensions of the plate are 1 m wide (a unit width) by 3.0 m long in the flow direction, corresponding to an ending Re_x of about 2.9×10^6 (a momentum Reynolds number of about 5400). Let the velocity boundary condition at the free stream be 15 m/s. The initial velocity profile appropriate to the starting x-Reynolds number (a fully turbulent boundary layer profile) can be supplied by using the *kstart*=3 choice in TEXSTAN. For a turbulence model, choose the mixing-length turbulence model with the Van Driest damping function (*ktmu*=5).

Calculate the boundary-layer flow and compare the friction coefficient results based on x Reynolds number and momentum thickness Reynolds number with the results in the text, Eqs. (11-20) and (11-23). Evaluate the virtual origin concept as described in Prob. 11-4, and observe whether this affects your ability to compare with Eq. (11-23). Calculate the friction coefficient distribution using momentum integral Eq. (5-11) and compare with the TEXSTAN calculations. Feel free to investigate any other attribute of the boundary-layer flow. For example, you can investigate the mixing-length distribution, comparing to Fig. 11-2, and the law of the wall, comparing to Fig. 11-5.

11-11. TEXSTAN *analysis of the turbulent momentum boundary layer over a flat plate with zero pressure gradient*: This problem is essentially a repeat of the previous problem, but choosing other turbulence models available in TEXSTAN. There exists a 1-equation model (*ktmu*=11) and four 2-equation (k-ε) models (*ktmu*=21,22,23,24). The initial velocity profile appropriate to the starting

x-Reynolds number (a fully turbulent boundary layer profile), along with turbulence profiles for k (and ε) can be supplied by using the *kstart*=3 choice in TEXSTAN. Choose an initial free-stream turbulence of 2 percent. Note that by setting the corresponding initial free-stream dissipation (for the two-equation model) equal to zero, TEXSTAN will compute an appropriate value.

Calculate the boundary-layer flow and compare the friction coefficient results based on x Reynolds number and momentum thickness Reynolds number with the results in the text, Eqs. (11-20) and (11-23). Calculate the friction coefficient distribution using momentum integral Eq. (5-11) and compare with the TEXSTAN calculations. Feel free to investigate any other attribute of the boundary-layer flow. For example, you can calculate the mixing-length model results from the previous problem and compare in a manner similar to Fig. 11-7. Likewise you can investigate the law of the wall, comparing to Fig. 11-6.

11-12. TEXSTAN *analysis of the transitional momentum boundary layer over a flat plate with zero pressure gradient*: Choose a starting x-Reynolds number of about 1000 (corresponding to a momentum Reynolds number of about 20) and pick fluid properties that are appropriate to air, evaluated at a free-stream temperature of 300 K. Use constant fluid properties, and note that the energy equation does not have to be solved. The geometrical dimensions of the plate are 1 m wide (a unit width) by 3.0 m long in the flow direction, corresponding to an ending Re_x of about 2.9×10^6 (a momentum Reynolds number of about 5400). Let the velocity boundary condition at the free stream be 15 m/s. The initial velocity profile appropriate to the starting x-Reynolds number (a laminar Blasius boundary-layer profile) can be supplied by using the *kstart*=4 choice in TEXSTAN. For a turbulence model, choose the mixing-length turbulence model with the Van Driest damping function (*ktmu*=5), along with the *abrupt transition model*, corresponding to *ktmtr*=1 and an appropriate momentum Reynolds number for transition, specified by the variable *gxx*, using the minimal value suggested by Eq. (11-1) or a larger value, say 200. Note that this value typically depends on the free-stream turbulence level.

Calculate the boundary-layer flow and compare the friction coefficient results based on x Reynolds number and momentum thickness Reynolds number with the laminar equations (9-13) and (9-16) and the turbulent equations (11-20) and (11-23). Note that, once again, you can evaluate the friction coefficient distribution by using momentum integral Eq. (5-11) and compare it with the TEXSTAN calculations. Feel free to investigate any other attribute of the boundary-layer flow.

REFERENCES

1. Anderson, P. S., W. M. Kays, and R. J. Moffat: *J. Fluid Mech.*, vol. 69, pp. 353–375, 1975.
2. Johnson, P. L., and J. P. Johnston: *Seventh Symposium on Turbulent Shear Flows, Stanford University*, August 21–23, 1989, pp. 20.2.1–20.2.6, Department of Mechanical Engineering, Stanford University, 1989.
3. Schultz-Grunow, F.: NACA (now NASA) TM-986, Washington, 1941.
4. Van Driest, E. R.: *J. Aero. Sci.*, vol. 23, p. 1007, 1956.

5. Kays, W. M., and R. J. Moffat: *Studies in Convection*, vol. 1, pp. 213–319, Academic Press, London, 1975.
6. Rodi, W., and D. B. Spalding: *Wärme- und Stoffübetragung*, Bd. 3, S. 85–95, 1970.
7. Harlow, F. H., and P. Nakayama: "Transport of Turbulence Decay Rate," Los Alamos Scientific Laboratory, University of California, Report LA-3854, 1968.
8. Jones, W. P., and B. E. Launder: *Int. J. Heat Mass Transfer*, vol. 15, p. 301, 1972.
9. Clauser, F. H.: *J. Aero. Sci.*, vol. 21, pp. 91–108, 1954.
10. Anderson, P. S., W. M. Kays, and R. J. Moffat: Report HMT-15, Thermosciences Division, Department of Mechanical Engineering, Stanford University, May 1972.
11. Simpson, R. L., W. M. Kays, and R. J. Moffat: Report HMT-2, Thermosciences Division, Department of Mechanical Engineering, Stanford University, December 1967.
12. Nikuradse, J.: *Forsch. Arb. Ing.-Wes.*, Nr. 361, 1933.
13. Schlichting, H.: *Ing.-Arch.*, vol. 7, pp. 1–34, 1936.
14. Pimenta, M. M., R. J. Moffat, and W. M. Kays: Report HMT-21, Thermosciences Division, Department of Mechanical Engineering, Stanford University, May 1979.
15. Hancock, P. E., and P. Bradshaw: *J. Heat Transfer*, vol. 105, pp. 284–289, 1983.

CHAPTER 12

Turbulent External Boundary Layers: Heat Transfer

The turbulent thermal boundary layer bears many similarities to the corresponding momentum boundary layer, the differences being attributable primarily to the variety of possible boundary conditions, and to the influence of the Prandtl number and the turbulent Prandtl number. However, the only new concept and new information required is that of the turbulent Prandtl number. This chapter will start by introducing the concept of eddy diffusivity for heat transfer, and then the turbulent Prandtl number. The Reynolds analogy will be developed as a very much simplified model for the latter. After the available experimental evidence for the turbulent Prandtl number has been examined, and following the development of a somewhat better model, a thermal law of the wall will be developed for a simple thermal boundary layer for air, and for water. This then leads to some useful though approximate algebraic solutions. Complete solutions to the energy differential equation using either the mixing-length or k–ε models of turbulence developed in Chap. 11, along with finite-difference calculations, are then discussed together with a comparison with experimental data for a variety of boundary conditions, roughly paralleling the turbulent momentum boundary layers considered in Chap. 11.

Throughout this chapter all fluid properties are treated as constant, and velocities are considered sufficiently low so that viscous energy dissipation is negligible.

THE CONCEPTS OF EDDY DIFFUSIVITY FOR HEAT TRANSFER, EDDY CONDUCTIVITY, AND TURBULENT PRANDTL NUMBER

In order to perform turbulent boundary-layer heat-transfer calculations, we need some method for evaluating $\overline{v'T'}$ in Eq. (5-34). A theory can be sought for direct evaluation of $\overline{v'T'}$ or alternatively an eddy diffusivity can be introduced, analogous to the eddy diffusivity for momentum. This is the course that will be followed here. $\overline{v'T'}$ is an apparent turbulent heat flux in the direction normal to the main flow. It seems plausible that it goes to zero if there is no mean temperature gradient in the normal direction. Thus it seems reasonable to state that

$$\overline{v'T'} \propto \frac{\partial \bar{T}}{\partial y}$$

As a proportionality factor we define the eddy diffusivity for heat transfer, ε_H:

$$\overline{v'T'} = \varepsilon_H \frac{\partial \bar{T}}{\partial y} \tag{12-1}$$

Substituting into Eq. (5-34), we obtain

$$\bar{u}\frac{\partial \bar{T}}{\partial x} + \bar{v}\frac{\partial \bar{T}}{\partial y} = \frac{\partial}{\partial y}\left[(\alpha + \varepsilon_H)\frac{\partial \bar{T}}{\partial y}\right] \tag{12-2}$$

As was the case for the momentum boundary layer, we often find that $\varepsilon_H \gg \alpha$ in the fully turbulent region, while $\alpha \gg \varepsilon_H$ in the viscous sublayer very close to the surface. However, this is not always the case, and the problem is not totally analogous to that of the momentum boundary layer.

It is sometimes convenient to speak of an eddy conductivity k_t, which can be defined as follows:

$$k_t = \rho c \varepsilon_H \tag{12-3}$$

Thus the turbulent heat flux becomes

$$\dot{q}'' = -\rho c \varepsilon_H \frac{\partial \bar{T}}{\partial y} = -k_t \frac{\partial \bar{T}}{\partial y} \tag{12-4}$$

Since we have now defined an eddy viscosity and an eddy conductivity, we can define a turbulent Prandtl number analogous to the molecular Prandtl number, which is of course a fluid property that we have previously found to have a profound influence on the laminar thermal boundary layer:

$$\mathrm{Pr}_t = \frac{\mu_t c}{k_t} = \frac{\varepsilon_M}{\varepsilon_H} \tag{12-5}$$

If we now substitute for ε_H in Eq. (12-2), we obtain the following form for the energy equation:

$$\bar{u}\frac{\partial \bar{T}}{\partial x} + \bar{v}\frac{\partial \bar{T}}{\partial y} = \frac{\partial}{\partial y}\left[\left(\alpha + \frac{\varepsilon_M}{\mathrm{Pr}_t}\right)\right] \tag{12-6}$$

From Eq. (12-6) it is now seen that if one has a solution to the momentum equation, so that ε_M is known at every point, the only new information needed to solve the thermal boundary layer is information on Pr_t. Of course, one may choose not to introduce the concept of Pr_t, in which case it is necessary to either attempt to evaluate $\overline{v'T'}$ directly, or else evaluate ε_H directly, and these are courses that some choose to follow. However, since the turbulent motions that give rise to $\overline{u'v'}$ also generate $\overline{v'T'}$ it might be hoped that a simple relationship exists between ε_M and ε_H, i.e., that Pr_t might be a reasonably simple function. If this is the case then the problem of calculating the thermal boundary layer is greatly simplified, because the momentum boundary layer must be solved in any case.

In the next section we will develop a very simple model for Pr_t, and following this we will examine some of the experimental evidence for Pr_t.

THE REYNOLDS ANALOGY

The oldest and simplest model for Pr_t is the Reynolds analogy. Let us propose and examine a physical model of the turbulent momentum and energy exchange process. Refer to Fig. 12-1 and imagine an element of fluid of mass δm that moves in the y direction a distance l (which is a "mixing length") as a consequence of turbulent motion. Let the element be originally in velocity and temperature equilibrium with the surrounding fluid at $\bar{u}$ and $\bar{T}$, and after the "event" let it come into equilibrium with the surrounding fluid at $\bar{u} + \delta\bar{u}$ and $\bar{T} + \delta\bar{T}$, assuming that gradients in $\bar{u}$ and $\bar{T}$ with respect to y exists. The net result of this "event" is the transfer of momentum and thermal energy in the y direction completely independent of that transferred by purely molecular processes.

A comment is in order about the mechanisms whereby the element comes into equilibrium with the surrounding fluid. The momentum exchange is evidently primarily through pressure forces acting on the element as a result of contact with the surrounding fluid. Viscous forces are obviously present, but apparently play a negligible role because it has already been observed in the development of Eq. (11-16) that the turbulent shear stress is independent of viscosity. On the other hand, the corresponding heat-exchange process must be by molecular conduction, since there is no mechanism for heat transfer analogous to

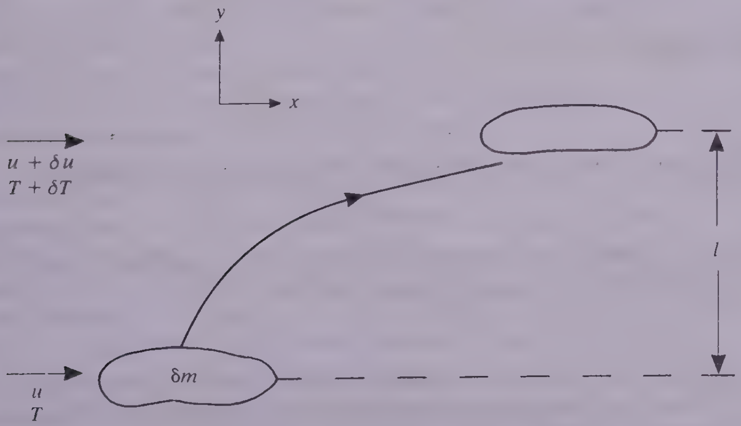

Figure 12-1 Turbulent exchange model on which the Reynolds analogy is based.

the pressure mechanism for momentum transfer. This difference in mechanisms, which is ignored in the Reynolds analogy, is considered later when we attempt to improve upon the latter.

Let us now compute the rate of x-momentum transfer, and the rate of heat transfer, implied by Fig. 12-1. Assume that the process at any one point in the flow is taking place continuously, i.e., one element following another, such that the effective continuous velocity of fluid in the y direction is $C\sqrt{\overline{v'^2}}$. Then consider the transfer rate across some area A parallel to the direction of the main flow. The rate of x-momentum transfer across A must be $(AC\sqrt{\overline{v'^2}}\rho)\,\delta\bar{u}$. Similarly, the rate of thermal energy transfer across A must be $(AC\sqrt{\overline{v'^2}}\rho)c\,\delta\bar{t}$.

According to the momentum theorem, the effective shear force F acting across a mean streamline is equal to the rate of momentum transfer. Then the effective shear stress must be

$$\tau_t = \frac{F}{A} = C\sqrt{\overline{v'^2}}\rho\,\delta\bar{u}$$

Similarly, the effective heat flux is

$$\dot{q}_t'' = C\sqrt{\overline{v'^2}}\rho c\,\delta\bar{T}$$

Now if l is small relative to the other dimensions of the system,

$$\delta\bar{u} \approx l\frac{d\bar{u}}{dy}, \qquad \delta\bar{t} \approx l\frac{d\bar{T}}{dy}$$

Substituting gives

$$\tau_t = C\sqrt{\overline{v'^2}}\rho l\frac{d\bar{u}}{dy}, \qquad \dot{q}_t'' = C\sqrt{\overline{v'^2}}\rho c l\frac{d\bar{T}}{dy}$$

Now rearrange to the *diffusivity* form:

$$\frac{\tau_t}{\rho} = C\sqrt{\overline{v'^2}}\,l\frac{d\bar{u}}{dy}, \qquad \frac{\dot{q}_t''}{\rho c} = C\sqrt{\overline{v'^2}}\,l\frac{d\bar{T}}{dy}$$

But, by definition of ε_M and ε_H,

$$\frac{\tau_t}{\rho} = \varepsilon_M\frac{d\bar{u}}{dy}, \qquad \frac{\dot{q}_t''}{\rho c} = \varepsilon_H\frac{d\bar{T}}{dy}$$

From comparison of terms in the two sets of expressions, it is apparent that

$$\varepsilon_H = \varepsilon_M$$

This equality of diffusivities is the Reynolds analogy. But, going back to Eq. (12-5), it is seen that the Reynolds analogy also implies that

$$\mathrm{Pr}_t = 1$$

Such a simple result, if true, would indeed be fortunate. As we shall see when we examine the experimental evidence, things are not quite so simple, but, on the other hand, the Reynolds analogy is not far wide of the mark.

The Reynolds analogy has some consequences that are in themselves sometimes called the Reynolds analogy. For the case of molecular Prandtl number Pr equal to unity, $u_\infty =$ constant, and $(T_s - T_\infty) =$ constant, it can be shown easily, just from examination of the differential equations, that $\text{Pr}_t = 1$ leads to similar velocity and temperature profiles. Under these conditions, it can then be shown that

$$\text{St} = c_f/2$$

This of course is exactly what obtains under the same conditions for the laminar boundary layer, and for basically the same reasons.

TURBULENT PRANDTL NUMBER

Experimental Evidence

From the definition of Pr_t, Eq. (12-5), and the definitions of the eddy diffusivities, Pr_t can be expressed in terms of quantities that can in principle be measured at each point in the boundary layer:

$$\text{Pr}_t = \overline{u'v'}\,\frac{d\bar{T}}{dy}\Big/\overline{v'T'}\,\frac{d\bar{u}}{dy}$$

Four quantities are required: the mean velocity and temperature gradients, the turbulent shear stress, and the turbulent heat flux. It is extremely difficult to measure all four of these quantities accurately, and for this reason reliable data on local values of Pr_t are relatively rare. We will examine some of the available data shortly, but before doing so we should note that there are indirect methods for obtaining at least average values for Pr_t. It will be seen later that when temperature profiles are plotted in semi-logarithmic *wall coordinates* for the simple case of constant free-stream velocity and constant surface temperature, there is a *straight-line* region similar to that observed for the velocity profiles. From the *slope* of this line, as compared with the slope of the corresponding line from the velocity profiles, Pr_t can be deduced, and it further follows that Pr_t is evidently a constant in the *logarithmic region* of the boundary layer. Table 12-1 shows some results using this technique for several cases where the fluid is air, and one case where the fluid is water.

It is evident that, at least for these fluids with Pr = 0.7 and 5.9, the turbulent Prandtl number in the logarithmic region, while not equal to 1 as implied by the Reynolds analogy, is certainly close to 1. The data range from about 0.7 to 0.9, with a preponderance of data around 0.85. Note that one case is for a "fully rough" surface, and roughness evidently has no effect. It is also worth noting that water with Pr = 5.9 yields about the same results as air with Pr = 0.7, so there is little if any effect of molecular Prandtl number, at least over this range.

Experiments with *liquid metals* flowing in pipes with Prandtl numbers in the range 0.001–0.02 suggest that Pr_t is considerably greater than 1.00 at low values of the Prandtl number. The evidence for this is very indirect—it is simply that it

Table 12-1 Turbulent Prandtl number from logarithmic-region profile slopes; zero pressure gradient

Experiment	Re_{δ_2}	Re_{Δ_2}	Pr_t
		Fluid: air, Pr = 0.7	
Reynolds[1]	Various to 6,400		0.73
Moffat[2]	4,419	4,756	0.85
Thielbahr[3]	1,572	1,684	0.85
Blackwell[4]	2,481	2,648	0.85
	2,609	3,008	0.78
	2,971	3,180	0.79
Gibson[5]	2,750	3,129	0.92
Simon[6]	4,445	1,756	0.77
	6,365	3,746	0.78
	4,957	4,261	0.82
Pimenta[7] (fully rough surface)	15,142	15,412	0.84
		Fluid: water, Pr = 5.9	
Hollingsworth[8]	1,552	287	0.85

is necessary to assume a high value for Pr_t in order to predict heat-transfer rates adequately by solution of the energy differential equation. Therefore there does appear to be a considerable Prandtl number effect, but it is confined to very low-Prandtl-number fluids.

Figure 12-2 shows some data for the logarithmic region presented by Zukaukas and Slanciauskas[9] for a fairly wide range of Prandtl number, all at constant free-stream velocity. These results are quite consistent with those in Table 12-1, but, most important, show little or no effect of Prandtl number up to $\mathrm{Pr} = 65$. From this it can be inferred that Pr_t is probably not affected by Prandtl number at high values of the latter.

Local point values of Pr_t, obtained using the preceding equation, are shown on Fig. 12-3 for air and for water, from constant free-stream velocity experiments. The data for water extend only to $y^+ = 30$ because the thermal boundary layer is very much thinner than the momentum boundary layer at this Prandtl number, and the measurements become very inaccurate at higher values of y^+. However, the log-slope in the outer region (see Fig. 12-10) suggests $\mathrm{Pr}_t = 0.85$. Several observations can be made. Although Pr_t is reasonably constant in the "logarithmic" or "law-of-the-wall" region, it apparently goes to much higher values in the sublayer, and air and water yield almost identical results.

In the "wake" region (and this refers only to the air data), Pr_t tends to decrease, and this and other experiments suggest that it approaches about 0.7 at the outer edge of the boundary layer. However, in calculating the thermal boundary layer, the behavior in the outer region is of minor significance.

Of much more significance is the sharp rise of Pr_t in the sublayer, indicating that the mechanisms of heat and momentum transfer differ greatly there, a conclusion that is probably not surprising. Successful calculation of the thermal

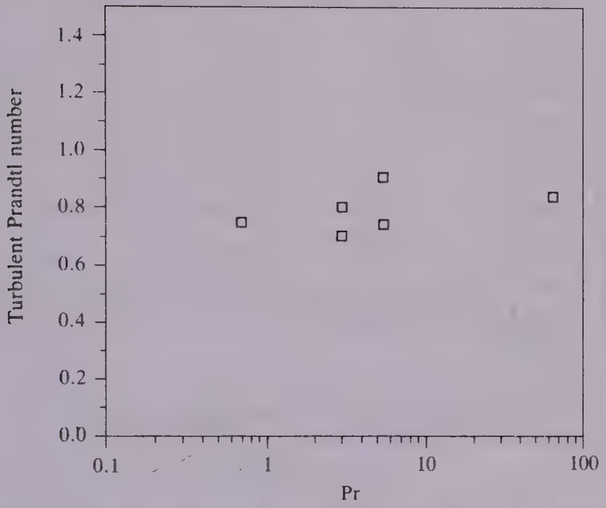

Figure 12-2 Turbulent Prandtl number measurements of Zukauskas and Stanciauskas[9] (data from logarithmic range of y^+).

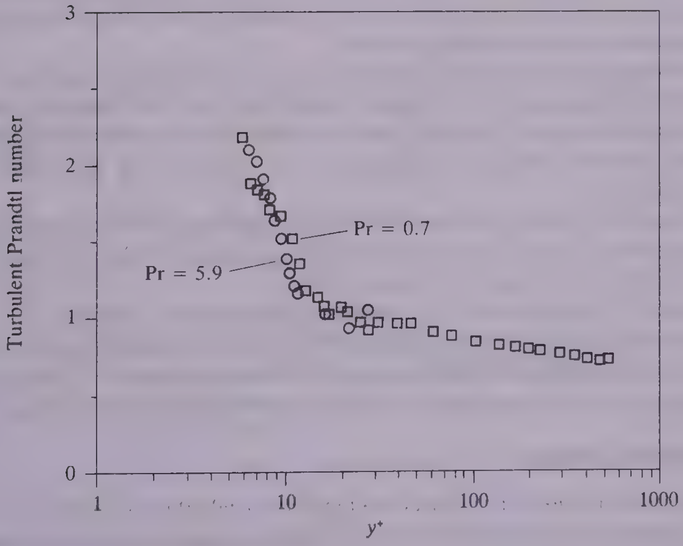

Figure 12-3 Point values for turbulent Prandtl number for air and water; constant u_∞ [data of Blackwell[4] (air) and Hollingsworth[8] (water)].

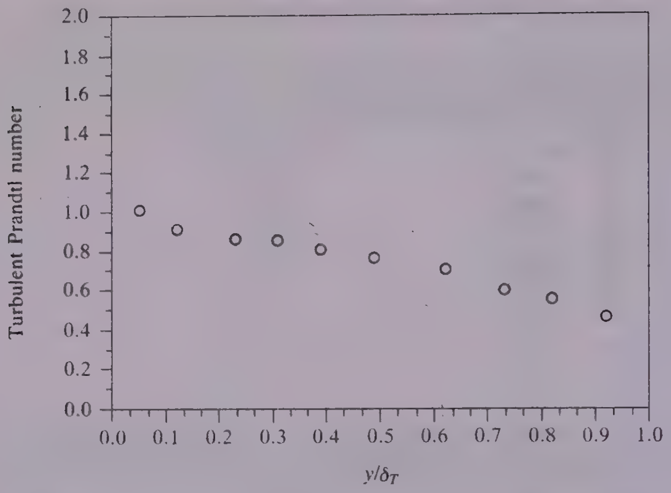

Figure 12-4 Point values for turbulent Prandtl number for air; constant u_∞ (data of Roganov *et al.*;[10] procedure and Reynolds number unknown).

boundary layer for moderate and high Prandtl numbers depends critically on including these high values of Pr_t. The data presented here extend only down to $y^+ = 6$. For $\mathrm{Pr} < 10$ the value of Pr_t for $y^+ < 6$ is not particularly important, but for higher-Prandtl-number fluids this region can become of critical importance, and at present there are simply no data.

Additional data on point values of Pr_t for air at constant free-stream velocity are given by Roganov *et al.*,[10] and are shown on Fig. 12-4. These are quite consistent with the data on Fig. 12-3. However, these data do not extend significantly into the sublayer, although a beginning of a rise in Pr_t as the surface is approached is seen.

Figure 12-5 shows the results of three experiments with positive transpiration (blowing). These are all very similar to the results on Fig. 12-3 and indicate that transpiration has little or no effect on Pr_t.

Figure 12-6 shows the effect on an adverse pressure gradient on Pr_t. It does appear that an adverse pressure gradient *decreases* Pr_t, and one would then infer that a favorable pressure gradient (negative) would *increase* Pr_t. This is not surprising, given the mechanisms that must be involved, but the evidence is scanty.

Analytical Evidence

Using supercomputers, it has become feasible to calculate turbulent flows over a limited domain through a full solution of the time-dependent Navier–Stokes and energy differential equations, i.e., to solve for the fluctuating velocities and temperatures as functions of time. From such solutions it is then possible to evaluate all of the statistical properties of the flow, including the turbulent Prandtl number.

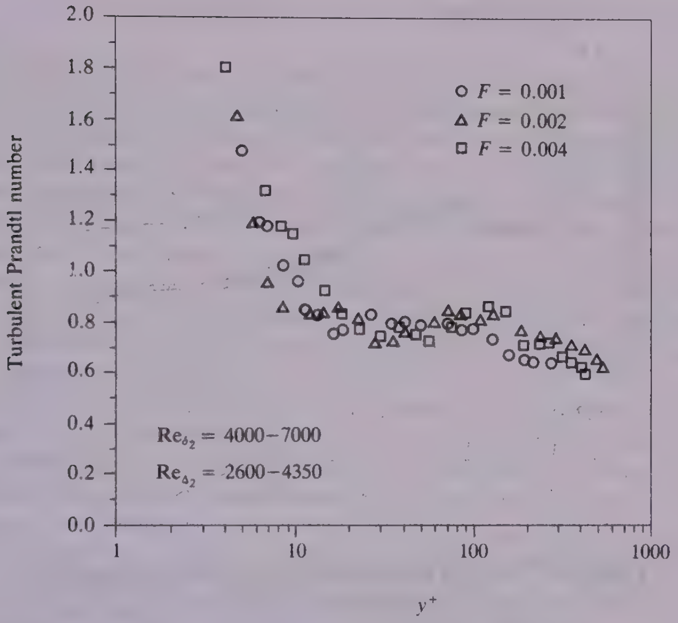

Figure 12-5 Effect of blowing on turbulent Prandtl number for air, with a mild pressure gradient (data of Blackwell[4]).

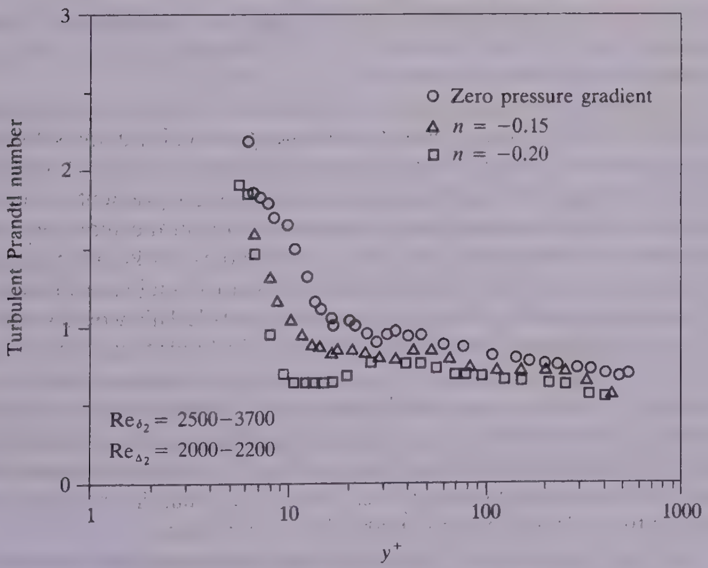

Figure 12-6 Effect of an adverse pressure gradient on turbulent Prandtl number for air (data of Blackwell[4]).

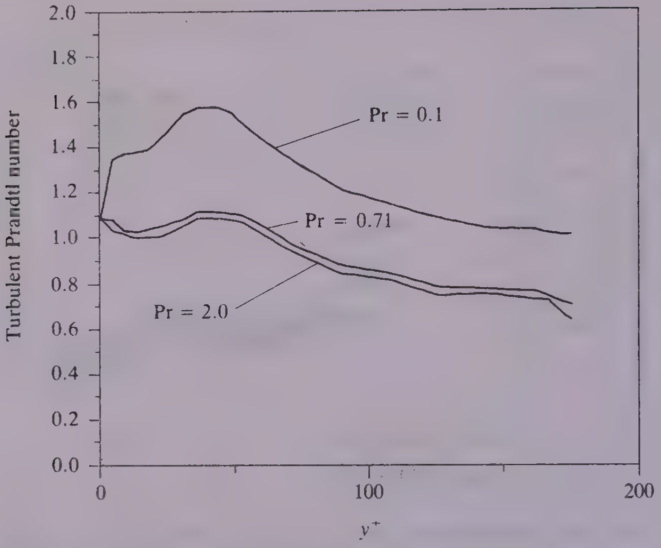

Figure 12-7 Turbulent Prandtl number for fully developed flow in a flat duct, calculated by direct numerical simulation.[12]

Rogers *et al.*[11] carried out such calculations for a uniform turbulent shear layer, which would correspond to the logarithmic region of the boundary layer, and found Pr_t to be about 0.85. Kim and Moin[12] carried out calculations for fully developed flow in a flat duct, and the results are shown on Fig. 12-7. Three different Prandtl numbers were considered: 0.1, 0.71, and 2.0.

These results show many of the characteristics seen in the experimental data—with the important exception that the steep rise in Pr_t in the sublayer does not appear. However, the calculations were made for a very low Reynolds number, which results in a relatively large *favorable* pressure gradient. It may be that a favorable pressure gradient has an influence on Pr_t in the sublayer. These results do show a substantial increase in Pr_t at low molecular Prandtl numbers, and confirm the idea that Pr_t can be considerably higher for liquid metals, which generally have molecular Prandtl numbers well below 0.1. This would seem to suggest that it is the *thermal conductivity* of the low-Pr fluids that causes a high Pr_t. (Note that high Pr_t implies a *low eddy conductivity.*) Of particular interest is the fact that at the surface Pr_t apparently approaches a value (about 1.09) that is independent of Prandtl number. It is almost impossible to make this kind of a measurement in a real boundary layer. Kim and Moin[12] call attention to the fact that Deissler[13] presents a turbulence analysis that predicts that Pr_t should approach 1, independently of Prandtl number, under these conditions.

More recent calculations[14] using the same techniques, but considering an actual external turbulent boundary layer with no pressure gradient, yield results very similar to those of Kim and Moin. However, once more the Reynolds numbers are very low: 653 for the momentum thickness and 773 for the enthalpy thickness. At these low Reynolds numbers there is only a very short "logarithmic" region in the velocity and temperature profiles, and a comparison with the law of the wall suggests that the sublayer is somewhat thicker than is the case at the higher Reynolds numbers where the experimental data on turbulent Prandtl number have been obtained. Thus it is not certain whether the relatively low values for turbulent Prandtl number in the sublayer observed in the calculated results do not result from these very low Reynolds numbers. Until full simulation calculations can be carried out at Reynolds numbers in the range 2000–3000, it may not be possible to explain this discrepancy between the calculations and experiments. However, as of this writing, the costs of full simulation calculations at such Reynolds numbers appear to be prohibitive.

Yakhot *et al.*[15] present a calculation of Pr_t, based on fundamental turbulence theory, that is entirely devoid of empirical input. At Prandtl numbers of 0.7 and higher, and/or at high Reynolds numbers, their result yields a constant Pr_t of about 0.85 (although a later consideration by the same authors suggests about 0.72). At very low Prandtl numbers (the liquid metal range) their results yield very much higher Pr_t, but values that decrease and approach 0.85 at high Reynolds number (or high y^+), all of which is consistent with the experimental data. However, the Yakhot equation does not yield the high values of Pr_t in the sublayer that one sees in the experimental data, suggesting that it is valid only in the logarithmic region of the boundary layer.

A CONDUCTION MODEL FOR TURBULENT PRANDTL NUMBER

At this point our concern is with the development of a simple computing equation for Pr_t that includes the sublayer effect, but that is also based on a physical model that is easy to comprehend. The Reynolds analogy was a first attempt to develop a model for the calculation of turbulent Prandtl number. The need for something better became evident when it was realized that Pr_t can become considerably higher than 1 for very low-Prandtl-number fluids.

A number of attempts have been made to predict turbulent Prandtl number through highly idealized analyses (see, for example, Ref. 16). Most prediction models for low Prandtl number fluids are modifications of an idea, first suggested by Jenkins,[17] that a turbulent eddy while moving transverse to the mean direction of flow might lose heat at a different rate than it loses momentum. Jenkins' original analysis assumed that the eddy lost heat by simple molecular conduction and lost momentum by the action of viscous shear. Thus the ratio of ν to α, that is, the molecular Prandtl number, became the primary parameter, and for $\mathrm{Pr} = 1$ the results came back to the simple Reynolds analogy. Further reflection on this problem suggests that turbulent eddies transfer momentum by the action of pressure forces, and that viscous forces are not involved. The success of the mixing-length theory, in which viscosity is not a variable, would suggest this to be the case. On the other hand, there is no mechanism other than molecular conduction whereby heat can be transferred to or from an eddy. Since the transfer mechanisms must be different, it is not surprising that Pr_t different from 1 is observed even for a fluid with $\mathrm{Pr} = 1$. It should be perfectly possible for an eddy to lose all its x momentum while it still has a velocity in the y direction, and thereby to carry heat a greater distance than momentum. This would account for observed values of Pr_t less than 1. On the other hand, if the fluid has a relatively *high thermal conductivity*, the eddy could lose a substantial amount of heat by conduction before it has traversed the distance of the momentum mixing length, and Pr_t would be greater than 1.

These ideas can be incorporated into a relatively simple *conduction model* for Pr_t. The algebraic details are somewhat lengthy, and the theoretical basis certainly rests on insecure footing, so only the final result is presented here. Suffice it to say that the model illustrated in Fig. 12-1 is modified to include *heat conduction* to or from the fluid element δm as it moves. The important point is that the following result contains the variables that intuitively seem correct, and when the two free constants are specified by comparison with experiment, the final equation fits the available experimental data reasonably well.

$$\mathrm{Pr}_t = \frac{1}{\dfrac{1}{2\,\mathrm{Pr}_{t\infty}} + C\,\mathrm{Pe}_t\sqrt{\dfrac{1}{2\,\mathrm{Pr}_{t\infty}}} - (C\,\mathrm{Pe}_t)^2\left[1 - \exp\left(-\dfrac{1}{C\,\mathrm{Pe}_t\sqrt{\mathrm{Pr}_{t\infty}}}\right)\right]} \tag{12-7}$$

where $\mathrm{Pe}_t = (\varepsilon_M/\nu)\,\mathrm{Pr}$, $\mathrm{Pr}_{t\infty}$ is the value of Pr_t far from the surface (an experimental constant), and C is an experimental constant.

Pe_t is a turbulent *Péclet number*, and although it is conveniently expressed as the product of the Prandtl number and the eddy-viscosity ratio (which is effectively a turbulent Reynolds number), note that the viscosity ν cancels.

Equation (12-7), with $C = 0.3$ and $\mathrm{Pr}_{t\infty} = 0.85$, is plotted on Fig. 12-8 for three Prandtl numbers: 0.7, 0.1, and 0.01. Also included is the experimental data for air from Fig. 12-3. Note that it fits the experimental data for air quite well, *including the rise in* Pr_t *in the sublayer.* The latter fact can only be fortuitous, because we have already seen that Pr_t in the sublayer is apparently independent of Prandtl number, and thus can have nothing to do with heat conduction. Furthermore, Eq. (12-7) with these constants yields $\mathrm{Pr}_t = 1.7$ at the surface, which is probably much too high. However, for fluids with $\mathrm{Pr} < 1$ the value of Pr_t at $y^+ < 7$ or 8 has a negligible effect on calculations. For very low-Prandtl-number fluids Eq. (12-7) with these constants yields values of Pr_t over the entire boundary layer that are quite consistent with the available data. As a consequence, this equation provides a reasonable way to evaluate Pr_t for any fluid for $\mathrm{Pr} < 1$. For gases it can be thought of as merely an empirical fit to the data; for low-Prandtl-number fluids it contains at least some theoretical basis. It can be used for fluids with Pr up to at least 6 (water), *provided that 0.7 is substituted for* Pr *in the equation,* since we have seen that the turbulent Prandtl number for water is virtually identical to that for air. For higher Prandtl numbers the values of Pr_t very close to the surface (i.e., $y^+ < 6$) become increasingly important, and there are simply no data at present available. The best procedure would probably be to patch on a function that goes to 1 at the surface.

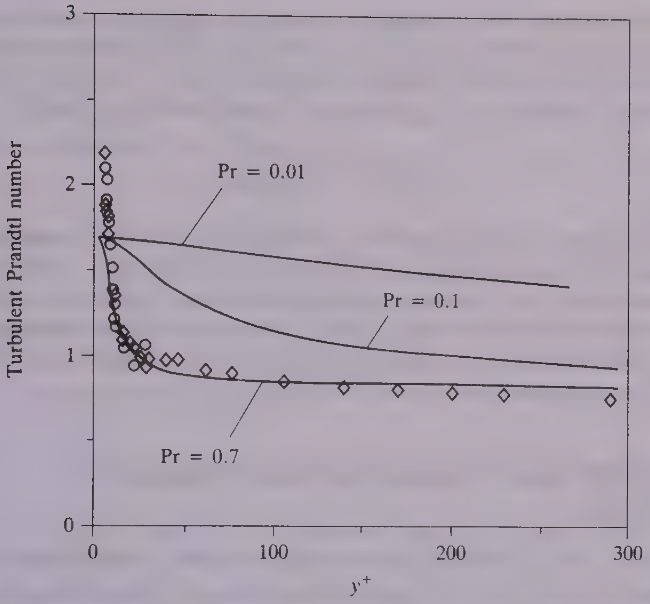

Figure 12-8 A plot of Eq. (12-7) for a boundary layer with no pressure gradient.

Although there may be a pressure-gradient effect on Pr_t, no attempt has been made to include such effects in Eq. (12-7).

The model given by Eq. (12-7) can be extended in its applicability range by the following considerations: Analyzing Eq. (12-7) again, it can be seen that $\mathrm{Pr}_t \rightarrow \mathrm{Pr}_{t\infty}$ for large values of Pe_t, which means far away from the surface. On the other side $\mathrm{Pr}_t \rightarrow 2\,\mathrm{Pr}_{t\infty}$ for $\mathrm{Pe}_t \rightarrow 0$, which is normally the case very close to the surface. If the value $\mathrm{Pr}_{t\infty} = 0.85$ is now exclusively used in Eq. (12-7), Pr_t will always be smaller or equal to 1.7. This might introduce an undesired behavior in the model for liquid metal flows for very low molecular Prandtl numbers, because for $\mathrm{Pr} \rightarrow 0$ (and a finite Re number) Pr_t should tend to large values, because heat will be transferred nearly exclusively by molecular conduction. Therefore, $\mathrm{Pr}_{t\infty}$ should depend on the Re and Pr number at least for very low values of the Prandtl number. Jischa and Rieke[31] developed a model for Pr_t from the modeled transport equations for k, ε and for the turbulent heat flux. As a final result of their analysis, they obtained a correlation for the turbulent Prandtl number for pipe and channel flows of the form

$$\mathrm{Pr}_t = E + \frac{F}{\mathrm{Pr}\,\mathrm{Re}^{0.888}}, \qquad E = 0.9, \qquad F = 182.4$$

In their model Pr_t is not dependent on the local distance from the surface, but on the Reynolds and Prandtl number. For a finite Re number, Pr_t tends to infinity for

$\mathrm{Pr} \rightarrow 0$ which reflects the correlation's behavior for the heat transfer for very low Prandtl numbers. The correlation can now be used to develop a model for Pr_{t_∞} for Eq. (12-7). For this, the two constants E and F have to be adjusted. Weigand *et al.*[32] obtained for Pr_{t_∞} for Eq. (12-7) the following equation

$$\mathrm{Pr}_{t_\infty} = 0.85 + \frac{100}{\mathrm{Pr}\,\mathrm{Re}^{0.888}}$$

This equation can be used instead of $\mathrm{Pr}_{t_\infty} = 0.85$ in Eq. (12-7). For moderate values of Pr and Re, the above equation will result in the value $\mathrm{Pr}_{t_\infty} = 0.85$ and the original model [Eq. (12-7)] will be recovered, whereas for very low molecular Prandtl numbers much higher values of Pr_{t_∞} are obtained. Some example calculations for liquid metal flows in ducts using the above modified model for the turbulent Prandtl number are shown in Weigand *et al.*[32]

COMPLETE SOLUTION OF THE ENERGY EQUATION

We now have all the ingredients needed to solve the energy differential equation of the boundary layer for a very large variety of boundary conditions, including all of those considered for the momentum equation in Chap. 11, and also virtually any kind of temperature boundary condition. It will always be necessary to solve the momentum equation, and its solution will provide values for ε_M. Then Pr_t is the only additional information required. However, before examining particular solutions, which involve finite-difference procedures and computer implementation, it will prove worthwhile to consider some simple cases where approximate algebraic closed-form solutions are obtainable, and at the same time some of the available experimental data will be examined.

A LAW OF THE WALL FOR THE THERMAL BOUNDARY LAYER

Equation (12-2) can be written in the following form if $\dot{q}''$ is used to represent the total heat flux, laminar plus turbulent:

$$\bar{u}\frac{\partial \bar{T}}{\partial x} + \bar{v}\frac{\partial \bar{T}}{\partial y} = \frac{1}{\rho c}\frac{\partial(-\dot{q}'')}{\partial y} \tag{12-8}$$

where

$$\dot{q}'' = -\rho c(\alpha + \varepsilon_H)\frac{\partial \bar{T}}{\partial y} \tag{12-9}$$

Let us now restrict consideration to the region near the surface, and then let the surface temperature T_s be a constant. The axial gradient $\partial \bar{T}/\partial \bar{x}$ must then be small, $\bar{T} = \bar{T}(y)$, and we are again introducing the Couette flow approximation.

Additionally, $v = v_s$, and thus Eq. (12-8) becomes

$$v_s \frac{d\bar{T}}{dy} = \frac{1}{\rho c} \frac{d(-\dot{q}'')}{dy}$$

Integrating between the limits $\bar{T} = T_s$, $\dot{q}'' = \dot{q}_s''$ at $y = 0$, and $\bar{T}$, $\dot{q}''$ at y, we obtain

$$v_s(\bar{T} - T_s) = \frac{1}{\rho c}(\dot{q}_s'' - \dot{q}'')$$

from which

$$\frac{\dot{q}''}{\dot{q}_s''} = 1 + \frac{\rho c v_s (T_s - \bar{T})}{\dot{q}_s''}$$

We then introduce the definition of v_s^+,

$$v_s^+ = \frac{v_s}{\sqrt{\tau_s/\rho}}$$

and let the remaining terms on the right-hand side, which must be nondimensional, be represented by a nondimensional temperature T^+:

$$T^+ = \frac{(T_s - \bar{T})\sqrt{\tau_s/\rho}}{\dot{q}_s''/\rho c} \tag{12-10}$$

Then

$$\frac{\dot{q}''}{\dot{q}_s''} = 1 + v_s^+ T^+ \tag{12-11}$$

Note the similarity to the comparable equation for τ/τ_s, Eq. (11-13), except that there is no p^+ term. In fact, the whole concept of analogous behavior between heat and momentum transfer breaks down in a pressure gradient. Remember, however, that Eq. (12-11) is applicable only relatively near the surface. At the outer edge of the boundary layer $\dot{q}''/\dot{q}_s''$ must go to zero.

Now let us consider a particular case, $v_s^+ = 0$. Then

$$\dot{q}'' = \dot{q}_s''$$

so that

$$\frac{\dot{q}_s''}{\rho c} = -(\alpha + \varepsilon_H)\frac{d\bar{T}}{dy}$$

and thus

$$\int_{T_s}^{\bar{T}} d\bar{T} = -\frac{\dot{q}_s''}{\rho c}\int_0^y \frac{dy}{\alpha + \varepsilon_H}$$

Let us now introduce y^+ as a variable. After rearrangement,

$$\frac{(T_s - \bar{T})\sqrt{\tau_s/\rho}}{\dot{q}_s''/(\rho c)} = \int_0^{y^+} \frac{dy^+}{1/\Pr + \varepsilon_H/\nu}$$

But the left-hand side is T^+, Eq. (12-10). Thus we obtain

$$T^+ = \int_0^{y^+} \frac{dy^+}{1/\mathrm{Pr} + \varepsilon_H/\nu} \tag{12-12}$$

Following the same procedures as were used for the momentum boundary layer in Chap. 11, let us first consider a *two-layer model* with a fully viscous sublayer and a fully turbulent region. For computer solution of the complete energy differential equation we will abandon the two-layer model in favor of a continuous model, but the two-layer model provides some easy insights into the structure of the thermal boundary layer, and also leads to some useful closed-form solutions.

For the simple momentum boundary layer (no pressure gradient, no transpiration) we found that the effective thickness of the sublayer was $y^+ = 10.8$. For a thermal boundary layer the effective thickness will vary with the Prandtl number of the fluid because the relative contribution of the eddy diffusivity to the heat-transfer conductance in the actual sublayer will vary with Prandtl number, as will be seen below. Only for a fluid with $\mathrm{Pr} = 1$ might one expect to find 10.8, but, because of the high and varying *turbulent Prandtl number* in the sublayer, even this would not be the case. Sufficient data are available to determine the effective sublayer thickness for the thermal boundary layer for air ($\mathrm{Pr} = 0.7$), and water at $\mathrm{Pr} = 5.9$ (Table 12-2).

Let us now split the integral of Eq. (12-12) into two parts corresponding to a viscous sublayer and a fully turbulent region. Then for the region $y^+ > y^+_{\mathrm{crit}}$,

$$T^+ = \int_0^{y^+_{\mathrm{crit}}} \frac{dy^+}{1/\mathrm{Pr} + \varepsilon_H/\nu} + \int_{y^+_{\mathrm{crit}}}^{y^+} \frac{dy^+}{1/\mathrm{Pr} + \varepsilon_H/\nu} \tag{12-13}$$

If we were to follow precisely the procedure used in Chap. 11, we would now neglect ε_H/ν in the first integral, and $1/\mathrm{Pr}$ in the second. But the term $1/\mathrm{Pr}$ can vary tremendously, depending on the particular fluid involved. Prandtl numbers for viscous fluids like oils can easily exceed 100, while those for liquid metals can be as low as 0.001. The magnitude of this term in each of these integrals can then have a large influence on the relative importance of all the terms in the denominators.

In Chap. 11 we noted that in reality the eddy diffusivity in the sublayer is not zero, it is merely small. But if Pr is large, a small diffusivity in the sublayer can be significant; and in fact if Pr is much greater than 1, significant error is introduced if ε_H/ν is neglected in the sublayer. For the present we would like to neglect this term. The use of a critical value of y^+ that is a function of Pr is a way of

Table 12-2 No pressure gradient, no transpiration

Pr	y^+_{crit}
0.7	13.2
5.9	7.55

compensating for this effect, but this means that we are restricted to just two Prandtl numbers, 0.7 and 5.9. However, at very low Pr the $1/\Pr$ term so dominates the first integral that the ε_H/ν term can be neglected in any case.

In the second integral, the fully turbulent region, the situation is reversed. The $1/\Pr$ term can become large for low-Pr fluids, and can become significantly larger than ε_H/ν. Physically, this means that *molecular conduction* is a significant and even the dominant mechanism in the fully turbulent region for a liquid metal, and thus cannot be neglected. The relative magnitude of these terms can be easily investigated by assuming that the Reynolds analogy is applicable and then evaluating the eddy diffusivity for momentum from the mixing-length theory developed in Chap. 11:

$$\varepsilon_M/\nu = \kappa y^+ \tag{12-14}$$

where $\kappa = 0.41$. For Pr greater than about 0.5 the molecular-conduction term can reasonably be neglected, but not for lower Prandtl numbers.

Let us now restrict consideration to air, $\Pr = 0.7$. In this case we can neglect ε_H/ν in the first integral, and the $1/\Pr$ term in the second. Substituting Eq. (12-14), the definition of $\Pr_t$, and a value of 13.2 for y^+_{crit}, Eq. (12-13) becomes

$$T^+ = \int_0^{13.2} \Pr\, dy^+ + \int_{13.2}^{y^+} \frac{\Pr_t\, dy^+}{\kappa y^+}$$

If we assume that $\Pr_t$ can be treated as a constant in the fully turbulent region, performing the integration in this equation gives

$$T^+ = 13.2\Pr + \frac{\Pr_t}{\kappa} \ln \frac{y^+}{13.2}$$

Assuming that a reasonable average value for $\Pr_t$ in the Couette flow region is 0.85, and that $\kappa = 0.41$, we obtain a thermal "law of the wall" for gases:

$$T^+ = 2.075 \ln y^+ + 13.2\Pr - 5.34 \tag{12-15}$$

Figure 12-9 shows a comparison of Eq. (12-15) with two temperature profiles for air—each from different experiments and for different Reynolds numbers. Note that, like the corresponding u^+–y^+ plot, there is a *wake*, and that the actual viscous sublayer extends to about $y^+ = 30$. As the Reynolds number increases, the wake extends to higher values of y^+, but in the *inner* region both profiles collapse onto the same function. Outside of the sublayer this function is very well represented by Eq. (12-15).

A comment about the Reynolds numbers should be made here. The Reynolds numbers indicated on Fig. 12-9 are based on *enthalpy thickness*. The data on the figure are from experiments for which the virtual origins of both the momentum boundary layers and the thermal boundary layers are at the same point. We will speak of such boundary layers as *equilibrium thermal boundary layers*. If the virtual origins differ, the temperature profiles will be affected, although most of the difference will generally be noted in the wake, or outer region. For equilibrium

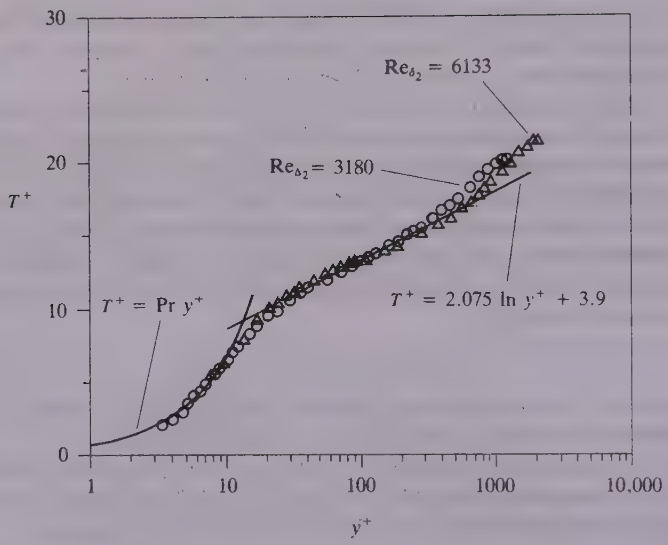

Figure 12-9 A thermal law of the wall for air: equilibrium thermal boundary layers; enthalpy thickness Reynolds numbers are indicated.

thermal boundary layers with *gases* the ratio of enthalpy thickness to momentum thickness tends to be approximately constant, about 1.10–1.15.

If we now repeat the same analysis for water with $\mathrm{Pr} = 5.9$ and $\mathrm{Pr}_t = 0.85$, we obtain

$$T^+ = 2.075 \ln y^+ + 7.55\,\mathrm{Pr} - 3.95 \qquad (12\text{-}16)$$

Figure 12-10 shows a comparison of Eq. (12-16) with experimental data for water at $\mathrm{Pr} = 5.9$. These data were obtained using very small temperature differences so that the effect of temperature on the Prandtl number and the viscosity is believed to have been small. This is a problem that besets heat-transfer experiments with liquids, and is discussed in more detail in Chap. 15.

Another potential difficulty with these data is that the *virtual origins* of the momentum and thermal boundary layers are not the same, and it is not clear what effect this might have. It will be noted that there is a *negative wake*, but this is to be expected because the thermal boundary layer is very much thinner than the momentum boundary layer at this Prandtl number, and does not effectively extend into the wake region of the momentum boundary layer. Note the very small enthalpy thickness Reynolds number as compared with the momentum thickness Reynolds number, and also the fact that a far greater part of the heat-transfer resistance is in the sublayer, as compared with the air boundary layer. Since the Prandtl number here is only 5.9, it can be appreciated that for very high-Prandtl-number fluids (say $\mathrm{Pr} = 100$) the heat-transfer resistance will be almost entirely in the sublayer, and the temperature profile in the fully turbulent part of the

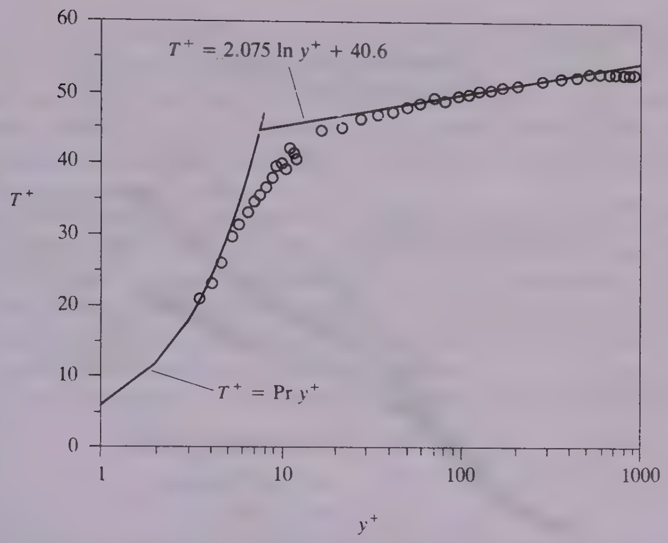

Figure 12-10 A thermal law of the wall for a fluid (water) with $\Pr = 5.9$; $\mathrm{Re}_{\delta_2} = 1552$, $\mathrm{Re}_{\Delta_2} = 287$.

boundary layer will be virtually flat. In that case the heat-transfer mechanisms in the fully turbulent region become irrelevant. Another conclusion is that at very high Prandtl numbers the eddy diffusivity in the sublayer, though small, can play a critical role, and it will be necessary to know accurately both the eddy diffusivity for momentum and the turbulent Prandtl number for very small values of y^+.

EFFECT OF PRESSURE GRADIENT ON TEMPERATURE PROFILES

Figure 12-11 shows the effect of axial pressure gradient on the nondimensional temperature profiles. Note that each of the temperature profiles has what could be called a "logarithmic" region, but—unlike the corresponding velocity profiles (Fig. 11-4)—the profiles *do not collapse* together in the logarithmic region. Thus the term thermal "law of the wall" does not have the same connotation as it does for the momentum equation. Equations (12-15) and (12-16) are applicable only for a constant free-stream velocity (no pressure gradient).

Also shown on Fig. 12-11 are temperature profiles predicted by solution of the energy differential equation using the mixing-length model previously discussed, and, in the case of the adverse pressure gradient, the k–ε model. These predictions all employ Eq. (11-26) for evaluation of A^+, and Eq. (12-7) for the turbulent Prandtl number. Note that there is only a minor improvement in the profile predicted by the k–ε model, but the use of Eq. (11-26) is critical, especially in the favorable-pressure-gradient case.

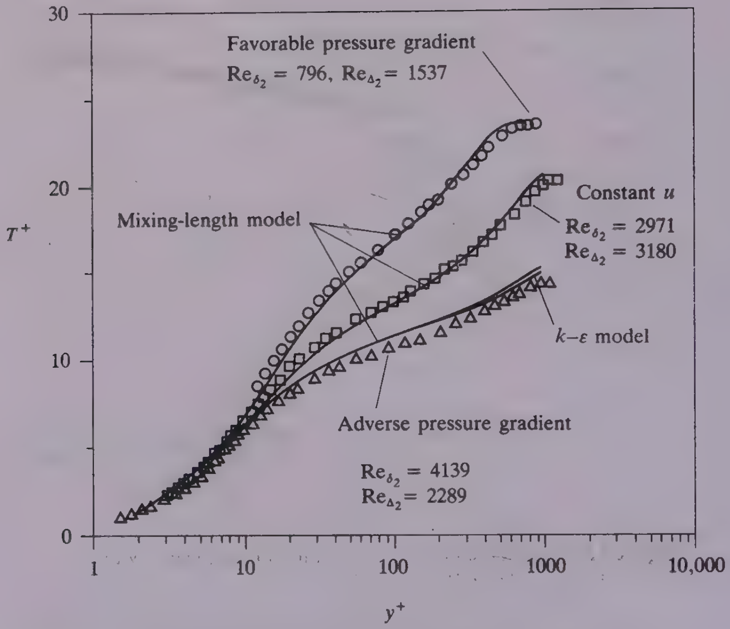

Figure 12-11 Effect of pressure gradient on temperature profiles (data of Thielbahr[3] and Blackwell[4]).

A HEAT-TRANSFER SOLUTION FOR CONSTANT FREE-STREAM VELOCITY AND SURFACE TEMPERATURE

With an algebraic "wall law" available for both the momentum boundary layer and the thermal boundary layer (at least for constant free-stream velocity), it becomes possible to develop an algebraic equation for the heat-transfer coefficient (i.e., the Stanton number) for the constant free-stream velocity case, and this will lead to algebraic solutions for even more complex cases However, it should be kept in mind that complete solution of the momentum and energy differential equations, using finite-difference techniques and the turbulence models already developed, can be used for any of these problems, and does not involve any of the approximations that characterize the algebraic solutions. Nevertheless, the algebraic solutions are extremely useful, both to provide quick answers to engineering problems and to provide insight into how the variables affect the answers.

The first assumption to be made here is that the momentum and thermal boundary layers have the same thickness. For a *laminar* boundary layer this is not the case, the relative thickness depending primarily on the Prandtl number. But since for the turbulent boundary layer the momentum layer provides the primary transport mechanism (the eddy diffusivity) in the outer region, it is not possible for the thermal layer to have a thickness that is significantly different, except for a very low-Prandtl-number fluid or for a case where the *virtual origins* of the two boundary layers are very different. We will *not* be considering a very low-Prandtl-number fluid, and we *will* be considering an equilibrium thermal boundary layer, i.e., a thermal boundary layer having the same virtual origin as the momentum boundary layer.

A second assumption will be that the "strength" of the wake for the thermal boundary layer for air is the same as that for the momentum boundary layer. For the latter, for constant free-stream velocity, it is 2.3, i.e., the departure of u^+ from the law of the wall at the outer edge of the boundary layer. Thus we will assume that the value of T^+ at the outer edge is 2.3 above the thermal wall law. The data on Fig. 12-9 indicate that this is a good assumption.

With these assumptions, u^+ at the outer edge, from Eq. (11-16), becomes

$$u_\infty^+ = 2.44 \ln y_\infty^+ + 5.00 + 2.3$$

Similarly, Eq. (12-15) becomes

$$T_\infty^+ = 2.075 \ln y_\infty^+ + 13.2\,\mathrm{Pr} - 5.34 + 2.3$$

We now solve each equation for $\ln y_\infty^+$ and equate. From the definition of u^+, it can be seen that

$$u_\infty^+ = \frac{1}{\sqrt{c_f/2}}$$

Similarly, from Eq. (12-10) it can be shown that

$$T_\infty^+ = \frac{\sqrt{c_f/2}}{\mathrm{St}}$$

We substitute and solve for St:

$$\mathrm{St} = \frac{c_f/2}{\sqrt{c_f/2}(13.2\,\mathrm{Pr} - 9.25) + 0.85}$$

We now substitute for $c_f/2$:

$$\mathrm{St} = \frac{0.0287\,\mathrm{Re}_x^{-0.2}}{0.169\,\mathrm{Re}_x^{-0.1}(13.2\,\mathrm{Pr} - 9.25) + 0.85} \tag{12-17}$$

For $0.5 < \mathrm{Pr} < 1.0$ and $5 \times 10^5 < \mathrm{Re}_x < 5 \times 10^6$ the denominator of the equation is quite well approximated by $\mathrm{Pr}^{0.4}$. Thus a much simpler expression for *gases* is

$$\mathrm{St}\,\mathrm{Pr}^{0.4} = 0.0287\,\mathrm{Re}_x^{-0.2} \tag{12-18}$$

We can now use the energy integral equation (5-24) to obtain an equation for St as a function of Re_{Δ_2}:

$$\mathrm{St} = \frac{d\Delta_2}{dx}$$

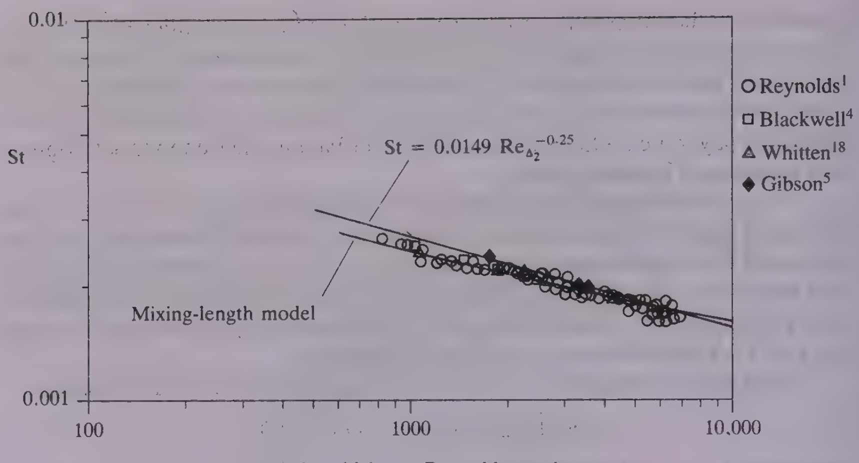

Figure 12-12 Experimental equilibrium boundary-layer data for air; constant free-stream velocity and constant surface temperature (data of Reynolds,[1] Blackwell,[4] Gibson,[5] and Whitten[18]).

We substitute for St from Eq. (12-18), solve for Δ_2 as a function of x, and then substitute for x in Eq. (12-18). The final result is

$$\mathrm{St}\,\mathrm{Pr}^{0.5} = 0.0125\,\mathrm{Re}_{\Delta_2}^{-0.25} \tag{12-19}$$

A comparison of Eq. (12-19) for Pr = 0.7 with experimental data for air is shown on Fig. 12-12. For Re_{Δ_2} from 2000 to 7000 it fits the data very well, although it tends to overpredict a bit at lower Reynolds numbers. Also shown on Fig. 12-12 are the results of a full solution to the energy differential equation using the mixing-length model and the turbulent Prandtl equation developed earlier. The k–ε model yields virtually the same result. As can be seen, the full solution fits the data somewhat better over a wider range of Reynolds number.

Since we also have available a thermal "law of the wall" for *water* with Pr = 5.9, the identical procedures can be used to develop equations for St for this value of Prandtl number. However, Pr for water varies greatly with temperature, from about 10 for cold water to near 1 for very hot water. Thus an equation for Pr = 5.9 is not very useful in and of itself. Hollingsworth[8] has developed a reasonable interpolation for Prandtl numbers from 0.7 to 5.9 using the two "wall laws" developed above as a basis and assuming that the critical thickness of the sublayer is a simple function of Pr. These equations are

$$\mathrm{St} = 0.02426\,\mathrm{Pr}^{-0.895}\,\mathrm{Re}_x^{-n}, \qquad n = 0.1879\,\mathrm{Pr}^{-0.18} \tag{12-20}$$

$$\mathrm{St} = C\left(\frac{1-n}{C}\right)^{n/(n-1)} \mathrm{Re}_{\Delta_2}^{n/(n-1)}, \qquad C = 0.02426\,\mathrm{Pr}^{-0.895} \tag{12-21}$$

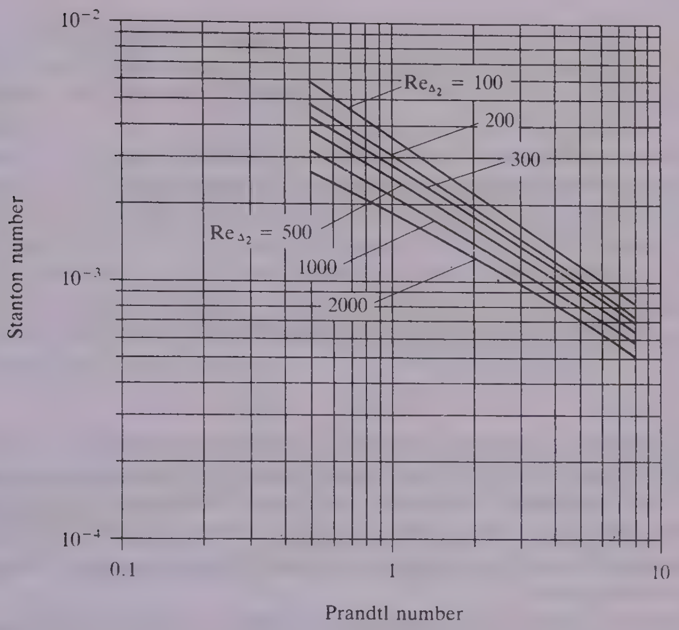

Figure 12-13 Stanton number for equilibrium turbulent thermal boundary layers at higher Prandtl numbers; enthalpy thickness Reynolds numbers are indicated.

From Eq. (12-21), St is plotted as a function of Prandtl number on Fig. 12-13 for various values of the enthalpy thickness Reynolds number. One point to note here is that the slopes of the curves for the higher Reynolds numbers vary from the approximately –0.5 indicated by Eq. (12-19) for gases to near –0.75 at $\text{Pr} = 6$. This larger slope is consistent with the larger slopes that have consistently been observed in pipe-flow experiments with high-Pr liquids. At $\text{Pr} = 0.7$ these equations reduce to the previously developed equations for air.

CONSTANT FREE-STREAM VELOCITY FLOW ALONG A SEMI-INFINITE PLATE WITH UNHEATED STARTING LENGTH

A number of approximate procedures have been proposed for determining heat transfer through a turbulent boundary layer with an unheated starting length, that is, on a plate on which the surface temperature is the same as that of the fluid up to some distance ξ, after which it is maintained at a different temperature, T_s. The problem is shown on Fig. 12-14.

This is the same problem that was solved for the laminar boundary layer in Chap. 10. The primary significance of this solution is that it provides a basic

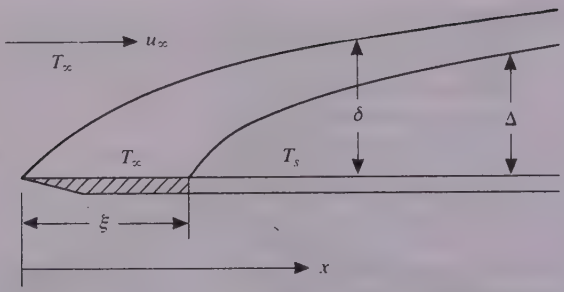

Figure 12-14 Boundary-layer development on a plate with an unheated starting length.

building block for constructing solutions for nonisothermal surfaces. Note, however, that this problem as well as the nonisothermal-surface problem can also be solved by finite-difference solution of the energy differential equation, and in that case no approximations need be introduced. But the objective here is to develop algebraic solutions, accepting some degree of approximation in return for a simply usable result.

To solve the laminar counterpart of this problem, the energy *integral* equation was used, and the same general procedure can be used here. One has to be careful in employing the energy integral equation for a turbulent boundary layer, however, because a simple assumed equation for the temperature profile may be quite adequate over most of the boundary layer but may give totally erroneous results in the sublayer and particularly at the surface. This same difficulty was encountered in obtaining a solution for the turbulent *momentum* boundary layer in Chap. 11. In the case a $\frac{1}{7}$-power equation was used to evaluate the integral; but since such a profile gives an infinite velocity gradient at the surface, it is obviously inadequate to describe the sublayer region, and a different procedure had to be used to evaluate the shear stress. The procedure used here, developed by Reynolds,[1] is one of several that have been proposed. It is developed for a fluid with Pr = 1, but the effect of unheated starting length is probably not highly dependent on Prandtl number, at least for Pr near 1, and the results are in good agreement with experiments with air.

A basic assumption is that the velocity and temperature profiles can be expressed by

$$\frac{\bar{u}}{u_\infty} = \left(\frac{y}{\delta}\right)^{1/7} \tag{12-22}$$

$$\frac{T_s - \bar{T}}{T_s - T_\infty} = \left(\frac{y}{\Delta}\right)^{1/7} \tag{12-23}$$

It is assumed that the local shear stress and heat flux can be expressed by Eqs. (11-9) and (12-9) and that the molecular Prandtl number is 1, so that $\alpha = \nu$.

It is also assumed that the turbulent Prandtl number is 1, so that $\varepsilon_H = \varepsilon_M$. The total diffusivities, $\alpha + \varepsilon_H$ and $\nu + \varepsilon_M$, are then the same for both momentum and heat transfer, and this is true in both the fully developed turbulent region and in the sublayer.

Since the algebraic details of this development are somewhat lengthy, only the method and the more important intermediate results will be discussed. As a first step, the momentum integral equation is developed in a form slightly different from that in Chap. 5. The momentum theorem is applied to a control volume extending from a point y in the boundary layer out to the free stream. Thus, if y is set equal to zero, the original momentum integral equation is obtained. Then substitution of Eq. (12-22) leads to an expression for the variation of *total* shear stress through the boundary layer:

$$\frac{\tau}{\tau_s} = 1 - \left(\frac{y}{\delta}\right)^{9/7} \tag{12-24}$$

The next step is to combine Eqs. (11-9), (12-22), and (12-24), and solve for the total diffusivity:

$$\nu + \varepsilon_M = 7\nu \frac{c_f}{2} \frac{\delta}{x} \mathrm{Re}_x \left[1 - \left(\frac{y}{\delta}\right)^{9/7}\right] \left(\frac{y}{\delta}\right)^{6/7} \tag{12-25}$$

In the sublayer this equation yields a *total* diffusivity that goes to zero at the surface, which is obviously incorrect. But when it is used together with Eq. (12-22), which is equally incorrect *at the surface*, a correct result can be obtained there.

For the next step Eq. (12-9) is solved for the heat flux, using Eq. (12-25) to supply the diffusivity and Eq. (12-23) to give the temperature gradient (thus the artificial diffusivity is again used to compensate for the equally artificial $\frac{1}{7}$-power profile in the sublayer):

$$\frac{\dot{q}''}{\rho c u_\infty (T_s - T_\infty)} = \frac{c_f}{2} \left[1 - \left(\frac{y}{\delta}\right)^{9/7}\right] \left(\frac{\Delta}{\delta}\right)^{-1/7} \tag{12-26}$$

We now set $y = 0$, and have an expression for the surface heat flux, and then the local Stanton number:

$$\mathrm{St} = \frac{\dot{q}_s''}{\rho c u_\infty (T_s - T_\infty)} = \frac{c_f}{2} \left(\frac{\Delta}{\delta}\right)^{-1/7} \tag{12-27}$$

For the final step the energy integral equation (5-24) is solved for Δ_2 as a function of x, using Eq. (12-27) for the Stanton number, and using Eqs. (12-22) and (12-23) to evaluate Δ_2 from Eq. (5-15). An ordinary differential equation results that is readily solved. Introducing the fact that the momentum boundary-layer thickness varies as the $\frac{4}{5}$ power of x, we obtain

$$\mathrm{St} = \frac{c_f}{2} \left[1 - \left(\frac{\xi}{x}\right)^{9/10}\right]^{-1/9} \tag{12-28}$$

The bracketed term contains the unheated starting-length effect; for $\xi = 0$ we obtain $\mathrm{St} = c_f/2$, which is precisely what Eqs. (11-23) and (12-18) reduce

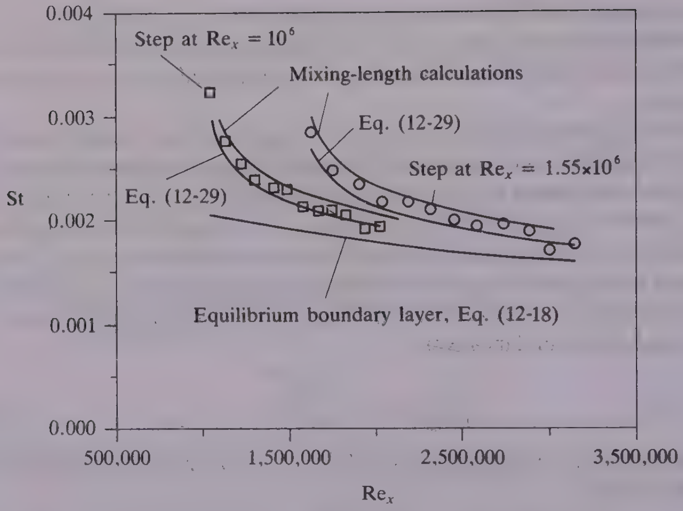

Figure 12-15 Effects of a step change in surface temperature (data of Reynolds[1]).

to for Pr = 1. If we then assume that the starting-length correction for a step-surface temperature is independent of Prandtl number, we can simply multiply the right-hand side of Eq. (12-18) by the correction term, and we have a simple equation applicable to *gases*:

$$\mathrm{St}\,\mathrm{Pr}^{0.4} = 0.0287\,\mathrm{Re}_x^{-0.2}\left[1 - \left(\frac{\xi}{x}\right)^{9/10}\right]^{-1/9} \qquad (12\text{-}29)$$

So many simplifying assumptions were introduced into this development that its validity must rest heavily on experimental verification. Fortunately, extensive experimental data are available.[1] A comparison of Eq. (12-29) with the data is shown on Fig. 12-15 for two cases. Also included on the figure are calculations based on the energy differential equation and the mixing-length model. The experimental uncertainty in these data is estimated at about ±5 percent; both methods of calculation fall within this band.

CONSTANT FREE-STREAM VELOCITY FLOW ALONG A SEMI-INFINITE PLATE WITH ARBITRARILY SPECIFIED SURFACE TEMPERATURE

The preceding step-function solution (unheated-starting-length solution) can now be used to solve the case of an *arbitrary* surface-temperature variation in exactly the same manner as was done for the laminar boundary layer. Again the method of superposition can be used to add step-function solutions to fit a prescribed surface temperature variation. Equation (10-31), previously derived, is directly applicable. Since the method of solution is identical to that used for the laminar boundary layer, only the final results for one particular type of problem are given.

Consider the case where the surface temperature can be expressed as a power series of the form

$$T_s = T_\infty + A + \sum_{n=1}^{\infty} B_n x^n \tag{12-30}$$

The heat flux at any point along the plate may then be expressed [using Eq. (12-29) for the step solution] as

$$\dot{q}_s''(x) = 0.0287\frac{k}{x}\,\mathrm{Pr}^{0.6}\,\mathrm{Re}_x^{0.8}\left(\sum_{n=1}^{\infty} nB_n x^n \frac{10}{9}\beta_n + A\right) \tag{12-31}$$

where β_n can be evaluated in terms of gamma functions:

$$\beta_n = \frac{\Gamma\left(\frac{8}{9}\right)\Gamma\left(\frac{10}{9}n\right)}{\Gamma\left(\frac{8}{9} + \frac{10}{9}n\right)}$$

Of course these results are restricted to the Prandtl-number range of *gases*, since Eq. (12-29) is so restricted.

CONSTANT FREE-STREAM VELOCITY FLOW ALONG A SEMI-INFINITE PLATE WITH ARBITRARILY SPECIFIED HEAT FLUX

This problem again can be handled in exactly the same manner as the laminar-boundary-layer problem. The step-function solution, Eq. (12-29), has the requisite form, and the function $g(\xi, x)$ evaluated from Eq. (10-39) becomes

$$g(\xi, x) = \frac{\frac{9}{10}\,\mathrm{Pr}^{-0.6}\,\mathrm{Re}_x^{-0.8}}{\Gamma\left(\frac{8}{9}\right)\Gamma\left(\frac{1}{9}\right)(0.0287k)}\left[1 - \left(\frac{\xi}{x}\right)^{9/10}\right]^{-8/9} \tag{12-32}$$

Substituting into Eq. (10-38), we obtain the expression for the surface temperature resulting from an arbitrarily specified heat-flux variation $\dot{q}_s''(\xi)$:

$$T_s(x) - T_\infty = \frac{3.42}{k}\,\mathrm{Pr}^{-0.6}\,\mathrm{Re}_x^{-0.8}\int_0^x \left[1 - \left(\frac{\xi}{x}\right)^{9/10}\right]^{-8/9} \dot{q}_s''(\xi)\,d\xi \tag{12-33}$$

The simplest example for which the heat flux is specified is that where it is taken as *constant*. With $\dot{q}_s''(\xi)$ a constant in Eq. (12-33), the integral can be readily evaluated by use of the beta function previously mentioned in connection with the laminar flow problem. The final result is

$$\mathrm{St}\,\mathrm{Pr}^{0.4} = 0.030\,\mathrm{Re}_x^{-0.2} \tag{12-34}$$

This result is approximately 4 percent higher than the comparable equation for constant surface temperature, Eq. (12-18). Recall that the difference was 36 percent for the laminar boundary layer. The turbulent boundary layer is thus much less sensitive to variations of surface temperature than the laminar boundary layer. For high-Prandtl-number fluids this is even more the case, while for very low Prandtl number fluids the large laminar-like effects begin to reappear.

AN APPROXIMATE SOLUTION FOR VARYING FREE-STREAM VELOCITY

The turbulent boundary-layer solutions considered up to this point have been concerned with a flat plate over which the free-stream velocity is constant. Obviously, more interesting problems occur when the velocity varies along the surface, such as flow over an airfoil, a turbine blade, or inside a variable-area passage such as a rocket nozzle.

For a laminar boundary layer a nearly exact solution was developed for this problem for a constant surface temperature, building from the wedge-flow solutions. For the turbulent boundary layer, no such convenient building blocks are available. On the other hand, a characteristic of the turbulent boundary layer is that it adjusts rather quickly to changes in boundary conditions, and this suggests that the integral boundary layer equations might be used to obtain at least approximate solutions for situations where the boundary conditions are not constant.

To be precise, it should be necessary to solve both the momentum and energy boundary-layer equations. A number of approximate procedures to do this have been proposed, but it turns out that for calculation of heat transfer the energy equation is by far the more important. Furthermore, a procedure based on the energy equation alone turns out to be remarkably adequate over a wide range of operating conditions. This procedure, suggested by Ambrok,[19] is described now.

For the case of constant free-stream velocity and constant surface temperature we developed Eq. (12-19) for gases, wherein the Stanton number is expressed as a function of the enthalpy thickness Reynolds number [Eq. (12-21) extends this idea to $\mathrm{Pr} = 6$]. In this equation the heat-transfer coefficient is expressed entirely in terms of *local* variables. If the thermal boundary layer responds very quickly to changes in boundary conditions, and if the local pressure gradient and local surface temperature gradient are not significant variables, then it is possible that Eq. (12-19) might be valid even if boundary conditions change in the flow direction. To test this hypothesis, let us examine some experimental data for a positive velocity gradient (favorable pressure gradient) and for a negative velocity gradient (adverse pressure gradient). Figure 12-16 shows the free-stream velocities for two such experiments. Both are for essentially *equilibrium* momentum and *equilibrium* thermal boundary layers. IDENT 51368 is a moderately strong acceleration, for which the acceleration parameter $K = 0.57 \times 10^{-6}$ and $\beta = -0.62$. IDENT 110871 is a moderately strong deceleration for which $\beta = 1.6$. Figure 12-17 shows a plot of Stanton number versus enthalpy thickness

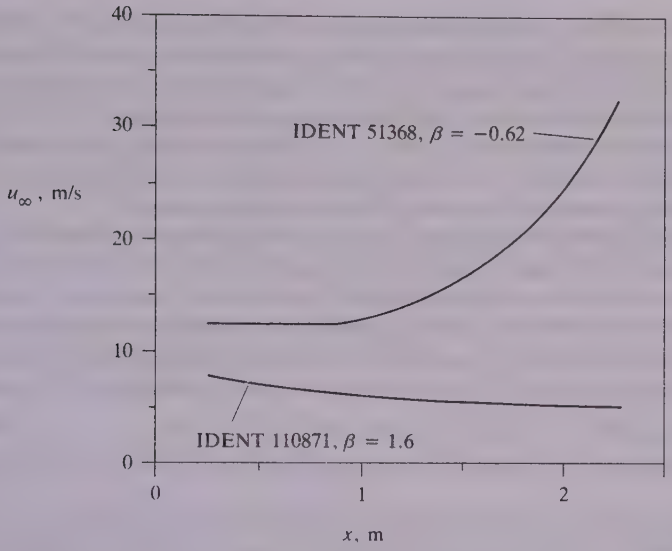

Figure 12-16 Free-stream velocity variations for two equilibrium boundary layers: IDENT 51368 (Thielbahr[3]) and IDENT 110871 (Blackwell[4]).

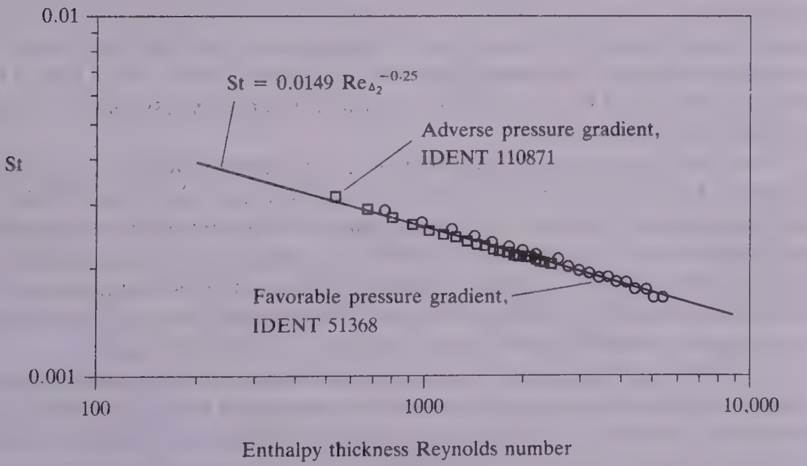

Figure 12-17 Demonstration of the generality of Eq. (12-19): effect of pressure gradient on St for air.

Reynolds numbers for these two experiments, together with Eq. (12-19) (for air). In both cases Eq. (12-19) represents the data remarkably well. Furthermore, if Eq. (12-29) for a step change in surface temperature is converted to enthalpy thickness Reynolds number (using the energy integral equation), it too will correlate quite well with the data on Fig. 12-17. All of this suggests that the range of approximate validity of Eq. (12-19) is far greater than for the simple case of constant free-stream velocity and constant surface temperature.

If this indeed is the case then the energy integral equation in its more general form, Eq. (5-20), can be used together with Eq. (12-19) to solve the thermal boundary layer for arbitrarily specified variations in free-stream velocity and surface temperature, and also for specified variations in the radius of a body of revolution such as a nozzle or flow over a body of revolution. If we substitute Eq. (12-19) into Eq. (5-20), we obtain, after some algebraic manipulation,

$$d[G_\infty \Delta_2 R(T_s - T_\infty)]^{1.25} = 0.0156 \, \mathrm{Pr}^{0.5} \, R^{1.25} \, \mu^{0.25} \, G_\infty (T_s - T_\infty)^{1.25} \, dx \tag{12-35}$$

Let $x = 0$ designate the *virtual origin* of the thermal boundary layer, which is essentially a point where any one of the variables within the exact differential is zero, and then integrate between the limits 0 and x. Introducing the definition of local Stanton number, we obtain

$$\mathrm{St} = 0.0287 \, \mathrm{Pr}^{-0.4} \frac{R^{0.25}(T_s - T_\infty)^{0.25}\mu^{0.2}}{\left[\int_0^x R^{1.25}(T_s - T_\infty)^{1.25} G_\infty \, dx\right]^{0.2}} \tag{12-36}$$

Alternatively, if a laminar boundary layer precedes the turbulent boundary layer, the enthalpy thickness of the laminar boundary layer at the presumed "point" of transition can be used as a lower limit of integration. (Note that the viscosity μ could have been left in the integrand, but it appears to such a small power that the error introduced by treating it as a constant is certainly less than the overall uncertainty of the analysis.)

The form of this result is similar to the comparable result for a laminar boundary layer, Eq. (10-53). Of particular interest is the fact that use of the energy equation has made it possible to account for a varying surface temperature, approximate though the result may be. Since we already have a reasonably accurate variable-surface-temperature solution for a constant free-stream velocity, we can at least check Eq. (12-36) for this case. It will be found that Eq. (12-36) provides a quite reasonable prediction for variable surface temperature.

It is now worth noting that the energy integral equation, upon which this result is based, is nothing more than a way of assuring that the first law of thermodynamics is satisfied in the boundary layer. The success of the method suggests that satisfying the first law in the boundary layer is of paramount importance.

Equation (12-36), despite the assumptions that went into its development, is in quite good agreement with experimental data for a wide range of applications, including rocket nozzles and missile bodies. It fails badly only for *strongly accelerated* flows, which can be characterized by large magnitudes of the acceleration parameter K defined by Eq. (11-45). For $K > 10^{-6}$ the favorable pressure gradient causes the viscous sublayer to thicken, which results in an increase in heat-transfer resistance in the sublayer and a decrease in Stanton number. This effect can be seen in Eq. (11-26) for A^+, the effective sublayer thickness. It was noted in Chap. 11 that for $K > 3.5 \times 10^{-6}$ the boundary layer begins to *relaminarize* as the viscous sublayer engulfs the entire boundary layer.

Note, of course, that Eq. (12-36) is based on *constant fluid properties* and *the absence of viscous dissipation.* We will see in Chaps. 15 and 16 how to take these effects into consideration quite simply. However, we have already taken account of one of the major compressible-flow effects, the variation of density ρ_∞ in the flow direction. We have done this by employing the free-stream mass velocity G_∞ as an independent variable. Since $G_\infty = \rho_\infty u_\infty$, the separate variations of ρ_∞ and u_∞ are immaterial.

STRONGLY ACCELERATED BOUNDARY LAYERS

Figure 12-18 shows some experimental data for a strongly accelerated boundary layer. For enthalpy thickness Reynolds numbers between 1000 and 2000 the free-stream is accelerated at $K = 2.0 \times 10^{-6}$. Note that the Stanton number decreases markedly as a result of the acceleration, although it recovers quickly when the acceleration is taken off. Also shown on the figure are the results of a calculation using the mixing-length model, including Eq. (11-26) for A^+, and the model obviously predicts the data quite well. It is worth noting that the same

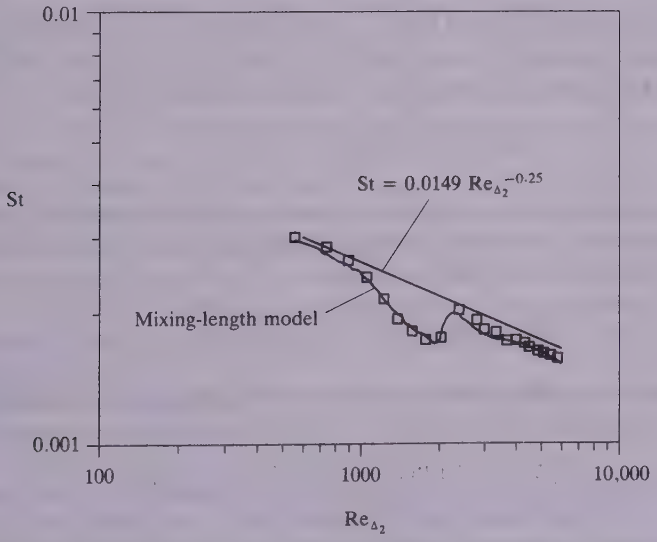

Figure 12-18 Heat transfer through a strongly accelerated turbulent boundary layer (data of Kearney,[20] IDENT 91069).

acceleration causes the friction coefficient to *increase* rather than decrease. The boundary layer shown on Fig. 12-18 is still a turbulent boundary layer, and it is not until K reaches about 3.5×10^{-6} that it will become entirely laminar, in which case the Stanton number simply continues to decrease. This boundary layer is an unusual turbulent boundary layer in that it has an abnormally thick sublayer.

The reduction in Stanton number caused by strong acceleration is frequently observed in the convergent section of small supersonic nozzles. In large nozzles it is seldom that K reaches these high values.

THE TRANSPIRED TURBULENT BOUNDARY LAYER

The effect of transpiration on the turbulent boundary layer is very similar to the effect on the momentum boundary layer described in Chap. 11. The *Couette flow* analysis described in Chap. 11 can be developed in precisely the same manner for the Stanton number as for the friction coefficient. The only difference is that a heat-transfer blowing parameter B_h is introduced rather than the friction blowing parameter B_f:

$$B_h = \frac{v_s/u_\infty}{\mathrm{St}} = \frac{\dot{m}''/G_\infty}{\mathrm{St}}$$

Then

$$\frac{\mathrm{St}}{\mathrm{St}_0} = \frac{\ln(1+B_h)}{B_h} \tag{12-37}$$

If comparison between St and St_0 is made at the same *x-Reynolds number* for the case of constant free-stream velocity, Eq. (12-37) fits the experimental data remarkably well. Thus, using Eq. (12-18), we obtain for a gas

$$\mathrm{St}\,\mathrm{Pr}^{0.4} = 0.0287\,\mathrm{Re}_x^{-0.2}\frac{\ln(1+B_h)}{B_h} \tag{12-38}$$

If we now use the energy integral equation, we can express the Stanton number as a function of the enthalpy thickness Reynolds number rather than the x-Reynolds number (holding B_h constant):

$$\mathrm{St}\,\mathrm{Pr}^{0.5} = 0.0125\,\mathrm{Re}_{\Delta_2}^{-0.25}\left[\frac{\ln(1+B_h)}{B_h}\right]^{1.25}(1+B_h)^{0.25} \tag{12-39}$$

It then follows that if St_0 is defined as the Stanton number for no transpiration at the *same value* of Re_{Δ_2} then

$$\left|\frac{\mathrm{St}}{\mathrm{St}_0}\right|_{\Delta_2} = \left[\frac{\ln(1+B_h)}{B_h}\right]^{1.25}(1+B_h)^{0.25} \tag{12-40}$$

The range of applicability of Eq. (12-40) is remarkable, and the same equation applies for c_f/c_{f_0} if B_h is replaced by B_f. Figure 12-19 shows a set of

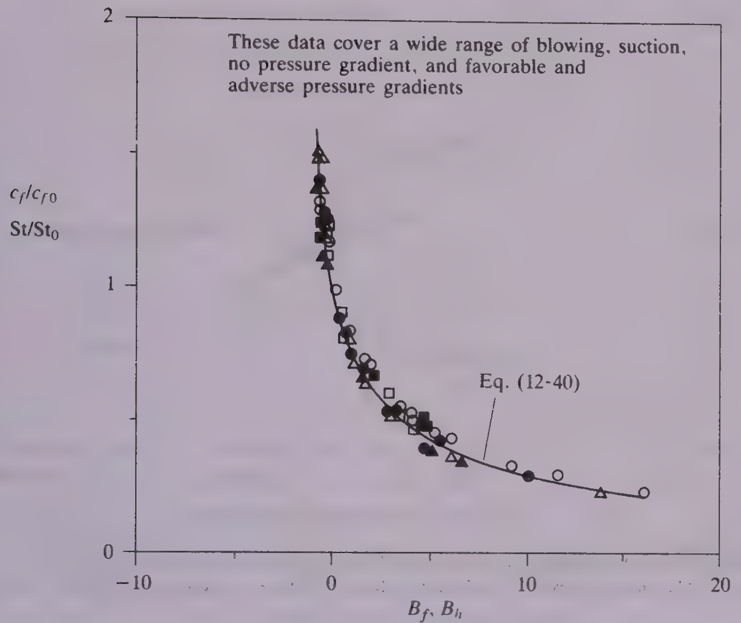

Figure 12-19 The effect of transpiration on Stanton number and friction coefficient for a wide range of flows (data of Kays and Moffat[21]).

experimental results for both St and c_f that include blowing, suction, free-stream acceleration, and deceleration. All are very well approximated by Eq. (12-40).

These results are based on experiments carried out with B_h and B_f held constant. These are the conditions for an *equilibrium thermal* boundary layer with blowing or suction, i.e., conditions that lead to outer-region similarity in both the velocity and temperature profiles. (Note that earlier we have used the term *equilibrium thermal boundary layer* for a thermal boundary layer at constant free-stream velocity having the same virtual origin as the momentum boundary layer.) However, the turbulent boundary layer comes to local equilibrium so quickly that any of Eqs. (12-38), (12-39), or (12-40) is quite applicable under conditions where B_h varies quite markedly along the surface. A rather extreme example is shown on Fig. 12-20, where a step in blowing is suddenly applied. The data are seen to closely approach the new equilibrium condition very soon after the step.

Also shown on Fig. 12-20 are the results of a full solution of the energy differential equation using the mixing-length model, which includes Eq. (11-26) for A^+. The mixing-length calculations do fit the data slightly better.

Experiments in which $\dot{m}''/G_\infty$ is held constant along the surface, rather than B_f and B_h, yield results for c_f and St that are virtually indistinguishable from the constant-B_f and constant-B_h experiments. This is in marked contrast to the behavior of the laminar boundary layer, where a substantial difference is seen.

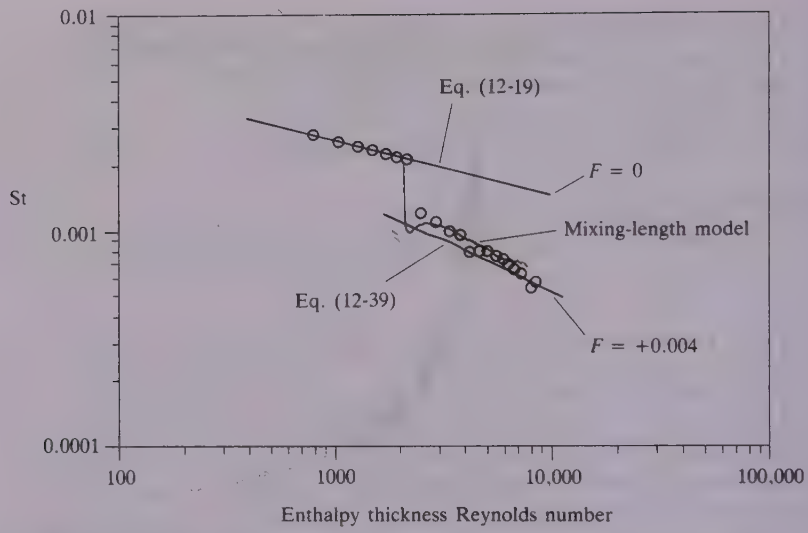

Figure 12-20 The response of Stanton number to a step increase in blowing, with $F = \dot{m}''/G_\infty$ going from 0 to +0.004; the fluid is air (data of Whitten, IDENT 50167).

By following the same procedures as for the friction coefficient in Chap. 11, an alternative blowing parameter b_h can be defined such that

$$\left.\frac{\mathrm{St}}{\mathrm{St}_0}\right|_x = \frac{b_h}{e^{b_h} - 1} \tag{12-41}$$

where

$$b_h = \frac{v_s/u_\infty}{\mathrm{St}_0} = \frac{\dot{m}''/G_\infty}{\mathrm{St}_0}$$

St_0 is here defined as the Stanton number for no transpiration at the same *x-Reynolds number*, and thus Eq. (12-41) is valid only for the case of constant free-stream velocity. But it does provide an explicit relation for St rather than the implicit equation (12-37).

For the more general case where free-stream velocity, temperature difference, and body radius, as well as transpiration rate, all vary in any arbitrary manner along a surface, a reasonable approximate procedure is to use Eq. (12-36) and simply multiply it by Eq. (12-37) to account for the effects of transpiration. A slightly more rational procedure would be to use Eq. (12-39) in place of Eq. (12-19) in the development of Eq. (12-36). However, if the pressure gradient is large, these approximate methods can lead to significant error.

Figure 12-21 shows an example of a somewhat unexpected effect of a combination of transpiration and varying free-stream velocity. From the beginning of the plate out to $\mathrm{Re}_{\Delta_2} = 4500$ the free-stream velocity is held constant, but

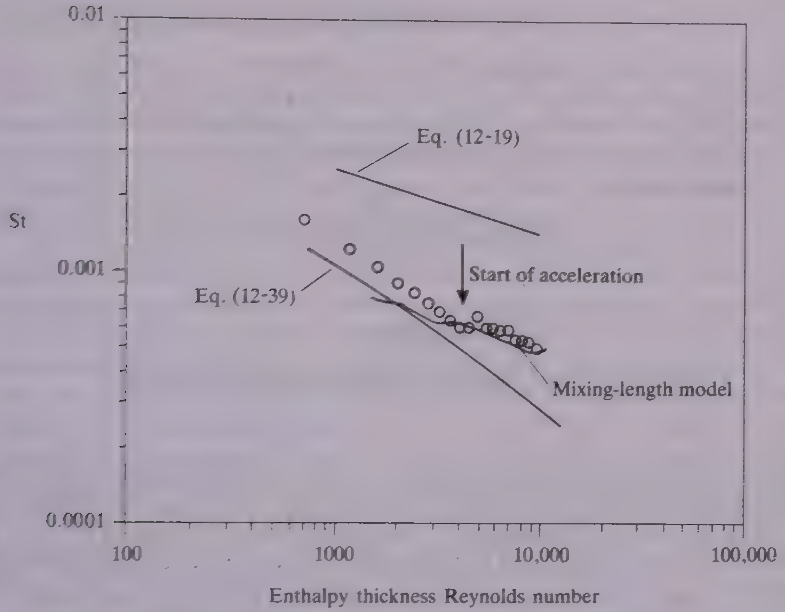

Figure 12-21 Combined effects of blowing and acceleration: blowing, $F = 0.0062$ (constant): constant u_∞, then $K = 0.77 \times 10^{-6}$ (data of Whitten, IDENT 30868).

$\dot{m}''/G_\infty$ is maintained constant at $+0.0062$. This is a quite high rate of blowing, and the experimental uncertainty for these data is at least ±10 percent. Nevertheless. Eq. (12-39) approximates the data reasonably well. At $\text{Re}_{\Delta_2} = 4500$ and thereafter the free-stream is accelerated at a constant rate $K = 0.77 \times 10^{-6}$. It was seen earlier that strong acceleration causes the Stanton number to *decrease*. Yet here it is seen that an acceleration superimposed on positive transpiration has the effect of *increasing* the Stanton number. Thus it is apparent that the various effects of changing boundary conditions are not necessarily additive.

Also shown in Fig. 12-21 are the results of a solution of the energy equation using the mixing-length model. This model does seem to show the increase in Stanton number accompanying acceleration.

There are two major areas of technical application of transpired turbulent boundary-layer theory: transpiration cooling and mass transfer. Positive transpiration, or blowing, through a porous surface provides a very effective way to cool a solid surface and protect it from a hot mainstream fluid. Not only does the transpired fluid absorb thermal energy from the porous surface as it passes through, but transpiration has the effect of substantially reducing the heat-transfer coefficient and therefore the heat-transfer rate.

Figure 12-22 shows the control volume that must be analyzed in order to employ the transpired boundary-layer solutions for transpiration cooling. Assuming that the transpiration rate $\dot{m}''$ is known and the heat transfer coefficient h

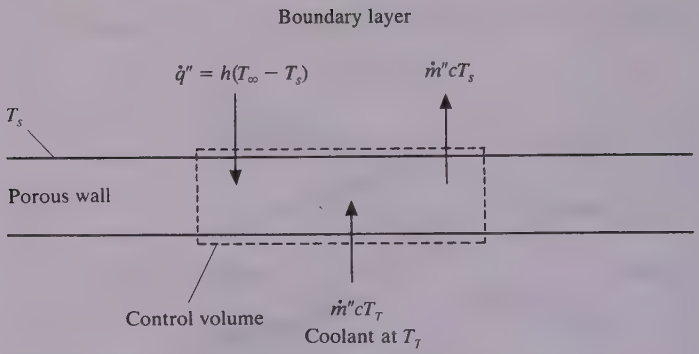

Figure 12-22 Control volume for analysis of transpiration cooling.

has been evaluated, an energy balance on the indicated control volume provides a relationship between the free-stream temperature T_∞, the surface temperature T_s, and the temperature of the coolant, which is denoted by T_T. (The enthalpy of the cooling fluid is represented as the product of the specific heat and the temperature.) But implicit in this analysis, as well as in all of the transpired boundary-layer solutions, including those for laminar boundary layers, is the assumption that the temperature of the transpired fluid is at T_s when it leaves the porous surface. In other words, it is assumed that the porous surface is a 100 percent effective heat exchanger. If the wall is thick and the pores, or holes, are very small, this may well be the case—but this is something that should be analyzed if the wall is very thin. Another critical assumption implicit in the transpired boundary-layer solutions is that the pores are infinitely small and infinitely close together. In the case of the turbulent boundary layer this effectively means that both the pores and the pore spacing are small relative to the sublayer thickness. Practically speaking, this probably means that the pore size and spacing should be no greater than one y^+ unit, although this is a problem that has not been investigated. It is related to a problem that is discussed in the next section.

In all of the previous development it has been assumed that the transpired fluid is chemically the same as the mainstream fluid. An important variation arises when the transpired fluid is chemically different, and this is sometimes a practicable cooling alternative. The associated momentum-transfer problem is basically unchanged, but the heat-transfer problem is altered, and a new transfer mechanism, *mass diffusion*, is introduced. In addition to solution of the momentum and energy equations of the boundary layer, the mass-diffusion equation of the boundary layer must be solved. But this then brings us to the general subject of mass transfer, which is the subject of Chaps. 18, 19, and 20. Since the transpired boundary layer does involve mass transfer across the fluid–solid interface, in reality it is part of the mass-transfer spectrum of problems, and the results developed in this section are used in the mass-transfer chapters even though the problem is formulated somewhat differently.

FULL-COVERAGE FILM COOLING

In cooling problems, of which the cooling of gas-turbine blades is a good example, it is often not practicable to construct the surface with a porous material. An alternative is to drill an array of small holes through the surface. The holes can be drilled normally to the surface, or a more effective arrangement is to drill them at an angle as in Fig. 12-23. But these holes are usually very large relative to the sublayer, or even the total boundary-layer thickness.

The term *full-coverage film cooling* is used here because a similar arrangement, but usually with one or two rows of holes only, is frequently used for cooling where the primary objective is to cool the surface *downstream* from the cooling holes by injecting a blanket of cool fluid into the boundary layer. The latter arrangement will be termed simply *film cooling*, and is discussed in the next section. The primary objective of full-coverage film cooling is to cool the surface *between* the cooling holes, and this may indeed involve the entire surface. Of course, if a full-coverage region is followed by an impermeable region, the latter will be cooled in the same manner as in simple film cooling, so the distinction is a bit academic. But full-coverage film cooling is obviously closely related to transpiration cooling, and, as the holes and hole spacing are made smaller, the behavior of the transpired boundary layer will be approached.

In Fig. 12-23 the temperature of the cooling fluid at the surface is denoted by T_2. Unlike the case of transpiration cooling, T_2 will usually be different from T_s because the tubes will be too short to provide sufficient heat-transfer surface area to bring the cooling fluid to surface temperature. Thus a new variable enters the problem. Fortunately, the linearity of the energy differential equation of the boundary layer provides a simple way to handle this difficulty. If experiments are performed at two different values of T_2, the behavior at any value of T_2 can be

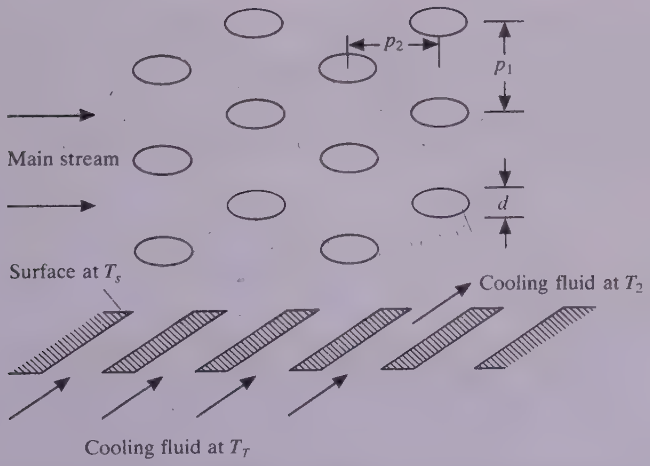

Figure 12-23 An example of a surface used for full-coverage film cooling.

determined. Let θ be defined by

$$\theta = \frac{T_2 - T_\infty}{T_s - T_\infty}$$

Now suppose two experiments are performed: one for $\theta = 0$ and the other for $\theta = 1$. It can be readily shown by superposition that at a particular point x along the surface

$$\mathrm{St}(\theta) = \mathrm{St}\,|_{\theta=0} - \theta(\mathrm{St}\,|_{\theta=0} - \mathrm{St}\,|_{\theta=1}) \tag{12-42}$$

Note that $\theta = 1$ corresponds to the case studied for the transpired boundary layer. With one other experiment, in this case letting the coolant enter at free-stream temperature, a heat-transfer coefficient for *any* value of T_2 can be evaluated.

It should be added that the heat-transfer coefficient implied is a local *average* over the solid surface between the holes; locally, the heat-transfer coefficient may vary considerably; but if the surface material has a reasonable thermal conductivity, the effect of local variations will damp out.

The number of geometric variables involved in an arrangement such as that illustrated in Fig. 12-23 is so large that it is not practicable to present any kind of comprehensive survey of the available data here. However, in order to illustrate the kind of results that are obtainable, one particular case at one Reynolds number will be presented. For more information the reader is referred to the report by Crawford, Kays, and Moffat.[22]

Figure 12-24 shows some results for a full-coverage plate with $p_1 = p_2$, $p_1/d = 5$, and the tubes at a 30° angle from the surface. This particular experiment

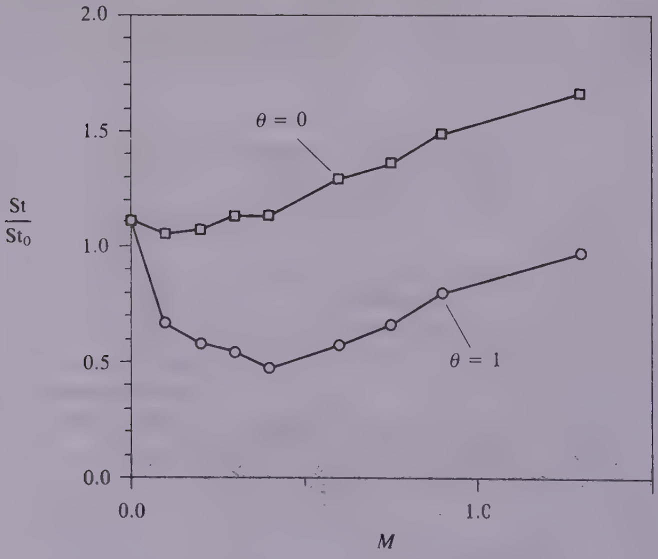

Figure 12-24 An example of experimental data for full-coverage film cooling (data of Crawford *et al.*,[22] taken at 11th row of holes).

was at constant free-stream velocity, at $\mathrm{Re}_x = 1{,}750{,}000$, and the thermal boundary layer had a delayed starting length with its origin at $\mathrm{Re}_x = 1{,}250{,}000$. This was also the point where the rows of injection holes started. The Reynolds number Re_d based on hole diameter and free-stream velocity was 12,971. The holes had $d = 1.03$ cm, and the boundary-layer total thickness at the start of injection was about 2 cm. Thus the holes were large relative to the boundary layer.

The St_0 on Fig. 12-24 is the Stanton number for no injection as given by Eq. (12-29). For this particular experiment there is a relatively large thermal boundary-layer starting-length effect, so it is appropriate to use Eq. (12-29) as a base. The ratio $\mathrm{St}/\mathrm{St}_0$ is plotted as a function of a blowing parameter M defined as

$$M = \frac{\rho_2 u_2}{\rho_\infty u_\infty} \tag{12-43}$$

M is thus similar to the transpiration mass-flux ratio $\dot{m}''/G_\infty$, but is much larger because it acts over a much smaller area.

It will be observed that the data for $\theta = 1$ initially *decrease* and behave very much like transpiration, i.e., the heat-transfer coefficient is decreased as blowing is increased. However, at about $M = 0.4$ it starts to rise, and continues to do so thereafter. The reason for this is that apparently the cooling fluid is beginning to pass completely through the sublayer instead of providing a blanket of cool fluid along the surface, and additionally it is increasing the turbulence in the boundary layer.

The effect of T_2 being less than T_s can be investigated through Eq. (12-42). A complete thermal analysis of the wall, including evaluation of heat transfer within the tubes and on its underside, is necessary before any conclusions can be drawn.

FILM COOLING

Another effective way to protect a surface from a hot fluid stream is to inject a cooler fluid under the boundary layer, thus forming a protective layer or film along the surface. The injected fluid can enter the boundary layer in a number of ways, and the number of possible geometrical arrangements is considerable. Figure 12-25 shows an example of the use of a *slot* in the surface through which

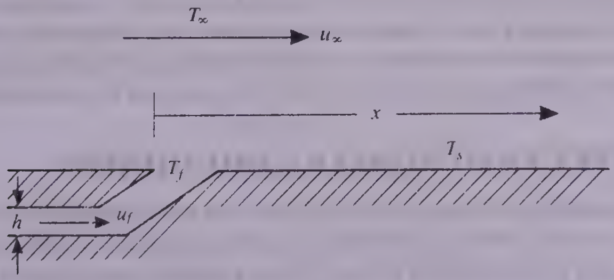

Figure 12-25 Example of a film-cooling scheme.

the cooling fluid may be injected. But the slot could be replaced by a row of holes, or two or three rows of holes, and the angle of injection could vary from normal to the surface to virtually parallel to it. Fluid could be injected through a section of *porous surface*, and also the region downstream of the *full-coverage* film-cooling region discussed in the preceding section has the same general characteristics as does the slot.

Most film-cooling experiments have been concerned with an *adiabatic* surface in the region downstream of the injection slot, and it is the temperature of this surface T_{aw} relative to the free-stream temperature T_∞ and the cooling-fluid temperature T_f that is of concern. A film-cooling effectiveness η is defined as

$$\eta = \frac{T_{\text{aw}} - T_\infty}{T_f - T_\infty} \tag{12-44}$$

It is found that η is primarily a function of a blowing-rate parameter $M = \rho_f u_f / \rho_\infty u_\infty$, the width or height of the injection slot h, and the distance x.

For essentially the scheme illustrated in Fig. 12-25, using air and a constant free-stream velocity, Weighardt[23] presents the correlation

$$\eta = 21.8(x/Mh)^{-0.8} \tag{12-45}$$

for $0.22 < M < 0.74$ and $x/h > 100$.

For applications where there is heat transfer to the surface downstream from the injection slot, the conventional procedure is to evaluate T_{aw} from η, and then calculate the heat-transfer rate using the heat-transfer coefficient that would obtain if there were no injection and the temperature difference were $T_{\text{aw}} - T_s$ rather than $T_\infty - T_s$. Metzger and Fletcher[24] have pointed out that this is not a good approximation immediately downstream of the point of injection, but high precision is generally not particularly important in that region.

Many other correlations for film-cooling are available in the literature, as well as many other geometric variations. A comprehensive review of the correlations is given by Goldstein[25] or Leontiev.[33] It is worth noting that if the slot in Fig. 12-25 is arranged parallel to the surface, and M is allowed to go to infinity, the problem of the *wall jet* is approached (see Ref. 26).

Transpiration cooling, full-coverage film cooling, film cooling by slot or hole injection, and the wall jet all obviously involve closely related phenomena. If the geometry is simple, complete solution of the boundary-layer equations is sometimes practicable, and when this is the case it is certainly the preferred method. However, if boundary-layer separation is involved, as is frequently the case, or three-dimensional effects are present, turbulence models developed for the particular application must be used, and this is beyond the scope of the present discussion.

THE EFFECTS OF SURFACE ROUGHNESS

All of the preceding discussion has been based on the assumption of an *aerodynamically smooth* surface. The effect of a rough surface on the momentum boundary layer is discussed in Chap. 11, and a mixing-length model for a *fully* *rough* surface ($\mathrm{Re}_k > 70$) is developed. The same procedure can now be applied to thermal boundary layer, but an important difference is encountered. Whereas a turbulent shear stress can be transmitted directly to the roughness elements as a result of dynamic or pressure forces on the area of the elements normal to the mean direction of flow, there exists no comparable mechanism for heat transfer. Thus heat can be transferred by *eddy conductivity* down to the plane of the roughness elements, but the actual final heat transfer to the solid surface must be through the mechanism of molecular conduction. A consequence of this fact is that, even in the fully rough regime, molecular thermal conductivity remains a significant variable; thus molecular Prandtl number remains a variable.

A mixing-length model incorporating this fact can be readily developed. Let us consider the fully rough regime for the elementary case of no pressure gradient and no transpiration. We develop a rough-surface thermal law of the wall paralleling the development of Eq. (12-15). We start with Eq. (12-12), but, since there is no sublayer, we assume that $\varepsilon_H \gg 1/\mathrm{Pr}$ all the way down to $y^+ = 0$, so we neglect $1/\mathrm{Pr}$. (This is obviously not valid for very low-Pr fluids, but for Pr of the order of magnitude of unity or larger this is an assumption of the same order as was made for the corresponding momentum-transfer problem in Chap. 11.) Next we take the lower limit of T^+ as a finite number δT_s^+ instead of zero. δT_s^+ represents the temperature difference (nondimensional) across which heat is transferred by conduction through what may be a semi-stagnant fluid in the roughness cavities at the surface. Thus Eq. (12-12) becomes

$$T^+ - \delta T_s^+ = \int_0^{y^+} \frac{dy^+}{\varepsilon_H/\nu}$$

The turbulent Prandtl number is then introduced to relate ε_H to ε_M, and ε_M is obtained from the corresponding development in Chap. 11:

$$\frac{\varepsilon_H}{\nu} = \frac{1}{\mathrm{Pr}_t}\frac{\varepsilon_M}{\nu} = \frac{\kappa}{\mathrm{Pr}_t}(y^+ + \delta y_s^+)$$

Integrating, and introducing Eq. (11-53) for δy_s^+ (treating Pr_t as constant), we have

$$T^+ = \delta T_s^+ + \frac{\mathrm{Pr}_t}{\kappa} \ln \frac{32.6 y^+}{\mathrm{Re}_k}$$

If we now examine the definition of δT_s^+ [defined similarly to T^+ in Eq. (12-10)] and define a local heat-transfer coefficient based on δT_s, we see that δT_s^+ can be expressed in terms of a Stanton number based on u_τ:

$$\delta T_s^+ = \frac{\rho c u_\tau}{h_k} = \frac{1}{\mathrm{St}_k}$$

Then

$$T^+ = \frac{1}{\mathrm{St}_k} + \frac{\mathrm{Pr}_t}{\kappa} \ln \frac{32.6 y^+}{\mathrm{Re}_k} \tag{12-46}$$

St_k must be determined from experiment, and it is undoubtedly a function of the type of roughness present. Dipprey and Sabersky[27] find that the available data can be correlated by an equation of the form

$$\mathrm{St}_k = C\,\mathrm{Re}_k^{-0.2}\,\mathrm{Pr}^{-0.44} \tag{12-47}$$

The data of Pimenta, Moffat, and Kays[7] for a rough surface composed of closely packed *spheres* yield a value of $C = 0.8$ when $\mathrm{Pr}_t = 0.9$ is used in Eq. (12-46).

Since we now have a thermal law of the wall for a fully rough surface for the case of constant u_∞ and $v_s = 0$, as well as the corresponding momentum law of the wall, Eq. (11-56), the conventional Stanton number under these conditions can be determined in precisely the same manner as was used to develop Eq. (12-17). The result is

$$\mathrm{St} = \frac{c_f/2}{\mathrm{Pr}_t + \sqrt{c_f/2}/\mathrm{St}_k} \tag{12-48}$$

Equation (11-57) can then be used to determine $c_f/2$.

Equation (12-48) would suggest that for a fully rough surface St is independent of Prandtl number. However, note that St_k is a function of Prandtl number, and as the latter becomes very large, this term can become the dominant one. Physically this means that the heat-transfer resistance offered by the molecular-conduction process in the cavities between the roughness elements becomes the major source of heat-transfer resistance in the boundary layer. Large values of $c_f/2$ have the same effect.

An example of the use of Eq. (12-48) is shown on Fig. 12-26. However, the value for C in Eq. (12-47) was *determined* from these data, so the close

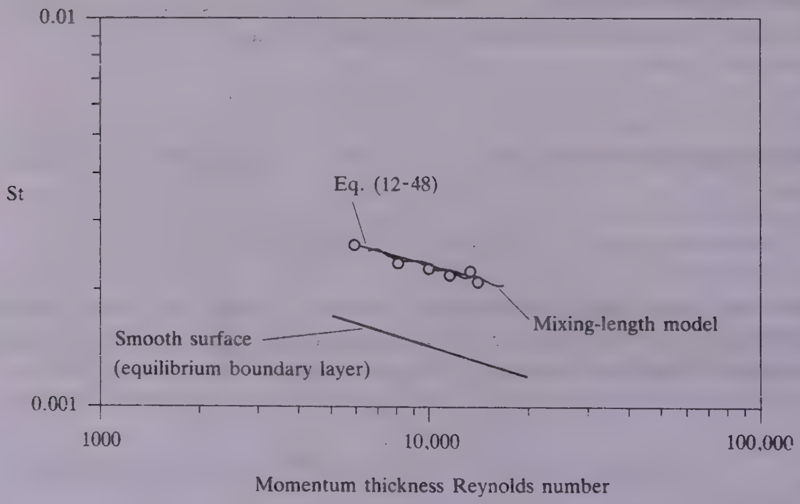

Figure 12-26 Comparison of fully rough-surface model with experiment (data from IDENT 71374; packed spheres, diameter 1.27 mm; $k_s = 0.787$ mm; air at constant u_∞).

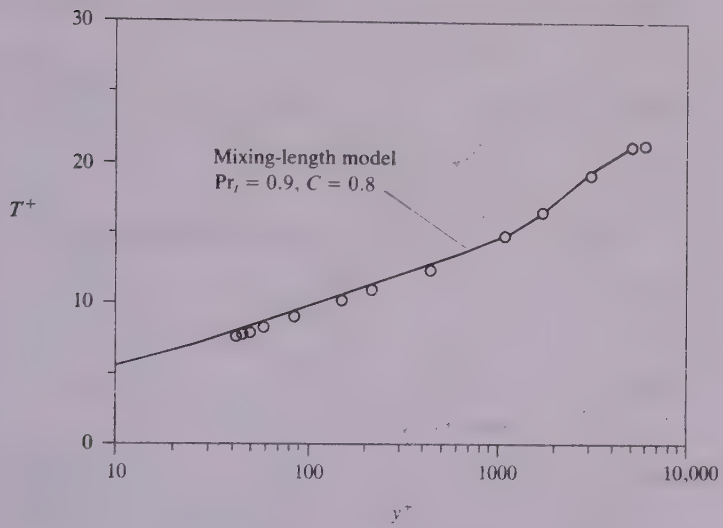

Figure 12-27 Comparison of a temperature profile calculated from the mixing-length model with experimental data (data from IDENT 71374; packed spheres, diameter 1.27 mm; $k_s = 0.787$; $\mathrm{Re}_{\delta_2} = 11{,}509$; $\mathrm{Re}_{\Delta_2} = 11{,}558$; $\mathrm{Re}_k = 101$).

correspondence between the data and Eq. (12-48) only demonstrates that C is indeed a constant. A better demonstration of the validity of the model is shown in the comparison of temperature profiles discussed below.

Note that a rough surface yields Stanton numbers significantly higher than a smooth surface—in this case about 60 percent higher. Thus roughening a surface is an effective way to increase heat-transfer rates.

The same mixing-length model can be used to solve the complete boundary-layer differential equations by finite-difference methods. The corresponding momentum boundary-layer problem is discussed in Chap. 11. The complete absence of a sublayer is modeled by setting $A^+ = 0$. Since there is no sublayer, the high values of Pr_t seen in the sublayer for a smooth surface are probably not present, and use of $\mathrm{Pr}_t = 0.9$ throughout the boundary layer seems appropriate. The results of such a calculation are also shown on Fig. 12-26. They are virtually the same as Eq. (12-48) (the "waviness" is the result of stability problems).

Figure 12-27 is of more significance. The model reproduces the nondimensional temperature profile extremely well.

THE EFFECTS OF AXIAL CURVATURE

The effects of axial curvature on the momentum boundary layer, and in particular on the friction coefficient, are discussed in Chap. 11. Curvature has a very similar effect upon the Stanton number. In fact, the data of Gibson[5] shown on Fig. 12-28 are based on the same experiments for which the friction coefficient is

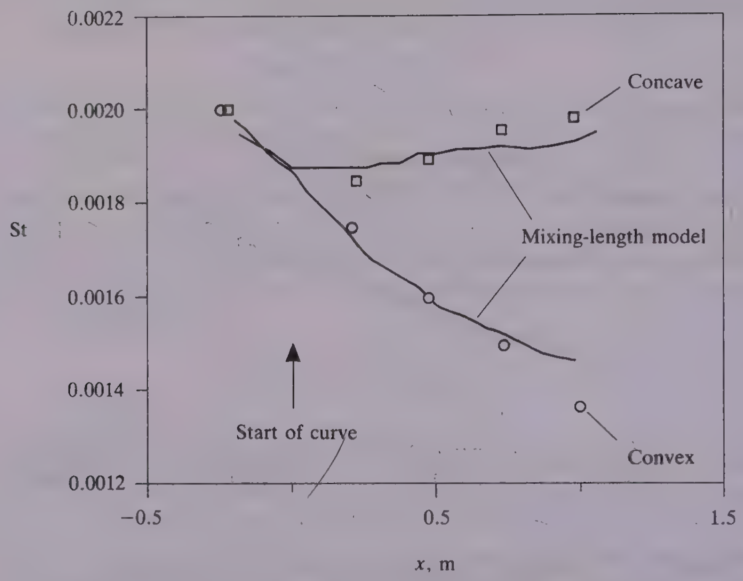

Figure 12-28 The effect of axial surface curvature on the Stanton number (data of Gibson,[5] IDENT 8000/8100; air at $u_\infty = 23.25$ m/s; $R = 0.41$ m; $\mathrm{Cr} = 0.26 \times 10^{-6}$; at $x = 0$, $\mathrm{Re}_{\delta_2} = 3540$, $\mathrm{Re}_{\Delta_2} = 4180$).

shown on Fig. 11-16, and the results are qualitatively the same. Convex curvature causes a *reduction* in St, while concave curvature has the opposite effect.

The same mixing-length model, in which the effective mixing length is reduced or increased by a linear function of the local Richardson number, and A^+ changes slightly, can be employed, i.e.,

$$l_{\mathrm{eff}} = l(1 - 10\,\mathrm{Ri})$$

$$A^+_{\mathrm{eff}} = \left(1 + \frac{1000\nu}{Ru_\tau}\right) A^+$$

Calculations employing this model, with no change in turbulent Prandtl number, are shown on Fig. 12-28, with quite reasonable results.

The data shown on Fig. 12-28 are for a relatively mild curvature. The strength of the curve can be expressed in terms of a curvature parameter Cr, which is simply the inverse of a Reynolds number based on the radius of curvature of the surface, R, and the free-stream velocity:

$$\mathrm{Cr} = \nu / u_\infty R$$

For both of the experiments shown on Fig. 12-28, $\mathrm{Cr} = 0.26 \times 10^{-6}$.

Figure 12-29 shows experimental data for a much stronger case of convex curvature, $\mathrm{Cr} = 1.21 \times 10^{-6}$. Precisely the same mixing-length model shown on this figure again yields quite satisfactory results.

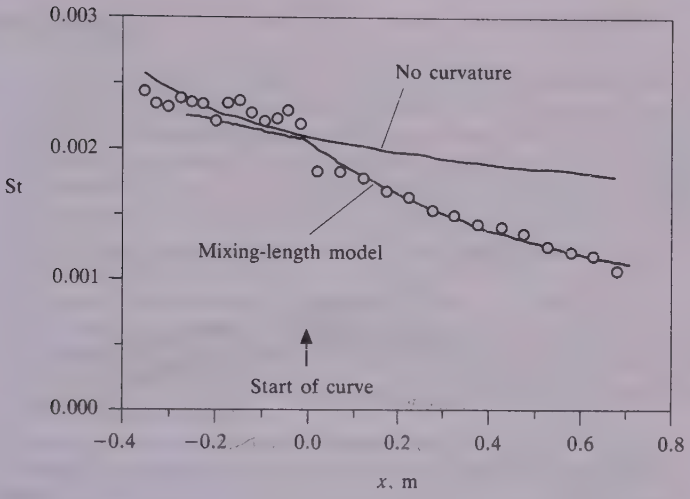

Figure 12-29 Effect of convex streamwise curvature (data of Simon;[6] air at $u_\infty = 28$ m/s; $R = 2.22$ m; $\mathrm{Cr} = 1.21 \times 10^{-6}$; at $x = 0$, $\mathrm{Re}_{\delta_2} = 4860$, $\mathrm{Re}_{\Delta_2} = 2500$).

Experiments by Hollingsworth[8] for concave curvature, using water, and with a considerably larger value of Cr, yield results for $c_f/2$ that can again be predicted quite well with the same model. However, Hollingsworth's heat-transfer results for strong concave curvature suggest that turbulent Prandtl number is affected by concave curvature, although the effect is not large in the early stages of a curved region. It should be recalled, however, that for water with $\mathrm{Pr} = 5.9$ the thermal boundary layer is largely within the sublayer, and this turbulent Prandtl-number effect may be unique to the sublayer.

An important question for technical applications is that of the range of validity of the flat-surface results; i.e., how much curvature can be tolerated before it is necessary to take it into consideration. This is similar to the question about the range of validity of the aerodynamically smooth surface correlations and models. Insufficient information is available to answer this question precisely, but the above results suggest that $\mathrm{Cr} \ll 0.26 \times 10^{-6}$ would be a necessary condition.

THE EFFECTS OF FREE-STREAM TURBULENCE

The effects of free-stream turbulence on the Stanton number are very similar to the corresponding effects on the friction coefficient (see Fig. 11-17). The wake is diminished, or completely eliminated, and St *increases*.

Some experimental results by Blair[28] are shown on Fig. 12-30, extending up to a nominal value of turbulent intensity $\mathrm{Tu} = 0.06$, indicating an increase in St

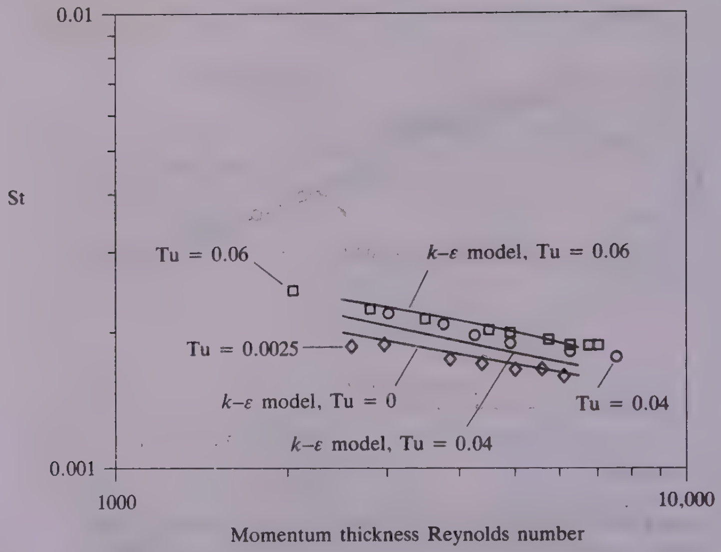

Figure 12-30 The effects of free-stream turbulence on heat transfer (data of Blair,[28] for air).

of about 20 percent. Also shown in this figure are the results of calculations using the k–ε model of turbulence, assuming isotropic free-stream turbulence. These results, together with the corresponding results for the friction coefficient (Fig. 11-17), suggest that the k–ε model is quite adequate up to least $\mathrm{Tu} = 0.075$. An interesting result of such calculations is that the increase in St resulting from free-stream turbulence seems to be relatively independent of free-stream turbulence length scale, despite experimental evidence that this may not be the case.[29]

The maximum value of Tu within the turbulent boundary layer with no free-stream turbulence is typically in the range 0.09–0.11. These experiments are for values of the free-stream turbulence that are below the turbulence level generated within the boundary layer as a result of sublayer instability. Thus free-stream turbulence has its major effect on the outer part of the boundary layer, i.e., on the wake. But when free-stream turbulence is greater than that naturally generated by the boundary layer itself, it is probably not surprising that the situation is changed.

At high values of the free-stream turbulence, Maciejewski[30] has found, from an examination of a large amount of data under widely varying conditions, that (for air) the heat-transfer coefficient is almost directly proportional to $\sqrt{\overline{u'^2}}$, and relatively independent of Reynolds number. If a Stanton number St′ is defined on the basis of $\sqrt{\overline{u'^2}}$ as the significant velocity, then Maciejewski suggests the following correlation:

$$\mathrm{St}' = 0.018 \quad \text{for } \mathrm{Tu} > 0.20 \tag{12-49}$$

PROBLEMS

12-1. The development leading to Eq. (12-17) was not expected to be applicable to a high-Prandtl-number fluid. The objective of this problem is to develop a heat-transfer solution for the turbulent boundary layer for no pressure gradient or transpiration, applicable at $\Pr = 100$. Use the Van Driest mixing-length equation and $\Pr_t = 0.9$, and integrate Eq. (12-12) out to about $y^+ = 100$ numerically. (It is desirable to use a programmable computer or calculator.) Then for $y^+ > 100$, neglect the $1/\Pr$ term and integrate as in the text. Compare the results with Eqs. (12-15) and (12-17).

12-2. Consider heat transfer to a turbulent boundary layer with no pressure gradient or transpiration but with a vanishingly small-Prandtl-number fluid. Why is this problem simpler than for the turbulent boundary layer at moderate and high Prandtl numbers? What closed-form solution already in hand should be a good approximation? Why?

12-3. The approximate solution in the text for the development of a thermal boundary layer under an already existing momentum boundary layer, Eq. (12-29), is not valid very close to the step in surface temperature. An alternative possibility in this region may be based on the fact that for a short distance from the step the thermal boundary layer is entirely within the almost completely laminar part of the sublayer, say out to $y^+ = 5$. A heat-transfer solution for this region can then be obtained in much the same manner as for a laminar boundary layer, but with the local turbulent boundary-layer surf shear stress used to establish the velocity profile. Develop a heat-transfer solution for this region, assuming that the shear stress is a constant throughout, and compare the results with Eq. (12-29). What is the range of validity of the result? What is the influence of the Prandtl number? This problem can be solved exactly using similarity methods or integral methods (see Chaps 8. and 10).

12-4. Starting with Eq. (12-34), determine the Stanton number as a function of the Prandtl number and *enthalpy thickness* Reynolds number for the case of *constant heat flux* along a surface. Compare with Eq. (12-19).

12-5. Using Eq. (12-29) and making any mathematical approximations that seem appropriate, determine the Stanton number as a function of the Prandtl number, *enthalpy thickness* Reynolds number, and *momentum thickness* Reynolds number. Note that Eq. (12-29) provides for the possibility of the ratio Δ_2/δ_2 varying from 0 to 1.

12-6. Consider the development of a turbulent boundary layer in a convergent axisymmetric nozzle. Let both the free-stream and surface temperatures be constant. As an approximation, treat the flow as one-dimensional, so that the mass velocity G may be calculated as the mass flow rate divided by the cross-sectional area of the duct, πR^2. Assume that the thermal boundary layer originates at the start of the convergence of the nozzle. Then take the case where the nozzle throat diameter is one-fifth the duct diameter at the start of convergence, x is a linear function of R, and the convergence angle is 45°. Derive an expression for the Stanton number at the nozzle throat as a function of the Prandtl number and a Reynolds number based on throat diameter and throat mass velocity. How sensitive is this expression to convergence angle? Would shapes other than the straight wall of this example yield significantly different results? Compare your results with the corresponding expression for fully developed turbulent flow in a circular pipe (see Chap. 14).

12-7. Air at a temperature of −7°C and 1 atm pressure flows along a flat surface (an idealized airfoil) at a constant velocity of 46 m/s. For the first 0.6 m the surface is heated at a constant rate per unit of surface area; thereafter, the surface is adiabatic. If the total length of the plate is 1.8 m, what must be the heat flux on the heated section so that the surface temperature at the trailing edge is not below 0°C? Plot the surface temperature along the entire plate. Discuss the significance of this problem with respect to wing deicing. (A tabulation of incomplete beta functions, necessary for this problem, is found in App. C.)

TEXSTAN can be used to confirm the results of this variable surface-heat-flux problem. Choose a starting x location near the leading edge, say 0.05 cm, and pick fluid properties that are appropriate to air, evaluated at the free-stream temperature. Use constant fluid properties and do not consider viscous dissipation. The piecewise surface heat flux boundary condition is modeled easily in TEXSTAN by providing heat flux values at four x locations, two for each segment, e.g., at $x = 0$, $x = 0.60$ m (over which there will be a heat flux), and at $x = 0.601$ m, $x = 1.8$ m (over which there will be a zero heat flux, adiabatic condition). Because TEXSTAN linearly interpolates the surface thermal boundary condition between consecutive x locations, a total of four boundary condition locations is sufficient to describe the surface temperature variation. The initial velocity and temperature profiles appropriate to the starting x location (fully turbulent boundary-layer profiles) can be supplied by using the *kstart*=3 choice in TEXSTAN. For a turbulence model, choose the mixing-length turbulence model with the Van Driest damping function (*ktmu*=5) and choose the variable turbulent Prandtl number model (*ktme*=3).

12-8. Work Prob. 12-7 but divide the heater section into two 0.3-m strips, with one at the leading edge and the other 0.9 m from the leading edge. What heat flux is required such that the plate surface is nowhere less than 0°C?

TEXSTAN can be used to confirm the results of this variable surface-heat-flux problem. Follow the general setup described in Prob. 12-7. The piecewise surface-heat-flux boundary condition will require a total of eight x locations, two for each segment, e.g., at $x = 0$, $x = 0.30$ m (over which there will be a heat flux), $x = 0.301$ m, $x = 0.90$ m (over which there will be a zero heat flux, adiabatic condition), $x = 0.901$ m, $x = 1.20$ m (over which there will again be a heat flux), and the pair $x = 1.201$ m, $x = 1.8$ m (over which there will be a zero heat flux, adiabatic condition).

12-9. In film cooling the primary effect is believed to be due to the energy put into or taken out of the boundary layer, rather than the mass of fluid injected. If this is the case, it should be possible to approximate the effect of slot injection by simulating the slot with a strip heater in which the total heat rate is set equal to the product of the injection mass flow rate and the enthalpy of the injected fluid. Using the methods of the preceding two problems, carry out an investigation of the case represented by Eq. (12-45).

12-10. Consider a film-cooling application of the type described in Prob. 12-9 (Fig. 12-25). The objective of this problem is to investigate methods of calculating heat transfer to or from the surface downstream of the injection slot (that is, the heater or heat extractor, if the above analogy is employed) when the surface temperature is maintained at some temperature different from the "adiabatic wall temperature." Since heat transfer is zero when the surface temperature is equal to T_{aw}, it would seem reasonable to define a heat-transfer coefficient based on $T_{aw} - T_s$. Such a coefficient would be useful if it turned out that it did not differ substantially from that given by, for example, Eq. (12-18). The investigation can be carried out by simulating the injection slot as in Prob. 12-9 and then specifying a constant but substantially smaller heat flux along the remainder of the plate.

12-11. An aircraft oil cooler is to be constructed using the skin of the wing as the cooling surface. The wing may be idealized as a flat plate over which air at 71 kPa and −4°C flows at 61 m/s. The leading edge of the cooler may be located 0.9 m from the leading edge of the wing. The oil temperature and oil-side heat-transfer resistance are such that the surface can be at approximately 54°C, uniform over the surface. How much heat can be dissipated if the cooler surface measures 60 by 60 cm? Would there be any substantial advantage in changing the shape to a rectangle 1.2 m wide by 0.3 m in flow length?

12-12. Consider a constant free-stream velocity flow of air over a constant-surface-temperature plate. Let the boundary layer be initially a laminar one, but let a transition to a turbulent boundary layer take place in one case at $\text{Re}_x = 300{,}000$ and in another at $\text{Re}_x = 10^6$. Evaluate and plot (on log–log paper) the Stanton number as a function of Re_x out to $\text{Re}_x = 3 \times 10^6$. Assume that the transition is abrupt (which is not actually very realistic). Evaluate the Stanton number for the turbulent part using the energy integral equation and an analysis similar to that used to develop Eq. (12-36), matching the enthalpy thicknesses of the laminar and turbulent boundary layers at the transition point. Also plot the Stanton number for a turbulent boundary layer originating at the leading edge of the plate. Where is the "virtual origin" of the turbulent boundary layer when there is a preceding laminar boundary layer? What is the effect of changing the transition point? How high must the Reynolds number be in order for turbulent heat-transfer coefficients to be calculated with 2 percent accuracy without considering the influence of the initial laminar portion of the boundary layer?

TEXSTAN can be used to confirm the results of this problem. Choose a starting x-Reynolds number of about 1000 (corresponding to a momentum Reynolds number of about 20) and pick fluid properties that are appropriate to air, evaluated at a free stream temperature of 300 K. Use constant fluid properties, and note that the energy equation does not have to be solved. The geometrical dimensions of the plate are 1 m wide (a unit width) by 3.0 m long in the flow direction, corresponding to an ending Re_x of about 3×10^6 (a momentum Reynolds number of about 5500). Let the velocity boundary condition at the free stream be 15 m/s. The initial velocity and temperature profiles appropriate to the starting x-Reynolds number (laminar Blasius boundary-layer profiles) can be supplied by using the *kstart*=4 choice in TEXSTAN. For a turbulence model, choose the mixing-length turbulence model with the Van Driest damping function (*ktmu*=5), along with the *abrupt transition model*, corresponding to *ktmtr*=1 and an appropriate momentum Reynolds number for transition, specified by the variable gxx. You will have to iterate on your gxx choice, using the ideas leading up to Eq. (11-1) to create the correct transition x-Reynolds numbers. Also, choose the variable turbulent Prandtl number model (*ktme*=3).

12-13. A 12-m-diameter balloon is rising vertically upward in otherwise still air at a velocity of 3 m/s. When it is at 1500 m elevation, calculate the heat-transfer coefficient over the entire upper hemispherical surface, making any assumptions that seem appropriate regarding the free-stream velocity distribution and the transition from a laminar to a turbulent boundary layer.

12-14. A round cylindrical body 1.2 m in diameter has a hemispherical cap over one end. Air flows axially along the body, with a stagnation point at the center of the end cap. The air has an upstream state of 1 atm pressure, 21°C, and 60 m/s. Under these conditions, evaluate the local heat-transfer coefficient along the cylindrical part of the surface to a point 4 m from the beginning of the cylindrical surface, assuming a constant-temperature surface. Make any assumptions that seem appropriate about an initial laminar boundary layer and about the free-stream velocity distribution around the nose. It may be assumed that the free-stream velocity along the cylindrical portion of the body is essentially constant at 60 m/s, although this is not strictly correct in the region near the nose.

Then calculate the heat-transfer coefficient along the same surface by idealizing the entire system as a flat plate with constant free-stream velocity from the stagnation point. On the basis of the results, discuss the influence of the nose on the boundary layer at points along the cylindrical section and the general applicability of the constant free-stream velocity idealization.

12-15. Problem 11-9 is concerned with the momentum boundary layer on a rough surface, and it involves analyzing some experimental data. The corresponding measured temperature profile is given in the following table. The surface temperature is 35.22°C, constant along the surface, and the free-stream temperature is 19.16°C. St = 0.00233. How do the results compare with the theory developed in the text?

y, cm	T, °C	y, cm	T, °C
0.020	29.02	0.660	24.17
0.030	28.64	1.10	22.84
0.051	28.14	1.61	21.62
0.081	27.57	2.12	20.36
0.127	26.97	2.82	19.46
0.191	26.36	3.58	19.16
0.279	25.76		
0.406	25.13		

12-16. Consider a flat surface that is 30 cm square. Hot air at 800 K is flowing across this surface at a velocity of 50 m/s. The hot-air density is 0.435 kg/m^3. The boundary layer on the plate is turbulent, and at the leading edge of the section of interest, the momentum thickness Reynolds number is 1100. There is no thermal boundary layer in the region preceding the 30 cm section of interest; i.e., the surface on which the momentum boundary layer has developed is adiabatic and thus at 800 K.

Cooling air is available at 290 K, at a rate of 0.0037 kg/s. The density of the coolant is 1.2 kg/m^3. Investigate what can be done with three methods of cooling the 30 cm section: (1) convection from the rear surface of the plate,

(2) transpiration, and (3) film cooling. In the first method assume that the surface is sufficiently thin, that the conduction resistance is negligible, that the effective heat-transfer coefficient on the rear surface is 25 W/(m^2 · K), and that the effective coolant temperature is 290 K over the whole surface. For the second method let $\dot{m}''$ be uniform everywhere.

Although the surface temperature varies in the direction of flow for each of the cooling methods used, ignore this effect on the heat-transfer coefficient; i.e., use constant-surface-temperature theory to determine h.

TEXSTAN PROBLEMS

12-17. TEXSTAN *analysis of the turbulent thermal boundary layer over a flat plate with constant surface temperature and with zero pressure gradient*: Choose a starting x-Reynolds number of about 2×10^5 (corresponding to a momentum Reynolds number of about 700) and pick fluid properties that are appropriate to air, evaluated at a free-stream temperature of 300 K. Use constant fluid properties and do not consider viscous dissipation. The geometrical dimensions of the plate are 1 m wide (a unit width) by 3.0 m long in the flow direction, corresponding to an ending Re_x of about 2.9×10^6 (a momentum Reynolds number of about 5400). Let the velocity boundary condition at the free stream be 15 m/s and let the energy boundary conditions be a free-stream temperature of 300 K and a constant surface temperature of 295 K. The initial velocity and temperature profiles appropriate to the starting x-Reynolds number (fully turbulent boundary-layer profiles) can be supplied by using the *kstart*=3 choice in TEXSTAN. For a turbulence model, choose the mixing-length turbulence model with the Van Driest damping function (*ktmu*=5) and choose the variable turbulent Prandtl number model (*ktme*=3) corresponding to Eq. (12-7).

Calculate the boundary layer flow and compare the Stanton number results based on x Reynolds number and enthalpy thickness Reynolds number with the results in the text, Eqs. (13-18) and (13-19). Calculate the Stanton number distribution using energy integral Eq. (5-24) and compare with the TEXSTAN calculations. Feel free to investigate any other attribute of the boundary-layer flow. For example, you can investigate the thermal law of the wall, comparing to Fig. 13-9.

12-18. TEXSTAN *analysis of the turbulent thermal boundary layer over a flat plate with constant surface temperature and with zero pressure gradient*: This is an extension to Prob. 12-17 to investigate the effect of Prandtl number on heat transfer. Examine fluids ranging from gases to light liquids and compare to Fig. 13-13. Compare Eqs. (13-17) through (13-21) with the TEXSTAN results.

12-19. TEXSTAN *analysis of the turbulent thermal boundary layer over a flat plate with constant surface temperature and with zero pressure gradient*: This problem is essentially a repeat of Prob. 12-17, but choosing higher-order turbulence models available in TEXSTAN. There exists a 1-equation model (*ktmu*=11) and four 2-equation (k–ε) models (*ktmu*=21,22,23,24). The initial velocity and temperature profiles appropriate to the starting x-Reynolds number (fully turbulent boundary-layer profiles), along with turbulence profiles for k (and ε) can be supplied by using the *kstart*=3 choice in TEXSTAN.

Choose an initial free-stream turbulence of 2 percent. Note that by setting the corresponding initial free-stream dissipation (for the 2-equation model) equal to zero, TEXSTAN will compute an appropriate value. For the 1- and 2-equation turbulence models it is best to choose a constant turbulent Prandtl number model (*ktme*=2), along with a choice for the turbulent Prandtl number, 0.9 is suggested, by setting *fxx*=0.9.

Calculate the boundary-layer flow and compare the Stanton number results based on x-Reynolds number and enthalpy thickness Reynolds number with the results in the text, Eqs. (13-18) and (13-19). Calculate the Stanton number distribution using energy integral Eq. (5-24) and compare with the TEXSTAN calculations. Feel free to investigate any other attribute of the boundary-layer flow. For example, you can investigate the thermal law of the wall, comparing to Fig. 13-9.

REFERENCES

1. Reynolds, W. C., W. M. Kays, and S. J. Kline: NASA Memo 12-1-58W, Washington, December 1958.
2. Moffat, R. J., and W. M. Kays: Report HMT-1, Thermosciences Division, Department of Mechanical Engineering, Stanford University, August 1967.
3. Thielbahr, W. H., W. M. Kays, and R. J. Moffat: Report HMT-5, Thermosciences Division, Department of Mechanical Engineering, Stanford University, April 1969.
4. Blackwell, B. F., W. M. Kays, and R. J. Moffat: Report HMT-16, Thermosciences Division, Department of Mechanical Engineering, Stanford University, August 1972.
5. Gibson, M. M., and C. A. Verriopoulos: *Experiments in Fluids*, vol. 2, pp. 73–80, Springer-Verlag, New York 1984.
6. Simon, T. W., R. J. Moffat, J. P. Johnston, and W. M. Kays: Report HMT-32, Thermosciences Division, Department of Mechanical Engineering, Stanford University, November 1980.
7. Pimenta, M. M., R. J. Moffat, and W. M. Kays: Report HMT-21, Thermosciences Division, Department of Mechanical Engineering, Stanford University, May 1975.
8. Hollingsworth, D. K., W. M. Kays, and R. J. Moffat: Report HMT-41, Thermosciences Division, Department of Mechanical Engineering, Stanford University, September 1989.
9. Zukauskas, A., and A. Slanciauskas: *Heat Transfer in Turbulent Fluid Flows*, p. 131, Hemisphere, Washington, 1987.
10. Roganov, P. S., V. P. Zabolotsky, E. V. Shihov, and A. I. Leontiev: *Int. J. Heat Mass Transfer*, vol. 27, pp. 1251–1259, 1984.
11. Rogers, M. M., P. Moin, and W. C. Reynolds: Report TF-25, Thermosciences Division, Department of Mechanical Engineering, Stanford University, August 1986.
12. Kim, J., and P. Moin: *Proceedings of 6th Symposium on Turbulent Shear Flows*, Toulouse, September 7–9, 1987, pp. 5-2-1–5-2-6.
13. Deissler, R. G.: *Int. J. Heat Mass Transfer*, vol. 6, p. 257, 1963.

14. Bell, D.: NASA–Ames Laboratories, Sunnyvale, California, personal communication, 1992.

15. Yakhot, V., S. A. Orszag, and A. Yakhot: *Int. J. Heat Mass Transfer*, vol. 30, pp. 15–22, 1987.

16. Reynolds, A. J.: *Int. J. Heat Mass Transfer*, vol. 18, pp. 1055–1068, 1975.

17. Jenkins, R.: *Proceedings of Heat Transfer and Fluid Mechanics Institute*, Stanford University, p. 147, 1951.

18. Whitten, D. G., W. M. Kays, and R. J. Moffat: Report HMT-3, Thermosciences Division, Department of Mechanical Engineering, Stanford University, December 1967.

19. Ambrok, G. S.: *Sov. Phys. Tech. Phys.*, vol. 2, p. 1979, 1957.

20. Kearney, D. W., R. J. Moffat, and W. M. Kays: Report HMT-12, Thermosciences Division, Department of Mechanical Engineering, Stanford University, April 1970.

21. Kays, W. M., and R. J. Moffat: *Studies in Convection*, pp. 223–319, Academic Press, London.

22. Crawford, M. E., W. M. Kays, and R. J. Moffat: Report HMT-30, Thermosciences Division, Department of Mechanical Engineering, Stanford University, August 1979; also NASA Report CR-3219, January 1980.

23. Wieghardt, K.: AAF Translation F-TS-919-RE, August 1946.

24. Metzger, D. E., and D. D. Fletcher: *J. Aircraft*, vol. 8, pp. 33–38, 1971.

25. Goldstein, R. J.: *Advances in Heat Transfer*, vol. 7, pp. 321–379, Academic Press, New York, 1971.

26. Meyers, G. E., J. J. Schauer, and R. H. Eustis: *J. Heat Transfer*, vol. 85, pp. 209–214, 1963.

27. Dipprey, D. F., and D. H. Sabersky: *Int. J. Heat Mass Transfer*, vol. 6, pp. 329–353, 1963.

28. Blair, M. F.: *J. Heat Transfer*, vol. 105, pp. 33–40, 1983.

29. Hancock, P. E., and P. Bradshaw: *J. Heat Transfer*, vol. 105, pp. 284–289, 1983.

30. Maciejewski, P. K., and R. J. Moffat: Report HMT-42, Thermosciences Division, Department of Mechanical Engineering, Stanford University, 1989.

31. Jischa, M., and H. B. Rieke: *Int. J. Heat Mass Transfer*, vol. 22, pp. 1547–1555, 1979.

32. Weigand, B., J. R. Ferguson, and M. E. Crawford: *Int. J. Heat Mass Transfer*, vol. 40, pp. 4191–4196, 1997.

33. Leontiev, A. I.: *J. Heat Transfer*, vol. 121, pp. 509–527, 1999.

13 CHAPTER

Turbulent Internal Flows: Momentum Transfer

In this chapter we are primarily concerned with fully developed flow in a circular tube or pipe, but we will examine briefly the problem of noncircular tubes and the effects of surface roughness. The turbulence phenomenon involved represents nothing substantially different from that discussed in Chap. 11 in connection with the turbulent external boundary layer, and therefore the material of that chapter is heavily drawn on. Similarly, the peculiarities of a fully developed flow in a constant-area tube or pipe are discussed in Chap. 7 in the context of laminar flow, and much of that material is also used here.

FULLY DEVELOPED FLOW IN A CIRCULAR TUBE

The geometry under consideration is shown in Fig. 7-1. The applicable momentum differential equation can be readily deduced from Eq. (4-11) simply by comparison with Eq. (11-3). For steady, constant-property flow we obtain

$$\bar{u}\frac{\partial \bar{u}}{\partial x} + \bar{v}_r \frac{\partial \bar{u}}{\partial r} = -\frac{1}{\rho}\frac{d\bar{P}}{dx} + \frac{1}{r}\frac{\partial}{\partial r}\left[(\nu + \varepsilon_M) r \frac{\partial \bar{u}}{\partial r}\right] \tag{13-1}$$

At and near the entrance to the tube, a turbulent boundary layer develops in much the same manner as an external boundary layer, provided that the Reynolds number is sufficiently high. But what happens in the entry region depends heavily on the geometric character of the entrance itself. If the tube is preceded by a smoothly converging nozzle, the boundary layer is often initially *laminar*, and then a *transition* to a turbulent boundary layer takes place somewhere farther downstream, assuming that the Reynolds number based on tube diameter, Eq. (7-14), is greater than the critical Reynolds number, about 2300. But if the entrance involves an abrupt or sharp-edged contraction, as is so often the case in engineering applications, no laminar boundary layer forms at all so long as

Re > 2300, but the eddy diffusivity in the turbulent developing region is very much higher than that given by the turbulence theories discussed in Chap. 11.

It is thus evident that the velocity-developing region for turbulent flow in a tube or pipe will only lend itself to an unambiguous analytical treatment for a highly idealized situation. If the entrance is a smoothly converging nozzle, so that the velocity is uniform at the beginning of the constant-area tube, and if it is assumed that a turbulent boundary layer originates at this point, then the entry region can be calculated by finite-difference solution of Eq. (13-1), using the same turbulence models as for the external boundary layer. The only thing new is the handling of the pressure gradient, which is now a dependent variable related to the acceleration of the fluid near the centerline of the tube caused by the displacement of fluid by the growing boundary layer.

Alternatively, the idealized entry region can be calculated by *integral methods* using an assumed velocity profile such as discussed in Chap. 11. A classic solution of this type is that developed by Latzko.[1] Of particular interest is the length of the developing region. Latzko's solution yields the following for the *entry length*:

$$(x/D)_{\text{entry}} = 0.623\,\text{Re}^{0.25} \tag{13-2}$$

where $\text{Re} = DG/\mu$ for a circular tube.

As an example, if $\text{Re}_D = 50{,}000$ then $x/D = 9.3$. This is obviously very much shorter than for a laminar flow, where up to 100 diameters is typical. Of course this is an idealized case, but in general the turbulent entry length is found to be of this order of magnitude. In most engineering applications, heat exchangers for example, the tubes are very much longer than this. For this reason the entry-length solution is usually not very important. The remainder of the chapter will be devoted to what will be termed *fully developed flow.*

The *unique feature* of flow in a constant-area tube is the fact that the growing boundary layers in the entry region must ultimately meet at the tube centerline (hence the *length* of the entry region). Thereafter no further growth is possible, the flow must adjust to this fact, and a *fully developed flow results.* Referring to Eq. (13-1), the radial velocity component $\bar{v}_r$ must be zero, and $\bar{u}$ must be a function of r alone. Then Eq. (13-1) becomes an ordinary differential equation:

$$0 = -\frac{1}{\rho}\frac{d\bar{P}}{dx} + \frac{1}{r}\frac{d}{dr}\left[(\nu + \varepsilon_M) r \frac{d\bar{u}}{dr}\right] \tag{13-3}$$

The problem is now much like the Couette flow problem considered for the region near the surface in Chap. 11. But, because of the pressure gradient, the shear stress cannot be independent of r; and, in fact, it is given by Eq. (7-12); i.e., it is the same as for a *laminar* flow.

Close to the surface, where r is near r_s and τ is near τ_s, the velocity profile outside the viscous sublayer should differ little from the law of the wall, Eq. (11-16). The experimental data over a substantial portion of the flow area, again excepting the sublayer, are quite well represented by a slight modification of Eq. (11-16):

$$u^+ = 2.5 \ln y^+ + 5.5 \tag{13-4}$$

where $y = r_s - r$. (This equation is frequently called the *Nikuradse equation.*)

In the context of the mixing-length theory, Eq. (13-4) implies a value of $\kappa = 0.40$, and a slightly thicker sublayer than for the simple external boundary layer, perhaps attributable to the negative pressure gradient that is always present for flow in a tube.

Equation (13-4) cannot be precisely valid at or near the tube centerline because the velocity gradient must there be zero because of symmetry. This is similar to the *wake* problem of the external boundary layer, although in this case the "wake" is smaller because of the negative pressure gradient. Furthermore, Eq. (13-4) implies $\varepsilon_M/\nu = 0$ at the centerline, which seems implausible. An empirical equation developed by Reichardt[2] for ε_M/ν for the entire region outside of the sublayer is

$$\frac{\varepsilon_M}{\nu} = \frac{\kappa y^+}{6}\left(1 + \frac{r}{r_s}\right)\left[1 + 2\left(\frac{r}{r_s}\right)^2\right] \tag{13-5}$$

where $r = r_s - y$. (Note that as $r \to r_s$, $\varepsilon_M/\nu \to \kappa y^+$, which is the same result as that obtained from simple mixing-length theory where there is no pressure gradient.) Note also that Eq. (13-5) provides a finite eddy diffusivity at the tube centerline.

Equation (13-5) is plotted in Fig. 13-1 for one particular value of Reynolds number. Note that the eddy diffusivity is finite at the tube centerline, although somewhat lower than its maximum. This is quite realistic; there is no *production* of turbulence at the centerline because there is no mean velocity gradient, but turbulence is continuously diffused toward the center of the tube from the region

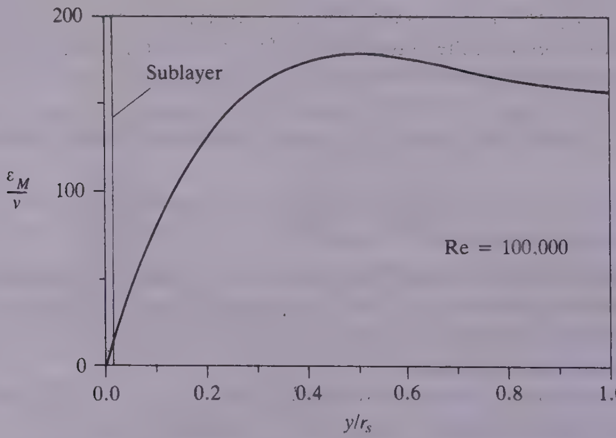

Figure 13-1 The distribution of eddy diffusivity for fully developed flow in a circular tube.

where it is produced, and it is dissipated near the centerline at the same rate. The k–ε model of turbulence can be used to calculate the velocity profile, and the turbulence kinetic energy will show the same characteristics as seen for the eddy diffusivity in Fig. 13-1.

If we now solve for the velocity using Eq. (11-9), but neglecting ν, using the linear shear-stress variation, Eq. (7-12), together with Eq. (13-5), and then using the same sublayer thickness as is implied by Eq. (13-4), with $\kappa = 0.4$, we obtain

$$u^+ = 2.5 \ln\left[y^+ \frac{1.5(1 + r/r_s)}{1 + 2(r/r_s)^2}\right] + 5.5 \qquad (13\text{-}6)$$

This equation is in slightly better agreement with experiment all the way to the centerline of the tube, and has zero slope there, which is at least more esthetically pleasing than Eq. (13-4). However the actual difference in the calculated values of u^+ is small and Eq. (13-4) is often preferred because of its simplicity.

Equation (13-3) can also be solved by finite-difference methods using essentially the same turbulence theories as discussed in Chap. 11. If the mixing-length theory is used, the sublayer can be calculated using the Van Driest function, although $A^+ = 26$ fits the data better than the value $A^+ = 25$ recommended for the simple external boundary layer. If Eq. (11-26) for A^+ is used, the pressure-gradient correction in that equation will in fact yield $A^+ \approx 26$ for Reynolds numbers (based on diameter) in the range 30,000–50,000, so the slightly higher value observed for A^+ for fully developed flow in a pipe or tube is probably due to the negative pressure gradient. For fully developed flow in a circular tube the following relationship for p^+ can be readily derived from the definition given in Chap. 11:

$$p^+ = \frac{14}{\mathrm{Re}\sqrt{c_f/2}}$$

If this equation is substituted into the equation for A^+, Eq. (11-26), it can be seen that A^+ increases at low Reynolds numbers. Although Eq. (11-26) is an empirical equation, a particularly interesting feature is that if the friction coefficient for fully developed *laminar* flow, $c_f/2 = 8/\mathrm{Re}$, is substituted, it will be found that A^+ becomes indefinitely large at $\mathrm{Re} = 2000$.

In the region near the center of the tube the assumption of a constant mixing length as recommended for external boundary layers is not a good one. A better alternative is Eq. (13-5), or a simpler and adequate scheme is to use the value given by Eq. (13-5) for $r = 0$ for the entire inner region, starting at the point where the same value of ε_M/ν is calculated using $l = \kappa y[1 - \exp(-y^+/A^+)]$.

A relatively simple algebraic equation for the friction coefficient for fully developed flow can be developed by approximating Eq. (13-6) with a power law. It will be recalled that this procedure is used to obtain a closed-form equation for the friction coefficient for the external boundary layer, Eq. (11-20). The following is quite a good fit for moderate Reynolds numbers:

$$u^+ = 8.6 y^{+1/7} \qquad (13\text{-}7)$$

Then at the centerline

$$u_c^+ = 8.6y_c^{+1/7} \tag{13-8}$$

and

$$\frac{u}{u_c} = \left(\frac{y}{r_s}\right)^{1/7} \tag{13-9}$$

The mean velocity can then be determined by substitution of Eq. (13-9) into Eq. (7-6) to yield the ratio of mean velocity to centerline velocity:

$$\frac{V}{u_c} = 0.817 \tag{13-10}$$

Then, from Eq. (13-8),

$$\frac{u_c}{u_\tau} = 8.6\left(\frac{r_s u_\tau}{\nu}\right)^{1/7}$$

But $u_\tau = \sqrt{\tau_s/\rho} = V\sqrt{c_f/2}$. Then

$$\frac{u_c}{V\sqrt{c\rho/2}} = 8.6\left(\frac{r_s V\sqrt{c_f/2}}{\nu}\right)^{1/7}$$

Introducing Eq. (13-10), and the definition of a Reynolds number based on tube diameter and mean velocity, $\mathrm{Re} = DV/\nu$, we obtain

$$c_f/2 = 0.039\,\mathrm{Re}^{-0.25} \tag{13-11}$$

(Note that henceforth Re will denote Reynolds number based on tube diameter.) Equation (13-11) fits the experimental data very well for $10^4 < \mathrm{Re} < 5 \times 10^4$.

For higher Reynolds numbers the logarithmic form of velocity profile is more precise. If we assume that Eq. (13-4) is a reasonable approximation for the *entire* velocity profile, we can go through precisely the same procedure as was used to derive Eq. (13-11) and obtain a logarithmic equation for the friction coefficient. With a small modification of the coefficients to provide a better fit to the experimental data, we then obtain the "classical" Kármán–Nikuradse equation:

$$\frac{1}{\sqrt{c_f/2}} = 2.46\ln(\mathrm{Re}\sqrt{c_f/2}) + 0.30 \tag{13-12}$$

This is a little awkward to use, and a commonly employed empirical equation that closely fits the Kármán–Nikuradse equation over the range $3 \times 10^4 < \mathrm{Re} < 10^6$ is

$$c_f/2 = 0.023\,\mathrm{Re}^{-0.2} \tag{13-13}$$

Another equation that fits the data (and the Kármán–Nikuradse equation) over the range $10^4 < \mathrm{Re} < 5 \times 10^6$ is that proposed by Petukhov[3]:

$$c_f/2 = (2.236\ln\mathrm{Re} - 4.639)^{-2} \tag{13-14}$$

The origin of this equation can be seen if for Eq. (13-12) a nominal value is given to $c_f/2$ in the logarithmic term, and then the equation is squared and inverted.

TUBES OF NONCIRCULAR CROSS SECTION

Most of the velocity change in a turbulent flow takes place very close to the surface and is relatively independent of the proximity of any other surfaces. For this reason, the shape of the flow tube cross-section has little effect on the shear stress at the surface, except where sharp corners are involved. Thus it would not be surprising if Eq. (13-12) were a good approximation for noncircular tubes, provided that some kind of equivalent tube diameter could be defined for evaluating the Reynolds number. A dimension that is independent of tube shape is the *hydraulic radius*, the ratio of flow area to surface perimeter:

$$r_h = \frac{\text{flow area}}{\text{wetted perimeter}} = \frac{A_c L}{A} \tag{13-15}$$

The hydraulic radius has the dimensions of length, and thus scales on system size, and for a circular tube is identically $\frac{1}{4}D$. Thus a *hydraulic diameter* can be defined as

$$D_h = 4r_h = \frac{4A_c L}{A} \tag{13-16}$$

If D_h is substituted for D in Eqs. (13-11), (13-12), (13-13), or (13-14), these equations hold quite well for noncircular cylindrical tubes.

This simplification obviously breaks down for passages with sharp corners, such as triangular passages with small angles at one or two corners, because the sublayer thickness becomes large relative to the distance to an opposite surface. The limits of applicability of the hydraulic diameter concept for triangular tubes are discussed by Carlson and Irvine.[4] Hartnett, Joh, and McCornas[5] find that for rectangular passages the circular-tube equations using the hydraulic diameter concept work very well.

Experimentally determined friction coefficients for a large variety of tube shapes, including passages with various types of boundary-layer interruptions, are given by Kays and London.[6] Another very extensive source of data is the *Handbook of Single-Phase Convective Heat Transfer.*[7]

EFFECTS OF SURFACE ROUGHNESS

The effects of surface roughness on fully developed flow in a tube are essentially the same as discussed in Chap. 11 in connection with the external boundary layer. The three roughness regimes—smooth, transitional, and fully rough—are observed as before, and the only differences are associated with the definitions of mean velocity V, the friction coefficient $c_f/2$, and the Reynolds number DV/ν.

For tube flow the *roughness Reynolds number* can be more conveniently expressed in terms of the tube-diameter Reynolds number and friction coefficient as follows:

$$\mathrm{Re}_k = \frac{k_s u_\tau}{\nu} = \frac{k_s V\sqrt{c_f/2}}{\nu} = \frac{k_s 2r_s V\sqrt{c_f/2}}{2r_s \nu}$$
$$= \frac{\mathrm{Re}\sqrt{c_f/2}}{D/k_s}$$

Thus the criterion for a *smooth* surface, $\mathrm{Re}_k < 5$, becomes

$$\frac{\mathrm{Re}\sqrt{c_f/2}}{D/k_s} < 5$$

and similarly the *fully rough* surface corresponds to

$$\frac{\mathrm{Re}\sqrt{c_f/2}}{D/k_s} > 70$$

An algebraic equation for friction coefficient for a *fully rough* surface can be developed from the fully rough surface law of the wall, say, Eq. (11-56), by essentially the same procedure as was used to derive the Kármán–Nikuradse equation (13-12), yielding

$$\frac{1}{\sqrt{c_f/2}} = 2.46 \ln \frac{D}{k_s} + 3.22$$

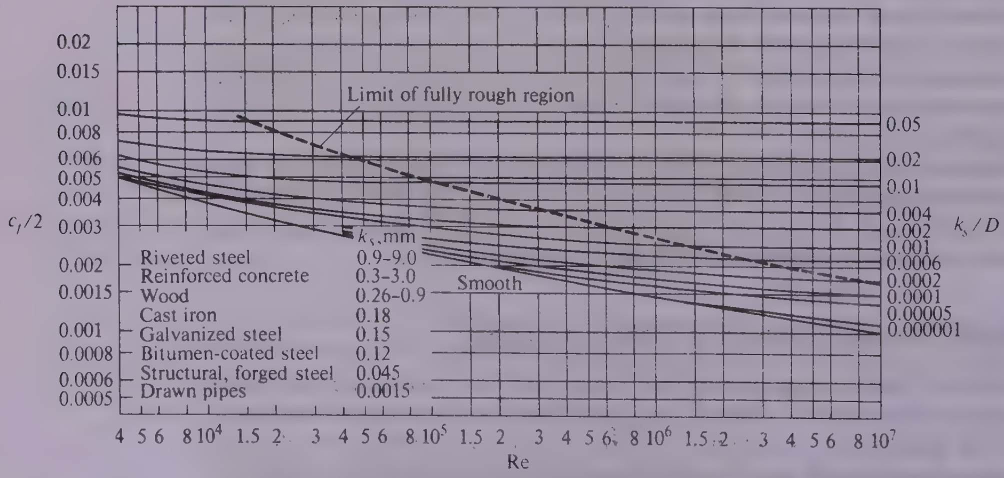

Figure 13-2 Friction coefficients for fully developed turbulent flow in smooth- and rough-walled circular tubes (Moody[8]).

from which

$$\frac{c_f}{2} = \left[2.46 \ln\left(\frac{D}{k_s}\right) + 3.22\right]^{-2} \tag{13-17}$$

Note that, as before, the friction coefficient for the fully rough case is independent of flow velocity and viscosity.

The friction coefficient for the entire range of roughness Reynolds numbers, together with data on values for k_s for typical types of pipe surface, are treated extensively by Moody.[8] An abstract of the Moody data is given in Fig. 13-2.

PROBLEMS

13-1. Develop an equation for the friction coefficient for fully developed turbulent flow between parallel planes, assuming that Eq. (13-7) is a reasonable approximation for the velocity profile.

13-2. Employing numerical integration to determine the ratio of mean velocity to centerline velocity, and Eq. (13-6) for the velocity profile, evaluate the friction coefficient for fully developed turbulent flow in a circular tube for two different Reynolds numbers: 30,000 and 150,000. Compare results with other relations for the friction coefficient given in the text. (It is presumed that a programmable computer is used for this problem.)

13-3. Develop a solution for the friction coefficient and velocity profile in the entry region of a flat duct, assuming that the velocity is uniform over the flow cross section at the entrance, that the boundary layer that develops on the two surfaces is turbulent from its very beginning, and that Eq. (13-7) is an adequate approximation for the velocity profile both in the entry region and in the fully developed region. Employ the momentum integral equation, and assume that the velocity profile in the entry region can be divided into two parts: a uniform-velocity core region and a boundary layer that ultimately engulfs the entire core. Note that the uniform velocity in the core region accelerates because of the displacement of the boundary layer, and that part of the pressure drop in the entry region is due to this acceleration. Determine the length of the entry region.

13-4. Develop Eq. (13-17) by the indicated procedures.

13-5. Employing Eq. (13-6), numerical integration, and a programmable computer, determine the ratio of mean velocity to centerline velocity for fully developed flow in a circular tube for a number of different Reynolds numbers, and compare with Eq. (12-10), which was developed assuming a $\frac{1}{7}$-power profile. Determine whether it is valid to neglect the contribution of the sublayer in these calculations.

13-6. The viscous sublayer behaves as if it were almost completely laminar out to a value of y^+ of about 5.0. With this idea in mind, calculate the ratio of such a sublayer thickness to pipe diameter for fully developed turbulent flow in a smooth-walled pipe. Using these results, discuss the significance of the data in Fig. 13-2.

13-7. Two water tanks, open to the atmosphere, are connected by a pair of parallel pipes each having an inside diameter of 2.5 cm. The pipes are 20 m long. One is a "smooth" tube, but the other is a galvanized iron pipe. What must be the elevation difference for the two tanks in order for the total flow rate for the two pipes to be 1.00 kg/s? (Neglect entrance and exit pressure-drop effects.)

TEXSTAN PROBLEMS

13-8. TEXSTAN *analysis of the turbulent momentum entry flow in a circular tube*: Investigate the entry-length region through the hydrodynamically fully developed region of flow in a circular tube with diameter Reynolds numbers of 30,000 and 150,000. Pick fluid properties that are appropriate to air, evaluated at a temperature of 300 K. Use constant fluid properties, and note that the energy equation does not have to be solved. Let the pipe diameter be 3.5 cm and the pipe length be 12.0 m. Let the velocity profile at the inlet to the tube be flat, which can be supplied by using the *kstart*=1 choice in TEXSTAN. For a turbulence model, choose the hybrid turbulence model having a constant eddy viscosity in the outer part of the flow ($\varepsilon_m/\nu = a\mathrm{Re}^b$ with $a = 0.005$ and $b = 0.9$) and a mixing-length turbulence model with the Van Driest damping function ($\kappa = 0.40$ and $A^+ = 26$) in the near-wall region (*ktmu*=7). This hybrid model tends to more closely fit Fig. 13-1, and thus better predict the fully developed friction coefficient for a given Reynolds number.

Compare the friction coefficient with the set of Eqs. (13-11) through (13-14). Feel free to investigate any other attribute of the boundary-layer flow. For example, you can examine a velocity profile at the hydrodynamically fully developed state to evaluate the *law of the wall* and the ratio of mean velocity to centerline velocity, and compare with Eqs. (13-6) and (13-10) respectively.

13-9. TEXSTAN *analysis of the turbulent momentum entry flow between parallel plates*: Investigate the entry-length region through the hydrodynamically fully developed region of flow in between parallel plates with hydraulic diameter Reynolds numbers of 30,000 and 150,000. Pick fluid properties that are appropriate to air, evaluated at a temperature of 300 K. Use constant fluid properties, and note that the energy equation does not have to be solved. Let the plate spacing be 7.0 cm and the plate length be 7.0 m. Let the velocity entry profile at the inlet to the plates be flat, which can be supplied by using the *kstart*=1 choice in TEXSTAN. For a turbulence model, choose the hybrid turbulence model having a constant eddy viscosity in the outer part of the flow ($\varepsilon_m/\nu = a\mathrm{Re}^b$ with $a = 0.0022$ and $b = 0.9$) and a mixing-length turbulence model with the Van Driest damping function ($\kappa = 0.40$ and $A^+ = 26$) in the near-wall region (*ktmu*=7). This hybrid model follows the circular pipe idea described in Prob. 13-8, and thus better predicts the fully developed friction coefficient for a given Reynolds number.

Compare the friction coefficient with the set of Eqs. (13-11) through (13-14), being careful to use the hydraulic diameter, Eq. (13-16). Feel free to investigate any other attribute of the boundary-layer flow. For example, you can compare the profile shape with that described as a part of Prob. 13-1.

REFERENCES

1. Latzko, H.: *Z. Angew. Math. Mach.*, vol. 1, pp. 268–290, 1921.
2. Reichardt, H.: *Arch. Ges. Warmetechnik*, vol. 6/7, pp. 129–143, 1951.

3. Petukhov, B. S.: *Advances in Heat Transfer*, vol. 6, pp. 503–504, Academic Press, New York, 1970.
4. Carlson, L. W., and T. F. Irvine, Jr: *J. Heat Transfer*, vol. 83, pp. 441–444, 1961.
5. Hartnett, J. P., J. C. Y. Koh, and S. T. McCornas: *J. Heat Transfer*, vol. 86, pp. 82–88, 1962.
6. Kays, W. M., and A. L. London: *Compact Heat Exchangers*, 3d ed., McGraw-Hill, New York, 1984.
7. Kakac, S., R. K. Shah, and W. Aung: *Handbook of Single-Phase Convective Heat Transfer*, Wiley, New York, 1987.
8. Moody, L. F.: *Trans ASME*, vol. 66, p. 671, 1944.

14 CHAPTER

Turbulent Internal Flows: Heat Transfer

For a turbulent flow in smooth tubes we will consider, as nearly as possible, all the same boundary conditions covered in Chap. 8 for a laminar flow. By employing the same nomenclature and essentially the same differential equations, we can use many of the results of the laminar flow analyses. The turbulent transport mechanism and some techniques for calculating heat-transfer rates in a turbulent shear layer have been discussed at considerable length in Chaps. 11 and 12 in the framework of the turbulent external boundary layer. Some of the peculiarities of the tube-flow problem were discussed in Chap. 13. Thus there is little that is fundamentally new to be discussed in this chapter; we are concerned primarily with analytic and experimental results for particular boundary conditions of interest, using techniques previously developed. We will restrict consideration to constant fluid properties and negligible viscous dissipation; these latter effects will be considered in later chapters.

To find an appropriate energy differential equation for the case of a *circular tube*, let us go back to the equation for a steady laminar flow in a circular tube, Eq. (4-35). We will evaluate the enthalpy from $di = c\,dT$ and restrict the problem to axisymmetric heating ($\partial T/\partial\phi = 0$) and negligible axial conduction ($\partial^2 T/\partial x^2 \approx 0$). Thus

$$\rho c u \frac{\partial T}{\partial x} + \rho c v_r \frac{\partial T}{\partial r} = \frac{1}{r}\frac{\partial}{\partial r}\left(rk\frac{\partial T}{\partial r}\right)$$

From this equation we simply *infer* the corresponding equation for a *turbulent* flow in a circular tube by comparison with Eq. (12-2), and at the same time we will restrict the problem to the case of constant fluid properties:

$$\bar{u}\frac{\partial \bar{T}}{\partial x} + \bar{v}_r\frac{\partial \bar{T}}{\partial r} = \frac{1}{r}\frac{\partial}{\partial r}\left[r(\alpha + \varepsilon_H)\frac{\partial \bar{T}}{\partial r}\right] \tag{14-1}$$

We already have at our disposal all the necessary tools to solve this equation for any desired thermal boundary conditions and any velocity initial conditions.

Either the Prandtl mixing-length or the k–ε method of Chap. 11 offer a method for evaluating ε_M, or, for the fully developed flow case, Eq. (13-5) can be used directly. The sublayer region can be calculated by using the Van Driest function, Eq. (11-25). The turbulent Prandtl number results of Chap. 13 should be equally applicable to flow in a tube, and thus offer a method for evaluating ε_H from ε_M. Of course the same methods must be used to solve the corresponding momentum equation (13-1) in order to evaluate $\bar{u}$ and $\bar{v}_r$. All of this requires use of finite-difference methods and a digital computer. But, given these tools, the problem can be solved for the most complex set of boundary conditions.

However, solutions for certain particular boundary conditions can frequently be obtained by simpler methods or directly from experiments, and very often such solutions are both quite adequate and more convenient for engineering analysis. Furthermore, the study of such solutions can enhance understanding of the phenomena involved in a way that is generally not possible from numerical solutions.

It was noted in Chap. 13 that for a turbulent flow, the velocity profile tends to become *fully developed* after an axial distance of 10–15 diameters, and that the behavior in the *entry region* is very dependent on the character of the tube entrance. Since the fully developed velocity region is often of much more importance than the entry region (and this is in sharp contrast to the behavior of a *laminar flow*), it is worthwhile taking advantage of the mathematical simplifications that obtain. For fully developed flow $\bar{v}_r = 0$, $\bar{u}$ is a function of r alone, and Eq. (14-1) reduces to

$$\frac{1}{r}\frac{\partial}{\partial r}\left[r(\alpha + \varepsilon_H)\frac{\partial \bar{T}}{\partial r}\right] = \bar{u}\frac{\partial \bar{T}}{\partial x} \tag{14-2}$$

Equation (14-2), and the corresponding momentum equation, can now be solved, using the turbulence models discussed above, and finite-difference computations, for *any thermal boundary conditions*, so long as the velocity profile is assumed to be *fully developed* at the point where heat transfer starts.

One class of problem that can be solved using Eq. (14-2) is the *thermal-entry-length problem*, where the entry fluid temperature is uniform, but the velocity profile is already fully developed at the point where heat transfer starts. This problem can be solved by finite-difference methods, but Eq. (14-2) can also be solved by the classical method of separation of variables in much the same manner as for the corresponding laminar flow problem, the so-called *turbulent Graetz problem.* (This procedure involves a numerical solution, but it is a "one-time" solution). The Graetz problem is considered later in this chapter for two cases—where the surface temperature is constant, and where the surface heat flux is constant.

But first let us consider a further simplification of Eq. (14-2). Refer to the section in Chap. 8 where the *fully developed temperature profile* is discussed. For the two thermal boundary conditions, *constant surface temperature* and *constant heat rate* (constant surface heat flux), a fully developed temperature profile, in a nondimensional sense, obtains following an entry region; again the axial distance required is usually not more than 10–15 diameters (exceptions to this rule are the very low-Prandtl-number fluids, the liquid metals). These two boundary conditions are commonly encountered in engineering applications, and the tubes are frequently very much longer than 10–15 diameters. Furthermore, it is shown in Chap. 8 that this situation leads to a heat-transfer coefficient h that is invariant with axial distance. *Heat-exchanger theory* is based on an assumption that h is independent of axial distance, since this is a commonly observed phenomenon. Thus the fully developed temperature-profile problem is worthy of study, and indeed more so for a turbulent flow than for a laminar flow, where entry lengths are often large.

CIRCULAR TUBE WITH FULLY DEVELOPED VELOCITY AND TEMPERATURE PROFILES, CONSTANT HEAT RATE, PRANDTL NUMBERS 0.6–6.0

This is the thermal boundary condition that occurs in a counterflow heat exchanger when the fluid capacity rates are the same, and it also occurs in a tube heated by electric resistance heating. It *can* occur as a result of nuclear heating or radiation from a high-temperature source. The axial temperature distribution is shown in Fig. 8-2.

When both the velocity and temperature profiles are fully developed, Eq. (8-8) is applicable and Eq. (14-2) becomes

$$\bar{u}\frac{dT_m}{dx} = \frac{1}{r}\frac{\partial}{\partial r}\left[r(\alpha + \varepsilon_H)\frac{\partial \bar{T}}{\partial r}\right] \tag{14-3}$$

Equation (14-3), and the associated momentum equation (13-3), are essentially ordinary differential equations, and are relatively easy to solve simultaneously by finite-difference methods using the mixing-length and eddy diffusivity methods of Chap. 13 and the turbulent Prandtl number, Eq. (12-7). Such calculations have been carried out for the Prandtl number range 0.7–5.9 using Eq. (12-7) but with the Prandtl number in that equation held at 0.7, because it was noted in Chap. 12 that the Pr_t distribution for water at $\mathrm{Pr} = 5.9$ is virtually identical to that for air, $\mathrm{Pr} = 0.7$. The resulting Nusselt numbers correspond closely to the generally accepted experimental data over this range of Prandtl number.

From these calculations it has then been possible to empirically fit a universal temperature profile in the same form as Eqs. (12-15) and (12-16), analogous to the Nikuradse equation (13-4) for velocity:

$$T^+ = 2.2 \ln y^+ + 13.39\,\mathrm{Pr}^{2/3} - 5.66 \tag{14-4}$$

Since this equation is based on turbulent Prandtl number data at just two points, $\mathrm{Pr} = 0.7$ and 5.9, it may not be valid far outside of this Prandtl number range; the $\frac{2}{3}$ power of the Prandtl number is somewhat arbitrary, but this is a function that has long been found to correlate experimental data to very high Prandtl number.

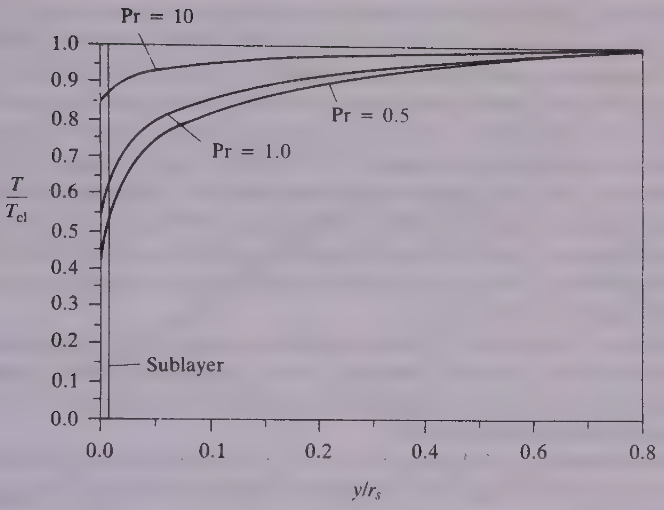

Figure 14-1 Effect of Prandtl number on turbulent flow temperature distribution; Re = 100,000.

Thus Eq. (14-4) is proposed as a *thermal law of the wall* for flow in a circular tube over the Prandtl number range 0.6–6.0, but one that may be reasonably valid at much higher Prandtl numbers. Note that this range covers all of the gases, as well as many light liquids, including water. It is certainly not valid for the very low-Prandtl-number fluids, the liquid metals. Note also that Eq. (14-4) is not valid inside the viscous sublayer, but this is also true of Eq. (13-4). Furthermore, neither Eq. (13-4) nor Eq. (14-4) is precisely valid at the tube centerline (see the discussion of this point in Chap. 13), but the manner in which these equations are now going to be used minimizes this discrepancy.

The temperature profiles implied by Eq. (14-4) are plotted on Fig. 14-1 for a single value of Reynolds number and three values of the Prandtl number. Note that the effect of increasing Prandtl number is to give a more "square" temperature profile, while a low Prandtl number yields a more rounded profile that is similar to that for laminar flow. Still higher and lower values of Prandtl number continue these trends. Note the location of the major source of heat-transfer resistance. At high Prandtl numbers the resistance is increasingly in the sublayer, whereas at low Prandtl numbers it is distributed over the entire flow cross section. The reasons for these differences can be seen in the "total conductance" term in Eq. (14-3), $\alpha + \varepsilon_H$. If this term is rendered nondimensional by dividing it by the kinematic viscosity ν, it becomes

$$1/\mathrm{Pr} + \varepsilon_H/\nu$$

The relative importance of turbulent eddy diffusion and molecular diffusion is seen to depend directly on the Prandtl number. Along any radius, the molecular-conduction term $1/\mathrm{Pr}$ is constant, while the eddy-conduction term ε_H/ν varies from a relatively large magnitude near the center of the tube to zero at the surface. The shape of the temperature profile and the whole character of turbulent flow heat transfer are determined by the relative magnitude of these two terms. At very low Prandtl numbers the conduction term dominates everywhere, and not only is the temperature profile similar to a laminar profile, but also the thermal-entry length and the response of the fluid to axial changes in surface temperature are both quite similar to laminar behavior. At higher Prandtl numbers we find very short thermal-entry lengths and quick response to axial surface-temperature changes, both attributable to the concentration of the thermal resistance close to the surface and the rapid diffusion of heat over the entire fluid once the sublayer has been penetrated.

The effect of increased Reynolds number is to decrease the thickness of the sublayer and increase the eddy diffusivity in the outer region, both of which lead toward more "square" temperature profiles with a still greater part of the resistance concentrated in the sublayer.

Let us now use Eq. (14-4) to develop an equation for the Nusselt number. Assuming that Eqs. (13-4) and (14-4) are valid at the tube centerline, we can write

$$u_\infty^+ = 2.5 \ln r_s^+ + 5.5$$

$$T_\infty^+ = 2.2 \ln r_s^+ + 13.39\,\mathrm{Pr}^{2/3} - 5.66$$

We now combine these equations, eliminating the term $\ln r_s^+$, and substitute the definitions of u_∞^+ and T_∞^+. Then we assume, for simplicity, that

$$\frac{T_{\mathrm{cl}} - T_s}{T_m - T_s} = 1, \qquad \frac{u_{\mathrm{cl}}}{V} = 1$$

where T_{cl} and u_{cl} are the centerline temperature and velocity, respectively, T_m is the mean temperature, and V is the mean velocity.

These ratios vary somewhat with both Re and Pr, but in any case are generally equal to or greater than 0.9. Then, if the definitions of c_f and St are introduced, we obtain

$$\frac{2.5\sqrt{c_f/2}}{\mathrm{St}} + 26.25 - 33.475\,\mathrm{Pr}^{2/3} = \frac{2.2}{\sqrt{c_f/2}}$$

Solving for the Stanton number,

$$\mathrm{St} = \frac{c_f/2}{0.88 + 13.39(\mathrm{Pr}^{2/3} - 0.78)\sqrt{c_f/2}}$$

or, in Nusselt number form,

$$\mathrm{Nu} = \frac{\mathrm{Re}\,\mathrm{Pr}\,c_f/2}{0.88 + 13.39(\mathrm{Pr}^{2/3} - 0.78)\sqrt{c_f/2}} \tag{14-5}$$

(Note that in this chapter Re will always denote the Reynolds number based on the tube diameter.)

Equation (13-13) can be used for the friction coefficient, with the result

$$\mathrm{Nu} = \frac{0.023\,\mathrm{Re}^{0.8}\,\mathrm{Pr}}{0.88 + 2.03(\mathrm{Pr}^{2/3} - 0.78)\mathrm{Re}^{-0.1}} \tag{14-6}$$

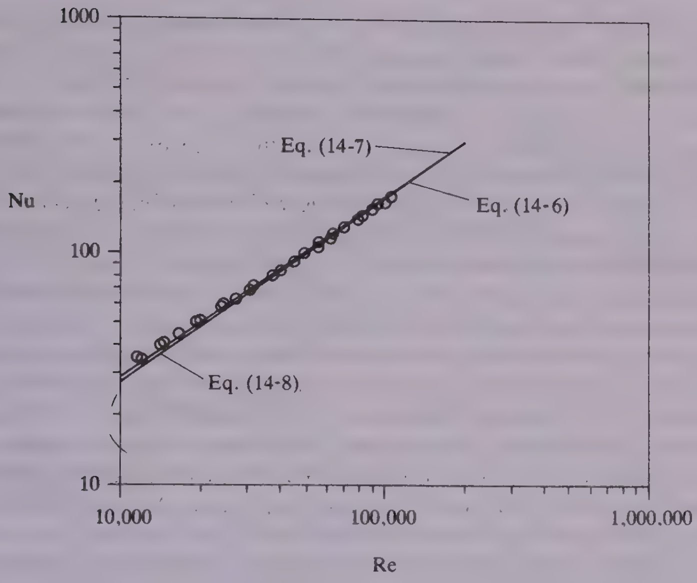

Figure 14-2 Comparison of analysis with experiment for fully developed velocity and temperature profiles in a circular tube, constant heat rate (data of Kays and Leung,[1] for air, Pr = 0.702).

This expression is unnecessarily cumbersome, and in the Prandtl number range of *gases* (0.5–1.0) is approximated quite well by

$$\mathrm{Nu} = 0.022\,\mathrm{Pr}^{0.5}\,\mathrm{Re}^{0.8} \tag{14-7}$$

A comparison of Eqs. (14-6) and (14-7) with some experimental data for air is shown in Fig. 14-2. The comparison is seen to be quite good, at least over the indicated range of Reynolds number.

CIRCULAR TUBE WITH FULLY DEVELOPED FLOW, HIGHER PRANDTL NUMBERS

A great many fluids of considerable technical interest have Prandtl numbers substantially higher than those considered in the preceding section. Oils, for example, frequently have Prandtl numbers in excess of 100, and for some very viscous fluids this figure may reach 1000. Essentially any fluid with Pr > 10 can be considered to have a "high" Prandtl number. The reason for treating these fluids separately lies in a fact pointed out in the preceding section: as the Prandtl number increases, the major part of the heat-transfer resistance appears closer and closer to the surface; i.e., the region where the temperature changes from its surface value to its centerline value is very close to the surface. For Prandtl numbers greater than about 10, almost the entire temperature profile is inside the sublayer, and in fact most of it is inside $y^+ = 5.0$. There is then a major difficulty in attempting to integrate the energy differential equation, because (1) it is not known how precisely the Van Driest equation (or any other turbulence theory) predicts eddy diffusivity close to the surface and (2) little or nothing is known about the turbulent Prandtl number in this region. Although the eddy diffusivity is very small for $y^+ < 5$, it becomes increasingly important as the Prandtl number increases, as can be seen in the total conduction term $1/\text{Pr} + \varepsilon_M/\nu$. The Van Driest equation is perfectly adequate for the *momentum equation* because it is not necessary to know the eddy diffusivity close to the surface with high precision; however, such is not the case for high-Prandtl-number heat transfer. The uncertainties in turbulent Prandtl number near the surface were discussed in Chap. 12. It is suspected that it has a value near 1, but it has not yet been practicable to measure it.

One can carry out calculations using the turbulence models that we have discussed, and the results for the Nusselt number appear reasonable, but there is usually sufficient discrepancy from the experimental data that one would like to correct the model. But it is not possible to say whether the difficulty is in the model used for the eddy diffusivity or in that used for the turbulent Prandtl number.

For these reasons we will not attempt to calculate temperature profiles for high-Prandtl-number fluids, but will instead simply examine what appear to be the most reliable experimental correlations for the Nusselt number. Later we will introduce techniques for calculating thermal-entry lengths and dealing with problems where surface temperature and/or heat flux vary axially, and we will then be obliged to use functions calculated on the basis of assumed models, uncertain as they may be. But in that case any model is better than none, because there is simply no other way to handle that kind of problem.

One of the conclusions that can be reached using crude models is that for $\text{Pr} > 1$ the Nusselt number becomes virtually independent of any but very substantial axial variations of surface temperature. Thus there is virtually no difference between a Nusselt number determined from a constant-surface-temperature experiment and one determined from a constant-heat-rate experiment. As will be recalled, this was definitely not true for laminar flows, and it is likewise not true for very low-Prandtl-number fluids in turbulent flow. The experimental correlations that will now be described are thus applicable to either of the two fundamental thermal boundary conditions, and will usually be adequate for still other variations of surface temperature or heat flux.

One further point should be noted. Most high-Prandtl-number fluids are liquids with high viscosity. The viscosity is virtually always a strong function of temperature. Unless experiments are performed with very small temperature differences, it is always difficult to infer what the Nusselt number would be for the case of constant fluid properties. Since most experiments have been performed with substantial temperature differences, the experimental uncertainty associated with this problem probably accounts for the considerable scatter of data in the literature. (The problems of the influence of temperature-dependent fluid properties are discussed in greater detail in Chap. 15.)

Kakac, Shah, and Aung[2] have examined a great many correlations for fully developed turbulent flow in a circular tube, and conclude that the following equation attributable to Gnielinski[3] correlates the available data somewhat better than any other over the range of Prandtl number from 0.5 to 2000, and Reynolds number from 2300 to 5×10^6:

$$\mathrm{Nu} = \frac{(\mathrm{Re} - 1000)\,\mathrm{Pr}\, c_f/2}{1.0 + 12.7\sqrt{c_f/2}(\mathrm{Pr}^{2/3} - 1.0)} \tag{14-8}$$

Note that the *form* of this equation is almost the same as that of Eq. (14-5). In fact, the only difference is what is apparently a low-Reynolds-number correction, so Eq. (14-8) has at least some theoretical foundation.

Sleicher and Rouse[4] suggest a somewhat more convenient empirical formulation that gives close to the same results:

$$\mathrm{Nu} = 5 + 0.015\,\mathrm{Re}^a\,\mathrm{Pr}^b \tag{14-9}$$

where

$$a = 0.88 - \frac{0.24}{4 + \mathrm{Pr}}, \qquad b = 0.333 + 0.5e^{-0.6\,\mathrm{Pr}}$$

The range of validity of this equation is stated to be

$$0.1 < \mathrm{Pr} < 10^4, \qquad 10^4 < \mathrm{Re} < 10^6$$

Equations (14-8) and (14-9) are stated to be valid for gases as well as high-Prandtl-number fluids. For air, $\mathrm{Pr} = 0.7$, Eq. (14-8) yields Nusselt numbers that are generally within 2 percent of Eqs. (14-6) and (14-7). A comparison of Eq. (14-8) with experiment and with Eqs. (14-6) and (14-7) is shown on Fig. 14-2. Equation (14-9) tends to be 3–4 percent low in this Prandtl number range.

Another equation that has long been popular is that of Dittus and Boelter,[5] as interpreted by Kakac *et al.*[2]:

$$\mathrm{Nu} = \begin{cases} 0.024\,\mathrm{Re}^{0.8}\,\mathrm{Pr}^{0.4} & \text{for heating} \\ 0.026\,\mathrm{Re}^{0.8}\,\mathrm{Pr}^{0.4} & \text{for cooling} \end{cases}$$

Of course the Dittus–Boelter equation contains a condition regarding the direction of heat-transfer (probably a variable-properties correction), but in any case it tends to overpredict the Nusselt number for gases by at least 20 percent, and to underpredict Nusselt number for the higher-Prandtl-number fluids by 7–10 percent. It is no longer recommended that this equation be used.

VERY LOW-PRANDTL-NUMBER HEAT TRANSFER, LIQUID METALS

The very low-Prandtl-number fluids are all liquid metals and have values of Prandtl number less than 0.1, ranging down to less than 0.001. The high thermal conductivity of these fluids accounts for the very low Prandtl number, since the viscosity and specific heat of liquid metals do not differ greatly from other common liquids. Also, the high thermal conductivity accounts for the unusual heat-transfer characteristics of liquid metals. These characteristics are related to the fact that often $\alpha \gg \varepsilon_H$, or nondimensionally $1/\mathrm{Pr} \gg \varepsilon_H/\nu$; that is, molecular conduction is the dominant diffusion mechanism even in the fully turbulent part of the flow field. As $\mathrm{Pr} \to 0$, turbulent eddy diffusion becomes unimportant. This means that a liquid metal has many of the heat-transfer characteristics of a laminar flow, while at the same time its momentum-transfer characteristics are no different from those of any other fluid. For example, fully developed temperature profiles tend to take on a parabolic shape, and this can be seen in Fig. 14-1, discussed earlier. The thermal-entry length tends to be large, similar to laminar flow, and axial variations in surface temperature and heat flux tend to have a substantial effect on the convective heat-transfer coefficient.

There is evidence that the turbulent Prandtl number Pr_t is considerably higher for a liquid metal than for other fluids, a fact discussed in Chap. 12 and that must be related to high molecular conductivity.

Although the Nusselt number tends to be low for a liquid metal, again like laminar flow, the heat-transfer coefficient tends to be very high because of the high molecular conductivity. In fact, this is one of the main reasons why liquid metals are of considerable interest as heat-transfer fluid media. High heat-transfer coefficients, however, mean that surface contamination can have a large influence on the effective heat-transfer coefficient, and surface wetting problems can be similarly important. These facts have led to difficulties and large uncertainties in experiments. The results discussed below are *believed* to represent the behavior of a clean system with complete wetting of the surface, but some uncertainty does persist.

Finally it should be noted that *longitudinal conduction* can be an important factor in liquid-metal heat transfer. It will be recalled that the term in the differential energy equation that accounts for longitudinal conduction, $\partial^2 \bar{T}/\partial x^2$, has been omitted in all of the equations that we have used. As a simple rule of thumb, longitudinal conduction may be a factor resulting in the changing of the effective heat-transfer coefficient if $\mathrm{Re\,Pr} < 100$.

Any of Eqs. (14-1)–(14-3) can be solved by computer-aided finite-difference calculations using the turbulent transport models that we have discussed. The only real uncertainty lies in the values of Pr_t used. Quite reasonable results for the Nusselt number are obtained using Eq. (12-7) for Pr_t, but, as discussed in Chap. 12, there is little direct information available on Pr_t.

An circular tube empirical equation that corresponds fairly well to the available experimental data is proposed by Sleicher and Rouse[4]:

$$\mathrm{Nu} = 6.3 + 0.0167\,\mathrm{Re}^{0.85}\,\mathrm{Pr}^{0.93} \quad \text{(constant heat rate)} \qquad (14\text{-}10)$$

In Fig. 14-3 the data of Skupinski, Tortel, and Vautrey[6] for a liquid metal with $\mathrm{Pr} = 0.0153$ and constant heat rate per unit of tube length are compared with Eq. (14-10) and with finite-difference calculations using Eq. (12-7) for Pr_t. The fact that the finite-difference calculations lie consistently about 15 percent above the data over the entire range of Reynolds number suggests that the discrepancy lies in the data rather than in the turbulent Prandtl number used in the calculations, because at the low-Reynolds-number end of the data the turbulent Prandtl number has little influence.

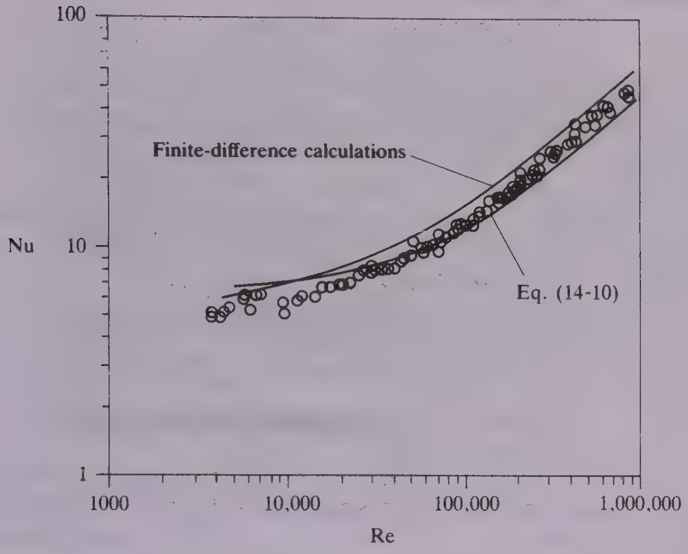

Figure 14-3 A comparison of the data of Skupinski *et al.*[6] with Eq. (14-10) and with the results of direct integration of the energy equation. These data were obtained using an NaK mixture having a Prandtl number of 0.0153.

Table 14-1 Nusselt number for fully developed turbulent flow in a circular tube with constant heat rate

		Re				
Pr	**Laminar**	**10,000**	**30,000**	**100,000**	**300,000**	**1,000,000**
0	4.364	6.30	6.30	6.30	6.30	6.30
0.001		6.37	6.47	6.78	7.53	9.71
0.003		6.49	6.78	7.64	9.70	15.77
0.01		6.88	7.77	10.40	16.73	35.32
0.03		7.91	10.39	17.69	35.27	86.92
0.5		22.91	56.90	146.99	345.90	883.02
0.7		27.42	69.51	182.99	436.91	1,130.64
1		32.81	84.86	227.70	552.05	1,449.75
3		53.82	146.10	411.93	1,041.71	2,855.87
10		86.45	242.16	707.11	1,846.82	5,246.01
30		128.74	366.12	1088.07	2,890.81	8,375.94
100		195.53	560.62	1682.54	4,514.18	13,233.20
1000		425.59	1226.81	3706.15	10,009.84	29,581.97

We now have equations covering the entire Prandtl number spectrum for *fully developed constant heat rate in a circular tube.* For convenience, results from Eqs. (14-8) and (14-10) are presented in Table 14-1 and Fig. 14-4.

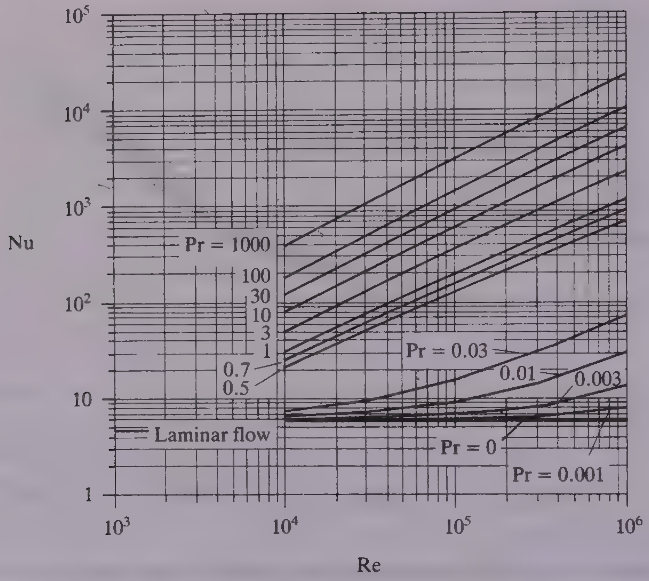

Figure 14-4 Nusselt number for fully developed velocity and temperature profiles; circular tube, constant heat rate.

Note that as the Prandtl number approaches very low values, the Nusselt number approaches a constant value. Lowering the Reynolds number has a similar effect. In either case the influence of the molecular-conduction mechanism is being observed, and, of course, for fully developed *laminar* flow the Nusselt number is indeed a constant.

CIRCULAR TUBE, FULLY DEVELOPED PROFILES, CONSTANT SURFACE TEMPERATURE

Following the pattern used in Chap. 8 for laminar flow in a tube, we have just considered the case of fully developed constant heat rate per unit of tube length. As was the case for laminar flow, another useful boundary condition for which a fully developed temperature profile is physically possible is that of a *constant surface temperature*. This condition is very frequently encountered in heat exchangers where one fluid capacity rate is very much greater than the other or when one fluid is boiling or condensing.

The applicable energy differential equation is derivable from Eq. (14-2) by comparison with Eq. (8-19):

$$\bar{u}\frac{T_s-\bar{T}}{T_s-T_m}\frac{dT_m}{dx}=\frac{1}{r}\frac{\partial}{\partial r}\left[r(\alpha+\varepsilon_H)\frac{\partial\bar{T}}{\partial r}\right] \qquad (14\text{-}11)$$

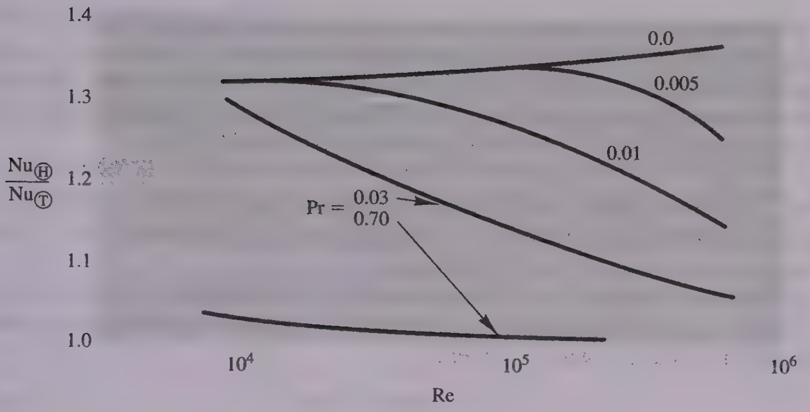

Figure 14-5 Ratio of Nusselt number for *constant heat rate* to Nusselt number for *constant surface temperature* for fully developed conditions in a circular tube (Sleicher and Tribus).[7]

This equation can be integrated numerically using the same turbulence models that have been used previously, although an iterative technique will have to be employed.

Alternatively, the fully developed constant-surface-temperature solutions may be obtained as special cases of the thermal-entry-length solutions to be described later, i.e., solutions to Eq. (14-2) for a uniform surface temperature and a uniform fluid temperature at the tube entrance. Sleicher and Tribus[7] were the first to present such a solution, and although the values of the turbulent Prandtl number used were higher than what is now believed to be correct at very low Prandtl numbers, this does not have a large effect on the particular results of interest here. The fully developed Nusselt numbers for both *constant surface temperature* and *constant heat rate* can be deduced from the Sleicher and Tribus results, and thus the ratio of Nusselt numbers for the two cases can be determined. These are presented in Fig. 14-5, where subscript Ⓗ refers to constant heat rate and Ⓣ to constant surface temperature.

Note that only at very low Prandtl number is there a significant difference between the constant-heat-rate and constant-surface-temperature results. At $Pr = 0.7$ the difference is only a few percent, and at higher Prandtl numbers the difference is even less significant. In the liquid-metal region (very low Prandtl number), however, the difference is substantial and actually in some cases becomes larger than the laminar flow difference [see Eqs. (8-17) and (8-21)]. The reasons lie again in the effect of Prandtl number on the distribution of thermal resistance. At very low Prandtl numbers, where the heat-transfer mechanism is predominantly molecular diffusion, the resistance is distributed over the entire flow cross section, and the different boundary conditions yield differently shaped temperature profiles. At high Prandtl numbers the resistance is primarily very close to the surface, yielding a quite "square" temperature profile regardless of the heating boundary condition. This fact suggests also that the Nusselt number for a high-Prandtl-number fluid is relatively insensitive to a variation of surface and/or heat flux in the direction of flow, whereas the Nusselt number for a low-Prandtl-number fluid is greatly affected by axial variation of surface temperature and/or heat flux. Such is indeed the case, as is shown later.

Figure 14-5 can now be used in conjunction with the data in Table 14-1, or Fig. 14-4, to completely establish the Nusselt numbers for fully developed velocity and temperature profiles for *constant surface temperature* over a wide range of Reynolds and Prandtl numbers.

Algebraic empirical correlations can also be developed for fully developed *constant surface temperature.* For *gases* Eq. (14-7) can be modified by lowering the coefficient a few percent to yield

$$\mathrm{Nu} = 0.021\,\mathrm{Pr}^{0.5}\,\mathrm{Re}^{0.8} \tag{14-12}$$

For very low-Prandtl-number fluids in a circular tube Sleicher and Rouse[4] suggest

$$\mathrm{Nu} = 4.8 + 0.0156\,\mathrm{Re}^{0.85}\,\mathrm{Pr}^{0.93} \tag{14-13}$$

EFFECT OF PERIPHERAL HEAT-FLUX VARIATION

In the examples previously considered, the heat flux and surface temperature have both been assumed to be uniform around the tube periphery. In many applications the heat flux and surface temperature are not uniform around the tube, and thus it becomes important to know how the heat-transfer coefficient varies around the tube.

This problem is discussed in Chap. 8 for laminar flow. The corresponding turbulent flow problem has been considered and treated in a similar manner by Gartner, Johannsen, and Ramm.[8] The energy equation for the case of fully developed constant heat rate per unit of tube length, but with nonaxisymmetric heating, becomes

$$\bar{u}\frac{dT_m}{dx} = \frac{1}{r}\frac{\partial}{\partial r}\left[r(\varepsilon_{Hr} + \alpha)\frac{\partial \bar{T}}{\partial r}\right] + \frac{1}{r^2}\frac{\partial}{\partial \phi}\left[(\varepsilon_{H\phi} + \alpha)\frac{\partial \bar{T}}{\partial \phi}\right] \tag{14-14}$$

where ε_{Hr} and $\varepsilon_{H\phi}$ are the eddy diffusivities for heat transfer in the radial and circumferential directions, respectively. There is experimental evidence that $\varepsilon_{H\phi}$ is greater than ε_{Hr}, especially near the surface, and this fact was taken into consideration in the development of a solution. A theoretical solution for the diffusivities was used, which compares reasonably with the experimental data, and also with the radial diffusivity and turbulent Prandtl number data used in this book.

In Ref. 8, Eq. (14-14) has been solved for any arbitrary heat-flux variation that can be expressed by a Fourier expansion. The complete solution for an arbitrarily prescribed heat flux around the periphery requires an extensive tabulation

Table 14-2 Circumferential heat-flux functions S_1 for fully developed turbulent flow in a circular tube with constant heat rate

		Re				
Pr	**Laminar**	**10^4**	**3×10^4**	**10^5**	**3×10^5**	**10^6**
0	1.000	1.000	1.000	1.000	1.000	1.000
0.001		0.9989	0.9937	0.9561	0.8059	0.4853
0.003		0.9929	0.9613	0.8005	0.5042	0.2300
0.01		0.9499	0.7915	0.4567	0.2185	0.0867
0.03		0.7794	0.4705	0.2055	0.0888	0.0336
0.7		0.1116	0.0442	0.0161	0.00644	0.00232
3		0.0440	0.0168	0.00594	0.00234	0.000824
10		0.0233	0.00879	0.00305	0.00120	0.000415
30		0.0145	0.00544	0.00184	0.000744	0.000250
100		0.00941	0.00354	0.00110	0.000484	0.000149

of functions. However, the simpler case of a *cosine* heat-flux variation may be presented very briefly, and since the thermal conductivity of the tube wall usually tends to smooth out peripheral temperature variations to a certain extent, most applications can at least be approximated by the simple cosine case.

Let the prescribed heat flux be

$$\dot{q}_s''(\phi) = \dot{q}_a''(1 + b\cos\phi) \tag{14-15}$$

Then the Nusselt number around the periphery is

$$\mathrm{Nu}(\phi) = \frac{1 + b\cos\phi}{1/\mathrm{Nu} + \frac{1}{2}S_1 b\cos\phi} \tag{14-16}$$

The functions S_1 are shown in Table 14-2 for a wide range of Reynolds and Prandtl numbers. The Nusselt number Nu in Eq. (14-16) is that for uniform peripheral temperature and heat flux as given in Table 14-1.

As an example, consider $\mathrm{Pr} = 0.7$ and $\mathrm{Re} = 100{,}000$, with $b = 0.20$. From Table 14-1, $\mathrm{Nu} = 183$; and from Table 14-2, $S_1 = 0.0161$. Substituting in Eq. (14-16), we find that the local Nusselt number will vary from 170 to 208. Thus the effect is rather pronounced even for only a 20 percent variation in heat flux. As might be expected, the effects are greater than this at low Prandtl numbers and less at high Prandtl numbers.

FULLY DEVELOPED TURBULENT FLOW BETWEEN PARALLEL PLANES AND IN CONCENTRIC CIRCULAR-TUBE ANNULI

The annulus geometry and its limiting case, flow between parallel planes, provide a particularly interesting heat-transfer problem because of the possibility of asymmetric heating from the two surfaces. Most applications do in fact involve asymmetry. The laminar flow annulus problem is discussed in Chap. 8, where the method of solution is outlined and the use of superposition for asymmetric heating is also treated.

The turbulent flow annulus problem can in principle be solved by the same superposition method. However, finding a satisfactory turbulence model presents new difficulties. A mixing-length model would be satisfactory near each of the two surfaces, but one has no basis for specifying the mixing length near the center of the passage, and this was also true for the simple circular tube. Presumably the k–ε model might be satisfactory, but most of the analytic work on turbulent flow in the circular-tube annulus was carried out before the k–ε model was invented.

Kays and Leung[1] carried out extensive calculations based on an empirical eddy-diffusivity equation, which was in turn based on empirical information on the ratio of the shear stresses at the two surfaces (which are, of course, different). It can readily be shown by a simple force balance on a fluid control volume that the point of zero shear stress in the flow, which is also the point of maximum velocity, is directly related to the surface shear-stress ratio. Measurements of the point of maximum velocity resulted in the following relation for the radius of maximum velocity (zero shear stress), which was found to be independent of Reynolds number:

$$\frac{r_m}{r_o} = r^{*0.343}(1 + r^{*0.657} - r^*) \tag{14-17}$$

where $r^* = r_i/r_o$ and r_m is the radius of maximum velocity.

With this information, a complete velocity profile could be constructed assuming that Eq. (13-4) is valid when applied separately, starting from each surface. The sublayer was modeled using an equation suggested by Deissler.[9] Finally an assumption was made that the eddy diffusivity in the region near the maximum-velocity point could be approximated by a linear connection between the maximum eddy diffusivities on either side of it, as determined from the velocity profile and the shear-stress distribution. It is necessary to make some kind of assumption about the central-region eddy diffusivity because asymmetric heating involves heat transfer across that region. Fortunately it is not a critical assumption.

Calculations were carried out over a wide range of Reynolds and Prandtl numbers for the case of one surface heated and the other insulated, and are presented in the same form as the analogous laminar annulus solutions. Thus Eqs. (8-28) and (8-29) are directly applicable, and any heat-flux ratio on the two surfaces can be solved. The results of these calculations are presented in Tables 14-3 to 14-5. They are in excellent agreement with experiments performed by Kays and Leung for air ($\mathrm{Pr} = 0.7$), including asymmetric heating. At high and low Prandtl numbers, the same uncertainty regarding Pr_t that was encountered for the circular tube still obtains. At very low Prandtl numbers the equation used for Pr_t yields values that are somewhat higher than are now

Table 14-3 Nusselt numbers and influence coefficients for $r^* = 0.20$; fully developed turbulent flow in a circular-tube annulus; constant heat rate

	Re											
	Laminar		10^4		3×10^4		10^5		3×10^5		10^6	
Pr	$\mathbf{Nu}_{ii}$	θ_i^*	$\mathbf{Nu}_{ii}$	θ_i^*	$\mathbf{Nu}_{ii}$	θ_i^*	$\mathbf{Nu}_{ii}$	θ_i^*	$\mathbf{Nu}_{ii}$	θ_i^*	$\mathbf{Nu}_{ii}$	θ_i^*
						Inner surface heated						
0.0	8.50	0.905	8.40	1.01	8.30	1.03	8.30	1.02	8.30	1.04	8.30	1.02
0.001			8.40	1.01	8.40	1.04	8.30	1.02	8.40	1.01	8.90	0.978
0.003			8.40	1.01	8.40	1.03	8.50	1.03	9.05	0.980	12.5	0.833
0.01			8.50	1.00	8.60	1.02	9.70	0.944	14.0	0.796	33.6	0.747
0.03			9.00	1.01	10.1	0.943	15.8	0.771	31.7	0.600	81.0	0.375
0.5			31.2	0.520	64.0	0.397	157	0.333	370	0.295	980	0.262
0.7			38.6	0.412	79.8	0.338	196	0.286	473	0.260	1270	0.235
1			46.8	0.339	99.0	0.284	247	0.248	600	0.228	1640	0.209
3			77.4	0.172	175	0.151	465	0.143	1150	0.137	3250	0.136
10			120	0.077	290	0.074	800	0.072	2050	0.073	6000	0.077
30			172	0.036	428	0.035	1210	0.035	3150	0.036	9300	0.038
100			243	0.014	617	0.014	1760	0.015	4630	0.016	13,800	0.016
1000			448	0.004	1140	0.002	3280	0.004	8800	0.004	26,000	0.003
Pr	$\mathbf{Nu}_{oo}$	θ_o^*	$\mathbf{Nu}_{oo}$	θ_o^*	$\mathbf{Nu}_{oo}$	θ_o^*	$\mathbf{Nu}_{oo}$	θ_o^*	$\mathbf{Nu}_{oo}$	θ_o^*	$\mathbf{Nu}_{oo}$	θ_o^*
						Outer surface heated						
0.0	4.88	0.104	5.83	0.140	5.92	0.146	6.10	0.151	6.16	0.152	6.35	0.157
0.001			5.83	0.140	5.92	0.144	6.10	0.151	6.30	0.154	6.92	0.153
0.003			5.83	0.140	6.00	0.146	6.22	0.150	6.90	0.150	10.2	0.135
0.01			5.95	0.141	6.20	0.146	7.40	0.144	11.4	0.131	24.6	0.089
0.03			6.22	0.140	7.55	0.140	12.7	0.125	26.3	0.098	80.0	0.086
0.5			22.5	0.071	51.5	0.064	130	0.055	310	0.049	823	0.044
0.7			29.4	0.063	64.3	0.055	165	0.049	397	0.044	1070	0.040
1			35.5	0.051	80.0	0.046	206	0.042	504	0.039	1390	0.035
3			60.0	0.026	145	0.026	390	0.024	980	0.024	2760	0.023
10			98.0	0.013	243	0.013	680	0.012	1750	0.012	4980	0.012
30			142	0.006	360	0.006	1030	0.006	2700	0.006	7850	0.006
100			205	0.003	520	0.003	1500	0.003	4000	0.003	12,000	0.003
1000			380	0.001	980	0.001	2830	0.001	7500	0.001	22,500	0.001

believed to be correct, so the results for the Nusselt number may be somewhat low. At $\text{Pr} \geq 0.7$, $\text{Pr}_t = 0.9$ was used.

Note that the Nusselt and Reynolds numbers for the circular-tube annulus are based on the *hydraulic diameter*. For flow between parallel planes the *hydraulic diameter* is then 2 × spacing.

A variation of heat flux around the periphery of either or both surfaces of an annular passage can have a larger effect than in the simple circular tube. Employing the method of Gartner *et al.*[8] and using the velocity and diffusivity data of Kays and Leung,[1] Sutherland and Kays[10] present the necessary functions to solve for any arbitrary variation of heat flux on both surfaces.

Table 14-4 Nusselt numbers and influence coefficients for $r^* = 0.50$; fully developed turbulent flow in a circular-tube annulus; constant heat rate

	Re											
	Laminar		10^4		3×10^4		10^5		3×10^5		10^6	
Pr	Nu_{ii}	θ_i^*	Nu_{ii}	θ_i^*	Nu_{ii}	θ_i^*	Nu_{ii}	θ_i^*	Nu_{ii}	θ_i^*	Nu_{ii}	θ_i^*
						Inner surface heated						
0.0	6.18	0.528	6.28	0.622	6.30	0.633	6.30	0.652	6.30	0.659	6.30	0.653
0.001			6.28	0.622	6.30	0.633	6.30	0.652	6.40	0.659	6.75	0.643
0.003			6.28	0.622	6.30	0.633	6.40	0.657	6.85	0.638	9.40	0.585
0.01			6.37	0.623	6.45	0.637	7.30	0.623	10.8	0.540	23.2	0.427
0.03			6.75	0.627	7.53	0.598	12.0	0.533	24.9	0.432	65.5	0.333
0.5			24.6	0.343	52.0	0.293	130	0.253	310	0.229	835	0.208
0.7			30.9	0.300	66.0	0.258	166	0.225	400	0.206	1080	0.185
1.0			38.2	0.247	83.5	0.218	212	0.208	520	0.182	1420	0.170
3.0			66.8	0.129	152	0.121	402	0.115	1010	0.114	2870	0.111
10.0			106	0.059	260	0.059	715	0.059	1850	0.059	5400	0.061
30.0			153	0.028	386	0.028	1080	0.028	2850	0.031	8400	0.032
100.0			220	0.006	558	0.006	1600	0.006	4250	0.007	12,600	0.007
1000.0			408	0.002	1040	0.002	3000	0.002	8000	0.002	24,000	0.002
Pr	Nu_{oo}	θ_o^*	Nu_{oo}	θ_o^*	Nu_{oo}	θ_o^*	Nu_{oo}	θ_o^*	Nu_{oo}	θ_o^*	Nu_{oo}	θ_o^*
						Outer surface heated						
0.0	5.04	0.216	5.66	0.281	5.78	0.294	5.80	0.297	5.83	0.303	5.95	0.310
0.001			5.66	0.281	5.78	0.294	5.80	0.297	5.92	0.303	6.40	0.304
0.003			5.66	0.281	5.78	0.294	5.85	0.294	6.45	0.301	9.00	0.278
0.01			5.73	0.281	5.88	0.289	6.80	0.289	10.3	0.264	22.6	0.217
0.03			6.03	0.279	7.05	0.284	11.6	0.258	24.4	0.214	64.0	0.163
0.5			22.6	0.162	49.8	0.142	125	0.123	298	0.111	795	0.098
0.7			28.3	0.137	62.0	0.119	158	0.107	380	0.097	1040	0.090
1.0			34.8	0.111	78.0	0.101	200	0.092	490	0.085	1340	0.078
3.0			60.5	0.059	144	0.058	384	0.055	960	0.054	2730	0.052
10.0			100	0.028	246	0.028	680	0.028	1750	0.028	5030	0.028
30.0			143	0.013	365	0.013	1030	0.014	2700	0.014	8000	0.015
100.0			207	0.006	530	0.006	1500	0.006	4000	0.006	12,000	0.006
1000.0			387	0.001	990	0.001	2830	0.001	7600	0.001	23,000	0.001

Some degree of eccentricity must usually be tolerated in an annular passage. Leung, Kays, and Reynolds[11] present experimental data on the effects of eccentricity. In general, the effects of eccentricity are (1) to decrease the average Nusselt number and (2) to yield a Nusselt number variation around the periphery. Heat conduction in the tube wall in the peripheral direction can alter this variation, but these experiments were carried out with negligible peripheral conduction. Table 14-6 presents an abstract of these results for two radius ratios and for various eccentricities, for the inner surface alone heated and for the outer surface alone heated, in the Reynolds number range 30,000–80,000. Further information will be found in Kakac *et al.*[2]

Table 14-5 Nusselt numbers and influence coefficients for fully developed turbulent flow between parallel plates; constant heat rate; one side heated and the other insulated

	Re											
	Laminar		10^4		3×10^4		10^5		3×10^5		10^6	
Pr	Nu	θ^*	Nu	θ^*	Nu	θ^*	Nu	θ^*	Nu	θ^*	Nu	θ^*
0.0	5.385	0.346	5.70	0.428	5.78	0.445	5.80	0.456	5.80	0.460	5.80	0.468
0.001			5.70	0.428	5.78	0.445	5.80	0.456	5.88	0.460	6.23	0.460
0.003			5.70	0.428	5.80	0.445	5.90	0.450	6.32	0.450	8.62	0.422
0.01			5.80	0.428	5.92	0.445	6.70	0.440	9.80	0.407	21.5	0.333
0.03			6.10	0.428	6.90	0.428	11.0	0.390	23.0	0.330	61.2	0.255
0.5			22.5	0.256	47.8	0.222	120	0.193	290	0.174	780	0.157
0.7			27.8	0.220	61.2	0.192	155	0.170	378	0.156	1030	0.142
1.0			35.0	0.182	76.8	0.162	197	0.148	486	0.138	1340	0.128
3.0			60.8	0.095	142	0.092	380	0.089	966	0.087	2700	0.084
10.0			101	0.045	214	0.045	680	0.045	1760	0.045	5080	0.046
30.0			147	0.021	367	0.022	1030	0.022	2720	0.023	8000	0.024
100.0			210	0.009	514	0.009	1520	0.010	4030	0.010	12,000	0.011
1000.0			390	0.002	997	0.002	2880	0.002	7650	0.002	23,000	0.002

Table 14-6 Effect of eccentricity on turbulent flow heat transfer in circular-tube annuli (experimental data for air, Leung *et al.*[11])

Radius ratio	e^*	$\frac{Nu_{ii,max}}{Nu_{ii,conc}}$	$\frac{Nu_{ii,min}}{Nu_{ii,conc}}$	$\frac{Nu_{oo,max}}{Nu_{oo,conc}}$	$\frac{Nu_{oo,min}}{Nu_{oo,conc}}$
0.255	0.27	0.99	0.97	1.02	0.93
	0.50	0.94	0.92	0.98	0.86
	0.77	0.92	0.88	0.93	0.77
0.500	0.54	0.96	0.87	1.01	0.78
	0.77	0.87	0.67	0.88	0.62

$e^* = e/(r_o - r_i)$, where e is the eccentricity of the tube centerlines.

$Nu_{ii,conc}$ and $Nu_{oo,conc}$ refer to the Nusselt numbers for the concentric annulus at the same Reynolds number and Prandtl number.

FULLY DEVELOPED TURBULENT FLOW IN OTHER TUBE GEOMETRIES

As long as Pr is greater than about 0.5, the greater portion of the heat-transfer resistance in tube flow is in the sublayer region near the surfaces, and if these surfaces are at a nearly uniform temperature then the temperature distribution over most of the cross-sectional flow area is relatively flat. Under these circumstances, one would expect that the heat-transfer rate from the surface would be reasonably independent of the cross-sectional shape of the tube. In other words, the computed behavior for circular tubes should be applicable to tubes of any cross-sectional shape. There remains, however, the problem of finding a characteristic dimension of a noncircular tube that has the same significance as the *diameter* of the circular tube.

An examination of the Reynolds number from a different point of view provides a suggestion. Consider a circular tube and let p be the tube surface perimeter and A_c the cross-sectional area. Then

$$\mathrm{Re} = \frac{DG}{\mu} = \frac{4A_cG}{p\mu} = \frac{4\dot{m}}{p\mu}$$

where $G = \rho V$. The Reynolds number is seen to be proportional to the ratio of the mass flow rate to the tube perimeter. If the heat-transfer resistance is primarily in the region close to the surface, it would seem reasonable that this ratio is more significant than the fact that the tube is circular and has diameter D. If this is the case, it should be possible to replace D in the circular-tube solutions and experimental correlations by $4A_c/p$; and since the latter is unambiguously defined for any cross-sectional shape, the results should be applicable to tubes of any cross-sectional shape. $4A_c/p$ is the hydraulic diameter D_h, or 4 times the hydraulic radius r_h:

$$D_h = 4r_h = \frac{4A_c}{p} \tag{14-18}$$

[See also a similar discussion in Chap. 13; note that this definition of D_h is identical to Eq. (13-16).]

Experimentally it is found that, with this substitution for D, the circular-tube results are indeed applicable quite accurately to many tubes of noncircular cross section. It was noted in Chap. 13 that this is also the case for the friction coefficient. At very low Prandtl numbers this approximation cannot be expected to apply, because the heat-transfer resistance is no longer confined to the region near the surface. This is also true in laminar flow; for laminar flow in tubes, the use of the hydraulic diameter does not correlate for different geometries. This approximation can also be expected to break down for tubes with very sharp corners, such as triangular tubes with one corner angle very small, because in the vicinity of the sharp corner the sublayer becomes large relative to the distance between the adjacent sides. It also does not apply for tubes with disconnected surfaces where the temperature is different on the different surfaces. With these exceptions, the approximation is very good, and the circular-tube solutions are applicable to rectangular tubes and any number of unusual shapes.

In this discussion the surface temperature is assumed everywhere uniform around the periphery, and the heat-transfer coefficient calculated is the mean coefficient around the periphery. The local coefficient around the periphery of a noncircular tube may vary considerably, but the hydraulic-diameter approximation sheds no light on this problem.

There is a considerable body of information in the heat-transfer literature, both analytic and experimental, on flow in noncircular tubes, including investigations of local coefficients around the periphery, nonuniform heating around the periphery, and many other variations. It is not practicable to summarize all of these investigations here. A comprehensive and excellent summary may be found in the *Handbook of Single-Phase Convective Heat Transfer* by Kakac *et al.*[2]

EXPERIMENTAL CORRELATIONS FOR FLOW IN TUBES

Until now, our major emphasis has been on analytic solutions to the energy equation, and experimental results have been referred to only when they serve to validate the assumptions used in building a mathematical model of the heat-transfer process, or where uncertainty in the information going into the mathematical models has been such that experimental data is probably more reliable. We encountered this kind of uncertainty when attempting to calculate heat transfer at very high and very low Prandtl numbers. However, experiments can and do form a primary source of convective heat-transfer data for engineering applications; if the flow geometry is complex, it is often far easier to perform experiments than to attempt to deduce heat-transfer rates by analysis. In fact, in many cases experiment is the only practicable approach.

A by-product of the analytic approach, in which we started with the applicable differential equations, is that we can now readily see how experimental results can be generalized by the use of nondimensional variables, so that it is not necessary to carry out experiments under the operating conditions of the proposed application or even with the same fluid. For example, in the absence of thermal- or hydrodynamic-entry effects, we have seen that for flow in a tube under, say, constant-heat-rate conditions, the heat-transfer performance can be expressed by a relation of the type

$$\mathrm{Nu} \text{ or } \mathrm{St} = f(\mathrm{Re}, \mathrm{Pr})$$

Experiments can be used to establish this functional relationship; and, since the variables are nondimensional, it does not matter if the dimensional variables making up the nondimensional groups are not the same in the application as in the experiment. The length dimension in the Reynolds number (and Nusselt number) can be any convenient length that characterizes the size of the passage (including the hydraulic diameter, if desired, but this is not mandatory). Since the experimental results are strictly applicable to geometrically similar systems only, all length dimensions bear the same relation to one another.

Frequently it is not possible or practicable to vary the Prandtl number over a wide range in a single experimental system in order to adequately establish the functional dependence on Prandtl number. For this reason experimenters often *assume* a Prandtl number dependence, based on experience with other geometries or on the analytic solutions. Thus one often finds experimental results presented in the form

$$\mathrm{St}\,\mathrm{Pr}^{0.6} = f(\mathrm{Re}) \quad \text{or} \quad \mathrm{Nu}\,\mathrm{Pr}^{-0.4} = f(\mathrm{Re})$$

(It should be noted that, regardless of the length variable in Nu and Re the following relation must apply: $\mathrm{Nu} = \mathrm{St}\,\mathrm{Pr}\,\mathrm{Re}$.)

Other powers of the Prandtl number are also frequently used, depending either on what is necessary to correlate the results or on some theoretical basis. For example, in some high-performance heat-exchanger flow passages, the surface is interrupted at frequent intervals so that each segment of surface sees essentially a laminar external boundary layer. In Chap. 10 it was seen that for a laminar boundary layer the Prandtl number dependence can be quite accurately represented by the group St $\mathrm{Pr}^{2/3}$ in the Prandtl number range 0.5–15. Thus there is a *theoretical* basis for using this group to generalize experimental data for such flow passages.

Obviously if there are other significant variables in the experiment, these can be included in the function, provided only that they are normalized with respect to some other variable (or variables) so as to provide an additional nondimensional group. For example, if the thermal- or hydrodynamic-entry length is significant (and this is discussed in sections to follow), the distance x from the entrance becomes significant, and an additional nondimensional parameter could be x/D. But it could just as well be xG/μ.

Such experimental correlations may be found throughout the literature for both laminar and turbulent flow in a large variety of types of flow passages and in different Prandtl number ranges. It is the intent of this book to place primary emphasis on the available analytic solutions, for it is felt that these should be thoroughly understood before the purely experimental data can be used intelligently. However, it is recognized that in engineering applications the reader will generally find it absolutely necessary to take advantage of the wealth of experimental data that exists. Typical of such available data is the compilation in *Compact Heat Exchangers*.[12] Other useful sources of data are the *Handbook of Single-Phase Convective Heat Transfer*,[2] and the *Handbook of Heat Transfer*.[13]

THERMAL-ENTRY LENGTH FOR TURBULENT FLOW IN A CIRCULAR TUBE

Consider the case of a fully developed velocity *profile*, but with a uniform fluid temperature at the point where heat transfer begins. We are concerned with the development of the temperature profile, that is, the *thermal-entry length*.

This problem can be readily solved by direct numerical integration of the energy differential equation, using the turbulence models previously discussed, for any particular problem. But it is also possible to obtain solutions in more generalized form, and this is often useful because it leads to closed-form results for certain particular cases and provides a technique for investigating certain effects that would involve multiple direct numerical solutions.

The differential equation that must be solved for the circular tube is again Eq. (14-2); but, of course, the derivative on the right-hand side is no longer a constant or a function of x alone, as was the case for a fully developed temperature profile. The problem is essentially the same as the corresponding laminar flow problem. Equation (14-2) can be expressed in the same (x^+, r^+) coordinate system, but now, since $\varepsilon_H + \alpha$ is a function of both Reynolds number and Prandtl number, rather than a constant, it is apparent that for given boundary conditions a family of solutions is obtained rather than a single solution.

Circular-tube solutions have been obtained for both *constant surface temperature* and *constant heat rate* by Notter and Sleicher.[14] These solutions follow the same procedures as were employed for the laminar flow counterpart to the problem. Separation of variables is first employed, but then it has been necessary to use a computer to evaluate the eigenvalues and constants in the resulting series solutions. Information on ε_H and $\bar{u}$ must be supplied. Notter and Sleicher used more recent information on Pr_t than was used in the earlier Sleicher and Tribus solution to the same problem, and their results are quite consistent with the Sleicher and Rouse equations cited earlier, Eqs. (14-9), (14-10), and (14-13).

These solutions can be put in precisely the same form as for laminar flow. Thus Eqs. (8-39), (8-40), and (8-41) for *constant surface temperature*, and Eq. (8-42) for *constant heat rate*, are all directly applicable. The *constant-heat-rate* solution yields the following equation for fully developed velocity *and* temperature profiles:

$$\mathrm{Nu}_\infty = \left(\frac{1}{2} \sum_{m=0}^{\infty} \frac{1}{A_m \gamma_m^4} \right)^{-1}$$

The series in this equation is very slowly convergent, and there are not sufficient eigenvalues and constants to evaluate it. An alternative equation for fully developed *constant heat rate*, based on variable-surface-temperature theory and the constant-surface-temperature functions, is Eq. (8-49).

An abstract of the Notter and Sleicher results is presented in Table 14-7. In addition, a set of functions for $\mathrm{Pr} = 10$ for the *constant-heat-rate* problem is tabulated there, based on the calculations of Sparrow, Hallman, and Seigel.[15] The latter used $\mathrm{Pr}_t = 1$ throughout their calculations. These functions must be used in conjunction with other data on Nu_∞ in order to be useful.

These series solutions, with the exception noted above, are very much more convergent than the corresponding laminar flow series, especially at higher Prandtl numbers, and the number of terms given is quite sufficient for most calculations.

Figures 14-6 to 14-8 show the thermal-entry-length effect for flow in a circular tube for constant heat rate for a number of different cases. At $\mathrm{Pr} = 0.01$ the effect is rather pronounced and increases with Reynolds number (Fig. 14-6). Figure 14-7 illustrates the strong influence of Prandtl number. At Prandtl numbers above 1 the thermal-entry-length effect becomes of decreasing importance. Note in Fig. 14-8 that at $\mathrm{Pr} = 0.7$ there is very little influence of Reynolds number.

We can also investigate the effect of thermal-entry length on the *length-mean* Nusselt number. In heat-exchanger design this is generally of more importance than the local Nusselt number. If we move sufficiently far downstream that the local Nusselt number has closely approached its asymptotic value (which also means that only the first term in the infinite-series solution is of importance), the mean Nusselt number for constant surface temperature is given by

$$\mathrm{Nu}_m = \frac{\lambda_0^2}{2} + \frac{1}{2x^+} \ln \frac{\lambda_0^2}{8G_0} \tag{14-19}$$

Table 14-7 Infinite-series-solution functions for thermal-entry length with turbulent flow in a circular tube

n, m	Pr	Re	λ_n^2	G_n	γ_m^2	A_m
0	0.002	50,000	10.61	0.975		
1			58.19	0.897	29.66	0.00773
2			144.6	0.862	98.51	0.01015
3			269.7	0.841	206.5	0.00105
4					353.4	0.000607
0	0.002	100,000	11.23	1.036		
1			61.74	0.943	31.6[illegible]	0.00725
2			153.6	0.903	104.7	0.00209
3			286.7	0.88	219.2	0.000977
4					374.9	0.00056
0	0.002	500,000	15.91	1.527		
1			90.19	1.246	48.83	0.00437
2			227.4	1.137	158	0.001202
3			426.8	1.08	331	0.000547
4					564.8	0.000307
0	0.01	50,000	13.39	1.277		
1			75.23	1.079	40.12	0.00431
2			188.9	0.996	131.8	0.00152
3			353.9	0.949	275	0.000696
4					469.3	0.000395
0	0.01	100,000	16.75	1.642		
1			96.15	1.29	53.11	0.00394
2			243.8	1.154	172.7	0.001068
3			458.5	1.085	358.8	0.000479
4						
0	0.01	500,000	39.31	4.2		
1			252.9	2.42	159.8	0.001152
2			665.6	1.93	504.6	0.000273
3			1,271	1.752	1,032	0.000112
4					1,737	0.0000591
0	0.03	50,000	21.28	2.17		
1			126.7	1.532	73.68	0.00272
2			325.2	1.32	237.8	0.000705
3			614.8	1.189	491.7	0.000306
4					835.3	0.000167
0	0.03	100,000	31.06	3.28		
1			194.2	2.03	119.4	0.0016
2			506.9	1.649	380.5	0.00039
3			964.8	1.488	781.4	0.000162
4					1,320	0.000087
0	0.03	500,000	91.5	10.38		
1			678.1	4.39	477.7	0.000362
2			1,844	3.22	1,490	0.000076
3			3,562	2.9	3,011	0.000029
4					5,027	0.000015

Table 14-7 *(continued)*

n, m	Pr	Re	λ_n^2	G_n	γ_m^2	A_m
0	0.72	10,000	64.38	7.596		
1			646.8	1.829	519.5	0.000301
2			1,870	1.217	1,624	0.0000513
3					3,202	0.0000149
0	0.72	50,000	219	26.6		
1			2,350	5.63	1,952	0.0000886
2			6,808	3.32	6,154	0.0000179
3					12,480	0.000006
0	0.72	100,000	375.9	45.8		
1			4,183	9.25	3,510	0.0000494
2			12,130	5.48	11,030	0.0000101
3					22,340	0.0000035
0	8	50,000	685.6	85.4		
		100,000	1,232	154		
		500,000	5,020	625		
1	10	50,000			2.736×10^4	5.02×10^{-6}
2					7.316×10^4	1.21×10^{-6}
3					1.373×10^5	4.36×10^{-3}
4					2.196×10^5	1.87×10^{-7}
5					3.198×10^5	8.79×10^{-8}
1	10	100,000			5.04×10^4	2.78×10^{-6}
2					1.346×10^5	6.97×10^{-7}
3					2.528×10^5	2.68×10^{-7}
4					4.046×10^5	1.26×10^{-7}
5					5.904×10^5	6.56×10^{-8}
0	50	100,000	2,570	321		
		200,000	4,778	598		
		500,000	10,800	1,350		
0	100	100,000	3,317	415		
		200,000	6,129	766		
		500,000	14,040	1,750		

But $\lambda_0^2 = 2\mathrm{Nu}_\infty$, from Eq. (9-41). Dividing this into Eq. (14-19), we obtain

$$\frac{\mathrm{Nu}_m}{\mathrm{Nu}_\infty} = 1 + \frac{1}{x + \lambda_0^2} \ln \frac{\lambda_0^2}{8G_0} \tag{14-20}$$

Now, for an example, consider Pr = 0.72 and Re = 50,000. From Table 14-7,

$$\lambda_0^2 = 219, \qquad G_0 = 26.6, \qquad x^+ = \frac{x/r_0}{\mathrm{Re\,Pr}} = \frac{x/D}{18{,}000}$$

$$\frac{\mathrm{Nu}_m}{\mathrm{Nu}_\infty} = 1 + \frac{17{,}500}{219x/D} \ln \frac{219}{8 \times 26.6} = 1 + \frac{2.36}{x/D} \tag{14-21}$$

Thus, even for a tube 100 diameters in length, there is still a 2 percent effect of the entry length, primarily due to the high heat-transfer coefficient in the first 10 diameters.

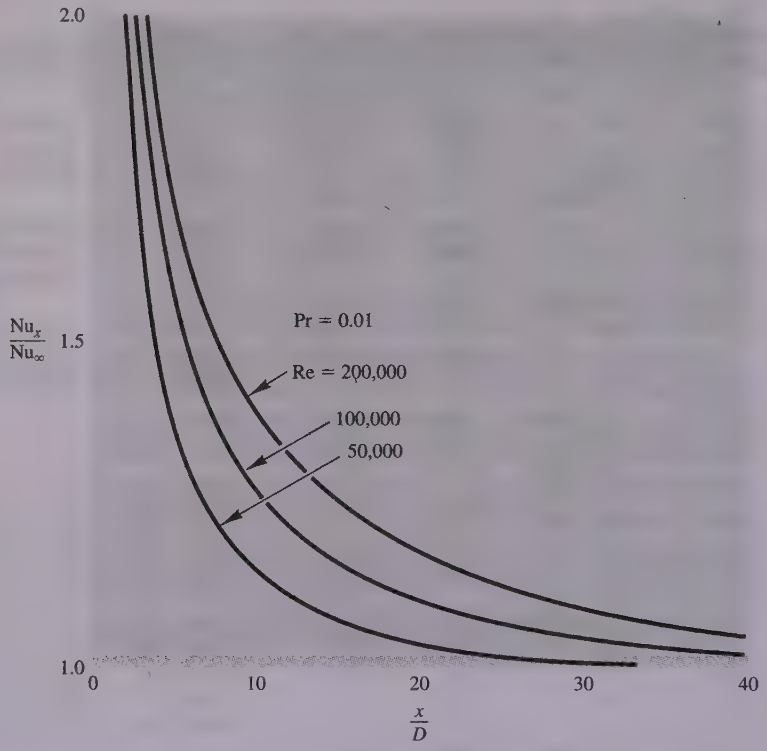

Figure 14-6 Nusselt numbers in the thermal-entry length of a circular tube, for constant heat rate: influence of Re at low Pr.

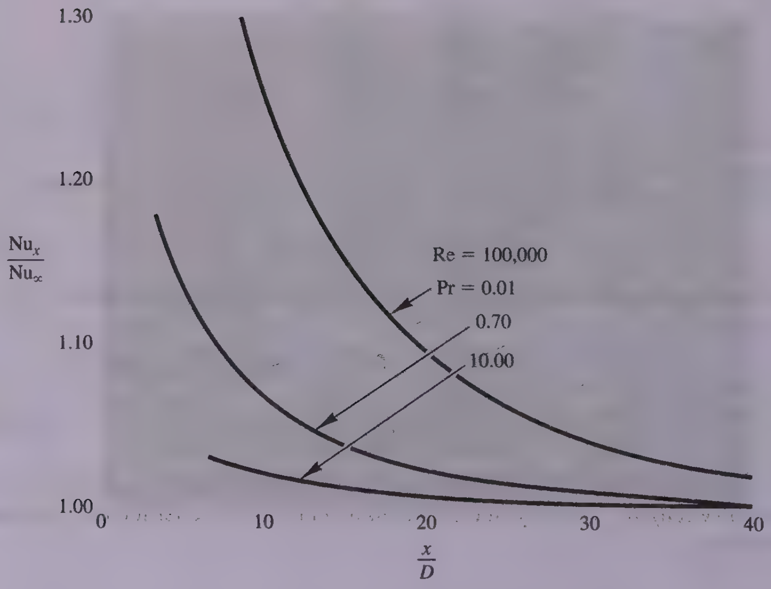

Figure 14-7 Nusselt numbers in the thermal-entry length of a circular tube, for constant heat rate: influence of Pr.

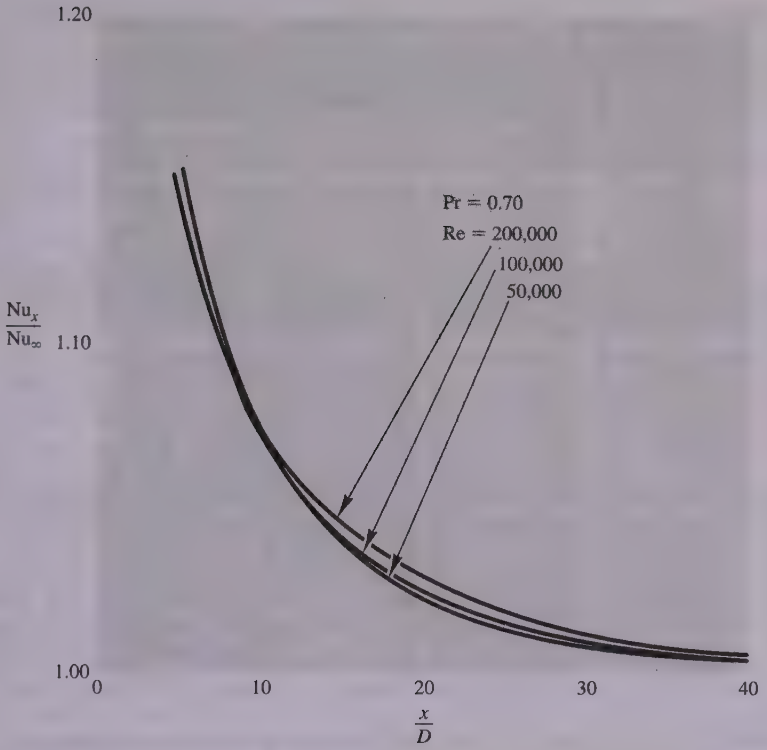

Figure 14-8 Nusselt numbers in the thermal-entry length of a circular tube, for constant heat rate: influence of Re at Pr = 0.7.

THERMAL-ENTRY LENGTH FOR TURBULENT FLOW BETWEEN PARALLEL PLANES

Hatton and Quarmby[16] developed eigenvalue solutions for turbulent flow between parallel planes for both the case of *constant temperature* on one surface with the other surface insulated, and the case of *constant heat rate* on one surface with the other surface insulated. $\mathrm{Pr}_t = 1$ was assumed throughout.

The resulting eigenvalues and constants for one surface at *constant temperature* are presented in Table 14-8 and are directly applicable to Eqs. (8-38)–(8-41). For *constant heat rate* on one surface the eigenvalues and constants are also available in the original paper, but it is more convenient to have the Nusselt numbers and influence coefficients as presented in Table 14-9. This table then corresponds to Table 8-11 for laminar flow; for asymmetric heating Eq. (8-28) is applicable. Note that these results overlap the fully developed temperature-profile results of Table 14-5, but, despite the use of somewhat different data on diffusivities and velocity profiles, they are quite consistent.

It is worth noting that these parallel-plane results are applicable with only small error to the concentric circular-tube annulus for $r^* > 0.5$, as can be seen by

Table 14-8 Infinite-series-solution functions for thermal-entry length with turbulent flow between parallel planes; one side at constant temperature and the other insulated

	Re = 7,096		Re = 73,612		Re = 494,576	
n	λ_n^2	G_n	λ_n^2	G_n	λ_n^2	G_n
			Pr = 0.1			
0	16.7	1.86	59.4	6.87	228	27.1
1	158	1.34	611	3.78	2,685	10.9
2	450	1.03	1,788	2.54	8,200	6.47
3	893	0.859	3,535	2.14	16,210	5.37
4	1,473	0.794	5,830	2.04	26,700	5.10
5	2,201	0.762	8,660	1.95	39,820	4.85
			Pr = 1			
0	52.1	6.28	296	36.1	1,303	160
1	656	2.17	4,400	9.44	2,244	33.0
2	2,067	1.16	14,100	4.85	7,360	16.3
3	4,175	0.939	22,150	3.73	14,890	12.6
4	6,775	0.936	46,850	3.27	24,530	10.9
5	9,945	0.981	70,100	2.87	36,660	9.55
			Pr = 10			
0	153	19.1	1,038	129.4	5,180	648
1	4,880	1.81	37,200	10.2	199,600	46.9
2	17,000	0.914	132,000	4.45	696,000	20.2
3	34,250	0.865	265,600	3.26	1,427,000	14.5
4	53,800	1.01	442,000	2.73	2,368,000	11.8
5	76,700	1.18	663,000	2.35	3,556,000	9.65

Table 14-9 Nusselt numbers and influence coefficients for turbulent flow between parallel planes; constant heat rate; one side heated and the other insulated

	Re = 7,096		Re = 73,612		Re = 494,576	
x/D_h	Nu_{11}	θ_1^*	Nu_{11}	θ_1^*	Nu_{11}	θ_1^*
			Pr = 0.1			
1	19.7	0.056	75.2	0.018	241	0.005
3	14.3	0.122	56.2	0.146	194	0.023
10	10.7	0.267	42.4	0.115	155	0.062
30	9.44	0.352	34.8	0.233	132	0.147
100	9.34	0.359	32.1	0.290	120	0.219
			Pr = 1.0			
1	47.3	0.013	234	0.005	940	0.000
3	37.9	0.033	203	0.018	851	0.009
10	31.5	0.089	177	0.049	761	0.030
30	28.0	0.173	160	0.114	697	0.077
100	27.1	0.200	152	0.155	661	0.123
			Pr = 10			
1	102	0.004	602	0.004	2925	0.000
3	88.6	0.012	575	0.008	2829	0.003
10	81.9	0.027	550	0.018	2724	0.010
30	78.6	0.057	532	0.041	2640	0.027
100	77.5	0.070	522	0.057	2590	0.045

comparing the asymptotic results for the annulus and parallel planes, Tables 14-4 and 14-5.

More extensive tables of eigenvalues and constants for flow between parallel planes may be found in Sakakibara and Endo.[17]

THE EFFECTS OF AXIAL VARIATIONS OF SURFACE TEMPERATURE AND HEAT FLUX

The axially varying surface temperature and the axially varying heat flux problems may be handled in exactly the same manner as for laminar flow. The caveat is still that any kind of boundary conditions can be solved just as easily by direct numerical integration of Eq. (14-1), but the classical solutions allow whole classes of problems to be generalized, and in some cases closed-form results can be obtained. The equations developed in Chap. 8 are directly applicable without alteration, but for turbulent flow the eigenvalues and constants from Tables 14-7 and 14-8 must now be used. Note also that Eqs. (8-28) and (8-29) are again applicable for the parallel-planes case, using Table 14-9.

The trends are found to be identical to those discussed for laminar flow. An increasing heat flux, or an increasing temperature difference in the flow direction, leads to higher heat-transfer coefficients, whereas the converse leads to lower heat-transfer coefficients. It is also possible to have zero or negative heat-transfer coefficients. However, the relative importance of axial variations is a strong function of Prandtl number. In the very low-Prandtl-number region (liquid metals) the effects can be very striking for a turbulent flow—even greater than those obtained for laminar flow. At Prandtl numbers near 1 and higher, the effects are usually negligible. Figure 14-5, which shows the relation between the Nusselt number for *constant heat rate* and the Nusselt number for *constant surface temperature*, provides a good indication of the regions where axial variations are of importance; it is noted that the effect at Prandtl number 0.7 is already quite small.

As an example of the significance of these results, consider the design of a nuclear reactor cooling system where the heat flux is a known function of length along the tube. Typically the heat flux is low near the entrance and exit, reaching a maximum at the midpoint. If the coolant is a liquid metal, considerable errors in the predicted surface temperatures can result unless variable-heat-flux theory is employed, that is, Eq. (8-55). On the other hand, if the coolant is a gas, or pressurized water, varying heat flux has very little influence, and it is perfectly adequate to use a Nusselt number based on *constant*-heat-flux theory or experiments to calculate the local temperature difference between the fluid and the surface. (Note, of course, that the *local* heat flux must be used to calculate the temperature difference, even though it is varying along the tube.)

COMBINED HYDRODYNAMIC- AND THERMAL-ENTRY LENGTH

In technical applications we are often more concerned about the development of the hydrodynamic and thermal boundary layers together than merely the thermal boundary layer alone. The turbulent tube-flow problem is further complicated by the fact that the turbulent-boundary-layer development is very strongly influenced by the character of the tube entrance. If the tube has a well-designed nozzle entrance so that the velocity profile is close to uniform at the tube entrance, and if a boundary-layer trip is provided, then the combined hydrodynamic- and thermal-entry-length behavior is close to that which can be predicted by numerical integration of Eq. (14-1). However, these are laboratory conditions that are seldom encountered in real applications. If the boundary layer is not tripped, a laminar boundary layer may develop, and, depending on the Reynolds number and the free-stream turbulence, it is even possible to get fully developed *laminar* flow before a transition to turbulent flow occurs. In typical heat-exchanger applications the entrance, far from being a nozzle, is either a sharp-edged contraction or is preceded by a bend in the tube. In either case there is a separated flow at the entrance, with sufficient vorticity shed into the main stream that the heat-transfer rate is very much higher than would be obtained in a developing turbulent boundary layer where the turbulence originates from the surface.

At present we must rely upon experimental data for the turbulent flow entry region of a pipe for most applications. Some rather extensive experiments were carried out by Boelter, Young, and Iverson[18] using air flowing through a steam-heated tube in which the steam jacket was sectioned in such a way that the local heat-transfer rate at each section could be determined from a measurement of the condensate rate. An abstract of these results is plotted in Fig. 14-9. The ratio of local Nusselt number to fully developed Nusselt number is plotted as a function of x/D for a tube-diameter Reynolds number close to 50,000. The lowest curve is for the case of a hydrodynamically fully developed flow, and thus would correspond to the curves of Fig. 14-8. The other curves are for various typical

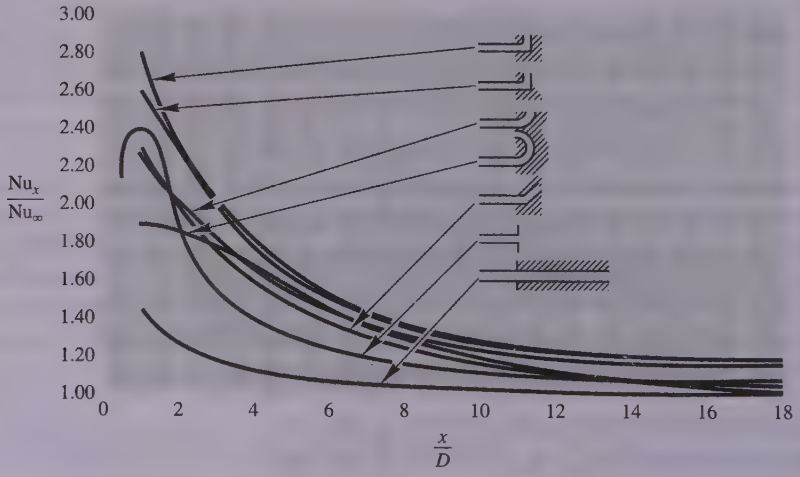

Figure 14-9 Measured local Nusselt numbers in the entry region of a circular tube for various entry configurations, air with constant surface temperature.[18]

heat-exchanger entrances: the abrupt contraction, and 45°, 90°, and 180° bends and angles.

When account is taken of the probable experimental uncertainty of data obtained in this manner, together with the fact that small changes in the geometry of the various bends may have considerable effects, a detailed quantitative comparison of the various curves is probably not warranted. What is important is the fact that all the curves for bends, and the abrupt contraction, lie substantially above the curve for the fully developed velocity profile. The interesting behavior of the abrupt-contraction curve (and this is probably the most common geometry encountered in heat exchangers) is apparently caused by the flow contraction and then reexpansion during the first diameter of tube length. The 180° bend shows similar behavior, possibly as a result of a stall region on the inside of the bend. The very high Nusselt number obtained for the 90° right-angled bend may be representative of the value that would be obtained for such a bend when preceded by a length of straight pipe; but the similar performance for the 45° round bend is probably attributable to a flow contraction rather than the bend itself, and thus would not be representative of such a bend following a section of straight pipe.

The curves of Fig. 14-9 all refer to the *local* Nusselt number. In many applications the *mean* Nusselt number with respect to tube length is of more use. For tubes with lengths greater than the entry length (and this means greater than about 20 diameters) it should be possible to express the mean Nusselt number in the form of Eq. (14-21), that is,

$$\frac{\mathrm{Nu}_m}{\mathrm{Nu}_\infty} = 1 + \frac{C}{x/D} \tag{14-22}$$

The following values of C have been evaluated by integration of the curves in Fig. 14-9:

Fully developed velocity profile	1.4
Abrupt-contraction entrance	6
90° right-angled bend	7
180° round bend	6

Note that C for the fully developed velocity profile comes out to be 1.4 rather than the predicted 2 in Eq. (14-21), but experimental uncertainty may account for this difference.

The effect on the mean Nusselt number of the abrupt-contraction and bend entrances is seen to be very substantial. For a tube of 100 diameters length the mean Nusselt number for the abrupt contraction is still 6 percent above the asymptotic value, although most of this effect is attributable to the first 10 diameters.

All of these data were obtained with a fluid with $\mathrm{Pr} = 0.7$. It is difficult to tell what the effect will be at very high and very low Prandtl numbers other than to say that it will be substantially greater in the liquid-metal region, and probably somewhat less at high Prandtl numbers.

THE INFLUENCE OF SURFACE ROUGHNESS

All the preceding discussion has been based on the assumption of an aerodynamically smooth surface. The effects of surface roughness have been discussed in some detail in connection with the external turbulent boundary layer (Chaps. 11 and 12) and with the hydrodynamics of flow in a tube or pipe. The effects of roughness on heat transfer for flow in a tube are essentially the same as described in Chap. 13 for the external boundary layer. The only difference arises from the fact that, for flow in a tube, the friction coefficient is based on the *mean* flow velocity, and the heat-transfer coefficient is based on the mixed *mean fluid* temperature.

The same mixing-length theory as discussed in Chap. 11 for rough surfaces is applicable to the tube-flow problem. The eddy diffusivity in the region far away from the surface differs little from that for a smooth surface. All the experiments (and these do not include the very low-Pr region) indicate a turbulent Prandtl number no different from that for a smooth surface. Thus numerical integration of Eq. (14-1) is quite feasible, and the more restricted cases of fully developed velocity profiles, Eq. (14-2), or fully developed velocity *and* temperature profiles, with constant heat rate, Eq. (14-3), all for circular tubes, can be readily handled. The surface resistance problem discussed in Chap. 13 is no different in a tube or pipe.

Dipprey and Sabersky[19] present correlations for heat transfer in tubes that take on essentially the same form as Eq. (13-48). A simpler empirical correlation is suggested by Norris:[20]

$$\frac{\mathrm{Nu}}{\mathrm{Nu}_{\mathrm{smooth}}} = \left(\frac{c_f}{c_{f_{\mathrm{smooth}}}}\right)^n \tag{14-23}$$

where $n = 0.68\,\mathrm{Pr}^{0.215}$. For $(c_f/c_{f_{\mathrm{smooth}}}) > 4.0$ Norris finds that the Nusselt number no longer increases with increasing roughness.

Equation (14-23) incorporates most of the effects of roughness that one would expect. The effect of roughness on heat transfer increases with Prandtl number because the sublayer becomes of dominant influence at high Prandtl numbers. On the other hand, one would expect little effect of roughness for liquid metals. The heat-transfer coefficient is not affected as strongly as the friction coefficient because of the additional conduction heat-transfer resistance at the surface. When the roughness effects on friction become very large, no further increase in heat transfer is observed because the heat-transfer resistance has become primarily a conduction resistance at the surface in the spaces between the roughness elements.

It should be noted that artificial roughness is frequently employed as a device to increase the heat-transfer coefficient. A popular and very effective scheme is to lay a small-diameter wire along the surface transverse to the flow direction (or else to machine a similar protrusion on the surface) so as to break up the sublayer. Typically the height of the protrusions should be about $y^+ = 50$, with protrusions spaced 10–20 heights along the surface. The friction coefficient is also increased because of pressure drag on the protrusion, but if the protrusion is small enough to be primarily in the sublayer region then the increase in friction is not disproportionate to the increase in heat transfer. Therefore this scheme is more effective than so-called *turbulence promoters* that are frequently inserted inside tubes to increase heat transfer at a large cost in pumping-power requirements. This whole problem is discussed in more detail in Chap. 19 in connection with a discussion of compact and high-performance heat-exchanger surfaces.

A comprehensive review of methods for augmentation of convective heat transfer is given by Bergles.[21,22]

PROBLEMS

14-1. Consider fully developed turbulent flow between parallel planes. Let the Reynolds number (based on hydraulic diameter) be 50,000 and let the Prandtl number of the fluid be 3.

The heat flux on one plate, *into* the fluid, is constant everywhere. The heat flux on the other plate is *out* of the fluid, is also constant everywhere, and is the same in magnitude as the heat flux on the first plate. The problem is to calculate and plot the temperature distribution across the fluid from plate to plate.

Use any equations for velocity distribution and or eddy diffusivity that you feel are reasonable. For simplicity, it is sufficiently precise to assume that the eddy diffusivity is constant across the center region of the duct at the value given at $r = 0$ by Eq. (13-5), and that Eq. (13-4) is valid over the remainder of the flow area, excepting the sublayer, which can be treated as in the development leading to Eq. (11-16).

Explain the shape of the temperature profile by referring to the basic mechanisms involved. How would this profile change with Prandtl number? What would the profile be if the flow were laminar?

14-2. Consider fully developed turbulent flow in a circular tube with heat transfer to or from the fluid at a constant rate per unit of tube length. Let there also be internal heat generation (perhaps from nuclear reaction) at a rate S, W/m^3, which is everywhere constant. If the Reynolds number is 50,000 and the Prandtl number is 4, evaluate the Nusselt number as a function of the pertinent parameters. The heat-transfer coefficient in the Nusselt number should be defined in the usual manner on the basis of the heat flux *at the surface*, the surface temperature, and the mixed mean fluid temperature. Use a two-layer model to handle the sublayer [see Chap. 11 and the development leading to Eq. (11-16)] and evaluate the eddy diffusivity as described for Prob. 14-1.

14-3. Consider turbulent flow between parallel planes with Reynolds number equal to 100,000. For a fluid with $\mathrm{Pr} = 10$, and then for a fluid with $\mathrm{Pr} = 0.01$, evaluate the Nusselt number for fully developed constant heat rate for only one side heated and then for both sides equally heated, using the solutions given in the text. Discuss the differences between the cases of one side heated and both sides heated, in terms of the heat-transfer mechanisms and the temperature profiles. How is the Nusselt number related to the "shape" of the temperature profile?

14-4. Consider fully developed flow in a circular tube with constant heat rate per unit of tube length. Let the mean flow velocity be 8 m/s. Evaluate the heat-transfer coefficient *h* for the following cases, and discuss the reasons for the differences:

a. air, 90°C, 1 atm pressure, 2.5-cm-diameter tube;
b. same with 0.6-cm-diameter tube;
c. hydrogen gas, 90°C, 1 atm pressure, 2.5-cm-diameter tube;
d. liquid oxygen, −200°C, 2.5-cm-diameter tube;
e. liquid water, 38°C, 2.5-cm-diameter tube;
f. liquid sodium, 200°C, 2.5-cm-diameter tube;
g. aircraft engine oil, 90°C, 2.5-cm-diameter tube;
h. air, 90°C, 1000 kPa pressure, 2.5-cm-diameter tube.

14-5. Consider a 1.20-cm-inside-diameter, 1.8-m-long tube wound by an electric resistance heating element. Let the function of the tube be to heat an organic fuel from 10 to 65°C. Let the mass-flow rate of the fuel be 0.126 kg/s, and let the following average properties be treated as constant:

$$\mathrm{Pr} = 10,\ \rho = 753\ \mathrm{kg/m^3},\ c = 2.10\ \mathrm{kJ/(kg \cdot K)},\ k = 0.137\ \mathrm{W/(m \cdot K)}$$

Calculate and plot both tube surface temperature and fluid mean temperature as functions of tube length.

TEXSTAN can be used to confirm this analysis. Use constant fluid properties and do not consider viscous dissipation. Let the velocity and thermal entry profiles at the inlet to the tube be flat, which can be supplied by using the *kstart*=1 choice in TEXSTAN. Let the energy boundary condition be a constant surface heat flux equal to the value from the analysis. For a turbulence model, choose the model described in Prob. 14-13.

14-6. Liquid potassium flows in a 2.5-cm-diameter tube at a mean velocity of 2.4 m/s and a mean temperature of 550°C. Suppose the tube is heated at a constant rate per unit of length but the heat flux varies around the periphery of the tube in a sinusoidal manner, with the maximum heat flux twice the minimum heat flux. If the maximum surface temperature is 700°C, evaluate the axial mean temperature gradient, °C/m, and prepare a plot of temperature around the periphery of the tube.

14-7. Consider the flow of first air ($\mathrm{Pr} = 0.7$) and then mercury ($\mathrm{Pr} = 0.01$) at a Reynolds number of 100,000 in a 2-cm-diameter circular tube with constant heat rate per unit of length. At a distance of 1.2 m from the tube entrance the heating stops, and the tube is insulated from then on. Using relative units of temperature, calculate and plot the decay of surface temperature as it approaches the mean fluid temperature in the insulated region. Discuss the difference in behavior of the two fluids in terms of the basic mechanisms involved.

TEXSTAN can be used to confirm this analysis. Use constant fluid properties and do not consider viscous dissipation. Let the velocity and thermal entry profiles at the inlet to the tube be flat, which can be supplied by using the *kstart*=1 choice in TEXSTAN. Let the energy boundary condition be a constant surface heat flux (you can arbitrarily choose 250 W/m^2). For a turbulence model, choose the model described in Prob. 14-13. The piecewise surface heat flux boundary condition is modeled easily in TEXSTAN by providing heat flux values at four x locations, two for each segment, e.g., at $x = 0$, $x = 1.2$ m (over which there will be a heat flux), and at $x = 1.201$ m, $x = 2.4$ m (arbitrary final tube length, over which there will be a zero heat flux, adiabatic condition). Because TEXSTAN linearly interpolates the surface thermal boundary condition between consecutive x locations, a total of four boundary-condition locations is sufficient to describe the surface heat-flux variation.

14-8. Let air at 21°C and 1 atm pressure flow at a Reynolds number of 50,000 in a 2.5-cm-diameter circular tube. The tube wall is insulated for the first 75 cm, but for the next 125 cm the tube surface temperature is constant at 40°C. Then it abruptly increases to 50°C and remains constant for another 125 cm. Plot the local heat-transfer coefficient h as a function of an axial distance. Does the abrupt increase in surface temperature to 50°C cause a significant change in the average heat-transfer coefficient over the entire 325 cm of heated length? In simple heat-exchanger theory a mean heat-transfer coefficient with respect to tube length is generally employed. In this case how much does the mean differ from the asymptotic value of h?

TEXSTAN can be used to confirm this analysis. Use constant fluid properties and do not consider viscous dissipation. Let the velocity and thermal entry profiles at the inlet to the tube be flat, which can be supplied by using the *kstart*=1 choice in TEXSTAN. Let the energy boundary condition be a surface temperature for this problem. For a turbulence model, choose the model described in Prob. 14-13. The piecewise surface temperature boundary condition is modeled easily in TEXSTAN by providing surface temperature values at six x locations. For the first interval from $x = 0$ to $x = 0.75$ m, set the surface temperature equal to the inlet temperature, effectively creating a zero-heat-flux boundary condition; over the interval $x = 1.7501$ m to $x = 2.0$ m set the surface temperature to be 40°C, and for the third interval $x = 2.001$ m to $x = 3.25$ m set the surface temperature to be 50°C.

14-9. Starting with the constant-surface-temperature thermal-entry-length solutions for a circular tube, calculate and compare the Nusselt numbers for constant surface temperature and for a linearly varying surface temperature, for very long tubes for a Reynolds number of 50,000 and a Prandtl number of 0.01. Repeat for a Prandtl number of 0.7 and discuss the reasons for the differences noted.

14-10. The following are the proposed specifications for the cooling tubes in a pressurized-water nuclear power reactor:

Tube configuration	Concentric circular-tube annulus, with heating from the inner tube (containing the uranium fuel), and the outer tube surface having no heat flux
Tube dimensions	Inner tube diameter, 2.5 cm Outer tube diameter, 5.0 cm Tube length, 5 m
Water temperature	Inlet, 275°C Outlet, 300°C
Water mean velocity	1 m/s
Axial heat-flux distribution	$\dot{q}''/\dot{q}''_{\max} = \frac{1}{3}[1 + 2\sin(\pi x/L)]$

Assume that the water properties may be treated as constant at 287°C

Calculate and plot heat flux, mean water temperature, and inner and outer tube surface temperatures as functions of x. Assume that the conductance h is independent of x and that the value for fully developed constant heat rate is a reasonable approximation. (Can you justify these assumptions?) How high must the water pressure be to avoid boiling? Or is it possible to avoid boiling with these specifications? What do you think would be the effect of local boiling at the highest-temperature parts of the system?

14-11. Repeat Prob. 14-10 for the case of liquid sodium in place of high-pressure water. Let the inlet and outlet sodium temperatures be 330 and 355°C, respectively. However, this time the effect of axially varying heat flux on the heat-transfer coefficient cannot be ignored.

14-12. Helium flows in a thin-walled circular tube of 2.5-cm inside diameter. Down the center of the tube is inserted a 5-mm-diameter circular electric heater. The Reynolds number of the flow, based on the hydraulic diameter of the resulting passage, is 30,000. Heat is generated and transferred through the heater surface at a rate of 30 kW/m^2. The outer surface of the outer tube is bare, exposed to an atmospheric environment at 21°C. Heat is transferred from the outer surface to the surroundings by both free convection and radiation. For the free convection, assume a heat-transfer coefficient h of 10 W/(m$^2 \cdot$ K). For the radiation, let the surface emissivity be 0.8.

At a particular point along the tube the mixed mean fluid temperature is 200°C. Assuming that the gas is transparent to thermal radiation and that the radiation emissivity of the two inner surfaces is 0.8, calculate the surface temperature of the heater and the temperature of the outer tube. Determine the fractions of the original heat generated in the core tube that are ultimately transferred to the helium and to the surroundings. Is radiation a major factor?

It may be assumed that the tube is sufficiently long that fully developed conditions are closely approached.

TEXSTAN PROBLEMS

14-13. TEXSTAN *analysis of the turbulent thermal entry flow in a circular tube with constant surface heat flux*: Investigate the entry length region through the thermally fully developed region of flow in a circular tube with diameter Reynolds numbers of 50,000 and 100,000 and fluids corresponding to Pr = 0.01, 0.7, and 10. Evaluate the properties at a fluid entry temperature of 280 K, use constant fluid properties, and do not consider viscous dissipation. Let the pipe diameter be 3.5 cm and the pipe length be 12.0 m. Let the velocity and thermal entry profiles at the inlet to the tube be flat, which can be supplied by using the *kstart*=1 choice in TEXSTAN. Let the energy boundary condition be a constant surface-heat flux of 250 W/m^2. For a turbulence model, choose the hybrid turbulence model composed of a constant eddy viscosity in the outer part of the flow ($\varepsilon_m/\nu = a\mathrm{Re}^b$ with $a = 0.005$ and $b = 0.9$) and a mixing-length turbulence model with the Van Driest damping function ($\kappa = 0.40$ and $A^+ = 26$) in the near-wall region (*ktmu*=7). This hybrid model tends to more closely fit Fig. 13-1, and thus better predict the fully developed friction coefficient and Nusselt number for a given Reynolds number. Choose the constant turbulent Prandtl number model (*ktme*=2) along with a choice for the turbulent Prandtl number, 0.9 is suggested, by setting *fxx*=0.9.

Compare the thermally fully developed Nusselt numbers for $\mathrm{Pr} = 0.7$ with the results from set of Eqs. (14-5) through (14-9). For $\mathrm{Pr} = -0.01$, compare with Eq. (14-10), and for $\mathrm{Pr} = 100$, compare with Eq. (14-8). Feel free to investigate any other attribute of the tube flow. For example, at $\mathrm{Pr} = 0.7$ you can examine a temperature profile at the thermally fully developed state to evaluate the *thermal law of the wall* and compare with Eq. (14-4). Compare your results for how Nusselt number varies in the thermal entry region, as appropriate, with Figs. 14-6, 14-7, and 14-8.

14-14. TEXSTAN *analysis of the turbulent thermal entry flow in a circular tube with constant surface temperature*: Investigate the entry length region through the thermally fully developed region of flow in a circular tube with diameter Reynolds numbers of 50,000 and 100,000 and fluids corresponding to $\mathrm{Pr} = 0.01$ and 0.7. Let the energy boundary condition be a constant surface temperature of 295 K. Follow the setup instructions of Prob. 14-13. Compare the thermally fully developed Nusselt number results with Eq. (14-12) for $\mathrm{Pr} = 0.7$ and Eq. (14-13) for $\mathrm{Pr} = 0.01$, and compare with Fig. 14-5. It is suggested you use TEXSTAN to compute the corresponding Nusselt number with a constant-heat-flux boundary condition to create the Nusselt number ratio in making the comparison in Fig. 14-5.

14-15. TEXSTAN *analysis of the turbulent thermal entry flow in a circular tube with constant surface heat flux*: This problem is essentially a repeat of Prob. (14-13), but choosing higher-order turbulence models available in TEXSTAN. For this problem there exists four 2-equation (k–ε) models (*ktmu*=21,22,23,24). The initial velocity and temperature profiles remain the flat profiles along with flat entry turbulence profiles for k and ε, all supplied by using the *kstart*=1 choice in TEXSTAN. Choose an entry turbulence of 10 percent. Note that by setting the corresponding entry dissipation equal to zero, TEXSTAN will compute an appropriate value. For the 2-equation turbulence models it is best to choose a constant turbulent Prandtl number model (*ktme*=2), along with a choice for the turbulent Prandtl number, 0.9 is suggested, by setting *fxx*=0.9.

14-16. TEXSTAN *analysis of the turbulent thermal entry flow between parallel plates with constant surface heat flux*: Investigate the entry length region through the thermally fully developed region of flow between parallel plates with hydraulic diameter Reynolds numbers of 30,000 and 100,000 and fluids corresponding to $\mathrm{Pr} = 0.01$, 0.7, and 10. Evaluate the properties at a fluid entry temperature of 280 K, use constant fluid properties, and do not consider viscous dissipation. Let the plate spacing be 7.0 cm and the plate length be 7.0 m. Let the velocity and thermal entry profiles at the inlet to the plates be flat, which can be supplied by using the *kstart*=1 choice in TEXSTAN. Let the energy boundary condition be a constant surface heat flux of 250 W/m^2. For a turbulence model, choose the hybrid turbulence model composed of a constant eddy viscosity in the outer part of the flow ($\varepsilon_m/\nu = a\mathrm{Re}^b$ with $a = 0.0022$ and $b = 0.9$) and a mixing-length turbulence model with the Van Driest damping function ($\kappa = 0.40$ and $A^+ = 26$) in the near-wall region (*ktmu*=7). This hybrid model follows the circular pipe idea described in Prob. 14-13, and thus better predicts the fully developed friction coefficient and Nusselt number for a given Reynolds number. Choose the constant turbulent Prandtl number model (*ktme*=2) along with a choice for the turbulent Prandtl number, 0.9 is suggested, by setting *fxx*=0.9.

Compare the thermally fully developed Nusselt numbers for $\mathrm{Pr} = 0.7$ with the results from set of Eqs. (14-5) through (14-9). For $\mathrm{Pr} = -0.01$, compare with Eq. (14-10), and for $\mathrm{Pr} = 100$, compare with Eq. (14-8). Be careful to use the hydraulic diameter, Eq. (14-18). Feel free to investigate any other attribute of the tube flow.

14-17. TEXSTAN *analysis of the turbulent thermally fully developed flow between parallel plates with asymmetrical surface heat flux*: Investigate the thermally fully developed Nusselt numbers of flow between parallel plates with hydraulic diameter Reynolds numbers of 30,000 and 100,000 and fluids corresponding to $\mathrm{Pr} = 0.01$, 0.7, and 10. Evaluate the properties at a fluid entry temperature of 280 K, use constant fluid properties, and do not consider viscous dissipation. Let the plate spacing be 7.0 cm and the plate length be 7.0 m. Start the flow at $x = 0$, as if it were entry flow. Let the velocity and thermal entry profiles at the inlet to the plates be flat, which can be done by using the *kstart*=1 choice in TEXSTAN. Let the energy boundary condition be a constant surface heat flux of 250 W/m^2 on one surface and a zero heat flux on the other surface. Note that in TEXSTAN this geometry will be *kgeom*=6 (it will be *kgeom*=5, corresponding to symmetric thermal boundary conditions, for Prob. 14-16). Compare the thermally fully developed Nusselt numbers with the results shown in Table 14-5.

REFERENCES

1. Kays, W. M., and E. Y. Leung: *Int. J. Heat Mass Transfer*, vol. 6, pp. 537–557, 1963.
2. Kakac, S., R. K. Shah, and W. Aung: *Handbook of Single-Phase Convective Heat Transfer*, Wiley, New York, 1987.
3. Gnielinski, V.: *Int. Chem. Engng.*, vol. 16, pp. 359–368, 1976.
4. Sleicher, C. A., and M. W. Rouse: *Int. J. Heat Mass Transfer*, vol. 18, pp. 677–683, 1975.
5. Dittus, P. W., and L. M. K. Boelter: *Univ. Calif. Publ. Engng.*, vol. 2, no. 13, pp. 443–461, October 17, 1930; reprinted in *Int. Commun. Heat Mass Transfer*, vol. 12, pp. 3–22, 1985.
6. Skupinski, E., J. Tortel, and L. Vautry: *Int. J. Heat Mass Transfer*, vol. 8, pp. 937–951, 1965.
7. Sleicher, C. A., and M. Tribus: *Proceedings of Heat Transfer and Fluid Mechanics Institute, Stanford University*, 1956, p. 59, Department of Mechanical Engineering, Stanford University, 1956.
8. Gartner, D., K. Johannsen, and H. Ramm: *Int. J. Heat Mass Transfer*, vol. 17, pp. 1003–1018, 1974.
9. Deissler, R. G.: NACA (now NASA) Report 1210, Washington, 1955.
10. Sutherland, W. A., and W. M. Kays: *Int. J. Heat Mass Transfer*, vol. 7, p. 1187, 1964.
11. Leung, E. Y., W. M. Kays, and W. C. Reynolds: Report AHT-4, Department of Mechanical Engineering, Stanford University, April 5, 1962.

12. Kays, W. M., and A. L. London: *Compact Heat Exchangers*, McGraw-Hill, New York, 1984.

13. Rohsenow, W. M., and J. P. Hartnett (eds.): *Handbook of Heat Transfer*, McGraw-Hill, New York, 1973.

14. Notter, R. H., and C. H. Sleicher: *Chem. Engng. Sci.*, vol. 27, pp. 2073–2093, 1972.

15. Sparrow, E. M., T. M. Hallman, and R. Speigel: *Appl. Sci. Res.*, ser. A, vol. 7, pp. 37–52, 1957.

16. Hatton, A. P., and A. Quarmby: *Int. J. Heat Mass Transfer*, vol. 6, pp. 903–914, 1963.

17. Sakakibara, M., and K. Endo: *Int. Chem. Engng.*, vol. 18, pp. 728–733, 1976.

18. Boelter, L. M. K., G. Young, and H. W. Iversen: NACA (now NASA) TN 1451, Washington, July 1948.

19. Dipprey, D. F., and R. H. Sabersky: *Int. J. Heat Mass Transfer*, vol. 6, pp. 329–353, 1963.

20. Norris, R. H.: *Augmentation of Convection Heat and Mass Transfer*, American Society of Mechanical Engineers, New York, 1971.

21. Bergles, A. E.: *Applied Mechanics Reviews*, vol. 26, pp. 675–682, 1973.

22. Bergles, A. E.: Report HTL-8, Engineering Research Institute, Iowa State University, Ames, 1975.

15 CHAPTER

Influence of Temperature-Dependent Fluid Properties

In all the heat-transfer and flow friction solutions considered in the previous chapters it has been assumed that the fluid properties remain constant throughout the flow field. When applied to real heat-transfer problems, this assumption is obviously an idealization, since the transport properties of most fluids vary with temperature and thus vary through the boundary layer or over the flow cross section of a tube. In this chapter we examine the results of a number of analytic solutions and experiments in which this influence has been investigated, and we propose methods whereby the constant-property solutions can be corrected in a simple manner to take this influence into consideration.

The temperature-dependent-property problem is further complicated by the fact that the properties of different fluids behave differently with temperature. For *gases* the specific heat varies only slightly with temperature, but the viscosity and thermal conductivity increase to about the 0.8 power of the absolute temperature (in the moderate temperature range). Furthermore, the density varies inversely with the first power of the absolute temperature. On the other hand, the Prandtl number $\mu c/k$ does not vary significantly with temperature.

For most *liquids* the specific heat and thermal conductivity are relatively independent of temperature, but the viscosity decreases very markedly with temperature. This is especially so for oils, but even for water the viscosity is very temperature dependent. The density of liquids, on the other hand, varies little with temperature. The Prandtl number of liquids varies with temperature in much the same manner as the viscosity.

A number of variable-property analyses are contained in the literature, as well as a considerable body of experimental data. The general effect of the variation of the transport properties with temperature is to change the velocity and temperature profiles, yielding different friction and heat-transfer coefficients than would be obtained if properties were constant.

For engineering applications it has been found convenient to employ the constant-property analytic solutions, or the experimental data obtained with small temperature differences, and then to apply some kind of correction to account for property variation. Fortunately, most of the variable-property results indicate that fairly simple corrections generally suffice over a moderate range of properties. Obviously, if the absolute value of the properties varies severalfold through the boundary layer, no simple correction scheme is going to be adequate, and thus a complete numerical integration of the applicable differential equations for each such application is required. Such cases are fortunately rare.

Two schemes for correction of the constant-property results are in common use. In the *reference temperature* method a characteristic temperature is chosen at which the properties appearing in the nondimensional groups (Re, Pr, Nu, etc.) may be evaluated such that the constant-property results at that temperature may be used to evaluate variable-property behavior. Typically, this may be the surface temperature or a temperature part way between the surface temperature and the free-stream or mixed mean temperature; there is no general rule. In the *property ratio* method all properties are evaluated at the free-stream temperature, or the mixed mean temperature, and then all the variable-property effects are lumped into a function of a ratio of some pertinent property evaluated at the surface temperature to that property evaluated at the free-stream or mixed mean temperature.

The *reference temperature* method, although extensively used, leads to a certain awkwardness—at least in internal flow applications—that is avoided by the property ratio method. For example, in evaluating the Reynolds number it becomes necessary to split the mass velocity $G = \rho V$ so that the density may be evaluated at the reference temperature. But for internal flows, such as flows in a pipe, G is also the mass-flow rate divided by the flow cross-sectional area; and it is one parameter about which there is no ambiguity regardless of density variation over the flow area.

The *property ratio* scheme involves a different kind of correction for liquids and for gases. For *liquids*, where the viscosity variation is responsible for most of the effect, it is found that equations of the following type are often excellent approximations:

$$\frac{\mathrm{Nu}}{\mathrm{Nu}_{\mathrm{CP}}} = \frac{\mathrm{St}}{\mathrm{St}_{\mathrm{CP}}} = \left(\frac{\mu_s}{\mu_m}\right)^n \quad \text{or} \quad \left(\frac{\mu_s}{\mu_\infty}\right)^n \tag{15-1}$$

$$\frac{c_f}{c_{f\,\mathrm{CP}}} = \left(\frac{\mu_s}{\mu_m}\right)^m \quad \text{or} \quad \left(\frac{\mu_s}{\mu_\infty}\right)^m \tag{15-2}$$

All properties in the nondimensional parameters are evaluated at local mixed mean fluid temperature (or free-stream temperature in the case of external flows), and the subscript CP refers to the appropriate constant-property solution or small-temperature-difference experimental results. The viscosity μ_s is evaluated at the surface temperature, while μ_m is evaluated at the mixed mean temperature (or the free-stream temperature in the case of external flows). The exponents m and n are functions of geometry and the type of flow.

For *gases* the viscosity, thermal conductivity, and density are functions of *absolute* temperature. Fortunately, the absolute temperature dependence tends to be similar for different gases, although the similarity does break down at the temperature extremes. Thus it is found that the temperature-dependent-property effects can usually be adequately correlated by the equations

$$\frac{\text{Nu}}{\text{Nu}_{\text{CP}}} = \frac{\text{St}}{\text{St}_{\text{CP}}} = \left(\frac{T_s}{T_m}\right)^n \quad \text{or} \quad \left(\frac{T_s}{T_\infty}\right)^n \tag{15-3}$$

$$\frac{c_f}{c_{f\,\text{CP}}} = \left(\frac{T_s}{T_m}\right)^m \quad \text{or} \quad \left(\frac{T_s}{T_\infty}\right)^m \tag{15-4}$$

Again, all properties in the nondimensional parameters are evaluated at the mixed mean temperature for internal flows or at the free-stream temperature for external flows.

In the remainder of this chapter we examine the evidence, both analytic and experimental, for values of the exponents m and n; and we also indicate some appropriate reference properties. We first consider flow inside tubes and then external boundary layers. In each case we consider laminar flow and then turbulent flow, and under these headings liquids and then gases. For one case—the laminar external boundary layer with a gas—we carry through a simple approximate analytic development.

In this chapter we are concerned with only low-velocity flow where viscous dissipation may be neglected; high-velocity effects are considered in Chap. 16.

LAMINAR FLOW IN TUBES: LIQUIDS

Fully developed laminar flow of a liquid in a tube with temperature-dependent properties is a relatively simple analytic problem. Only the variation of viscosity with temperature is significant. The momentum and energy differential equations for fully developed, constant-heat-rate conditions in a circular tube follow directly from Eq. (7-1) and the variable-property formulation of Eq. (8-10):

$$0 = -\frac{dP}{dx} + \frac{1}{r}\frac{\partial}{\partial r}\left(r\mu\frac{\partial u}{\partial r}\right) \tag{15-5}$$

$$\rho c u\frac{dT_m}{dx} = \frac{1}{r}\frac{\partial}{\partial r}\left(rk\frac{\partial T}{\partial r}\right) \tag{15-6}$$

Equations (15-5) and (15-6) can be integrated by an iterative procedure in which the temperature distribution for constant properties is used as a first approximation. Then using the appropriate viscosity variation with temperature, the momentum equation is integrated numerically to yield a second approximation for the velocity distribution. This velocity distribution is employed in a numerical integration of the energy equation to yield a second approximation for the temperature distribution. The procedure is repeated until the velocity and temperature distributions do not change. Then the mean velocity, the mixed mean temperature, the friction coefficient, and the convection conductance are evaluated as in the constant-property solutions.

Deissler[1] carried out such calculations for a circular tube for a fluid for which the viscosity varies with temperature as

$$\mu \propto T^{-1.6}$$

which corresponds approximately to the behavior of liquid metals. When the results are put in the form of Eqs. (15-1) and (15-2), we obtain

$$n = -0.14$$

which is a number that has also been used extensively to correlate experimental data for laminar flow of moderate- and high-Prandtl-number liquids.

For the friction coefficient Deissler's results indicate a slightly different exponent, depending on whether the liquid is being heated or cooled:

$$\frac{\mu_s}{\mu_m} > 1, \quad m = 0.50 \quad \text{(cooling)}$$

$$\frac{\mu_s}{\mu_m} < 1, \quad m = 0.58 \quad \text{(heating)}$$

Yang[2] considered the laminar thermal-entry-length problem in a circular tube for both a constant surface temperature and a constant heat rate. He employed an integral method that yielded results very close to the exact eigenvalue solution for constant viscosity, and he assumed that the viscosity dependence on temperature could be expressed as

$$\frac{\mu}{\mu_s} = \frac{1}{1+\gamma\theta}$$

where $\theta = (T_s - T)/(T_s - T_e)$ and γ is a parameter.

Yang considered only the heat-transfer behavior, and his results for both constant surface temperature and constant heat rate can be very well approximated by

$$n = -0.11$$

and this result (which refers to the local heat-transfer coefficient) applies to both the thermal-entry length and the subsequent fully developed region. The difference in exponent, −0.11 as compared with −0.14, is evidently related to the different form of viscosity–temperature function employed. The difference is small, and in either case the influence of viscosity ratio on Nusselt number is evidently not great. Also, there appears to be little effect due to different types of thermal boundary conditions. The influence on the friction coefficient, on the other hand, is very substantial.

Calculations by the authors using a finite-difference code and the real properties of *water* yield substantially the same conclusions.

This problem has apparently not been handled for other than a circular tube.

LAMINAR FLOW IN TUBES: GASES

In this case reasonably complete analytic solutions are available as well as a considerable body of experimental data. Deissler[1] first investigated this problem analytically, assuming fully developed velocity and temperature profiles and employing an iterative procedure similar to that described for the liquid case. However, experimental data[3,4] are only in moderate agreement with these results. The difficulty apparently is that, because of density changes with temperature, there is always a radial component of velocity and under large-temperature-difference conditions it is not possible to have a fully developed velocity profile. Worsøe-Schmidt[5] has solved the applicable differential equations using a finite-difference technique for a gas with the properties of air in the temperature range 300–1700 K. A circular tube is considered, with a developed velocity profile and uniform temperature at the tube entrance. Heating and cooling with a constant surface temperature and heating with a constant heat rate are considered. In this solution the radial velocity is included.

Worsøe-Schmidt's results show a rather small effect of temperature ratio on Nusselt number but a substantial effect on friction coefficient. Near the entrance, and also well downstream, the results can be satisfactorily correlated for both heating and cooling by

$$n = 0, \qquad m = 1$$

Experiments by Kays and Nicoll[3] verify the conclusion that n is approximately zero over the temperature ratio range 0.5–2. Experiments by Davenport[4] for temperature ratios from 1.0 to 2.2 yield $m = 1.35$, but this is a difficult experiment to carry out accurately and the conclusion from the analysis is probably to be preferred.

Calculations (by the authors) for flow between parallel planes, using the fully developed flow assumption and employing essentially the procedure of Deissler, yield substantially the same results for the friction coefficient as were obtained for the circular tube under the same assumptions. However, the results for the Nusselt number are substantially different.

TURBULENT FLOW IN TUBES: LIQUIDS

The mixing-length methods developed in Chap. 11 can be used to find solutions for the variable-property problem provided only that the variable-property forms of the momentum and energy differential equations are employed, i.e., the turbulent flow versions of Eqs. (7-1) and (8-10). It is necessary to evaluate fluid properties at the local temperature, which then requires a simultaneous solution of the momentum and energy equations. However, extensive experimental data are also available, and these are used for the recommendations to follow because the validity of any turbulent flow analytic solutions of this problem must rely heavily on experimental verification anyway.

Petukhov[6] has examined heat-transfer data covering these ranges: $\mathrm{Pr} = 2$–140; $\mathrm{Re} = 5000$–$123{,}000$; and $\mu_s/\mu_m = 0.025$–12.5. He finds that the data are quite well correlated by

$$\frac{\mu_s}{\mu_m} > 1, \quad n = -0.25 \quad \text{(cooling)}$$

$$\frac{\mu_s}{\mu_m} < 1, \quad n = -0.11 \quad \text{(heating)}$$

Allen and Eckert[7] conducted experiments with water at $\mathrm{Pr} = 8$ for the Reynolds number range 13,000–111,000 for the heating case and found that the friction coefficient results are reasonably correlated by

$$\frac{\mu_s}{\mu_m} < 1, \quad m = 0.25 \quad \text{(heating)}$$

Friction data for the cooling case appear to be rare, but the very early data of Rohonczy[8] for $\mathrm{Re} = 33{,}000$–$225{,}000$, $\mathrm{Pr} = 1.3$–5.8, and $\mu_s/\mu_m = 1$–2 are quite well correlated by the same value of m:

$$\frac{\mu_s}{\mu_m} > 1, \quad m = 0.25 \quad \text{(cooling)}$$

TURBULENT FLOW IN TUBES: GASES

There is a considerable body of experimental data for $T_s/T_m > 1$. The data of Humble, Lowdermilk, and Desmon[9] for air yield $n = -0.55$. The extensive data of McCarthy and Wolf[10] for helium and hydrogen yield $n = -0.55$. The experiments of Barnes[11] for air, helium, and carbon dioxide yield values of n that differ for the different gases and are somewhat lower. Petukhov[6] presents an excellent summary of these and many other experiments, which yield roughly the same conclusions but which also suggest that the absolute value of n increases with temperature ratio, Sleicher and Rouse[18] examined a large amount of data and concluded that

$$\text{for } 1 < \frac{T_s}{T_m} < 5, \qquad n = -\left(\log_{10}\frac{T_s}{T_m}\right)^{1/4} + 0.3 \quad \text{at } \frac{x}{D} > 40$$

Calculations by the authors using a finite-difference procedure and the mixing-length theory developed in Chap. 11 are in quite good agreement with this equation for $x/D > 30$ but yield smaller absolute values of n for shorter lengths, which means that there is a considerable entry-length effect. One of the difficulties with this problem is that for either a constant heating rate or a constant surface temperature there is a continuous axial variation of T_s/T_m, a continuous flow acceleration, and the radial component of velocity is never zero, so that a fully developed flow never exists. It is worth noting that in evaluating the Van Driest damping function for the sublayer (see Chap. 11), *local* values of viscosity and density were used to evaluate y^+ in the term y^+/A^+, although the shear stress is the surface value. $A^+ = 26$ was used throughout. Since the major portion of the heat-transfer resistance is in the sublayer, this procedure is critical.

The cooling experiment, $T_s/T_m < 1$, is more difficult to carry out, especially if local heat-transfer coefficients are desired, and few results have been reported. Humble, Lowdermilk, and Desmon[9] report a small amount of data for T_s/T_m varying from 1 to 0.46; there appears to be a negligible effect of temperature ratio; that is, $n = 0$. Nicoll and Kays[12] carried out similar experiments and could detect no effect over the range of temperature ratio 0.63 to 0.38. Brim and Eustis[19] carried out experiments with a mixture of combustion gases and nitrogen and measured local heat-transfer coefficients at $x/D = 50$ for values of T_s/T_m as low as 0.25, with the conclusion that $n = 0$. Kays' analytic solutions yield n between 0 and -0.1, that is, very close to 0.

Experimental data on the friction coefficient are not extensive, and they are difficult to interpret because of the pressure drop caused by flow acceleration or deceleration. McEligot[13] concludes that $m = -0.1$ on the basis of his own experiments and an examination of the data of Lel'chuk and Dyadyakin,[14] all for $T_s/T_m > 1$. There have apparently been few experiments for $T_s/T_m < 1$. Kays' analytic results suggest a value of m between -0.1 and -0.2 for both heating and cooling.

On the basis of this evidence, the following are recommended as simple correlations for turbulent flow of a gas in a circular tube for $x/D > 30$:

$$\text{for } T_s/T_m > 1, \quad m = -0.1, \quad n = -0.5 \quad \text{(heating)}$$

$$\text{for } T_s/T_m < 1, \quad m = -0.1, \quad n = 0.0 \quad \text{(cooling)}$$

The equation recommended by Sleicher and Rouse is probably a better approximation for n for the heating case.

It seems unlikely that tube cross-sectional shape is a significant parameter for turbulent flow, and thus these conclusions should be applicable for noncircular tubes.

THE LAMINAR EXTERNAL BOUNDARY LAYER: GASES

Consider a steady-flow, laminar, low-velocity, two-dimensional boundary layer with no pressure gradient and with constant but different surface and free-stream temperatures. The applicable differential equations under the conditions of variable-fluid properties are as follows:

Continuity, from Eq. (4-1),

$$\frac{\partial(\rho u)}{\partial x} + \frac{\partial(\rho v)}{\partial y} = 0 \tag{15-7}$$

Momentum, from Eq. (4-10),

$$\rho u \frac{\partial u}{\partial x} + \rho v \frac{\partial u}{\partial y} = \frac{\partial}{\partial y}\left(\mu \frac{\partial u}{\partial y}\right) \tag{15-8}$$

Energy, from (4-37), omitting the viscous dissipation term,

$$\rho c u \frac{\partial T}{\partial x} + \rho c v \frac{\partial T}{\partial y} = \frac{\partial}{\partial y}\left(k \frac{\partial T}{\partial y}\right) \tag{15-9}$$

The boundary conditions are

$$\begin{aligned} u, v &= 0, & T &= T_s & \text{at } y &= 0 \\ u &= u_\infty, & T &= T_\infty & \text{at } y &\to \infty \\ u &= u_\infty, & T &= T_\infty & \text{at } x &= 0 \end{aligned}$$

Similarity solutions may be obtained for this system of equations. Consider the following transformation of variables. First define a stream function ψ that satisfies the continuity equation:

$$\rho u = \rho_\infty \frac{\partial \psi}{\partial y}, \qquad \rho v = -\rho_\infty \frac{\partial \psi}{\partial x} \tag{15-10}$$

Next define

$$\eta = \sqrt{\frac{u_\infty}{\nu_\infty x}} \int_0^y \frac{\rho}{\rho_\infty}\, dy, \qquad \zeta(\eta) = \frac{\psi}{\sqrt{u_\infty \nu_\infty x}}, \qquad T = T(\eta) \tag{15-11}$$

As in the constant-property case, we find that these changes of variables reduce the momentum and energy equations to ordinary differential equations:

$$\frac{d}{d\eta}\left(\frac{\mu\rho}{\mu_\infty \rho_\infty} \frac{d^2\zeta}{d\eta^2}\right) + \frac{1}{2}\zeta \frac{d^2\zeta}{d\eta^2} = 0 \tag{15-12}$$

$$\frac{d}{d\eta}\left(k \frac{\rho}{\rho_\infty} \frac{dT}{d\eta}\right) + c\mu_\infty \frac{\zeta}{2} \frac{dT}{d\eta} = 0 \tag{15-13}$$

Thus it is apparent that similarity solutions can be obtained regardless of how the properties vary with temperature.

Let us first consider a hypothetical gas for which Pr is a constant, c is a constant, μ varies directly as T, and ρ varies as T^{-1}. This is not very far from the room-temperature behavior of air, although the temperature dependence of μ (and by implication k) is a little large. (The properties of low-pressure steam and NH_3 correspond closely to these approximations.)

Under these conditions, Eq. (15-13) can be rewritten as

$$\frac{d}{d\eta}\left(\frac{\mu\rho}{\mu_\infty \rho_\infty} \frac{1}{\mathrm{Pr}} \frac{dT}{d\eta}\right) + \frac{1}{2}\zeta \frac{dT}{d\eta} = 0$$

Since $\mu\rho$ is a constant under these assumptions, the momentum and energy equations reduce to

$$\zeta''' + \tfrac{1}{2}\zeta\zeta'' = 0$$
$$T'' + \tfrac{1}{2}\,\mathrm{Pr}\,\zeta T' = 0$$

These are, of course, exactly the equations obtained for the corresponding constant-property problem, Eqs. (9-8) and (10-4) [where T is replaced by θ, as in Eq. (10-1)]. We already have the desired solutions. Let us evaluate a Nusselt number and friction coefficient, evaluating all properties in the nondimensional parameters at the free-stream temperature T_∞:

$$\dot{q}_s'' = -k_s\left(\frac{\partial T}{\partial y}\right)_s = -k_s(T_\infty - T_s)\left(\frac{\partial \theta}{\partial y}\right)_s$$

We recall that

$$\theta = \theta(\eta), \qquad \frac{\partial \theta}{\partial y} = \frac{d\theta}{d\eta}\frac{\partial \eta}{\partial y} = \theta'\sqrt{\frac{u_\infty}{\nu_\infty x}}\frac{\rho}{\rho_\infty}$$

$$\dot{q}_s'' = k_s(T_s - T_\infty)\theta'(0)\sqrt{\frac{u_\infty}{\nu_\infty x}}\frac{\rho_s}{\rho_\infty}$$

$$= h(T_s - T_\infty)$$

$$h = k_s\frac{\rho_s}{\rho_\infty}\sqrt{\frac{u_\infty}{\nu_\infty x}}\theta'(0)$$

$$\mathrm{Nu}_\infty = \frac{hx}{k_\infty} = \frac{k_s}{k_\infty}\frac{\rho_s}{\rho_\infty}\mathrm{Re}_{\infty,x}^{1/2}\theta'(0)$$

But, since $\mathrm{Pr} = \mu c/k$ and c are constants, k must vary as μ, that is, as T. Thus the property ratios cancel, and we obtain

$$\mathrm{Nu}_\infty = \mathrm{Re}_{\infty,x}^{1/2}\theta'(0)$$

In other words, our constant-property solutions are applicable if all properties are evaluated at the free-stream temperature. (In fact, under these property variations, $\mathrm{Nu}/\mathrm{Re}^{1/2}$ has the same value regardless of what temperature is used to evaluate properties.) In terms of Eq. (15-3), we conclude that $n = 0$.

Similar evaluation of the friction coefficient leads to an identical result if free-stream properties are used in the definition of friction coefficient, as well as in the Reynolds number. That is,

$$c_f = \frac{\tau_s}{\frac{1}{2}\rho_\infty u_\infty^2}$$

$$= 2\zeta''(0)\mathrm{Re}_{\infty,x}^{1/2} = 0.664\,\mathrm{Re}_{x,\infty}^{-1/2}$$

In terms of Eq. (15-4), we conclude that $m = 0$. (However, in this case, had properties been evaluated at T_s, a substantial temperature-ratio effect would have been noted.)

This approximate analysis illustrates how the temperature variation of the properties of a gas tends to compensate, so that, despite large property variations in a real gas, the constant-property solutions have a remarkable range of validity.

Solutions based on more realistic gas properties are presented by Brown and Donoughe[15] for the family of wedge solutions and the blowing and suction solutions. Reshotko and Cohen[16] include the axisymmetric stagnation point. For these solutions a slightly different transformation of variables is used, in addition to Eqs. (15-10) and (15-1):

$$\eta = y\sqrt{\frac{u_\infty}{\nu_s x}}, \qquad \zeta(\eta) = \frac{\psi}{\sqrt{u_\infty \nu_s x}} \tag{15-14}$$

Again Eqs. (15-8) and (15-9) reduce to ordinary differential equations. For property variations with temperature the following relations, which approximate for air in the 600–1600 K range, are used:

$$\frac{\mu}{\mu_s} = \left(\frac{T}{T_s}\right)^{0.70}, \qquad \frac{c}{c_s} = \left(\frac{T}{T_s}\right)^{0.19}, \qquad \frac{k}{k_s} = \left(\frac{T}{T_s}\right)^{0.85}$$

The density variation is taken as $\rho/\rho_s = (T/T_s)^{-1}$, and $\mathrm{Pr}_s = 0.70$. Note that, under these assumptions, Pr varies as $T^{0.04}$. With these relations substituted for the properties, the equations were integrated numerically and the results presented in tabular form. When put in the form of Eqs. (15-3) and (15-4), the data in Table 15-1 are a good approximation for $\mu_\infty =$ constant and for the two-dimensional stagnation point. Other cases, including blowing and suction, are found in the indicated references.

For $\mu_\infty =$ constant, these results are very close to the results of the approximate solution described above; in fact, the only case for which there is a significant effect is for the friction coefficient for the stagnation point.

Experimental data appear to be lacking, but there are data for *flow normal to a cylinder.*[3] For $T_s/T_\infty > 1$ it is found that $n = 0.02$, which is quite consistent with the results in Table 15-1 since, on a cylinder, there is a two-dimensional stagnation point, followed by a laminar boundary layer approaching $u_\infty =$ constant. Thus a value between 0.10 and −0.01 would be expected. Similar results would be expected for the cylinder for $T_s/T_\infty < 1$, and for a *bank of tubes*, such as are frequently used in heat exchangers.

As an alternative to the temperature-ratio corrections suggested above, Eckert[17] suggests the use of a reference temperature scheme for gases. He finds that if the specific heat does not vary markedly through the boundary layer, the constant-property, laminar boundary-layer solutions for constant free-stream

Table 15-1 Temperature-ratio exponents for the laminar external boundary layer with a gas

	$T_s/T_\infty > 1$ (heating)		$T_s/T_\infty < 1$ (cooling)	
	m	n	m	n
$u_\infty =$ constant	−0.10	−0.01	−0.05	0
Two-dimensional stagnation point	0.40	0.10	0.30	0.07

velocity can be correlated with the variable-property calculations by introducing *all* properties at a *reference temperature* T_R:

$$T_R = T_\infty + 0.5(T_s - T_\infty) \tag{15-15}$$[†]

Under this scheme, the Reynolds number in both the constant-property heat-transfer and friction coefficient equations becomes

$$\mathrm{Re}_{x,R} = \frac{\rho_R u_\infty x}{\mu_R}$$

and similarly for the Nusselt, Stanton, and Prandtl numbers. The local surface shear stress is evaluated from Eq. (9-13), but with ρ_R replacing ρ.

For extremely large temperature differences the *specific heat* can no longer be treated as constant, and a formulation of the heat-transfer problem based on enthalpies rather than temperatures become more convenient. However, this problem is of more concern at high velocities and thus is discussed in Chap. 16.

THE LAMINAR EXTERNAL BOUNDARY LAYER: LIQUIDS

The laminar external boundary layer with liquids has evidently not been investigated experimentally. However, calculations by the authors using a finite-difference code and the real properties of *water* yielded the following results when comparison is made at the same *x-Reynolds* number:

$$\begin{aligned}
&\text{for } \mu_s/\mu_\infty > 1, && n = -0.25 && \text{(cooling)}\\
&\text{for } \mu_s/\mu_\infty < 1, && n = -0.25 && \text{(heating)}\\
&\text{for } \mu_s/\mu_\infty > 1, && m = 0.09 && \text{(cooling)}\\
&\text{for } \mu_s/\mu_\infty < 1, && m = 0.20 && \text{(heating)}
\end{aligned}$$

If comparison is made at the same *enthalpy thickness* and *momentum thickness* Reynolds numbers, respectively, then the exponents become $n = -0.5, m = 0.18$ for cooling, and $n = -0.5, m = 0.4$ for heating.

THE TURBULENT EXTERNAL BOUNDARY LAYER: LIQUIDS

No experimental results for the turbulent boundary layer for liquids with large temperature differences exist. However, calculations by the authors using a finite-difference code, the real properties of water, and the mixing-length models described in Chaps. 11 and 12 yielded the following results when comparison is made at the same *enthalpy thickness* (for n) and *momentum thickness* (for m)

[†] Extension of this scheme to the high-velocity boundary layer is given in Chap. 16 and specifically in Eq. (16-40).

Reynolds numbers:

$$\begin{array}{lll} \text{for } \mu_s/\mu_\infty > 1, & n = -0.12 & \text{(cooling)} \\ \text{for } \mu_s/\mu_\infty < 1, & n = -0.23 & \text{(heating)} \\ \text{for } \mu_s/\mu_\infty > 1, & m = 0.26 & \text{(cooling)} \\ \text{for } \mu_s/\mu_\infty < 1, & m = 0.26 & \text{(heating)} \end{array}$$

Note that these results are very close to the experimental results for turbulent flow in a tube with liquids. This is not unexpected, but it does provide additional confidence in the mixing-length models discussed in Chaps. 11 and 12.

The exponents for the case where comparison is made at the same *x-Reynolds* number can be obtained by *subtracting* approximately 0.25 from each of the above.

THE TURBULENT EXTERNAL BOUNDARY LAYER: GASES

The turbulent external boundary layer with temperature-dependent properties has received little attention, either analytic or experimental. Most of the available experimental data involve high Mach numbers, which introduces the additional complication of viscous energy dissipation, a subject that is discussed in Chap. 16. However, it is difficult to see how the effect of temperature ratio on Stanton number (or Nusselt number) can be materially different from that for flow in a tube. In fact, the principal difference must be simply that the temperature ratio on which n is based for the external boundary layer, T_s/T_∞, is analogous in the case of flow in a tube to T_s/T_{cl}, rather than T_s/T_m. Recall that in Chap. 14 it was suggested that $(T_s - T_m)/(T_s - T_{\mathrm{cl}})$ is about 0.90. For the heating case this suggests that the absolute value of n should be less than the value 0.5 recommended for flow in a tube. A check of some representative values of T_s and T_m yields a value for n for the external boundary layer between -0.35 and -0.40. This is presumably the correction that should be made when the comparison between constant and variable properties is made at the same *enthalpy thickness* Reynolds number.

Calculations by the authors using a finite-difference code, the real properties of *air*, and the mixing-length theory discussed in Chaps. 11 and 12, with constant free-stream velocity, yield the following results when comparison is made at the same *momentum thickness* Reynolds number for c_f, and the same *enthalpy thickness* Reynolds number for St:

$$\begin{array}{llll} \text{for } T_s/T_\infty > 1, & m = -0.33, & n = -0.30 & \text{(heating)} \\ \text{for } T_s/T_\infty < 1, & m = -0.22, & n = -0.14 & \text{(cooling)} \end{array}$$

When these results are converted to an *x Reynolds number* basis, they become

$$\begin{array}{llll} \text{for } T_s/T_\infty > 1, & m = -0.58, & n = -0.55 & \text{(heating)} \\ \text{for } T_s/T_\infty < 1, & m = -0.47, & n = -0.39 & \text{(cooling)} \end{array}$$

As was seen for flow in a tube, the exponents tend to increase somewhat with temperature ratio; the results are valid for $T_s/T_\infty \approx 2.00$ and 0.75.

Eckert[17] recommends the same *reference temperature* for the turbulent boundary layer for a gas as for the laminar boundary layer, i.e., Eq. (15-15). Such a procedure gives somewhat smaller values of m and n, as do the results of Spalding and Chi.[20]

PROBLEMS

15-1. Consider fully developed laminar flow between symmetrically heated parallel plates with constant heat rate per unit of duct length. The plate spacing is 1 cm, the fluid is an aircraft engine oil, and the heat flux is 1.4 kW/m^2. The mass velocity G is 600 kg/(s · m^2). At a particular point in question the surface temperature is 110°C. Assuming that the viscosity is the only temperature-dependent property of significance, carry out the necessary calculations (numerical integration is necessary) to evaluate the friction coefficient and the heat-transfer conductance. Compare the results with the recommended procedures given in the text.

15-2. For air as a working substance and using the actual tabulated properties, compare the recommended temperature ratio and reference property schemes for evaluating heat-transfer coefficients and friction coefficients for a laminar boundary layer with constant free-stream velocity for both heating and cooling.

15-3. Repeat Prob. 15-2 but for a turbulent boundary layer with constant free-stream velocity.

REFERENCES

1. Deissler, R. C.: NACA (now NASA) TN 2410, Washington, July 1951.
2. Yang, K. T.: *J. Heat Transfer*, vol. 84, pp. 353–362, 1962.
3. Kays, W. M., and W. B. Nicoll: *J. Heat Transfer*, vol. 85, pp. 329–338, 1963.
4. Davenport, M. E., Ph.D. dissertation, Stanford University, 1962.
5. Worsøe-Schmidt, P. M.: Technical Report 247-8. Thermosciences Division, Department of Mechanical Engineering, Stanford University, November 1964.
6. Petukhov, B. S.: *Advances in Heat Transfer*, vol. 6, Academic Press, pp. 503–564, 1970.
7. Allen, R. W., and E. R. C. Eckert: *J. Heat Transfer*, vol. 86, pp. 301–310, 1964.
8. Rohonczy, G.: *Schweitzer Arch.*, no. 5, 1939.
9. Humble, L. V., W. H. Lowdermilk, and L. G. Desmon: NACA (now NASA) Report 1020, Washington, 1951.
10. McCarthy, J. R., and H. Wolf: Research Report RR-60-12, Rocketdyne Corporation. Canoga Park, California, 1960.
11. Barnes, J. F.: National Gas Turbine Establishment Report R, 241, Pyestock, Hants, England, 1960.
12. Nicoll, W. B., and W. M. Kays: Technical Report 43, Department of Mechanical Engineering, Stanford University, 1959.

13. McEligot, D. M.: Ph.D. dissertation, Stanford University, 1963.

14. Lel'chuk, V. D., and B. V. Dyadyakin: AEC-TR-4511, Atomic Energy Commission Translation, 1962.

15. Brown, W. B., and P. L. Donoughe: NACA (now NASA) TN 2379, Washington, September 1951.

16. Reshotko, E., and C. B. Cohen: NACA (now NASA) TN 3513, Washington, July 1955.

17. Eckert, E. R. G.: *J. Aero. Sci.*, vol. 22, pp. 585–587, 1955.

18. Sleicher, C. A., and M. W. Rouse: *Int. J. Heat Mass Transfer*, vol. 18, pp. 677–683, 1975.

19. Brim, L. H., and R. H. Eustis: ASME Paper 70-HT/SpT-44, 1970.

20. Spalding, D. B., and S. W. Chi: *J. Fluid Mech.*, vol. 18, p. 117, 1964.

16 CHAPTER

Convective Heat Transfer at High Velocities

In all the forced-convection solutions considered up to this point, the velocities and velocity gradients have been assumed sufficiently small that the effects of kinetic energy and viscous energy dissipation could be neglected. We now consider the influence of high velocities and viscous energy dissipation. Although these effects can be of importance in internal tube flow, we are primarily concerned with external boundary layers, where the more important applications appear.

High-velocity convection involves essentially two different phenomena:

1. Conversion of mechanical energy to thermal energy, resulting in temperature variations in the fluid
2. Variation of the fluid properties as a result of the temperature variation

Extremely high velocities in gases like air lead to very high temperatures, dissociation, mass concentration gradients, and thus mass diffusion, which further complicates the problem. However, at present we restrict our attention to the boundary layer with no chemical reaction; this means that for air, at least, we do not deal with temperatures greater than about 2000 K, or Mach numbers greater than about 5.

Generally the high-velocity effects are of most importance in high-speed aerodynamics. However, the effects of the mechanical-to-thermal energy conversion can actually be of considerable importance at quite moderate velocities of a liquid if the Prandtl number is sufficiently high. We restrict attention to fluids with Prandtl number near 1, with primary emphasis on gases.

Much of the literature on high-velocity convection involves a consideration of both mechanical energy conversion and the effects of temperature-dependent fluid properties, so that it is often difficult to see what are the separate effects. Here we first consider the energy conversion problem and then take up the variable-property effects.

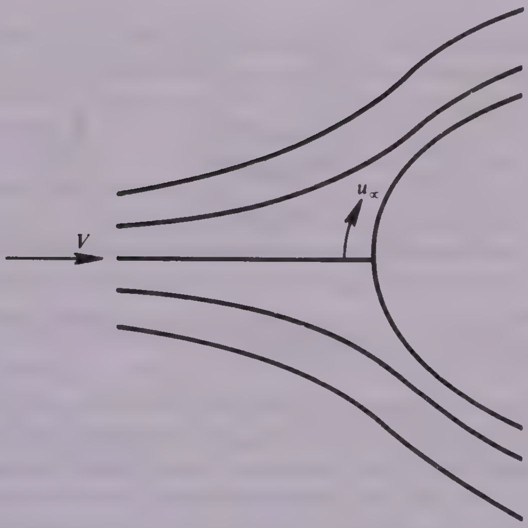

Figure 16-1 Flow at a stagnation point.

The energy conversion process can take place either reversibly or irreversibly. Shock waves and viscous interaction (such as in a boundary layer) give rise to irreversible interchanges of mechanical and thermal energy. Inviscid velocity changes (such as the deceleration of the fluid approaching a subsonic stagnation point) yield reversible, or very nearly reversible, exchanges.

The significant differences in the two types of behavior are well illustrated by a comparison of the stagnation point with the high-speed boundary layer. At a stagnation point (Fig. 16-1) the velocity decreases, and both the pressure and the temperature rise, *outside* the boundary layer. For subsonic flow the process is close to isentropic, and the viscosity of the fluid plays no part.

Regardless of whether the deceleration is reversible or irreversible, the temperature of the fluid *outside* the stagnation-region boundary layer is the *stagnation temperature*, that is, the fluid temperature resulting from an adiabatic deceleration:

$$T_\infty^* = T_\infty + \frac{V^2}{2c} \qquad (16\text{-}1)^\dagger$$

Thus the *high-velocity stagnation-point problem* involves nothing that has not already been discussed. The low-velocity stagnation-point solutions are applicable (although a correction for the influence of temperature-dependent properties may be required), and it is only necessary to replace T_∞ by T_∞^* in the convection rate equation, that is,

$$q_s'' = h(T_s - T_\infty^*) \qquad (16\text{-}2)$$

[†] This equation is valid only as long as the specific heat may be treated as constant.

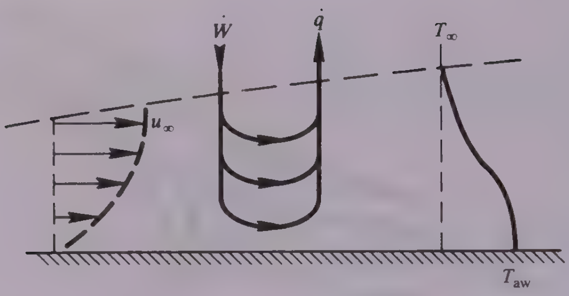

Figure 16-2 Velocity and adiabatic wall-temperature profile in a high-velocity boundary layer.

The *high-velocity boundary-layer problem*, on the other hand, is somewhat different. If the free-stream velocity is large, there will be large velocity gradients *within* the boundary layer and a substantial conversion of mechanical energy to thermal energy by viscous shear within the boundary layer. If we consider for the moment a body that is *insulated*, as in Fig. 16-2, it is apparent that the thermal energy generated can escape from the region close to the surface only by the mechanism of molecular or eddy conduction. In the steady state an equilibrium is established between viscous energy dissipation and heat conduction, and the result is a temperature distribution such as shown in Fig. 16-2. The surface temperature under these conditions is known as the *adiabatic wall temperature* T_{aw}.

It is apparent that determination of this adiabatic wall temperature is going to be of importance in the calculation of heat transfer, since whether heat is transferred to or from the surface must depend on whether the surface temperature is above or below T_{aw}.

It is also apparent that the Prandtl number of the fluid is going to have some bearing on the adiabatic wall temperature. The Prandtl number is the ratio of the viscosity (responsible for the energy dissipation) to the thermal diffusivity (associated with the mechanism whereby heat escapes from the boundary layer). In fact, other things being equal, this argument would suggest that a high Prandtl number should lead to a high adiabatic wall temperature, and that a low Prandtl number should lead to a low adiabatic wall temperature.

We now concentrate attention on the high-velocity *boundary-layer problem* and in particular on high-velocity *gas* flow, so that we are concerned with Prandtl numbers near 1. First we develop a particular form of the energy equation of the boundary layer, and then we consider two special cases that lend themselves to simple and direct solution, before going on to the more general problem.

THE STAGNATION ENTHALPY EQUATION

Referring to Chap. 4, note that two basic forms of the laminar energy equation of the boundary layer are developed. The first, which might be called the *total* energy equation, is Eq. (4-26). The second is Eq. (4-27), followed by some particularizations of it, namely Eqs. (4-37) and (4-38). These latter equations were developed from Eq. (4-26) by combining it with the momentum equation. Equation (4-27) is a *thermal* energy equation, every term representing thermal energy or conversion of mechanical to thermal energy. Actually, we make use of both forms of the energy equation in the developments to follow, and it is well to note that the shear-stress term has a different meaning in the two equations. In Eq. (4-26) it represents work done against viscous forces, part of which is a reversible mechanical work rate and part of which is dissipation into thermal energy. In Eq. (4-27) the viscous term represents conversion of mechanical to thermal energy resulting from the viscous work term, and this term is thus called the *viscous dissipation term.*

Let us first make use of Eq. (4-26) and develop a laminar energy equation with *stagnation enthalpy* as the dependent variable, because at Prandtl numbers at or near 1 this turns out to be a particularly convenient form. Let us neglect work against body forces, internal heat sources, and mass concentration gradients. Then we introduce the *stagnation enthalpy* i^*, the perfect-gas relation between enthalpy and temperature, and the relation between the shear stress and the viscosity coefficient:

$$i^* = i + \tfrac{1}{2}u^2$$

$$di = c\,dT$$

(c is the specific heat at constant pressure)

$$\tau_{yx} = \mu\frac{\partial u}{\partial y}$$

$$\rho u\frac{\partial i^*}{\partial x} + \rho v\frac{\partial i^*}{\partial y} = \frac{\partial}{\partial y}\left(\frac{k}{c}\frac{\partial i}{\partial y}\right) + \frac{\partial}{\partial y}\left(u\mu\frac{\partial u}{\partial y}\right) \tag{16-3}$$

But

$$\frac{\partial i^*}{\partial y} = \frac{\partial i}{\partial y} + u\frac{\partial u}{\partial y} \tag{16-4}$$

We solve for $\partial i/\partial y$ and substitute into Eq. (16-3). After transposing and introducing the definition of the Prandtl number, we obtain

$$\rho u\frac{\partial i^*}{\partial x} + \rho v\frac{\partial i^*}{\partial y} = \frac{\partial}{\partial y}\left(\frac{k}{c}\frac{\partial i^*}{\partial y}\right) + \frac{\partial}{\partial y}\left[\mu\left(1-\frac{1}{\mathrm{Pr}}\right)\frac{\partial(\frac{1}{2}u^2)}{\partial y}\right] \tag{16-5}$$

For *turbulent flows* the boundary-layer form of the stagnation enthalpy equation was developed in Chap. 6, and it can be recast using the same ideas leading to Eq. (16-5) for the laminar boundary layer. Neglecting the body force and source terms in Eq. (6-32), and substituting for the molecular heat flux and shear stress, leads to

$$\begin{aligned}\rho\bar{u}\frac{\partial\bar{i^*}}{\partial x} + \rho\bar{v}\frac{\partial\bar{i^*}}{\partial y} &= \frac{\partial}{\partial y}\left(\frac{k}{c}\frac{\partial\bar{i^*}}{\partial y} - \rho\overline{v'i'}\right)\\ &\quad + \frac{\partial}{\partial y}\left[\mu\left(1-\frac{1}{\mathrm{Pr}}\right)\frac{\partial(\frac{1}{2}\bar{u}^2)}{\partial y} - \rho\overline{u'v'}\,\bar{u}\right]\end{aligned} \tag{16-6}$$

Note that for inclusion of density fluctuation terms in Eq. (16-6), the reader is referred to Cebeci and Smith.[1]

The eddy diffusivity models developed in the previous turbulence chapters can now be applied to Eq. (16-6). First, the turbulent heat flux and Reynolds stress are recast using mean field closure:

$$-\rho\overline{v'i'} = \rho\varepsilon_H \frac{\partial \bar{i}}{\partial y} = \frac{k_t}{c}\frac{\partial \bar{i}}{\partial y} = \frac{k_t}{c}\left[\frac{\partial \overline{i^*}}{\partial y} - \frac{\partial(\frac{1}{2}\bar{u}^2)}{\partial y}\right]$$

$$-\rho\overline{u'v'}\,\bar{u} = \rho\varepsilon_M \frac{\partial(\frac{1}{2}\bar{u}^2)}{\partial y} = \mu_t \frac{\partial(\frac{1}{2}\bar{u}^2)}{\partial y}$$

Then the definitions of effective viscosity, conductivity, and Prandtl number are introduced:

$$k_{\text{eff}} = k + k_t = k + \rho c \varepsilon_H$$

$$\mu_{\text{eff}} = \mu + \mu_t = \mu + \rho\varepsilon_M$$

$$\text{Pr}_{\text{eff}} = \frac{\mu_{\text{eff}}}{k_{\text{eff}}/c} = \frac{1 + \varepsilon_M/v}{1/\text{Pr} + (\varepsilon_M/v)/\text{Pr}_t}$$

Using these, the resulting turbulent boundary-layer equation for the stagnation enthalpy becomes

$$\rho\bar{u}\frac{\partial \overline{i^*}}{\partial x} + \rho\bar{v}\frac{\partial \overline{i^*}}{\partial y} = \frac{\partial}{\partial y}\left(\frac{k_{\text{eff}}}{c}\frac{\partial \overline{i^*}}{\partial y}\right) + \frac{\partial}{\partial y}\left[\mu_{\text{eff}}\left(1 - \frac{1}{\text{Pr}_{\text{eff}}}\right)\frac{\partial(\frac{1}{2}\bar{u}^2)}{\partial y}\right] \tag{16-7}$$

Given a solution to Eq. (16-5) or Eq. (16-7), the heat flux at the surface $\dot{q}''_s$ can be evaluated as follows (for turbulent flows the time-averaged quantities replace the laminar quantities):

$$\dot{q}''_s = -\left(k\frac{\partial T}{\partial y}\right)_s$$

From Eq. (16-4),

$$\left(\frac{\partial i^*}{\partial y}\right)_s = \left(\frac{\partial i}{\partial y}\right)_s = \left(\frac{di}{dT}\frac{\partial T}{\partial y}\right)_s = \left(c\frac{\partial T}{\partial y}\right)_s$$

Thus

$$\dot{q}''_s = -\left(\frac{k}{c}\frac{\partial i^*}{\partial y}\right)_s \tag{16-8}$$

The advantage of this particular formulation of the energy equation for use at Pr near 1 is apparent when one notes that at Pr = 1 the entire right-hand side goes to zero. Further, it is worth noting that, even for a low-velocity flow (where $i^* = i$), it is perfectly feasible to develop convective heat-transfer theory on the basis of enthalpy rather than temperature; and if the specific heat is not constant, this is a more natural formulation. In Chap. 18 such a formulation is introduced since it is particularly useful when mass transfer is present or when there is chemical reaction in the boundary layer. In using Eq. (16-5), or Eq. (16-7), it becomes convenient to define an *enthalpy conductance* g_i as an alternative to the heat-transfer coefficient h:

$$g_i = \frac{[(k/c)\,\partial i^*/\partial y]_s}{i_\infty^* - i_s^*}$$

from which

$$\dot{q}_s'' = g_i(i_s^* - i_\infty^*) \qquad (16\text{-}9)^\dagger$$

Then, if the velocity is low ($i^* = i$) and the specific heat c is constant, the following relation exists between g_i and h:

$$g_i = h/c \qquad (16\text{-}10)$$

THE HIGH-VELOCITY THERMAL BOUNDARY LAYER FOR A FLUID WITH Pr = 1

Let us now examine some particular features of the high-velocity boundary layer by using Eq. (16-5) and considering a fluid with Pr = 1. Let us further assume a fluid with constant specific heat so that we can employ the *stagnation temperature* T^* rather than the stagnation enthalpy; this, in turn, permits some useful comparisons with previously obtained low-velocity solutions.

By definition,

$$T^* = T + \frac{u^2}{2c}$$

Then, with Pr = 1 and c constant, Eq. (16-5) becomes

$$\rho c u \frac{\partial T^*}{\partial x} + \rho c v \frac{\partial T^*}{\partial y} = \frac{\partial}{\partial y}\left(k \frac{\partial T^*}{\partial y}\right) \qquad (16\text{-}11)$$

With Pr = 1 and c constant, μ and k can still be temperature-dependent, although they must be the same functions of temperature. These are reasonable approximations for most gases.

Equation (16-11) is precisely the same as Eq. (15-9), which was developed and solved for a low-velocity boundary layer. One need only replace T by T^* in the solutions. If all properties are treated as constant, Eq. (16-11) becomes identical with Eq. (4-39) or Eq. (10-2), for which solutions already exist.

The preceding argument is based on a laminar boundary layer, but if it is assumed that $\text{Pr}_t = 1$ as well as Pr = 1, the same conclusion is reached for a turbulent boundary layer as for a laminar boundary layer.

Note that the momentum equation is unaffected by viscous dissipation, except insofar as the resulting static temperature distribution affects the fluid properties.

[†] See also the development of Eq. (18-33) in the chapter on mass transfer (Chap. 18).

The boundary conditions for the low-velocity boundary-layer solutions under discussion (the constant-surface-temperature solutions) have been

$$\begin{aligned} &u, v = 0, \quad && T = T_s \quad && \text{at } y = 0 \\ &u \to u_\infty, && T \to T_\infty && \text{as } y \to \infty \\ &u = u_\infty, && T = T_\infty && \text{at } x = 0 \end{aligned}$$

When T is replaced by T^*, the corresponding boundary conditions for Eq. (16-11) are

$$\begin{aligned} &u, v = 0, \quad && T^* = T_s^* \quad && \text{at } y = 0 \\ &u \to u_\infty, && T^* \to T_\infty^* && \text{as } y \to \infty \\ &u = u_\infty, && T^* = T_\infty^* && \text{at } x = 0 \end{aligned}$$

These are, of course, exactly the boundary conditions desired for a constant-temperature plate in a high-velocity stream.

In the low-velocity case the solutions were reduced to a local convection conductance h such that

$$\dot{q}_s'' = -k\left(\frac{\partial T}{\partial y}\right)_s = h(T_s - T_\infty)$$

The corresponding solutions to Eq. (16-11) can be expressed as follows, where h is obviously the same function of the system variables as for the low-velocity case:

$$-k\left(\frac{\partial T^*}{\partial y}\right)_s = h(T_s^* - T_\infty^*)$$

However, $(\partial T^*/\partial y)_s = (\partial T/\partial y)_s$ and $T_s^* = T_s$ because $u = 0$ at $y = 0$. Thus

$$-k\left(\frac{\partial T}{\partial y}\right)_s = \dot{q}_s'' = h(T_s^* - T_\infty^*) \tag{16-12}$$

Evidently we can calculate surface heat-transfer rates, at least for Pr = 1, by merely replacing the free-stream temperature in the convection rate equation by the free-stream stagnation temperature; this, then, is the *major influence of high-velocity viscous dissipation.*

We can now evaluate the adiabatic wall temperature under this condition of Pr = 1 by merely letting $\dot{q}_s'' = 0$ in Eq. (16-12):

$$h(T_s - T_\infty^*) = 0$$

$$T_{\text{aw}} = T_s = T_\infty^* = T_\infty + \frac{u_\infty^2}{2c} \tag{16-13}$$

From these results, a diagram of the temperature distribution in the boundary layer, shown in Fig. 16-3, can be readily constructed.

Since the Prandtl number for all gases does not differ greatly from 1, we really do not expect substantially different results for real gases.

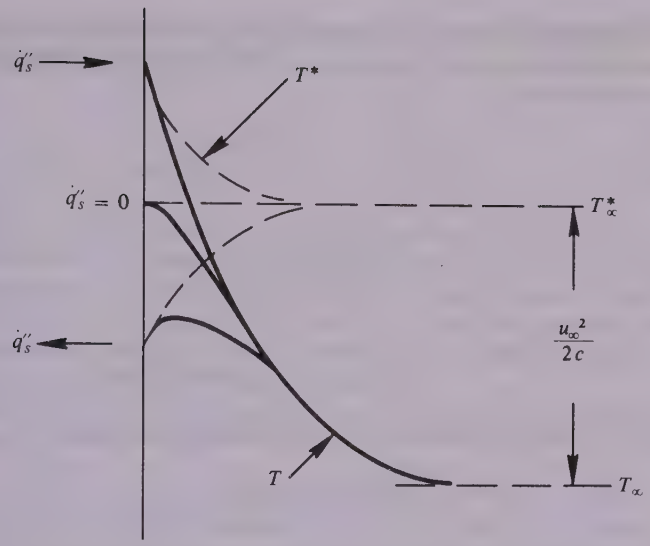

Figure 16-3 Temperature distribution in the high-velocity boundary layer for a fluid with Pr = 1.

THE LAMINAR CONSTANT-PROPERTY BOUNDARY LAYER FOR Pr ≠ 1

Let us now consider the problem of a laminar high-velocity boundary layer on a flat plate with T_∞ and u_∞ constant but with Prandtl number different from 1. So that we may more clearly see the influence of viscous dissipation, and the effect of the Prandtl number on this influence, we consider first the rather hypothetical case of *constant* fluid properties.

The applicable differential equations are the same continuity and momentum equations employed for the corresponding low-velocity problem, Eqs. (9-1) and (9-2), but the energy equation must contain a viscous dissipation term. A convenient form of the energy equation is Eq. (4-38). Thus we have

$$\frac{\partial u}{\partial x} + \frac{\partial v}{\partial y} = 0 \tag{16-14}$$

$$u\frac{\partial u}{\partial x} + v\frac{\partial u}{\partial y} = \nu\frac{\partial^2 u}{\partial y^2} \tag{16-15}$$

$$u\frac{\partial T}{\partial x} + v\frac{\partial T}{\partial y} = \alpha\frac{\partial^2 T}{\partial y^2} + \frac{\alpha\,\mathrm{Pr}}{c}\left(\frac{\partial u}{\partial y}\right)^2 \tag{16-16}$$

Since the continuity and momentum equations are the same as for the low-velocity boundary layer discussed in Chap. 9, and the velocity boundary conditions are likewise the same, it is quite apparent that similarity solutions for the velocity field exist; in fact, the solution is simply Table 9-1.

For the energy equation one is tempted to again seek similarity solutions, employing the same similarity parameter as was used for the momentum equation. If we assume that

$$\zeta = \zeta(\eta), \qquad T = T(\eta)$$

where

$$\eta = \frac{y}{\sqrt{\nu x / u_\infty}}$$

and that

$$u = \frac{\partial \psi}{\partial y}, \qquad v = -\frac{\partial \psi}{\partial x}, \qquad \psi = \sqrt{\nu x u_\infty}\,\zeta$$

then Eq. (16-16) indeed reduces to an ordinary differential equation:

$$T'' + \frac{u_\infty^2}{c} \Pr \zeta''^2 + \tfrac{1}{2} \Pr \zeta T' = 0 \tag{16-17}$$

It is now convenient to define a new dependent variable such that

$$\Theta(\eta) = \frac{T - T_\infty}{u_\infty^2 / 2c} \tag{16-18}$$

Then Eq. (16-17) becomes

$$\Theta'' + \tfrac{1}{2} \Pr \zeta \Theta' + 2 \Pr \zeta''^2 = 0 \tag{16-19}$$

Our first concern is a *particular solution* to Eq. (16-19) for the case where there is an *adiabatic wall*, that is, $\dot{q}_s'' = 0$. We call this solution Θ_{aw}, and the boundary conditions on Eq. (16-19) must then be

$$\Theta(\infty) = 0, \qquad \Theta'(0) = 0$$

Equation (16-19) is a linear equation that is readily solved for Θ_{aw} by use of an integrating factor.

Of special interest is the surface temperature under adiabatic wall conditions, and it is a straightforward process to obtain

$$\Theta_{\text{aw}}(0) = \int_0^\infty \frac{\int_0^\eta \exp\left(\int_0^\eta \frac{1}{2} \Pr \zeta \, d\eta\right) 2 \Pr (\zeta'')^{1/2} \, d\eta}{\exp\left(\int_0^\eta \frac{1}{2} \Pr \zeta \, d\eta\right)} \, d\eta \tag{16-20}$$

Equation (16-20) can be readily integrated numerically for various values of the Prandtl number, employing $\zeta(\eta)$ from Table 9-1. The results (following Pohlhausen[2]) are then in the form of a table of $\Theta_{\text{aw}}(0)$ as a function of Pr. However, in the range of Pr from 0.5 to 10 the solution is quite well represented by

$$\Theta_{\text{aw}}(0) \approx \Pr^{1/2} \tag{16-21}$$

Usually $\Theta_{\text{aw}}(0)$ is known as the *recovery factor* r_c. The adiabatic wall temperature T_{aw} can be evaluated from

$$T_{\text{aw}} = T_\infty + r_c \frac{u_\infty^2}{2c} \tag{16-22}$$

where $r_c \approx \Pr^{1/2}$. Note that at $\Pr = 1$, $r_c = 1$, and Eq. (16-22) reduces to Eq. (16-13).

Next we would like to obtain a complete solution to Eq. (16-19) for any surface temperature. We already have one particular solution, Θ_{aw}, but this, of course, gives us only the temperature field when there is no heat transfer at the surface. We can develop a complete solution if we can find a general solution to the homogeneous part of Eq. (16-19), since then the complete solution is the sum of the general solution and the particular solution.

We already have such a solution from the low-velocity problem. Recall Eq. (10-4):

$$\theta'' + \tfrac{1}{2}\Pr \zeta \theta' = 0$$

We have $\theta(\eta)$ for boundary conditions $\theta(0) = 0$ and $\theta(\infty) = 1$. Then a complete solution to Eq. (16-19) is

$$\Theta = \Theta_{\text{aw}} + C_1\theta + C_2 \tag{16-23}$$

as substitution into Eq. (16-19) readily demonstrates.

We would now like to satisfy the boundary conditions

$$\Theta(\infty) = 0, \qquad \Theta(0) = \frac{T_s - T_\infty}{u_\infty^2/2c}$$

For the first boundary condition,

$$0 = 0 + C_1 \times 1 + C_2, \qquad C_1 = -C_2$$

From the second boundary condition,

$$\frac{T_s - T_\infty}{u_\infty^2/2c} = \Theta_{\text{aw}}(0) + 0 + C_2$$

$$C_2 = \frac{T_s - T_\infty}{u_\infty^2/2c} - \Theta_{\text{aw}}(0)$$

Substituting the constants into Eq. (16-23), and rearranging, gives

$$\Theta = \frac{T - T_\infty}{u_\infty^2/2c} = \Theta_{\text{aw}} + \left(\frac{T_s - T_\infty}{u_\infty^2/2c} - \frac{T_{s,\text{aw}} - T_\infty}{u_\infty^2/2c}\right)(1 - \theta)$$

from which

$$T - T_\infty = \Theta_{\text{aw}} \frac{u_\infty^2}{2c} + (T_s - T_{s,\text{aw}})(1 - \theta)$$

But $T_{s,\text{aw}}$ is simply T_{aw}.

We can now evaluate the heat flux at the surface:

$$\dot{q}_s'' = -k\left(\frac{\partial T}{\partial y}\right)_s$$

$$\frac{\partial T}{\partial y} = \frac{\partial \Theta_{\mathrm{aw}}}{\partial y}\frac{u_\infty^2}{2c} - (T_s - T_{\mathrm{aw}})\frac{\partial \theta}{\partial y}$$

$$\left(\frac{\partial T}{\partial y}\right)_s = 0 - (T_s - T_{\mathrm{aw}})\left(\frac{\partial \theta}{\partial y}\right)_0$$

$$\dot{q}_s'' = -k\left(\frac{\partial T}{\partial y}\right)_s = k(T_s - T_{\mathrm{aw}})\frac{\theta'(0)}{\sqrt{\nu x/u_\infty}}$$

But, from Eqs. (10-9) and (10-10),

$$\theta'(0) = \left[\int_0^\infty \exp\left(-\frac{1}{2}\,\mathrm{Pr}\int_0^\eta \zeta\, d\eta\right) d\eta\right]^{-1} \approx 0.332\,\mathrm{Pr}^{1/3}$$

Then

$$\dot{q}_s'' = k(T_s - T_{\mathrm{aw}})\frac{0.332\,\mathrm{Pr}^{1/3}}{\sqrt{\nu x/u_\infty}}$$

This result immediately suggests that for a high-velocity boundary layer we should define a convection conductance h on the basis of the difference between surface temperature and *adiabatic wall temperature*. This is perfectly consistent with the $\mathrm{Pr} = 1$ results of the preceding section, because in that case $T_{\mathrm{aw}} = T_\infty^*$, and it is also perfectly consistent with the low-velocity problem, since then $T_{\mathrm{aw}} = T_\infty$. Thus let

$$\dot{q}_s'' = h(T_s - T_{\mathrm{aw}}) \tag{16-24}$$

Substituting,

$$h = k\frac{0.332\,\mathrm{Pr}^{1/3}}{\sqrt{\nu x/u_\infty}}$$

or

$$\mathrm{Nu}_x = 0.332\,\mathrm{Pr}^{1/3}\,\mathrm{Re}_x^{1/2} \tag{16-25}$$

Note that this is identical to the low-velocity result given in Eq. (10-10). We see that if fluid properties are constant, the effects of viscous dissipation are entirely taken care of by the simple expedient of substituting T_{aw} for T_∞ in the defining equation for the conductance h. Although we have demonstrated this fact only for the laminar boundary layer with constant u_∞ and T_s, it is actually a far more general conclusion and is applicable also to the turbulent boundary layer. Of course, there remains the problem of evaluating the recovery factor for other situations so that T_{aw} may be determined.

THE LAMINAR BOUNDARY LAYER FOR A GAS WITH VARIABLE PROPERTIES

We first examine an approximate solution and then discuss a more refined analysis. In both cases we consider the case of constant free-stream velocity and constant surface temperature.

If the fluid properties are variable, the three applicable differential equations, corresponding to Eqs. (16-14), (16-15), and (16-16), are

$$\frac{\partial(\rho u)}{\partial x}+\frac{\partial(\rho v)}{\partial y}=0 \tag{16-26}$$

$$\rho u\frac{\partial u}{\partial x}+\rho v\frac{\partial u}{\partial y}=\frac{\partial}{\partial y}\left(\mu\frac{\partial u}{\partial y}\right) \tag{16-27}$$

and, from Eq. (4-37),

$$\rho c u\frac{\partial T}{\partial x}+\rho c v\frac{\partial T}{\partial y}=\frac{\partial}{\partial y}\left(k\frac{\partial T}{\partial y}\right)+\mu\left(\frac{\partial u}{\partial y}\right)^2 \tag{16-28}$$

In Chap. 15 we found that similarity solutions are obtainable from this system of equations when the dissipation term in the energy equation is omitted. Therefore it is suggested that the same change of variables be tried here. Substituting Eqs. (15-10) and (15-11), the momentum and energy equations are found to reduce to the following ordinary differential equations:

$$\frac{d}{d\eta}\left(\frac{\mu\rho}{\mu_\infty\rho_\infty}\frac{d^2\zeta}{d\eta^2}\right)+\frac{1}{2}\zeta\frac{d^2\zeta}{d\eta^2}=0 \tag{16-29}$$

$$\frac{d}{d\eta}\left(k\frac{\rho}{\rho_\infty}\frac{dT}{d\eta}\right)+\frac{\mu\rho}{\rho_\infty}u_\infty^2\left(\frac{d^2\zeta}{d\eta^2}\right)^2+c\mu_\infty\frac{\zeta}{2}\frac{dT}{d\eta}=0 \tag{16-30}$$

If we now make the only slightly restrictive assumption that c is a constant, Eq. (16-30) can be rewritten as

$$\frac{d}{d\eta}\left(\frac{\mu\rho}{\mu_\infty\rho_\infty}\frac{1}{\mathrm{Pr}}\frac{dT}{d\eta}\right)+\frac{\mu\rho}{\mu_\infty\rho_\infty}\frac{u_\infty^2}{c}\left(\frac{d^2\zeta}{d\eta^2}\right)^2+\frac{1}{2}\zeta\frac{dT}{d\eta}=0 \tag{16-31}$$

As a first approximation we could assume $\mathrm{Pr}=$ constant and $\mu\rho=$ constant, as was discussed in Chap. 15. This is not a bad approximation for a gas, but then Eq. (16-29) again becomes the same as Eq. (9-8), the Blasius equation obtained for the corresponding constant-property problem. Equation (16-31) becomes the same as Eqs. (16-17) and (16-19), the constant-property energy equations for high-velocity flow.

Thus, under the assumptions of $\mu\rho=$ constant and $\mathrm{Pr}=$ constant, we find that the solution for constant u_∞ and constant T_s is identical to the corresponding constant-property solution. We can evaluate all properties at free-stream static temperature, and the high-velocity viscous dissipation effects are again entirely taken care of by merely introducing the adiabatic wall temperature into the convection rate equation.

The second approximation to this problem must obviously involve insertion of more nearly correct functions of T/T_∞ for μ/μ_∞ and ρ/ρ_∞ in Eqs. (16-29) and (16-31). Under these conditions, it is not possible to absorb the free-stream velocity in the dependent variable, as was done using Eq. (16-18).

In order to see more clearly the form that the final solution must take, let us introduce a nondimensional free-stream velocity, the Mach number M:

$$\mathrm{M} = \frac{u_\infty}{\sqrt{\gamma R T_\infty}} \tag{16-32}$$

where γ is the ratio of the specific heats and R is the gas constant. Then letting $\theta = T/T_\infty$ and $f(\theta) = \mu\rho/\mu_\infty\rho_\infty$, Eq. (16-31) becomes

$$\frac{d}{d\eta}\left[f(\theta)\frac{1}{\Pr}\frac{d\theta}{d\eta}\right] + f(\theta)\mathrm{M}^2(\gamma-1)\zeta''^2 + \frac{1}{2}\zeta\theta' = 0 \tag{16-33}$$

We then seek the family of solutions $\theta(\eta)$ for the boundary conditions

$$\theta(\infty) = 1, \qquad \theta'(0) = \text{constant}$$

Again an important particular solution θ_{aw} is obtained for the condition $\theta'(0) = 0$. From this a recovery factor can be obtained, defined again by Eq. (16-22).

For the solutions for $\theta'(0)$ other than zero we can evaluate the heat flux at the surface from $\theta'(0)$, define a convection conductance again by Eq. (16-24), and evaluate a Nusselt number. If we refer all fluid [illegible]rties in the Nusselt and Reynolds numbers to free-stream static temperatu[illegible]n readily be shown that

$$\frac{\mathrm{Nu}_{x,\infty}}{\mathrm{Re}_{x,\infty}^{1/2}} = f(\theta(0))\frac{\theta'(0)}{\theta_{\text{aw}}(0) - \theta(0)} \tag{16-34}$$

Since the Mach number, as well as the Prandtl number, is a parameter in Eq. (16-33) and $\theta(0)$ is an additional parameter (uniquely determined by the specification of $\theta'(0)$ as a parameter), it is apparent that the final result is in the form

$$\frac{\mathrm{Nu}_{x,\infty}}{\mathrm{Re}_{x,\infty}^{1/2}} = F\left(\mathrm{M}, \frac{T_s}{T_\infty}, \Pr\right) \tag{16-35}$$

Alternatively, the Mach number can be replaced by T_{aw}/T_∞, since if we combine Eqs. (16-32) and (16-22), we obtain

$$\frac{T_{\text{aw}}}{T_\infty} = 1 + \frac{1}{2}r_c(\gamma - 1)\mathrm{M}^2 \tag{16-36}$$

Thus we can also express the final result as

$$\frac{\mathrm{Nu}_{x,\infty}}{\mathrm{Re}_{x,\infty}^{1/2}} = F\left(\frac{T_{\text{aw}}}{T_\infty}, \frac{T_s}{T_\infty}, \Pr\right) \tag{16-37}$$

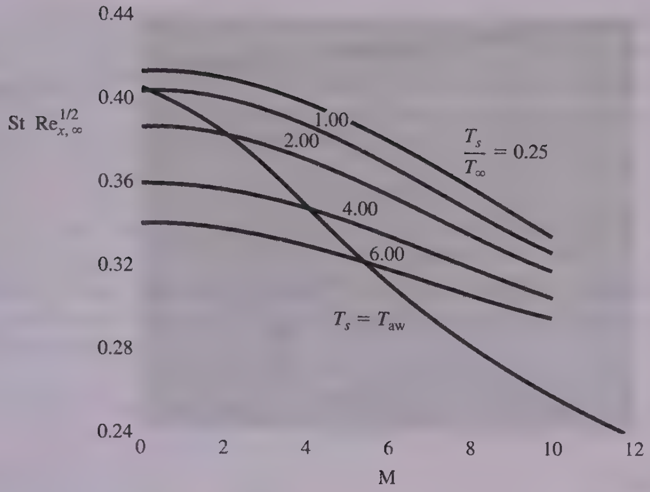

Figure 16-4 Heat transfer to or from the laminar high-velocity boundary layer; air with $\mathrm{Pr} = 0.75$ and $T_\infty = 217.82$ K.

Van Driest[3] presents an extension of a solution to Eqs. (16-29) and (16-33) developed by Crocco. In this method the $\mu\rho =$ constant assumption is used as a first approximation, and a method of successive approximations is employed. The solution is developed for a gas with $\mathrm{Pr} = 0.75$, constant c, $\gamma = 1.40$, and the Sutherland law for viscosity.

Despite the temperature dependence of the fluid properties, it is again found that to a good approximation

$$r_c \approx \mathrm{Pr}^{1/2}$$

The remainder of the solution is shown graphically in Fig. 16-4. (Note that $\mathrm{St}\,\mathrm{Re}_{x,\infty}^{1/2} = \mathrm{Pr}^{-1}\,\mathrm{Nu}_{x,\infty}\,\mathrm{Re}_{x,\infty}^{-1/2}$.) The friction coefficient behaves in the same manner as the Stanton number, except, of course, $(c_f/2)\mathrm{Re}_{x,\infty}^{1/2} = 0.332$ at $\mathrm{M} = 0$ and $T_s/T_\infty = 1$.

Note that the curve for $T_s = T_{\mathrm{aw}}$ is derivable from the others through Eq. (16-36). This tendency of the Stanton number (and the friction coefficient) to decrease with Mach number is quite characteristic of the high-velocity boundary layer for both laminar and turbulent flow when the fluid properties are temperature-dependent. On the other hand, there is no such influence of Mach number when the properties are constant.

These results suggest that the phenomenon under discussion here is basically the same as in the low-velocity, large-temperature-difference problem discussed in Chap. 15. In fact, if T_{aw}/T_∞ is used to replace M through Eq. (16-36), a fair approximation to Fig. 16-4 can be constructed using temperature ratios raised to a power:

$$\frac{\mathrm{St}}{\mathrm{St}_{\mathrm{CP}}} = \left(\frac{T_s}{T_\infty}\right)^{-0.08} \left(\frac{T_{\mathrm{aw}}}{T_\infty}\right)^{-0.04} \qquad (16\text{-}38)$$

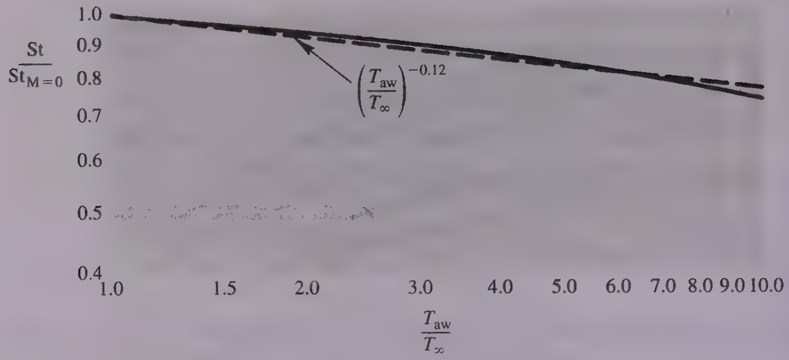

Figure 16-5 Correlation of the results of Fig. 16-4 on a temperature-ratio basis.

or, alternatively,

$$\frac{\mathrm{St}}{\mathrm{St}_{\mathrm{CP}}} = \left(\frac{T_s}{T_{\mathrm{aw}}}\right)^{-0.08}\left(\frac{T_{\mathrm{aw}}}{T_\infty}\right)^{-0.12} \quad \text{for } T_s > T_\infty,\ \mathrm{M} \le 6 \tag{16-38a}$$

For the particular case of $T_s = T_{\mathrm{aw}}$, Eq. (16-38) becomes

$$\frac{\mathrm{St}}{\mathrm{St}_{\mathrm{CP}}} = \left(\frac{T_{\mathrm{aw}}}{T_\infty}\right)^{-0.12} = \left(\frac{T_s}{T_\infty}\right)^{-0.12} \tag{16-39}$$

How well Eq. (16-39) fits Fig. 16-4 is illustrated in Fig. 16-5.

Note that these exponents are small, which is again consistent with the low-velocity, large-temperature-difference problem. However, note that when Eq. (16-38) is reduced to low velocities where $T_{\mathrm{aw}} = T_\infty$, the exponent on T_s/T_∞ is -0.08, whereas in Chap. 15 exponents of -0.01 for heat transfer and -0.10 for friction were suggested. The difference is simply due to the slightly different property variation with temperature used in the two analyses. In dealing with a real gas the most important conclusion is that the effects are small, and Eq. (16-38) is probably as good an approximation as Fig. 16-4.

THE USE OF REFERENCE PROPERTIES FOR HIGH-VELOCITY LAMINAR BOUNDARY-LAYER CALCULATIONS

In the preceding section it was shown that the constant-property boundary-layer solutions can be used for approximate calculation of high-velocity boundary layers by evaluating all properties in the constant-property solutions at free-stream static temperature and then including an empirical temperature-ratio correction in the equations. Many engineers prefer to make this correction by simply evaluating the properties in the constant-property solutions at some *reference temperature* different from the free-stream temperature.

On the basis of examination of a number of "exact" laminar boundary-layer solutions for constant u_∞, T_∞, and T_s, Eckert[4] concludes that if the specific heat may be treated as constant, the following reference temperature correlates the available solutions within a few percent for Mach numbers up to 20 and over a wide range of free-stream and surface temperatures:

$$T_R = T_\infty + 0.5(T_s - T_\infty) + 0.22(T_{\text{aw}} - T_\infty) \tag{16-40}$$

The adiabatic wall temperature T_{aw} is again evaluated from Eq. (16-22), and the recovery factor from Eq. (16-21), but the Prandtl number in Eq. (16-21) is evaluated at T_R. Equations (16-24) and (16-25) are employed, but *all* properties in Eq. (16-25) are evaluated at T_R. In other words, the Reynolds number in Eq. (16-25) becomes

$$\text{Re}_{x,R} = \frac{\rho_R u_\infty x}{\mu_R}$$

and, similarly,

$$\text{Nu}_{x,R} = \frac{hx}{k_R} \quad \text{or} \quad \text{St}_R = \frac{h}{u_\infty \rho_R c}$$

The friction coefficient can be evaluated from the constant-property equation (9-15), but using $\text{Re}_{x,R}$ in place Re_x. The local surface shear stress is evaluated from Eq. (9-12) but with ρ_R replacing ρ.

For very large temperature differences through the boundary layer the assumption of constant specific heat, which has been made in all the preceding solutions and discussion, is no longer valid. It was shown earlier in the development of Eq. (16-5), and the subsequent discussion, that stagnation enthalpy can be used as the dependent variable in the energy equation, and the entire problem can be formulated in terms of enthalpy rather than temperature. If the specific heat cannot be treated as constant, this is a more natural formulation. Eckert's reference property method is again applicable, and, following a development completely analogous to the previous one, we obtain

$$\dot{q}_s'' = g_i(i_s - i_{\text{aw}}) \tag{16-41}$$

where i_{aw} is the adiabatic wall or recovery enthalpy

$$i_{\text{aw}} = i_\infty + \tfrac{1}{2} r_c u_\infty^2, \qquad r_c = \text{Pr}_R^{1/2}$$

and g_i is an enthalpy conductance evaluated from the Stanton number

$$\text{St}_R = \frac{g_i}{\rho_R u_\infty} = \frac{\text{Nu}_R}{\text{Re}_R \, \text{Pr}_R}$$

St_R is the *constant-property* Stanton number evaluated with all properties at a temperature corresponding to a *reference enthalpy* i_R:

$$i_R = i_\infty + 0.5(i_s - i_\infty) + 0.22(i_{\text{aw}} - i_\infty) \tag{16-42}$$

This scheme is thus virtually identical to that based on temperatures.

THE TURBULENT BOUNDARY LAYER FOR A GAS WITH VARIABLE PROPERTIES

Equation (16-7) can be quite readily and satisfactorily solved for a turbulent boundary layer for any desired boundary conditions using the mixing-length theory developed in Chaps. 11 and 12, but with fluid properties *variable*, employing a finite-difference computing technique. For many applications, especially those involving complex boundary conditions, this is undoubtedly the most satisfactory procedure. However, in order to appreciate the influence of high velocity on a turbulent boundary layer, it is useful to examine some results for simple boundary conditions: constant free-stream velocity and constant surface temperature. For this purpose we could examine either some finite-difference solutions of Eq. (16-7) or some of the solutions available in the literature that involve various degrees of approximation.

The semiempirical results of Spalding and Chi[5] are a very thorough and probably accurate summary of the available data on friction coefficient. For heat transfer the results of Deissler and Loeffler[6] are less complete, but are convenient for present purposes and are in reasonably good agreement with experiment.

Deissler and Loeffler reduced the boundary-layer equations to Couette flow form and then used a mixing-length theory for their solution. The Stanton number is determined as a function of the local momentum thickness Reynolds number. The Prandtl number is considered constant at 0.73, the specific heat is held constant, and

$$\frac{\mu}{\mu_s} = \frac{k}{k_s} = \left(\frac{T}{T_s}\right)^{0.68}$$

The analysis covers the Mach number range 0–8 and momentum thickness Reynolds numbers from 10^3 to 10^5, corresponding to length Reynolds numbers from 0.5×10^6 to 0.6×10^9. Only two heat-transfer cases are considered: $T_s \to T_{\text{aw}}$ and $T_s/T_{\text{aw}} = 0.5$.

Both the recovery factor and the Stanton number are determined in the analysis. For Mach numbers from 0 to 8 and Re_x from 10^6 to 10^8, the recovery factor is found to vary from about 0.87 to 0.91. Experimental values for air generally lie in this range. It has been frequently proposed that for a turbulent boundary layer

$$r_c \approx \text{Pr}^{1/3} \qquad (16\text{-}43)$$

This is in reasonably good agreement with Deissler's result.

The Stanton number is strongly affected by the Mach number, but this effect is only slightly dependent on the Reynolds number. The results for $\text{Re}_{\delta_2} = 10^4$ alone are described here. The approximate nature of the analysis probably does not warrant including a Reynolds number influence in the correlations to be proposed.

In Fig. 16-6, $\text{St}/\text{St}_{\text{M}=0}$ is plotted as a function of Mach number for $T_s/T_{\text{aw}} = 0.5$ and 1. Also shown are two experimental test points obtained by Pappas and Rubesin.[7] $\text{St}_{\text{M}=0}$ is the Stanton number at $\text{M} = 0$ at the same

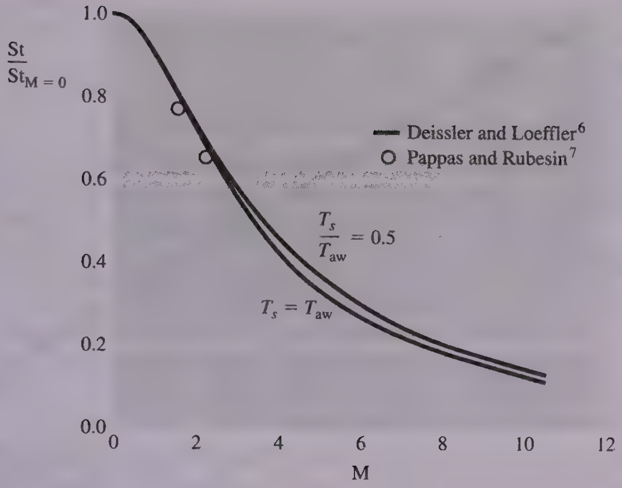

Figure 16-6 Heat transfer to or from the turbulent high-velocity boundary layer; air, $Pr = 0.73$, $Re_{\delta_2} = 10^4$ (analysis of Deissler and Loeffler[6]; data of Pappas and Rubesin[7]).

momentum thickness Reynolds number.[†] The Pappas and Rubesin data are based on a comparison at the same x Reynolds number, but the difference is probably within the experimental uncertainty. Note that the correlation between analysis and experiment is quite good. Calculations by the authors using the mixing-length models discussed in Chaps. 11 and 12 and a finite-difference computer code yield substantially the same results.

Two facts are immediately evident. Although the influence of Mach number is qualitatively similar to that seen for the laminar boundary layer, it is at the same time very much greater. This is quite similar to the effect of temperature-dependent properties at low velocities noted in Chap. 15. Furthermore, the influence of the Mach number is approximately the same regardless of T_s/T_{aw}, although, of course, only two values of T_s/T_{aw} are considered.

The nature of the Mach number influence can be better appreciated if the Mach number is replaced by T_{aw}/T_∞, using Eq. (16-36), and then $St/St_{M=0}$ is plotted as shown in Fig. 16-7.

On logarithmic coordinates the result is very close to a straight line for T_{aw}/T_∞ up to about 7, corresponding to Mach numbers up to about 6.

Of particular interest is the exponent -0.6, which is close to the -0.4 power of T_s/T_∞ that was found in Chap. 15 to correlate most of the large-temperature-difference results for heating. In fact, some experimental *pipe* data for air yield

---

[†] *Enthalpy thickness* Reynolds number is not a very useful parameter for compressible boundary layers because thermal energy is generated within the boundary layer in addition to that transferred to or from the boundary layer at the surface.

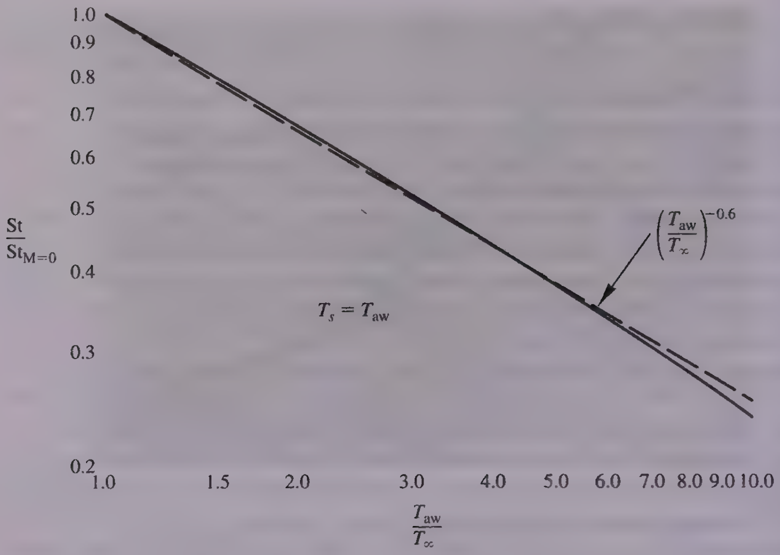

Figure 16-7 Correlation of the results of Fig. 16-6 on a temperature-ratio basis.

exponents as high as −0.575. It thus appears that the Mach number effect for high-velocity convection differs little from the large-temperature-difference effect at low velocities.

The fact that the curve for $T_s/T_{aw} = 0.5$ is very close to the curve for $T_s/T_{aw} = 1$ in Fig. 16-6 suggests that the influence of T_s/T_{aw} can be separately correlated. Since only two points on the curve are available, it is not possible to tell whether a simple power of T_s/T_{aw} would be adequate. However, all our previous experience with these effects suggests that this might be the case. The Deissler and Loeffler results indicate that the ratio of Stanton number to Stanton number at the same Mach number but with $T_s/T_{aw} = 1$ is about 1.32 over the entire Mach number range of the analysis. Then

$$\frac{\mathrm{St}}{\mathrm{St}_{aw}} = \left(\frac{T_s}{T_{aw}}\right)^{-0.4}$$

Finally, putting both the Mach number and surface-temperature effects together, we obtain

$$\frac{\mathrm{St}}{\mathrm{St}_{CP}} = \left(\frac{T_{aw}}{T_\infty}\right)^{-0.6}\left(\frac{T_s}{T_{aw}}\right)^{-0.4} \qquad (16\text{-}44)$$

where all properties in the equation used to evaluate St_{CP} are presumed to be evaluated at the free-stream static temperature.

Examination of Eq. (16-44) indicates that T_{aw} has only a minor influence, and a simplified version of Eq. (16-44) is

$$\frac{\mathrm{St}}{\mathrm{St}_{\mathrm{CP}}} = \left(\frac{T_s}{T_\infty}\right)^{-0.5} \tag{16-45}$$

This is, of course, identical to the correlation recommended in Chap. 15 for a *low*-velocity gas being *heated* in a tube, as well as close to the exponents recommended for an external boundary layer.

The friction coefficient is found to behave in a quite similar manner to the Stanton number, so to a good approximation

$$\frac{c_f}{c_{f\,\mathrm{CP}}} = \frac{\mathrm{St}}{\mathrm{St}_{\mathrm{CP}}} \tag{16-46}$$

REFERENCE PROPERTIES FOR HIGH-VELOCITY TURBULENT BOUNDARY-LAYER CALCULATIONS

As an alternative to the temperature-ratio corrections to the constant-property solutions, in order to account for the influence of temperature-dependent properties, the properties in the constant-property solutions can be introduced at a reference temperature, or a reference enthalpy, as suggested for the laminar boundary layer. Eckert[4] shows that, in fact, the available data can be satisfactorily correlated with the same reference properties as given for the laminar boundary layer. In other words, Eq. (16-40) should be used where the specific heat can be treated as approximately constant, and Eq. (16-42) where it is also temperature-dependent.

MACH NUMBER AND LARGE-TEMPERATURE-DIFFERENCE CORRECTIONS FOR VARIABLE FREE-STREAM VELOCITY AND VARIABLE TEMPERATURE DIFFERENCES

We have considered only the case of a constant free-stream velocity and constant free-stream and surface temperature. In applications where these parameters vary in the flow direction, i.e., in most applications, there is no doubt that direct integration of the momentum and energy equations using finite-difference procedures provides the most direct and accurate route to an engineering solution. For the laminar boundary layer there are no real difficulties, and many computer codes are available. For the turbulent boundary layer there are codes available, but their applicability depends on the adequacy of the turbulence models employed. The authors have found that the turbulence models discussed in Chaps. 11 and 12 are actually quite adequate for Mach numbers up to 3 or 4.

In the absence of finite-difference computer procedures, a reasonable approximation is to use the constant-property procedures discussed in the preceding chapters and then to apply a local correction, i.e., Eq. (16-38) or Eq. (16-44), for the compressible-flow effects. Equation (16-24) should, of course, be used as the defining equation for the heat-transfer coefficient, and Eqs. (16-21) and (16-43) are generally adequate approximations for the recovery factor. Alternatively, the reference property corrections can be used.

Such a procedure is undoubtedly not accurate for a laminar boundary layer, but fortunately we have seen that the influence of the temperature ratio for a typical gas is quite small, so that the accuracy of the correction is not of great importance.

On the other hand, the correction for a turbulent boundary layer can be substantial. But we have seen that, except for very low-Prandtl-number fluids, the turbulent boundary layer responds very quickly to axial changes in boundary conditions. Thus a local correction for the influence of the temperature dependence of the fluid properties appears justified.

Equation (12-16) for a turbulent boundary layer, when corrected as indicated above, has been found to provide a remarkably good approximation for heat transfer in supersonic nozzles.

PROBLEMS

16-1. Consider an aircraft flying at Mach 3 at an altitude of 17,500 m. Suppose the aircraft has a hemispherical nose with a radius of 30 cm. If it is desired to maintain the nose at 80°C, what heat flux must be removed at the stagnation point by internal cooling? As a fair approximation, assume that the air passes through a normal detached shock wave and then decelerates isentropically to zero at the stagnation point; then the flow near the stagnation point is approximated by low-velocity flow about a sphere.

16-2. In Prob. 16-1 it is desired to cool a particular rectangular section of the aircraft body to 65°C. The section is to be 60 cm wide by 90 cm long (in the flow direction) and is located 3 m from the nose. Estimate the total heat-transfer rate necessary to maintain the desired surface temperature. As an approximation, the boundary layer may be treated as if the free-stream velocity were constant along a flat surface for the preceding 3 m. It may also be assumed that the preceding 3 m of surface is adiabatic. To obtain the state of the air just outside the boundary layer, it is customary to assume that the air accelerates from behind the normal shock wave at the nose, isentropically to the free-stream static pressure. In this case the local Mach number then becomes 2.27, and the ratio of local absolute static temperature to free-stream stagnation temperature is 0.49. The local static pressure is the same as the free-stream, that is, the pressure at 17,500 m altitude.

16-3. Consider a laminar constant-property boundary layer on a flat plate with constant free-stream velocity. Evaluate the recovery factor for a fluid with $\mathrm{Pr} = 100$, using Eq. (16-20). The correct answer is 7.63. Why is it difficult to obtain accuracy in solving this problem numerically?

16-4. Consider a supersonic nozzle with radius, mass velocity, temperature, and pressure specified as functions of *axial* distance within the nozzle. The fluid is air. It is desired to maintain the nozzle surface uniformly at 200°C. Calculate the necessary heat flux along the nozzle surface. Assume that a turbulent boundary layer originates at the start of the nozzle.

Axial distance, cm	Radius, cm	Mass velocity, kg/(s · m^2)	Pressure, kPa	T, K
0	9.70	0	2068	893
1.94	8.59	98	2068	893
6.07	6.15	366	2068	891
8.14	4.95	561	2048	890
10.20	3.81	879	2013	886
12.26	2.62	1733	1841	856
13.50	2.13	2734	1262	806
14.33	2.06	2710	931	669
15.15	2.29	1855	331	518
16.39	2.84	1318	172	446
18.45	3.76	928	96.5	380
20.51	4.57	698	62.1	334
22.58	5.28	586	48.3	308
24.64	5.92	464	34.5	287
26.72	6.48	391	27.6	265
28.75	6.99	352	20.7	250
30.81	7.44	322	17.3	237
34.95	8.20	249	13.8	219

16-5. In Prob. 16-4 the nozzle is to be constructed of 0.5-cm-thick stainless-steel walls. The entire nozzle is to be surrounded by a bath of water, maintained at 27°C by constant changing. The heat-transfer coefficient on the water side of the nozzle walls is estimated to be 1100 W/(m^2 · K) uniformly. Calculate the temperature along the inner surface of the nozzle wall and the local heat flux. Assume that heat conduction in the nozzle wall is significant in the radial direction only.

16-6. Repeat Prob. 16-4 but assume that the nozzle is constructed with a uniformly porous wall so that transpiration cooling may be used. Air is available as a coolant at 30°C. Determine the transpiration air rate, as a function of position along the surface, to maintain the surface at 200°C.

16-7. A particular rocket ascends vertically with a velocity that increases approximately linearly with altitude, reaching 3000 m/s at 60,000 m. Consider a point on the cylindrical shell of the rocket 5 m from the nose. Calculate and plot, as functions of altitude, the adiabatic wall temperature, the local convection conductance, and the internal heat flux necessary to prevent the skin temperature from exceeding 50°C (see Prob. 16-2 for remarks about the state of the air just outside the boundary layer in such a situation).

16-8. Consider again Prob. 16-7, but let the skin be of 3-mm-thick stainless steel, insulated on the inner side. Treating the skin as a single element of capacitance, calculate the skin temperature as a function of altitude. [The specific heat of stainless steel is 0.46 kJ/(kg · K).]

16-9. Consider the gas turbine blade on which Prob. 11-8 is based (see Fig. 11-19). It is desired to maintain the blade surface uniformly at 650°C by internal cooling. Calculate the necessary heat flux around the periphery of the blade.

16-10. In Prob. 16-9 the turbine blade is 15-cm-long, and for present purposes it may be assumed that blade dimensions and operating conditions are the same along the entire blade length. It appears feasible to allocate up to 0.03 kg/s of air at 200°C to cool the blade. Assuming a hollow blade of mild-steel construction, a minimum wall thickness of 0.75 mm, and any kind of internal inserts desired (a solid core leaving a narrow passage just inside the outer wall could be used, for example), make a study of the feasibility of internally cooling this blade. Assume that the cooling air can be introduced at the blade root and discharged through the tip. Treat the blade as a simple heat exchanger.

16-11. The gas turbine blade of Prob. 11-8 is to be cooled to a uniform surface temperature of 650°C by transpiration of air through a porous surface. If the cooling air is available at 200°C, calculate the necessary cooling-air mass-transfer rate per unit of surface area as a function of position along the blade surface. Discuss the probable surface temperature distribution if it is mechanically feasible only to provide a transpiration rate that is uniform along the surface.

16-12. Consider the rocket nozzle described in Prob. 11-6 (Fig. 11-18). Calculate the heat flux along the nozzle surface necessary to maintain the surface at 1100°C. If the convergent part of the nozzle is exposed to black-body radiation at 2200°C (the reactor core) and the nozzle surface itself is a black body, will thermal radiation contribute significantly to the heat flux through the nozzle walls?

16-13. Suppose the nozzle of Prob. 16-12 is constructed of 6-mm-thick molybdenum. Copper cooling tubes are then to be wrapped around the nozzle and bonded to the surface. Room-temperature water is available as a coolant. Make a study of the feasibility of water cooling in this manner, after first choosing a tubing size, flow arrangement, and reasonable water velocity.

16-14. The helium rocket nozzle of Probs. 11-6 and 16-12 is to be cooled to a uniform surface temperature of 800°C by transpiration of additional helium that is available at 38°C. Calculate the necessary local transpiration rates if this turns out to be a feasible scheme. What is the total necessary coolant rate? How does this compare with the total hot-helium rate passing through the nozzle?

16-15. Consider again Prob. 12-11, but let the aircraft speed be 300 m/s. At what airspeed does direct cooling become impossible?

REFERENCES

1. Cebeci, T., and A. M. O. Smith: *Analysis of Turbulent Boundary Layers*, pp. 47–79, Academic Press, New York, 1974.
2. Pohlhausen, E.: *Z. Angew. Math. Mech.*, vol. 1, pp. 115–121, 1921.
3. Van Driest, E. R.: NACA (now NASA) TN 2597, Washington, January 1952.
4. Eckert, E. R. G.: *J. Aero. Sci.*, vol. 22, pp. 585–587, 1955.
5. Spalding, D. B., and S. W. Chi: *J. Fluid Mech.* vol. 18, pp. 117–143, 1964.
6. Deissler, R. G., and A. L. Loeffler, Jr.: NACA (now NASA) TN 4262, Washington, April 1958.
7. Pappas, C. C., and M. W. Rubesin: *Heat Transfer and Fluid Mechanics Institute Papers*, pp. 19–28, Stanford University, California, 1953.

CHAPTER 17

Convective Heat Transfer with Body Forces

In Chap. 1 convection was defined as the transport of mass and energy by potential gradients and by bulk fluid motion. If the fluid motion is induced by some external means such as fluid machinery or vehicle motion, the process is generally called *forced convection.* In contrast, fluid motion can also be induced by body forces such as gravitational, centrifugal, or Coriolis forces, and this process is generally called *natural convection.* Natural flows occur in atmospheric and oceanic circulation, electric machinery and nuclear reactor cooling systems, heated or cooled enclosures, electronic power supplies, and so forth. The flow is a buoyancy-induced motion resulting from body forces acting on density gradients, which, in turn, arise from mass concentration and/or temperature gradients in the fluid. In this chapter we consider primarily temperature-induced buoyancy from a single surface within quiescent surroundings. Natural flow on such a surface, unbounded by other surfaces, is usually called *free convection*, and it has many of the characteristics of forced-convection boundary-layer flows.

In this chapter we deal primarily with free-convection solutions which are of boundary layer form, consistent with the treatment for forced convection flows. However, because of the importance of natural convection flows in enclosures, we also briefly summarize some of the recent work on this topic. More in-depth presentations can be found in Ostrach[1] or Ede.[2] An introduction to the various aspects of external natural convection flows is given by Gebhart.[3] For detailed discussions of natural convection in enclosures the reader is referred to Yang[43], Ostrach[44,60] and Catton.[45]

We start with the mass, momentum, and energy equations that govern laminar free-convection boundary-layer flows. We then develop similarity solutions to the equations for constant-wall-temperature, constant-wall-heat-flux, and transpiration boundary conditions, and an approximate integral solution for the constant-wall-temperature case. The effects of variable properties are then discussed. For turbulent free convection we present approximate solutions and recommended correlations based on experimental data. Then, heat-transfer correlations for other geometries are presented, and mixed free and forced convection is discussed. Finally, natural convection in enclosures is briefly discussed.

BOUNDARY-LAYER EQUATIONS FOR FREE CONVECTION

The equations governing external laminar-flow-free convection are essentially the same as those for forced convection. We assume the fluid to be of one species and Newtonian, and the flow field two-dimensional and steady. The applicable equations from Chap. 4 are *continuity*, from Eq. (4-1),

$$\frac{\partial(\rho u)}{\partial x}+\frac{\partial(\rho v)}{\partial y}=0 \tag{17-1}$$

momentum, from Eq. (4-10), including $X=-\rho g$ (a gravitational body force oriented in the negative x direction),

$$\rho u\frac{\partial u}{\partial x}+\rho v\frac{\partial u}{\partial y}=-\frac{dP}{dx}-\rho g+\frac{\partial}{\partial y}\left(\mu\frac{\partial u}{\partial y}\right) \tag{17-2}$$

and *energy*, from Eq. (4-37), assuming constant specific heat. Note that work done against external force fields uX does not appear, because this equation is the combination of the total energy equation and the momentum equation. We also neglect viscous dissipation and the pressure-gradient term:

$$\rho cu\frac{\partial T}{\partial x}+\rho cv\frac{\partial T}{\partial y}=\frac{\partial}{\partial y}\left(k\frac{\partial T}{\partial y}\right) \tag{17-3}$$

The pressure-gradient term in the momentum equation is due to the hydrostatic pressure field outside the boundary layer.[†] From hydrostatics, the gradient is

$$\frac{dP}{dx}=-\rho_\infty g$$

Thus the body force and pressure-gradient terms combine, and the momentum equation becomes

$$\rho u\frac{\partial u}{\partial x}+\rho v\frac{\partial u}{\partial y}=g(\rho_\infty-\rho)+\frac{\partial}{\partial y}\left(\mu\frac{\partial u}{\partial y}\right) \tag{17-4}$$

These equations can be further simplified by making the *Boussinesq approximation* for free-convection flows. It is a two-part approximation: (1) it neglects all variable-property effects in the three equations, except for density in the momentum equation, and (2) it approximates the density difference term with a simplified equation of state. To derive this approximation, the density is expanded into a Taylor series. Because $\rho = \rho(P, T)$, one obtains:

[†] The pressure is assumed to be a function of x. If the gravitational field is not aligned with the principal direction of motion or if the surface is curved or rotating, the pressure field is two-dimensional. For surface inclinations at a small angle γ to the gravitational field, g can usually be replaced by $g\cos\gamma$, the component along the surface.

$$\rho = \rho_\infty + \left(\frac{\partial \rho}{\partial T}\right)_p (T - T_\infty) + \left(\frac{\partial \rho}{\partial P}\right)_T (P - P_\infty) + \cdots$$

Normally, the last term in this equation, which represents the dependence of the density on the pressure difference, can be neglected compared to the other terms. This is especially true for boundary layers, where the pressure is constant across the boundary layer. After introducing the volumetric coefficient of thermal expansion

$$\beta = -\frac{1}{\rho}\left(\frac{\partial \rho}{\partial T}\right)_p$$

one obtains the following simple equation showing the dependence of the density difference on the temperature ratio in the boundary layer

$$\rho_\infty - \rho = \rho\beta(T - T_\infty) \tag{17-5}$$

Note that for ideal gases $\beta = 1/T_\infty$, where T is the absolute temperature in kelvins, and for incompressible liquids $\rho\beta$ is nearly constant. This approximation is good for gravity-induced flows over nearly vertical surfaces with negligible temperature variation of T_∞ with x. For further discussion of these restrictions see Gebhart.[4]

It should be noted here that Eq. (17-5) should not be applied if the dependence between density and temperature is nonlinear in the temperature range of interest. This might be the case if a larger temperature range has to be considered. One other situation where the dependence of the density on the temperature has to be considered by a nonlinear function, also for small temperature differences, is the free convection water flow near 4°C, where a density maximum of the water appears. For such problems it is better to approximate the density difference in Eq. (17-4) directly by a function. For the case of water flow, the water density depends mainly on temperature, and one might use

$$\frac{\rho(T_F)}{\rho(T)} = 1 + a_1\left(\frac{T - T_F}{T_F}\right) + a_2\left(\frac{T - T_F}{T_F}\right)^2 + a_3\left(\frac{T - T_F}{T_F}\right)^3 + a_4\left(\frac{T - T_F}{T_F}\right)^4$$

with the constants

$$a_1 = -0.01854592$$
$$a_2 = +0.67694068$$
$$a_3 = -1.96578728$$
$$a_4 = +4.86372082$$
$$\rho(T_F) = 999.8396 \text{ kg/m}^3$$
$$T_F = 273.15 \text{ K}$$

The above expression approximates the density of water in the range between 0°C and 20°C to about four digits (see Cheng[38]).

If we invoke the Boussinesq approximation, the free-convection equations become

$$\frac{\partial u}{\partial x}+\frac{\partial v}{\partial y}=0 \tag{17-6}$$

$$u\frac{\partial u}{\partial x}+v\frac{\partial u}{\partial y}=g\beta(T-T_\infty)+\nu\frac{\partial^2 u}{\partial y^2} \tag{17-7}$$

$$u\frac{\partial T}{\partial x}+v\frac{\partial T}{\partial y}=\alpha\frac{\partial^2 T}{\partial y^2} \tag{17-8}$$

with boundary conditions

$$\begin{aligned} u,v&=0, & T&=T_s(x) & &\text{at } y=0\\ u&=0, & T&=T_\infty & &\text{as } x=0\\ u&\to 0, & T&\to T_\infty & &\text{as } y\to\infty \end{aligned} \tag{17-9}$$

SCALING AND FLOW REGIMES IN FREE CONVECTION

Before developing specific solutions for free convection boundary layer flows, it is important to investigate the general scaling behavior of the free convective flows and how the flow regimes are defined. This will be done for a free convection flow on a vertical heated plate of length L, which has a constant wall temperature T_s and a constant temperature T_∞ outside the boundary layer. Figure 17-1 shows isotherms around a vertical flat plate as recorded by Eckert and Soehngen[46] using an interferometer. In this figure, the development of the boundary layer at the vertical flat plate can be seen clearly. It is also obvious from Fig. 17-1 that the free convection boundary layer is relatively thick.

The typical shapes of the velocity and the temperature profiles for this problem are shown in Figs. 17-2 and 17-3. Although we will focus on the flow over a vertical flat plate, the results are applicable to all other free convection problems on external surfaces.

In forced convection we find that a length Reynolds number arises when the Navier–Stokes equations are nondimensionalized. For Re → 0 the inertial terms are no longer important and the flow is termed *slow viscous* or "creeping" flow. At moderate Re the flow is still laminar, but viscous and inertial effects are important, and for high Re the flow is turbulent. These same flow regimes are observed in free convection. To define a Reynolds number for free convection, we need a characteristic velocity to describe the inertial forces within the boundary layer. Consider the region of the boundary layer where the velocity profile reaches a maximum. If we ignore the effects of diffusion and cross-stream convection in this region and assume that T can be approximated by T_s, the momentum Eq. (17-7) reduces to

$$\rho U\frac{dU}{dx}=\rho g\beta(T_s-T_\infty)$$

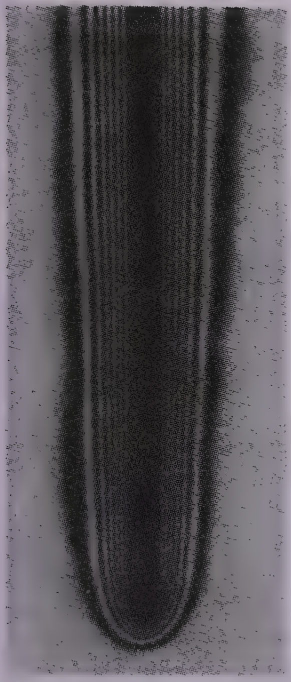

Figure 17-1 Isotherms recorded by a Mach-Zehnder interferometer by Eckert and Soehngen (photograph taken from Ref. 46).

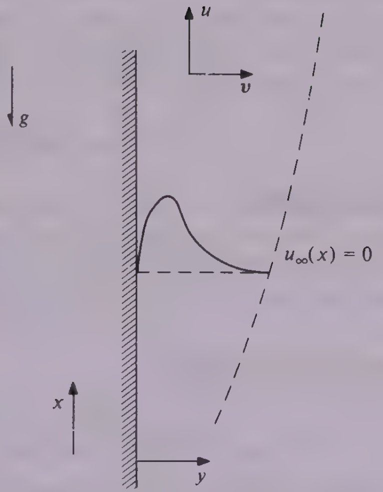

Figure 17-2 Coordinate system and velocity components for a free-convection momentum boundary layer.

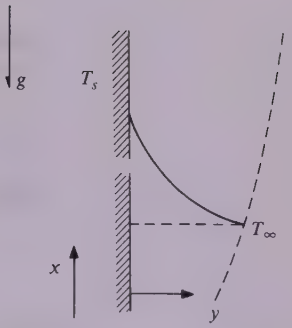

Figure 17-3 A free-convection thermal boundary layer.

This equation relates the convective acceleration of the fluid to the buoyancy driving force. By integrating the equation, we obtain a characteristic velocity for the flow:

$$U \propto \sqrt{g\beta(T_s - T_\infty)x}$$

A Reynolds number for the flow then follows:

$$\mathrm{Re}_x = \frac{Ux}{\nu} = \sqrt{\frac{g\beta(T_s - T_\infty)x^3}{\nu^2}}$$

In order to understand the functional dependence of the solutions for free convective flows, one can introduce dimensionless quantities into the boundary layer equations (17-6)–(17-8). Suitable dimensionless quantities are:

$$\tilde{x} = \frac{x}{L}, \quad \tilde{y} = \frac{y}{L}, \quad \tilde{u} = \frac{u}{U}, \quad \tilde{v} = \frac{v}{U}, \quad \theta = \frac{T - T_\infty}{T_s - T_\infty}, \quad U = \sqrt{g\beta(T_s - T_\infty)L}$$

Here it has been assumed that the characteristic velocity U for $x = L$ is a suitable choice for scaling the velocity components u and v. Introducing these dimensionless quantities into Eqs. (17-6)–(17-9) results in:

$$\frac{\partial \tilde{u}}{\partial \tilde{x}} + \frac{\partial \tilde{v}}{\partial \tilde{y}} = 0 \tag{17-10}$$

$$\tilde{u}\frac{\partial \tilde{u}}{\partial \tilde{x}} + \tilde{v}\frac{\partial \tilde{u}}{\partial \tilde{y}} = \theta + \frac{1}{\sqrt{\mathrm{Gr}_L}}\frac{\partial^2 \tilde{u}}{\partial \tilde{y}^2} \tag{17-11}$$

$$\tilde{u}\frac{\partial \theta}{\partial \tilde{x}} + \tilde{v}\frac{\partial \theta}{\partial \tilde{y}} = \frac{1}{\mathrm{Pr}\sqrt{\mathrm{Gr}_L}}\frac{\partial^2 \theta}{\partial \tilde{y}^2} \tag{17-12}$$

with boundary conditions

$$\begin{aligned} \tilde{u}, \tilde{v} &= 0, \quad \theta = 1 \quad \text{at } \tilde{y} = 0 \\ \tilde{u} &= 0, \quad \theta = 0 \quad \text{as } \tilde{x} = 0 \\ \tilde{u} &\to 0, \quad \theta \to 0 \quad \text{as } \tilde{y} \to \infty \end{aligned} \tag{17-13}$$

and the dimensionless quantity

$$\mathrm{Gr}_L = \frac{g\beta(T_s - T_\infty)L^3}{\nu^2}$$

which is called the *Grashof number*, generally interpreted as the ratio of the buoyancy forces to the viscous forces. Comparing the obtained Grashof number with the free-convection-formulated Reynolds number shows that

$$\mathrm{Re}_L = \sqrt{\mathrm{Gr}_L}$$

Thus the Grashof number can serve as the length Reynolds number for free convection from vertical flat surfaces. For gases and moderate Pr liquids the slow viscous flow regime is generally found below about $\mathrm{Gr}_x = 10^4$. Transition to turbulent flow occurs between $\mathrm{Gr}_x = 10^9$ and 10^{10}, with a tendency toward higher Gr_x for higher Pr. Surface inclination and surface heating rate also affect transition. A discussion of transition phenomena is given by Gebhart.[3]

Frequently the *Rayleigh number*

$$\mathrm{Ra}_x = \mathrm{Gr}_x\mathrm{Pr}$$

is used in place of Gr_x for defining these flow regimes. It also appears in many heat-transfer correlations. However, most experimental evidence indicates that Ra_x does not entirely reflect the Pr dependence. Le Fevre[15] points out that the *Boussinesq number*,

$$\mathrm{Bo} = \mathrm{Gr}_x\mathrm{Pr}^2$$

is the proper functional dependence for large Gr_x or small Pr, one that eliminates the effect of viscosity.

From Eqs. (17-10)–(17-13) it can be seen that the Nusselt number in case of free convective flows with constant fluid properties will depend only on the Grashof (or the Rayleigh) number and on the Prandtl number; thus

$$\mathrm{Nu}_L = f(\mathrm{Gr}_L, \mathrm{Pr}) \quad \text{or} \quad \mathrm{Nu}_L = f(\mathrm{Ra}_L, \mathrm{Pr}) \tag{17-14}$$

The thickness of the boundary layer for free convection flows can be approximated very easily. Because we know that the thickness of the boundary layer, divided by the length scale L, for a laminar forced convective flow over a flat plate is proportional to $1/\sqrt{\mathrm{Re}_L}$, one obtains for free convection

$$\frac{\delta}{L} \propto 1/(\mathrm{Gr}_L)^{1/4}$$

If the velocity outside of the boundary layer u_∞ is nonzero and buoyancy forces are still important, one speaks of a *mixed convection flow.* For such a flow over a flat vertical plate with $u_\infty =$ constant, we could use the following dimensionless quantities to nondimensionalize the boundary layer equations (17-6)–(17-9)

$$\tilde{x} = \frac{x}{L}, \quad \tilde{y} = \frac{y}{L}, \quad \bar{u} = \frac{u}{u_\infty}, \quad \bar{v} = \frac{v}{u_\infty}, \quad \theta = \frac{T - T_\infty}{T_s - T_\infty}, \quad \mathrm{Re}_L = \frac{u_\infty L}{\nu}$$

Introducing these quantities into Eqs. (17-6)–(17-9) results in

$$\frac{\partial \bar{u}}{\partial \tilde{x}} + \frac{\partial \bar{v}}{\partial \tilde{y}} = 0 \tag{17-15}$$

$$\bar{u}\frac{\partial \bar{u}}{\partial \tilde{x}} + \bar{v}\frac{\partial \bar{u}}{\partial \tilde{y}} = \frac{\mathrm{Gr}_L}{\mathrm{Re}_L^2}\theta + \frac{\partial^2 \bar{u}}{\partial \tilde{y}^2} \tag{17-16}$$

$$\bar{u}\frac{\partial \theta}{\partial \tilde{x}} + \bar{v}\frac{\partial \theta}{\partial \tilde{y}} = \frac{1}{\mathrm{Pr}\,\mathrm{Re}_L}\frac{\partial^2 \theta}{\partial \tilde{y}^2} \tag{17-17}$$

with boundary conditions

$$\begin{aligned} \bar{u}, \bar{v} = 0, \quad & \theta = 1 \quad \text{at } \tilde{y} = 0 \\ \bar{u} = 0, \quad & \theta = 0 \quad \text{as } \tilde{x} = 0 \\ \bar{u} \to 1, \quad & \theta \to 0 \quad \text{as } \tilde{y} \to \infty \end{aligned} \tag{17-18}$$

From the above equations one sees that in case of mixed convection flow the Nusselt number depends additionally on the Reynolds number, thus

$$\mathrm{Nu}_L = f(\mathrm{Gr}_L, \mathrm{Pr}, \mathrm{Re}_L) \tag{17-19}$$

Frequently, the relative importance of the free convection effects $(\mathrm{Gr}_L/\mathrm{Re}_L^2)$ is used directly as a dimensionless group.

From the above analyses the differences and similarities of the governing equations for free convection flows compared to forced convection flows with constant fluid properties can be seen clearly.

SIMILARITY SOLUTIONS: LAMINAR FLOW ON A CONSTANT-TEMPERATURE, VERTICAL, AND SEMI-INFINITE FLAT PLATE

One of the earliest analytic and experimental investigations of free convection over isothermal vertical plates was by Schmidt and Beckmann (see Ref. 5). Their experimental results confirm the boundary-layer character of the flow. Figures 17-2 and 17-3 depict the shapes of the velocity and temperature profiles obtained from the experiments.[†]

The experimental profiles suggest the possibility of profile similarity and the possibility that similarity solutions might exist for the governing equations. There are several methods for obtaining these solutions if they exist, and the one outlined here is similar to that used in Chap. 9, leading to the Blasius solution.

Because the continuity, momentum, and energy equations contain the v component of velocity, it becomes convenient to transform the boundary-layer equations by defining a stream function. It is also convenient to nondimensionalize the temperature. Let

$$u = \frac{\partial \psi}{\partial y}, \qquad v = -\frac{\partial \psi}{\partial x}, \qquad \theta = \frac{T - T_\infty}{T_s - T_\infty}$$

Then the momentum equation becomes

$$\frac{\partial \psi}{\partial y}\frac{\partial^2 \psi}{\partial x \partial y} - \frac{\partial \psi}{\partial x}\frac{\partial^2 \psi}{\partial y^2} = g\beta(T_s - T_\infty)\theta + \nu\frac{\partial^3 \psi}{\partial y^3} \tag{17-20}$$

and the energy equation becomes

$$\frac{\partial \psi}{\partial y}\frac{\partial \theta}{\partial x} - \frac{\partial \psi}{\partial x}\frac{\partial \theta}{\partial y} = \alpha\frac{\partial^2 \theta}{\partial y^2} + \theta\frac{\partial \psi}{\partial y}\frac{dT_s}{dx} \tag{17-21}$$

with the boundary conditions

$$\begin{aligned} \frac{\partial \psi}{\partial x}, \frac{\partial \psi}{\partial y} &= 0, \quad \theta = 1 \quad \text{at } y = 0 \\ \frac{\partial \psi}{\partial y} &= 0, \quad \theta = 0 \quad \text{as } x = 0 \\ \frac{\partial \psi}{\partial y} &\to 0, \quad \theta \to 0 \quad \text{as } y \to \infty \end{aligned} \tag{17-22}$$

The premise that the velocity and temperature profiles are geometrically similar, differing only by stretching factors in the x direction, suggests that we define a similarity variable as

$$\eta = y \cdot H(x)$$

[†] Note that Figs. 17-2 and 17-3 depict the case $T_s > T_\infty$, which induces a vertically upward flow. The leading edge of the plate ($x = 0$) is at the bottom and g is in the $-x$ direction. For the case of $T_s < T_\infty$ the buoyancy-induced flow would be downward, with the leading edge at the top. For either case the heat-transfer solutions are identical.

Under the transformation, two partial differential equations for $\psi(x, \eta)$ and $\theta(x, \eta)$ are obtained. The objective now is to reduce these partial differential equations to ordinary differential equations, and a classical technique is to separate variables. Thus we assume

$$\psi(x, \eta) = \nu F(\eta) \cdot G(x) \tag{17-23}$$

Furthermore, we assume that

$$\theta(x, \eta) = \theta(\eta)$$

Introducing the new similarity variable and the stream function into the equations, one obtains the following set of equations

$$\begin{aligned} &H\frac{dH}{dx}G^2(F')^2 + H^2G\frac{dG}{dx}(F')^2 - G\frac{dG}{dx}H^2FF'' \\ &= \frac{g\beta(T_s - T_\infty)}{\nu^2}\theta + H^3GF''' \end{aligned} \tag{17-24}$$

$$\Pr F\frac{dG}{dx}\theta' + H\theta'' = 0 \tag{17-25}$$

where the prime symbol denotes the derivative with respect to η. Because one is interested in finding similar solutions of the momentum and energy equation, all functions that depend on x in Eqs. (17-24)–(17-25) have to drop out. This is possible only if

$$H^3G = \text{constant}$$

$$\frac{dH}{dx}HG^2 = \text{constant}$$

$$H^2G\frac{dG}{dx} = \text{constant}$$

$$\frac{1}{H}\frac{dG}{dx} = \text{constant}$$

From the above four conditions it can be seen that the third condition can be obtained by multiplying the fourth condition by the first condition. Taking the derivative from the first condition and multiplying this equation by $G(x)$, a combination of the second and third condition can be obtained. Satisfying therefore the first and the fourth condition is sufficient. This leads to the following expressions for $G(x)$ and $H(x)$ according to (see Gebhart[4])

$$G(x) = 4\left(\frac{1}{4}\mathrm{Gr}_x\right)^{1/4}$$

$$H(x) = \frac{1}{x}\left(\frac{1}{4}\mathrm{Gr}_x\right)^{1/4}$$

where

$$\mathrm{Gr}_x = \frac{g\beta x^3(T_s - T_\infty)}{\nu^2}$$

is the *Grashof number* based on x.

The ordinary differential equations for $T_s(x) =$ constant become

$$F''' + \theta + 3FF'' - 2F'^2 = 0 \tag{17-26}$$

$$\theta'' + 3\,\mathrm{Pr}\,F\theta' = 0 \tag{17-27}$$

The boundary conditions on these equations transform as follows:

$$y = 0\colon u = 0 = \frac{\partial\psi}{\partial y} = \nu H(x)G(x)F'(0) \qquad \Rightarrow F'(0) = 0$$

$$y = 0\colon v = 0 = \frac{\partial\psi}{\partial x} = \nu(H(x)G(x))'F(0) \qquad \Rightarrow F(0) = 0$$

$$y = 0\colon T = T_s \qquad \Rightarrow \theta(0) = 1$$

$$y \to \infty\colon u \to 0 = \frac{\partial\psi}{\partial y} = \nu H(x)G(x)F'(\infty) \qquad \Rightarrow F'(\infty) \to 0$$

$$y \to \infty\colon T \to T_\infty \qquad \Rightarrow \theta(\infty) \to 0$$

Equations (17-26) and (17-27) are coupled, nonlinear ordinary differential equations that were initially solved by approximate methods. The first complete numerical solution was carried out by Ostrach[6] for a range of Prandtl numbers from 0.01 to 1000. Heat-transfer results from the numerical solution can be defined in terms of a local heat-transfer coefficient

$$h_x = \frac{\dot{q}_s''}{T_s - T_\infty} \qquad \text{(positive } \dot{q}'' \text{ in positive } y \text{ direction)}$$

where

$$\dot{q}_s'' = -k\left(\frac{\partial T}{\partial y}\right)_{y=0} = -k(T_s - T_\infty)\left(\frac{\partial\theta}{\partial y}\right)_{y=0} = -k(T_s - T_\infty)\left(\frac{d\theta}{d\eta}\frac{\partial\eta}{\partial y}\right)_{y=0}$$

$$\dot{q}_s'' = -k(T_s - T_\infty)\theta'(0)H(x)$$

A local Nusselt number is then defined to put h_x into nondimensional form:

$$\mathrm{Nu}_x = \frac{xh_x}{k} = -\theta'(0)xH(x) = -\frac{\theta'(0)}{\sqrt{2}}\mathrm{Gr}_x^{1/4} \tag{17-28}$$

As expected, the local Nusselt number is thus found to be a function of Pr and Gr_x. Solutions for $-\theta'(0)/\sqrt{2}$ from Ostrach and others are presented in Table 17-1. Ede[2] also gives a function that is a very satisfactory correlation to the

Table 17-1 Values of $\mathrm{Nu}_x\mathrm{Gr}_x^{-1/4}$ for various Prandtl numbers; laminar heat transfer to a vertical free-convection boundary layer with $T_s =$ constant, adapted from Refs. 2, 4, 6, and 7

Pr	**0.01**	**0.1**	**0.72**	**1.0**	**10**	**100**	**1000**
$\mathrm{Nu}_x\mathrm{Gr}_x^{-1/4}$	0.0570	0.164	0.357	0.401	0.827	1.55	2.80

entries in this table:

$$\mathrm{Nu}_x = \frac{3}{4}\left[\frac{2\,\mathrm{Pr}}{5(1+2\,\mathrm{Pr}^{1/2}+2\,\mathrm{Pr})}\right]^{1/4}(\mathrm{Gr}_x\,\mathrm{Pr})^{1/4} \tag{17-29}$$

As stated above, Eq. (17-29) can also be expressed by using the Rayleigh number instead of the Grashof number. This results in

$$\mathrm{Nu}_x = \frac{3}{4}\left[\frac{2\,\mathrm{Pr}}{5(1+2\,\mathrm{Pr}^{1/2}+2\,\mathrm{Pr})}\right]^{1/4}\mathrm{Ra}_x^{1/4}$$

Solutions also exist for the limiting cases of Pr → 0 and Pr → ∞. Le Fevre[8] obtained these solutions by transforming Eqs. (17-26) and (17-27). For this, the similarity variable η as well as the stream function F and the temperature θ will be transformed according to

$$\eta_1 = \eta z_1(\mathrm{Pr})$$
$$F_1 = F/z_2(\mathrm{Pr})$$
$$\theta_1 = \theta$$

with the yet unknown scaling coefficients z_1 and z_2. These coefficients shall now be determined in a way that the physical character of the flow for Pr → 0 and Pr → ∞ are apparent. This means that for Pr → 0 the viscous term in the momentum equation becomes unimportant and needs to cancel out, whereas for Pr → ∞ the inertial terms will cancel out of the momentum equation.

Introducing the above quantities into Eq. (17-27) results in

$$\theta_1'' z_1^2 + 3\,\mathrm{Pr}\,\theta_1' F_1 z_1 z_2 = 0$$

where the prime symbol indicates the derivative with respect to η_1. From the above equation it follows that

$$z_2(\mathrm{Pr}) = z_1(\mathrm{Pr})/(3\,\mathrm{Pr})$$

if one wants the equation for θ_1 to not explicitly contain the Prandtl number. Using this result, one obtains from Eq. (17-26) after introducing F, η_1 and θ_1

$$\frac{F_1'''}{3\,\mathrm{Pr}} + \frac{3F_1F_1'' - 2(F_1')^2}{9\,\mathrm{Pr}^2} + \frac{\theta_1}{z_1^4} = 0$$

For this equation Le Fevre[8] determined z_1 to be

$$z_1^4 = \frac{3\,\mathrm{Pr}^2}{1+\mathrm{Pr}}$$

because for this value of z_1 the correct behavior of the momentum equation (17-26) can be guaranteed for Pr → 0 (vanishing effect of the viscous forces, proportional to F_1''') and for Pr → ∞ (vanishing effect of the inertia term, proportional to $3F_1F_1'' - 2(F_1')^2$). One finally obtains

$$\mathrm{Pr}\,(F_1''' + \theta_1) + \theta_1 + F_1F_1'' = \tfrac{2}{3}F_1^2 \tag{17-30}$$

$$\theta_1'' + \theta_1' F_1 = 0 \tag{17-31}$$

In this form the differential equations can be simplified for Pr → 0 and Pr → ∞. One obtains for Pr → 0:

$$\theta_1 + F_1 F_1'' = \tfrac{2}{3} F_1^2$$

$$\theta_1'' + \theta_1' F_1 = 0$$

and for Pr → ∞:

$$F_1''' + \theta_1 = 0$$

$$\theta_1'' + \theta_1' F_1 = 0$$

The solutions of these equations result finally in

$$\mathrm{Nu}_x = \begin{cases} 0.600(\mathrm{Gr}_x\,\mathrm{Pr}^2)^{1/4} = 0.600\,\mathrm{Bo}^{1/4} & \text{as Pr} \to 0 \qquad (17\text{-}32) \\ 0.503(\mathrm{Gr}_x\,\mathrm{Pr})^{1/4} = 0.503\,\mathrm{Ra}^{1/4} & \text{as Pr} \to \infty \qquad (17\text{-}33) \end{cases}$$

These asymptotic results compare favorably with the $\mathrm{Pr} = 0.01$ and $\mathrm{Pr} = 1000$ entries in Table 17-1. They also indicate a variation in the Prandtl number exponent. By plotting $-\theta'(0)/\sqrt{2}$ versus Prandtl number, it can be shown that the $\frac{1}{2}$-power dependence holds to about $\mathrm{Pr} = 0.1$. In addition it is interesting to note that Eqs. (17-32)–(17-33) seem to indicate that for Pr → 0 the Nusselt number depends only on the Boussinesq number, whereas for Pr → ∞ the Nusselt number depends only on the Rayleigh number.

Frequently the total plate heat transfer is of interest rather than the local heat transfer. To calculate the total rate, we need a mean Nusselt number with respect to x. Thus

$$h = \frac{1}{x}\int_0^x h_x\,dx = \frac{1}{x}\int_0^x \frac{k}{x}\left[\frac{-\theta'(0)}{\sqrt{2}}\mathrm{Gr}_x^{1/4}\right]dx$$

$$= \frac{1}{x}\int_0^x \frac{k}{x}Cx^{3/4}\,dx = \frac{4}{3}\frac{k}{x}Cx^{3/4} = \frac{4}{3}h_x$$

or

$$\mathrm{Nu} = \tfrac{4}{3}\mathrm{Nu}_x \qquad (17\text{-}34)$$

The coefficient $\frac{4}{3}$ in Eq. (17-34) for free convection on a vertical surface compares with a coefficient of 2 in Eq. (10-14) for laminar forced convection over a flat plate. This reflects the fact that h varies as $x^{-1/4}$ for free convection, compared with $x^{-1/2}$ for forced convection.

SIMILARITY SOLUTIONS WITH VARIABLE SURFACE TEMPERATURE

Similarity solutions can also be obtained for certain $T_s(x)$ functions. Again the requirement is to have the governing equations reduce to ordinary differential equations. Yang[9] and Sparrow and Gregg[10] have shown that the power-law form of $T_s(x)$ leads to similarity solutions.

Consider the power-law variation

$$T_s - T_\infty = Ax^n$$

For the same method and variables as outlined in the previous section, Eqs. (17-26) and (17-27) become

$$F''' + \theta + (n+3)FF'' - (2n+2)F'^2 = 0 \tag{17-35}$$

$$\theta'' + \Pr[(n+3)F\theta' - 4nF'\theta] = 0 \tag{17-36}$$

with the same boundary conditions

$$F(0) = F'(0) = 0, \qquad \theta(0) = 1$$
$$F'(\infty) = 0, \qquad \theta(\infty) = 0$$

Recall that the wall heat flux is

$$\dot{q}_s'' = -k(T_s - T_\infty)\theta'(0)H(x) = -k(T_s - T_\infty)\frac{\theta'(0)}{\sqrt{2}}\frac{1}{x}\mathrm{Gr}_x^{1/4}$$

$$= k\left(\frac{g\beta}{\nu^2}\right)^{1/4}\frac{-\theta'(0)}{\sqrt{2}}(T_s - T_\infty)^{5/4}\frac{x^{3/4}}{x}$$

$$= C(T_s - T_\infty)^{5/4}x^{-1/4}$$

If $T_s - T_\infty$ now varies as $x^{1/5}$, a constant-heat-flux boundary condition $\dot{q}_s''$ = constant is obtained: The heat flux can be recast in terms of a heat-transfer coefficient and Nusselt number, and Eq. (17-28) is again obtained. Actually, the constant wall temperature is a special case where $n = 0$.

Table 17-2 gives solutions for $-\theta'(0)/\sqrt{2}$ for the constant-heat-flux case. Comparison of the constant-heat-flux values with the constant-wall-temperature values in Table 17-1 reveals that the constant-heat-flux Nusselt number is about 15 percent higher. This compares with ratios of about 36 percent for laminar forced-convection boundary layers. A correlating equation for the entries in Table 17-2 is given by Fujii and Fujii[11] in a form similar to Eq. (17-29):

$$\mathrm{Nu}_x = \left(\frac{\Pr}{4 + 9\Pr^{1/2} + 10\Pr}\right)^{1/5}(\mathrm{Gr}_x^*\Pr)^{1/5} \tag{17-37}$$

In Eq. (17-37) heat-flux data are correlated using a modified Grashof number containing $\dot{q}_s''$ explicitly:

$$\mathrm{Gr}_x^* = \frac{g\beta}{k\nu^2}\dot{q}_s''x^4$$

Table 17-2 Values of $\mathrm{Nu}_x\mathrm{Gr}_x^{-1/4}$ for various Prandtl numbers; laminar heat transfer to a vertical free-convection boundary layer with $\dot{q}_s''$ = constant, adapted from Refs. 2, 4, 6, 7, and 11

Pr	**0.01**	**0.1**	**0.72**	**1.0**	**10**	**100**	**1000**
$\mathrm{Nu}_x\mathrm{Gr}_x^{-1/4}$	0.0669	0.189	0.406	0.457	0.931	1.74	3.14

SIMILARITY SOLUTIONS WITH WALL SUCTION OR BLOWING

Heat-transfer solutions exist for the case of vertical free-convection flow over a porous surface with mass transfer at the wall. As with the variable-surface-temperature problems, the transpired fluid velocity v_s needs to be a particular function of x for similar velocity and temperature profiles. Eichhorn[12] obtained similarity solutions for prescribed $v_s(x)$ and $T_s(x)$. The applicable equations are Eqs. (17-35) and (17-36), with

$$T_s - T_\infty = Ax^n$$

Eichhorn's $v_s(x)$ function that leads to similarity can be derived using the same procedures as in the previous sections. From the stream function definition for v, Eq. (17-23) for ψ, and the previously determined $G(x)$ and $H(x)$ functions, we have

$$v = -\frac{\partial \psi}{\partial x} = -\nu F\frac{dG}{dx} - \nu G\frac{dF}{d\eta}\frac{\partial \eta}{\partial x} = -\nu F\frac{dG}{dx} - \nu GF'y\frac{dH}{dx}$$

At the wall, $y = 0$ and $T_s - T_\infty = Ax^n$:

$$v_s = -\nu F(0)\frac{dG}{dx} = -\nu F(0)\frac{d}{dx}\left[4\left(\frac{\mathrm{Gr}_x}{4}\right)^{1/4}\right]$$

$$= -\frac{\nu}{x}\left(\frac{\mathrm{Gr}_x}{4}\right)^{1/4}(n+3)F(0) \qquad (17\text{-}38)$$

For similarity solutions to exist, the ordinary differential equations and boundary conditions must have constant coefficients. Similarity results if, in Eq. (17-38),

$$F(0) = \text{constant}$$

Therefore

$$v_s \propto \frac{1}{x}\left(\frac{\mathrm{Gr}_x}{4}\right)^{1/4} \propto x^{(n-1)/4}$$

The requirement $F(0) = \text{constant}$ becomes the boundary condition corresponding to $v = v_s$ at $y = 0$. For $F(0) > 0$ there will be wall suction, while $F(0) < 0$ corresponds to blowing. The Nusselt number is exactly the same as for the variable-temperature case:

$$\mathrm{Nu}_x = \frac{-\theta'(0)}{\sqrt{2}}\mathrm{Gr}_x^{1/4}$$

Table 17-3 gives solutions for $-\theta'(0)/\sqrt{2}$ for the constant-wall-temperature boundary condition, $n = 0$, and for $\mathrm{Pr} = 0.73$.

In Table 17-3 we see that blowing reduces heat transfer, while suction has the opposite effect. The blowing limit is $\theta'(0) \to 0$, corresponding to a zero

Table 17-3 Values of $\mathrm{Nu}_x\mathrm{Gr}_x^{-1/4}$ for $\mathrm{Pr} = 0.73$ and wall suction and blowing; laminar heat transfer to a vertical free-convection boundary layer with T_s = constant, adapted from Ref. 12

	Suction			**Blowing**			
***F*(0)**	**+1.0**	**+0.8**	**+0.4**	**0**	**−0.4**	**−0.8**	**−1.0**
$\mathrm{Nu}_x\mathrm{Gr}_x^{-1/4}$	1.55	1.27	0.758	0.359	0.115	0.0187	0.00529

wall-temperature gradient. The suction limit is the case where the wall heat transfer equals the change in enthalpy of the fluid being sucked. These limits correspond to those for the laminar forced-convection case in Chap. 10. However, for the free-convection case, the $\theta'(0) = 0$ limit does not result in a zero wall shear stress because the blowing increases the temperature gradient, and this increases the buoyant driving force, which accelerates and stabilizes the flow. For more discussion see Eichhorn.[12]

APPROXIMATE INTEGRAL SOLUTION: LAMINAR FLOW ON A CONSTANT-TEMPERATURE, VERTICAL, AND SEMI-INFINITE FLAT PLATE

The free-convection integral solution technique can be developed by following the same procedures outlined in Chap. 8 for the forced-convection laminar boundary layer. The idea is to solve the integral momentum and energy equations by assuming velocity and temperature profile shapes and laws for wall shear stress and heat transfer. The resulting differential equations are coupled through the density, and their solutions follow that outlined by Eckert.[13]

The momentum integral equation to be used is Eq. (5-4) with an added body force term, $v_s = u_\infty = 0$, R constant, and the Boussinesq approximation:

$$
\begin{aligned}
-\tau_s &= \frac{d}{dx}\int_0^Y \rho u^2\,dy + Y\frac{dP}{dx} + \int_0^Y \rho g\,dy \\
&= \frac{d}{dx}\int_0^Y \rho u^2\,dy - g\beta\int_0^Y \rho(T - T_\infty)\,dy \qquad (17\text{-}39)
\end{aligned}
$$

The applicable energy integral equation is Eq. (5-13) with the enthalpy $i = c(T - T_\infty)$, $v_s = 0$, R constant, and the Boussinesq approximation:

$$
\dot{q}_s'' = \frac{d}{dx}\int_0^Y \rho u c(T - T_\infty)\,dy = \rho c\frac{d}{dx}\int_0^Y u(T - T_\infty)\,dy \qquad (17\text{-}40)
$$

To solve these equations, we require profile shapes that approximate the velocity and temperature profiles in Figs. 17-2 and 17-3. Eckert assumed the following shapes, along with the assumption that the momentum and thermal

Table 17-4 Comparison between the exact similarity solution for laminar heat transfer to a vertical free-convection boundary layer with T_s = constant with the approximation given by Eq. (17-42)

Pr	0.01	0.1	0.72	1.0	10	100	1000
$\mathrm{Nu}_x\mathrm{Gr}_x^{-1/4}$ (exact)	0.0570	0.164	0.357	0.401	0.827	1.55	2.80
$\mathrm{Nu}_x\mathrm{Gr}_x^{-1/4}$ [Eq. (17-42)]	0.0513	0.159	0.379	0.430	0.883	1.60	2.86

boundary layers are of equal thickness:

$$\frac{u}{U} = \frac{y}{\delta}\left(1-\frac{y}{\delta}\right)^2$$

$$\frac{T-T_\infty}{T_s-T_\infty} = \left(1-\frac{y}{\delta}\right)^2$$

These profiles are substituted into the integral equations, along with Newton's law of viscosity and Fourier's conduction law for τ_s and $\dot{q}_s''$. This results in a set of coupled ordinary differential equations involving the characteristic velocity U and δ. Eckert solved these equations by assuming them to be power-law functions in x. The resulting expression for the boundary-layer thickness is

$$\frac{\delta}{x} = 3.93\left(\frac{0.952+\mathrm{Pr}}{\mathrm{Pr}^2}\right)^{1/4}\mathrm{Gr}_x^{-1/4} \tag{17-41}$$

The expression for δ can now be substituted into the temperature profile to evaluate the wall heat flux, and the resulting Nusselt number is

$$\mathrm{Nu}_x = 0.508\left(\frac{\mathrm{Pr}^2}{0.952+\mathrm{Pr}}\right)^{1/4}\mathrm{Gr}_x^{1/4} = 0.508\left(\frac{\mathrm{Pr}}{0.952+\mathrm{Pr}}\right)^{1/4}\mathrm{Ra}_x^{1/4} \tag{17-42}$$

Table 17-4 compares the values for $\mathrm{Nu}_x\mathrm{Gr}_x^{-1/4}$ from Eq. (17-42) to the exact similarity solution given in Table 17-1. For example, for Pr = 0.72, Eq. (17-42) gives a value for $\mathrm{Nu}_x\mathrm{Gr}_x^{-1/4}$ of 0.379. This result is within 6 percent of the exact similarity solution, as can be seen from Table 17-4.

THE EFFECT OF VARIABLE PROPERTIES

Up to this point, we have considered heat-transfer solutions derived using the Boussinesq approximation, which assumed, in part, that properties except for the density in the momentum equation were constant. From Chap. 15 we know that for gases μ, k, and ρ are functions of the *absolute temperature*. Since the free-convection motion itself is derived from a temperature gradient across the boundary layer, we expect variable properties to influence the Nusselt number.

Clearly the influence of variable properties depends on how μ and k vary with T. We can assume ρ to obey the ideal-gas equation of state, and $\beta = 1/T_\infty$. The simplest case for analysis is the hypothetical ideal gas in which c is constant and μ and k vary directly as T. Sparrow and Gregg[14] studied this problem and showed that the governing equations reduce to the constant-property equations. Thus the $\mathrm{Nu}_x = f(\mathrm{Pr}, \mathrm{Gr}_x)$ relations are exactly the same as those we obtained from the constant-property solutions. An analogous conclusion was obtained for the laminar forced-convection boundary layer in Chap. 15.

Sparrow and Gregg[14] obtained numerical solutions for a number of other hypothetical fluid-property variations. They included $\mu \propto T^{3/4}$ and $k \propto T^{3/4}$, which is close to the 0.8-power law for gases in the moderate temperature range. The major conclusion from their work was that a *reference temperature* could satisfactorily be used to correct the constant-property solutions. They proposed that all properties in the constant-property correlations be evaluated at a reference temperature

$$T_R = T_s - 0.38(T_s - T_\infty) \tag{17-43}$$

For gases they recommend $\beta = 1/T_\infty$ and for low Pr fluids $\beta = 1/T_R$. Later Miyamoto[50] investigated the effect of variable properties on heat transfer for laminar gas flows along a vertical flat plate. He assumed that the fluid properties are such that $\rho \propto T^{-1}$, $\mu \propto T^{\omega}$ and $k \propto T^{\omega}$. Specific heat was assumed to be constant. He suggested for $\mathrm{Pr} = 0.7$ the use of the reference temperature

$$T_R = T_\infty + 0.73(T_s - T_\infty) = T_s - 0.27(T_s - T_\infty) \tag{17-44}$$

for $\omega = 3/4$, $-0.3 < (T_s - T_\infty)/T_\infty < 3$. If the fluid properties are evaluated according to Eq. (17-44), Miyamoto[50] found that the effect of variable properties could satisfactorily be corrected and the constant property solutions can be used. However, almost all Nu_x data and data correlation reported in the open literature, and in this chapter, are formulated using $T_R = 0.5(T_s + T_\infty)$, the average film temperature. For the heat-flux boundary condition, T_R is an unknown. To evaluate Gr_x and Nu_x, the wall temperature must be guessed and iterated until the T_s used in T_R is the same as that calculated from $\dot{q}_s''$ and Nu_x.

TURBULENT FLOW ON A VERTICAL AND SEMI-INFINITE FLAT PLATE

After a certain distance from the leading edge of the vertical plate, the boundary layer becomes unstable. This can be observed in Fig. 17-4, which is a photograph taken with a Mach–Zehnder interferometer by Eckert and Soehngen.[46] The numbers shown in Fig. 17-4 indicate the distance from the leading edge of the plate in inches. It can be observed that as the boundary layer becomes unstable, waves appear, which increase in amplitude for larger distances. Finally, the waves transform into turbulence, which is shown on the photograph in Fig. 17-4.

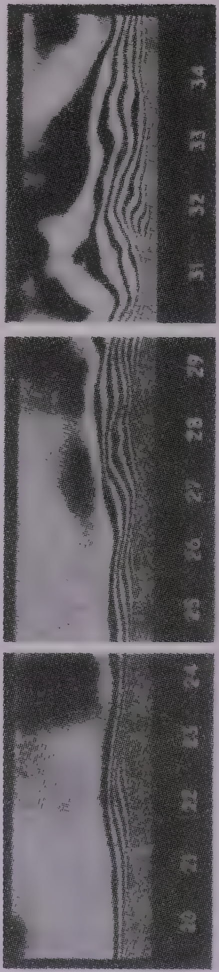

Figure 17-4 Interference photograph of transition to turbulence at a vertical flat plate after Eckert and Soehngen.[46]

An early analysis for the turbulent boundary layer was carried out by Eckert and Jackson[16] using precisely the same technique that Eckert[13] used for laminar free-convection flow. Equations (17-39) and (17-40) are again applicable. According to available experimental velocity and temperature profile data, the profile shapes used by Eckert and Jackson were

$$\frac{u}{U} = \left(\frac{y}{\delta}\right)^{1/7}\left(1 - \frac{y}{\delta}\right)^4$$

$$\frac{T - T_\infty}{T_s - T_\infty} = 1 - \left(\frac{y}{\delta}\right)^{1/7}$$

In these profile shapes U is a characteristic velocity, T_s is constant, and δ is the outer edge of the boundary layer. Note that differentiating the velocity profile gives $u_{\max} = 0.537U$. Thus U is defined to eliminate the constant obtained in curve-fitting the experimental velocity profile data.

To solve the integral equations, the laws for wall shear stress and heat flux need to be modeled. Eckert and Jackson argued that in the near-wall region τ_s would be similar to that for forced convection. The shear-stress law they used follows from the power-law form of the wall law for the near-wall region, Eq. (11-17). Because $u = 0$ at $y = \delta$, Eckert and Jackson used the characteristic velocity U in place of u_∞ at $y = \delta$. The resulting equation for the shear stress becomes

$$\tau_s = 0.0225\rho U^2 \left(\frac{\nu}{U\delta}\right)^{1/4}$$

The wall heat flux is obtained by using an analogy between momentum and heat transfer with a Prandtl number function for fluids with Prandtl numbers near unity:

$$\mathrm{St} = \frac{\dot{q}_s''}{\rho c U (T_s - T_\infty)} = 0.0225 \left(\frac{\nu}{U\delta}\right)^{1/4} \mathrm{Pr}^{-2/3}$$

Solution for the turbulent case follows exactly the solution procedure for the laminar case. The profiles and expressions for τ_s and $\dot{q}_s''$ are substituted into Eqs. (17-39) and (17-40). This results in two ordinary differential equations for U and δ. The equations are solved by assuming the power-law functions

$$U = C_u x^m, \qquad \delta = C_\delta x^n$$

These functions are substituted into the differential equations, and the exponents and constants are obtained directly. The resulting Nusselt number is found to be

$$\mathrm{Nu}_x = 0.0295 \left[\frac{\mathrm{Pr}^7}{(1 + 0.494\,\mathrm{Pr}^{2/3})^6}\right]^{1/15} \mathrm{Gr}_x^{2/5} \tag{17-45}$$

This analysis suggests that h varies as $x^{0.2}$. To obtain an average heat-transfer coefficient, we follow the same procedure used with Eq. (17-34) for the laminar solution, which leads to

$$\mathrm{Nu} = 0.834\,\mathrm{Nu}_x$$

Bailey[17] carried out a turbulent integral analysis using Eqs. (17-39) and (17-40) and the same velocity profile and τ_s expression as Eckert and Jackson. For the temperature profile, and therefore $\dot{q}_s''$, Bailey used a two-layer temperature model with a laminar sublayer out to $y^+ = 15$ and then a constant-diffusivity turbulent region. He found that

$$\begin{aligned} \mathrm{Pr} &= 0.73, & \mathrm{Nu}_x &= 0.10(\mathrm{Gr}_x\mathrm{Pr})^{1/3} \\ \mathrm{Pr} &= 0.01, & \mathrm{Nu}_x &= 0.060\,\mathrm{Gr}_x^{1/4} \end{aligned} \tag{17-46}$$

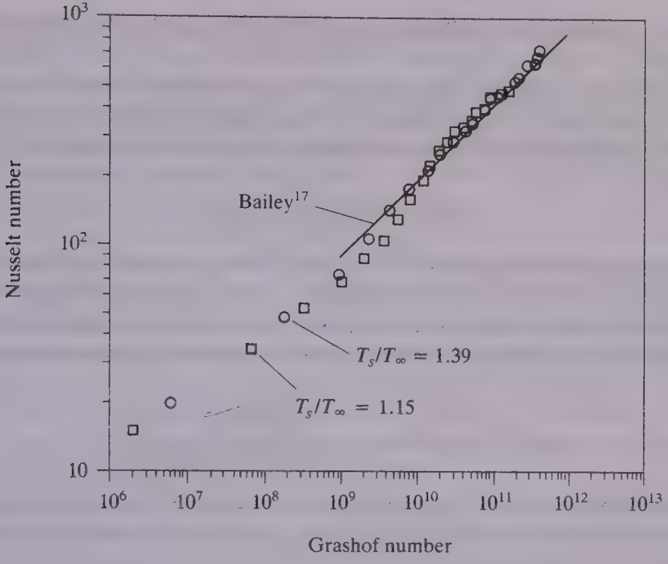

Figure 17-5 Turbulent free convection; air, constant surface temperature (data of Seibers, Schwind, and Moffat[37]).

This analysis suggests that h is independent of x for gases (Pr about unity) and that $\mathrm{Nu} = \mathrm{Nu}_x$.

By comparing the Eckert and Jackson solution with the Bailey solution for air ($\mathrm{Pr} = 0.73$), we find the Bailey solution to consistently predict a lower Nusselt number. Experimental data can be found in the literature to support both analyses. The Eckert and Jackson analysis is supported by Cheesewright,[18] and the data of Warner and Arpaci[19] fit the Bailey correlation. Numerical predictions of turbulent free convection have been reported in the literature, and the prediction trend is for the Nusselt number to lie between the two correlations.

Figure 17-5 shows the experimental data of Seibers, Schwind, and Moffat,[37] together with the Bailey equation for air. These data also show the transition from a laminar free-convection boundary layer to a turbulent free-convection boundary layer, and in addition provide some idea of the effects of temperature-dependent fluid properties on a turbulent free-convection boundary layer. The two sets of data were obtained at wall-to-free-stream temperature ratios of 1.15 and 1.39.

Experimental heat-transfer data for turbulent free convection with a constant wall heat flux have been reported by Vliet and Ross.[20] They found that their air data correlate using

$$\mathrm{Nu}_x = 0.0942(\mathrm{Gr}_x \mathrm{Pr})^{1/3} \tag{17-47}$$

This equation is nearly identical to the Bailey equation and suggests that the Nusselt numbers for a turbulent flow for constant-heat-flux and constant-temperature boundary conditions are similar for gases. The same conclusion is found in forced convection.

A study of numerous sets of experimental data has been carried out by Churchill and Chu.[21] They presented several simple but quite general correlations. The correlations have been developed in terms of the model of Churchill and Usagi[47]

$$\mathrm{Nu}^n\{z\} = \mathrm{Nu}_0^n\{z\} + \mathrm{Nu}_\infty^n\{z\}$$

and require appropriate expressions for the limiting behavior for both large and small values of the independent variable z, which could be, for example, the Rayleigh or Prandtl number. They proposed the following general correlation for the mean Nusselt number for turbulent free convection on an isothermal vertical surface:

$$\mathrm{Nu}^{1/2} = 0.825 + \frac{0.387\,\mathrm{Ra}^{1/3}}{[1 + (0.492/\mathrm{Pr})^{9/16}]^{8/27}} \tag{17-48}$$

The correlation is valid for all Pr and for Gr up to 10^{12}. For a uniform-heat-flux boundary condition Churchill and Chu suggested a very similar correlation for the mean Nusselt number

$$\mathrm{Nu}^{1/2} = 0.825 + \frac{0.387\,\mathrm{Ra}^{1/3}}{[1 + (0.437/\mathrm{Pr})^{9/16}]^{8/27}} \tag{17-49}$$

By comparing Eqs. (17-48) and (17-49), it can be seen that only the coefficient in the denominator of the equation has been changed from 0.492 to 0.437.

HEAT-TRANSFER SOLUTIONS FOR OTHER GEOMETRIES

When heated plates are inclined from the vertical, the buoyancy force can be decomposed into $g \sin \gamma$ and $g \cos \gamma$ components. Here γ is the angle of inclination from the vertical, and $+\gamma$ refers to an upward-facing heated surface (Fig. 17-6b). For this case the density of the fluid is smaller near the heated surface than in the colder free stream, a buoyancy component exists in the direction away from the

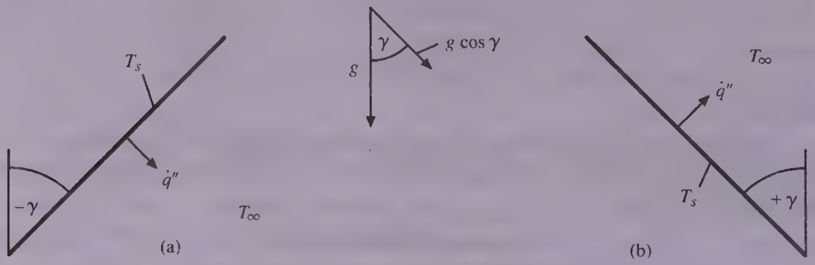

Figure 17-6 Heat transfer at inclined surfaces.

surface, and the flow may become unstable, leading to flow separation. The $-\gamma$ refers to a downward-facing heated flat plate (Fig. 17-6a). Here, no flow separation occurs, because there exists a buoyancy component that pushes the fluid toward the wall. If the plate is cooled, then these cases are reversed: the downward-facing cooled plate gives rise to flow separation, while the upward-facing cooled plate has a stable flow situation. Moran and Lloyd[22] and Fujii and Imura[48] recommend replacing g with $g \cos \gamma$ in the Grashof number,

$$\mathrm{Gr}_\gamma = \mathrm{Gr}_L \cos \gamma$$

and in the vertical-surface Nusselt number correlations can be used in the range from $+20^\circ$ to -60° relative to the vertical. This applies to laminar flow on constant-surface-temperature and constant-heat-flux surfaces for the case where the surface span is wide enough to neglect edge effects. Vliet and Ross[20] indicate that the Nusselt number is independent of angle for turbulent flow and $0^\circ < \gamma < +30^\circ$. For the stable condition, $-80^\circ < \gamma < 0^\circ$, they indicate that the Grashof number should be computed using $g \cos^2 \gamma$.

For completeness, we include results from available experimental data correlations for horizontal surfaces and horizontal and vertical cylinders. The reader is referred to Raithby and Hollands[23] for an approximate integral method for predicting free-convection coefficients for these and numerous other geometries. The concept of local similarity and local nonsimilarity can also be applied to obtain approximate heat-transfer solutions for nonsimilar free-convection boundary layers. For reference to the method (similar to that outlined in Chap. 9) see Minkowycz and Sparrow.[24]

Average Nusselt number correlations for gases over isothermal *horizontal surfaces* with the heated surface facing *upward* are given by Fishenden and Saunders.[25] The Rayleigh numbers in the correlation are based on the length of a square plate:

$$\begin{aligned} \mathrm{Nu} &= 0.54\,\mathrm{Ra}_L^{1/4} && \text{for } 10^5 < \mathrm{Ra}_L < 2 \times 10^7 && \text{(laminar)} \\ \mathrm{Nu} &= 0.14\,\mathrm{Ra}_L^{1/3} && \text{for } 2 \times 10^7 < \mathrm{Ra}_L < 3 \times 10^{10} && \text{(turbulent)} \end{aligned} \tag{17-50}$$

Lloyd and Moran[26] have also studied the horizontal-surface free-convection problem using the heat–mass-transfer analogy, and they find about the same results as those given in Eq. (17-50). The differences are as follows: in the laminar equation the limits are $2.2 \times 10^4 \leq \mathrm{Ra}_L \leq 8 \times 10^8$; in the turbulent equation the coefficient is 0.15 and the limits are $8 \times 10^6 \leq \mathrm{Ra}_L \leq 1.6 \times 10^9$. The length scale in their Grashof number is that developed by Goldstein, Sparrow, and Jones[27]: $L = A/P$, where A is the surface area and P is the surface perimeter. Lloyd and Moran showed that with this definition of L, Eq. (17-50) correlates data for circular, square, rectangular, and right-angled triangular surfaces.

For average Nusselt numbers on isothermal *horizontal cylinders* Kuehn and Goldstein[28] recommend a slightly modified form of the laminar correlation by Churchill and Chu[29] and the turbulent correlation by Fishenden and Saunders[25] for $\mathrm{Ra}_D > 10^9$:

$$\mathrm{Nu}_D = 0.518\left[1+\left(\frac{0.599}{\mathrm{Pr}}\right)^{3/5}\right]^{-5/12}\mathrm{Ra}_D^{1/4} \qquad \text{for } \mathrm{Ra}_D \le 10^9 \quad \text{(laminar)}$$

$$\mathrm{Nu}_D = 0.1\,\mathrm{Ra}_D^{1/3} \qquad \text{for } \mathrm{Ra}_D > 10^9 \quad \text{(turbulent)} \tag{17-51}$$

To account for curvature effects or low Gr_D when the boundary layer is thick compared with the cylinder diameter, the Nusselt number correlation is modified by using

$$\overline{\mathrm{Nu}} = \frac{2}{\ln(1+2/\mathrm{Nu})} \tag{17-52}$$

An extensive survey of free-convection data from horizontal cylinders can be found in a study by Fand, Morris, and Lum[30] for $0.7 < \mathrm{Pr} < 3090$. They also discuss the effects of reference temperature on correlations.

Vertical circular cylinders have average Nusselt numbers that depend on the ratio D/L for the surface and on the number $\mathrm{Gr}_D\,\mathrm{Pr}$. In a study for laminar flow, Sparrow and Gregg[31] conclude that the vertical flat-plate solution is acceptable for air when

$$(\mathrm{Gr}_D\,\mathrm{Pr})^{1/4}\frac{D}{L} > 38 \tag{17-53}$$

Raithby and Hollands[23] recommend Eq. (17-52) to correct the flat-surface Nusselt number for curvature effects or low Gr_D when the boundary layer is thick compared to the cylinder diameter. Note that Eq. (17-52) yields a larger Nusselt number, so the flat-surface value will always be conservative. Ede[2] presents data for turbulent flow on vertical cylinders that indicate a marked increase in Nusselt number for $D/L < 0.05$.

The heat transfer for different orientation of cubes has been studied by Sparrow and Stretton.[49] They performed experiments in water and air, yielding natural convection heat-transfer coefficients for cubes positioned in 13 different orientations in the gravity field. They proposed the following correlation for their results:

$$\mathrm{Nu} = 6.65 + 0.625\left\{\frac{\mathrm{Ra}_{L^*}}{[1+(0.492/\mathrm{Pr})^{9/16}]^{16/9}}\right\}^{0.261} \tag{17-54}$$

where the Nusselt and Rayleigh numbers are based on a new characteristic length

$$L^* = \frac{A}{D^*}, \qquad \pi(D^*)^2/4 = A_{\text{horiz}}$$

This is the same length scale that has been used in Eq. (17-54). L^* is based on the surface area of the body and on the square root of the area projection of the body on the horizontal plane. Equation (17-54) was found to correlate the data of Sparrow and Stretton very well for $200 < \mathrm{Ra}_{L^*} < 10^9$.

MIXED FREE AND FORCED CONVECTION

Combined forced and free convection or mixed free and forced convection flows arise in many transport processes in engineering devices and in nature. Consider the case of upward forced convection over a vertical surface (or vertical tube). If the surface is heated such that $T_s > T_\infty$, the resulting buoyancy force aids the convective motion, especially in the near-wall region, and we would expect the Nusselt number to be greater than the forced-convection value at that Reynolds number. Likewise, for $T_s < T_\infty$ the buoyancy force would oppose the flow, and the Nusselt number is found to decrease. For flow over a horizontal surface a similar enhancement or decrease of the Nusselt number occurs. In this case the buoyancy effect appears as a pressure gradient because the isotherms are not parallel to the surface. Forced convection in heated horizontal tubes can result in enhanced Nusselt numbers if the buoyancy sets up a secondary flow.

Fully established turbulent flows and laminar flows with low Gr have negligible buoyancy effects. *Mixed* convection primarily occurs with laminar and transitional flows and moderate to large Gr, and its onset depends on the relative magnitudes of Gr and Re. A review of mixed convection in internal flows is given by Kays and Perkins[32] and by Aung[42] for external mixed convection flows (see Gebhart[4] and Chen *et al.*[57]).

From Eqs. (17-15)–(17-18) it can be seen that the effects of free convection on the forced convection flow are often expressed by the ratio $\mathrm{Gr}/\mathrm{Re}^2$. Sparrow et al.[39] carried out an analysis of the boundary layer equations, where similarity solutions for combined forced- and free-convection flows have been investigated. The result of their study was that the flow can be classified by using the parameter $\mathrm{Gr}/\mathrm{Re}^2$. For a 5 percent deviation in Nusselt number for the pure (either forced or free) convection flow they obtained the following limits for $\mathrm{Pr} = 0.7$:

$0 < \mathrm{Gr}_x/\mathrm{Re}_x^2 < 0.3$	forced convection flow
$0.3 < \mathrm{Gr}_x/\mathrm{Re}_x^2 < 16$	mixed flow
$16 < \mathrm{Gr}_x/\mathrm{Re}_x^2$	free convection

These criteria were derived for the case of aiding flow. For opposing flow, they obtained

$0 < \mathrm{Gr}_x/\mathrm{Re}_x^2 < 0.3$	forced convection flow
$0.3 < \mathrm{Gr}_x/\mathrm{Re}_x^2$	mixed flow

where no criterion for purely free convection flow was available, since solutions were not obtained beyond the separation point.

Later, Lloyd and Sparrow[33] carried out a local similarity analysis for forced convection over isothermal vertical surfaces with aided buoyancy. They compared $\mathrm{Nu}_x/\mathrm{Re}_x^{1/2}$ with the ratio $\mathrm{Gr}_x/\mathrm{Re}_x^2$ for various Prandtl number fluids to show the effects of buoyancy. For a 5 percent increase in Nusselt number the $\mathrm{Gr}_x/\mathrm{Re}_x^2$ values were 0.24, 0.13, 0.08, and 0.056 at $\mathrm{Pr} = 100$, 10, 0.72, and 0.08. They also presented the effects of buoyancy on velocity and temperature profiles.

Mixed-convection flow on horizontal plates with $\mathrm{Pr} = 0.7$ was studied by Chen *et al.*[34] using local similarity and nonsimilarity analyses. They found that for a heated surface facing upward, a 5 percent increase in Nusselt number occurred when $\mathrm{Gr}_x/\mathrm{Re}_x^{2.5}$ was about 0.05. Their study also shows the effects of buoyancy on velocity and temperature profiles.

An analytical and experimental study of convection heat transfer with buoyancy inside heated horizontal tubes was carried out by Mori and Futagami.[35] For air with $\mathrm{Pr} = 0.72$, they found that the Nusselt number for forced convection begins to increase when the product (Re Gr Pr) exceeds 10^3, with a 50 percent increase by 10^5. The Grashof number is defined using the tube radius, while the Reynolds number is defined in terms of the tube diameter. The main cause of the increased heat transfer is the secondary flow, similar to that found in curved-tube flow. Mixed convection on the external surface of horizontal tubes is discussed by Morgan.[36]

Ramachandran et al.[58] provided a correlation for laminar mixed convection adjacent to an inclined flat plate

$$\mathrm{Nu}_x\,\mathrm{Re}^{-1/2}/F_1(\mathrm{Pr}) = \left\{1 \pm \left[F_2(\mathrm{Pr})\left(\frac{\mathrm{Gr}_x}{\mathrm{Re}_x^2}\cos\gamma\right)^{1/4} \Big/ F_1(\mathrm{Pr})\right]^3\right\}^{1/3} \tag{17-55}$$

$$F_1(\mathrm{Pr}) = 0.332\,\mathrm{Pr}^{1/3},\quad F_2(\mathrm{Pr}) = 0.75\{2\,\mathrm{Pr}^2/[5 + 10(\mathrm{Pr} + \mathrm{Pr}^{1/2})]\}^{1/4}$$

where the angle γ is measured positive from the vertical. This correlation has been obtained by using the concept of Churchill,[59] which is to correlate the mixed convection local Nusselt number Nu_x by using the pure forced convection value Nu_F and the pure free convection value Nu_N as limiting values. These expressions are then combined via

$$\mathrm{Nu}_x^n = \mathrm{Nu}_F^n \pm \mathrm{Nu}_N^n$$

where $n = 3$ has been used and the plus sign denotes buoyancy assisting flow whereas the minus sign denotes buoyancy opposing flow. The obtained correlation by Ramachandran et al.[58] is in good agreement with predictions and measurements for assisting flow and $0.1 < \mathrm{Gr}_x/\mathrm{Re}_x^2 < 7$ and for buoyancy opposing flow and $0.06 < \mathrm{Gr}_x/\mathrm{Re}_x^2 < 0.25$.

Extensive correlations for the Nusselt number in laminar mixed convection inside vertical tubes have been presented by Kessler.[40] These correlations have been developed by numerical calculations for aiding laminar flows, and the derived correlations are in agreement with experimental data from Hallmann.[41] Kessler[40] also included the effect of variable fluid properties into the given correlations for the Nusselt number.

NATURAL CONVECTION IN ENCLOSURES

Natural convection flows in enclosures are good examples of complicated flow types. These flows have a number of technical applications, ranging from cooling of electronic equipment to the thermal design of furnaces to energy storage systems. One of the characteristics of buoyancy-driven flows in enclosures is that for the most part the velocity components are all essentially of the same order of magnitude, except in some subregions of the flow. This means that for the description of such flows, the complete set of conservation equations (Navier–Stokes plus energy equation) has to be used. For most of the technical applications the flow can be considered to be incompressible and the Boussinesq approximation can be made. As the main focus of the present chapter is on boundary-layer-type flows, the natural convection flows in enclosures will be discussed here only very briefly. No attempt will be made to present a complete literature review of the topic, which would by far exceed the scope of the present book. The reader who wants to get a more detailed discussion about the interesting topic of natural convection flows in enclosures is referred to the excellent review articles by Yang,[43] Ostrach,[44] Ostrach,[60] and Catton.[45]

In order to elucidate the large number of geometries that are possibly important in natural convection flows in enclosures, Fig. 17-7 shows some examples of two-dimensional and three-dimensional enclosures from Yang.[43] If the extension of the enclosure in the third dimension is large and the two side walls are thermally insulated, two-dimensional problems are obtained. From Fig. 17-7a to c, the geometry of these enclosures can be described by the height H and the width W. In Fig. 17-7d, a more complex example is shown, where the enclosure contains a vertical partition, and Fig. 17-7e shows an annular enclosure bounded by two concentric cylinders, which are held at different temperatures. In most of the technical applications the enclosures are three-dimensional; Fig. 17-7f to h shows three simple examples of such arrangements. Fig. 17-7h represents a three-dimensional enclosure formed by two eccentric spheres.

The flow in the enclosures is driven by a temperature difference $T_H > T_C$, and the flow structure can be extremely complicated. The flow and heat transfer in a vertical two-dimensional enclosure with $H/W > 1$ (Fig. 17-7b) has been investigated by Mac Gregor and Emery[51] and others. This type of geometry has important application in computing the heat loss through the double-pane window, which is affected by natural convection between the window panels, and in modeling the performance of solar collectors. Mac Gregor and Emery present a schematic diagram showing the Nusselt number behavior for increasing Grashof number in the enclosure with $H/W > 1$. Figure 17-8 shows this diagram, taken from Ref. 51.

As the temperature of the hot wall begins to rise, energy is first transferred to the cold wall by conduction (the conduction regime) and a linear temperature distribution is obtained (see Fig. 17-8). Increasing the temperature difference $(T_H - T_C)$ between the hot and the cold wall for $\mathrm{Ra}_W > 10^3$ (where the Rayleigh number is based on the length scale W) results in a moderate circulation flow that is invariant over most of the height of the enclosure (the asymptotic flow regime). Further increasing the temperature difference so that $\mathrm{Ra}_W > 10^4$ causes the growth of laminar boundary layers, and the heat is primarily transferred by convection in the boundary layer with only very minor heat transferred by conduction through the central core. There are basically three different flow areas in

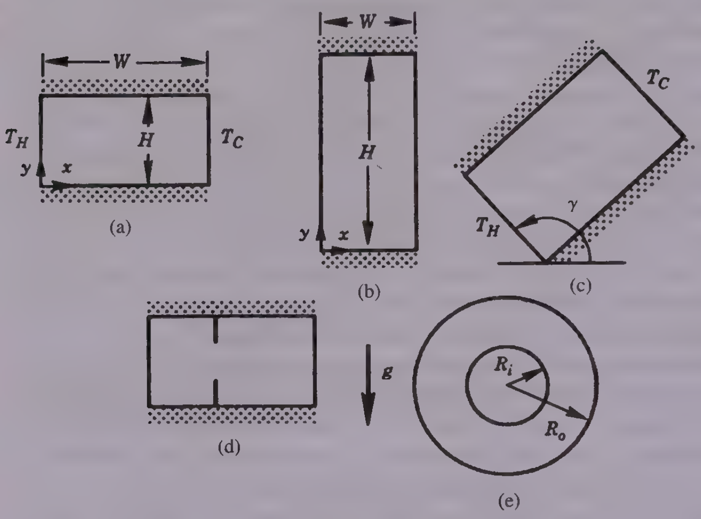

Two-dimensional enclosures

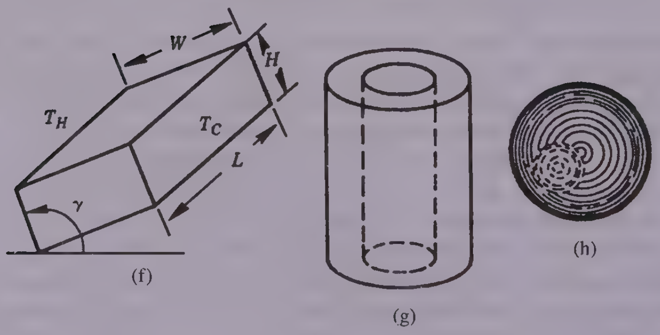

Three-dimensional enclosures

Figure 17-7 Different geometries for two- and three-dimensional enclosures (taken from Yang[43]). This material is used by permission of John Wiley & Sons, Inc.

the enclosure: the wall boundary layers, the central core, and the end areas near the top and the bottom of the enclosure. In the wall area, large temperature gradients are present, and the flow is similar to that of a vertical flat plate. Between $10^6 < \mathrm{Ra}_W < 10^7$, the boundary layers become unstable, and for $\mathrm{Ra}_W > 10^7$, a turbulent flow is established. The whole flow structure and the transition from one flow regime to the other are dependent not only on the Rayleigh number, but also on the aspect ratio H/W (see Yin et al.[52]). Mac Gregor and Emery provided a correlation for the Nusselt number for different aspect ratios for vertical enclosures. For laminar flow they gave the correlation

$$\mathrm{Nu}_W = 0.42(\mathrm{Ra}_W)^{1/4}\,\mathrm{Pr}^{0.012}\left(\frac{H}{W}\right)^{-0.3}, \qquad \dot{q}_s'' = \text{constant} \tag{17-56}$$

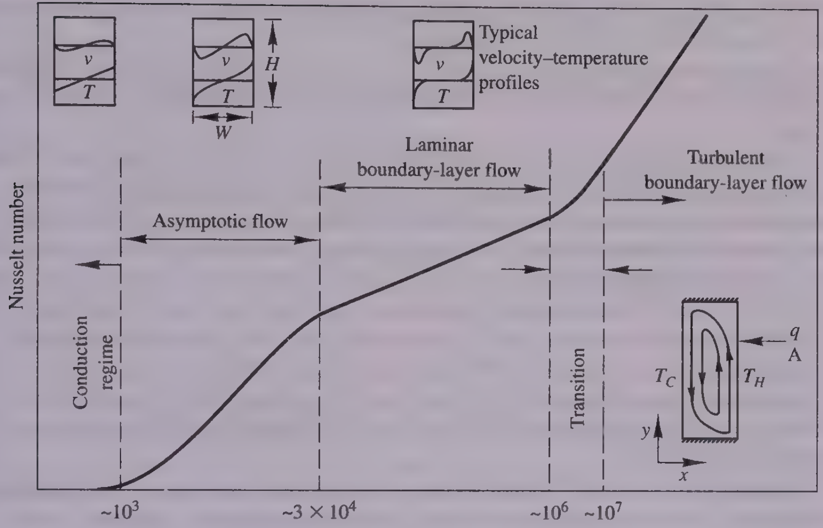

Figure 17-8 Schematic diagram and flow regimes for vertical enclosures with $H/W > 1$ (taken from Mac Gregor and Emery[51]).

which is valid for $10^4 < \mathrm{Ra}_W < 10^7$, $1 < \mathrm{Pr} < 2000$ and $10 < H/W < 40$. For the turbulent regime they recommend

$$\mathrm{Nu}_W = 0.046(\mathrm{Ra}_W)^{1/3}, \quad \dot{q}_s'' = \text{constant} \tag{17-57}$$

which is valid for $10^6 < \mathrm{Ra}_W < 10^9$, $1 < \mathrm{Pr} < 20$ and $1 < H/W < 40$. For both correlations, the Nusselt and the Rayleigh number are based on the characteristic length W and both correlations have been obtained for a constant-heat-flux boundary condition.

Catton[45] noted that Berkovsky and Polevikov provided a correlation, which Catton found in good agreement with experimental data and numerical calculations

$$\mathrm{Nu}_W = 0.18\left(\frac{\mathrm{Pr}}{0.2+\mathrm{Pr}}\right)^{0.29}(\mathrm{Ra}_W)^{0.29} \tag{17-58}$$

which is valid for $1 < H/W < 2$, $10^{-3} < \mathrm{Pr} < 10^5$ and $10^3 < \mathrm{Pr}/(0.2+\mathrm{Pr})\mathrm{Ra}_W$, and

$$\mathrm{Nu}_W = 0.22\left(\frac{\mathrm{Pr}}{0.2+\mathrm{Pr}}\right)^{0.28}\left(\frac{H}{W}\right)^{-1/4}(\mathrm{Ra}_W)^{0.28} \tag{17-59}$$

which is valid for $2 < H/W < 10$, $\mathrm{Pr} < 10^5$ and $\mathrm{Ra}_W < 10^{10}$.

The heat-transfer characteristics in tilted enclosures have been discussed by Yang[43] and Catton.[45] The tilt angle can have a dramatic effect on the flow and heat transfer characteristics. Inaba[53] presented a detailed investigation on tilted enclosures for $5 < H/W < 83$ and inclination angles from $0° < \gamma < 180°$. The flow behavior has been visualized on two orthogonal planes, and correlations for the Nusselt number have been provided.

Horizontal enclosures with $H/W < 1$ have also been extensively investigated in the past. Correlations for the heat transfer can be found, for example, in Yang.[43]

For laminar flow and heat transfer in two-dimensional enclosures for $H/W \gg 1$ and $H/W \ll 1$, many of the physical characteristics could be clarified by asymptotic analysis for the different limiting flow regimes (see for example Graebel,[54] Cormack et al.[55]). A very good review of the different methods used and the available work is given in Yang.[43] However, for gas flows for $H/W = 1$, most of these theories can not be used. Therefore, numerous numerical studies have been carried out for this special case. This also motivated experimentalists to provide very detailed measurements in a square cavity, which can be used as an "experimental benchmark case" for numerical solutions. One of such an example has been provided by Ampofo and Karayiannis[56] for a Rayleigh number of about 10^9.

In contrast to natural convection on a vertical wall, the natural convection in a horizontal fluid layer of finite thickness, heated from below, starts only after a critical temperature gradient is reached. Then, regular cell structures can be observed, which have first been experimentally investigated by Bénard.[61] The related stability problem was solved later by Lord Rayleigh[62] and by Jeffreys.[63] Since then, the Rayleigh-Bénard problem has attracted many researchers because of its importance in understanding the laminar–turbulent transition mechanism and because of its importance for astrophysical and meteorological applications. The reader is referred to Catton[45] for a good review on this topic.

Natural convection between horizontal circular cylinders has many technical applications. A good review of the available literature on this subject is given in Ostrach.[60] Kuehn and Goldstein[28] developed a correlation for heat transfer by conduction, laminar flow, and turbulent flow in the cylindrical, horizontal enclosure, where the two cylinders each have a uniform temperature. Their results approach the correlation for heat transfer from a free horizontal cylinder as the outer cylinder diameter becomes infinite.

Many physical situations of buoyant enclosure flows are three-dimensional, and numerous applications have geometries that are far more complicated than the one shown in Fig. 17-7. Because of the increased complexity of this type of flow, only a limited number of experimental and numerical investigations have been carried out in the past. This is especially true for the important case of turbulent flow in three-dimensional enclosures. The reader is referred to Yang[43] for a discussion of this subject.

PROBLEMS

17-1. Investigate Eq. (17-29) for very large values of Pr. Compare your result to Eq. (17-33). What is your conclusion? What result do you obtain by using Eq. (17-42) instead of Eq. (17-29)?

17-2. Investigate Eq. (17-29) for very small values of Pr. Compare your result to Eq. (17-32). What is your conclusion? What result do you obtain by using Eq. (17-42) instead of Eq. (17-29)?

17-3. Show that the volumetric coefficient of thermal expansion $\beta = -1/\rho(\partial\rho/\partial T)_P$ is equal to $1/T$ for an ideal gas.

17-4. Consider a flat plate surrounded by a fluid at rest (at rest outside the boundary layer) and oriented vertically to a gravity field of strength g. If the plate is heated to a temperature above that of the fluid, the fluid immediately adjacent to the plate will be heated, its density will decrease below that of the surrounding fluid, the resulting buoyancy force will put the fluid in motion, and a free-convection boundary layer will form. If the thermal expansion coefficient for the fluid is defined as

$$\beta = -\frac{1}{\rho}\left(\frac{\partial\rho}{\partial T}\right)_P$$

develop the applicable momentum integral equation of the boundary layer under conditions where the density variation through the boundary layer is small relative to the free-fluid density.

17-5. For laminar flow over a constant-heat-flux surface, develop two expressions for the mean Nusselt number. In the first case base the heat-transfer coefficient on the temperature difference between the average surface temperature and the ambient; in the second case let the temperature difference be the surface minus the ambient at $\frac{1}{2}L$. Compare the two mean Nusselt numbers with those for a constant-wall-temperature surface, Eq. (17-34), at Prandtl numbers of 0.1, 0.72, 1.0, and 100.0, and discuss.

17-6. Develop an analytic solution for the laminar temperature profile and Nusselt number for the case of large wall suction. Start with Eq. (17-36). The final expression will contain n, $F(0)$, and Pr as parameters. Compare this asymptotic expression for Nusselt number with the results in Table 17-3.

17-7. A flat ribbon heat strip is oriented vertically on an insulating substrate. Let the ribbon be 1 m wide by 3 m long. Its energy dissipation is 0.5 W/cm^2 to air at 25°C. What are the average heat-transfer coefficient and surface temperature of the ribbon? Where will transition to turbulent flow occur? Would you be justified in neglecting the laminar contribution to the heat transfer?

17-8. Using the approximate integral solution method for turbulent free convection over a vertical and constant-temperature surface, develop an equation for δ/x. Compare and discuss how the boundary-layer thickness varies with x for laminar and turbulent free and forced convection.

17-9. Consider the free-convection cooling of a thick, square plate of copper with one surface exposed to air and the other surfaces insulated. Let the air temperature be 25°C and the copper temperature be 45°C. The copper is 10 cm on a side. Compare the average heat-transfer coefficients for three exposed face orientations: vertical, inclined 45° to the vertical, and horizontal.

17-10. Consider the wire on a constant-temperature hot-wire anemometer sensor. The wire diameter is 0.00038 cm and its length is 580 diameters. Let the wire temperature be 260°C and the air temperature be 25°C. Compare the heat-transfer coefficients for the wire placed in the horizontal and vertical positions. Note that the effects of the wire support prongs are neglected.

REFERENCES

1. Ostrach, S.: *Theory of Laminar Flows*, pp. 528–615, Princeton University Press, Princeton, NJ, 1964.
2. Ede, A. J.: *Advances in Heat Transfer*, vol. 4, pp. 1–64. Academic Press, New York, 1967.
3. Gebhart, B.: *J. Fluids Engng.*, vol. 101, pp. 5–28, 1979.
4. Gebhart, B.: *Heat Transfer*, 2d ed., pp. 316–402, McGraw-Hill, New York, 1971.
5. Eckert, E. R. G., and E. E. Soehngen: Tech. Rep. 5747, ATI 44580, Air Material Company, Dayton, Ohio, December 1948.
6. Ostrach, S.: NASA Report 1111, Washington, 1953.
7. Sparrow, E. M., and J. L., Gregg: *Trans. ASME*, vol. 78, pp. 435–440, 1956.
8. Le Fevre, E. J.: *Proceedings of 9th International Congress of Applied Mechanics, Brussels, 1956*, vol. 4, pp. 168–174.
9. Yang, K.-T.: *J. Appl. Mech.*, vol. 27, p. 230, 1960.
10. Sparrow, E. M., and J. L. Gregg: *Trans. ASME*, vol. 80, pp. 379–386, 1958.
11. Fujii, T., and M. Fujii: *Int. J. Heat Mass Transfer*, vol. 19, pp. 121–122, 1976.
12. Eichhorn, R.: *J. Heat Transfer*, vol. 82, pp. 260–263, 1960.
13. Eckert, E. R. G.: *Introduction to the Transfer of Heat and Mass*, pp. 158–164. McGraw-Hill, New York, 1950.
14. Sparrow, E. M., and J. K. Gregg: *Trans. ASME*, vol. 80, pp. 879–886, 1958.
15. Le Fevre, E. J.: *Int. J. Heat Mass Transfer*, vol. 19, pp. 1215–1216, 1976.
16. Eckert, E. R. G., and T. W. Jackson: NACA (now NASA) TN 2207, Washington, 1950.
17. Bailey, F. J.: *Proc. Inst. Mech. Engrs*, vol. 169, pp. 361–368, 1955.
18. Cheesewright, R.: *J. Heat Transfer*, vol. 89, pp. 1–8, 1968.
19. Warner, C. Y., and V. S. Arpaci: *Int. J. Heat Mass Transfer*, vol. 11, pp. 397–406, 1968.
20. Vliet, G. C., and D. C. Ross: *J. Heat Transfer*, vol. 97, pp. 549–555, 1975.
21. Churchill, S. W., and H. H. S. Chu: *Int. J. Heat Mass Transfer*, vol. 18, pp. 1323–1329, 1975.
22. Moran, W. R., and J. R. Lloyd: *J. Heat Transfer*, vol. 97, pp. 472–474, 1975.
23. Raithby, G. D., and K. G. T. Hollands: *J. Heat Transfer*, vol. 98, pp. 72–80, 1976.
24. Minkowycz, W. J., and E. M. Sparrow: *J. Heat Transfer*, vol. 96, pp. 178–183, 1974.
25. Fishenden, M., and O. A. Saunders: *An Introduction to Heat Transfer*, Oxford University Press, London, 1950.
26. Lloyd, J. R., and W. R. Moran: *J. Heat Transfer*, vol. 96, pp. 443–447, 1974.
27. Goldstein, R. J., Sparrow, E. M., and D. C. Jones: *Int. J. Heat Mass Transfer*, vol. 16, pp. 1025–1034, 1973.
28. Kuehn, T. H., and R. J. Goldstein: *Int. J. Heat Mass Transfer*, vol. 19, pp. 1127–1134, 1976.
29. Churchill, S. W., and H. H. S. Chu: *Int. J. Heat Mass Transfer*, vol. 18, pp. 1049–1053, 1975.

30. Fand, R. M., Morris, E. W., and M. Lum: *Int. J. Heat Mass Transfer*, vol. 20, pp. 1173–1184, 1977.
31. Sparrow, E. M., and J. L. Gregg: *Trans. ASME*, vol. 78, pp. 1823–1828, 1956.
32. Kays, W. M., and H. C. Perkins: *Handbook of Heat Transfer*, pp. 7-37–7-46, McGraw-Hill, New York, 1973.
33. Lloyd, J. R., and E. M. Sparrow: *Int. J. Heat Mass Transfer*, vol. 13, pp. 434–438, 1970.
34. Chen, T. S., E. M. Sparrow, and A. Mucoglu: *J. Heat Transfer*, vol. 99, pp. 66–71, 1977.
35. Mori, Y., and K. Futagami: *Int. J. Heat Mass Transfer*, vol. 10, pp. 1801–1813, 1967.
36. Morgan, V. T.: *Advances in Heat Transfer*, vol. 11, pp. 199–264, Academic Press, New York, 1975.
37. Seibers, D. L., R. G. Schwind, and R. J. Moffat: Report HMT-36, Thermosciences Division, Department of Mechanical Engineering, Stanford University, February 1983.
38. Cheng, K. C.: *J. of Heat Transfer*, vol. 98, pp. 581–587, 1976.
39. Sparrow, E. M., Eichhorn, R., and J. L. Gregg: *The Physics of Fluids*, vol. 2, pp. 319–328, 1959.
40. Kessler, J.: *Forschung im Ingenieurwesen*, vol. 55, pp. 69–76, 1989.
41. Hallmann, T. M.: *Combined and Free Convection in a Vertical Tube*, Ph.D. Thesis, Purdue University, 1958.
42. Aung, W.: *Mixed Convection in Internal Flows*, Handbook of Single-Phase Convective Heat Transfer, eds. S. Kakac, R. K. Shah, and W. Aung, pp. 15.1–15.51, John Wiley & Sons, New York, 1987.
43. Yang, K. T.: *Natural Convection in Enclosures*, Handbook of Single-Phase Convective Heat Transfer, eds. S. Kakac, R. K. Shah, and W. Aung, pp. 13.1–13.51, John Wiley & Sons, New York, 1987.
44. Ostrach, S.: *Advances in Heat Transfer*, vol. 8, pp. 161–227, Academic Press, New York, 1972.
45. Catton, I.: *Proc. 6th Heat Transfer Conference*, Toronto, vol. 6, pp. 13–31, 1978.
46. Eckert, E. R. G., *Wärme- und Stoffaustausch*, Springer, Berlin, 1959.
47. Churchill, S. W., and R. Usagi: *AICHE Journal*, vol. 18, pp. 1121–1128, 1972.
48. Fujii, T., and H. Imura: *Int. J. Heat Mass Transfer*, vol. 15, pp. 755–767, 1972.
49. Sparrow, E. M., and A. J. Stretton: *Int. J. Heat Mass Transfer*, vol. 28, pp. 741–752, 1985.
50. Miyamoto, M.: *Int. J. Heat Mass Transfer*, vol. 20, pp. 1258–1261, 1977.
51. Mac Gregor, R. K., and A. F. Emery: *J. of Heat Transfer*, vol. 91, pp. 391–402, 1969.
52. Yin, S. H., Wung, T. Y., and K. Chen: *Int. J. Heat Mass Transfer*, vol. 21, pp. 307–315, 1978.
53. Inaba, H.: *Int. J. Heat Mass Transfer*, vol. 27, pp. 1127–1139, 1984.
54. Graebel, W. P.: *Int. J. Heat Mass Transfer*, vol. 24, pp. 125–131, 1981
55. Cormack, D. E., L. G. Leal, and J. Imberger: *J. Fluid Mechanics*, vol. 65, pp. 209–229, 1974.

56. Ampofo, F., and T. G. Karayiannis: *Int. J. Heat Mass Transfer*, vol. 46, pp. 3551–3572, 2003.
57. Chen, T. S., B. F. Armaly, and W. Aung: *Mixed Convection in Laminar Boundary-Layer Flow*, Natural Convection: Fundamentals and Applications, eds. S. Kakac, W. Aung, and R. Viskanta, pp. 699–725, Hemisphere, 1985.
58. Ramachandran, N., B. F. Armaly, and T. S. Chen: *J. Heat Transfer*, vol. 109, pp. 146–150, 1987.
59. Churchill, S. W.: *AICHE Journal*, vol. 23, pp. 10–16, 1977.
60. Ostrach, S.: *J. Heat Transfer*, vol. 110, pp. 1175–1190, 1988.
61. Bénard, H.: *Ann. Chimie Phys.*, vol. 23, p. 61, 1901.
62. Rayleigh, J. W. S., Lord: *Scientific Papers.*, vol. 6, pp. 432–446, 1916.
63. Jeffreys, H.: *Philos. Mag.*, vol. 2, pp. 833–844, 1926.

CHAPTER 18

Convective Mass Transfer: Basic Definitions and Formulation of a Simplified Theory

Convective mass transfer problems play an important role in nature and in many engineering activities. For example: evaporation of water at the surface of the oceans, cooling towers of power stations, ablation cooling for reentry vehicles, combustion processes, or the dissolving of a sugar cube in a cup of coffee. The next three chapters are concerned with fluid systems in which concentration gradients of two or more components of the fluid exist, so that mass diffusion takes place within the fluid. Mass transfer is an extremely large and complex subject, thus these chapters are intended to serve as a convenient introductory route into the subject. After this introduction, the reader who wants to study the fascinating subject of mass transfer in a greater detail might be referred to the books of Spalding[1], Bird, Stewart, Lightfoot[2] or to Mills.[3]

Our primary concern is the calculation of mass- and energy-transfer rates at the interface between a mass-transferring surface and a fluid flow.

The object of this chapter is to introduce the reader to the subject by showing several important definitions and by discussing the general equations for a mass-transfer problem for laminar and turbulent flows and their associated boundary conditions. Furthermore, Chap. 18 will show a simplified theory for predicting mass-transfer rates. Chapter 19 is concerned with the solution of the simplified diffusion equation. Here it will be shown how the mass-transfer conductance can be evaluated. Additionally, the chapter presents analogies between heat and mass transfer. With these analogies, most of the theories and correlations developed in the previous chapters of this book can be used to solve mass-transfer problems. Finally, Chap. 20 is devoted to a number of examples to show the wide range of engineering problems related to convective mass transfer.

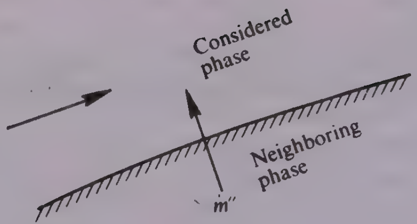

Figure 18-1

DEFINITIONS

Our ultimate concern is with the total rate of mass transfer $\dot{m}''$, kg/(s · m^2), across a phase boundary under steady-flow conditions, as shown in Fig. 18-1. However, in any particular application we may be more interested in a heat-transfer rate, or we may want to consider the heat transfer where there is mass diffusion within the boundary layer but with $\dot{m}'' = 0$. The formulation that we develop is sufficiently general that such problems are merely special cases.

The primary variables within the boundary layer (in addition to the spatial coordinates) are

$m_j = \rho_j / \rho$	mass concentration of component j, kg/kg mixture, where ρ is the density of the mixture, kg/m^3. It follows from this definition that $\sum_j m_j = 1$
$\dot{m}_j'''$	mass-creation rate of component j at some point in the boundary layer due to chemical reaction, kg/(s · m^3). Because of mass conservation, it follows that $\sum_j \dot{m}_j''' = 0$
n_α	mass concentration of element α, kg element α per kg of total mixture.
$n_{\alpha,j}$	a constant fixed by the chemical formula for compound j, (kg of element α)/(kg of substance j). From the above definitions it follows: $n_\alpha = \sum_j n_{\alpha,j} m_j$ For example: $n_{\mathrm{C,CO}} = 12/30$ and $n_{\mathrm{C,C}} = 1/1$ $\sum_\alpha n_\alpha = 1, \quad \sum_j n_{\alpha,j}\, \dot{m}_j''' = 0$
$\mathbf{G} = \rho \mathbf{V}$	net mass-flux vector, kg/(s · m^2). Note that this includes all components of the mixture, some of which may be

	moving at different velocities than others because of diffusion. Note further that
$\mathbf{V} = \mathbf{G}/\rho$	the "mixture velocity" vector with the components $u = G_x/\rho,\ v = G_y/\rho,\ w = G_z/\rho.$
$\dot{m}'' = G_{y,s}$	the normal component of the net mass flux vector at the interface; $\dot{m}''$ is then the *net mass-transfer* rate at the interface, including all components, and is defined as *positive* into the considered phase.
$m_j\mathbf{G}$	convected component of the flux of component j.
$\dot{m}_j'' = m_j \dot{m}''$	convected flux of component j at or below the interface (this is further subscripted later).
i	specific enthalpy of mixture, J/kg.
i_j	specific enthalpy of component j, J/kg, thus $i = \sum_j m_j i_j$.
$c_j = \left(\dfrac{\partial i_j}{\partial T}\right)_{P,m_j,m_k}$	specific heat at constant pressure for component j. For perfect-gas mixtures the specific heat is a function only of temperature, so that $c_j = di_j/dT$.
$c = \sum_j m_j c_j$	specific heat of mixture. Note that $c \neq di/dT$, except where composition is uniform (no mass diffusion) or where the specific heats of all components are equal and there is no chemical reaction.
$\gamma_j = \rho D_j$	product of the diffusion coefficient D_j and the density.
$\Gamma = k/c$	ratio of thermal conductivity to specific heat, kg/(m · s).
$\Phi = \Gamma, \gamma_j$	a diffusion coefficient; see Eq. (18-17).
$\mathcal{P}$	conserved property, $\mathcal{P} = m_j, n_\alpha, \ldots, i, T, \left(m_f - \dfrac{m_o}{r}\right)$; see Eq. (18-16).
$B = \dfrac{\mathcal{P}_\infty - \mathcal{P}_s}{\mathcal{P}_s - \mathcal{P}_T}$	Mass transfer driving force, see Eq. (18-32)
$\mathrm{Sc}_j = \dfrac{\mu}{\gamma_j} = \dfrac{\mu}{\rho D_j}$	Schmidt number of component j
$\mathrm{Le}_j = \dfrac{\gamma_j}{\Gamma} = \dfrac{\mathrm{Pr}}{\mathrm{Sc}_j}$	Lewis number of component j
$\mathrm{Sh} = \dfrac{gx}{\gamma}$	Sherwood number

THE DIFFERENTIAL EQUATIONS OF THE CONCENTRATION BOUNDARY LAYER

Consider a two-dimensional boundary layer in (x, y) coordinates within the considered phase. Let us restrict our analysis to steady flow in the absence of body forces, and let velocities be sufficiently low that we can neglect viscous energy dissipation and the influence of pressure gradients on the energy equation. Then, from the differential equations developed in Chap. 4, the following must be the differential equations to be satisfied within the laminar boundary layer:

Diffusion of component j, Eq. (4-18),

$$G_x \frac{\partial m_j}{\partial x} + G_y \frac{\partial m_j}{\partial y} - \frac{\partial}{\partial y}\left(\gamma_j \frac{\partial m_j}{\partial y}\right) = \dot{m}_j''' \tag{18-1}$$

Diffusion of chemical elements α, Eq. (4-24),

$$G_x \frac{\partial n_\alpha}{\partial x} + G_y \frac{\partial n_\alpha}{\partial y} - \frac{\partial}{\partial y}\left(\sum_j \gamma_j \frac{\partial}{\partial y}(n_{\alpha,j} m_j)\right) = 0 \tag{18-2}$$

Energy, from Eq. (4-26) or (4-27),

$$G_x \frac{\partial i}{\partial x} + G_y \frac{\partial i}{\partial y} - \frac{\partial}{\partial y}\left(\sum_j \gamma_j \frac{\partial m_j}{\partial y} i_j\right) - \frac{\partial}{\partial y}\left(k \frac{\partial T}{\partial y}\right) = 0 \tag{18-3}$$

Continuity, from Eq. (4-1),

$$\frac{\partial G_x}{\partial x} + \frac{\partial G_y}{\partial y} = 0 \tag{18-4}$$

Momentum, from Eq. (4-10),

$$G_x \frac{\partial u}{\partial x} + G_y \frac{\partial u}{\partial y} = -\frac{dP}{dx} + \frac{\partial}{\partial y}\left(\mu \frac{\partial u}{\partial y}\right) \tag{18-5}$$

These five equations then form the basis for the solution of the steady-flow, low-velocity, laminar-boundary-layer problem. As an illustrative example, we consider a binary mixture with no chemical reactions (inert) with constant fluid properties ($\dot{m}_j''' = 0,\ m_1 + m_2 = 1,\ \gamma_1 = \gamma_2 = \gamma$). For this case, one obtains from the above equations:

Diffusion of component 1,

$$G_x \frac{\partial m_1}{\partial x} + G_y \frac{\partial m_1}{\partial y} - \frac{\partial}{\partial y}\left(\gamma_1 \frac{\partial m_1}{\partial y}\right) = 0$$

Energy,

$$G_x \frac{\partial i}{\partial x} + G_y \frac{\partial i}{\partial y} - \frac{\partial}{\partial y}\left(\gamma \frac{\partial m_1}{\partial y} i_1 + \gamma \frac{\partial m_2}{\partial y} i_2\right) - \frac{\partial}{\partial y}\left(k \frac{\partial T}{\partial y}\right) = 0$$

Noting that (for $c_j = \text{constant}$) $i = m_1 i_1 + m_2 i_2 = cT = m_1 c_1 T + m_2 c_2 T = m_1(c_1 - c_2)T + c_2 T$ results in

$$(c_2 + m_1(c_1 - c_2))\left(G_x \frac{\partial T}{\partial x} + G_y \frac{\partial T}{\partial y}\right) + (c_1 - c_2)T\left(G_x \frac{\partial m_1}{\partial x} + G_y \frac{\partial m_1}{\partial y}\right)$$
$$- \frac{\partial}{\partial y}\left(\gamma \frac{\partial m_1}{\partial y}\right)(c_1 - c_2)T - (c_1 - c_2)\gamma \frac{\partial T}{\partial y}\frac{\partial m_1}{\partial y} - \frac{\partial}{\partial y}\left(k \frac{\partial T}{\partial y}\right) = 0$$

By applying the diffusion equation for component 1 it can be seen that the second and the third terms cancel out and one obtains for the energy equation

$$c\left(G_x\frac{\partial T}{\partial x}+G_y\frac{\partial T}{\partial y}\right)-(c_1-c_2)\gamma\frac{\partial T}{\partial y}\frac{\partial m_1}{\partial y}-\frac{\partial}{\partial y}\left(k\frac{\partial T}{\partial y}\right)=0 \tag{18-6}$$

In addition, one has to satisfy *continuity*,

$$\frac{\partial G_x}{\partial x}+\frac{\partial G_y}{\partial y}=0 \tag{18-4}$$

and the *momentum* balance,

$$G_x\frac{\partial u}{\partial x}+G_y\frac{\partial u}{\partial y}=-\frac{dP}{dx}+\frac{\partial}{\partial y}\left(\mu\frac{\partial u}{\partial y}\right) \tag{18-5}$$

The turbulent boundary layer can be handled in much the same way. If we replace the viscosity and the diffusion coefficients by their corresponding effective quantities (laminar + turbulent values), we obtain the equations for an inert binary mixture for a steady-flow, low-velocity, turbulent boundary layer with constant properties as^5:

Diffusion of component 1,

$$G_x\frac{\partial m_1}{\partial x}+G_y\frac{\partial m_1}{\partial y}-\frac{\partial}{\partial y}\left(\gamma_{\text{eff}}\frac{\partial m_1}{\partial y}\right)=0 \tag{18-7}$$

Energy,

$$c\left(G_x\frac{\partial T}{\partial x}+G_y\frac{\partial T}{\partial y}\right)-(c_1-c_2)\gamma_{\text{eff}}\frac{\partial T}{\partial y}\frac{\partial m_1}{\partial y}-\frac{\partial}{\partial y}\left(k_{\text{eff}}\frac{\partial T}{\partial y}\right)=0 \tag{18-8}$$

Continuity,

$$\frac{\partial G_x}{\partial x}+\frac{\partial G_y}{\partial y}=0 \tag{18-9}$$

Momentum,

$$G_x\frac{\partial u}{\partial x}+G_y\frac{\partial u}{\partial y}=-\frac{dP}{dx}+\frac{\partial}{\partial y}\left(\mu_{\text{eff}}\frac{\partial u}{\partial y}\right) \tag{18-10}$$

where the effective values (for an eddy viscosity concept) are given by:

$$\begin{aligned}\mu_{\text{eff}}&=\mu+\mu_t=\mu+\rho\varepsilon_M\\ k_{\text{eff}}&=k+k_t=k+\rho c\varepsilon_H=k+\rho c\frac{\varepsilon_M}{\text{Pr}_t}\\ \gamma_{\text{eff}}&=\gamma+\gamma_t=\gamma+\rho\varepsilon_D=\gamma+\rho\frac{\varepsilon_M}{\text{Sc}_t}\end{aligned} \tag{18-11}$$

The turbulent Prandtl number Pr_t has been discussed in Chap. 12. Experimental information on the turbulent Schmidt number Sc_t is very scarce, but what little there is seems to suggest a considerable similarity to the turbulent Prandtl number. Because of this, the ratio $\mathrm{Pr}_t/\mathrm{Sc}_t$ can often be set to 1; i.e., $\mathrm{Le}_t = 1$.

In the following analysis, we will focus for simplicity mainly on the set of Eqs. (18-1)–(18-5) for laminar flow. However, all derivations presented below are equally applicable to turbulent flow if the fluid properties are replaced by their effective values.

SIMPLIFIED EQUATIONS FOR THE CONCENTRATION BOUNDARY LAYER

As can be seen from Eqs. (18-1)–(18-5), the boundary layer equations for the energy transport and the mass diffusion look similar. It is therefore possible to show that these equations will lead to the same differential equation if some simplifications are invoked (see for a detailed explanation App. E).

Let us first focus on the mass-diffusion equation (18-1). This equation can be simplified, for example, for an inert substance ($\dot{m}_j''' = 0$):

$$G_x \frac{\partial m_j}{\partial x} + G_y \frac{\partial m_j}{\partial y} - \frac{\partial}{\partial y}\left(\gamma_j \frac{\partial m_j}{\partial y}\right) = 0 \tag{18-12}$$

Consider a simple chemical reaction, in which a *fuel* (subscript f) combines with an *oxidant* (subscript o) to form a single *product* (subscript p), without intermediates

$$1 \text{ kg fuel} + r \text{ kg oxidant} \rightleftarrows (1+r) \text{ kg product}$$

For example:

$$1\,\mathrm{C} + 1\,\mathrm{O_2} \rightleftarrows 1\,\mathrm{CO_2}$$

$$1 \text{ kmol C} + 1 \text{ kmol } \mathrm{O_2} \rightleftarrows 1 \text{ kmol } \mathrm{CO_2}$$

$$12 \text{ kg C} + 32 \text{ kg } \mathrm{O_2} \rightleftarrows 44 \text{ kg } \mathrm{CO_2}$$

and $r = 32/12 = 8/3$.

Equation (18-1) can be simplified under the assumption that $\gamma_f = \gamma_o = \gamma_p = \gamma$ to

$$G_x \frac{\partial}{\partial x}\left(m_f - \frac{m_o}{r}\right) + G_y \frac{\partial}{\partial y}\left(m_f - \frac{m_o}{r}\right) - \frac{\partial}{\partial y}\left[\gamma \frac{\partial}{\partial y}\left(m_f - \frac{m_o}{r}\right)\right] = 0 \tag{18-13}$$

Similarly, the energy equation (18-3) can be simplified under the assumption that the Lewis number Le = 1 or under the assumption of simple chemical

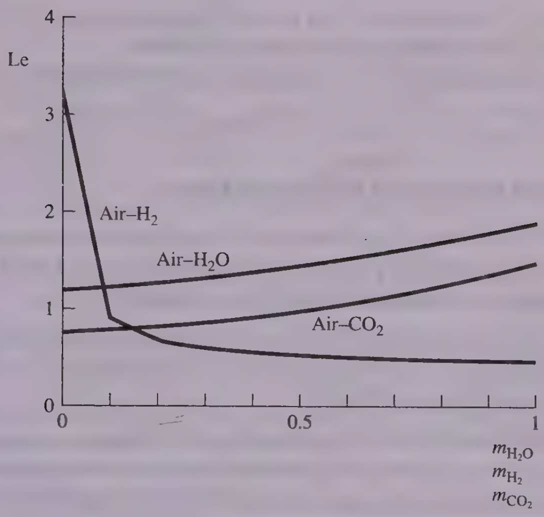

Figure 18-2 Lewis number variation for binary gas mixtures ($P = 101.325$ kPa, $T = 290$ K) as a function of mixture composition (see App. A, Table A-19).

reactions with equal specific heats (see App. E). This results in

$$G_x \frac{\partial i}{\partial x} + G_y \frac{\partial i}{\partial y} - \frac{\partial}{\partial y}\left(\Gamma \frac{\partial i}{\partial y}\right) = 0 \tag{18-14}$$

For gases and gas mixtures, both Pr and Sc are of the order of magnitude of unity, so the assumption of Le $= 1$ for a gas mixture is normally reasonably valid. As an example, Fig. 18-2 shows the Lewis number for binary mixtures of air with CO_2, H_2O, and H_2.

From Eqs. (18-12)–(18-14) it can be seen that these equations can be written in the same form by using a variable $\mathcal{P}$, which is called a conserved property

$$G_x \frac{\partial \mathcal{P}}{\partial x} + G_y \frac{\partial \mathcal{P}}{\partial y} - \frac{\partial}{\partial y}\left(\Phi \frac{\partial \mathcal{P}}{\partial y}\right) = 0 \tag{18-15}$$

where $\mathcal{P}$ stands for one of the following functions

$$\mathcal{P} = m_j, n_\alpha, \ldots, i, T, \left(m_f - \frac{m_o}{r}\right) \tag{18-16}$$

This means that the transport of energy or concentration will be identical in the boundary layer, if the resulting boundary conditions for the differential equations will be the same. The quantity Φ, which appears in Eq. (18-15) is a diffusion coefficient and is equal to

$$\Phi = \Gamma, \gamma_j \tag{18-17}$$

depending on the $\mathcal{P}$ function. If $\mathcal{P} = i$, for, example in Eq. (18-15), Φ has to be set to Γ and Eq. (18-15) becomes the energy equation.

If we now generalize Eq. (18-15) to three-dimensional space, we obtain[1]

$$G \cdot \nabla\mathcal{P} - \nabla \cdot \Phi\nabla\mathcal{P} = 0 \tag{18-18}$$

The Conserved Property of the Second Kind

Following D. B. Spalding,[4] any property that satisfies the above given $\mathcal{P}$ equation is defined as a *conserved property of the second kind.* A useful feature of this conserved property is contained in the following theorem:

> If, in any steady flow, there are two conserved properties of the second kind, $\mathcal{P}_{\mathrm{I}}$ and $\mathcal{P}_{\mathrm{II}}$, and at each point $\Phi_{\mathrm{I}} = \Phi_{\mathrm{II}}$, then a linear combination of $\mathcal{P}_{\mathrm{I}}$ and $\mathcal{P}_{\mathrm{II}}$ is a conserved property of the second kind.

This can easily be understood by substituting the linear combination into the $\mathcal{P}$ equation. This theorem allows us to build up new conserved properties and thus additional solutions by combining properties that we already know.

BOUNDARY CONDITIONS

The simplified equations have to be solved, along with appropriate boundary conditions. Let us first consider the boundary conditions for the momentum equation. Here the following boundary conditions have to be satisfied:

$$\begin{aligned} y = 0&: u = 0,\ v = v_s \\ y \to \infty&: u = u_\infty(x) \end{aligned} \tag{18-19}$$

One sees clearly from Eq. (18-19) that for the process of convective mass transfer a velocity component $v_s \neq 0$ at the interface $y = 0$ might be present because of the mass transferred from one phase to the other. For very small mass-flow rates from the interface at $y = 0$, the velocity component v_s might be negligible. For this case one can achieve a *complete* analogy between the transport of energy and diffusion in the boundary layer. This case is normally called *low mass transfer rate convection.* It can be used to obtain the heat-transfer coefficient by measuring the mass transfer coefficient. One experimental technique used for this purpose, the naphthalene sublimation technique, will be described in more detail in Chaps. 19 and 20. If the velocity component v_s cannot be ignored, one might refer to this situation as to *high mass transfer rate convection.* For the various $\mathcal{P}$ equations, the boundary conditions can easily be formulated for the edge of the boundary layer ($y \to \infty$). Here the temperature, enthalpy, or concentration is known, which gives rise to boundary conditions of the form

$$y \to \infty: T = T_\infty,\ i = i_\infty,\ m_j = m_{j\infty}, \ldots \tag{18-20}$$

The formulation of the boundary condition at the interface is somewhat more complicated. In order to develop a uniform representation of the boundary

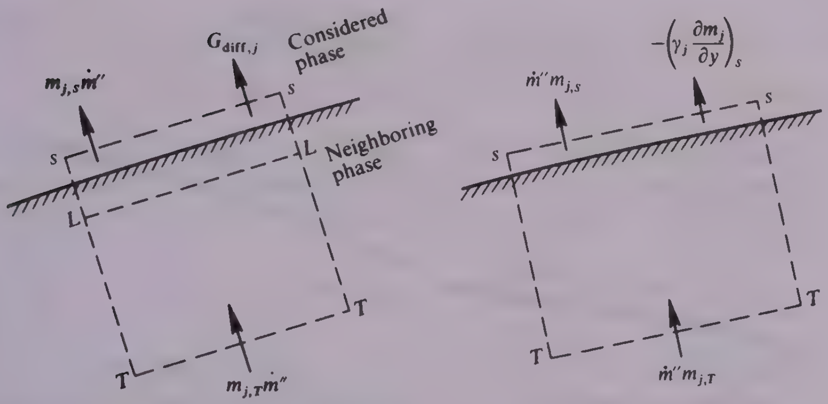

Figure 18-3 Control volumes at the phase interface for the mass-diffusion equation.

conditions at the interface, it is useful to follow the suggestions of Spalding[4] and introduce a purely fictitious T surface.

Figure 18-3 shows the interface between the considered and the neighboring phase. Mass is transferred from one to another phase. Let s be an infinitesimal distance inside the considered boundary layer and the L surface be an infinitesimal distance inside the neighboring phase. The T surface is considered to be some finite distance inside the neighboring phase, and the fluid state at this surface is termed the *transferred-substance state*. The principal characteristic of the T state is that there are no gradients of either concentration or temperature at the T-state location. Therefore, the T state will be in most cases totally fictitious, and the only reason to introduce this additional state is that the integral balance equations can be simplified if one considers that one surface is present where all mass and energy is transferred only by convection.

The normal (y-direction) component of the net mass flux vector at the interface $\dot{m}'' = (\rho V)_{y,s}$ is unknown. This component at the interface can be expressed by the mass flux of component j across the T surface:

$$\dot{m}''_{j,T} = m_{j,T}\dot{m}'' \tag{18-21}$$

This defines a fictitious T-state "concentration"

$$m_{j,T} = \dot{m}''_{j,T}/\dot{m}'' \tag{18-22}$$

From Eq. (18-21) it is immediately clear that if $j = 1$ (which means that there is only one transferred substance) then $m_{j,T} = 1$. Both $\dot{m}''$ and $\dot{m}''_{j,T}$ are defined to be positive if flowing toward the considered phase.

If we now apply conservation of mass for component j, we obtain

$$\dot{m}'' m_{j,s} - \left(\gamma_j \frac{\partial m_j}{\partial y}\right)_s - \dot{m}'' m_{j,T} = 0 \tag{18-23}$$

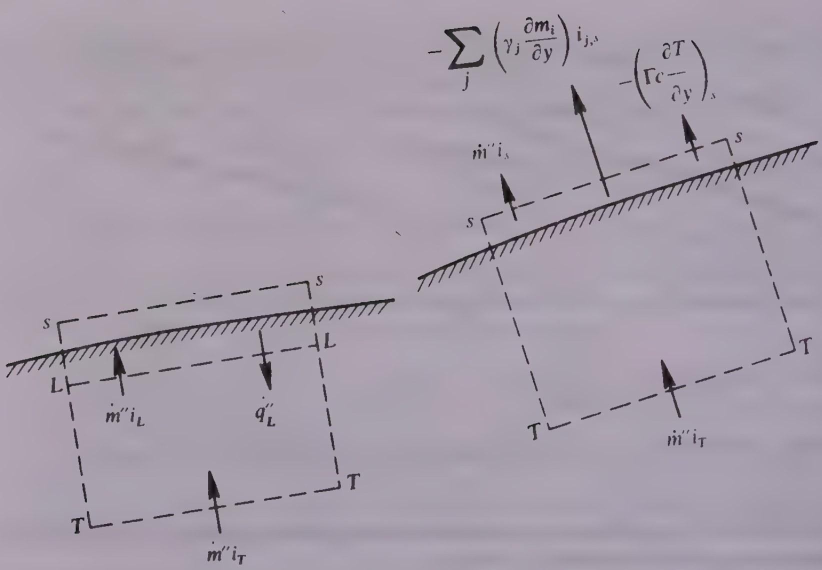
$-\sum_j \left(\gamma_j \frac{\partial m_i}{\partial y}\right) i_{j,s}$
$-\left(\Gamma c \frac{\partial T}{\partial y}\right)_s$
$\dot{m}'' i_s$
s
s
T
T
$\dot{m}'' i_T$
s
s
L
L
$\dot{m}'' i_L$
$\dot{q}''_L$
T
T
$\dot{m}'' i_T$

Figure 18-4 Control volumes at the phase interface.

This equation can be solved for the unknown mass-flow rate $\dot{m}''$ at the interface, which results in

$$\dot{m}'' = \frac{(\gamma_j\, \partial m_j/\partial y)_s}{m_{j,s} - m_{j,T}} \tag{18-24}$$

Consider next the control volume indicated in Fig. 18-4 and the steady-flow energy fluxes flowing across the L and T surfaces. The indicated heat flux $\dot{q}''_L$ is by conduction within the transferred substance, fluid or solid, or within any solid structural materials present. Again, the T surface is fictitious, and we will assume that at this surface no temperature gradients are present. This means that heat is transferred only by convection through this surface. If the conservation of energy principle is now applied to the control volume bounded by the L and T surfaces, a formal definition of the transferred-substance enthalpy i_T is obtained:

$$\dot{m}''\, i_L - \dot{q}''_L - \dot{m}''\, i_T = 0$$

$$i_T = i_L - \frac{\dot{q}''_L}{\dot{m}''} \tag{18-25}$$

Applying conservation of energy across the s and T surfaces, one obtains

$$\dot{m}''\, i_s - \sum_j \left(\gamma_j \frac{\partial m_j}{\partial y}\right)_s i_{j,s} - \left(\Gamma c \frac{\partial T}{\partial y}\right)_s - \dot{m}''\, i_T = 0 \tag{18-26}$$

from which

$$\dot{m}'' = \frac{\sum_j [\gamma_j(\partial m_j/\partial y)]_s\, i_{j,s} + [\Gamma c\,(\partial T/\partial y)]_s}{i_s - i_T} \tag{18-27}$$

The numerator of Eq. (18-27) can be simplified under the assumption that the Lewis number is 1 or under the assumption of no chemical reaction and equal specific heats for all components (see for a detailed explanation in App. E). This results in

$$\dot{m}'' = \frac{[\Gamma(\partial i/\partial y)]_s}{i_s - i_T} \tag{18-28}$$

Comparing Eq. (18-24) with Eq. (18-28), it is obvious that both equations have a very similar structure. It can now be shown by some simple analysis (see App. E) that the boundary condition at the interface for all $\mathcal{P}$ equations will attain always the same form The general form of the boundary condition at the interface can be written as

$$\dot{m}'' = \frac{(\Phi\partial\mathcal{P}/\partial y)_s}{\mathcal{P}_s - \mathcal{P}_T} \tag{18-29}$$

DEFINITION OF THE MASS-TRANSFER CONDUCTANCE AND DRIVING FORCE

As stated above, our interest is to solve the $\mathcal{P}$ equation for various boundary conditions. Examining the $\mathcal{P}$ equation indicates that it is *almost* linear in $\mathcal{P}$. The nonlinearity arises in two ways. First, Φ may be a function of $\mathcal{P}$. This is the same kind of nonlinear effect that arises in the convective-heat-transfer problem resulting from the influence of temperature on the transport properties. However, we have to contend with the possible influence of composition.

The other source of nonlinearity is the normal velocity component at the interface, v_s, which is directly proportional to the mass transfer rate at the interface $\dot{m}''$, which is, in turn, functionally related to $\mathcal{P}_\infty - \mathcal{P}_s$. Thus the whole velocity field is strongly coupled with the diffusion equation.

As it has been stated before, the *low-mass-transfer problem* is characterized by the fact that the mass-transfer rate $\dot{m}'' \to 0$. If we further restrict our considerations to constant properties, then the $\mathcal{P}$ equation will be linear for this special case. This motivates the definition of a mass-transfer conductance (similar to the heat-transfer conductance) given by

$$\left(\Phi\frac{\partial\mathcal{P}}{\partial y}\right)_s = g(\mathcal{P}_\infty - \mathcal{P}_s), \quad \text{or} \quad g = \frac{\left(\Phi\dfrac{\partial\mathcal{P}}{\partial y}\right)_s}{(\mathcal{P}_\infty - \mathcal{P}_s)} \tag{18-30}$$

The conductance g is independent of $\dot{m}''$ in the limit of $\dot{m}''$ tending to zero, but may become a strong function of $\dot{m}''$ as $\dot{m}''$ becomes large. However, this does not invalidate the above definition of g.

If we now combine Eqs. (18-30) and (18-29), we obtain

$$\dot{m}'' = g\frac{\mathcal{P}_\infty - \mathcal{P}_s}{\mathcal{P}_s - \mathcal{P}_T} \tag{18-31}$$

Let us now define a mass transfer driving force B such that

$$B = \frac{\mathcal{P}_\infty - \mathcal{P}_s}{\mathcal{P}_s - \mathcal{P}_T} \tag{18-32}$$

With Eq. (18-32) we can write Eq. (18-31) as

$$\dot{m}'' = gB \tag{18-33}$$

Thus, to calculate the mass transfer rate $\dot{m}''$, we evaluate B from given values of $\mathcal{P}$ at the s, T, and ∞ states, and g from the solution of the suitable boundary layer equations (momentum, continuity, diffusion, and energy). B can be calculated from mass concentrations, but it can also be calculated from any other conserved properties under suitable restricted conditions.

The dimension of g is the same as the dimension of $\dot{m}''$, that is, it has dimensions kg/(s · m^2), because B is a nondimensional parameter. The driving force can be positive or negative, which determines the direction of $\dot{m}''$, where a positive B corresponds to mass transfer *into* the boundary layer from the surface. The conductance g is always positive.

From Eq. (18-33) it is obvious that the case of $\dot{m}'' \to 0$ requires that $B \to 0$, because the conductance g will be always positive and finite. As it was stated above, the case $\dot{m}'' \to 0$ is the limiting case where the equation for $\mathcal{P}$ is essentially linear and where no coupling exists between the momentum equation and the diffusion equation because v_s is negligible. The conductance g for $B \to 0$ will be denoted by g^* and is given by Eq. (18-33) as

$$g^* = \lim_{B\to 0} \frac{\dot{m}''}{B} \tag{18-34}$$

The ratio g/g^* is frequently useful because it tends to be primarily a function of B alone (this will be shown in more detail in Chap. 19). That is, for a given class of boundary layers, g/g^* is often moderately, or completely, independent of such parameters as Reynolds or Prandtl number. The relationship between g/g^* and B is qualitatively shown in Fig. 18-5.

The nature of the conductance g is closely related to the nature of the heat-transfer conductance h. This can be understood if we write Eq. (18-30) with h replacing g and T replacing $\mathcal{P}$:

$$h = \frac{\left(\Gamma c \dfrac{\partial T}{\partial y}\right)_s}{(T_\infty - T_s)} \tag{18-35}$$

Previously we defined the heat transfer conductance h such that

$$\dot{q}_s'' = h(T_s - T_\infty) = \left(-k\frac{\partial T}{\partial y}\right)_s = \left(-\Gamma c\frac{\partial T}{\partial y}\right)_s \tag{18-36}$$

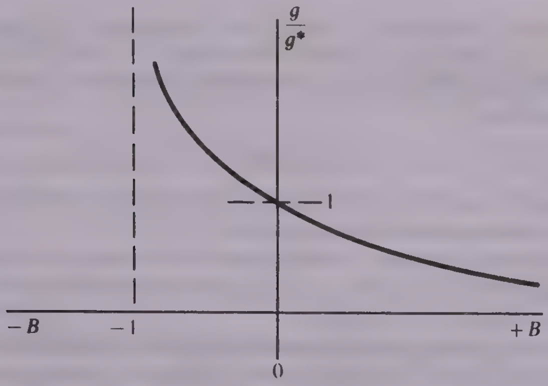

Figure 18-5 Typical variation of g/g^* with B.

As has been shown in the previous chapters dealing with convective heat transfer, it is usual to represent the heat-transfer conductance h in a nondimensional form by the Nusselt number ($\mathrm{Nu}_x = hx/k$) or by the Stanton number ($\mathrm{St} = \mathrm{Nu}_x/(\mathrm{Re}_x\,\mathrm{Pr})$). A similar approach is also very useful for the mass-transfer conductance. So one obtains:

$$\mathrm{Sh}_x = \frac{gx}{\gamma} \tag{18-37}$$

$$\mathrm{St} = \frac{g}{(\rho u)_\infty} \tag{18-38}$$

Equation (18-37) gives the definition of the Sherwood number Sh_x, which is similar to the Nusselt number for heat-transfer problems. Equation (18-38) gives the definition of the mass-transfer Stanton number.

The parameter B has been developed here as a driving force, or potential, in terms of the values of conserved properties in the free stream and at the interface, but it can also be recognized as the boundary-layer "blowing" parameter B_h discussed in Chap. 12.

$$B = \frac{\dot{m}''}{g} = \frac{\dot{m}''}{(\rho u)_\infty}\frac{(\rho u)_\infty}{g} = \frac{(\rho v)_s}{(\rho u)_\infty}\frac{1}{\mathrm{St}} = \frac{v_s}{u_\infty}\frac{1}{\mathrm{St}} \tag{18-39}$$

where it has been assumed that the density is constant across the boundary layer.

PROBLEMS

18-1. Consider a binary-mixture-gas mass-transfer system in which the considered phase is a mixture of gases 1 and 2. Let gas 2 be injected into the mixture at the interface; that is, gas 2 is the only transferred substance. Show that if there is no phase change from the L state to the s state, then $\dot{q}_s'' = \dot{q}_L''$, regardless of the mass-transfer aspects of the problem [start with Eq. (18-27)].

18-2. Consider the same problem as in Prob. 18-1. In addition to no phase change at the interface, let the Lewis number be everywhere 1. At the outer edge of the boundary layer let the mixture be exclusively component 1. Show that under these conditions,

$$\dot{q}_L'' = \dot{q}_s'' = g(h_{1,\infty} - h_{1,s})$$

If the specific heat of component 1 may be considered as constant, what is the implied relationship between St and g/G_∞?

18-3. Show that for the case $\dot{m}'' = 0$, the heat flux at the interface is proportional to the enthalpy differences between the s and ∞ states, for any case for which enthalpy is a conserved property.

18-4. Demonstrate, with the aid of a suitable model, that in a turbulent flow, under the assumption of the Reynolds analogy, the "turbulent" Lewis number is equal to 1.

18-5. Starting with the energy equation of the boundary layer in the form of Eq. (4-26), show that for the case of a fluid with Pr = 1 the stagnation enthalpy is a conserved property of the second kind.

18-6. Prove the theorem for the conserved property of the second kind, given after Eq. (18-18), by introducing a linear combination of two conserved properties of the second kind ($\mathcal{P}_{\text{I}}$, $\mathcal{P}_{\text{II}}$) into Eq. (18-15).

18-7. Consider a chemical reaction of C_2H_5OH with O_2. It is assumed that the fuel combines with the oxidant and forms a product consisting of CO_2 and H_2O. Write down the reaction equation in kmol and in kg of the reactants. What value has the stoichiometric ratio r?

REFERENCES

1. Spalding, D. B.: *Convective Mass Transfer*, McGraw-Hill, New York, 1963.
2. Bird, R. B., W. E. Stewart, and E. N. Lightfoot: *Transport Phenomena*, John Wiley & Sons, New York, 2002.
3. Mills, A. F.: *Mass Transfer*, Prentice Hall, Englewood Cliffs, N.J., 2001.
4. Spalding, D. B.: *Int. J. Heat Mass Transfer*, vol. 1, pp. 192–207, 1960.
5. Landis, R. B., and A. F. Mills: *Int. J. Heat Mass Transfer*, vol. 15, pp. 1905–1932, 1972.

CHAPTER 19

Convective Mass Transfer: Evaluation of the Mass-Transfer Conductance from the Conserved Property ($\mathcal{P}$) Equation

As stated in Chap. 18, our main interest is to obtain the mass flux rate $\dot{m}''$ from the interface into the boundary layer. From Eq. (18-33) it is obvious that this requires first the determination of the driving force B from given information of the problem description and second that the mass-transfer conductance g has to be obtained by solving the (conserved-property) $\mathcal{P}$ equation, (18-15) or (18-18). Therefore, the solution of this equation will be the primary interest of the present chapter.

Most of the material presented here will focus on solutions of the $\mathcal{P}$ equation for simple cases where analytical or semianalytical solutions are possible. Many of these solutions are restricted to constant fluid properties. However, there might be a rather substantial influence of mixture composition on the transport properties in a multicomponent system. This is very much different from heat-transfer problems without mass transfer, where the change in fluid properties is mostly small and the resulting effect on the Nusselt number might be negligible. Nevertheless, the constant-property solutions will form the basic starting point, and thus constitute our primary concern here.

Of course, one always has the option to solve the $\mathcal{P}$ equation for any desired variable properties and boundary conditions using a numerical solution technique such as a finite-difference method; indeed this might turn out to be the only practicable procedure for more complex problems. However, one should also then consider the validity of the various approximations and simplifications that went into the development of the $\mathcal{P}$ equation. Therefore, it might be preferable for a numerical approach to the problem to go back to the original underlying differential equations (see Chap. 4) without simplifications and solve them numerically.

On the other hand, the simplified approach developed in the last and the present chapter will lead, for a large number of technical problems, to approximate results that might be fully satisfactory for the engineer. Moreover, these solutions will be obtainable very quickly, therefore the engineer has the chance to estimate first by a simple method whether there is any problem in design and maybe later initiate a more detailed numerical analysis of the problem.

THE PREDICTION OF THE MASS-TRANSFER CONDUCTANCE g^* FOR LOW MASS-TRANSFER RATES

In Chap. 18 it has been shown that the mass-transfer conductance g is normally referred to the value g^*, for which $B \to 0$. Further, it has been noted that in several cases, the ratio of g/g^* is a strong function of B, but only a weak or no function of other parameters. Additionally, for very low mass transfer rates ($B \to 0$), the interface velocity v_s is approximately zero. In such cases, the fluid properties change only very little, because the transferred-substance concentration is not large enough within the boundary layer. Because of these facts, we will start our analysis by first looking at the case of *low-mass-transfer rates*, before we move to *high-mass-transfer* convection.

THE LAMINAR CONSTANT-PROPERTY BOUNDARY LAYER FOR LOW MASS-TRANSFER RATES

We will start our investigations with the very simple case of a laminar flow over a flat plate subjected to a constant free-stream velocity $u_\infty =$ constant. It is assumed that the mass transfer rate from the interface into the boundary layer is relatively small. If constant properties are assumed, Eq. (18-15) becomes

$$u\frac{\partial \mathcal{P}}{\partial x} + v\frac{\partial \mathcal{P}}{\partial y} = \frac{\partial}{\partial y}\left(\frac{\Phi}{\rho}\frac{\partial \mathcal{P}}{\partial y}\right) \tag{19-1}$$

The velocity components are given from a solution of the *momentum* and *continuity* equations:

$$u\frac{\partial u}{\partial x} + v\frac{\partial u}{\partial y} = \frac{\partial}{\partial y}\left(\frac{\mu}{\rho}\frac{\partial u}{\partial y}\right) \tag{19-2}$$

$$\frac{\partial u}{\partial x} + \frac{\partial v}{\partial y} = 0 \tag{19-3}$$

These equations have to be solved together with the following boundary conditions:

$$\begin{aligned}
x = 0:\quad & u = u_\infty; & \mathcal{P} &= \mathcal{P}_\infty \\
y = 0:\quad & u = 0, & \mathcal{P} &= \mathcal{P}_s \\
& v = v_s(v_s \to 0) & & \\
y \to \infty:\quad & u \to u_\infty, & \mathcal{P} &\to \mathcal{P}_\infty
\end{aligned} \tag{19-4}$$

Because of the low mass-transfer rates assumed, the velocity component v_s at the interface will be sufficiently small and can be neglected within the following analysis. This sort of problem has been mentioned in Chap. 18 as *low-mass-transfer-rate convection.* The solution will lead to the mass-transfer conductance g^* for which $B \to 0$.

If we set $\mathcal{P} = T$ in Eq. (19-1), then we have already generated an exact solution for the above given problem in Chap. 10. For the nondimensional heat-transfer conductance, the Nusselt number,

$$\mathrm{Nu}^* = \frac{x\,(\partial T/\partial y)_s}{(T_\infty - T_s)} \tag{19-5}$$

a correlation was obtained in Chap. 10, which showed the dependence of the Nusselt number on the Reynolds and Prandtl number:

$$\mathrm{Nu}^* = 0.332\,\mathrm{Pr}^{1/3}\,\mathrm{Re}_x^{1/2} \tag{10-10}$$

Substituting $\mathcal{P}$ for T and using the definition of the mass-transfer conductance, according to Eq. (18-35), results in

$$\mathrm{Sh}^* = \frac{g^* x}{\Phi} = \frac{x(\partial \mathcal{P}/\partial y)_s}{(\mathcal{P}_\infty - \mathcal{P}_s)} \tag{19-6}$$

The * in the above equations denotes again that $B \to 0$ and $v_s \to 0$.

Because Eqs. (19-1)–(19-3) have the identical structure for $\mathcal{P} = T$ or any other $\mathcal{P}$ (for example $\mathcal{P} = m_j$, $\Phi = \gamma_j$) and also the boundary conditions, according to Eq. (19-4) are the same, it can be concluded that the dependence of the Sherwood number on Re and Sc will be the same as the dependence of the Nusselt number on Re and Pr. This means that we have simply to replace in Eq. (10-10) Nu by Sh and Pr by Sc. This results in

$$\mathrm{Sh}^* = 0.332\,\mathrm{Sc}^{1/3}\,\mathrm{Re}_x^{1/2} \tag{19-7}$$

From Eq. (10-10) and Eq. (19-7) one sees very clearly that a simple analogy between heat and mass transfer exists for the case of low mass-transfer rates. By taking the ratio between Nusselt and Sherwood number from the two equations, one obtains:

$$\frac{\mathrm{Nu}^*}{\mathrm{Sh}^*} = \left(\frac{\mathrm{Pr}}{\mathrm{Sc}}\right)^{1/3} = \mathrm{Le}^{1/3} \tag{19-8}$$

or more generally

$$\frac{\mathrm{Nu}^*}{\mathrm{Sh}^*} = \left(\frac{\mathrm{Pr}}{\mathrm{Sc}}\right)^n = \mathrm{Le}^n \tag{19-9}$$

where the exponent n will vary with the acceleration of the mainstream flow. If $u_\infty = Cx^m$, the exponent n can be approximated according to Eckert[1] by

$$n = 0.35 + 0.02\frac{2m}{1+m} \tag{19-10}$$

Eq. (19-8) shows that for a Lewis number of unity, the Nusselt number takes the same value as the Sherwood number and a *complete analogy* between heat and mass transfer exists within the boundary layer. This is because the Prandtl number is a nondimensional measure for the ratio of the thickness of the thermal and the hydrodynamic boundary layer, whereas the Schmidt number is a measure for the ratio between the thickness of the concentration and the hydrodynamic boundary layer. Therefore, the Lewis number compares directly the thickness of the concentration to the thermal boundary layer.

However, the simple analogy given by Eqs. (19-8)–(19-10) is applicable only for the case of $B \to 0$ which means for low mass-transfer rates, when the velocity component v_s at the interface is negligible. For this case, all correlations that have been obtained in the previous chapters for the heat-transfer processes can simply been used for calculating g^* by replacing the Prandtl number by the Schmidt number.

THE TURBULENT CONSTANT-PROPERTY BOUNDARY LAYER FOR LOW MASS-TRANSFER RATES

For the turbulent constant-property boundary layer with a constant free-stream velocity and a negligible interface velocity $v_s \to 0$ (*for low mass-transfer rates*) one can follow the above approach by replacing the fluid properties Φ by their effective values according to Eq. (18-11). By doing so, the solutions obtained in Chap. 12 for the turbulent boundary layer can be used if we assume that the ratio $\mathrm{Pr}_t/\mathrm{Sc}_t$ is unity. If we focus first on the most simple case of the flow over a flat plate with a constant free-stream velocity u_∞, the correlation derived for the Nusselt number in Chap. 12 for the flow along a flat plate with a constant surface temperature was:

$$\mathrm{Nu}^* = \frac{0.0287\,\mathrm{Pr}\,\mathrm{Re}_x^{0.8}}{0.169\,\mathrm{Re}_x^{-0.1}(13.2\,\mathrm{Pr} - 8.66) + 0.85} \tag{12-17}$$

For $0.5 < \mathrm{Pr} < 1.0$ and $5 \times 10^5 < \mathrm{Re}_x < 5 \times 10^6$, a much simpler expression for gases has also been developed from this equation in Chap. 12

$$\mathrm{Nu}^* = 0.0287\,\mathrm{Pr}^{0.6}\,\mathrm{Re}_x^{0.8} \tag{12-18}$$

If we now follow the procedure developed in the previous paragraph, the Sherwood number for the *low-mass-transfer case* is simply obtained by replacing the Nusselt number by the Sherwood number and the Prandtl number by the Schmidt number in Eq. (12-17). Thus

$$\mathrm{Sh}^* = \frac{0.0287\,\mathrm{Sc}\,\mathrm{Re}_x^{0.8}}{0.169\,\mathrm{Re}_x^{-0.1}(13.2\,\mathrm{Sc} - 8.66) + 0.85} \tag{19-11}$$

These equations show that the ratio between Nusselt and Sherwood number is given by

$$\frac{\mathrm{Nu}^*}{\mathrm{Sh}^*} = \left(\frac{\mathrm{Pr}}{\mathrm{Sc}}\right)\frac{0.169\,\mathrm{Re}_x^{-0.1}(13.2\,\mathrm{Sc} - 8.66) + 0.85}{0.169\,\mathrm{Re}_x^{-0.1}(13.2\,\mathrm{Pr} - 8.66) + 0.85} \tag{19-12}$$

Comparing Eq. (19-12) with Eq. (19-9) shows that for turbulent boundary-layer flows, the ratio $\mathrm{Nu}^*/\mathrm{Sh}^*$ might still depend on the Reynolds number. Furthermore, it is interesting to note that if $\mathrm{Pr} = \mathrm{Sc}$, which means that $\mathrm{Le} = 1$, Eq. (19-12) shows that also for turbulent flows (for which $\mathrm{Pr}_t/\mathrm{Sc}_t = 1$) the ratio $\mathrm{Nu}^*/\mathrm{Sh}^*$ is independent of Re_x and equal to 1. This result is easy to understand because the conserved property equations for T and m_j are identical for $\mathrm{Le} = 1$ and therefore also the dimensionless gradients at the wall (the Nusselt and the Sherwood numbers) must be the same.

The two paragraphs above show that for *low-mass-transfer-rate convection problems*, all the correlations developed in the previous chapters for heat-transfer problems can be used to obtain the mass-transfer conductance g^* by simply replacing the Prandtl number in these correlations with the Schmidt number. Some more functions describing the analogy between heat and mass transfer for *low mass-transfer rates* (e.g., naphthalene–air mixtures) can be found in Goldstein and Cho.[2]

The analogy between heat and mass transfer for low mass-transfer rates is very useful in order to obtain accurate experimental data for heat-transfer coefficients on bodies of complicated shape. For this, a body (for which the heat-transfer characteristics shall be obtained) is coated with a thin naphthalene layer. After this, the thickness of the layer is measured precisely. Then the body is exposed to a forced convection flow for a certain time, so that the naphthalene is transferred from the interface into the flow. After the test, the thickness of the layer is recorded again and the Sherwood number is predicted from the difference in thickness, the elapsed measurement time, and the fluid properties. From the known Sherwood number, the Nusselt number can finally be calculated by using, for example, Eq. (19-9) or (19-12). Figure 19-1 shows some results for a flow over a flat plate.[3] It can be seen that the experimental data are in good agreement with the correlation, Eq. (12-18). The advantage of this experimental method is that only the change in thickness with time has to be measured. This gives rise to very accurate experimental data. Furthermore, a high resolution can be obtained and, because of the analogy, boundary conditions simulating a constant wall temperature (naphthalene coated = constant concentration) or an adiabatic wall (uncoated = no mass flux at the wall) can be obtained easily.

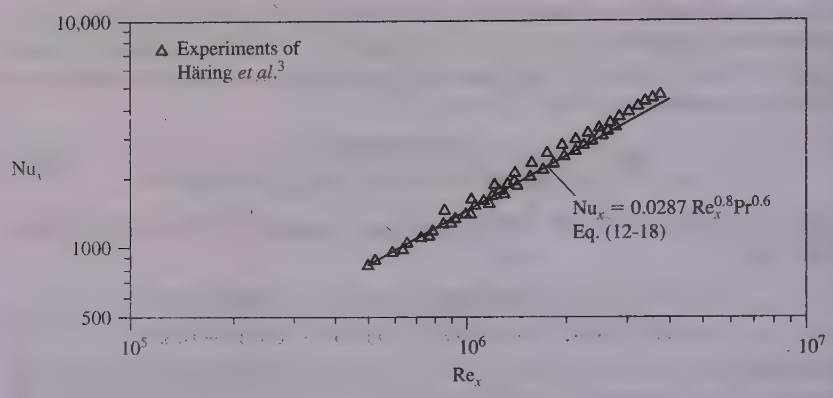

Figure 19-1 Nusselt numbers for the flow over a flat plate obtained from mass transfer experiments by using the naphthalene sublimation technique (taken from Häring *et al.*[3]).

THE PREDICTION OF THE MASS-TRANSFER CONDUCTANCE *g* FOR HIGH MASS-TRANSFER RATES

In contrast to the low mass-transfer rate cases, the interface velocity v_s can not be neglected if the mass-transfer rate is high. For this case, the additional mass transferred into the boundary layer will lead to noticeable changes in the thickness of the boundary layer and will change, therefore, the heat- and mass-transfer conductance. Additionally, the changes in the fluid properties might be no longer negligible and have to be taken into account.

As has been stated in Chap. 18, we are interested in deriving expressions for the ratio of the mass-transfer conductance g/g^* of the form

$$\frac{g}{g^*} = f(B, \ldots) \tag{19-13}$$

where g/g^* will depend strongly on B and weakly on other parameters.

HIGH MASS-TRANSFER-RATE CONVECTION IN A LAMINAR COUETTE FLOW

In order to elucidate the dependence of g/g^* on the mass-transfer driving force B, consideration will be given to a steady-state laminar Couette flow with mass transfer through one surface (a Couette flow is a fully developed flow between two parallel plates, where the lower plate is fixed and the upper one is moved with the constant velocity u_∞). It is assumed that at the surface at $y = 0$ an evaporating liquid is placed with the temperature T_s. For $y = \delta$, the mass concentration m_1 is equal to $m_{1,\infty}$. Further, it will be assumed that species 1 is chemically inert. The configuration under investigation is shown in Fig. 19-2.

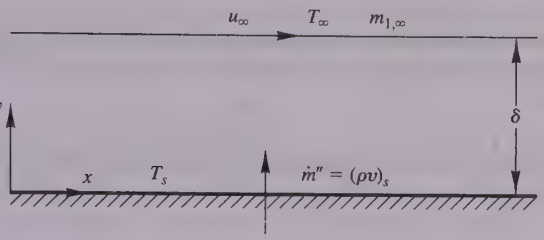

Figure 19-2 Configuration and coordinate system.

Because only one component is transferred into the boundary layer, one obtains from a mass balance between $y = 0$ and $y = \delta$ that

$$\dot{m}'' = (\rho v)_s = \text{constant} \tag{19-14}$$

throughout the boundary layer. Consider now a control volume within the flow field between $y = 0$ and an arbitrary position y (similar to the one considered in Fig. 18-3) and apply again the conservation of mass for the component 1 (the evaporating liquid), which is transferred. One obtains, with $m_{1,T} = 1$ (see also the derivation of Eq. (18-23)),

$$\dot{m}'' m_1 - \gamma_1 \frac{dm_1}{dy} - \dot{m}'' = 0 \tag{19-15}$$

This is an ordinary differential equation for the mass concentration of component 1. This differential equation has to be solved with the boundary condition that m_1 is specified at the interface $y = 0$ by the prescribed temperature T_s from the vapor pressure data of the evaporating liquid. Solving Eq. (19-15) results in:

$$\frac{m_1 - 1}{m_{1,s} - 1} = \exp\left(\frac{\dot{m}'' y}{\gamma_1}\right) \tag{19-16}$$

Evaluating Eq. (19-16) at $y = \delta$, where $m_1 = m_{1,\infty}$, one obtains

$$\frac{m_{1,\infty} - 1}{m_{1,s} - 1} = 1 + \frac{m_{1,\infty} - m_{1,s}}{m_{1,s} - 1} = \exp\left(\frac{\dot{m}'' \delta}{\gamma_1}\right) \tag{19-17}$$

From this equation it can be seen that the term $(m_{1,\infty} - m_{1,s})/(m_{1,s} - 1)$ is identical to the mass-transfer driving force B given by Eq. (18-32) (where $m_{1,T} = 1$ because only one component is transferred). Therefore, Eq. (19-17) might also be written as

$$1 + B = \exp\left(\frac{\dot{m}'' \delta}{\gamma_1}\right) \Rightarrow \dot{m}'' = \frac{\gamma_1}{\delta} \ln(1 + B) \tag{19-18}$$

Comparing Eq. (19-18) with the definition of g according to Eq. (18-33) shows that the mass-transfer conductance g is given by

$$g = \frac{\gamma_1}{\delta} \frac{\ln(1 + B)}{B} \tag{19-19}$$

The mass-transfer conductance g^* for the case of negligible mass transferred from the interface to the flow follows for $B \to 0$ from Eq. (19-19) by using l'Hospital's rule:

$$g^* = \lim_{B\to 0}\left(\frac{\gamma_1}{\delta}\frac{\ln(1+B)}{B}\right) = \frac{\gamma_1}{\delta}\lim_{B\to 0}\frac{(\ln(1+B))'}{(B)'} = \frac{\gamma_1}{\delta}\lim_{B\to 0}\left(\frac{1}{1+B}\right) = \frac{\gamma_1}{\delta} \tag{19-20}$$

One finally obtains

$$\frac{g}{g^*} = \frac{\ln(1+B)}{B} \tag{19-21}$$

Eq. (19-21) shows nicely that for the laminar Couette flow the ratio of the conductance g/g^* is only dependent on the mass-transfer driving force B and not on any other parameter.

THE LAMINAR CONSTANT-PROPERTY BOUNDARY LAYER, SIMILARITY SOLUTIONS FOR HIGH MASS-TRANSFER RATES

Under the stipulation of constant properties, Eq. (18-15) becomes

$$u\frac{\partial \mathcal{P}}{\partial x} + v\frac{\partial \mathcal{P}}{\partial y} - \frac{\partial}{\partial y}\left(\frac{\Phi}{\rho}\frac{\partial \mathcal{P}}{\partial y}\right) = 0 \tag{19-1}$$

The velocity components u and v must come again from a solution of the corresponding momentum and continuity equations:

$$u\frac{\partial u}{\partial x} + v\frac{\partial u}{\partial y} = \frac{\partial}{\partial y}\left(\frac{\mu}{\rho}\frac{\partial u}{\partial y}\right) \tag{19-2}$$

$$\frac{\partial u}{\partial x} + \frac{\partial v}{\partial y} = 0 \tag{19-3}$$

The above set of equations has to be solved together with the following boundary conditions:

$$\begin{aligned} x = 0:&\quad u = u_\infty, & \mathcal{P} &= \mathcal{P}_\infty \\ y = 0:&\quad u = 0,\ v = v_s, & \mathcal{P} &= \mathcal{P}_s, \\ y \to \infty:&\quad u \to u_\infty, & \mathcal{P} &\to \mathcal{P}_\infty \end{aligned} \tag{19-22}$$

We already have a group of exact solutions to the above given equations (19-1)–(19-3) and (19-22) for certain boundary conditions, namely the similarity solutions for $u_\infty = Cx^m$, in Chap. 10, where the boundary conditions include additional specifications that $\mathcal{P}_s$ and $\mathcal{P}_\infty$ are constant along the surface, and $(v_s/u_\infty)\sqrt{\mathrm{Re}_x}$ is constant along the surface. However, the similarity solutions in Chap. 10 employ temperature T as dependent variable, rather than $\mathcal{P}$. These solutions were presented in nondimensional form (see Tables 10-3 to 10-5) as

$$\frac{\mathrm{Nu}}{\sqrt{\mathrm{Re}_x}} = f\left(m, \mathrm{Pr}, \frac{v_s}{u_\infty}\sqrt{\mathrm{Re}_x}\right) \tag{19-23}$$

Now, following the approach from the last paragraphs, the Prandtl number in the above equation will be replaced by the Schmidt number ($\mathrm{Sc} = \mu/\Phi = \mu/\gamma$) and the Nusselt number has to be replaced by the Sherwood number

$$\mathrm{Sh} = \frac{gx}{\Phi} \quad \text{and} \quad \mathrm{St} = \frac{g}{G_\infty} \tag{19-24}$$

Finally, the blowing parameter must be interpreted in terms of mass-transfer parameters:

$$\frac{v_s}{u_\infty}\sqrt{\mathrm{Re}_x} = \frac{\dot{m}''}{G_\infty}\sqrt{\mathrm{Re}_x} \quad \text{(since the density is assumed to be constant)}$$

But, since $\dot{m}'' = gB$,

$$\frac{v_s}{u_\infty}\sqrt{\mathrm{Re}_x} = \frac{gB}{G_\infty}\sqrt{\mathrm{Re}_x} = \frac{xg}{\Phi}\frac{\mu}{xG_\infty}\frac{\Phi}{\mu}B\sqrt{\mathrm{Re}_x} = \frac{B}{\mu/\Phi}\frac{\mathrm{Sh}}{\sqrt{\mathrm{Re}_x}} \tag{19-25}$$

or

$$B = \frac{v_s}{u_\infty}\sqrt{\mathrm{Re}_x}\,\frac{\mu}{\Phi}\frac{\sqrt{\mathrm{Re}}}{\mathrm{Sh}} \tag{19-26}$$

Thus we see that we can express the similarity solutions from Eq. (19-23) in the form

$$\frac{\mathrm{Sh}}{\sqrt{\mathrm{Re}_x}} = f\left(m, \frac{\mu}{\Phi}, B\right) \tag{19-27}$$

where the functions f in Eqs. (19-23) and (19-27) are identical.

An interesting and perhaps unforeseen result is that the similarity solutions yield a constant value B along the surface. Since $\mathcal{P}_s$ and $\mathcal{P}_\infty$ have already been assumed constant in the above development, it is apparent that in this case constant B implies that $\mathcal{P}_T$ is constant.

Using the relation derived above, we can now convert all the similarity solutions presented in Chap. 10 to the form of Eq. (19-27). For example, consider Table 10-3 for $m = 0$ and $\mathrm{Pr} = 0.7$. With the indicated change of parameters, it becomes Table 19-1, a family of solutions to the $\mathcal{P}$ equation for $\mu/\Phi = 0.7$.

The other results in Tables 10-3 to 10-5 can be similarly modified. Spalding and Evans[4] present much more extensive tabulations of these solutions.

In Figs. 19-3 and 19-4 some of the constant-property similarity solutions for $m = 0$ (constant u_∞) are plotted in the form g/g^* as a function of B, where g^* is the limiting value of g as B approaches zero. Of particular interest in these plots is the fact that g/g^* is not only independent of Re_x, but is also only mildly dependent on μ/Φ.

Table 19-1 Solutions to the $\mathcal{P}$ equation for a laminar constant-property boundary layer for $m = 0$, $\mu/\Phi = 0.7$, and $B =$ constant ($v_s/u_\infty\sqrt{\mathrm{Re}_x} < 0$ indicates a mass flux into the interface, whereas $v_s/u_\infty\sqrt{\mathrm{Re}_x} > 0$ indicates a mass flux into the boundary layer)

$\dfrac{v_s}{u_\infty}\sqrt{\mathrm{Re}_x}$	$\dfrac{gx/\Phi}{\sqrt{\mathrm{Re}_x}}$	B
−2.500	1.8500	−0.946
−0.750	0.7220	−0.728
−0.250	0.4290	−0.408
0	0.2920	0
0.250	0.1660	1.054
0.375	0.1070	2.455
0.500	0.0517	6.780

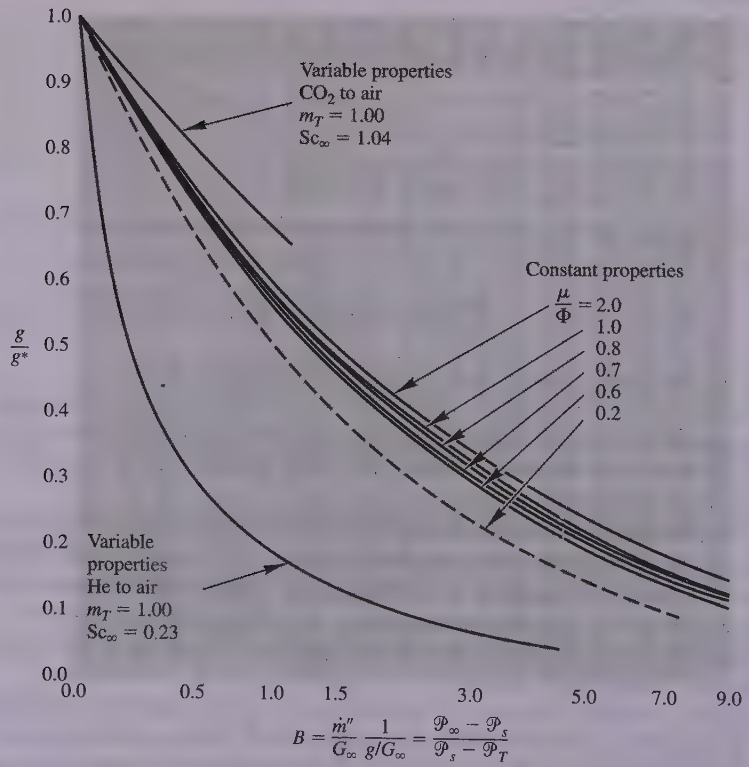

Figure 19-3 Solution of the $\mathcal{P}$ equation for a laminar boundary layer with constant free-stream velocity and $B \geq 0$.

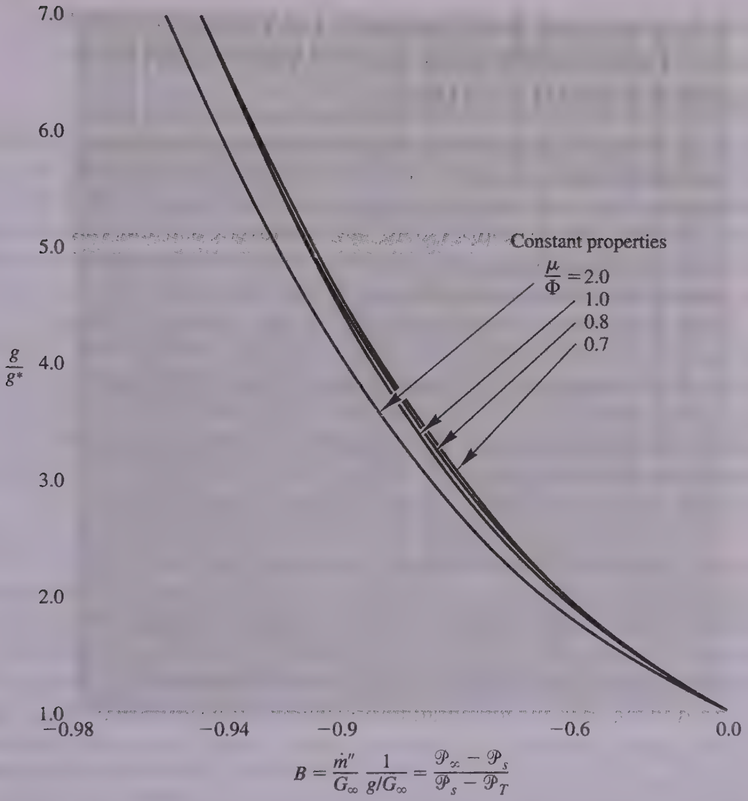

Figure 19-4 Solution of the $\mathcal{P}$ equation for a laminar boundary layer with constant free-stream velocity and $B \leq 0$.

A word regarding the useful applicability of the constant-property solutions is in order here. Obviously, in real problems the properties are not precisely constant. However, the constant-property mass-transfer solutions do provide a fair approximation for many applications, and they are accurately applicable under any of the following three conditions:

1. Applications where Φ, μ, and ρ are truly close to constant through the boundary layer because of the peculiar combination of fluids involved.
2. Low mass-transfer rates ($B \to 0$), as discussed at the beginning of this chapter. Here the transferred-substance concentration might never be large enough to change properties substantially.
3. High mass-transfer rates where most of the fluid transferred across the interface is the same as the free-stream fluid, but there is a small concentration of the fluid of interest in the transferred fluid. In other words, if $\mathcal{P} = m_j$, this would be the case of $m_{j,T} \ll 1$.

THE LAMINAR BOUNDARY LAYER FOR HIGH MASS-TRANSFER RATES: SOME VARIABLE-PROPERTY SOLUTIONS

In Fig. 19-3 there are also plotted some calculated results of Baron[5] for which helium and carbon dioxide, respectively, are injected from the surface into a laminar boundary layer with air as the free-stream fluid. The actual properties of the binary mixtures He–air and CO_2–air are employed, and the concentration of the helium or the carbon dioxide varies from zero in the free stream to a value at the s state that is a function of the mass-transfer rate [in fact, $m_s = B/(1+B)$]. In either case, mass concentration m_j is the conserved property $\mathcal{P}$, and $\mu/\Phi = \mu/\gamma = \mathrm{Sc}$. At very small values of B, the concentration of the He or CO_2 is small throughout the boundary layer, the constant-property situation is approached, and g^* can be taken as the result corresponding to the constant-property solution for the value of Sc for a dilute mixture. At high values of B, the Schmidt number varies markedly through the boundary layer, especially in the case of He–air; the results of property variation are shown in Fig. 19-3.

For engineering calculations it would be very convenient if constant-property solutions could be applied to variable-property applications by making some empirical correction to the former in much the same manner as was suggested in Chap. 15. Here, however, we are discussing variable properties caused by variation of mixture ratio through the boundary layer, whereas in Chap. 15 the variable properties were caused by temperature variations.

As was the case for temperature-dependent property effects, two empirical schemes appear possible. A *reference-property* scheme can be used whereby the appropriate constant-property solution is employed, and the fluid properties are evaluated at some defined reference composition. Or, alternatively, the constant-property solution can be employed at the free-stream state, and then the result is corrected by multiplying by a function of the ratio of some appropriate property evaluated at the s state and the ∞ state; this is the *property-ratio* scheme.

Knuth[6] has investigated the use of reference compositions for binary gas mixtures, employing, as a basis, an analysis of variable-property mass transfer to a Couette flow. Knuth finds that the few available variable-property laminar boundary-layer solutions can be satisfactorily correlated with the constant-property solutions if the fluid properties are all evaluated at a reference composition defined as follows: Let component A be injected into a boundary-layer in which the fluid is a mixture of component A and component B. Then the desired mean composition for correlation, expressed in terms of component B, is m_B^* and is given by

$$m_B^* = \frac{\mathfrak{M}_B}{\mathfrak{M}_B - \mathfrak{M}_A} \frac{\ln(\mathfrak{M}_\infty/\mathfrak{M}_s)}{\ln[m_{B,\infty}\mathfrak{M}_\infty/(m_{B,s}\mathfrak{M}_s)]} \tag{19-28}$$

where $\mathfrak{M}_A$ and $\mathfrak{M}_B$ are the molecular weights of components A and B, respectively, and $\mathfrak{M}_\infty$ and $\mathfrak{M}_s$ are the molecular weights of the mixture at the free-stream and s states, respectively. The molecular weight of a binary mixture of

A and *B* can be expressed as

$$\mathfrak{M} = \frac{\mathfrak{M}_A \mathfrak{M}_B}{\mathfrak{M}_B + (\mathfrak{M}_A - \mathfrak{M}_B) m_B} \tag{19-29}$$

It is evident that molecular weight is the dominant variable here, and an alternative scheme that empirically correlates the data in Fig. 19-3 equally satisfactorily is to replace the ordinate of Fig. 19-3 (and also presumably Fig. 19-4) by

$$\frac{g}{g^*}\left(\frac{\mathfrak{M}_\infty}{\mathfrak{M}_s}\right)^{2/3}$$

In this scheme all properties are otherwise introduced at the free-stream, or ∞, state. This is, of course, a *property-ratio* scheme.

Note that for a gas the density of the mixture varies directly with the molecular weight. In a binary gas mixture the diffusion coefficient D_j is virtually independent of mixture ratio, so that $\gamma_j = \rho D_j$ varies directly with density and thus directly with mixture molecular weight. The viscosity also varies with mixture ratio, but not nearly so much as ρ and γ_j. Thus the density variation is primarily responsible for the variable-property influence, and this is why correlations can be approximately obtained by use of a molecular-weight ratio.

THE LAMINAR CONSTANT-PROPERTY BOUNDARY LAYER WITH ARBITRARY VARYING FREE-STREAM VELOCITY AND HIGH MASS-TRANSFER RATES

In Chap. 10 an approximate scheme was described for extending the exact wedge-flow solutions to flow over a body of revolution with any arbitrarily varying free-stream velocity. It was shown in Fig. 10-6 that the necessary function could be approximated by a linear relation, which then yields a particularly simple equation for predicting the local Stanton number. Precisely the same technique can be used to extend the exact similarity solutions for blowing and suction to the variable-free-stream-velocity problem. In terms of the mass-transfer variables, the computing equation becomes [see also Eq. (10-52)]

$$\mathrm{St} = \frac{g}{G_\infty} = \frac{C_1 \mu^{1/2} R G_\infty^{C_2}}{\left(\int_0^x G_\infty^{C_3} R^2\, dx\right)^{1/2}} \tag{19-30}$$

The constants C_1, C_2, and C_3, as computed by Spalding and Chi,[7] are functions of μ/Φ and B and are given in Table 19-2.

Equation (19-30) and Table 19-2 then constitute a laminar flow constant-property solution to the $\mathcal{P}$ equation. Actually everything in Table 19-1 and Figs. 19-3 and 19-4, as well as in the earlier Tables 10-3 to 10-6, is incorporated in this result. These results are exact for the family of wedge-flow solutions and are presented as a useful approximation for the arbitrarily varying free-stream velocity problem.

Table 19-2 Constants for Eq. (19-30) for various values of μ/Φ for a laminar constant-property boundary layer

μ/Φ	B	C_1	C_2	C_3
0.7	−0.9	1.850	0.050	1.10
	−0.6	0.812	0.150	1.30
	0.0	0.418	0.435	1.87
	1.0	0.244	0.650	2.30
	3.0	0.136	1.150	3.30
	9.0	0.060	1.900	4.80
1.0	−0.9	1.430	0.150	1.30
	−0.6	0.633	0.250	1.50
	0.0	0.332	0.475	1.95
	1.0	0.200	0.650	2.30
	3.0	0.113	1.000	3.00
	9.0	0.052	1.450	3.90
5.0	−0.9	0.431	0.450	1.90
	−0.6	0.205	0.500	2.00
	0.0	0.117	0.595	2.19
	1.0	0.073	0.650	2.30
	3.0	0.045	0.750	2.50
	9.0	0.023	0.900	2.80
>5.0	−0.9	$1.037(\mu/\Phi)^{-2/3}$	0.900	2.80
	−0.6	$0.568(\mu/\Phi)^{-2/3}$	0.900	2.80
	0.0	$0.339(\mu/\Phi)^{-2/3}$	0.900	2.80
	1.0	$0.230(\mu/\Phi)^{-2/3}$	0.900	2.80
	3.0	$0.145(\mu/\Phi)^{-2/3}$	0.900	2.80
	9.0	$0.077(\mu/\Phi)^{-2/3}$	0.900	2.80

THE TURBULENT CONSTANT-PROPERTY BOUNDARY LAYER WITH CONSTANT FREE-STREAM VELOCITY AND HIGH MASS-TRANSFER RATES

For the case of *low mass-transfer rates* we have derived at the beginning of this chapter some correlations for the Sherwood number and therefore for the mass-transfer conductance g^* for $B \to 0$. A larger rate of mass transfer to or from the surface leads to the transpired boundary-layer problem discussed in Chaps. 11 and 12. If all fluid properties are assumed constant, it makes no difference if the fluid crossing the surface is chemically the same or different from the free-stream fluid. Thus Eqs. (12-37) and (12-38) should be applicable. The blowing parameter B_h is, of course, the same as B when g/G_∞ is substituted for St. Thus

$$\frac{g}{g^*} = \frac{\ln(1+B)}{B} \tag{19-31}$$

with g^* given by Eq. (19-11). Therefore, the mass-transfer conductance is given by

$$\frac{g}{G_\infty} = \frac{\ln(1+B)}{B} \frac{0.0287\,\mathrm{Re}_x^{-0.2}}{0.169\,\mathrm{Re}_x^{-0.1}[13.2(\mu/\Phi) - 8.66] + 0.85} \tag{19-32}$$

It is interesting to note that the relation between g and g^* given in Eq. (19-31) is the same as for the laminar Couette flow, which has been derived in one of the previous paragraphs [see Eq. (19-21)].

THE TURBULENT BOUNDARY LAYER: SOME VARIABLE-PROPERTY SOLUTIONS

The effects of property variations that results from large concentration differences through the boundary layer can be readily investigated if the $\mathcal{P}$ equation is solved by a numerical method, but, of course, the possible variations are enormous and little attempt has been made to generalize results. Rubesin and Pappas[8] presented two variable-property solutions for a constant free-stream velocity, employing a Couette flow approximation. In one, helium is injected into an air stream; in the other, hydrogen is injected. The conserved property is the concentration of helium, or hydrogen, in a binary mixture with air. In both cases $m_T = 1$.

The effect of the property variations proves to be very substantial, and serious error is introduced if it is ignored. However, a fairly satisfactory correlation is obtained if Eq. (19-31) is modified to

$$\frac{g}{g^*}\left(\frac{\mathfrak{M}_\infty}{\mathfrak{M}_0}\right)^{0.4} = \frac{\ln(1+B)}{B} \tag{19-33}$$

and all properties are otherwise evaluated at the free-stream state.

Knuth and Dershin[9] have investigated the use of reference composition to correlate variable-property turbulent boundary-layer solutions for binary gas mixtures with the constant-property solutions. They conclude that the same reference composition can be used as was suggested for the laminar boundary layer, that is, Eq. (19-28).

PROBLEMS

19-1. Consider a laminar Couette flow with mass transfer through the s surface. Let the transferred substance be CO_2 alone (this means that $m_T = 1$), and let the considered phase be a binary mixture of CO_2 and air, all at 1.013-bar pressure and 16°C. Let the thickness of the layer be such that the concentration of CO_2 at the ∞ state is always effectively zero. Using actual properties that vary with concentration, evaluate g/g^* as a function of B. Compare with the results given in Fig. 19-3.

19-2. Consider again Prob. 19-1, but let $m_T \ll 1$ so that γ can be treated as constant. Let the remainder of the transferred substance be air. Compare the results of both problems. Can you suggest an empirical correlation of the variable-property results with the constant property results?

19-3. Consider mass transfer from a fuel droplet, which can be approximated as a sphere. Let there be no effects of transverse flow; that is, the mass flows out symmetrically in all directions. Solve the $\mathcal{P}$ equation under the assumption of constant fluid properties to obtain an expression for g. What is the result for g/g^*?

19-4. Let the transferred substance of Prob. 19-3 be benzene and the surrounding fluid be air. Using the concentration of the benzene as the conserved property, calculate g/g^* as a function of B using the actual variable properties, assuming that the system is isothermal. Let the temperature be 150°C. (Note that the Schmidt number for the dilute mixture is relatively independent of temperature and pressure, that D_j is relatively independent of composition, and that γ_j is relatively independent of pressure. On this basis, γ_j can be estimated as a function of composition.) Compare the results with those of Prob. 19-3.

19-5. Prepare a plot of g/g^* as a function of B for a laminar constant-property boundary layer at an axisymmetric stagnation point, and at a two-dimensional stagnation point, for $\mathrm{Sc} = 0.5$. Compare with the similar results on the flat plate, $m = 0$.

19-6. It is required to estimate the average mass-transfer rate per unit area of benzene evaporating from the outer surface of a circular cylinder across which air is flowing at 6 m/s. The driving force B has been evaluated to be 0.9. It is found that if a cylinder of the same diameter is placed in the same air stream, the heat-transfer coefficient is $h = 85\ \mathrm{W/(m^2 \cdot K)}$. Estimate the mass-transfer rate explaining in detail the reasons for any assumptions that you build into the analysis. Evaluate the concentrations of benzene in the S state, assuming no chemical reaction.

REFERENCES

1. Eckert, E. R. G.: *VDI Forsch.-Heft*, no. 416, 1942.
2. Goldstein, R. J., and H. H. Cho: *Exp. Thermal and Fluid Sci.*, vol. 10, pp. 416–434, 1995.
3. Häring, M., A. Hoffs, A. Bölcs, and B. Weigand: Int. Gas Turbine and Aeroengine Congress and Exposition, Houston, USA, 95-GT-16, 1995.
4. Spalding, D. B., and H. L. Evans: *Int. J. Heat Mass Transfer*, vol. 2, pp. 314–341, 1960.
5. Baron, J. R.: Technical Report 160, Naval Supersonic Laboratory, MIT, Cambridge, Mass., 1956.
6. Knuth, E. L.: *Int. J. Heat Mass Transfer*, vol. 6, pp. 1–22, 1963.
7. Spalding, D. B., and S. W. Chi: *Int. J. Heat Mass Transfer*, vol. 6, pp. 363–385, 1963.
8. Rubesin, M. W., and C. C. Pappas: NACA (now NASA) TN 4149, Washington, February 1958.
9. Knuth, E. L., and H. Dershin: *Int. J. Heat Mass Transfer*, vol. 6, pp. 999–1018, 1963.

CHAPTER 20

Convective Mass Transfer: Examples for Application of the Simplified Method

This chapter is devoted to the solution of several mass transfer problems to further develop the applicability of the method presented in the last two chapters. The examples are selected in a way to show the reader how to best become familiar with the method. To provide guidance, the general problem solution method is reviewed before the various examples are solved.

GENERAL PROBLEM SOLUTION PROCEDURE

In Chap. 18 the mass transfer rate per unit area was shown to be proportional to B, the driving force based on the conserved property $\mathcal{P}$, such as the mass concentration of a mass species or chemical element, or an enthalpy or a temperature. In its generalized form, B is written as

$$B = \frac{\mathcal{P}_\infty - \mathcal{P}_s}{\mathcal{P}_s - \mathcal{P}_T} \tag{18-32}$$

With this, the mass transfer rate per unit area is written as

$$\dot{m}'' = gB \tag{18-33}$$

If we want to use Eq. (18-33), there are two different issues involved: one is the evaluation of the driving force B, and the other is the evaluation of the conductance g.

Choice of the Driving Force

The convective-mass-transfer methodology requires a choice of the driving force that is very much dependent on the type of mass-transfer problem under consideration and the information available. When we are concerned with the mass transfer of a single inert species, and we base the driving force on the mass concentration of the transferred substance, then we obtain always the simplification that $m_{1T} = 1$. The following examples show the reader how to choose and evaluate B from the given information in the problem. The examples range from air–water-vapor systems to combustion of volatile fuels.

Evaluation of the Conductance

Evaluation of the conductance g, corresponding to the chosen driving force B, has been developed in detail in Chap. 19. The evaluation of this quantity requires knowledge of the flow configuration and the physical properties involved. In the last chapter, the conductance g was based on the value g^* for $B \to 0$ which corresponds to a negligible low mass transfer rate at the interface. Therefore, the customary procedure is to develop the value for g^* and then adapt it to higher mass-transfer rates.

THERMODYNAMICS OF THE AIR–WATER-VAPOR SYSTEM

The thermodynamics of the air–water-vapor mixture system are simple and provide a particularly convenient vehicle for illustrating mass-transfer problems where the L state is a liquid phase while the s and ∞ states are gas phases. A familiar example is moist atmospheric air, which may be regarded as a mixture of dry air (treated as a single component) and water vapor. An adequate description of the thermodynamic state of this system can be obtained by assuming perfect-gas mixtures. a table of vapor pressure of water as a function of temperature, the latent heat of vaporization of H_2O at some reference temperature, and specific heat data for H_2O in the liquid and vapor forms and for air.

The following mixture relations are based on the definitions of the quantities involved. These basic definitions are summarized here because of their importance in understanding air–water-vapor systems.

The mass concentration of species j has been defined in Chap. 3 by

$$m_j = \frac{\rho_j}{\rho}$$

The molar concentration of species j is given by

$$c_j = \frac{\rho_j}{\mathfrak{M}_j} \tag{20-1}$$

The molar concentration of species j is the number of moles of this species per unit volume. The total molar concentration is

$$c = \sum_j c_j \tag{20-2}$$

The mole fraction of component j in the mixture is

$$x_j = \frac{c_j}{c} = \frac{\rho_j/\mathfrak{M}_j}{\sum_j \rho_j/\mathfrak{M}_j} = \frac{m_j/\mathfrak{M}_j}{\sum_j m_j/\mathfrak{M}_j} = \frac{m_j \mathfrak{M}}{\mathfrak{M}_j} \tag{20-3}$$

where $\mathfrak{M}$ is the equivalent molecular weight of the mixture. This quantity is defined by

$$\mathfrak{M} = \sum_j x_j \mathfrak{M}_j = \left(\sum_j \frac{m_j}{\mathfrak{M}_j}\right)^{-1} \tag{20-4}$$

The following summation rules exist for the mole fraction and the mass concentration:

$$\sum_j m_j = 1, \qquad \sum_j x_j = 1 \tag{20-5}$$

In the examples that follow, it will be necessary to have the mass concentration of species j be expressed explicitly in terms of mole fractions and molar weights. This can be done by using the following equations:

$$m_j = \frac{x_j \mathfrak{M}_j}{\mathfrak{M}} \Rightarrow x_j = \frac{m_j \mathfrak{M}}{\mathfrak{M}_j} \tag{20-6}$$

The mixture pressure P equals the sum of the partial pressures P_j of its constituents

$$P = \sum_j P_j \tag{20-7}$$

where P_j is given by the ideal gas law $P_j = \rho_j R_j T = \rho_j (\mathfrak{R}/\mathfrak{M}_j) T$. From Eq. (20-7) it follows for a mixture of ideal gases in thermodynamic equilibrium

$$x_j = \frac{c_j}{c} = \frac{m_j \mathfrak{M}}{\mathfrak{M}_j} = \frac{\rho_j \mathfrak{M}}{\mathfrak{M}_j \rho} = \frac{P_j}{\mathfrak{R}T}\frac{\mathfrak{R}T}{P} = \frac{P_j}{P} \tag{20-8}$$

when we assume that all components of the gas mixture are at the same mixture temperature.

For an air–water-vapor mixture the above equations combine to give the following relation for the mass concentration of the water vapor in the mixture:

$$\begin{aligned} m_{H_2O} &= \frac{x_{H_2O}\mathfrak{M}_{H_2O}}{x_{Air}\mathfrak{M}_{Air} + x_{H_2O}\mathfrak{M}_{H_2O}} \\ &= \frac{P_{H_2O}}{P\mathfrak{M}_{Air}/\mathfrak{M}_{H_2O} + P_{H_2O}\left(1 - \mathfrak{M}_{Air}/\mathfrak{M}_{H_2O}\right)} \end{aligned} \tag{20-9}$$

and with the ratio of the molecular weights of air (28.96 kg/kmol) and H_2O (18.016 kg/kmol) one finally obtains

$$m_{H_2O} = \frac{P_{H_2O}}{1.61P - 0.61P_{H_2O}} \tag{20-10}$$

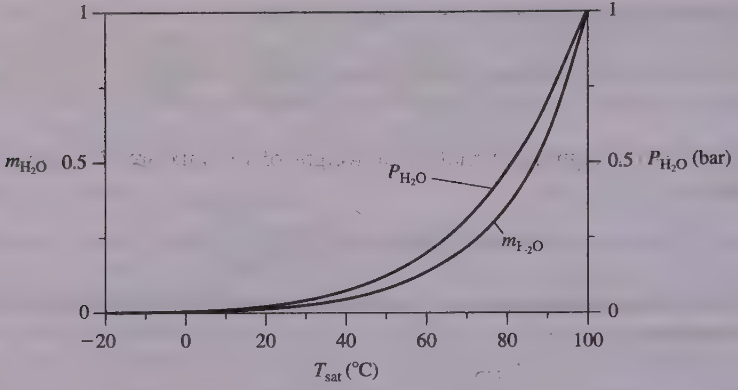

Figure 20-1 Vapor pressure of H_2O and mass concentration of H_2O in saturated air at $P = 1.013$ bar (compiled from App. A, Table A-20).

where P is the mixture pressure of the air–water-vapor mixture and P_{H_2O} is the partial pressure of the water vapor. If there is an interface in the boundary layer between the liquid H_2O and the air–water-vapor mixture, and if thermodynamic equilibrium is assumed to exist at the interface, then P_{H_2O} in Eq. (20-10) is the saturated vapor pressure of H_2O at the interface temperature $T_s = T_L$. This fact is important, because it will help us to define the correct driving force B for our problem.

Figure 20-1 shows the vapor pressure of H_2O and the mass concentration of H_2O in saturated air at $P = 1.013$ bar (see also App. A, Table A-20). It can be seen that there is a steep increase in P_{H_2O} and in m_{H_2O} for temperatures T_{sat} larger than about 60°C.

For specifying the moisture content of air, one can use the *absolute humidity* ω, kg H_2O/kg dry air. Here the amount of water in the air is related to the amount of dry air. This has the advantage that the amount of dry air will not change if, for example, some water is condensed from the flow and is taken out afterwards. The absolute humidity ω is related to the mass concentration of H_2O by

$$m_{H_2O} = 1 - \frac{1}{1+\omega} \tag{20-11}$$

Additionally, the *relative humidity* φ is defined by:

$$\varphi = \frac{P_{H_2O}}{P_{H_2O,sat}} \tag{20-12}$$

where $P_{H_2O,sat}$ is the saturated vapor pressure of H_2O at the mixture temperature. For $\varphi = 0$, the air is completely dry, whereas for $\varphi = 1$, the air is saturated with water vapor.

There are a number of different ways in which we could express the enthalpy of an air–water-vapor mixture, depending on the datum states chosen. The following scheme is adequate for present purposes, but otherwise has no advantages over any other scheme.

Air: The enthalpy model for air is based on the ideal-gas enthalpy model

$$i_{\text{air}} - i_{\text{air},0} = c_{\text{air}}(T - T_0)$$

Express T in °C and let 0°C be the datum ($T_0 = 0°\text{C}$). Then we obtain for a constant value of the specific heat

$$i_{\text{air}} = c_{\text{air}} T\,(°\text{C})$$

where $c_{\text{air}} = 1.005\ \text{kJ/(kg} \cdot \text{K)}$.

H_2O: For the water-vapor enthalpy model, let the datum be liquid H_2O at 0°C. Then for H_2O vapor with a constant value of the specific heat, we obtain

$$i_{\text{H}_2\text{O}} = i_{fg,0} + c_{\text{H}_2\text{O}} T\,(°\text{C})$$

where $i_{fg,0} = 2503\ \text{kJ/kg}$ and $c_{\text{H}_2\text{O}} = 1.880\ \text{kJ/(kg} \cdot \text{K)}$.

Now, the enthalpy for a air–water-vapor mixture is

$$i = \sum_j m_j\, i_j = m_{\text{air}}\, i_{\text{air}} + m_{\text{H}_2\text{O}}\, i_{\text{H}_2\text{O}} = \left(1 - m_{\text{H}_2\text{O}}\right) i_{\text{air}} + m_{\text{H}_2\text{O}}\, i_{\text{H}_2\text{O}} \qquad (20\text{-}13)$$

Combining Eq. (20-13) with the enthalpy models for air and water yields

$$i = \left(1.005 + 0.875\, m_{\text{H}_2\text{O}}\right) T\,(°\text{C}) + 2503\, m_{\text{H}_2\text{O}}, \ \text{kJ/kg mixture} \qquad (20\text{-}14)$$

Note that for the pure liquid phase, the water enthalpy is given by

$$i_{\text{liquid}} = c_{\text{liquid}} T\,(°\text{C})$$

where $c_{\text{liquid}} = 4.2\ \text{kJ/(kg} \cdot \text{K)}$.

ANALYSIS OF THE WET-BULB PSYCHROMETER

Consider a thermometer, the bulb of which is surrounded by a cloth wick that has been dipped in water. Then allow moist air, the humidity of which is to be determined, to flow over the bulb (Fig. 20-2). If the system is allowed to come to equilibrium and if the wick remains moist, the thermometer will indicate a temperature T_{wb} lower than the free-stream, or dry-bulb, temperature T_{db}, which can be measured independently by another thermometer. At equilibrium, $\dot{q}''_L = 0$, and in terms of our formulation of the mass-transfer problem $T_{\text{wb}} = T_s = T_L$ and $T_{\text{db}} = T_\infty$.

The concentration of H_2O in the mixture is a conserved property, since this problem involves the mass diffusion of the inert substance H_2O. Because only one substance is transferred, we know that $m_{\text{H}_2\text{O},T} = 1$. With this, we can express the driving force as

$$B = \frac{m_{\text{H}_2\text{O},\infty} - m_{\text{H}_2\text{O},s}}{m_{\text{H}_2\text{O},s} - m_{\text{H}_2\text{O},T}} = \frac{m_{\text{H}_2\text{O},\infty} - m_{\text{H}_2\text{O},s}}{m_{\text{H}_2\text{O},s} - 1} \qquad (20\text{-}15)$$

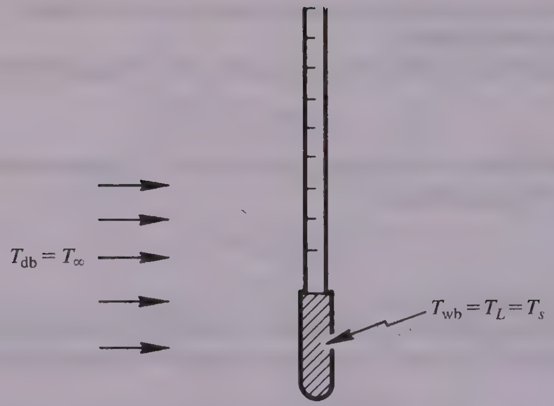

Figure 20-2 The wet-bulb psychrometer.

In this equation, $m_{H_2O,\infty}$ is the concentration of H_2O in the free stream, which we want to predict. The value of $m_{H_2O,s}$ can be determined if we know T_{wb}, because this temperature determines the saturation pressure $P_{H_2O,sat}$ at the interface for the case of thermodynamic equilibrium, and we can evaluate $m_{H_2O,s}$ from Eq. (20-10) for a given pressure $P = 1.013$ bar (see App. A, Table A-20 and Fig. 20-1).

To appreciate the order of magnitude of the numbers involved, consider the case of $T_{wb} = 16°C$, $T_{db} = T_\infty = 27°C$ and $P = 1.013$ bar. Then we find from App. A that $m_{H_2O,s} = 0.011$. Because $m_{H_2O,\infty}$ must be lower or equal to $m_{H_2O,s}$, we find from Eq. (20-15) values for B in the range between 0 and 0.01. This shows clearly that we consider here a low-mass-transfer problem, where $B \to 0$. Furthermore, it is clear from the above values that one can approximate the driving force B for the case under consideration by

$$B = m_{H_2O,s} - m_{H_2O,\infty} \tag{20-16}$$

because the value of $m_{H_2O,s}$ is negligible compared to 1 in the denominator of Eq. (20-15). Inserting Eq. (20-16) into Eq. (18-33) results in

$$\dot{m}'' = g(m_{H_2O,s} - m_{H_2O,\infty})$$

leading to

$$m_{H_2O,\infty} = m_{H_2O,s} - \frac{\dot{m}''}{g} \tag{20-17}$$

For the present example, we want to predict $m_{H_2O,\infty}$ and the humidity of the air stream. Therefore, the mass transfer rate per unit area $\dot{m}''$ in Eq. (20-17) needs to be replaced by known quantities. This can be done by considering an energy balance at the interface. If we reexamine the general form of the boundary condition for the energy equation [Eqs. (18-25) to (18-27)], we note that the second term in the numerator of Eq. (18-27) is simply the convection heat flux $\dot{q}_s''$. Because the concentration of H_2O is everywhere small, $\dot{q}_s''$ is virtually unaffected by the presence of the water vapor and can be calculated as if there is no mass transfer. The first term in the numerator of Eq. (18-27) can be obtained from the solution to the mass-diffusion equation by using Eq. (18-23). If we now let i_{H_2O} be zero at the s state, so that $i_L = i_{fg,s}$, and express i_T in terms of i_L and $\dot{q}_L''/\dot{m}''$ by Eq. (18-25), we readily obtain the following expression for $\dot{q}_L''$

$$\dot{q}_L'' = h(T_\infty - T_s) - \dot{m}'' i_{fg,0} \tag{20-18}$$

where h is the conductance for heat transfer in the absence of mass transfer. In this equation the latent heat of vaporization of water $i_{fg,s} = i_{fg}(T_s)$ has been replaced by $i_{fg,0} = i_{fg}(T_0 = 0°\text{C})$ because the latent heat of vaporization of water changes only by about 2 percent between 0 and 20°C, which is roughly the temperature range of interest for T_s for our application.

At equilibrium, $\dot{q}_L'' = 0$, and in terms of our formulation of the mass-transfer problem $T_{\text{wb}} = T_s = T_L$ and $T_{\text{db}} = T_\infty$. Then Eq. (20-18) states the simple fact that the heat generated by phase change has to be transported away from the interface by convection. Inserting Eq. (20-18) into Eq. (20-17) results in

$$m_{H_2O,\infty} = m_{H_2O,s} - \frac{h}{g i_{fg,0}}(T_{\text{db}} - T_{\text{wb}}) \tag{20-19}$$

Because of the low mass-transfer rates from the interface into the flow, g can be replaced by g^*, and the ratio h/g^* might be obtained from an appropriate geometric shape of the thermometer. Assuming, for example, laminar flow and that the flow around the thermometer can be approximated by a flow around a cylinder, one obtains h and g^* from Eq. (10-22):

$$\frac{h}{g^*} = c_{\text{air}} \left(\frac{\text{Pr}}{\text{Sc}}\right)^{0.4} \tag{20-20}$$

Combining Eq. (20-19) with Eq. (20-20) yields

$$m_{H_2O,\infty} = m_{H_2O,s} - \frac{c_{\text{air}}}{i_{fg,0}} \left(\frac{\text{Pr}}{\text{Sc}}\right)^{0.4} (T_{\text{db}} - T_{\text{wb}}) \tag{20-21}$$

where $m_{H_2O,s}$ is determined by the temperature measured at the wet bulb thermometer for a fixed pressure by App. A, Table A-20. Therefore

$$m_{H_2O,s} = m_{H_2O,s}(T_{\text{wb}}, P) \tag{20-22}$$

where P in the case considered here is standard atmospheric pressure, 1.013 bar. The prediction of the relative humidity $\varphi = P_{H_2O}/P_{H_2O,\text{sat}}$ according to Eq. (20-12) requires that the partial pressure of H_2O be known. The partial pressure can be determined by using the mass concentration predicted from Eq. (20-21), then using Eqs. (20-6) and (20-8).

The above procedure will now be illustrated by an example: Assume air at a pressure of 1.013 bar flows over a combination wet-dry bulb thermometer. The wet bulb thermometer measures a temperature of $T_{\text{wb}} = 16°\text{C}$, whereas the dry bulb thermometer measures $T_{\text{db}} = T_\infty = 27°\text{C}$. The objective is to determine the relative humidity of the air. From App. A, Table A-20, one obtains: $m_{H_2O,s} = 0.011$,

$P_{H_2O,\text{sat}} = 1831$ Pa. With $c_{\text{air}} = 1005$ J/(kg · K), $i_{fg,0} = 2503$ kJ/kg and with Pr = 0.716, Sc = 0.599 from App. A, Table A-19, we obtain from Eq. (20-21):

$$m_{H_2O,\infty} = 0.011 - \frac{1005}{2503000}\left(\frac{0.716}{0.599}\right)^{0.4}(27 - 16) = 0.00628$$

From Eq. (20-6) we get

$$\begin{aligned} x_{H_2O,\infty} &= \frac{m_{H_2O,\infty}/\mathfrak{M}_{H_2O}}{m_{H_2O,\infty}/\mathfrak{M}_{H_2O} + m_{\text{air},\infty}/\mathfrak{M}_{\text{air}}} \\ &= \frac{m_{H_2O,\infty}/\mathfrak{M}_{H_2O}}{m_{H_2O,\infty}/\mathfrak{M}_{H_2O} + \left(1 - m_{H_2O,\infty}\right)/\mathfrak{M}_{\text{air}}} \\ &= \frac{0.00628/18.016}{0.00628/18.016 + (1 - 0.00628)/28.96} = 0.01 \end{aligned}$$

and the partial pressure is

$$P_{H_2O,\infty} = x_{H_2O,\infty} P = 1013\,\text{Pa}$$

With this we finally obtain for the relative humidity

$$\varphi = \frac{P_{H_2O}}{P_{H_2O,\text{sat}}} = \frac{1013}{1831} = 0.55$$

In the analysis of the example we did not assume that the Lewis number is unity. In Chap. 18 it was shown that several simplifications could be developed for the solution of the mass diffusion and the energy equation. From the calculation shown above it can be seen that the air–water-vapor mixture system is close to a unity-Lewis-number system. Thus the simplified form of the energy equation is a reasonable approximation, and the enthalpy is also a conserved property. Furthermore, if Le = 1 then $\Gamma = \gamma_j$, and it follows that the same value of g applies to both the energy- and mass-diffusion problems. The B values are thus the same, because $\dot{m}''$ is common to both equations. We thus can write, from the energy equation

$$B = \frac{i_\infty - i_s}{i_s - i_T}$$

Equating this expression with Eq. (20-16) results in

$$\frac{i_\infty - i_s}{i_s - i_T} = m_{H_2O,s} - m_{H_2O,\infty} \tag{20-23}$$

The enthalpies are given by

$$i_\infty = \left(1.005 + 0.875\, m_{H_2O,\infty}\right)T_{\text{db}} + 2503\, m_{H_2O,\infty}$$

$$i_s = \left(1.005 + 0.875\, m_{H_2O,s}\right)T_{\text{wb}} + 2503\, m_{H_2O,s}$$

$$i_T = i_L - \frac{\dot{q}''_L}{\dot{m}''} = i_L = 4.2T_{\text{wb}}$$

Solving Eq. (20-23) for $m_{H_2O,\infty}$ in the example gives $m_{H_2O,\infty} = 0.00654$, $x_{H_2O,\infty} = 0.01047$, and $\varphi = 0.58$, which shows very nicely that only slightly higher values for the relative humidity will be obtained with the assumption of $Le = 1$ for the wet-dry bulb thermometer system.

DRYING

Suppose we have a wet surface that we want to dry by blowing air over it while at the same time supplying heat to the surface (Fig. 20-3). It is assumed that the surface can be estimated by a flat plate. The external flow speed is such that the flow is laminar.

Let $T_\infty = 27°\text{C}$ and $m_{H_2O,\infty} = 0.02$. Suppose we supply heat sufficient to hold the surface at 82°C, that is, $T_s = T_L = 82°\text{C}$. Let $P = 1.013$ bar. The objective of the analysis is to determine the drying rate per unit area $\dot{m}''$ during the period the surface is completely wet and to determine the heat flux $\dot{q}_L''$ necessary to hold the surface at 82°C.

From App. A, Table A-20, we obtain $m_{H_2O,s} = 0.393$. For an inert substance m_{H_2O} is a conserved property and we can predict the driving force

$$B = \frac{m_{H_2O,\infty} - m_{H_2O,s}}{m_{H_2O,s} - m_{H_2O,T}} = \frac{m_{H_2O,\infty} - m_{H_2O,s}}{m_{H_2O,s} - 1} = \frac{0.02 - 0.393}{0.393 - 1} = 0.615$$

Thus

$$\dot{m}'' = gB \tag{18-33}$$

Note that in this example the H_2O concentration is no longer small and B is sufficiently large such that g/g^* is no longer near unity. This means that the present example falls into the class of the high-mass-transfer-rate problems. In order to evaluate the mass-transfer conductance g, we first need to predict g^* for the flow over a flat plate.

For the above conditions it is known that the flow is laminar. Therefore g^* can be predicted from Eq. (10-15) by replacing Nu_m with Sh_m and Pr with Sc. For a plate with the length l in the flow direction,

$$Sh_m = \frac{g^* l}{\gamma} = 0.664\, Sc^{1/3}\, Re_l^{1/2}$$

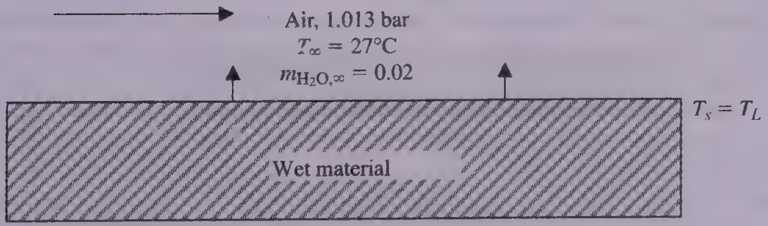

Figure 20-3 Example of drying of a wet surface.

leading to

$$g^* = \frac{\gamma}{l} 0.664\,\mathrm{Sc}^{1/3}\,\mathrm{Re}_l^{1/2}$$

where the fluid properties have to been taken from App. A, Table A-19. The ratio of g/g^* can be obtained from Fig. 19-3 to be 0.69 for $B = 0.615$. Therefore, the mass-transfer rate per unit area at the interface (drying rate) is given by

$$\dot{m}'' = 0.69\left(\frac{\gamma}{l} 0.664\,\mathrm{Sc}^{1/3}\,\mathrm{Re}_l^{1/2}\right) B$$

To evaluate the necessary heat flux, we turn to the energy equation and the unit-Lewis-number simplification (from App. A, Table A-19 it can be seen that this is a reasonable engineering assumption, because the Lewis number for the present case is about 1.38). Then enthalpy is a conserved property and we obtain

$$B = \frac{i_\infty - i_s}{i_s - i_T} = \frac{i_\infty - i_s}{i_s - i_L + \dot{q}_L''/\dot{m}''} = 0.615$$

Solving for $\dot{q}_L''$ gives

$$\dot{q}_L'' = \dot{m}''(1.63 i_\infty - 2.63 i_s + i_L)$$

where $\dot{m}''$ has been predicted above and the enthalpies can be evaluated from Eqs. (20-13) and (20-14).

EVAPORATIVE COOLING

Suppose we have a uniformly porous surface exposed to a hot dry gas and we would like to keep the surface cool by forcing water through the surface at a sufficient rate to keep the surface wet. Consider the example shown in Fig. 20-4. The objective is to determine the necessary cooling rate at the equilibrium surface temperature $T_s = T_L$.

For an inert substance

$$B = \frac{m_{\mathrm{H_2O},\infty} - m_{\mathrm{H_2O},s}}{m_{\mathrm{H_2O},s} - m_{\mathrm{H_2O},T}} = \frac{-m_{\mathrm{H_2O},s}}{m_{\mathrm{H_2O},s} - 1}$$

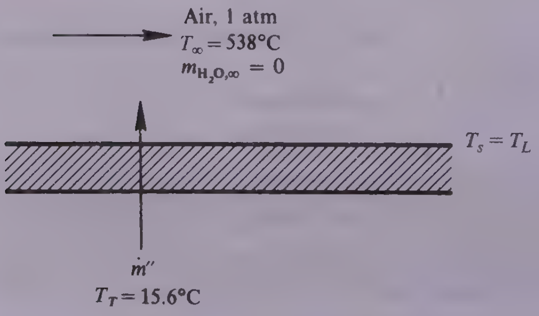

Figure 20-4 Example of evaporative cooling.

Again, we will assume that the Lewis number is equal to 1 for the analysis, enthalpy becomes the conserved property, and

$$B = \frac{i_\infty - i_s}{i_s - i_T}$$

For the present case we are not interested in $\dot{q}_L''$, but we do know the T-state temperature, 15.6°C. Equating the two expressions for B and substituting Eqs. (20-13) and (20-14) for the enthalpies, we obtain an equation with $m_{H_2O,s}$ and T_s as unknowns:

$$\frac{m_{H_2O,s}}{1 - m_{H_2O,s}} = \frac{1.005T_\infty - (1.005 + 0.875\,m_{H_2O,s})T_s - 2503\,m_{H_2O,s}}{(1.005 + 0.875\,m_{H_2O,s})T_s + 2503\,m_{H_2O,s} - 4.2T_T}$$

The two unknowns are related by the equation of state and can be separately evaluated. The solution is an iterative one, yielding

$$T_s = 63.2^\circ\text{C}, \qquad m_{H_2O,s} = 0.157$$

Finally we obtain

$$B = \frac{-m_{H_2O,s}}{m_{H_2O,s} - 1} = \frac{-0.157}{0.157 - 1} = 0.187$$

and

$$\dot{m}'' = gB = 0.187g$$

We now investigate the low-mass-transfer assumption that would permit the use of g^* instead of g. This requires evaluation of Eq. (19-21), leading to

$$\frac{g}{g^*} = \frac{\ln(1 + B)}{B} = 0.92$$

This ratio is significantly close to unity, and thus we can use g^* in the above equation with sufficient accuracy to predict the necessary cooling water rate.

NAPHTHALENE SUBLIMATION FROM A FLAT PLATE

As outlined in the previous chapter, the naphthalene ($C_{10}H_8$) sublimation technique can be used for determining the convective heat transfer by using the analogy between heat and mass transfer. Therefore, this method is usually called an indirect method for determining the heat transfer coefficient. For this method, the mass-flow rate at the interface is always selected to be very small, in order to avoid any influence of blowing at the wall on the mass transfer coefficient.

As an example of the method, let us consider a flat plate, which is coated with a 0.5-mm-thick naphthalene layer. The model is exposed to air flow with a free-stream velocity of 10 m/s, a free-stream temperature of 20°C and a pressure of 1.013 bar. The plate temperature is held constant at 20°C. The configuration and the coordinate system are shown in Fig. 20-5.

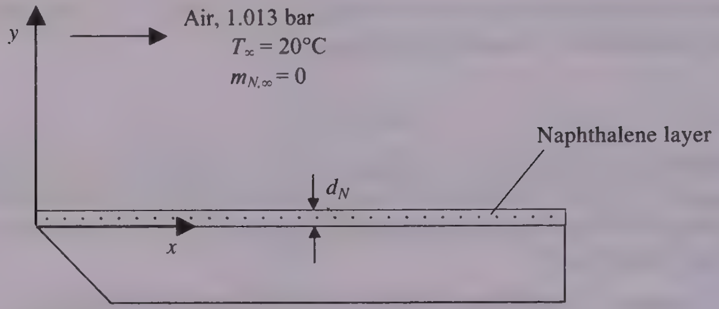

Figure 20-5 Naphthalene sublimation on a flat plate.

Table 20-1 Thickness of the naphthalene layer after 3 hours exposure to a free stream

Axial position x, m	**0.1**	**0.2**	**0.3**	**0.4**	**0.5**
Naphthalene thickness d_N, mm	0.477	0.484	0.485	0.488	0.490

After exposing the plate to the free stream for 3 hours, some of the naphthalene has been sublimated and the thickness of the layer has decreased. At that time the new thickness of the layer is described in Table 20-1. The objective is to determine the heat-transfer coefficient at the given axial positions of the flat plate from the decrease in naphthalene thickness.

The properties of naphthalene ($C_{10}H_8$) are (Presser[5]):

Saturated vapor pressure (Pa)	$\log P_{N,\text{sat}} = \left(13.57 - \dfrac{3734}{T}\right)$ $(273\text{ K} < T < 323\text{ K})$
Solid density	$\rho_N = 1145\text{ kg/m}^3$ $(280\text{ K} < T < 300\text{ K})$
Molecular weight	$\mathfrak{M}_N = 128.16\text{ kg/kmol}$
Schmidt number (in air at 20°C):	$\text{Sc} = 2.53$

From Eq. (18-33) one obtains

$$g = \frac{\dot{m}''}{B}$$

where B is given by Eq. (18-32). For an inert substance

$$B = \frac{m_{N,\infty} - m_{N,s}}{m_{N,s} - m_{N,T}} = \frac{m_{N,\infty} - m_{N,s}}{m_{N,s} - 1}$$

Now, the mass concentration of naphthalene at the infinite state, subscript ∞, is negligible and can be set to zero. Furthermore, we will assume that the properties of the free stream (air) do not change because of the very small amount of naphthalene that mixes with the air (the properties of the air flow can be taken from

Table A-1: $\rho = 1.2047\ \text{kg/m}^3$, $\nu = 15.08 \times 10^{-6}\ \text{m}^2/\text{s}$, $k = 0.02563\ \text{W/(m}\cdot\text{K)}$, $\text{Pr} = 0.712$). The mass concentration at the surface is determined by the saturated vapor pressure and can be calculated from the ideal gas law

$$m_{N,s} = \frac{\rho_N}{\rho_{\text{air}}} = \frac{P_{N,\text{sat}}}{P_{\text{air}}} \frac{T_{\text{air}}}{T_{N,s}} \frac{\mathfrak{M}_N}{\mathfrak{M}_{\text{air}}}$$

because the plate is held isothermal at the free-stream temperature, causing the naphthalene–air boundary layer and the free stream to be the same temperature. From the above equation

$$m_{N,s} = \frac{P_{N,\text{sat}}}{P_{\text{air}}} \frac{\mathfrak{M}_N}{\mathfrak{M}_{\text{air}}} = \frac{6.8}{101300} \frac{128.16}{28.96} = 2.97 \times 10^{-4}$$

which confirms that naphthalene sublimation is a very low-mass-transfer-rate problem. Thus the driving force B can be simplified to

$$B = \frac{m_{N,\infty} - m_{N,s}}{m_{N,s} - 1} = (m_{N,s} - m_{N,\infty}) = 2.97 \times 10^{-4}$$

In order to determine the mass-transfer conductance g, which is equal to g^* because $B \to 0$, the mass rate per unit area $\dot{m}''$ needs to be predicted. This can be done from the thickness change in the naphthalene layer and the measurement time:

$$\dot{m}'' = \frac{1}{A} \frac{\Delta m}{\Delta \tau} = \rho_N \frac{d_N(\tau = 0) - d_N(\tau = 10800s)}{\Delta \tau}$$

Finally, the mass-transfer Stanton number can be predicted from Eq. (18-38) according to

$$\text{St}^*_{\text{mass}} = \frac{g^*}{(\rho u)_\infty}$$

Table 20-2 shows the predicted values for g^* and St^* at various x-Reynolds numbers. As can be seen from this table, the flow is laminar over the entire plate. Because the flow is laminar, the heat-transfer coefficient can be formulated by using the heat- and mass-transfer analogy equation from Chap. 19,

$$\frac{\text{Nu}^*}{\text{Sh}^*} = \left(\frac{\text{Pr}}{\text{Sc}}\right)^{1/3} \tag{19-8}$$

Table 20-2 Mass-transfer conductance and mass-transfer Stanton number for the flat plate

Axial position x, m	0.1	0.2	0.3	0.4	0.5
Naphthalene thickness d_N, mm	0.477	0.484	0.485	0.488	0.490
Mass transfer conductance g^*, kg/(m$^2\cdot$s)	8.210	5.710	5.355	4.284	3.569
Mass transfer Stanton number $\text{St}^*/10^{-3}$	0.6815	0.4741	0.4444	0.3555	0.2964
Local Reynolds number Re_x	66,312	132,626	198,939	265,251	331,564

Table 20-3 Heat-transfer Stanton and Nusselt numbers obtained from the thickness change of the naphthalene layer by the analogy between heat and mass transfer

Axial position x, m	**0.1**	**0.2**	**0.3**	**0.4**	**0.5**
Local Reynolds number Re_x	66,312	132,626	198,939	265,251	331,564
Heat transfer Stanton number $\mathrm{St}^*/10^{-3}$	1.586	1.104	1.035	0.8277	0.6901
Nu^* from analogy	74.9	104.3	146.6	156.4	162.9

Using the definitions of the heat and mass transfer Stanton numbers gives

$$\mathrm{St}^*_{\mathrm{mass}} = \frac{\mathrm{Sh}^*}{\mathrm{Re}_x \mathrm{Sc}} \quad \text{and} \quad \mathrm{St}^*_{\mathrm{heat}} = \frac{\mathrm{Nu}^*}{\mathrm{Re}_x \mathrm{Pr}}$$

Eq. (19-8) becomes the defining equation for the heat- and mass-transfer analogy,

$$\frac{\mathrm{St}^*_{\mathrm{heat}}}{\mathrm{St}^*_{\mathrm{mass}}} = \left(\frac{\mathrm{Sc}}{\mathrm{Pr}}\right)^{2/3}$$

For this example, predicted values for the heat-transfer Stanton number $\mathrm{St}^*_{\mathrm{heat}}$ and the Nusselt number Nu^* are given in Table 20-3, and the results show how the analogy between heat and mass transfer can be used for obtaining heat-transfer coefficients from *low-mass-transfer-rate convection* results.

BURNING OF A VOLATILE FUEL IN AIR

Let us consider the rate of burning of a droplet of ethyl alcohol (C_2H_5OH) in air (Fig. 20-6). We are concerned with the mass-transfer rate per unit area $\dot{m}''$ at which alcohol leaves the surface.

As a first approximation, let us assume that the rate of chemical reaction is so much greater than the rate at which components are diffused through the boundary layer that the reaction can be assumed to be instantaneous, and the burning rate is then *diffusion-controlled*. This assumption allows us to specify

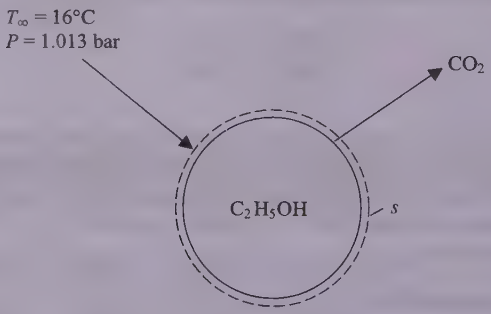

Figure 20-6 Burning of a droplet of ethyl alcohol.

rather simple boundary conditions, since there can then be no oxygen at the s state and no fuel at the ∞ state.

Next we assume that the "simple chemical reaction" is a valid approximation, that all specific heats are equal and $\gamma_{O_2} = \Gamma$, and that for the mass-diffusion equation $\gamma_{O_2} = \gamma_{C_2H_5OH}$. These are admittedly rather gross approximations, but the alternative is a complete solution of the basic differential equations of the boundary layer. Our objective here is an approximate solution, obtained by reducing the problem to a solution of the $\mathcal{P}$ equation.

A complete solution of this problem requires both the energy equation and the mass-diffusion equation, but we find it most convenient to use the former. To a close approximation, the energy equation alone will give us the driving force B.

Let us first investigate the chemical reaction of the fuel. It is assumed that the fuel will react to CO_2 and H_2O:

$$\begin{array}{llll}
C_2H_5OH & + 3\,O_2 & \rightarrow 2\,CO_2 & + 3\,H_2O \\
1\,\text{kmol } C_2H_5OH & + 3\text{ kmol } O_2 & \rightarrow 2\text{ kmol } CO_2 & + 3\text{ kmol } H_2O \\
46\text{ kg } C_2H_5OH & + 3\cdot 32\text{ kg } O_2 & \rightarrow 2\cdot 44\text{ kg } CO_2 & + 3\cdot 18\text{ kg } H_2O
\end{array}$$

and $r = (3\cdot 32)/46 = 2.09$.

Because we are considering atmospheric air, $m_{O_2,\infty} = 0.232$. The further constants for this problem are as follows:

$T_\infty = 16°C$

$H_0 = 28{,}145$ kJ/(kg fuel vapor), heat of combustion of fuel at $T_0 = 78°C$

$i_{fg,0} = 854$ kJ/(kg fuel), latent heat of vaporization of fuel at $T_0 = 78°C$

$c = 1.005$ kJ/(kg · K)

$P = 1.013$ bar

As a first step, let us assume that the entire droplet is uniformly at the same temperature $T_s = T_L = T_T = 78°C$, the boiling point of C_2H_5OH at 1.013-bar pressure. The actual surface temperature is somewhat lower and must be established by iteration. However, we will see that we do not need to know this temperature very accurately to evaluate B.

For a simple chemical reaction we have previously seen that we can express the enthalpy of the system by Eq. (F-17):

$$i = m_{O_2}\frac{H_0}{r} + \int_{T_0}^{T} c\,d\tilde{T} \tag{F-17}$$

If we assume that c is approximately constant for the temperature range considered, it follows

$$i = m_{O_2}\frac{H_0}{r} + c\,(T - T_0)$$

For convenience, let us set the s state as the datum for enthalpy, so that $T_0 = T_s$.

Since C_2H_5OH is a volatile fuel, the reaction is a gas-phase reaction and takes place somewhere between the s state and the ∞ state. Under the assumption of instantaneous reaction, we can conclude that $m_{O_2,s} = 0$.

Then

$$\begin{aligned} i_s &= 0 \text{ kJ/kg} \\ i_\infty &= 0.232\frac{28{,}145}{2.09} + 1.005(16 - 78) = 3062 \text{ kJ/kg} \\ i_T &= i_L \quad (\text{since } \dot{q}''_L = 0 \text{ by conditions of this problem}) \\ &= -i_{fg,0} = -854 \text{ kJ/kg} \end{aligned}$$

With these values we can evaluate the driving force B:

$$B = \frac{i_\infty - i_s}{i_s - i_T} = \frac{3062 - 0}{0 - (-854)} = 3.59$$

Finally, $\dot{m}'' = gB$ can be obtained. For this example one has to notice the large value of B. This indicates that there is a large mass transferred from the interface into the flow. Therefore, g will take values far away from g^*.

Finally, it should be noted that a proper evaluation of the surface temperature would require that we need to know the mixture composition at the s state, so that the partial pressure of the fuel at the s state may be evaluated. To do this, we can turn to the mass-diffusion equation for a simple chemical reaction, but we can see from the above calculations that the result for B is not very sensitive to small changes of T_s.

SIMPLE GRAPHITE BURNING IN AIR

Let us consider the rate of burning of carbon from a graphite surface in an atmospheric-air environment. The surface shall be approximated by a flat plate (see Fig. 20-7). It is assumed that the only chemical reaction taking place in the vicinity of the surface is

$$\begin{array}{ccccc} 2\,C & + & O_2 & \rightarrow & 2\,CO \\ 2 \cdot 12 \text{ kg C} & + & 32 \text{ kg } O_2 & \rightarrow & 2 \cdot 28 \text{ kg CO} \end{array}$$

and $r = 32/(2 \cdot 12) = 1.33$.

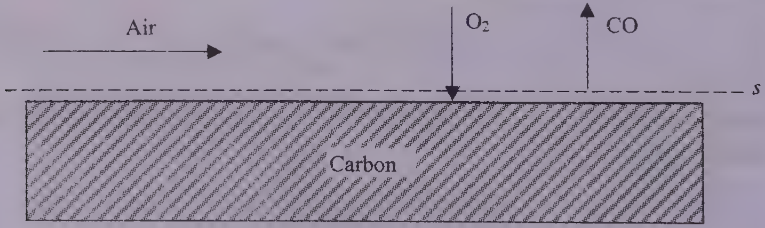

Figure 20-7 Graphite burning in air.

The vapor pressure of carbon is so low at any reasonable surface temperature that we are forced to conclude that the reaction must take place at the surface. Unlike with the volatile substance just considered, it appears that the surface temperature is going to be very high and will contribute materially to the enthalpy evaluation. In the absence of any initial basis for estimating this temperature, it appears that the mass-diffusion equation for a simple chemical reaction provides a more direct route to the evaluation of the driving force B. The expected high surface temperature also provides the basis for the assumption of a reaction to CO rather than CO_2. This is obviously related to the thermodynamic equilibrium state of the carbon–oxygen system at the temperature and pressure at the surface.

On the assumption of the above simple chemical reaction, the quantity $m_C - m_{O_2}/r$ is a conserved property. This has been shown in detail in App. E. Thus, from App. E, Eq. (E-7) and Eq. (18-13), a possible formulation for the driving force is

$$B = \frac{(m_C - m_{O_2}/r)_\infty - (m_C - m_{O_2}/r)_s}{(m_C - m_{O_2}/r)_s - (m_C - m_{O_2}/r)_T}$$

Whether this expression will be adequate depends on whether values of $m_C - m_{O_2}/r$ can be found at the ∞, s, and T states.

If carbon is the only transferred substance,

$$\left(m_C - \frac{m_{O_2}}{r}\right)_T = 1$$

At the ∞ state there is obviously no carbon and the concentration of oxygen is 0.232. Thus

$$\left(m_C - \frac{m_{O_2}}{r}\right)_\infty = 0 - \frac{0.232}{1.333} = -0.174$$

The most sensitive state is the s state. It has already been assumed that the surface temperature is such that the vapor pressure of carbon is negligible, and thus $m_{C,s} = 0$. The concentration of oxygen presents a further problem. If thermodynamic equilibrium is obtained, we must conclude that at an elevated temperature uncombined oxygen cannot exist at the s surface, thus

$$\left(m_C - \frac{m_{O_2}}{r}\right)_s = 0$$

This result assumes, of course, that reaction rates are sufficiently high that thermodynamic equilibrium obtains, and it also assumes that no other reactions are involved. These are simply the approximations that we make in order to obtain a simple solution. Obviously a more precise result is obtained if the reaction rates of all possible reactions are considered.

On the basis of the various approximations introduced, we then conclude that

$$B = \frac{-0.174 - 0}{0 - 1} = 0.174$$

Thus

$$\dot{m}'' = gB = 0.174\,g$$

Note that the magnitude of B is quite small compared with the volatile fuel example.

GRAPHITE ABLATION WITH MORE THAN ONE REACTION

Let us consider a chemically reacting boundary layer where more than one reaction is of importance, so that the simple-chemical-reaction idealization is inadequate. In this case we find it necessary to consider the diffusion of each element. If we can accept the assumption that the diffusion coefficients for all components are the same, then the applicable diffusion equation is Eq. (18-15) [see also App. E, Eq. (E-10)], where the concentration of chemical element α is a conserved property.

Consider a combustion-products mixture containing by mass 40 percent CO_2 and 20 percent H_2O, with the remainder products assumed to be inert. Let this mixture flow over a graphite surface at 1650°C. The gas mixture could be the products from a rocket motor, and the graphite surface could be a nozzle. The problem is to compute the rate of erosion of the graphite surface.

Again, because of the low vapor pressure of carbon, any reaction between the gas and the graphite can be expected to take place at the surface. However, there is more than one possible reaction at the surface. Let us examine the equilibrium constants K_P, at 1650°C, for some of these reactions.

For a reaction

$$l_1 A + l_2 B = l_3 C + l_4 D$$

we have

$$K_P = \frac{P_C^{l_3} P_D^{l_4}}{P_A^{l_1} P_B^{l_2}}$$

where P is the partial pressure of the component of the mixture.

The following are possible reactions, with the corresponding equilibrium constants at 1650°C, with carbon as a solid:

$$\begin{aligned}
&C(s) + CO_2 = 2\,CO, && K_P = 4000\\
&C(s) + H_2O = CO + H_2, && K_P = 1234\\
&C(s) + 2\,H_2 = CH_4, && K_P = 1/790\\
&CO_2 = CO + 0.5\,O_2, && K_P = 1/18{,}000\\
&H_2O = H_2 + 0.5\,O_2, && K_P = 1/40{,}000\\
&C(s) + 0.5\,O_2 = CO, && K_P \to \infty
\end{aligned}$$

A large value of K_P means that the thermodynamic equilibrium lies on the right-hand side of the equation, while a very small value means that equilibrium lies on the left-hand side. With these equations (and two of them are redundant), we could calculate the equilibrium composition at the s state, but merely by inspection it is apparent that at the s state the mixture can contain only CO and H_2, plus the inerts. On the other hand, at the ∞ state only CO_2 and H_2O are present. The T state is entirely carbon. The complete mixture under consideration then contains (excluding CH_4, which evidently cannot exist anywhere at this temperature)

$$CO_2, \quad H_2O, \quad CO, \quad H_2, \quad C(s)$$

Let us now express the concentration of the elements carbon, oxygen, and hydrogen at any point in the system, employing the definition of n_α from Chap. 4:

$$n_\alpha = \sum_j n_{\alpha,j} m_j$$

The mass concentration of chemical element α in species j is denoted by $n_{\alpha,j}$ and is obtained directly from the chemical formula for the species. For example: $n_{C,CO} = 12/30$ and $n_{C,C} = 1/1$. For the present example we obtain:

$$\begin{aligned} n_C &= n_{C,CO_2} m_{CO_2} + n_{C,CO} m_{CO} + n_{C,C} m_C \\ &= \tfrac{12}{44} m_{CO_2} + \tfrac{12}{28} m_{CO} + m_C \\ n_O &= n_{O,CO_2} m_{CO_2} + n_{O,H_2O} m_{H_2O} + n_{O,CO} m_{CO} \\ &= \tfrac{32}{44} m_{CO_2} + \tfrac{16}{18} m_{H_2O} + \tfrac{16}{28} m_{CO} \\ n_H &= n_{H,H_2O} m_{H_2O} + n_{H,H} m_{H_2} \\ &= \tfrac{2}{18} m_{H_2O} + m_{H_2} \end{aligned}$$

Any one of these element concentrations could be used for a conserved property in the $\mathcal{P}$ equation. However, we need a conserved property that can be evaluated from presently known data at the s, ∞, and T states, and none of these qualify. Specially, we do not know the concentration of CO and H_2 at the s state. But it is recalled from Chap. 18 that any linear combination of conserved properties is again a conserved property, provided that diffusion coefficients are the same. This suggests that a combination of several different n_α may be found containing only quantities that are known at the s, ∞, and T states. Both n_C and n_O contain the unknown m_{CO}, but the following combination does not:

$$n_C - \tfrac{3}{4} n_O = m_C - \tfrac{3}{11} m_{CO_2} - \tfrac{2}{3} m_{H_2O}$$

This quantity is a conserved property that can be evaluated at all the necessary states. Thus

$$\mathcal{P}_s = \left(n_{\mathrm{C}} - \tfrac{3}{4} n_{\mathrm{O}}\right)_s = 0$$

$$\mathcal{P}_\infty = 0 - \tfrac{3}{11}(0.40) - \tfrac{2}{3}(0.20) = -0.242$$

$$\mathcal{P}_T = 1$$

Then

$$B = \frac{\mathcal{P}_\infty - \mathcal{P}_s}{\mathcal{P}_s - \mathcal{P}_T} = \frac{-0.242 - 0}{0 - 1} = 0.242$$

and

$$\dot{m}'' = gB = 0.242g$$

It should be evident that the simple chemical reaction is merely a special case of this more general procedure.

THE HIGH-TEMPERATURE BOUNDARY LAYER WITH DISSOCIATION

Consider a boundary layer in which there is chemical reaction, and thus concentration gradients and mass diffusion, but in which there is no mass transfer across the s and L surfaces. An example might be the nose cone surface of a body entering Earth's atmosphere, but cooled so that there is no ablation. The air behind the bow shock wave is at such a high temperature that dissociation occurs. But if the body is cooled to a moderately low temperature, recombination tends to occur within the boundary layer, and the equilibrium state at the s surface tends toward the state of the original free-stream air (although the process can occur sufficiently fast that thermodynamic equilibrium is not established). If the unit-Lewis-number approximation, or any of the other energy-equation simplifications, is applicable, the boundary condition to the energy equation becomes that of the $\mathcal{P}$ equation:

$$\dot{m}'' = gB = g\,\frac{i_\infty - i_s}{i_s - i_T} = g\,\frac{i_\infty - i_s}{i_s - i_L + \dot{q}''_L/\dot{m}''}$$

Transposing gives

$$\dot{m}''(i_s - i_L) + \dot{q}''_L = g(i_\infty - i_s)$$

But if $\dot{m}'' = 0$ (no ablation), the first term drops out, and $g = g^*$. Thus

$$\dot{q}''_L = g^*(i_\infty - i_s) \tag{20-24}$$

The surface heat flux to a chemically reacting boundary layer is then seen to be proportional to the *enthalpy difference* across the boundary layer.

Note, however, that for the nose of a high-velocity vehicle, the free-stream enthalpy i_∞ must include the specific free-stream kinetic energy $u_\infty^2/2$. This term may be so large that the other enthalpy terms can be neglected.

TRANSPIRATION COOLING BY GAS INJECTION

An effective way to cool a surface over which a hot gas is flowing is to construct it from a porous material and force a cool gas through it from the rear surface.

The injected cooling gas can be the same as the hot mainstream fluid, in which case the boundary-layer problem is that of heat transfer with simple blowing (see Chap. 12); or it can be of a *different* composition, in which case we have a combined heat- and mass-transfer problem. The two types of problems are, however, closely related, since they both involve mass transfer at the surface.

If the injected gas is the same as the mainstream gas, or if it is different but one of the simplifications to the energy equation is applicable, enthalpy is a conserved property and the complete solution is contained in the standard formulation

$$\dot{m}'' = gB = g\frac{i_\infty - i_s}{i_s - i_T}$$

where i is a function of temperature (and composition in the second case), and the problem is generally to evaluate $\dot{m}''$ to attain a given T_s or vice versa.

It is sometimes preferred, however, to express the solution in terms of the heat flux $\dot{q}_s''$ rather than to use the simplified mass-transfer formulation, because if properties of the injected gas and the mainstream gas are such that none of the simplifications to the energy equation are approximated, enthalpy is no longer a conserved property of the second kind and the standard formulation is no longer valid. In fact, we are forced all the way back to Eq. (18-27) and Fig. 18-4 for a valid expression of the boundary condition at the surface.

In either case, it can be readily demonstrated that if there is no phase change between the L and s surfaces then $\dot{q}_L'' = \dot{q}_s''$. And of course,

$$\dot{q}_s'' = -\left(\Gamma c \frac{\partial T}{\partial y}\right)_s$$

Consider first the case where the injected gas is the same as the mainstream gas. Then the standard formulation yields

$$\dot{m}'' = g\frac{i_\infty - i_s}{i_s - i_L + \dot{q}_L''/\dot{m}''} = g\frac{i_\infty - i_s}{i_s - i_L + \dot{q}_s''/\dot{m}''}$$

But in the case $i_s = i_L$, this equation simplifies to

$$\dot{q}_s'' = g(i_\infty - i_s)$$

If the specific heat may be treated as constant in the considered phase, we can then define a heat-transfer convection coefficient in the conventional manner and

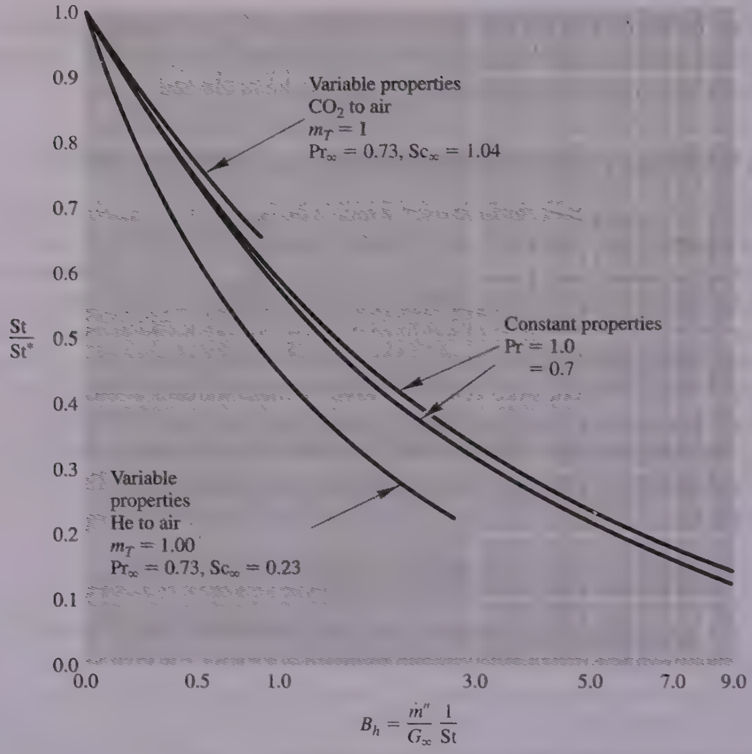

Figure 20-8 Heat transfer to a laminar boundary layer with transpiration cooling and constant free-stream velocity.

evaluate a heat-transfer Stanton number:

$$\dot{q}_s'' = gc(T_\infty - T_s) = h(T_\infty - T_s), \qquad h = gc$$

$$\frac{h}{G_\infty c} = \mathrm{St} = \frac{g}{G_\infty}$$

If we denote again the Stanton number for $B \to 0$ by St* then

$$\frac{\mathrm{St}}{\mathrm{St}^*} = \frac{g}{g^*} = f(B, \text{other parameters})$$

For the constant-property laminar boundary layer for u_∞ = constant, this result is plotted in Fig. 20-8 for Pr = 0.7 and 1.0, and the curves are taken from Fig. 19-3. Similarly, a corresponding turbulent-boundary-layer constant-property result is plotted in Fig. 20-9. Note, however, that g/G_∞ in the definition of B has been replaced by its equivalent for this case, St, and the resulting parameter has been denoted by B_h, the transpiration parameter introduced in Chap. 12.

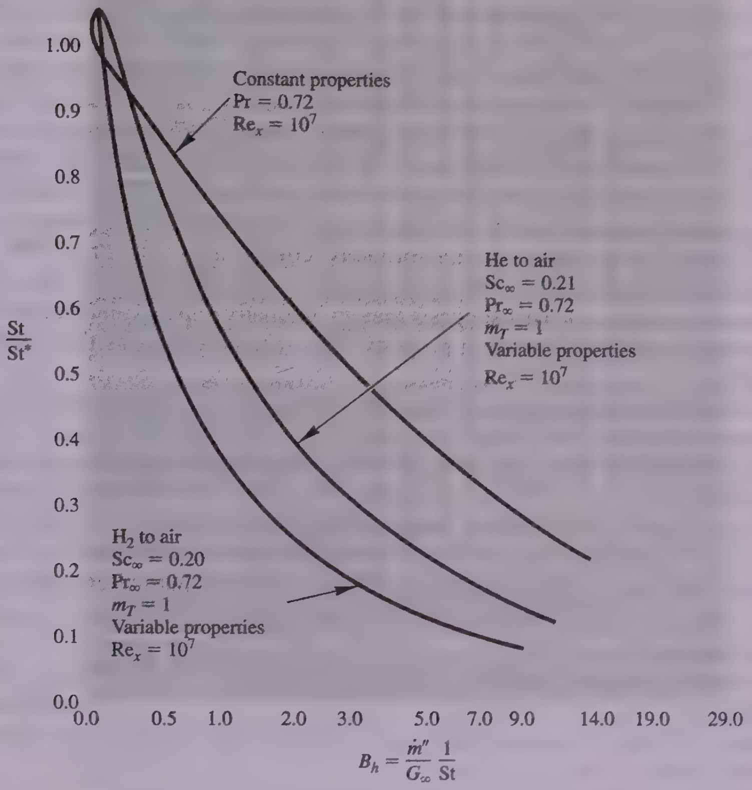

Figure 20-9 Heat transfer to a turbulent boundary layer with transpiration cooling and constant free-stream velocity.

A few solutions, based on the "exact" energy equation rather than the simplified energy equation, have been developed for transpiration cooling in which some other gas is injected into an air boundary layer. Not only do these solutions involve simultaneous heat and mass transfer through the boundary layer, but the transport properties of the mixture (including the Lewis number) vary markedly through the boundary layer, especially at high blowing rates where the concentration of the injected gas is high at the *s* state. (Note that as $B \rightarrow 0$, the Stanton number must approach its value for the simple constant-property air boundary layer, regardless of whether the injected fluid is the same as or different from the free-stream fluid.) The results of these variable-property solutions can be presented in graphical form on the same coordinate system as employed in Figs. 20-8 and 20-9. However, B_h will no longer be related to conserved properties.

Results for helium injection and CO_2 injection, both into a laminar air boundary layer,[1] are plotted in Fig. 20-8. Similar results for helium and hydrogen injection into a turbulent boundary layer[2] are plotted in Fig. 20-9. The variable-property effects are seen to be quite substantial, especially in the case of light-gas injection. A correlation of the variable-property results with the constant-property solutions, using the reference property concept, is presented by Knuth[3] and by Knuth and Dershin.[4] The latter authors employ a Couette flow model as a basis for determining a reference composition that correlates the variable-property results with constant-property solutions. Analysis of the Couette flow heat-transfer problem with foreign gas injection indicates that the property most responsible for the large variable-property effects shown in Figs. 20-8 and 20-9 is the specific heat of the injected fluid c_T (if different from that of the mainstream fluid c_∞). This suggests that an alternative approximate correlation procedure might be based on a property ratio scheme c_T/c_∞ as the additional variable.

A fairly good correlation of the data in Fig. 20-8 is indeed obtained if all properties are based on the ∞ state and B_h is replaced by $B_h(c_T/c_\infty)^{1/3}$. Similarly, the turbulent flow data in Fig. 20-9 can be approximately correlated if B_h is replaced by $B_h(c_T/c_\infty)^{0.6}$. This correlation does not work well at very low blowing rates, where the hydrogen and helium curves are seen to rise before they decrease. This effect occurs because the very high thermal conductivity of the injected fluid tends to substantially increase the mixture thermal conductivity in the sublayers, and this initially offsets the normal effect of blowing to decrease heat-transfer rate.

In applying these solutions, where the problem is to determine the surface temperature for a given mass-transfer rate per unit area, or vice versa, an energy balance on the L–T control volume yields the desired relation. Thus, referring to Fig. 18-4,

$$\dot{m}''i_L - \dot{m}''i_T = \dot{q}''_L = \dot{q}''_s = h(T_\infty - T_s)$$

$$i_L - i_T = c_T(T_L - T_T) = c_T(T_s - T_T)$$

$$\dot{m}'' = \frac{h(T_\infty - T_s)}{c_T(T_s - T_T)}$$

Thermal radiation can, of course, be included in this energy balance as desired (see App. F).

PROBLEMS

20-1. Consider the burning of a droplet of ethyl alcohol (or a wet wick) in an atmosphere of pure oxygen. How does the burning rate compare with the same droplet in atmospheric air, assuming that the logarithmic equation for g/g^* is applicable, other things being equal?

20-2. Suppose you dip the wick of a wet-bulb thermometer in ethyl ether and expose it to atmospheric air at 20°C. What equilibrium temperature will the thermometer record under the unit-Lewis-number assumption?

20-3. Dry air at 315°C flows along a flat wet surface (water) at 9 m/s. The pressure is 1.013 bar. If the surface is insulated (except for exposure to the air) and radiation is neglected, what equilibrium temperature will the surface assume? If the boundary layer is turbulent, what is the mass-transfer rate per unit area at a point 1.5 m from the virtual origin of the boundary layer?

20-4. Consider flow of air normal to a cylinder as described in Prob. 19-4. Let the air be at 20°C, 1.013-bar pressure, and 60 percent relative humidity. Inside the cylinder there is water at 90°C. The surface is porous so that the water can be forced out at a rate sufficient to keep the outer surface moist. What is the average surface temperature and the average mass-transfer rate per unit of surface area?

20-5. A thin plate of solid salt (NaCl), 0.15 m by 0.15 m, is to be dragged through seawater (edgewise) at 20°C at a velocity of 5 m/s. Seawater has a salt concentration of about 3 percent by weight. Saturated NaCl–H_2O at 20°C has a concentration of 0.036 kg NaCl/0.1 kg H_2O. Estimate the total rate at which salt goes into solution.

20-6. Consider an axisymmetric stagnation point on a missile traveling through the atmosphere at 5500 m/s where the static air temperature is near zero degrees absolute. It is desired to maintain the surface at 1200°C by transpiration of hydrogen through the wall. The hydrogen is available from a reservoir at 38°C. If the heat of combustion of hydrogen is approximately 116,000 kJ/kg at 1200°C and the mean specific heats of hydrogen and air are, respectively, 15 kJ/(kg · K) and 1.1 kJ/(kg · K), evaluate the driving force B from the energy equation under the unit-Lewis-number assumption for the conditions of (1) reaction of H_2 with O_2 and (2) no reaction. *Suggestion*: Use the surface temperature as the temperature datum for enthalpy. Note that the free-stream enthalpy must include the very large contribution of the stagnation enthalpy.

20-7. In Prob. 16-9 the cooling of a gas turbine blade is considered. Considering only the stagnation point at the leading edge of the blade, evaluate the surface temperature and the necessary water rate per square foot of stagnation area to cool by water injection through a porous surface. Assume that the water is available at 38°C and that the mass concentration of water vapor in the products of combustion is 0.01.

20-8. Continue Prob. 20-7 to include the entire blade surface, using what you feel to be the best available approximations for various parts of the surface.

20-9. A rocket nozzle is to be constructed with dimensions as shown in Fig. 11-18. The following table gives the composition of the exhaust products.

Compound	m_j, **kg/(kg mixture)**
CO_2	0.278
CO	0.279
H_2O	0.209
H_2	0.022
N_2	0.212

The stagnation pressure is 3400 kPa and the stagnation temperature is 3000°C. The nozzle is to be constructed of graphite. The objective of the problem is to estimate the rate of erosion (ablation) of the graphite at the throat, and particularly to estimate the time elapsed for a 10 percent increase in throat diameter.

20-10. Consider an axisymmetric blunt-nosed vehicle entering Earth's atmosphere. At 60,000 m altitude the velocity is 6100 m/s. The radius of curvature of the nose is 1.8 m. Calculate the convective heat flux to the vehicle at the stagnation point. (Note that this calculation neglects radiation from the very high temperature dissociated gases behind the shock wave). If the surface is insulated, calculate the equilibrium surface temperature assuming that the surface radiates as a black body to the surroundings. Suppose the surface is a graphite heat shield; calculate the rate of ablation of the graphite in millimeters per minute.

20-11. Let a piece of ice uniformly at 0°C be immersed in water at 27°C. Evaluate the rate at which melting occurs in terms of the conductance g. How would you evaluate g?

20-12. Consider a 1.2-m-square wet towel hanging from a clothes line. Let sunlight fall on one side at an angle of 45°C. The normal solar flux is 946 $\mathrm{W/m^2}$, and the absorptivity and emissivity of the towel are 1. The surrounding air is at 21°C, with a relative humidity of 65 percent. At the equilibrium temperature of the system, it is determined that an equivalent system with no mass transfer would have a free-convection coefficient of 8.5 $\mathrm{W/(m^2 \cdot K)}$. What is the drying rate during the period when the towel is sufficiently wet that the surface can be idealized as a liquid surface? (Note that, in addition to the high-frequency solar flux, the 21°C surroundings radiate to *both* sides of the towel, and the towel radiates to the surroundings. Assume that the towel is at a uniform temperature throughout its thickness.)

20-13. In a diesel engine the fuel is injected as small droplets, and, after an initial ignition delay, during which time part of the fuel vaporizes and then burns rather abruptly, the remainder of the fuel burns as fast as the fuel vaporizes from each individual droplet. The objective of this problem is to estimate the time required for complete consumption of a spherical droplet 5 μm in diameter.

20-14. During this period, let it be assumed that the combustion chamber pressure is 6200 kPa and the air temperature is 800°C. The fuel may be idealized as $C_{12}H_{26}$, with heat of combustion of 44,000 kJ/kg and latent heat of vaporization 358 kJ/kg. It may be assumed that these values are relatively independent of temperature. The boiling point of the fuel is approximately 427°C at this pressure.

20-15. Calculate the evaporation (sublimation) rate from a snow bank if the ambient air temperature is −23°C, solar energy is falling on the bank at a rate per unit area of 600 $\mathrm{W/m^2}$, the underside of the bank is effectively insulated, and the heat-transfer coefficient for free convection from an equivalent surface with no mass transfer is 6 $\mathrm{W/(m^2 \cdot K)}$. The absorptivity *and* emissivity of snow may be assumed to be 1. The absolute humidity of the air is 0.0003 kg H_2O/kg dry air.

20-16. At a particular region in a steam condenser the fluid is a mixture of 80 percent steam (by mass) and 20 percent air. The total pressure is 6.75 kPa, and the temperature is that of saturated steam at that pressure. What is the necessary condition at the surface of the tubes for condensation to take place? In simple condensation the resistance to heat transfer is usually considered to be entirely that of the liquid film that forms on the surface. How does the present problem differ? Suppose the liquid film has an average thickness of 0.1 mm; investigate the effect of the air on the overall resistance to heat transfer between the tube metal surfaces and the free-stream mixture.

20-17. A wet surface is to be dried by blowing dry air at 32°C over it, while at the same time electrically heating it from the rear with a fixed heat flux of 25,000 W/m^2. Investigate the variation of the drying rate per unit area $\dot{m}''$ as the conductance g is varied (presumably by varying the air velocity).

20-18. In Prob. 20-16 the heat is to be supplied from the rear by condensing steam. Let the steam be available at 110°C, and let it be assumed that the *overall conductance* for heat transfer from the steam to the L surface (including the condensing resistance, the wall resistance, and the resistance of the material being dried) is 280 $W/(m^2 \cdot K)$. Investigate the influence of the mass-transfer conductance g on the drying rate.

20-19. Consider a laundry convective clothes dryer for which there is available dry air at 20°C and 1.013-bar pressure. There is also available superheated steam at 1.013 bar pressure and 260°C. Considering only the "constant-drying-rate" period during which the cloth surface is totally wet, investigate whether it is possible to increase the drying rate by mixing some of the steam with the air. That is, how does drying rate vary with steam-air ratio?

20-20. In a part of a solar-operated seawater desalting plant, air saturated with water vapor at 1.013 bar and 55°C passes into a condenser where the fresh water is recovered. The condenser is built up of a bank of circular tubes with cooling seawater flowing inside the tubes and the saturated air flowing normally. The heat-transfer coefficient on the inside of the tubes is estimated to be 1400 $W/(m^2 \cdot K)$. The tube wall is 0.75 mm thick and has a thermal conductivity of 100 $W/(m \cdot K)$. On the outside of the tubes, it is estimated that if there were no mass transfer, the average heat-transfer coefficient would be 70 $W/(m^2 \cdot K)$. If the cooling-water temperature in the first row of tubes (the tubes over which the 55°C saturated air is flowing) is 46°C, calculate the rate of condensation per unit of surface area and the rate of heat transfer to the coolant. Neglect the resistance of the condensate film on the tubes. (Would it be significant if the film thickness was, say, 0.1 mm?)

20-21. Air, saturated with water vapor, at 1.013 bar and 77°C, flows downward along a flat, smooth plate at a velocity of 3 m/s. The plate is 30 cm high (flow direction) and 1.8 m wide. It is cooled by circulating water on its back side. The cooling water circulates so that its average temperature is effectively 18°C over the entire back surfaces. The heat-transfer coefficient between the coolant and the back surface is estimated to be 1100 $W/(m^2 \cdot K)$. The wall is 1.3 mm thick and has a thermal conductivity of 26 $W/(m \cdot K)$. Estimate the total rate of condensation of water and the total heat-transfer rate to the coolant, assuming that the condensate on the plate surface runs off fast enough that its heat-transfer resistance may be neglected.

20-22. Is B a constant along the surface? What are the necessary conditions for B to be a constant? Describe how you would propose to analyze the problem, taking into consideration the liquid condensate film on the plate surface.

20-23. Air at 1100°C and 1013 kPa pressure flows along a flat surface at a uniform velocity of 30 m/s. Investigate the problem of cooling this surface by transpiration cooling. At a point 1 m from the leading edge of the surface, consider the use of first air, then helium, as coolants, both of which are assumed to be available at 20°C. Prepare a plot of surface temperature as a function of coolant mass-flow rate per unit of surface area. Also calculate the surface temperature as a function of coolant mass-flow rate if the coolant were used merely to absorb heat rather than to pass into the boundary layer, assuming that the coolant leaves the system at surface temperature.

REFERENCES

1. Baron, J. R.: Technical Report 160, Naval Supersonic Laboratory, MIT, Cambridge, Mass., 1956.

2. Rubesin, M. W., and C. C. Pappas: NACA (now NASA) TN 4149, Washington, February 1958.

3. Knuth, E. L.: *Int. J. Heat Mass Transfer*, vol. 6, pp. 1–22, 1963.

4. Knuth, E. L., and H. Dershin: *Int. J. Heat Mass Transfer*, vol. 6, pp. 999–1018, 1963.

5. Presser, K. H.: *Wärme- und Stoffübertragung*, vol. 1, pp. 225–236, 1968.

APPENDIX A

Property Values

In this appendix the transport properties of a variety of gaseous and liquid fluids are presented. The primary purpose of this compilation is to support the problems at the end of each chapter and to provide material for additional problems.

The data are presented in the International System of Units (SI), and the units should be compatible with the various presently accepted national and international standards for SI. An introduction to SI can be found at the website for the National Institute of Standards and Technology (NIST), an agency of the US Department of Commerce: http://physics.nist.gov/cuu/Units/introduction.html. The units in the data tables include the base units of meter (length), kilogram (mass), second (time), mole (amount of substance), and kelvin (temperature). The algebraically derived units used in the tables are the joule (energy), pascal (pressure), and watt (power). For convenience in some of the tables, the SI prefixes *kilo* ($k = 10^3$), *milli* ($m = 10^{-3}$), and *micro* ($\mu = 10^{-6}$) are used. The balance of the tables use an abbreviated scientific notation (for powers of 10) that has been found useful with hand calculators (for example, $-07 = 10^{-7}$, $+00 = 10^0$, and $+04 = 10^4$). Conversion of the table entries from SI to the English Engineering System of Units can be easily made using the conversion factors on the inside covers of the textbook.

Tables A-1 to A-7 contain the properties of a representative group of gases at standard atmospheric pressure, $P = 101.325$ kPa. For many applications these gases may be treated as perfect gases for which the transport properties are independent of pressure, and the densities may be computed from $P/\rho = (\Re/\mathfrak{M})T$, where $\Re = 8314.34$ J/(kmol · K) is the universal gas constant and $\mathfrak{M}$ is the molecular weight, kg/kmol. The gas data for Tables A-1 to A-5 have been primarily obtained from three volumes of *Thermophysical Properties of Matter*, published by the Thermophysical Properties Research Center (TPRC) at Purdue University.[1–3] The table entries for specific heat and density are ideal-gas values, except near the critical temperature of the gas. For air, oxygen, and nitrogen the first three table entries, and for carbon dioxide the first four table entries,

Table A-1 Properties of air at $P = 101.325$ kPa; $\mathfrak{M} = 28.966$ kg/kmol

T, K	ρ, kg/m^3	μ, Pa · s		ν, m^2/s		c_p, kJ/(kg · K)	k, W/(m · K)		Pr	$g\beta/\nu^2$, 1/(K · m^3)	
100	3.5985	70.60	−07	19.62	−07	1.028	92.20	−04	0.787	25.5	+09
150	2.3673	10.38	−06	43.85	−07	1.011	13.75	−03	0.763	34.0	+08
200	1.7690	13.36	−06	75.52	−07	1.006	18.10	−03	0.743	85.9	+07
250	1.4119	16.06	−06	11.37	−06	1.003	22.26	−03	0.724	30.3	+07
263	1.3421	16.70	−06	12.44	−06	1.003	23.28	−03	0.720	24.1	+07
273	1.2930	17.20	−06	13.30	−06	1.004	24.07	−03	0.717	20.3	+07
283	1.2473	17.69	−06	14.18	−06	1.004	24.86	−03	0.714	17.2	+07
293	1.2047	18.17	−06	15.08	−06	1.004	25.63	−03	0.712	14.7	+07
300	1.1766	18.53	−06	15.75	−06	1.005	26.14	−03	0.711	13.2	+07
303	1.1650	18.64	−06	16.00	−06	1.005	26.37	−03	0.710	12.6	+07
313	1.1277	19.11	−06	16.95	−06	1.005	27.09	−03	0.709	10.9	+07
323	1.0928	19.57	−06	17.91	−06	1.006	27.80	−03	0.708	94.6	+06
333	1.0600	20.02	−06	18.89	−06	1.007	28.51	−03	0.707	82.5	+06
343	1.0291	20.47	−06	19.89	−06	1.008	29.21	−03	0.706	72.2	+06
350	1.0085	20.81	−06	20.63	−06	1.008	29.70	−03	0.706	65.8	+06
353	1.0000	20.91	−06	20.91	−06	1.008	29.89	−03	0.705	63.5	+06
363	0.9724	21.34	−06	21.95	−06	1.009	30.58	−03	0.704	56.1	+06
373	0.9463	21.77	−06	23.01	−06	1.010	31.26	−03	0.703	49.6	+06
400	0.8825	22.94	−06	26.00	−06	1.013	33.05	−03	0.703	36.3	+06
450	0.7844	24.93	−06	31.78	−06	1.020	36.33	−03	0.700	21.6	+06
500	0.7060	26.82	−06	37.99	−06	1.029	39.51	−03	0.699	13.6	+06
550	0.6418	28.60	−06	44.56	−06	1.039	42.60	−03	0.698	89.7	+05
600	0.5883	30.30	−06	51.50	−06	1.051	45.60	−03	0.699	61.6	+05
650	0.5431	31.93	−06	58.80	−06	1.063	48.40	−03	0.701	43.6	+05
700	0.5043	33.49	−06	66.41	−06	1.075	51.30	−03	0.702	31.7	+05
750	0.4706	34.98	−06	74.32	−06	1.087	54.10	−03	0.703	23.7	+05
800	0.4412	36.43	−06	82.56	−06	1.099	56.90	−03	0.703	18.0	+05
850	0.4153	37.83	−06	91.10	−06	1.110	59.70	−03	0.703	13.9	+05
900	0.3922	39.18	−06	99.90	−06	1.121	62.50	−03	0.702	10.9	+05
950	0.3716	40.49	−06	10.90	−05	1.131	64.90	−03	0.705	86.9	+04
1000	0.3530	41.77	−06	11.83	−05	1.141	67.20	−03	0.709	70.0	+04
1100	0.3209	44.4	−06	13.8	−05	1.160	73.2	−03	0.705		
1200	0.2942	46.9	−06	15.9	−05	1.177	78.2	−03	0.705		
1300	0.2715	49.3	−06	18.2	−05	1.195	83.7	−03	0.705		
1400	0.2521	51.7	−06	20.5	−05	1.212	89.1	−03	0.704		
1500	0.2353	54.0	−06	22.9	−05	1.230	94.6	−03	0.704		
1600	0.2206	56.3	−06	25.5	−05	1.248	10.0	−02	0.703		
1700	0.2076	58.5	−06	28.2	−05	1.266	10.5	−02	0.702		
1800	0.1961	60.7	−06	31.0	−05	1.286	11.1	−02	0.701		
1900	0.1858	62.9	−06	33.9	−05	1.307	11.7	−02	0.700		
2000	0.1765	65.0	−06	36.8	−05	1.331	12.4	−02	0.699		
2100	0.1681	67.2	−06	40.4	−05	1.359	13.1	−02	0.696		
2200	0.1605	69.3	−06	43.2	−05	1.392	13.9	−02	0.693		
2300	0.1535	71.4	−06	46.5	−05	1.434	14.9	−02	0.688		
2400	0.1471	73.5	−06	50.0	−05	1.487	16.1	−02	0.681		
2500	0.1412	75.7	−06	53.6	−05	1.556	17.5	−02	0.673		

Table A-2 Properties of O_2 at $P = 101.325$ kPa; $\mathfrak{M} = 31.999$ kg/kmol

T, K	ρ, kg/m^3	μ, Pa · s	ν, m^2/s	c_p, kJ/(kg · K)	k, W/(m · K)	Pr	$g\beta/\nu^2$, 1/(K · m^3)
100	3.9906	76.80 −07	19.25 −07	0.947	90.50 −04	0.804	26.5 +09
150	2.6186	11.27 −06	43.04 −07	0.918	13.76 −03	0.754	35.3 +08
200	1.9557	14.65 −06	74.91 −07	0.914	18.24 −03	0.735	87.3 +07
250	1.5598	17.77 −06	11.39 −06	0.912	22.54 −03	0.718	30.2 +07
300	1.2998	20.67 −06	15.90 −06	0.918	26.74 −03	0.710	12.9 +07
350	1.1141	23.37 −06	20.98 −06	0.929	30.56 −03	0.710	63.6 +06
400	0.9749	25.89 −06	26.56 −06	0.942	34.20 −03	0.713	34.7 +06
450	0.8665	28.28 −06	32.64 −06	0.956	37.70 −03	0.717	20.4 +06
500	0.7799	30.54 −06	39.16 −06	0.971	41.20 −03	0.720	12.8 +06
600	0.6499	34.70 −06	53.39 −06	1.002	48.00 −03	0.725	57.3 +05
700	0.5571	38.50 −06	69.11 −06	1.031	54.40 −03	0.730	29.3 +05
800	0.4874	42.10 −06	86.37 −06	1.054	60.30 −03	0.736	16.4 +05
900	0.4333	45.40 −06	10.48 −05	1.074	66.10 −03	0.737	99.2 +04
1000	0.3899	48.50 −06	12.44 −05	1.090	71.70 −03	0.737	63.3 +04
1100	0.3545	51.40 −06	14.50 −05	1.103	77.10 −03	0.736	42.4 +04
1200	0.3250	54.20 −06	16.68 −05	1.115	82.10 −03	0.736	29.4 +04
1300	0.3000	56.90 −06	18.97 −05	1.125	87.10 −03	0.735	20.9 +04
1400	0.2785	59.50 −06	21.36 −05	1.134	92.10 −03	0.733	15.3 +04

Table A-3 Properties of N_2 at $P = 101.325$ kPa; $\mathfrak{M} = 28.018$ kg/kmol

T, K	ρ, kg/m^3	μ, Pa · s	ν, m^2/s	c_p, kJ/(kg · K)	k, W/(m · K)	Pr	$g\beta/\nu^2$, 1/(K · m^3)
100	3.4800	68.70 −07	19.74 −07	1.072	94.10 −04	0.783	25.1 +09
150	2.2890	10.00 −06	43.69 −07	1.047	13.85 −03	0.756	34.2 +08
200	1.7107	12.86 −06	75.20 −07	1.043	18.26 −03	0.734	86.7 +07
250	1.3657	15.46 −06	11.32 −06	1.039	22.22 −03	0.724	30.6 +07
300	1.1381	17.86 −06	15.69 −06	1.039	25.98 −03	0.714	13.3 +07
350	0.9755	20.08 −06	20.58 −06	1.040	29.39 −03	0.711	66.1 +06
400	0.8536	22.14 −06	25.94 −06	1.044	32.52 −03	0.711	36.4 +06
450	0.7587	24.08 −06	31.74 −06	1.049	35.64 −03	0.709	21.6 +06
500	0.6829	25.90 −06	37.93 −06	1.056	38.64 −03	0.708	13.6 +06
600	0.5691	29.27 −06	51.44 −06	1.075	44.10 −03	0.713	61.7 +05
700	0.4878	32.35 −06	66.32 −06	1.097	49.30 −03	0.720	31.8 +05
800	0.4268	35.20 −06	82.48 −06	1.122	54.10 −03	0.730	18.0 +05
900	0.3794	37.86 −06	99.80 −06	1.145	58.70 −03	0.739	10.9 +05
1000	0.3414	40.36 −06	11.82 −05	1.167	63.10 −03	0.746	70.1 +04
1100	0.3104	42.70 −06	13.76 −05	1.186	67.20 −03	0.754	47.1 +04
1200	0.2845	45.00 −06	15.82 −05	1.204	71.30 −03	0.760	32.6 +04
1300	0.2626	47.10 −06	17.93 −05	1.219	75.40 −03	0.761	23.4 +04
1400	0.2439	49.20 −06	20.17 −05	1.232	79.70 −03	0.761	17.2 +04

Table A-4 Properties of CO_2 at $P = 101.325$ kPa; $\mathfrak{M} = 44.010$ kg/kmol

T, K	ρ, kg/m^3	μ, Pa · s	ν, m^2/s	c_p, kJ/(kg · K)	k, W/(m · K)	Pr	$g\beta/\nu^2$, 1/(K · m^3)
220	2.4728	11.19 −06	45.25 −07	0.778	10.83 −03	0.804	21.8 +08
250	2.1652	12.63 −06	58.33 −07	0.806	12.89 −03	0.790	11.5 +08
300	1.7967	14.99 −06	83.43 −07	0.852	16.62 −03	0.768	46.9 +07
350	1.5369	17.26 −06	11.23 −06	0.897	20.50 −03	0.755	22.2 +07
400	1.3408	19.42 −06	14.48 −06	0.938	24.41 −03	0.746	11.7 +07
450	1.1918	21.50 −06	18.04 −06	0.977	28.34 −03	0.741	66.9 +06
500	1.0726	23.48 −06	21.89 −06	1.013	32.28 −03	0.737	40.9 +06
600	0.8939	27.20 −06	30.43 −06	1.075	40.30 −03	0.726	17.6 +06
700	0.7662	30.60 −06	39.94 −06	1.125	48.70 −03	0.707	87.8 +05
800	0.6704	33.90 −06	50.57 −06	1.168	56.00 −03	0.707	47.9 +05
900	0.5959	36.90 −06	61.92 −06	1.204	62.10 −03	0.715	28.4 +05
1000	0.5363	39.70 −06	74.02 −06	1.234	68.00 −03	0.720	17.9 +05
1100	0.4876	42.40 −06	86.96 −06	1.259	73.30 −03	0.728	11.8 +05
1200	0.4469	44.90 −06	10.05 −05	1.280	78.00 −03	0.737	80.9 +04
1300	0.4125	47.40 −06	11.49 −05	1.298	82.50 −03	0.746	57.1 +04
1400	0.3831	49.70 −06	12.97 −05	1.313	86.70 −03	0.753	41.6 +04

Table A-5 Properties of H_2 at $P = 101.325$ kPa; $\mathfrak{M} = 2.016$ kg/kmol

T, K	ρ, kg/m^3	μ, Pa · s	ν, m^2/s	c_p, kJ/(kg · K)	k, W/(m · K)	Pr	$g\beta/\nu^2$, 1/(K · m^3)
100	0.2457	42.10 −07	17.14 −06	11.16	67.60 −03	0.695	33.4 +07
150	0.1638	55.70 −07	34.01 −06	12.61	98.60 −03	0.712	56.5 +06
200	0.1228	67.80 −07	55.20 −06	13.52	12.80 −02	0.716	16.1 +06
250	0.0983	79.00 −07	80.39 −06	14.03	15.60 −02	0.711	60.7 +05
300	0.0819	89.40 −07	10.92 −05	14.27	18.15 −02	0.703	27.4 +05
350	0.0702	99.40 −07	14.16 −05	14.38	20.33 −02	0.703	14.0 +05
400	0.0614	10.91 −06	17.76 −05	14.49	22.12 −02	0.715	77.6 +04
450	0.0546	11.84 −06	21.69 −05	14.49	23.89 −02	0.718	46.3 +04
500	0.0491	12.74 −06	25.93 −05	14.50	25.64 −02	0.720	29.2 +04
600	0.0409	14.50 −06	35.41 −05	14.53	29.10 −02	0.724	13.0 +04
700	0.0351	16.10 −06	45.87 −05	14.60	32.50 −02	0.723	66.5 +03
800	0.0307	17.70 −06	57.64 −05	14.71	36.00 −02	0.723	36.9 +03
900	0.0273	19.20 −06	70.34 −05	14.83	39.40 −02	0.723	22.0 +03
1000	0.0246	20.70 −06	84.26 −05	14.99	42.80 −02	0.725	13.8 +03
1100	0.0223	22.20 −06	99.40 −05	15.17	46.20 −02	0.729	90.2 +02
1200	0.0205	23.60 −06	11.53 −04	15.36	49.50 −02	0.732	61.5 +02
1300	0.0189	25.00 −06	13.23 −04	15.57	52.80 −02	0.737	43.1 +02
1400	0.0175	26.30 −06	14.99 −04	15.80	56.20 −02	0.739	31.2 +02

Table A-6 Properties of He-4 at $P = 101.325$ kPa; $\mathfrak{M} = 4.003$ kg/kmol

T, K	ρ, kg/m^3	μ, Pa · s	ν, m^2/s	c_p, kJ/(kg · K)	k, W/(m · K)	Pr	$g\beta/\nu^2$, 1/(K · m^3)
100	0.4870	97.80 −07	20.05 −06	5.194	73.60 −03	0.690	24.4 +07
150	0.3252	12.50 −06	38.44 −06	5.194	96.90 −03	0.670	44.2 +06
200	0.2439	15.10 −06	61.91 −06	5.193	11.80 −02	0.665	12.8 +06
250	0.1951	17.60 −06	90.20 −06	5.193	13.70 −02	0.667	48.2 +05
300	0.1626	19.90 −06	12.24 −05	5.193	15.50 −02	0.667	21.8 +05
350	0.1394	22.20 −06	15.93 −05	5.193	17.20 −02	0.670	11.0 +05
400	0.1220	24.30 −06	19.93 −05	5.193	18.90 −02	0.668	61.7 +04
450	0.1084	26.40 −06	24.35 −05	5.193	20.50 −02	0.669	36.7 +04
500	0.0976	28.40 −06	29.11 −05	5.193	22.10 −02	0.667	23.1 +04
600	0.0813	32.20 −06	39.61 −05	5.193	25.10 −02	0.666	10.4 +04
700	0.0697	35.90 −06	51.52 −05	5.193	28.00 −02	0.666	52.8 +03
800	0.0610	39.40 −06	64.62 −05	5.193	30.70 −02	0.666	29.3 +03
900	0.0542	42.80 −06	78.97 −05	5.193	33.40 −02	0.665	17.5 +03
1000	0.0488	46.20 −06	94.71 −05	5.193	36.00 −02	0.666	10.9 +03
1100	0.0443	49.40 −06	11.14 −04	5.193	38.50 −02	0.666	71.8 +02
1200	0.0407	52.50 −06	12.91 −04	5.193	41.00 −02	0.665	49.0 +02
1300	0.0375	55.60 −06	14.82 −04	5.193	43.40 −02	0.665	34.3 +02
1400	0.0348	58.60 −06	16.82 −04	5.193	45.70 −02	0.666	24.7 +02

Table A-7 Properties of NH_3 at $P = 101.325$ kPa; $\mathfrak{M} = 17.033$ kg/kmol

T, K	ρ, kg/m^3	μ, Pa · s	ν, m^2/s	c_p, kJ/(kg · K)	k, W/(m · K)	Pr
250	0.8469	85.29 −07	10.07 −06	2.213	19.68 −03	0.959
300	0.6971	10.27 −06	14.73 −06	2.170	24.55 −03	0.908
350	0.5948	12.06 −06	20.28 −06	2.211	30.21 −03	0.883
400	0.5193	13.90 −06	26.77 −06	2.289	36.48 −03	0.872
450	0.4610	15.76 −06	34.19 −06	2.381	43.24 −03	0.868
500	0.4146	17.63 −06	42.52 −06	2.477	50.42 −03	0.866
550	0.3768	19.51 −06	51.78 −06	2.572	57.97 −03	0.866
600	0.3453	21.38 −06	61.92 −07	2.665	65.63 −03	0.868
650	0.3187	23.24 −06	72.92 −06	2.755	73.24 −03	0.874
700	0.2959	25.09 −06	84.79 −06	2.844	81.20 −03	0.878

contain real-gas specific heat and density values obtained from the National Bureau of Standards Circular 564.[4] For all gas tables the volume coefficient of thermal expansion for an ideal gas was assumed, $\beta = 1/T$. Table entries for air above 1000 K are from Ref. 5.

The properties of helium gas (Table A-6) were obtained from National Bureau of Standards Technical Note 631.[6]

Tables A-7 and A-10 give gaseous and saturated liquid data for ammonia. Density and specific heat data were obtained from Haar and Gallagher,[7] and the other properties were obtained from the 1976 ASHRAE Handbook.[8]

The properties of steam in the superheated state at two different pressures are given in Table A-8, and the properties of saturated liquid water are given in

Table A-8 Properties of steam

T, °C	200	250	300	350	400	450	500	550	600
Density, kg/m^3									
$P = 100$ kPa	0.460	0.416	0.379	0.348	0.322	0.300	0.280	0.263	0.248
$P = 7500$ kPa			37.4	30.8	27.1	24.4	22.4	20.7	19.3
Viscosity, μPa · s									
$P = 100$ kPa	16.2	18.2	20.3	22.4	24.5	26.5	28.6	30.6	32.6
$P = 7500$ kPa			19.7	22.1	24.4	26.6	28.8	30.9	32.9
Thermal conductivity, mW/(m · K)									
$P = 100$ kPa	33.4	38.3	43.5	49.0	54.7	60.7	66.9	73.3	79.9
$P = 7500$ kPa			64.1	60.6	62.9	67.5	72.8	78.7	84.8
Specific heat, kJ/(kg · K)									
$P = 100$ kPa	1.979	1.990	2.010	2.037	2.067	2.099	2.132	2.166	2.201
$P = 7500$ kPa			4.686	3.228	2.726	2.512	2.420	2.386	2.379
Prandtl number									
$P = 100$ kPa	0.959	0.947	0.938	0.930	0.924	0.917	0.910	0.905	0.989
$P = 7500$ kPa			1.443	1.179	1.057	0.990	0.956	0.936	0.924

Table A-9 Properties of saturated liquid water

T, °C	ρ, kg/m^3	μ, Pa · s	ν, m^2/s	c_p, kJ/(kg · K)	k, W/(m · K)	Pr
0.01	999.8	17.91 −04	17.91 −07	4.217	0.562	13.44
10	999.8	13.08 −04	13.08 −07	4.193	0.582	9.42
20	998.2	10.03 −04	10.05 −07	4.182	0.600	6.99
30	995.6	79.77 −05	80.01 −08	4.179	0.615	5.42
40	992.2	65.31 −05	65.80 −08	4.179	0.629	4.34
50	988.0	54.71 −05	55.37 −08	4.181	0.640	3.57
60	983.2	46.68 −05	47.48 −08	4.185	0.651	3.00
70	977.7	40.44 −05	41.36 −08	4.190	0.659	2.57
80	971.8	35.49 −05	36.52 −08	4.197	0.667	2.23
90	965.3	31.50 −05	32.63 −08	4.205	0.673	1.97
100	958.3	28.22 −05	29.45 −08	4.216	0.677	1.76
140	926.1	19.61 −05	21.17 −08	4.285	0.685	1.23
180	886.9	14.94 −05	16.85 −08	4.408	0.674	0.98
220	840.3	12.10 −05	14.40 −08	4.613	0.648	0.86
260	784.0	10.15 −05	12.95 −08	4.983	0.606	0.83

Table A-9. For these tables the density and specific heat values come from the equations of the 1967 IFC Formulation for Industrial Use, given in the ASME Steam Tables.[9] Viscosity and thermal conductivity values are those issued by the International Association for the Properties of Steam.[10,11]

The properties of saturated liquid oxygen (Table A-11), were obtained from NASA SP-3071,[12] and similar properties for liquid parahydrogen (Table A-12) were obtained from NASA SP-3089.[13]

Table A-10 Properties of saturated liquid ammonia

T, °C	ρ, kg/m^3	μ, Pa · s	ν, m^2/s	c_p, kJ/(kg · K)	k, W/(m · K)	Pr
−30	677	26.3 −05	38.9 −08	4.447	0.609	1.92
−20	665	23.7 −05	35.6 −08	4.501	0.586	1.82
−10	652	21.2 −05	32.4 −08	4.556	0.562	1.72
0	639	19.0 −05	29.7 −08	4.618	0.539	1.63
10	625	17.0 −05	27.2 −08	4.683	0.516	1.54
20	610	15.2 −05	24.9 −08	4.758	0.493	1.47
30	595	13.6 −05	22.9 −08	4.843	0.470	1.40
40	580	12.2 −05	21.0 −08	4.943	0.447	1.35
50	563	11.0 −05	19.5 −08	5.066	0.423	1.32
60	545	98.7 −06	15.7 −08	5.225	0.400	1.29

Table A-11 Properties of saturated liquid oxygen

T, K	ρ, kg/m^3	μ, Pa · s	ν, m^2/s	c_p, kJ/(kg · K)	k, W/(m · K)	Pr
56	1299	58.5 −05	45.0 −08	1.664	0.191	5.10
62	1273	47.5 −05	37.3 −08	1.664	0.186	4.25
68	1246	38.8 −05	31.1 −08	1.666	0.179	3.61
76	1209	30.0 −05	24.8 −08	1.672	0.170	2.95
82	1181	24.9 −05	21.1 −08	1.679	0.162	2.58
90.2	1141	19.6 −05	17.2 −08	1.696	0.151	2.20
100	1091	15.1 −05	13.8 −08	1.732	0.138	1.90
112	1024	11.4 −05	11.1 −08	1.814	0.122	1.70
126	933	87.1 −06	93.4 −09	2.029	0.102	1.73
138	833	72.3 −06	86.8 −09	2.537	0.0838	2.19
150	675	53.7 −06	79.6 −09	5.598	0.0724	4.15

Table A-12 Properties of saturated liquid parahydrogen

T, K	ρ, kg/m^3	μ, Pa · s	ν, m^2/s	c_p, kJ/(kg · K)	k, W/(m · K)	Pr
14	76.9	24.8 −06	32.2 −08	6.47	0.0746	2.15
16	75.1	19.4 −06	25.8 −08	7.36	0.0889	1.61
18	73.2	15.9 −06	21.7 −08	8.42	0.0954	1.40
20.3	70.8	13.2 −06	18.6 −08	9.66	0.0989	1.29
22	68.7	11.6 −06	16.9 −08	10.82	0.1010	1.24
24	66.0	10.1 −06	15.3 −08	12.52	0.1008	1.25
26	62.8	88.0 −07	14.0 −08	14.80	0.0984	1.32
28	59.0	76.2 −07	12.9 −08	18.48	0.0938	1.50
30	53.9	64.6 −07	12.0 −08	26.59	0.0866	1.98
32	46.0	51.3 −07	11.2 −08	65.37	0.0915	3.67

Table A-13 Properties of mercury, sodium, 22 percent sodium/78 percent potassium, and potassium

T, °C	0	50	100	200	300	400	500	600	700
Density, kg/m^3									
Hg	13,600	13,460	13,350	13,110	12,880				
Na	—	—	927	905	882	858	834	809	783
NaK	—	—	847	823	799	775	751	727	703
K	—	—	819	795	771	747	723	701	676
Viscosity, mPa · s									
Hg	1.68	1.39	1.21	1.01	0.862				
Na	—	—	0.705	0.450	0.345	0.284	0.243	0.210	0.186
NaK	—	—	0.529	0.354	0.276	0.229	0.195	0.168	0.146
K	—	—	0.463	0.298	0.227	0.190	0.169	0.145	0.134
Specific heat, kJ/(kg · K)									
Hg	0.140	0.140	0.140	0.136	0.135				
Na	—	—	1.384	1.339	1.305	1.280	1.264	1.255	1.255
NaK	—	—	0.941	0.908	0.887	0.879	0.874	0.874	0.883
K	—	—	0.812	0.791	0.774	0.766	0.761	0.766	0.774
Thermal conductivity, W/(m · K)									
Hg	8.2	9.3	10.4	12.4	14.0				
Na	—	—	—	81.5	75.7	71.2	66.8	62.7	59.0
NaK	—	—	—	24.7	25.9	26.2	26.2	25.9	25.5
K	—	—	—	44.1	42.0	39.4	37.2	34.9	32.5
Prandtl number									
Hg	0.029	0.021	0.016	0.011	0.0083				
Na	—	—	—	0.0074	0.0059	0.0051	0.0046	0.0042	0.0039
NaK	—	—	—	0.013	0.0095	0.0077	0.0065	0.0057	0.0051
K	—	—	—	0.0053	0.0042	0.0037	0.0035	0.0032	0.0036

The liquid-metal properties in Table A-13 were obtained primarily from *Liquid Metals Handbook*[14,15] and supplemented from Ref. 16.

The properties of some typical hydrocarbon fuels and oils (Tables A-14 to A-16) were adapted from data presented in *SAE Aerospace Allied Thermodynamics Manual.*[16]

Table A-17 contains properties of the atmosphere, taken from the 1976 U.S. Standard Atmosphere published by NOAA.[17]

Table A-18 gives values of the Schmidt number for a number of dilute bindary mixtures, based on data in *International Critical Tables*[18] and *Chemical Engineer's Handbook.*[19] From the Schmidt number the binary diffusion coefficient $\mathcal{D}_{12} = \mathcal{D}_{21}$ may be deduced, since the viscosity and density are the values for the medium of diffusion. The Schmidt number for gases varies only slightly with pressure and does not vary greatly with temperature; it does, however, vary significantly with mixture ratio. With these facts, it is thus possible to estimate

Table A-14 Properties of engine oil (unused)

T, °C	ρ, kg/m^3	μ, Pa · s	ν, m^2/s	c_p, kJ/(kg · K)	k, W/(m · K)	Pr
0	898	38.3 −01	42.7 −04	1.788	14.7 −02	46,540
15	889	10.6 −01	12.0 −04	1.845	14.5 −02	13,530
30	881	36.9 −02	41.9 −05	1.905	14.3 −02	4,912
45	872	15.3 −02	17.5 −05	1.969	14.1 −02	2,130
60	863	73.2 −03	84.8 −06	2.035	14.0 −02	1,065
75	855	39.4 −03	46.1 −06	2.101	13.8 −02	598
100	840	17.2 −03	20.5 −06	2.214	13.6 −02	280
125	826	91.5 −04	11.1 −06	2.328	13.4 −02	159
150	811	56.4 −04	69.5 −07	2.440	13.2 −02	104

Table A-15 Properties of hydraulic fluid (MIL-H-5606, $P = 101.325$ kPa)

T, °C	ρ, kg/m^3	μ, Pa · s	ν, m^2/s	c_p, kJ/(kg · K)	k, W/(m · K)	Pr
−15	879	70.6 −03	80.3 −06	1.737	12.7 −02	962
0	868	34.2 −03	39.4 −06	1.788	12.6 −02	483
15	858	19.2 −03	22.4 −06	1.845	12.4 −02	286
30	847	12.2 −03	14.4 −06	1.905	12.1 −02	192
45	836	84.4 −04	10.1 −06	1.969	11.7 −02	143
60	826	63.0 −04	76.3 −07	2.035	11.2 −02	114
75	815	49.9 −04	61.2 −07	2.101	10.8 −02	97

Table A-16 Properties of JP-4 fuel

T, °C	ρ, kg/m^3	μ, Pa · s	ν, m^2/s	c_p, kJ/(kg · K)	k, W/(m · K)	Pr
−15	802	15.3 −04	19.1 −07	1.858	14.1 −02	20
0	789	11.2 −04	14.2 −07	1.926	14.0 −02	15
15	776	86.8 −05	11.2 −07	1.995	13.8 −02	13
30	763	70.1 −05	91.9 −08	2.063	13.7 −02	11
45	750	58.6 −05	78.2 −08	2.132	13.6 −02	9
60	737	50.4 −05	68.4 −08	2.201	13.5 −02	8
75	724	44.4 −05	61.3 −08	2.269	13.3 −02	8

$\mathcal{D}_{12}$ and γ_{12} over a wide range of pressure, temperature, and mixture ratio. The Schmidt number for liquids varies considerably with temperature, although it is not significantly affected by pressure. Little data appear to be available on the variation of Schmidt number with mixture ratio.

Table A-19 has been prepared to provide an idea of the variation of properties with mixture composition in binary gas mixtures. The molecular weight, mole fraction, mass fraction, and specific heat for a gas mixture are given in the mass-transfer chapters. The mixture density was calculated according to the ideal-gas law. For the table air was the medium of diffusion, and the binary

Table A-17 Properties of the atmosphere

Geometric altitude, m	Temperature, K	Pressure, Pa	Density, kg/m^3	Viscosity, μPa · s	Thermal conductivity, mW/(m · K)	Speed of sound, m/s
0	288.2	1.01325 +05	1.225 +00	17.89	25.36	340.3
250	286.5	9.836 +04	1.196 +00	17.82	25.23	339.3
500	284.9	9.546 +04	1.167 +00	17.74	25.11	338.4
750	283.3	9.263 +04	1.139 +00	17.66	24.97	337.4
1,000	281.7	8.988 +04	1.112 +00	17.58	24.85	336.4
1,250	280.0	8.719 +04	1.085 +00	17.50	24.72	335.5
1,500	278.4	8.456 +04	1.058 +00	17.42	24.59	334.5
3,000	268.7	7.012 +04	9.093 −01	16.94	23.81	328.6
4,500	258.9	5.775 +04	7.770 −01	16.45	22.03	322.6
6,000	249.2	4.722 +04	6.601 −01	15.95	22.23	316.5
7,500	239.5	3.830 +04	5.572 −01	15.44	21.44	310.2
10,000	223.3	2.650 +04	4.135 −01	14.58	20.09	299.5
12,500	216.7	1.793 +04	2.884 −01	14.22	19.53	295.1
15,000	216.7	1.211 +04	1.948 −01	14.22	19.53	295.1
17,500	216.7	8.182 +03	1.316 −01	14.22	19.53	295.1
20,000	216.7	5.529 +03	8.891 −02	14.22	19.53	295.1
25,000	221.6	2.549 +03	4.008 −02	14.48	19.95	298.4
30,000	226.5	1.197 +03	1.841 −02	14.75	20.36	301.7
45,000	264.2	1.491 +02	1.966 −03	16.71	23.45	325.8
60,000	247.0	2.196 +01	3.097 −04	15.84	22.06	315.1
75,000	208.4	2.388 +00	3.992 −05	13.76	18.83	289.4

diffusion coefficient $\mathscr{D}_{12}$ was calculated using the viscosity of air and the Schmidt number from Table A-18. This allowed calculation of γ_{12} from $\mathscr{D}_{12}$ and the mixture density.

The mixture viscosity was calculated using the Wilke[20] method and the mixture thermal conductivity was calculated using the Lindsay-Bromley[21] method, as reviewed by Gambill.[22] References 1, 3, and 23 contain a review of these and other methods of computing mixture thermophysical properties.

Table A-20 has been prepared as an aid in mass-transfer problems involving the air–water-vapor system. The vapor pressure of H_2O as a function of temperature is taken from Ref. 9, and then the concentration of H_2O in a *saturated* air–water-vapor mixture at 1 atm total pressure is plotted. The latter has been prepared from Eq. (20-10). Similar curves can be prepared for other total pressures, using the same vapor-pressure curve; and, of course, other gas–vapor systems can be handled in the same way if vapor-pressure data are available.

Table A-18 Some values of the Schmidt number for dilute binary mixtures at approximately normal atmospheric conditions

Diffusing substance	**Medium of diffusion**	**Schmidt number** $Sc = \frac{\mu}{\gamma_{12}} = \frac{\mu}{\rho\mathcal{D}_{12}} = \frac{\nu}{\mathcal{D}_{12}}$
Ammonia	Air (gas)	0.61
Ammonia	Water (liquid)	570
Benzene	Air (gas)	1.71
Benzene	Carbon dioxide (gas)	1.37
Carbon dioxide	Air (gas)	0.96
Carbon dioxide	Hydrogen (gas)	1.58
Carbon dioxide	Water (liquid)	559
Carbon dioxide	Ethyl alcohol (liquid)	445
Carbon disulfide	Air (gas)	1.48
Carbon tetrachloride	Air (gas)	2.13
Chlorine	Air (gas)	1.42
Chlorine	Water (liquid)	824
Ethane	Air (gas)	1.22
Ethyl alcohol	Air (gas)	1.30
Ethyl alcohol	Water (liquid)	1005
Ethyl ether	Air (gas)	1.70
Glycerol	Water (liquid)	1630
Helium	Air (gas)	0.22
Hydrochloric acid	Water (liquid)	381
Hydrogen	Air (gas)	0.22
Hydrogen	Oxygen (gas)	0.182
Methane	Air (gas)	0.84
Methyl alcohol	Air (gas)	1.00
Nitrogen	Air (gas)	0.98
Nitrogen	Water (liquid)	613
Oxygen	Air (gas)	0.74
Oxygen	Nitrogen (gas)	0.681
Oxygen	Water (liquid)	558
n-Octane	Air (gas)	2.62
Sodium chloride	Water (liquid)	745
Sodium hydroxide	Water (liquid)	665
Sucrose	Water (liquid)	2230
Sulfuric acid	Water (liquid)	580
Water (vapor)	Air (gas)	0.60

Table A-19 Binary gas mixtures ($P = 101.325$ kPa, $T = 290$ K)

m_{H_2O} m_{H_2} m_{CO_2}	$\mathfrak{M}$, kg/kmol	c_p, kJ/(kg · K)	γ, kg/(m · s)	Pr	Sc	Le
			Air–H_2O			
0.00	28.97	1.003	0.3008 −04	0.714	0.600	1.189
0.10	27.31	1.089	0.2836 −04	0.729	0.597	1.220
0.20	25.82	1.175	0.2682 −04	0.751	0.595	1.264
0.30	24.50	1.261	0.2544 −04	0.780	0.592	1.318
0.40	23.30	1.347	0.2419 −04	0.813	0.589	1.381
0.50	22.21	1.433	0.2307 −04	0.850	0.586	1.451
0.60	21.22	1.518	0.2204 −04	0.890	0.583	1.528
0.70	20.32	1.604	0.2110 −04	0.934	0.580	1.611
0.80	19.49	1.690	0.2024 −04	0.980	0.576	1.701
0.90	18.72	1.776	0.1944 −04	1.030	0.573	1.797
1.00	18.01	1.862	0.1870 −04	1.083	0.570	1.900
			Air–H_2			
0.00	28.97	1.003	0.8204 −04	0.714	0.220	3.244
0.10	12.40	2.326	0.3511 −04	0.425	0.472	0.900
0.20	7.88	3.648	0.2233 −04	0.448	0.664	0.674
0.30	5.78	4.970	0.1637 −04	0.482	0.819	0.588
0.40	4.56	6.292	0.1292 −04	0.517	0.951	0.544
0.50	3.77	7.614	0.1068 −04	0.550	1.066	0.516
0.60	3.21	8.937	0.0909 −04	0.583	1.171	0.498
0.70	2.80	10.259	0.0792 −04	0.614	1.268	0.484
0.80	2.48	11.581	0.0702 −04	0.644	1.359	0.474
0.90	2.22	12.903	0.0630 −04	0.674	1.446	0.466
1.00	2.02	14.226	0.0571 −04	0.703	1.529	0.460
			Air–CO_2			
0.00	28.97	1.003	0.1880 −04	0.714	0.960	0.743
0.10	29.99	0.986	0.1947 −04	0.711	0.911	0.780
0.20	31.09	0.969	0.2018 −04	0.709	0.862	0.822
0.30	32.28	0.952	0.2095 −04	0.708	0.815	0.869
0.40	33.55	0.935	0.2178 −04	0.708	0.768	0.923
0.50	34.94	0.918	0.2268 −04	0.711	0.722	0.984
0.60	36.44	0.901	0.2365 −04	0.715	0.677	1.056
0.70	38.08	0.884	0.2471 −04	0.722	0.634	1.139
0.80	39.87	0.867	0.2588 −04	0.731	0.591	1.238
0.90	41.84	0.850	0.2715 −04	0.745	0.549	1.356
1.00	44.01	0.833	0.2856 −04	0.763	0.509	1.501

Table A-20 Vapor pressure of H_2O and mass concentration of H_2O in saturated air at $P = 101.325$ kPa

T_{sat}, °C	Vapor pressure, Pa	m_{H_2O}	T_{sat}, °C	Vapor pressure, Pa	m_{H_2O}
−20	103	0.00064	40	7,378	0.0468
−15	165	0.00102	45	9,585	0.0614
−10	260	0.00160	50	12,339	0.0799
−5	401	0.00248	55	15,745	0.1033
0	611	0.00377	60	19,925	0.1330
5	872	0.00539	65	25,014	0.1705
10	1,227	0.00760	70	31,167	0.2180
15	1,704	0.0106	75	38,554	0.2784
20	2,337	0.0145	80	47,365	0.3556
25	3,167	0.0198	85	57,809	0.4554
30	4,243	0.0266	90	70,112	0.5861
35	5,623	0.0354	100	101,325	1.0000

REFERENCES

1. Touloukian, Y. S., P. E. Liley, and S. C. Saxena: *Thermophysical Properties of Matter*, vol. 3: *Thermal Conductivity. Nonmetallic Liquids and Gases*. IFI/Plenum, New York, 1970.
2. Touloukian, Y. S., and T. Makita: *Thermophysical Properties of Matter*, vol. 6: *Specific Heat. Nonmetallic Gases and Liquids*, IFI/Plenum, New York, 1970.
3. Touloukian, Y. S., S. C. Saxena, and P. Hestermans: *Thermophysical Properties of Matter*, vol. 11: *Viscosity*, IFI/Plenum, New York, 1970.
4. Hilsenrath, J., *et al.*: "Tables of Thermal Properties of Gases," NBS Circular 564, Washington, November 1955.
5. Poferl, D. J., R. A. Svehla, and K. Lewandowski: "Thermodynamic and Transport Properties of Air and the Combustion Products of Natural Gas and of ASTM-A-1 Fuel with Air," NASA Technical Note D-5452, Washington, 1969.
6. McCarty, R. D.: "Thermophysical Properties of Helium-4 from 2 to 1500 K with Pressures to 1000 Atmospheres," NBS Tech. Note 631, Washington, November 1972.
7. Haar, L., and J. S. Gallagher: "Thermodynamic Properties of Ammonia," *J. Phys. Chem. Ref. Data*, vol. 7, p. 635, 1977.
8. *ASHRAE Thermophysical Properties of Refrigerants*, American Society of Heating, Refrigeration, and Air-Conditioning Engineers, New York, 1976.
9. *ASME Steam Tables*, 3d ed., American Society of Mechanical Engineers, New York, 1977.
10. Nagashima, A.: "Viscosity of Water Substance—New International Formulation and Its Background," *J. Phys. Chem. Ref. Data*, vol. 6, p. 1133, 1977.
11. "Release of Thermal Conductivity of Water Substance," International Association for the Properties of Steam, December 1977.
12. Roder, H. M., and L. A. Weber: *Thermophysical Properties*, vol. 1: *ASRDI Oxygen Technology Survey*, NASA SP-3071, Washington, 1972.

13. McCarty, R. D.: *Hydrogen Technological Survey—Thermophysical Properties*, NASA SP-3089, Washington, 1975.
14. Lyon, R. N. (ed.): *Liquid Metals Handbook*, 2d ed., Atomic Energy Commission and Department of the Navy, Washington, 1952.
15. Jackson, C. B. (ed.): *Liquid Metals Handbook*, 3d ed., Atomic Energy Commission and Department of the Navy, Washington, 1955.
16. *SAE Aerospace Applied Thermodynamics Manual*, 2d ed., Society of Automotive Engineers, New York, 1969.
17. *U.S. Standard Atmosphere*, 1976, NOAA, NASA, and USAF, Washington, October 1976.
18. *International Critical Tables*, McGraw-Hill, New York, 1926–1930.
19. Perry, J. H.: *Chemical Engineer's Handbook*, McGraw-Hill, New York, 1950.
20. Wilke, C. R.: *J. Chem. Phys*. vol. 18, p. 157, 1950.
21. Lindsay, A. L., and L. A. Bromley: *Ind. Engng Chem*., vol. 42, p. 508, 1950.
22. Gambill, W. R.: *Chem. Engng*, vol. 64, p. 277, 1957.
23. Reid, R. C., J. M. Prausnitz, and T. K. Sherwood: *The Properties of Gases and Liquids*, 3d ed., McGraw-Hill, New York, 1977.

APPENDIX B

Dimensions and Conversion to SI

BASIC UNITS

Length	meter (m)
Mass	kilogram (kg)
Time	second (s)
Electric current	ampere (A)
Thermodynamic temperature	kelvin (K)
Luminous intensity	candela (cd)
Amount of substance	mole (mol)

DERIVED UNITS

See Table B-2.

PHYSICAL CONSTANTS

Gas constant	$\Re = 8314.34\ \mathrm{J/(kmol \cdot K)}$
Stefan–Boltzmann constant	$\sigma = 5.66961 \times 10^{-8}\ \mathrm{W/(m^2 \cdot K^4)}$
Freefall, standard	$g = 9.806650\ \mathrm{m/s^2}$

Table B-1 SI prefixes

Factor	Prefix	Symbol
10^{18}	exa	E
10^{15}	peta	P
10^{12}	tera	T
10^{9}	giga	G
10^{6}	mega	M
10^{3}	kilo	k
10^{2}	hecto	h
10	deka	da
10^{-1}	deci	d
10^{-2}	centi	c
10^{-3}	milli	m
10^{-6}	micro	μ
10^{-9}	nano	n
10^{-12}	pico	p
10^{-15}	femto	f
10^{-18}	atto	a

Table B-2 Conversion factors

Physical quantity	Unit	SI equivalent†
Acceleration, m/s^2	foot/second^2	3.048 000‡ −01
Area, m^2	foot^2	9.290 304‡ −02
	inch^2	6.451 600‡ −04
Density, kg/m^3	gram/centimeter^3	1.000 000‡ +03
	pound-mass/inch^3	2.767 990 +04
	pound-mass/foot^3	1.601 846 +01
	slug/foot^3	5.153 788 +02
Energy, $J = N \cdot m$	Btu_{IT}	1.055 056 +03
	Btu_{th} (thermochemical)	1.054 350 +03
	$\text{calorie}_{\text{IT}}$	4.186 800‡ +00
	$\text{calorie}_{\text{th}}$ (thermochemical)	4.184 000‡ +00
	erg	1.000 000‡ −07
	foot pound-force	1.355 818 +00
	foot-poundal	4.214 011 −02
	watt-hour	3.600 000‡ +03
Enthalpy, J/kg	$\text{Btu}_{\text{IT}}/\text{lb}_m$	2.326 000‡ +03
	$\text{Btu}_{\text{th}}/\text{lb}_m$	2.324 444 +03
Force, $N = kg \cdot m/s^2$	dyne	1.000 000‡ −05
	kilogram-force	9.806 650‡ +00
	pound-force	4.448 222 +00
	poundal	1.382 550 −01
Heat flux, $W/m^2 = J/(s \cdot m^2)$	$\text{Btu}_{\text{IT}}/(\text{s} \cdot \text{ft}^2)$	1.135 653 +04
	$\text{Btu}_{\text{IT}}/(\text{h} \cdot \text{ft}^2)$	3.154 591 +00
	$\text{cal}_{\text{th}}/(\text{s} \cdot \text{cm}^2)$	4.186 800‡ +04
Heat-transfer coefficient, $W/(m^2 \cdot K)$	$\text{Btu}_{\text{TH}}/(\text{s} \cdot \text{ft}^2 \cdot \text{F})$	2.044 175 +04
	$\text{Btu}_{\text{IT}}/(\text{h} \cdot \text{ft}^2 \cdot {}^\circ\text{F})$	5.678 263 +00
	$\text{cal}_{\text{TH}}/(\text{s} \cdot \text{cm}^2 \cdot {}^\circ\text{C})$	4.186 800‡ +04

Table B-2 *Continued*

Physical quantity	Unit	SI equivalent†
Heat transfer rate, W = J/s	Btu$_{\text{IT}}$/hour	2.930 711 −01
	Btu$_{\text{th}}$/hour	2.928 751 −01
	Btu$_{\text{IT}}$/second	1.055 056 +03
	cal$_{\text{IT}}$/second	4.186 800‡ +00
	cal$_{\text{th}}$/second	4.184 000‡ +00
Kinematic viscosity, m^2/s	centistoke	1.000 000‡ −06
	foot^2/second	9.290 304‡ −02
	stoke	1.000 000‡ −04
Length, m	foot	3.048 000‡ −01
	inch	2.540 000‡ −02
	mile (US)	1.609 344‡ +03
Mass, kg	pound-mass	4.535 924 −01
	slug	1.459 390 +01
	ton (metric)	1.000 000 +03
Mass flow rate, kg/s	lb$_m$/second	4.535924 −01
	lb$_m$/hour	1.259979 −04
Power, W = J/s	ft · lb$_f$ /s	1.355 818 +00
	horsepower (550 ft · lb$_f$ /s)	7.456 999 +02
Pressure, Pa = N/m^2	atmosphere (normal = 760 Torr)	1.013 250‡ +05
	atmosphere (technical = 1 kg$_f$ /cm^2)	9.806 650‡ +04
	bar	1.000 000‡ +05
	dyne/centimeter^2	1.000 000‡ −01
	inch of Hg (0°C)	3.386 389 +03
	inch of Hg (60°F)	3.376 85 +03
	inch of H_2O (4°C)	2.490 82 +02
	inch of H_2O (60°F)	2.488 4 +02
	mmHg (0°C) = Torr	1.333 22 +02
	poundal/foot^2	1.488 164 +00
	pound-force/foot^2	4.788 026 +01
	pound-force/inch^2	6.894 757 +03
Specific heat, kJ/(kg · K)	Btu$_{\text{IT}}$/(lb$_m$ · °F)	4.186 800‡ +00
	Btu$_{\text{th}}$ /(lb$_m$ · °F)	4.184 000‡ +00
	cal$_{\text{IT}}$/(g · °C)	4.186 800‡ +00
	cal$_{\text{th}}$/(g · °C)	4.184 000‡ +00
Temperature, K	$T\,(\mathrm{K}) = T\,(^\circ\mathrm{C}) + 273.15$	
	$T\,(\mathrm{K}) = T\,(^\circ\mathrm{R})/1.8$	
	$T\,(\mathrm{K}) = [T\,(^\circ\mathrm{F}) + 459.67]/1.8$	
	$T\,(^\circ\mathrm{C}) = [T(^\circ\mathrm{F}) - 32]/1.8$	
Thermal conductivity, W/(m · K) = J/(s · m · K)	Btu$_{\text{IT}}$/(h · ft · °F)	1.730 735 +00
	Btu$_{\text{IT}}$ · in/(h · ft^2 · °F)	1.442 279 −01
	Btu$_{\text{th}}$/(h · ft · °F)	1.729 577 +00
	cal$_{\text{th}}$/(s · cm · C)	4.184 000‡ +02
Thermal diffusivity, m^2/s	foot^2/second	9.290 304‡ −02
	foot^2/hour	2.580 640‡ −05
Velocity, m/s	foot/second	3.048 000‡ −01
	kilometer/hour	2.777 778 −01
	mile (US)/hour	0.447 04‡ +00

Table B-2 *Continued*

Physical quantity	Unit	SI equivalent†
Viscosity, $Pa \cdot s = N \cdot s/m^2$	centipoise	1.000 000‡ −03
	poise	1.000 000‡ −01
	$lb_m/(s \cdot ft)$	1.488 164 +00
	$lb_m/(h \cdot ft)$	4.133 789 −04
	$lb_f \cdot s/ft^2$	4.788 026 +01
	$slug/(s \cdot ft)$	4.788 026 +01
Volume, m^3	$foot^3$	2.831 685 −02
	in^3	1.638 706 −05
	gallon (US liquid)	3.785 412 −03
	liter	1.000 000‡ −03
	ounce (US fluid)	2.957 353 −05
Volume flow rate, m^3/s	$foot^3$/minute	4.719 474 −04
	$foot^3$/second	2.831 685 −02
	gallon (US liquid)/minute	6.309 020 −05

† As in App. A, an abbreviated notation is used: $-01 = 10^{-1}$ etc.

‡ An exact definition.

REFERENCES

Mechtly, E. A.: *The International System of Units—Physical Constants and Conversion Factors*, 2d ed., NASA SP-7012, Washington, 1973.

Metric Manual, McDonnell Douglas Corporation, 1976.

APPENDIX C

Some Tables of Functions Useful in Boundary-Layer Analysis

Table C-1 Gamma function

$$\Gamma(n) = \int_0^\infty x^{n-1} e^{-x}\, dx, \quad \Gamma(n+1) = n\Gamma(n)$$

n	$\Gamma(n)$	n	$\Gamma(n)$	n	$\Gamma(n)$
1.00	1.000	1.35	0.891	1.70	0.909
1.05	0.974	1.40	0.887	1.75	0.919
1.10	0.951	1.45	0.886	1.80	0.931
1.15	0.933	1.50	0.886	1.85	0.946
1.20	0.918	1.55	0.889	1.90	0.962
1.25	0.906	1.60	0.894	1.95	0.980
1.30	0.897	1.65	0.900	2.00	1.00

Table C-2 Beta function and incomplete beta function

$$\beta_1(m, n) = \int_0^1 Z^{m-1}(1 - Z)^{n-1}\, dz$$

$$= \beta_1(n, m) = \frac{\Gamma(m)\Gamma(n)}{\Gamma(m+n)}$$

Incomplete beta function

$$\beta_r(m, n) = \int_0^r Z^{m-1}(1 - Z)^{n-1}\, dZ$$

$$= \beta_1(m, n) - \beta_{1-r}(n, m)$$

Table C-3 Tabulation of $\beta_1(m, n)$ for some particular values of m and n encountered in Chaps. 10 and 12 and values of β_r/β_1 as a function of r for the same values of m and n†

m	$\frac{1}{3}$	$\frac{1}{3}$	$\frac{1}{3}$	$\frac{2}{3}$	$\frac{1}{9}$	$\frac{1}{9}$	$\frac{1}{9}$	$\frac{8}{9}$
n	$\frac{2}{3}$	$\frac{4}{3}$	$\frac{8}{3}$	$\frac{4}{3}$	$\frac{8}{9}$	$\frac{10}{9}$	$\frac{20}{9}$	$\frac{10}{9}$
$\beta_1(m, n)$	**3.628**	**2.650**	**2.015**	**1.209**	**9.185**	**8.844**	**7.984**	**1.021**
r				β_r/β_1				
0	0	0	0	0	0	0	0	0
0.02	0.225	0.307	0.402	0.0912	0.635	0.659	0.728	0.0432
0.06	0.325	0.441	0.568	0.189	0.717	0.744	0.819	0.0917
0.10	0.387	0.521	0.663	0.264	0.760	0.787	0.862	0.142
0.20	0.492	0.651	0.801	0.312	0.821	0.849	0.920	0.261
0.40	0.634	0.804	0.928	0.634	0.890	0.915	0.970	0.477
0.60	0.745	0.900	0.980	0.800	0.934	0.954	0.990	0.673
0.80	0.850	0.964	0.997	0.924	0.968	0.981	0.998	0.851
1.00	1.000	1.000	1.000	1.000	1.000	1.000	1.000	1.000

† *Taken from Baxter and Reynolds.*[1]

Table C-4 Error function

$$\operatorname{erf}(x) = \frac{2}{\sqrt{\pi}} \int_0^x e^{-\eta^2}\, d\eta = \frac{2}{\sqrt{\pi}} \int_{-x}^0 e^{-\eta^2}\, d\eta$$

x	**erf(x)**	x	**erf(x)**	x	**erf(x)**
0.00	0.0000	0.45	0.475	1.10	0.880
0.02	0.0226	0.50	0.521	1.20	0.910
0.04	0.0451	0.55	0.563	1.30	0.934
0.06	0.0676	0.60	0.604	1.40	0.952
0.08	0.0901	0.65	0.642	1.50	0.966
0.10	0.1125	0.70	0.678	1.60	0.976
0.15	0.168	0.75	0.711	1.80	0.989
0.20	0.223	0.80	0.742	2.00	0.995
0.25	0.276	0.85	0.771	3.00	1.000
0.30	0.329	0.90	0.797	∞	1.000
0.35	0.379	0.95	0.821		
0.40	0.428	1.00	0.843		

REFERENCE

1. Baxter, D. C., and W. C. Reynolds: *J. Aero. Sci.*, vol. 25, no. 6, 1958.

APPENDIX D

Operations Implied by the ∇ Operator

Let **V** represent a vector quantity and S a scalar quantity. Subscripts designate the scalar magnitudes of the components of a vector in the indicated direction. Note that

∇S	is a vector
$\nabla \cdot \mathbf{V}$	is a scalar
$\nabla^2 S$	is a scalar
$\nabla^2 \mathbf{V}$	is a vector
$\mathbf{V} \cdot \nabla S$	is a scalar

RECTANGULAR COORDINATES (x, y, z)

See Fig. D-1.

$$\nabla \cdot \mathbf{V} = \frac{\partial V_x}{\partial x} + \frac{\partial V_y}{\partial y} + \frac{\partial V_z}{\partial z}$$

$$\nabla^2 S = \frac{\partial^2 S}{\partial x^2} + \frac{\partial^2 S}{\partial y^2} + \frac{\partial^2 S}{\partial z^2}$$

$$(\nabla S)_x = \frac{\partial S}{\partial x}, \qquad (\nabla S)_y = \frac{\partial S}{\partial y}, \qquad (\nabla S)_z = \frac{\partial S}{\partial z}$$

$$\mathbf{V} \cdot \nabla S = V_x \frac{\partial S}{\partial x} + V_y \frac{\partial S}{\partial y} + V_z \frac{\partial S}{\partial z}$$

$$\nabla \cdot \alpha \nabla S = \frac{\partial}{\partial x}\left(\alpha \frac{\partial S}{\partial x}\right) + \frac{\partial}{\partial y}\left(\alpha \frac{\partial S}{\partial y}\right) + \frac{\partial}{\partial z}\left(\alpha \frac{\partial S}{\partial z}\right)$$

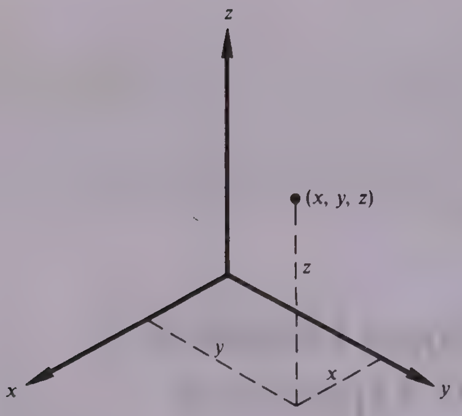

Figure D-1

$$(\nabla^2 \mathbf{V})_x = \frac{\partial^2 V_x}{\partial x^2} + \frac{\partial^2 V_x}{\partial y^2} + \frac{\partial^2 V_x}{\partial z^2}$$

$$(\nabla^2 \mathbf{V})_y = \frac{\partial^2 V_y}{\partial x^2} + \frac{\partial^2 V_y}{\partial y^2} + \frac{\partial^2 V_y}{\partial z^2}$$

$$(\nabla^2 \mathbf{V})_z = \frac{\partial^2 V_z}{\partial x^2} + \frac{\partial^2 V_z}{\partial y^2} + \frac{\partial^2 V_z}{\partial z^2}$$

CYLINDRICAL COORDINATES (r, ϕ, x)

See Fig. D-2.

$$\nabla \cdot \mathbf{V} = \frac{1}{r}\frac{\partial}{\partial r}(rV_r) + \frac{1}{r}\frac{\partial V_\phi}{\partial \phi} + \frac{\partial V_x}{\partial x}$$

$$\nabla^2 S = \frac{1}{r}\frac{\partial}{\partial r}\left(r\frac{\partial S}{\partial r}\right) + \frac{1}{r^2}\frac{\partial^2 S}{\partial \phi^2} + \frac{\partial^2 S}{\partial x^2}$$

$$(\nabla S)_r = \frac{\partial S}{\partial r}, \qquad (\nabla S)_\phi = \frac{1}{r}\frac{\partial S}{\partial \phi}, \qquad (\nabla S)_x = \frac{\partial S}{\partial x}$$

$$\mathbf{V} \cdot \nabla S = V_r \frac{\partial S}{\partial r} + \frac{V_\phi}{r}\frac{\partial S}{\partial \phi} + V_x \frac{\partial S}{\partial x}$$

$$\nabla \cdot \alpha \nabla S = \frac{1}{r}\frac{\partial}{\partial r}\left(r\alpha\frac{\partial S}{\partial r}\right) + \frac{1}{r}\frac{\partial}{\partial \phi}\left(\frac{\alpha}{r}\frac{\partial S}{\partial \phi}\right) + \frac{\partial}{\partial x}\left(\alpha\frac{\partial S}{\partial x}\right)$$

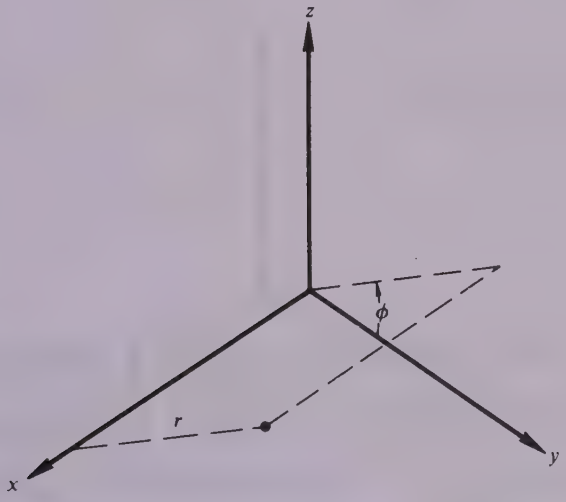

Figure D-2

$$(\nabla^2 \mathbf{V})_r = \frac{\partial}{\partial r}\left[\frac{1}{r}\frac{\partial}{\partial r}(rV_r)\right] + \frac{1}{r^2}\frac{\partial^2 V_r}{\partial \phi^2} - \frac{2}{r^2}\frac{\partial V_\phi}{\partial \phi} + \frac{\partial^2 V_r}{\partial x^2}$$

$$(\nabla^2 \mathbf{V})_\phi = \frac{\partial}{\partial r}\left[\frac{1}{r}\frac{\partial}{\partial r}(rV_\phi)\right] + \frac{1}{r^2}\frac{\partial^2 V_\phi}{\partial \phi^2} + \frac{2}{r^2}\frac{\partial V_r}{\partial \phi} + \frac{\partial^2 V_\phi}{\partial x^2}$$

$$(\nabla^2 \mathbf{V})_x = \frac{1}{r}\frac{\partial}{\partial r}\left(r\frac{\partial V_x}{\partial r}\right) + \frac{1}{r^2}\frac{\partial^2 V_x}{\partial \phi^2} + \frac{\partial^2 V_x}{\partial x^2}$$

SPHERICAL COORDINATES (r, θ, ϕ)

See Fig. D-3.

$$\nabla \cdot \mathbf{V} = \frac{1}{r^2}\frac{\partial}{\partial r}(r^2 V_r) + \frac{1}{r\sin\theta}\frac{\partial}{\partial \theta}(V_\theta \sin\theta) + \frac{1}{r\sin\theta}\frac{\partial V_\phi}{\partial \phi}$$

$$\nabla^2 S = \frac{1}{r^2}\frac{\partial}{\partial r}\left(r^2\frac{\partial S}{\partial r}\right) + \frac{1}{r^2\sin\theta}\frac{\partial}{\partial \theta}\left(\sin\theta\frac{\partial S}{\partial \theta}\right) + \frac{1}{r^2\sin^2\theta}\frac{\partial^2 S}{\partial \phi^2}$$

$$(\nabla S)_r = \frac{\partial S}{\partial r}, \quad (\nabla S)_\theta = \frac{1}{r}\frac{\partial S}{\partial \theta}, \quad (\nabla S)_\phi = \frac{1}{r\sin\theta}\frac{\partial S}{\partial \phi}$$

$$\mathbf{V} \cdot \nabla S = V_r\frac{\partial S}{\partial r} + \frac{V_\theta}{r}\frac{\partial S}{\partial \theta} + \frac{V_\phi}{r\sin\theta}\frac{\partial S}{\partial \phi}$$

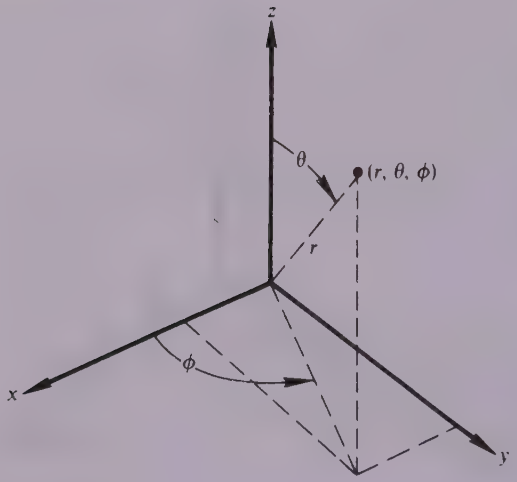

Figure D-3

$$\nabla \cdot \alpha \nabla S = \frac{1}{r^2}\frac{\partial}{\partial r}\left(r^2 \alpha \frac{\partial S}{\partial r}\right) + \frac{1}{r^2 \sin\theta}\frac{\partial}{\partial \theta}\left[(\sin\theta)\alpha \frac{\partial S}{\partial \theta}\right]$$

$$+ \frac{1}{r^2 \sin^2\theta}\frac{\partial}{\partial \phi}\left(\alpha \frac{\partial S}{\partial \phi}\right)$$

$$(\nabla^2 \mathbf{V})_r = \nabla^2 V_r - \frac{2V_r}{r^2} - \frac{2}{r^2}\frac{\partial V_\theta}{\partial \theta} - \frac{2V_\theta \cot\theta}{r^2} - \frac{2}{r^2 \sin\theta}\frac{\partial V_\phi}{\partial \phi}$$

$$(\nabla^2 \mathbf{V})_\theta = \nabla^2 V_\theta + \frac{2}{r^2}\frac{\partial V_r}{\partial \theta} - \frac{V_\theta}{r^2 \sin\theta} - \frac{2\cos\theta}{r^2 \sin^2\theta}\frac{\partial V_\phi}{\partial \phi}$$

$$(\nabla^2 \mathbf{V})_\phi = \nabla^2 V_\phi - \frac{V_\phi}{r^2 \sin^2\theta} + \frac{2}{r^2 \sin\theta}\frac{\partial V_r}{\partial \phi} + \frac{2\cos\theta}{r^2 \sin^2\theta}\frac{\partial V_\theta}{\partial \phi}$$

APPENDIX E

Detailed Derivation of the Simplified Mass-Diffusion and Energy Equation ($\mathcal{P}$ Equation) for Convective Mass Transfer Problems and the Corresponding Boundary Conditions

In this appendix, the various simplifications are discussed that finally lead to the conserved property equation (18-15) and the boundary condition at the interface according to Eq. (18-29).

Consider a two-dimensional boundary layer in (x, y) coordinates within the considered phase. Let us restrict consideration to steady-flow in the absence of body forces, and let velocities be sufficiently low so that we can neglect viscous energy dissipation and the influence of pressure gradients on the energy equation. Then the differential equations to be satisfied within the laminar boundary layer are:

diffusion of component j, Eq. (4-18),

$$G_x \frac{\partial m_j}{\partial x} + G_y \frac{\partial m_j}{\partial y} - \frac{\partial}{\partial y}\left(\gamma_j \frac{\partial m_j}{\partial y}\right) = \dot{m}_j''' \tag{18-1}$$

diffusion of chemical elements α, Eq. (4-24),

$$G_x \frac{\partial n_\alpha}{\partial x} + G_y \frac{\partial n_\alpha}{\partial y} - \frac{\partial}{\partial y} \sum_j \gamma_j \frac{\partial}{\partial y}(n_{\alpha,j} m_j) = 0 \tag{18-2}$$

energy, from Eq. (4-26) or (4-27),

$$G_x \frac{\partial i}{\partial x} + G_y \frac{\partial i}{\partial y} - \frac{\partial}{\partial y}\left(k \frac{\partial T}{\partial y}\right) - \frac{\partial}{\partial y}\left(\sum_j \gamma_j \frac{\partial m_j}{\partial y} i_j\right) = 0 \tag{18-3}$$

continuity, from Eq. (4-1),

$$\frac{\partial G_x}{\partial x} + \frac{\partial G_y}{\partial y} = 0 \tag{18-4}$$

momentum, from Eq. (4-10),

$$G_x \frac{\partial u}{\partial x} + G_y \frac{\partial u}{\partial y} = -\frac{dP}{dx} + \frac{\partial}{\partial y}\left(\mu \frac{\partial u}{\partial y}\right) \tag{18-5}$$

In the following process of simplification we are obviously going to lose some generality. In applications where we are not satisfied with the validity of these simplifications we have no resource but to return to the original five equations and attempt a solution by other means (for example with the help of a numerical solution method). If, in a multicomponent system, the binary diffusion coefficients differ sufficiently to invalidate the use of Fick's law, or if the Dufour or Soret effects are deemed to be of importance (see Chap. 3), we must obviously retreat even further before attempting a solution. Whether the increased accuracy is worth the time and effort is one of the classic problems of engineering analysis.

SIMPLIFICATIONS OF THE MASS-DIFFUSION EQUATIONS OF THE BOUNDARY LAYER

Within this section we are discussing first various simplifications of the mass-diffusion equation, which will lead to the same simplified equation.

CASE 1: Diffusion of an Inert Substance

In this case there is no chemical reaction, and $\dot{m}_j''' = 0$. Thus Eq. (18-1) becomes

$$G_x \frac{\partial m_j}{\partial x} + G_y \frac{\partial m_j}{\partial y} - \frac{\partial}{\partial y}\left(\gamma_j \frac{\partial m_j}{\partial y}\right) = 0 \tag{18-12}$$

Eq. (18-12) is the standard form that we seek for all the other simplifications.

CASE 2: Simple Chemical Reaction with Equal Diffusion Coefficients

Consider a simple reaction taking place within the considered phase in which a fuel combines with an oxidant to form a single product, without intermediaries. Then from stoichiometric considerations, we can write

$$1 \text{ kg fuel} + r \text{ kg oxidant} \rightleftarrows (1 + r) \text{ kg product}$$

We can now apply Eq. (18-1) independently to the fuel (Index f) and the oxidant (Index o), or to the product (Index p), if we prefer:

$$G_x \frac{\partial m_f}{\partial x} + G_y \frac{\partial m_f}{\partial y} - \frac{\partial}{\partial y}\left(\gamma_f \frac{\partial m_f}{\partial y}\right) = \dot{m}_f''' \tag{E-1}$$

$$G_x \frac{\partial m_o}{\partial x} + G_y \frac{\partial m_o}{\partial y} - \frac{\partial}{\partial y}\left(\gamma_o \frac{\partial m_o}{\partial y}\right) = \dot{m}_o''' \tag{E-2}$$

From the stoichiometric relation we obtain

$$\dot{m}_f''' = \dot{m}_o'''/r \tag{E-3}$$

If we combine Eqs. (E-1)–(E-2) and use Eq. (E-3), we obtain

$$\begin{aligned} G_x \frac{\partial m_f}{\partial x} + G_y \frac{\partial m_f}{\partial y} - \frac{\partial}{\partial y}\left(\gamma_f \frac{\partial m_f}{\partial y}\right) \\ = \frac{1}{r}\left(G_x \frac{\partial m_o}{\partial x} + G_y \frac{\partial m_o}{\partial y}\right) - \frac{1}{r}\frac{\partial}{\partial y}\left(\gamma_o \frac{\partial m_o}{\partial y}\right) \end{aligned} \tag{E-4}$$

Rearranging gives

$$G_x \frac{\partial}{\partial x}\left(m_f - \frac{m_o}{r}\right) + G_y \frac{\partial}{\partial y}\left(m_f - \frac{m_o}{r}\right) - \frac{\partial}{\partial y}\left(\gamma_f \frac{\partial m_f}{\partial y} - \frac{\gamma_o}{r}\frac{\partial m_o}{\partial y}\right) = 0 \tag{E-5}$$

If we now suppose that $\gamma_f = \gamma_o = \gamma$ (and this is the first of our major simplifications), then

$$G_x \frac{\partial}{\partial x}\left(m_f - \frac{m_o}{r}\right) + G_y \frac{\partial}{\partial y}\left(m_f - \frac{m_o}{r}\right) - \frac{\partial}{\partial y}\left[\gamma \frac{\partial}{\partial y}\left(m_f - \frac{m_o}{r}\right)\right] = 0 \tag{18-13}$$

Similar equations can obviously be developed for

$$m_f + \frac{m_p}{1+r} \quad \textit{if} \quad \gamma_f = \gamma_p \tag{E-6}$$

$$\frac{m_o}{r} + \frac{m_p}{1+r} \quad \textit{if} \quad \gamma_o = \gamma_p \tag{E-7}$$

Note that in assuming equality of the diffusion coefficients, we are not introducing significantly more of an approximation than is already incorporated in the differential equations. In the development of the latter, Fick's law was assumed to be valid, and from Chap. 3 Fick's law is accurately applicable to the components of a multicomponent mixture only if the binary diffusion coefficients for each pair of components in the mixture are the same.

CASE 3: Diffusion of Chemical Elements α with Equal Diffusion Coefficients

In a chemically reacting boundary layer in which simple reaction is not applicable we can still consider conservation of the separate elements. Consider Eq. (18-2) under the assumption that $\gamma_j = \gamma_k = \gamma$ (note that the diffusion coefficients refer to the compounds m_j and not to the elements α). Then we obtain from Eq. (18-2)

$$G_x \frac{\partial n_\alpha}{\partial x} + G_y \frac{\partial n_\alpha}{\partial y} - \frac{\partial}{\partial y}\left[\gamma \frac{\partial}{\partial y} \sum_j (n_{\alpha,j} m_j)\right] = 0 \qquad \text{(E-8)}$$

This equation can be simplified further, because

$$\sum_j (n_{\alpha,j} m_j) = n_\alpha \qquad \text{(E-9)}$$

Thus

$$G_x \frac{\partial n_\alpha}{\partial x} + G_y \frac{\partial n_\alpha}{\partial y} - \frac{\partial}{\partial y}\left(\gamma \frac{\partial n_\alpha}{\partial y}\right) = 0 \qquad \text{(E-10)}$$

From the three cases considered for the mass-diffusion equation it can be seen that the equation always attains the following form:

$$G_x \frac{\partial \mathcal{P}}{\partial x} + G_y \frac{\partial \mathcal{P}}{\partial y} - \frac{\partial}{\partial y}\left(\Phi \frac{\partial \mathcal{P}}{\partial y}\right) = 0 \qquad \text{(18-15)}$$

where $\Phi = \gamma$ and $\mathcal{P}$ stands for one of the following functions:

$$\mathcal{P} = m_j, n_\alpha, \left(m_f - \frac{m_o}{r}\right), \left(m_f + \frac{m_p}{1+r}\right), \left(\frac{m_o}{r} + \frac{m_p}{1+r}\right) \qquad \text{(E-11)}$$

SIMPLIFICATIONS OF THE ENERGY EQUATION OF THE BOUNDARY LAYER

Now we investigate the energy equation in detail in order to see if also this equation can be simplified to the same form as given by Eq. (18-15).

CASE 1: The Unit-Lewis-Number Simplification

The case of Le = 1 means that the Prandtl and Schmidt numbers are equal. This gives rise to the fact that the thickness of the concentration boundary layer and the thermal boundary layer are identical. Therefore, it can be assumed that this case will lead to substantial simplifications in the energy equation.

First let us write the energy equation (18-3) in a slightly different form. The last term may be written

$$\frac{\partial}{\partial y}\left(k \frac{\partial T}{\partial y}\right) = \frac{\partial}{\partial y}\left(\Gamma c \frac{\partial T}{\partial y}\right) \doteq \frac{\partial}{\partial y}\left(\Gamma \sum_j m_j c_j \frac{\partial T}{\partial y}\right)$$

But for a perfect gas $c_j dT = di_j$, and we have previously indicated an intention to use this expression as an approximation for a liquid. Thus

$$\frac{\partial}{\partial y}\left(k \frac{\partial T}{\partial y}\right) \doteq \frac{\partial}{\partial y}\left(\Gamma \sum_j m_j \frac{\partial i_j}{\partial y}\right)$$

and Eq. (18-3) becomes

$$G_x \frac{\partial i}{\partial x} + G_y \frac{\partial i}{\partial y} - \frac{\partial}{\partial y}\left(\sum_j \gamma_j \frac{\partial m_j}{\partial y} i_j\right) - \frac{\partial}{\partial y}\left(\Gamma \sum_j m_j \frac{\partial i_j}{\partial y}\right) = 0 \qquad \text{(E-11)}$$

From this equation it is now apparent that a great simplification will result if we set $\gamma_j = \Gamma$, which is the assumption that $\mathrm{Le}_j = \gamma_j / \Gamma = 1$. This simplification is valid if the Lewis number for each of the various fluids in the mixture is equal to unity at all points in the boundary layer. Of course, this does not preclude γ_j and Γ from varying through the boundary layer. As it has been stated in Chap. 18, the assumption that the Lewis number of gas mixtures is equal to unity is reasonably valid, because Pr and Sc are of the order of magnitude of unity.

Note further that under the unit-Lewis-number assumption, no restriction is placed on chemical reaction within the boundary layer, so that the resulting simplified differential equation is applicable to a chemically reacting boundary layer.

Applying now the assumption that $\gamma_j = \Gamma$ for all components, we find that Eq. (E-11) becomes

$$G_x \frac{\partial i}{\partial x} + G_y \frac{\partial i}{\partial y} - \frac{\partial}{\partial y}\left(\Gamma \sum_j \frac{\partial m_j}{\partial y} i_j + \Gamma \sum_j m_j \frac{\partial i_j}{\partial y}\right) = 0 \qquad \text{(E-12)}$$

The last term of this equation can be further simplified as follows

$$\Gamma\left(\sum_j \frac{\partial m_j}{\partial y} i_j + \sum_j m_j \frac{\partial i_j}{\partial y}\right) = \Gamma \sum_j \frac{\partial}{\partial y}(m_j i_j) = \Gamma \frac{\partial}{\partial y} \sum_j (m_j i_j) = \Gamma \frac{\partial i}{\partial y} \qquad \text{(E-13)}$$

Thus Eq. (E-12) reduces finally to

$$G_x \frac{\partial i}{\partial x} + G_y \frac{\partial i}{\partial y} - \frac{\partial}{\partial y}\left(\Gamma \frac{\partial i}{\partial y}\right) = 0 \qquad \text{(E-14)}$$

CASE 2: No Chemical Reaction, with Equal Specific Heats for All Components

We express the enthalpy of a component of the mixture by integrating the defining expression for the specific heat at constant pressure:

$$i_j = i_{j,0} + \int_{T_0}^{T} c_j \, d\tilde{T}$$

The temperature T_0 is an arbitrary datum temperature associated with $i_{j,0}$, the enthalpy of the j component at the datum temperature. If no chemical reaction is permitted then all the $i_{j,0}$ can be arbitrarily set to zero. If, in addition, the specific heats are all equal, that is, $c_j = c_k = c$, then

$$i_j = \int_{T_0}^{T} c \, d\tilde{T}$$

The third term of Eq. (18-3) then becomes

$$\frac{\partial}{\partial y}\left(\sum_j \gamma_j \frac{\partial m_j}{\partial y} i_j\right) = \frac{\partial}{\partial y}\left(\int_{T_0}^{T} c\,d\tilde{T} \sum_j \gamma_j \frac{\partial m_j}{\partial y}\right)$$

But, from Eq. (4-29), $\sum_j \gamma_j\,\partial m_j/\partial y = 0$. Thus the entire mass-diffusion term in Eq. (18-3) is equal to zero.

Under the condition of equal specific heats, one obtains for the enthalpy of the mixture

$$i = \sum_j m_j i_j = \sum_j \left(m_j \int_{T_0}^{T} c_j\,d\tilde{T}\right) = \int_{T_0}^{T} c\,d\tilde{T} \sum_j m_j = \int_{T_0}^{T} c\,d\tilde{T}$$

and $di = c\,dT$. Thus Eq. (18-3) can be simplified to

$$G_x \frac{\partial i}{\partial x} + G_y \frac{\partial i}{\partial y} - \frac{\partial}{\partial y}\left(\Gamma \frac{\partial i}{\partial y}\right) = 0 \qquad \text{(E-14)}$$

CASE 3: Simple Chemical Reaction, with Equal Specific Heats for All Components

Consider a boundary layer in which the same simple reaction is taking place as discussed above under the simplifications of the mass diffusion equation. Employing the subscripts *f*, *o*, *p*, and *oc* for the *fuel*, *oxidant*, *products*, and *all other components*, respectively, the enthalpy of the mixture can be expressed as

$$i = \sum_j m_j i_j = m_f i_f + m_o i_o + m_p i_p + m_{oc} i_{oc} \qquad \text{(E-15)}$$

The enthalpy of each component can be expressed in various ways, depending on the chemical state of the system chosen for enthalpy datum. A frequently chosen datum scheme is to let the enthalpy of the elements be zero at some reference temperature, and then the enthalpy of a compound at the same temperature is the *change* of enthalpy associated with the reaction forming the compound from its elements, the so-called "heat of formation" of a compound. Such a scheme could be convenient to define and derive a heat of combustion H_0, J/(kg of fuel), which is actually the negative of the enthalpy difference between the products of combustion and fuel and oxidant entering the reaction, all at T_0.

For calculation purposes H_0 can be attached to the fuel, oxidant, or product, since it is a property of a chemical system and not merely a property of the fuel. It cancels out of calculations unless a reaction actually takes place, in which case all three components are involved in a fixed stoichiometric ratio. Thus if we employ H_0, there are three possible schemes for expressing the enthalpy of the components, and thereby the enthalpy of the mixture, as follows:

Scheme 1:

$$i_f = \int_{T_0}^{T} c_f\, d\tilde{T} + H_0, \qquad i_o = \int_{T_0}^{T} c_o\, d\tilde{T}$$

$$i_p = \int_{T_0}^{T} c_p\, d\tilde{T}, \qquad i_{oc} = \int_{T_0}^{T} c_{oc}\, d\tilde{T}$$

Scheme 2:

$$i_f = \int_{T_0}^{T} c_f\, d\tilde{T}, \qquad i_o = \int_{T_0}^{T} c_o\, d\tilde{T} + \frac{H_0}{r}$$

$$i_p = \int_{T_0}^{T} c_p\, d\tilde{T}, \qquad i_{oc} = \int_{T_0}^{T} c_{oc}\, d\tilde{T}$$

Scheme 3:

$$i_f = \int_{T_0}^{T} c_f\, d\tilde{T}, \qquad i_o = \int_{T_0}^{T} c_o\, d\tilde{T}$$

$$i_p = \int_{T_0}^{T} c_p\, d\tilde{T} - \frac{H_0}{1+r}, \qquad i_{oc} = \int_{T_0}^{T} c_{oc}\, d\tilde{T}$$

For present purposes let us employ scheme 2. Then the enthalpy of the mixture becomes

$$i = m_f \int_{T_0}^{T} c_f\, d\tilde{T} + m_o \int_{T_0}^{T} c_o\, d\tilde{T} + m_o \frac{H_0}{r} + m_p \int_{T_0}^{T} c_p\, d\tilde{T} + m_{oc} \int_{T_0}^{T} c_{oc}\, d\tilde{T} \tag{E-16}$$

Now, we will consider the case, where all the specific heats are equal ($c_j = c$). Then the above equation simplifies to

$$i = m_o \frac{H_0}{r} + \int_{T_0}^{T} c\, d\tilde{T} \tag{E-17}$$

Employing the scheme 2 and the above made assumption of equal specific heats, the third term in Eq. (18-3) can be written as follows:

$$\sum_j \gamma_j \frac{\partial m_j}{\partial y} i_j = \gamma_f \frac{\partial m_f}{\partial y} \int_{T_0}^{T} c\, d\tilde{T} + \gamma_o \frac{\partial m_o}{\partial y} \int_{T_0}^{T} c\, d\tilde{T} + \gamma_o \frac{\partial m_o}{\partial y} \frac{H_0}{r}$$
$$+ \gamma_p \frac{\partial m_p}{\partial y} \int_{T_0}^{T} c\, d\tilde{T} + \gamma_{oc} \frac{\partial m_{oc}}{\partial y} \int_{T_0}^{T} c\, d\tilde{T}$$

Because the four integral terms are identical, the equation can be rewritten in the following way

$$\sum_j \gamma_j \frac{\partial m_j}{\partial y} i_j = \int_{T_0}^{T} c\, d\tilde{T} \sum_j \gamma_j \frac{\partial m_j}{\partial y} + \gamma_o \frac{\partial m_o}{\partial y} \frac{H_0}{r}$$

By using now Eq. (4-29) we conclude that

$$\sum_j \gamma_j \frac{\partial m_j}{\partial y} i_j = \gamma_o \frac{\partial m_o}{\partial y} \frac{H_0}{r}$$

Finally, the last term in Eq. (18-3) may be developed as follows. From Eq. (E-17),

$$\frac{\partial i}{\partial y} = \frac{H_0}{r} \frac{\partial m_o}{\partial y} + c \frac{\partial T}{\partial y} \tag{E-18}$$

and

$$\Gamma \frac{\partial i}{\partial y} = \Gamma \frac{H_0}{r} \frac{\partial m_o}{\partial y} + \Gamma c \frac{\partial T}{\partial y} = \Gamma \frac{H_0}{r} \frac{\partial m_o}{\partial y} + k \frac{\partial T}{\partial y}$$

we obtain

$$k \frac{\partial T}{\partial y} = \Gamma \frac{\partial i}{\partial y} - \Gamma \frac{H_0}{r} \frac{\partial m_o}{\partial y}$$

Now substituting for the last term of Eq. (18-3),

$$G_x \frac{\partial i}{\partial x} + G_y \frac{\partial i}{\partial y} - \frac{\partial}{\partial y} \left(\gamma_o \frac{\partial m_o}{\partial y} \frac{H_0}{r} + \Gamma \frac{\partial i}{\partial y} - \Gamma \frac{\partial m_o}{\partial y} \frac{H_0}{r} \right) = 0 \tag{E-19}$$

If we now suppose that $\gamma_o = \Gamma$, Eq. (E-19) reduces to

$$G_x \frac{\partial i}{\partial x} + G_y \frac{\partial i}{\partial y} - \frac{\partial}{\partial y} \left(\Gamma \frac{\partial i}{\partial y} \right) = 0 \tag{E-14}$$

In some cases this result may be less restricting than the unit-Lewis-number simplification, since only the diffusion coefficient for the oxidant must be equal to the heat-diffusion coefficient, although, of course, the equality of specific heats must be assumed. Note that the unit-Lewis-number simplification includes the possibility of "simple" chemical reactions, as well as multiple reactions.

Eq. (E-14) is obviously also derivable under enthalpy schemes 1 and 3. The expression for the enthalpy of the mixture and the diffusion coefficient assumption are then

Scheme 1: $$i = m_f H_0 + \int_{T_0}^{T} c\, d\tilde{T}, \quad \text{with } \gamma_f = \Gamma \tag{E-20}$$

Scheme 3: $$i = -m_P \frac{H_0}{1+r} + \int_{T_0}^{T} c\, d\tilde{T}; \quad \text{with } \gamma_P = \Gamma \tag{E-21}$$

This is an interesting result, because it shows that these assumptions might always be very useful, if only one of the diffusion coefficients γ_j is equal to the heat-diffusion coefficient.

CASE 4: Uniform Composition

The final simplification of the energy equation to the standard form results when the composition is everywhere uniform. There is thus no mass diffusion, since $\partial m_j/\partial y = 0$ everywhere. This, of course, simply brings us back to the single-component boundary layer problem, which was the subject matter of Chap. 10 and Chap. 12. However, this can still be a *mass-transfer* problem, since fluid of the same composition as the mainstream fluid can flow through the interface (boundary-layer blowing or suction).

Under these conditions, the third term in Eq. (18-3) drops out, and we can also express $di = c\,dT$. Then noting that $k = c\Gamma$, Eq. (18-3) becomes

$$G_x \frac{\partial i}{\partial x} + G_y \frac{\partial i}{\partial y} - \frac{\partial}{\partial y}\left(\Gamma \frac{\partial i}{\partial y}\right) = 0 \tag{E-14}$$

An alternative form of Eq. (E-14) is

$$G_x c \frac{\partial T}{\partial x} + G_y c \frac{\partial T}{\partial y} - \frac{\partial}{\partial y}\left(c\Gamma \frac{\partial T}{\partial y}\right) = 0 \tag{E-22}$$

Then if we consider the case of constant specific heat, c drops out and we obtain another equation in the standard form

$$G_x \frac{\partial T}{\partial x} + G_y \frac{\partial T}{\partial y} - \frac{\partial}{\partial y}\left(\Gamma \frac{\partial T}{\partial y}\right) = 0 \tag{E-23}$$

From the four cases considered for the energy equation it can be seen that the equation always attains the following form

$$G_x \frac{\partial \mathcal{P}}{\partial x} + G_y \frac{\partial \mathcal{P}}{\partial y} - \frac{\partial}{\partial y}\left(\Phi \frac{\partial \mathcal{P}}{\partial y}\right) = 0 \tag{18-15}$$

where $\Phi = \Gamma$ and $\mathcal{P}$ stands for one of the following functions

$$\mathcal{P} = i, T \tag{E-24}$$

GENERAL FORM OF THE SIMPLIFIED EQUATIONS

All the above simplifications of the mass diffusion and the energy equations have led to the same differential equation:

$$G_x \frac{\partial \mathcal{P}}{\partial x} + G_y \frac{\partial \mathcal{P}}{\partial y} - \frac{\partial}{\partial y}\left(\Phi \frac{\partial \mathcal{P}}{\partial y}\right) = 0 \tag{18-15}$$

where $\Phi = \Gamma$ or γ_j and the function $\mathcal{P}$ stands for one of the following functions

$$\mathcal{P} = m_j, n_\alpha, \left(m_f - \frac{m_o}{r}\right), \left(m_f + \frac{m_p}{1+r}\right), \left(\frac{m_o}{r} + \frac{m_p}{1+r}\right), i, T, \ldots \tag{E-25}$$

BOUNDARY CONDITIONS AT THE INTERFACE

After we have shown that the simplified mass-diffusion equations and the energy equation will attain the same form, it will now be shown that the boundary conditions of these equations can be written in the same way. Of course, we will only be concerned here with the boundary condition at the interface, because the other boundary conditions (for $x = 0$ and at free-stream) can easily be shown to be the same [see Eqs. (18-19)–(18-20)].

We will focus again first on the mass-diffusion equation and later on the energy equation.

THE BOUNDARY CONDITION AT THE INTERFACE FOR THE MASS-DIFFUSION EQUATIONS

As has been shown in Chap. 18, the general form of the boundary condition for the mass-diffusion equation at the interface can be obtained by applying conservation of mass for component j for a control volume including the s and T state (see Fig. 18-3).

In Chap. 18 we obtained

$$\dot{m}'' = \frac{(\gamma_j\, \partial m_j/\partial y)_s}{m_{j,s} - m_{j,T}} \tag{18-24}$$

This is of course the boundary condition for diffusion of an inert substance (*CASE 1*). Now we will consider all the other above discussed cases for the mass-diffusion equation. The goal will be to show that the boundary condition at the surface can always be expressed in the same form as Eq. (18-24).

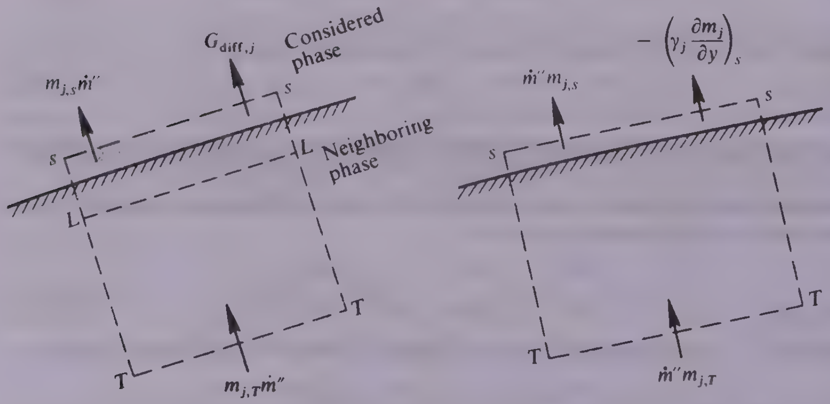

Figure 18-3 Control volumes at the phase interface for the mass-diffusion equation.

CASE 2: Simple Chemical Reaction with Equal Diffusion Coefficients

Considering the same control volume and applying conservation of mass separately for the *fuel* and the *oxidant*, we obtain for the fuel

$$\dot{m}''m_{f,s} - \left(\gamma_f \frac{\partial m_f}{\partial y}\right)_s - \dot{m}''m_{f,T} = 0 \qquad \text{(E-26)}$$

and for the oxidant

$$\dot{m}''m_{o,s} - \left(\gamma_o \frac{\partial m_o}{\partial y}\right)_s - \dot{m}''m_{o,T} = 0 \qquad \text{(E-27)}$$

Dividing Eq. (E-27) by r and subtracting from Eq. (E-26),

$$\dot{m}''\left(m_f - \frac{m_o}{r}\right)_s - \left(\gamma_f \frac{\partial m_f}{\partial y} - \gamma_0 \frac{\partial}{\partial y}\left(\frac{m_o}{r}\right)\right)_s - \dot{m}''\left(m_f - \frac{m_o}{r}\right)_T = 0 \qquad \text{(E-28)}$$

We now let $\gamma_f = \gamma_o = \gamma$, and obtain

$$\dot{m}'' = \frac{\left[\gamma \frac{\partial}{\partial y}\left(m_f - \frac{m_o}{r}\right)\right]_s}{\left(m_f - \frac{m_o}{r}\right)_s - \left(m_f - \frac{m_o}{r}\right)_T} \qquad \text{(E-29)}$$

CASE 3: Diffusion of Chemical Elements α

If we apply conservation of chemical element α to the same control volume and let $\gamma_j = \gamma_k = \gamma$, we obtain

$$\dot{m}'' = \frac{(\gamma_j\, \partial n_\alpha / \partial y)_s}{n_{\alpha,s} - n_{\alpha,T}} \qquad \text{(E-30)}$$

From these three cases it is obvious that the boundary condition at the interface can generally be written as

$$\dot{m}'' = \frac{(\Phi\, \partial \mathcal{P} / \partial y)_s}{\mathcal{P}_s - \mathcal{P}_T} \qquad \text{(18-29)}$$

where $\Phi = \gamma_j$ and $\mathcal{P}$ is one of the following functions

$$\mathcal{P} = m_j, n_\alpha, \left(m_f - \frac{m_o}{r}\right), \left(m_f + \frac{m_p}{1+r}\right), \left(\frac{m_o}{r} + \frac{m_p}{1+r}\right), \ldots \qquad \text{(E-31)}$$

THE BOUNDARY CONDITION AT THE INTERFACE FOR THE ENERGY EQUATION

In Chap. 18 we considered the control volume indicated in Fig. 18-4 and the steady flow energy fluxes flowing across the L and T surfaces. Applying conservation of energy across the s and T surfaces led to the following boundary

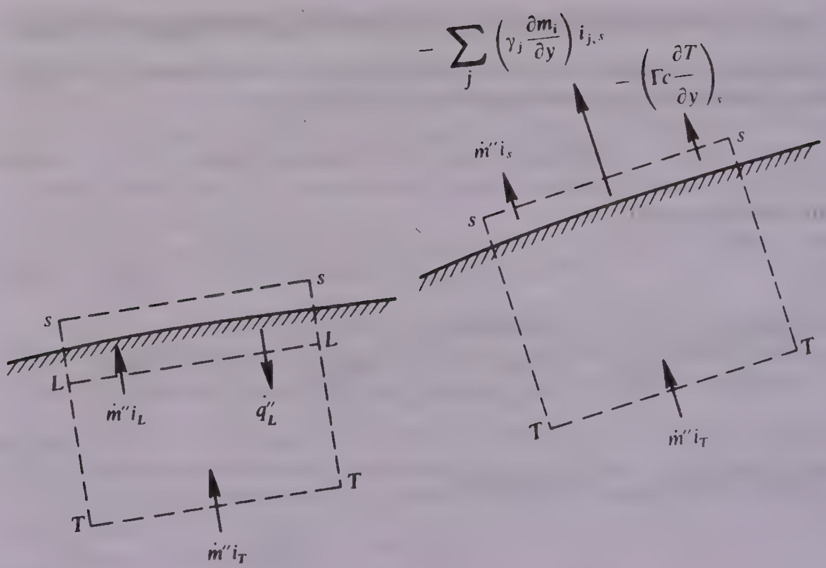
$-\sum_j \left(\gamma_j \frac{\partial m_i}{\partial y}\right) i_{j,s}$
$-\left(\Gamma c \frac{\partial T}{\partial y}\right)_s$
$\dot{m}'' i_s$
s
s
T
T
$\dot{m}'' i_T$
s
s
L
L
$\dot{m}'' i_L$
$\dot{q}''_L$
T
T
$\dot{m}'' i_T$

Figure 18-4 Control volumes at the phase interface.

condition at the interface for the energy equation

$$\dot{m}'' = \frac{\sum_j [\gamma_j\,(\partial m_j/\partial y)]_s\, i_{j,s} + [\Gamma c\,(\partial T/\partial y)]_s}{i_s - i_T} \tag{18-27}$$

It will be shown now that the various simplifications of the energy equations will lead to a form of Eq. (18-27), which is identical to the standard form.

CASE 1: The Unit-Lewis-Number Simplification

The second term in the numerator of Eq. (18-27) may be rewritten as follows:

$$\begin{aligned}\left(\Gamma c \frac{\partial T}{\partial y}\right)_s &= \left(\Gamma \frac{\partial T}{\partial y}\right)_s \left(\sum_j m_j c_j\right)_s \\ &= \left(\Gamma \sum_j m_j c_j \frac{\partial T}{\partial y}\right)_s = \left(\Gamma \sum_j m_j \frac{\partial i_j}{\partial y}\right)_s\end{aligned}$$

Thus, Eq. (18-27) results in

$$\dot{m}'' = \frac{\sum_j [\gamma_j\,(\partial m_j/\partial y)]_s\, i_{j,s} + \Gamma \sum_j m_j (\partial i_j/\partial y)_s}{i_s - i_T} \tag{E-32}$$

Under the unit-Lewis-number assumption $\gamma_j = \gamma_k = \cdots = \Gamma$, Eq. (E-32) can be simplified to

$$\dot{m}'' = \frac{\Gamma \sum_j [(\partial(m_j i_j)/\partial y)]_s}{i_s - i_T} = \frac{\Gamma \dfrac{\partial}{\partial y} \sum_j [m_j i_j]_s}{i_s - i_T}$$

Thus

$$\dot{m}'' = \frac{(\Gamma \partial i/\partial y)_s}{i_s - i_T} \tag{18-28}$$

CASE 2: No Chemical Reaction, with Equal Specific Heats for All Components

We have already seen that under these conditions

$$\frac{\partial}{\partial y}\left(\sum_j \gamma_j \frac{\partial m_j}{\partial y} i_j\right) = \frac{\partial}{\partial y}\left(\int_{T_0}^{T} c\, d\tilde{T} \sum_j \gamma_j \frac{\partial m_j}{\partial y}\right) = 0$$

and also

$$\Gamma c \frac{\partial T}{\partial y} = \Gamma \frac{\partial i}{\partial y}$$

for equal specific heats. Thus Eq. (18-27) becomes

$$\dot{m}'' = \frac{(\Gamma \partial i/\partial y)_s}{i_s - i_T} \tag{18-28}$$

CASE 3: Simple Chemical Reaction, with Equal Specific Heats

In applying this simplification to the energy equation, it was shown that if the enthalpy of the mixture is expressed by Eq. (E-17)

$$i = m_o \frac{H_0}{r} + \int_{T_0}^{T} c\, d\tilde{T} \tag{E-17}$$

then

$$\sum_j \gamma_j \frac{\partial m_j}{\partial y} i_j = \gamma_o \frac{\partial m_o}{\partial y} \frac{H_0}{r}$$

It was similarly shown that

$$k \frac{\partial T}{\partial y} = \Gamma \frac{\partial i}{\partial y} - \Gamma \frac{H_0}{r} \frac{\partial m_o}{\partial y}$$

If these two expressions are substituted into Eq. (18-27) and we make the additional stipulation that $\gamma_o = \Gamma$, we obtain again

$$\dot{m}'' = \frac{(\Gamma \partial i/\partial y)_s}{i_s - i_T} \tag{18-28}$$

Obviously, the other enthalpy schemes lead to the same result.

CASE 4: Uniform Composition

If the composition is uniform, the first term in the numerator of Eq. (18-27) is zero, and $dT = di/c$. Thus Eq. (18-27) reduces to

$$\dot{m}'' = \frac{(\Gamma \partial i/\partial y)_s}{i_s - i_T} \tag{18-28}$$

Finally, if c is everywhere the same (and this includes the transferred substance):

$$\dot{m}'' = \frac{(\Gamma \partial T/\partial y)_s}{T_s - T_T} \tag{E-33}$$

GENERAL FORM OF THE BOUNDARY CONDITION AT THE INTERFACE

All the above simplifications of the boundary condition at the interface for the mass-diffusion equations and the energy equation have led to the same equation

$$\dot{m}'' = \frac{(\Phi\, \partial \mathcal{P}/\partial y)_s}{\mathcal{P}_s - \mathcal{P}_T} \tag{18-29}$$

where $\Phi = \Gamma$ or γ_j and the function $\mathcal{P}$ stands for one of the following functions

$$\mathcal{P} = m_j, n_\alpha, \left(m_f - \frac{m_o}{r}\right), \left(m_f + \frac{m_p}{1+r}\right), \left(\frac{m_o}{r} + \frac{m_p}{1+r}\right), i, T, \ldots \tag{E-25}$$

In summary, we can conclude that it is possible to show that the simplified mass-diffusion equations, the energy equation as well as the corresponding boundary conditions can be brought to the same form.

MODIFICATION OF THE DEFINITION OF *B* TO ACCOUNT FOR THERMAL RADIATION

In the derivation of the driving force B we ignored the possible influence of thermal radiation. If g is large, radiation could be negligible, but there are obviously many applications where it is not negligible.

It is assumed that thermal radiation is absorbed and emitted at least an infinitesimal distance inside the L surface and that the considered phase fluid is transparent. Then the boundary layer is totally unaffected by radiation. However, the energy balance on the L-T control volume that leads to the definition of B must be modified.

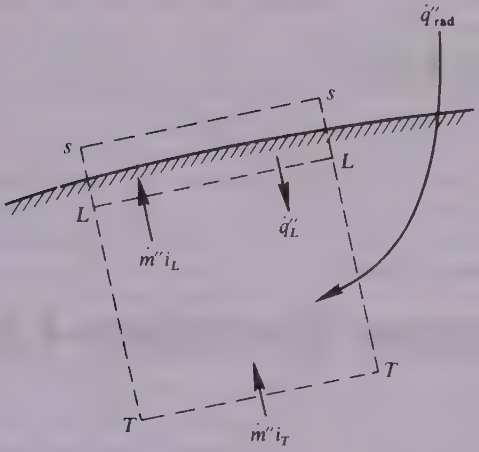

Figure E-1 Modification of the energy balance at the phase interface to account for thermal radiation.

Consider the control volume shown in Fig. E-1, in which a net radiant heat flux is included. Without radiation, the original definition of B from the simplified energy equation is

$$B = \frac{i_\infty - i_s}{i_s - i_T}$$

If we retain the original definition of i_T, Eq. (18-25), we obtain

$$B = \frac{i_\infty - i_s}{i_s - \left[i_L - \dot{q}''_L/\dot{m}''\right]}$$

But this definition of B is still valid for radiation, if the radiant flux is assumed to act below the L surface. Then we apply the conservation-of-energy principle to the L-T control volume

$$\dot{m}'' i_L - \dot{m}'' i_T - \dot{q}''_L - \dot{q}''_{\rm rad} = 0$$

$$i_L - \frac{\dot{q}''_L}{\dot{m}''} = i_T - \frac{\dot{q}''_{\rm rad}}{\dot{m}''}$$

Thus a modified form of the definition of B for applications of the energy equation involving thermal radiation is

$$B = \frac{i_\infty - i_s}{i_s - i_L + \dot{q}''_{\rm rad}/\dot{m}''} \qquad \text{(E-34)}$$

In applications where it is more convenient to work with i_L than i_T, the original definition is, of course, still valid, and radiation is handled as a separate effect.

F APPENDIX

The Texstan Boundary-Layer Code

TEXSTAN OVERVIEW

This appendix describes the features of the TEXSTAN computer simulation code. It was primarily developed to enhance analysis and understanding of the flow fields that accompany surface friction, heat, and mass transfer and to solve boundary layer flows with convective boundary conditions that do not permit analytical or approximate solutions. We have developed a website for downloading the compiled academic version of the TEXSTAN code, and the compiled version is made freely available to the academic community. The site also provides the student of convective heat and mass transfer with numerous data sets that reflect the spirit of this textbook. In addition, an input manual is available at the website which explains the flags and variables which are used in the input file. This manual, along with manuals for six key data sets will help the reader become familiar with the code.

TEXSTAN is the outgrowth of a long development period that was carried out at Stanford University in the period from the early 1960s through the mid-1970s, with further development at The University of Texas at Austin since 1980. The genesis of the Stanford code was a sabbatical taken by Professor William M. Kays (now Professor Emeritus at Stanford University), which allowed him to work with Professor Brian Spalding at the Imperial College–London (now retired, and managing director of CHAM, Ltd., England) and his student, Suhas Patankar (now Professor Emeritus at the University of Minnesota). Kays was given a copy of Patankar's thesis code, and the Stanford version of the Patankar-Spalding boundary-layer code was started. Several of Kay's students contributed to the development of the early code, with a primary contribution by Dr. Howard Julien, and other contributions by Dr. Ben Blackwell and Dr. Peter Andersen. In the early 1970s, Dr. Michael Crawford completely revised the code while developing a film cooling model for simulation of full-coverage film cooling. At the urging of Dr. Ray Colladay, then at NASA–Lewis Research Center, Dr. Crawford documented the non-film-cooled version of the code, naming it STAN5 (acknowledging there were earlier versions), and NASA published it as a NASA-CR.[12] The companion film-cooled version, STANCOOL, was turned over to NASA–Lewis Research Center for utilization by the aeropropulsion industry. Commencing in 1980, the code was further developed at UT–Austin by Professor Crawford, and his most recent version was renamed TEXSTAN to reflect the blending of the codes developed while at Texas and earlier at Stanford. Significant contributors to TEXSTAN at UT–Austin include Dr. Joe Pietrzyk, Dr. Huei Chen, and Dr. Sriram Neelakantan.

TEXSTAN is a boundary-layer finite-difference computer code, with the source code written in FORTRAN. It is basically a parabolic partial differential equation solver for equations of the form: convection = diffusion ± source. Currently within the code the momentum sources include pressure gradient, free convection body force, and a generalized body force. For the stagnation enthalpy equation (or temperature, if low speed), the sources include viscous dissipation, body force work, and a generalized volumetric source. For convective mass transfer, there are currently no source terms implemented for combustion, but in principle the appropriate source terms can be defined.

A large variety of flow geometries can be analyzed by TEXSTAN, including the *external wall shear flow family* of flat plates, airfoil-shaped surfaces, two-dimensional and axisymmetric converging-diverging nozzles, and bodies of revolution of the missile shape. The *internal wall shear flow family* include circular pipes, planar ducts, and annular ducts.

Turbulence models in TEXSTAN include three levels of mean field closure via the eddy viscosity model. These include the Prandtl mixing length with Van Driest damping a one-equation turbulence kinetic energy model, and numerous low-turbulence Reynolds number two-equation k–ε models. The turbulent heat flux closure is via a turbulent Prandtl (or Schmidt) number concept. In principle, higher level turbulence closure models such as algebraic and full Reynolds stress models, along with turbulent heat flux transport models, could be adapted to the code.

TEXSTAN can handle a variety of different boundary conditions. For the energy equation the flow-direction variation of either the wall heat flux or the wall temperature may be specified. The mass flux at a wall may also vary in the flow direction for certain geometries. For geometries with two different walls, such as annular or planar ducts, asymmetric thermal boundary conditions can be accommodated. For external wall shear flows, the free-stream velocity, rather than the pressure, is treated as a variable boundary condition, while the free-stream stagnation enthalpy is held constant. The user may specify the initial profiles of the dependent variables, or an automatic initial profile generator may be used.

Fluid properties in TEXSTAN may be treated as constant or variable. Constant fluid properties are user-supplied via the input data set. Variable fluid properties are supplied through subroutines. The current routines include those for air at both low and elevated pressures, water, nitrogen, helium, and products of combustion.

BOUNDARY-LAYER EQUATIONS

The equations for solution within TEXSTAN are for the transport of momentum, heat, and mass concentration within flows that obey the boundary layer approximations. The equations presented here are formulated in their turbulent axisymmetric form appropriate to mean field closure. To conform to the nature of the numerical solver within TEXSTAN, the equations are formulated as

$$\text{convection}\,(\phi) = \text{diffusion}\,(\phi) \pm \{\text{sources}\,(\phi)\}$$

For the boundary layer momentum equation has $\phi = u$, based on Chap. 11, with an added x-direction body force term

$$\rho u \frac{\partial u}{\partial x} + \rho v \frac{\partial u}{\partial y} = \frac{1}{r}\frac{\partial}{\partial y}\left(r\mu_{\text{eff}}\frac{\partial u}{\partial y}\right) + \left\{-\frac{dP}{dx} + X\right\}$$

where

$$\mu_{\text{eff}} = \mu + \mu_t = \rho(\nu + \varepsilon_M)$$

The boundary layer stagnation enthalpy equation has $\phi = i^*$, based on Chap. 16, with added x-direction body force work and volumetric energy source terms

$$\rho u \frac{\partial i^*}{\partial x} + \rho v \frac{\partial i^*}{\partial y} = \frac{1}{r}\frac{\partial}{\partial y}\left(r\frac{\mu_{\text{eff}}}{\text{Pr}_{\text{eff}}}\frac{\partial i^*}{\partial y}\right)$$

$$+ \left\{\frac{1}{r}\frac{\partial}{\partial y}\left[r\mu_{\text{eff}}\left(1 - \frac{1}{\text{Pr}_{\text{eff}}}\right)\frac{\partial\left(\frac{1}{2}u^2\right)}{\partial y}\right] + uX + S\right\}$$

where the diffusion coefficient term is redefined using $(\mu_{\text{eff}}/\text{Pr}_{\text{eff}}) = (k_{\text{eff}}/c)$, and

$$k_{\text{eff}} = k + k_t = k + \rho c \varepsilon_H$$

$$\text{Pr}_{\text{eff}} = \frac{\mu_{\text{eff}}}{k_{\text{eff}}/c} = \frac{1 + \varepsilon_M/\nu}{1/\text{Pr} + (\varepsilon_M/\nu)/\text{Pr}_t}$$

The temperature-equation counterpart has $\phi = T$, where the velocity-pressure gradient term, body force work, and volumetric energy source terms are neglected,

$$\rho u \frac{\partial T}{\partial x} + \rho v \frac{\partial T}{\partial y} = \frac{1}{r}\frac{\partial}{\partial y}\left(r\frac{\mu_{\text{eff}}}{\text{Pr}_{\text{eff}}}\frac{\partial T}{\partial y}\right) + \left\{\frac{\mu_{\text{eff}}}{c}\left(\frac{\partial u}{\partial y}\right)^2\right\}$$

The boundary-layer mass-transfer equation for an inert substance has $\phi = m_j$, in accordance with Eq. (18-12), and is written for laminar flow (the turbulent version has had limited testing):

$$\rho u \frac{\partial m_j}{\partial x} + \rho v \frac{\partial m_j}{\partial y} = \frac{1}{r}\frac{\partial}{\partial y}\left(r\frac{\mu}{\text{Sc}_j}\frac{\partial m_j}{\partial y}\right)$$

where the diffusion coefficient term is redefined using $(\mu/\mathrm{Sc}_j) = \gamma_j$. A typical example of m_j would be water vapor or naphthalene in an air–water vapor or air–naphthalene boundary layer.

In the strictest sense TEXSTAN is a parabolic partial differential equation solver for equations of a common form

$$r\rho u \frac{\partial \phi}{\partial x} + r\rho v \frac{\partial \phi}{\partial y} = \frac{\partial}{\partial y}\left(r \frac{\mu_{\text{eff}}}{C} \frac{\partial \phi}{\partial y}\right) + \{S_\phi\}$$

where C represents the appropriate nondimensional effective transport coefficient for scalar variables such as stagnation enthalpy, temperature, or mass concentration, and S_ϕ becomes the collective source and sink terms for the dependent variable in question.

These equations are presented in axisymmetric coordinates to accommodate axisymmetric flows, where there is a well-defined relationship between the variable r and y. For example, in pipe flow, $y = (r_s - r)$ and y is measured from the no-slip surface. With this formulation, when the radius is set to unity, the Cartesian form is recovered.

BOUNDARY CONDITIONS

Boundary conditions for both planar and axisymmetric flows depend on whether the flow is considered an internal flow or an external wall shear flow. The difference is in the handling of the pressure gradient in the boundary layer momentum equation which governs both types of flows. For the external flows, the pressure gradient is predetermined using a potential flow solver to obtain the free-stream velocity distribution and Bernoulli's equation to convert it to a pressure-gradient distribution. For the internal flows, the pressure gradient can not be predetermined. Therefore, it is guessed during the numerical solution and iterated until the integral form of the conservation of mass is satisfied.

For external wall shear flows the momentum boundary conditions include the surface and the free stream. For the surface the no-slip is standard, although TEXSTAN can be easily modified to accommodate a slip boundary condition. The wall-normal velocity is either zero, to reflect no fluid penetration, or it is nonzero for the case of wall transpiration. Acceptable values of wall transpiration correspond to that described in Chap. 9 for blowing and suction.

$$u(x, y = 0) = 0$$

$$v(x, y = 0) = v_s(x) = \dot{m}_s''(x)/\rho_s$$

$$u(x, y \to \infty) = u_\infty(x)$$

The corresponding thermal boundary conditions for the energy equation include the surface and the free stream. For the surface the choice is either to the surface temperature or the surface heat flux

$$T(x, y = 0) = T_s(x) \quad \text{or} \quad \dot{q}''(x, y = 0) = \dot{q}_s''(x)$$

The surface boundary condition is appropriately converted by TEXSTAN into a Dirichlet mathematical form when the surface temperature is specified and into a Neumann form when the wall heat flux is specified and then further converted, depending on whether the dependent variable is stagnation enthalpy or temperature. For the free stream, when the user chooses to solve the stagnation enthalpy form of the energy equation, the stagnation temperature is all that is needed to determine the free-stream stagnation enthalpy boundary condition, and for the low-speed choice of temperature as the dependent variable, the free-stream static temperature is appropriate.

$$i^*(x, y \to \infty) = i^*_\infty = \left(cT_\infty + u^2_\infty/2\right) \quad \text{or} \quad T(x, y \to \infty) = T_\infty$$

The corresponding boundary conditions for the mass concentration equation include the surface and the free stream.

$$m_j(x, y = 0) = m_{j,s}$$
$$m_j(x, y \to \infty) = m_{j,\infty}$$

For internal wall shear flows the boundary conditions are geometry dependent. For pipe flows, where the flow is axisymmetric, the momentum boundary conditions are no-slip and no penetration at the wall and symmetry line at the pipe centerline. The latter converts mathematically into a Neumann condition of zero gradient of the axial velocity with respect to radius at the centerline. The corresponding thermal boundary conditions for a pipe of radius r_s are

$$T(x, r = r_s) = T_s(x) \quad \text{or} \quad \dot{q}''(x, r = r_s) = \dot{q}''_s(x)$$

The thermal boundary condition for the symmetry line follows that for the momentum equation, being converted mathematically into a Neumann condition of zero gradient of the temperature with respect to radius at the centerline, and then further converted, depending on whether the dependent variable is stagnation enthalpy or temperature.

For planar ducts, where the aspect ratio is such that the *b/a* ratio of Table 8-2 in Chap. 8 approaches infinity, two geometry configurations are available in TEXSTAN. The first configuration is for the case where the thermal boundary conditions are symmetrical with respect to the duct centerline, and the second configuration is for when the thermal boundary conditions are asymmetrical with respect to the duct centerline. The first has momentum and thermal boundary conditions that match that of the pipe, and the second has momentum boundary conditions that are no-slip and no-penetration for both surfaces, and surface thermal boundary conditions similar to that for the pipe wall. The momentum and thermal boundary conditions for the annular duct match the second configuration for the planar duct.

INITIAL CONDITIONS

The flow or solution domain where the boundary-layer equations are solved will depend on the flow geometry. For external wall shear flows, the flow domain is bounded in the cross direction to the principal flow direction between the no-slip surface (called the I-surface in TEXSTAN) and the free stream (called the E-surface). The domain starts where the initial conditions are specified and is essentially unbounded as the flow proceeds in the flow direction. For internal wall shear flows, the flow domain is likewise bounded in the cross direction, the flow starts where the initial conditions are specified, and the flow is unbounded in the flow direction. For pipe flows and the first geometry configuration for planar ducts, the centerline is the I-surface and the no-slip surface is the E-surface. For the second geometry configuration for planar ducts and for the annular geometry, the I- and E-surfaces are the inner and outer no-slip surfaces respectively.

For both the external and internal wall shear flow geometries, there are basically two types of initial profile choices: either the user provides TEXSTAN with "experimental" initial profiles or the user permits TEXSTAN to generate initial profiles. For internal flows, which often start at the entrance to a channel, the most obvious choice is for TEXSTAN to generate flat initial profiles corresponding to the classic combined entry problem. Fully developed initial flow profiles for channels, either laminar or turbulent, can also be fairly accurately generated by TEXSTAN. The same is true for laminar boundary layer flows using Blasius or Falkner-Skan analytical profiles. For turbulent boundary layer flows, the user can either choose to have TEXSTAN generate initial profiles, or the user can supply experimental profiles. If the latter is chosen, TEXSTAN interpolates the experimental data to provide enough points to permit an appropriately fine computing grid for the finite-difference solver.

FLUID PROPERTIES

In TEXSTAN the choice of whether to model a convective problem using constant or variable properties is primarily based on the ratio of the expected surface temperature to mean temperature for internal flows, or ratio of surface-to-free-stream temperature for external flows, where the temperatures are absolute (kelvins or degrees Rankine). When this ratio falls outside the interval from 0.95 to 1.05, the use of variable properties should be considered. Note that TEXSTAN does not require the use of variable properties to compute the effect of viscous work (or the effect of viscous dissipation). This is an independent effect. For constant properties, the user supplies quantities such as density, dynamic viscosity, and Prandtl number.

TEXSTAN contains a number of variable-property property tables or curve-fit functions, obtained from a variety of sources. There are three variable-property models for dry air. The first model derives from tables for air in the open literature for the temperature range 100–2800 K (or 243–5040° R), with the effect of pressure on all properties except density ignored. The tables are interpolated. The second model incorporates from the ideal gas law for density, a constant Prandtl number, a constant specific heat, and the Sutherland dynamic viscosity law. The third model supports the approximation introduced in the high-velocity chapter of this text, where the density-dynamic viscosity product is assumed constant. To achieve this model, the density and viscosity are computed at a reference temperature of 300 K, then density is computed via the ideal gas law, and viscosity is computed such that the density-viscosity product at a given temperature equates to the same product at 300 K. Variable-property tables are also available for nitrogen and helium, and for liquids, water properties and oil properties are available.

TURBULENCE MODELS

In TEXSTAN internal flows are forced to be either laminar or turbulent. For external flows, the boundary layer can be forced to be either laminar or turbulent over the entire surface, or the flow can be transitional, with a laminar starting flow, followed by the transition region, followed by turbulent flow.

For turbulent flows the mixing-length model and corresponding turbulent Prandtl number are mostly described in Chap. 11 and Chap. 12, respectively. The mixing length incorporates the Van Driest damping function, with the A^+ model being a function of both pressure gradient and transpiration, and damped by a first-order lag equation. For internal flows, the A^+ model constant is typically 25 and for internal flows it is typically 26. For internal flows, there is also a provision to compute a constant eddy diffusivity for momentum as a function of hydraulic diameter Reynolds number for the outer layer away from a wall. With this option, the constant eddy diffusivity is used when its value exceeds the mixing-length model value or when the distance from the wall exceeds ($\kappa \times$ channel half-width). This hybrid model is valid only for fully developed pipe flow and fully developed flow between parallel planes. For both internal and external flows, the turbulent Prandtl number is described by Eq. (12-7), with Pr_{t_∞}, the value of Pr_t far from the surface, being equal to 0.85.

A model for curvature can be used in conjunction with the external-flow mixing-length, following that described in Chap. 11 and by Adams and Johnston.[1] The radius of curvature is allowed to vary in the x direction, and it is first converted to curvature, with a damping function controlling the rate of change of the curvature to create an effective curvature, and then back-converted into an effective radius of curvature. The procedure is to then compute the external flow mixing-length distribution for all y locations and modify it for the effects of curvature according to the local Richardson number, for both convex and concave curvatures.

A model for roughness can also be used in conjunction with the mixing-length model for both internal and external flows, following that described in Chap. 11. The roughness model is based on the roughness Reynolds number; thus the model is valid only for uniformly distributed roughness of the Nikuradse type. For fully rough surfaces, $\text{Re}_k > 43$, the mixing length in the inner region is modified by using a mixing-length offset described by Eqs. (11-51) to (11-53), along with $A^+ = 0$ in the Van Driest damping function. For the transitionally rough surfaces, $5 \leq \text{Re}_k \leq 43$, the mixing-length offset is used, along with a Van Driest damping function, with both the offset and A^+ linearly changed over the transitional range of roughness Reynolds numbers. Below $\text{Re}_k = 5$ the offset is not used, and the Van Driest damping function is the same as that for a smooth surface.

The one-equation turbulence-kinetic-energy can be used with the external-flow mixing-length providing the length scale. This model is really only suitable for boundary layer flows as it is currently programmed. It is an extension of what is described in Chap. 11, and additional documentation can be found in Dawes,[2] Hassid and Poreh,[3] and Birch,[4] with the primary source being Hassid and Poreh. Because the one-equation model uses the mixing length, it is adapted to the curvature model. A primary advantage of this model is to incorporate the effects of the free-stream turbulence via the outer boundary condition for the k-equation.

For both internal and external flows, the TEXSTAN code has a choice of 4 two-equation (k–ε) models by Launder and Sharma,[5] Chien,[6] Lam-Bremhorst, as described by Schmidt and Patankar,[7] and Jones-Launder.[8] These models vary in subtle details, and one of the constants in the Jones-Launder model is changed from the literature citation to permit better agreement with benchmark test cases. All other constants and functionals agree with the citations. A constant turbulent Prandtl number is most often used with two-equation turbulence models.

The free-stream boundary condition on the k equation is based on the assumption of isotropic turbulence as described in Chap. 11 for the one-equation model. Thus its initial value is $k_\infty = 1.5[(\mathrm{Tu}/100) \times V_{\mathrm{app}}]^2$ where Tu and V_{app} are the values of the turbulence intensity and free-stream velocity that approach the no-slip surface for the external flow. The free-stream boundary condition on the ε equation is set equal to $k_\infty^{1.5}/L_e$, where k_∞ is the local value of free-stream flow-direction turbulence and L_e is the corresponding local free-stream turbulence length scale. Several choices exist for the L_e scale. The most appropriate is the streamwise integral length scale obtained from the streamwise velocity autocorrelation. Note this should be about twice the vertical spatial scale if the flow is nearly isotropic. A second choice is the dissipation length scale, which relies heavily on the flow being homogeneous and isotropic. The dissipation scale is typically a factor of 2–3 larger than the integral scale. A third choice is to compute the length scale from a correlation if the turbulence was produced using a standard grid-generation scheme, similar to the procedure described by Van Fossen, Simoneau, and Ching.[9] Whatever the choice, the resulting free stream ε should be on the order of 100 to 10,000 $\mathrm{m}^2/\mathrm{s}^3$. The ideal situation is to have the distribution of free-stream k versus x, thus permitting the L_e scale to be the unique value that matches the decay of k versus x. Note that the initial value of k is permitted to change by solving the k–ε equations as ordinary differential equations, neglecting diffusion and production terms.

For external boundary layer transitional flows, the mixing-length and one-equation turbulence models are controlled by starting the flow in a laminar state, and turbulent viscosity is computed and added to the laminar viscosity when the flow exceeds some criterion such as a critical Reynolds number. For abrupt transition, the switch occurs at a prescribed momentum Reynolds number, typically in the range of 200, being smaller if the surface is rough and larger if the free-stream turbulence intensity (Tu) is below 2–3 percent. There are three smoothly varying transition models in TEXSTAN. For intermittency-based transition models, turbulent viscosity is computed, multiplied by the intermittency factor, and added to the laminar viscosity when the flow exceeds a criteria based on Tu and pressure gradient. The intermittency models in TEXSTAN are from Abu-Ghannam and Shah[10] and Mayle.[11] A third model, described by Crawford and Kays,[12] uses a smoothly varying Van Driest A^+ function to simulate transition.

With two-equation models, the flow is started turbulent at a very low x Reynolds number, and the k–ε equations are computed along with the x-momentum equation. The turbulent viscosity is added to the laminar viscosity from the start of computations, and as the k–ε profiles develop, the turbulent viscosity becomes significant, causing the friction and heat transfer to move from a laminar value and approach a turbulent value. This type of transition is called a *natural two-equation transition*. Typically this results in early transition, and the transition length (from the point where the friction is 10 percent greater than its laminar value to the point where it is within 90 percent of its fully turbulent value) is too short. To change this, the k-equation is modified to control the production of (k). The model was developed by Schmidt and Patankar[8] using the Abu-Ghannam and Shah[10] database; therefore, it can reproduce that database quite accurately for start and length of transition. It works fairly well for turbine blade transition, but probably needs further adjustments.

NUMERICAL METHOD FOR TEXSTAN

Recall that the boundary-layer equations for TEXSTAN have a generalized form

$$r\rho u\frac{\partial\phi}{\partial x}+r\rho v\frac{\partial\phi}{\partial y}=\frac{\partial}{\partial y}\left(r\frac{\mu_{\text{eff}}}{C}\frac{\partial\phi}{\partial y}\right)+\{S_\phi\}$$

If we define the diffusion term to be

$$j_\phi=\frac{\mu_{\text{eff}}}{C}\frac{\partial\phi}{\partial y}$$

then the generalized form becomes

$$r\rho u\frac{\partial\phi}{\partial x}+r\rho v\frac{\partial\phi}{\partial y}=\frac{\partial}{\partial y}(rj_\phi)+\{S_\phi\}$$

The independent variables in this generalized equation are now transformed from (x, y) to (x, ψ) coordinates using the following derivative transformation operators

$$\frac{\partial()}{\partial x}=\left.\frac{\partial()}{\partial\xi}\frac{\partial\xi}{\partial x}\right|_y+\left.\frac{\partial()}{\partial\psi}\frac{\partial\psi}{\partial x}\right|_y$$

and

$$\frac{\partial()}{\partial y}=\left.\frac{\partial()}{\partial\xi}\frac{\partial\xi}{\partial y}\right|_x+\left.\frac{\partial()}{\partial\psi}\frac{\partial\psi}{\partial y}\right|_x$$

Let $\xi=x$. Using this partial transformation, the derivative operators become

$$\frac{\partial()}{\partial x}=\frac{\partial()}{\partial\xi}1+\left.\frac{\partial()}{\partial\psi}\frac{\partial\psi}{\partial x}\right|_y \quad \text{and} \quad \frac{\partial()}{\partial y}=\frac{\partial()}{\partial\xi}0+\left.\frac{\partial()}{\partial\psi}\frac{\partial\psi}{\partial y}\right|_x$$

Now, introduce the stream function, ψ, to define the von Mises stream-function transformation that identically satisfies the variable-density conservation of mass,

$$\left.\frac{\partial \psi}{\partial x}\right|_y = -r\rho V \quad \text{and} \quad \left.\frac{\partial \psi}{\partial y}\right|_x = r\rho U$$

The final form of the derivative operators become

$$\frac{\partial()}{\partial x} = \frac{\partial()}{\partial \xi} + (-r\rho V)\frac{\partial()}{\partial \psi} \quad \text{and} \quad \frac{\partial()}{\partial y} = (r\rho U)\frac{\partial()}{\partial \psi}$$

Now, transform the generalized boundary-layer equation, preserving the ξ variable for clarity

$$r\rho U\left[\frac{\partial \phi}{\partial \xi} - r\rho V\frac{\partial \phi}{\partial \psi}\right] + r\rho V\left[r\rho U\frac{\partial \phi}{\partial \psi}\right] = r\rho U\frac{\partial}{\partial \psi}[rj_\phi] + \{S_\phi\}$$

or

$$\frac{\partial \phi}{\partial \xi} = \frac{\partial}{\partial \psi}(rj_\phi) + \left\{\frac{1}{r\rho U}S_\phi\right\}$$

The independent variables in this generalized equation are now transformed from (x, ψ) coordinates to (x, ω) coordinates using the following derivative transformation operators

$$\frac{\partial()}{\partial \xi} = \left.\frac{\partial()}{\partial \eta}\frac{\partial \eta}{\partial \xi}\right|_\psi + \left.\frac{\partial()}{\partial \omega}\frac{\partial \omega}{\partial \xi}\right|_\psi$$

and

$$\frac{\partial()}{\partial \psi} = \left.\frac{\partial()}{\partial \eta}\frac{\partial \eta}{\partial \psi}\right|_\xi + \left.\frac{\partial()}{\partial \omega}\frac{\partial \omega}{\partial \psi}\right|_\xi$$

Let $\eta = \xi = x$. Using this partial transformation, the derivative operators become

$$\frac{\partial()}{\partial \xi} = \frac{\partial()}{\partial \eta}1 + \left.\frac{\partial()}{\partial \omega}\frac{\partial \omega}{\partial \xi}\right|_\psi$$

and

$$\frac{\partial()}{\partial \psi} = \frac{\partial()}{\partial \eta}0 + \left.\frac{\partial()}{\partial \omega}\frac{\partial \omega}{\partial \psi}\right|_\xi$$

Define the nondimensional stream function, ω, bounded by the stream function values at the domain bounding surfaces I and E. For an external boundary layer flow over a flat or curved surface I is a solid surface and E is the free stream; for internal pipe flows, I is a symmetry line and E is a solid surface.

$$\omega = \frac{\psi - \psi_I}{\psi_E - \psi_I}$$

The derivative of ω with respect to ξ is

$$\begin{aligned}
\left.\frac{\partial \omega}{\partial \xi}\right|_{\psi} &= \left\{ (\psi_E - \psi_I)^{-1} \left.\frac{\partial(\psi - \psi_I)}{\partial \xi}\right|_{\psi} + (\psi - \psi_I) \left.\frac{\partial}{\partial \xi}[(\psi_E - \psi_I)^{-1}]\right|_{\psi} \right\} \\
&= \left\{ (\psi_E - \psi_I)^{-1} \left[0 - \left.\frac{\partial \psi_I}{\partial \xi}\right|_{\psi} \right] + (\psi - \psi_I) \right. \\
&\qquad \left. \left[-(\psi_E - \psi_I)^{-2} \left(\left.\frac{\partial \psi_E}{\partial \xi}\right|_{\psi} - \left.\frac{\partial \psi_I}{\partial \xi}\right|_{\psi} \right) \right] \right\} \\
&= \left\{ \frac{1}{(\psi_E - \psi_I)} [0 - (-r_I \dot{m}''_I)] - \frac{(\psi - \psi_I)}{(\psi_E - \psi_I)^2} [(-r_E \dot{m}''_E) - (-r_I \dot{m}''_I)] \right\} \\
&= \frac{a + b\omega}{\Delta \psi}
\end{aligned}$$

where

$$\begin{aligned}
a &= r_I \dot{m}''_I \\
b &= \left(r_E \dot{m}''_E - r_I \dot{m}''_I \right) \\
\Delta \Psi &= (\psi_E - \psi_I)
\end{aligned}$$

and the derivative of ω with respect to ψ is

$$\left.\frac{\partial \omega}{\partial \psi}\right|_{\xi} = \frac{1}{\psi_E - \psi_I} = \frac{1}{\Delta \Psi}$$

With the ω transformation, the final forms of the derivative operators are:

$$\frac{\partial()}{\partial \xi} = \frac{\partial()}{\partial \eta} + \left(\frac{a + b\omega}{\Delta \Psi} \right) \frac{\partial()}{\partial \omega} \quad \text{and} \quad \frac{\partial()}{\partial \psi} = \left(\frac{1}{\Delta \Psi} \right) \frac{\partial()}{\partial \omega}$$

Transformation of the generalized equation to the (x, ω) coordinate system is straightforward. For simplicity, replace both the ξ and η variables by x, and the finalized form becomes

$$\frac{\partial \phi}{\partial x} + \left(\frac{a + b\omega}{\Delta \Psi} \right) \frac{\partial \phi}{\partial \omega} = \left(\frac{1}{\Delta \Psi} \right) \frac{\partial}{\partial \omega}(r j_{\phi}) + \left\{ \frac{1}{r \rho U} S_{\phi} \right\}$$

Solution to this generalized ϕ equation is carried out using the *method of finite differences* over the solution domain that is bounded between the I and E surfaces in the cross-stream direction and the x location where the initial conditions are specified. This domain is called a parabolic domain, from the mathematics, because it is unbounded in the flow direction.

To obtain the solution, four basic steps are required:

1. Subdivide the solution domain into numerous subdomains, called *finite volumes.*

2. For each finite volume, identify a location within the volume that will represent the dependent variable (ϕ).
3. Develop an algebraic equation that links this dependent variable to the values of the dependent variables that are in the neighboring finite volumes.
4. Solve the set of algebraic equations to determine $\phi(x, \omega)$ and then transform it back to $\phi(x, y)$.

Because the problem is parabolic, the two-dimensional solution can be started at any initial x location and marched in the x direction, rather than having to solve for the complete (x, y) field as is required for, say, two-dimensional conduction heat transfer problems. Typical starting x locations would be close to the leading edge of a flat plate for the Blasius problem or at the entrance for a pipe-flow problem. Note that external flows can not be started at a singularity where the velocity field is zero because of the nature of the von Mises transformation.

There exists several methods to develop the algebraic equation that links the dependent variable to its nearest neighbors. With each of these methods the governing differential equations are replaced with difference equations, which become the algebraic equations for solution.

The method of Patankar[13] is to integrate the governing differential equation over a finite volume. This method creates integrals for each term of the differential equation, and to carry out the integration, one or more assumptions must be made as to how the variable ϕ_i will vary in the cross-stream direction. On the basis of these assumptions each integral is evaluated, and the result is a linearized algebraic equation for each node location i

$$a_i\phi_i = b_i\phi_{i+1} + c_i\phi_{i-1} + d_i$$

These equations are then assembled into a set and solved by a tridiagonal matrix algorithm, and iterated as needed. Boundary conditions on the set of difference equations depends on whether their mathematical form is Dirichlet or Neumann.

DATA SETS FOR TEXSTAN

The website for the TEXSTAN code contains numerous data sets to help the new user with understanding a variety of different geometries available for study. These are summarized in App. H. For most of the sample data sets there is a corresponding output file that is generated by TEXSTAN, and the output is typically formatted to contain nondimensional results that compare the calculations to accepted laminar or turbulent correlations. At this time there are no graphics associated with TEXSTAN, although the output files are suitable for importing into various graphical packages.

The following data sets have extensive documentation on the website to permit the new user to understand their construction, and App. G describes in detail the construction of the data set *s10.dat.txt*.

s10.dat.txt	laminar Blasius flow on a flat plate
s31.dat.txt	laminar combined entry flow in a circular pipe
s200_5.dat.txt	turbulent flow on a flat plate
s400_7.dat.txt	turbulent combined entry flow in a circular pipe
s800_5e.dat.txt	transitional flow on a flat plate
s700_5e.dat.txt	flow on the suction side of an airfoil

TEXSTAN FOR RESEARCH

For more than 25 years TEXSTAN and its predecessor codes STAN5 and STANCOOL have been used worldwide in academia and industry. Research versions of this code have extended turbulence modeling closure to include full Reynolds stress models, turbulent heat flux models, and multiple-time-scale k–ε models. The performance of various two-equation models with transition is described in Harasgama et al.[14] for the highly-loaded transonic turbine guide vane data of Arts et al.[15] They discovered the models are generally adequate for the laminar and fully turbulent portions of the vane surfaces over the various Mach and Reynolds numbers and free-stream turbulence levels of the experiments, but predictions indicate a somewhat inconsistent model performance for a given model in the start/end of the transition region, especially at lower Reynolds numbers. To model stochastic surface roughness in TEXSTAN, the Taylor-Coleman-Hodge[16] discrete roughness model and it's modification for heat transfer by Tarada[17] have been incorporated into the research version of TEXSTAN. Tolpadi and Crawford[18] used this model to predict the suction and pressure side heat transfer data of airfoils for heat transfer data by Abuaf, Bunker, and Lee[19] at four Reynolds numbers and high free-stream turbulence. The roughness elements were simulated using full-height right-circular cones, with parameters of the elements being matched to the airfoil's roughness statistical profile measurements. Both the heat transfer level and transition locations were in good agreement for all but the lowest of the Reynolds number cases.

The film cooling models of TEXSTAN have evolved since the early version described by Miller and Crawford.[20] The revised film cooling models are derived based on the early work of Tafti and Yavuzkurt[21] and the extensions to that work by Neelakantan and Crawford.[22,23] Those references show extensive validation of the models for flat-plate conditions. For film-cooled airfoils, very little validation of the Crawford models has been carried out. Weigand, Bonhoff, and Ferguson[24] evaluated TEXSTAN and a 3-D Navier–Stokes code for predicting heat transfer on a fully film-cooled vane data for both film cooling effectiveness and heat transfer. They found the boundary layer program provided good agreement with the data, providing the appropriate boundary conditions are used for the velocity loading. Weigand, Crawford, and Lutum[25] evaluated TEXSTAN for the combined effects of its roughness and film cooling models using the flat plate data included in Hoffs, Drost, and Boelcs.[26] The combined effects were successfully modeled for both the effectiveness and heat transfer.

REFERENCES

1. Adams, E. W., and Johnston, J. P.: ASME Paper Number 83-GT-80, 1983.
2. Dawes, W. N.: ASME Paper Number 90-GT-303, 1990.
3. Hassid, S., and Poreh, M.: *ASME J. Fluids Engrg.*, vol. 97, p. 234, 1975.
4. Birch, N. T.: ASME Paper Number 87-GT-22, 1987.
5. Launder, B. E., and Sharma, B. I.: *Letters in Heat and Mass Transfer*, vol. 1, pp. 131–138, 1974.
6. Chien, K-Y, (1982): AIAA, Vol. 20, pp. 33–38, 1982.
7. Schmidt, R. C., and Patankar, S. V., (1991): *ASME J. of Turbomachinery*, vol. 113, pp. 13–26, 1991.
8. Jones, W. P., and Launder, B. E: *Int. J. Heat Mass Transfer*, vol. 16, pp. 1119–1129, 1973.
9. Van Fossen, G. J., Simoneau, R. J., and Ching, C. Y.: *ASME J. Heat Transfer*, vol. 117, pp. 597–603, 1995.
10. Abu-Ghannam, B. J., and Shah, R.: *J. Mech. Eng. Sci.*, vol. 22, pp. 213–228, 1980.
11. Mayle, R. E.: *ASME J. Turbomachinery*, vol. 113, pp. 509–537, 1991.
12. Crawford, M. E., and Kays, M. E.: NASA CR-2742, 1976.
13. Patankar, S.: *Numerical Heat Transfer and Fluid Flow*, Hemisphere Publishing, 1980.
14. Harasgama, S. P., Tarada, F. H., Baumann, R., Crawford, M. E., and Neelakantan, S.: ASME Paper 93-GT-79, 1993.
15. Arts, T., Lambert de Rouvroit, M., and Rutherford, A.W.: von Karman Institute (Belgium) Technical Note 174, 1990.
16. Taylor, R. P., Coleman, H. W., and Hodge, B. K.: *ASME J. Fluids Engrg.*, vol. 107, pp. 251–257, 1985.
17. Tarada, F.: *Int. J. Heat and Fluid Flow*, vol. 11, pp. 331–345, 1990.
18. Tolpadi, A. K., and Crawford, M. E.: ASME Paper 98-GT-87, 1998.
19. Abuaf, N., Bunker, R. S., and Lee, C. P.: *ASME J. Turbomachinery*, vol. 120, pp. 522–529, 1997.
20. Miller, K. L., and Crawford, M. E.: ASME Paper 84-GT-112, 1984.
21. Tafti, D. K., and Yavuzkurt, S.: ASME Paper 89-GT-139, 1989.
22. Neelakantan, S., and Crawford, M. E.: American Society of Mechanical Engineers Paper 95-GT-151, 1995.
23. Neelakantan, S., and Crawford, M. E.: ASME Paper 96-GT-224, 1996.
24. Weigand, B., Bonhoff, B., and Ferguson, J. R.: ASME National Heat Transfer Conference, HTD-Vol. 350, pp. 213–221, 1997.
25. Weigand, B., Crawford, M. E., and Lutum, E.: ISROMAC-7 Conference, Honolulu, HI., 1998.
26. Hoffs, A., Drost, U., and Boelcs, A.: ASME Paper 96-GT-169, 1996.

G APPENDIX

Blasius Flow—A Sample Data Set for Texstan

We present the construction of the s10.dat.txt data set to provide a feel for what is needed by TEXSTAN as an input data set to describe a convective problem. This data set is the Blasius problem for laminar flow over a flat plate with constant wall temperature and constant free-stream velocity. The problem permits comparison with analytical solutions for local shear stress (Pa or N/m^2), local heat flux (W/m^2), and total heat transfer rate (W), along with confirmation of the similarity of profiles for velocity and temperature using the Blasius similarity variable and confirmation of the variation of friction coefficient, Nusselt number, and/or Stanton number with the square-root dependence on Reynolds number. At the end of this appendix is a discussion of modifications that can be carried out to incorporate variable-property effects, high-velocity effects, and a discussion on implementation of a variable-surface-temperature boundary condition.

For the Blasius problem let the free-stream velocity be 15 m/s, free-stream temperature be 300 K, and wall temperature be 295 K; let the fluid be air at 1 atm (101,325 Pa); the plate geometry is 0.2 m long in the flow direction by 1 m wide; assume constant properties and start calculations at an x-Reynolds number of about 1000; neglect viscous dissipation. The input file (s10.dat.txt) for this problem will contain a total of 16 sets of data lines:

```
c= #1 --------------------------------------------------------
    title
s10.dat.txt lam bl, flat plate, twall(I)=c

c= #2 --------------------------------------------------------
      kgeom    neq   kstart   mode   ktmu   ktmtr   ktme
          1      2        4      1      0       0      0
```

kgeom=1 applies to geometries that include flow over flat plates, over 2-D airfoils, and inside high aspect ratio 2-D converging-diverging nozzles (either subsonic or supersonic isentropic). Computations are carried out from the wall (I surface) to the free stream (E surface). The flow is computed per unit width.

neq=2 tells TEXSTAN to solve two partial differential equations (pde's). The first pde must be the x-momentum equation (boundary layer form). To determine what the second pde will be, TEXSTAN will have to examine the variable *jsor*.

kstart=4 is a flag to select the type of initial profiles to generate. This value of the flag tells TEXSTAN to create Blasius profiles to start the calculations.

mode=1 is a flag to start the flow as laminar flow.

ktmu=*ktmtr*=*ktme*=0 tells TEXSTAN that the flow will remain laminar (that is, no turbulence models will be used, regardless of Reynolds number).

```
c= #3 ------------------------------------------------------
      kbfor      jsor(1)      jsor(2)      jsor(3)      jsor(4)      jsor(5)
        1           1
```

kbfor=1 tells TEXSTAN to calculate only the pressure gradient in the momentum equation; other flag values would cause calculation of a body force or an arbitrary source introduced through the variable *aux3*.

jsor(1)=1 tells TEXSTAN that diffusion equation (1) will be the thermal energy equation (actually, any value between 1–10 will be a thermal energy equation), and =1 means do not calculate any viscous or body-force work for the energy equation.

Note: The *jsor* variables are subscripted from 1 to 5; this is because there can be up to five diffusion equations being solved along with the momentum equation. Because *neq*=2, the variables *jsor*(2) through *jsor*(5) are left blank.

```
c= #4 ------------------------------------------------------
      kfluid      kunits
        1            1
```

kfluid=1 tells TEXSTAN to use constant properties; other values of the flag activate variable property routines. Constant properties are generally used for small temperature difference problems involving gases and low-viscosity liquids, and with gases at low speeds.

kunits=1 tells TEXSTAN that all physical units will be in SI units (using only meters, kilograms, joules, newtons, kelvins or degrees Celsius, and seconds); the flag can also be set to use British units.

```
c= #5 ------------------------------------------------------
        po          rhoc          viscoc      amolwt      gam/cp
  101325.0       1.17700     1.838E-05        0.00      1005.0
```

po=pressure in Pa (N/m^2); this will be considered static pressure if *kfluid*=1 and stagnation pressure if *kfluid*>1

rhoc=density in kg/m^3 (user can set =0 if *kfluid*>1)

viscoc=dynamic viscosity in kg/(m · s) or Pa · s (user can set =0 if *kfluid*>1)

amolwt=molecular weight (user can set =0 unless *kfluid*=14,15)

gam/cp has a dual meaning. For *kfluid*=1, it is the specific heat in J/(kg · K) for all other *kfluid* values (except =14,15) user can set =0; for *kfluid*=14,15 it is the ratio of specific heats. User also can set =0 if *neq*=1 (solving only the momentum equation).

```
c= #6 --------------------------------------------------------------------
    prc(1)      prc(2)      prc(3)      prc(4)      prc(5)
     0.707
```

prc(1)=Prandtl number for the (1) equation; recall that setting *jsor*(1) between the value of 1–10 flagged TEXSTAN that the (1) equation will be a thermal energy equation. If the (1) equation were a mass diffusion equation (*jsor*(1)=31), then the *prc*(1) would be technically called a Schmidt number.

Note: Because *neq*=2, the variables *prc*(2) through *prc*(5) are left blank.

The following data blocks begin the boundary condition information for the I and E surfaces. They are supplied to TEXSTAN in 3 blocks. The first block is a set of two data lines representing the I and E surfaces. The variable *nxbc* tells how many boundary condition points to expect for the I surface and for the E surface (they must be equal in value). The *jbc* variable tells TEXSTAN how to interpret the boundary conditions for each diffusion equation (Dirichlet or Neumann type or symmetry).

```
c= #7 --------------------------------------------------------------------
c= #8 --------------------------------------------------------------------
   nxbc(I)    jbc(I,1)    jbc(I,2)    jbc(I,3)    jbc(I,4)    jbc(I,5)
         2           1
   nxbc(E)    jbc(E,1)    jbc(E,2)    jbc(E,3)    jbc(E,4)    jbc(E,5)
         2           1
```

nxbc(I)=2 is the number of bc locations, I surface; note that 2 is the minimum and 100 is the maximum; this will become the number of *x*(m) locations and the number of other bc values read by TEXSTAN's input logic.

nxbc(E)=*nxbc*(I)

jbc(I,1)=1 tells TEXSTAN that the type of boundary condition at the I surface for equation (1) is Dirichlet; since the *jsor*(1) variable tells TEXSTAN that the (1) equation is the thermal energy equation, this will be the wall temperature, since the I surface for *kgeom*=1 is a wall.

jbc(E,1)=1 tells TEXSTAN that the type of boundary condition at the E surface for equation (1) is Dirichlet; again, since the *jsor*(1) variable tells TEXSTAN that the (1) equation is the thermal energy equation, this will be the free-stream temperature, since the E surface for *kgeom*=1 is a free stream.

Note: Because *neq*=2, the variables *jbc*(I,2) through *jbc*(I,5) and *jbc*(E,2) through *jbc*(E,5) are left blank.

The second data block is a set of lines (m=1,*nxbc*) representing the *x* locations of the boundary condition points, the wall radius (*rw*) at each of these locations, and the values of pre-defined variables (*aux1*, *aux2*, and *aux3*) at these locations. Note that TEXSTAN will linearly interpolate the *rw* and *aux1*, *aux2*, and *aux3* variables between the various *x*(m) locations.

c= #9 --

x(m)	*rw*(m)	*aux1*(m)	*aux2*(m)	*aux3*(m)
0.0000000	1.0000	0.0000	0.0000	0.0000
0.2000000	1.0000	0.0000	0.0000	0.0000

x(m)=*x* locations, in meters, where boundary conditions will be specified; two *x* locations are sufficient to define the s10.dat.txt geometry. If either the I- or E-surface boundary conditions were varying with *x*, then enough points would be required to resolve the distribution using linear interpolation (spline for velocity).

rw(m)=1.000 is the required wall radius for a plane surface, *kgeom*=1.

aux1(m)=*aux2*(m)=*aux3*(m)=0.000 because these arrays are not used.

The third data block is a set of 2**nxbc* lines representing the I- and E-surface boundary conditions for each of the *x*(m) locations, including the velocity (*ub*), mass flux (*am*), and boundary conditions (*fj*) for all equations other than the momentum equation. TEXSTAN will linearly interpolate the *am* and *fj* variables between the various *x*(m) locations, and it will spline-interpolate the *ub* variable. Note that many of the boundary condition values can be set zero because they are either not needed or defined using some other variable.

c= #10 --

ubI(m) *ubE*(m)	*am*(I,m) *am*(E,m)	*fj*(I,1,m) *fj*(E,1,m)	*fj*(I,2,m) *fj*(E,2,m)	*fj*(I,3,m) *fj*(E,3,m)	*fj*(I,4,m) *fj*(E,4,m)	*fj*(I,5,m) *fj*(E,5,m)
0.00	0.000	295.0				
15.00	0.0	0.0				
0.00	0.000	295.0				
15.00	0.0	0.0				

ubI(m)=0.00, the no-slip velocity, I surface

ubE(m)=15.00, free-stream velocity in m/s, E surface

am(I,m)=0.000, mass transfer, I surface (only non-zero for blowing or suction)

am(E,m)=0.0, mass transfer, E surface (always =0 for free stream)

fj(I,1,m)=295.0, the wall temperature (I surface), because *jbc*(I,1)=1, in units of kelvins (can be °C for *kfluid*=1). Note if *jbc*(I,1)=2, this would be interpreted as a wall heat flux in units of W/m^2.

fj(E,1,m)=0.0, the free steam (E surface) energy equation variable is set =0 because it will be defined using the variable *tstag*. Note that *tstag* is interpreted as static temperature for *kfluid*=1, and interpreted as stagnation temperature for *kfluid*>1 and converted to stagnation enthalpy.

Note: Because *neq*=2, the variables *fj*(I,2,m) through *fj*(I,5,m) and *fj*(E,2,m) through *fj*(E,5,m) can be left blank.

```
c= #11--------------------------------------------------------------------------------
               xstart           xend          deltax          fra           enfra
     0.0010410       0.200000       0.100          0.010        1.000E-06
```

xstart=user-calculated value, in meters, to produce (approximately) the starting x-Reynolds number; *xstart* must be $\geq x(1)$. It is important to note that TEXSTAN cannot start at a free-stream velocity singularity, such as x=0 for a Blasius or Falkner–Skan problem (the F–S m=1 problem is the cylinder in crossflow, approximating the leading edge of a turbine blade).

xend=user specified value, $\leq x(nxbc)$, in meters, where integration is stopped.

deltax=recommended value, =0.1. This is a nondimensional ratio of the true integration stepsize divided by the boundary layer thickness. When one is checking effect of integration stepsize, this value is tested. A value of 0.1 means integration in the flow direction proceeds at a stepsize no larger than 10 percent of the 99 percent boundary-layer thickness.

fra=recommended value, =0.01. This is a complicated parameter relating to controlling stepsize in the event the boundary layer starts to grow rapidly, which is often the case in an adverse pressure gradient, or when large blowing is prescribed.

enfra=recommended value, =1.0E-06. This controls how close to zero TEXSTAN keeps the gradient of the velocity profile at the E surface (if the flag *kent*=0) or for all dependent variables (if the flag *kent*=1). In effect, this is controlling the mesh expansion in the +y direction by creating entrainment. Changing this value to 1.000E-03, for example, would result in the numerical answers deviating from the Blasius solution to some degree.

Note: Numerical simulations always require testing to ensure the solution is grid and stepsize independent. In TEXSTAN testing is carried out by refining the resolution of the initial profile by changing *dyi* and *rate*, by changing *deltax*, and by changing *enfra*. We recommend you use *kstart*>0 (which allows TEXSTAN to generate initial profiles that have been well tested for grid spacing) and use the recommended values for *dyi*, *rate*, *deltax* and *enfra*.

```
c= #12 --------------------------------------------------------
     kout      kspace      kdx      kent
       8        100          0        1
```

kout=8 causes output to be formatted to compare friction (and heat transfer) results with accepted academic correlations; this is most frequently chosen when testing the various TEXSTAN *sxxx.dat* benchmark data sets; otherwise use *kout*=2 as a general external flow output format; output is always printed to a file named *out.txt*.

kspace=print interval in terms of integration steps in the file *out.txt*.

kdx=recommended value; =0. Rarely is this set =1, and if so, it is used in conjunction with the *aux1*(m) variable; typically useful if step changes in boundary conditions are being studied and one wants to vary stepsize immediately after the step.

kent=recommended value; =1. Rarely is this set =0, except for free convection profiles.

c= #13 ---

k1	*k2*	*k3*	*k4*	*k5*	*k6*
0	0	0	0	50	0

k1>0 permits defining a virtual origin for the *x*-Reynolds number using the *gxx* variable. Rarely necessary for laminar flows.

k2>0 permits using a recovery factor in the definition of the heat transfer coefficient and Stanton number.

k3>0 sets the print interval for diagnostics when the user sets *k8*>0.

k4 is useful only with analytical laminar flows. It allows the user to select various analytical free-stream velocity distributions built into TEXSTAN, such as the Falkner–Skan *m*=1 or the potential flow over a cylinder.

k5=print interval for various files that contain useful information that can be easily plotted using plot software. For the external boundary layer with heat transfer these files include:

ftn84.txt: *x/s, yl, uinf, del2, h12, del3*
ftn85.txt: *x/s, rex, rem, cf/2, reh, st, htc*
ftn86.txt: *intg, x/s, htc, qflux, twall, tinf*
ftn87.txt: *intg, x/s, htc, uinf, st*

where:

cf/2	friction coefficient
del1	boundary layer displacement thickness, m
del2	boundary layer momentum thickness, m
del3	boundary layer enthalpy thickness (meters)
h12	shape factor, *del1/del2*
htc	heat transfer coefficient, W/(m^2 · K)
intg	integration step
qflux	wall heat flux, W/m^2
reh	enthalpy thickness Reynolds number
rem	momentum thickness Reynolds number
rex	*x*-Reynolds number

st	Stanton number
tinf	free stream temperature, kelvins or °C
twall	surface temperature, kelvins or °C
uinf	free-stream velocity, m/s
x/s	*x* location, normalized by *s*=*exx*; *exx*=0.0 sets *s* to its default value, *s*=1.0
yl	boundary layer thickness, where *u/uinf* =0.99, m

k6>0 permits the user to stop TEXSTAN at integration step =*k6*.

```
c= #14 ----------------------------------------------------------------
          k7          k8          k9          k10          k11          k12
           0           0           0            0            0            0
```

k7 is not used in academic TEXSTAN.

k8 permits special diagnostics to be printed (see the input manual). The two that are really useful are:

=35 to print diagnostics to files *ftn35* and to *ftn74* (and to the screen) from subroutines that create starting profiles when *kstart*>0.

=36 to print analysis of various boundary conditions, as interpolated by TEXSTAN. The user should use this option if any input data vary with *x*, including free-stream velocity, wall temperature, or wall curvature. Be sure to plot the interpolated data to check for smoothness. Note: *x* distribution can be scaled to be *x/s*, where *s* is the input variable *exx*.

k9 is not used for laminar flows.

k10 permits profiles of velocity and other variables to be printed to files that can be easily plotted using plot software. Two options exist:

First option: print profiles to the output file: *out.txt*. For this option:

=10 to print non-dimensional forms of the profiles at each *x*(m) bc

=11 to print dimensional forms of the profiles at each *x*(m) bc

Note: If the user needs profiles at locations other than the *x*(m) values, then the user can add additional values to the *x*(m) array; this option works only for *kout* =2 (bl flow) or *kout*=4(internal flow).

Second option: print one set of profiles to *ftn74* at a location defined by the input variable *bxx*.

=21 to print profiles at *x*-Reynolds number =*bxx*

=22 to print profiles at momentum Reynolds number =*bxx*

=23 to print profiles at enthalpy Reynolds number =*bxx*

k11 is not used in academic TEXSTAN.

k12 is not used in laminar flows.

```
c= #15 -------------------------------------------------------
        axx          bxx          cxx          dxx          exx          fxx          gxx
0.000E+00  0.000E+00  0.000E+00  0.000E+00  0.000E+00  0.000E+00  0.000E+00
```

axx is used (*k4*>0) to define an analytic free-stream velocity distribution built into TEXSTAN.

bxx is used (*k4*>0) to define an analytic free-stream velocity distribution.
or if (*k10*>0) to define where to print profiles.
or if (*k2*>0) to define a special recovery factor.

cxx is used (*k4*>0) to define an analytic free-stream velocity distribution built into TEXSTAN.

dxx is used (*k4*>0) to define an analytic free-stream velocity distribution built into TEXSTAN.

exx is used (*k5*>0 or *k8*=36) as a scaling coefficient, *s*, to convert *x* to *x*/*s*.

fxx not used with laminar flows.

gxx is used (*k1*=1) to define the *x*-virtual origin in the Reynolds number.
or if (*kbfor*=4) to define an alternative gravitational constant.

The initial profiles in TEXSTAN typically come from within the code or they are user-specified for *kstart*=1,10. The input manual describes how to provide user-specified profiles. For laminar boundary layer flows, *kstart*=4 generates Blasius profiles for velocity and temperature for use with constant free-stream velocity. Use of *kstart*=5,6 provide either the Falkner–Skan *m*=1 profiles or the cylinder in crossflow profiles. These profiles are documented in the input manual. The following input variables apply only for *kgeom*=1,2,3 (the external wall shear flows where free-stream velocity is supplied as a boundary condition), and an alternate set of variables will be presented for *kgeom*=4,5,6,7 (the internal wall shear flows where the pressure gradient is iterated to conserve mass flow rate).

```
c= #16 ---------------------------------------------------------
       dyi         rate       tstag      vapp     tuapp    epsapp
5.000E-05     0.0900     300.0      0.00      0.0      0.00
```

dyi=recommended value for *kstart*=4

rate=recommended value for *kstart*=4

tstag is interpreted as the free stream static temperature (kelvins or °C) for *kfluid*=1, and it is interpreted as the stagnation temperature (kelvins) for *kfluid*>1

vapp=turbulence variable; set =0.0

tuapp=turbulence variable; set =0.0

epsapp=turbulence variable; set =0.0

Output file for *s10.dat.txt*

The following output data set (*s10.bm.txt*) was produced by TEXSTAN for this *s10.dat.txt* input data set.

```
=======================================================
  TEXSTAN(academic)
  dat: s10.dat.txt lam bl, flat plate, twall(I)=c
  stepsize: const, dx= 0.100
  entrainment based only on mom + energy eqns; enfra= 1.00E-06 fra= 0.010
  dpdx: not-a-knot spline curve fit
  energy eqn: solved, no source terms
  props: const
    po= 1.01325E+05 den= 1.17700E+00 vis= 1.83800E-05 sp_ht= 1.00500E+03
    prc(je)=    0.707
  initial profiles: kstart=  4  dyi= 5.000E-05  rate= 0.0900
  laminar flow at xstart, transition not possible
  axx= 0.0000E+00  bxx= 0.0000E+00  cxx= 0.0000E+00  dxx= 0.0000E+00
  exx= 0.0000E+00  fxx= 0.0000E+00  gxx= 0.0000E+00
  Stanton number and htc based on (twall-tinf)
  ====================================================
   Laminar flat plate flow benchmark
   cf/2,theo = 0.332/sqrt(rex)
   nux,theo = 0.332*(rex**0.5)*(pr(je,np1)**0.33)
  ====================================================
  intg rex       rem       cf2         nu   cfrat nurat h12   reh
     5 1.008E+03 2.108E+01 1.046E-02   9.4 1.000 0.995 2.590 2.598E+01
   100 2.180E+03 3.103E+01 7.110E-03  13.8 1.000 0.995 2.590 3.846E+01
   200 5.074E+03 4.735E+01 4.658E-03  21.0 0.999 0.993 2.590 5.893E+01
   300 9.175E+03 6.367E+01 3.464E-03  28.2 0.999 0.993 2.590 7.940E+01
   400 1.448E+04 7.999E+01 2.757E-03  35.4 0.999 0.993 2.590 9.985E+01
   500 2.100E+04 9.632E+01 2.290E-03  42.6 1.000 0.992 2.590 1.203E+02
   600 2.873E+04 1.126E+02 1.958E-03  49.8 1.000 0.992 2.590 1.407E+02
   700 3.766E+04 1.290E+02 1.710E-03  57.0 1.000 0.992 2.590 1.612E+02
   800 4.780E+04 1.453E+02 1.518E-03  64.2 1.000 0.992 2.590 1.816E+02
   900 5.915E+04 1.616E+02 1.365E-03  71.4 1.000 0.992 2.590 2.020E+02
  1000 7.171E+04 1.779E+02 1.240E-03  78.7 1.000 0.992 2.590 2.225E+02
  1100 8.547E+04 1.942E+02 1.135E-03  85.9 1.000 0.992 2.590 2.429E+02
  1200 1.004E+05 2.106E+02 1.047E-03  93.1 1.000 0.992 2.590 2.633E+02
  1300 1.166E+05 2.269E+02 9.721E-04 100.3 1.000 0.992 2.590 2.837E+02
  1400 1.340E+05 2.432E+02 9.068E-04 107.5 1.000 0.992 2.590 3.042E+02
  1500 1.526E+05 2.595E+02 8.498E-04 114.7 1.000 0.992 2.590 3.246E+02
  1600 1.724E+05 2.759E+02 7.995E-04 122.0 1.000 0.992 2.590 3.450E+02
  1694 1.921E+05 2.912E+02 7.574E-04 128.7 1.000 0.992 2.590 3.642E+02
```

where:

intg	integration
rex	x-Reynolds number
rem	momentum thickness Reynolds number
cf2	friction coefficient
nu	Nusselt number
cfrat	ratio cf2/cf2,theo where cf2,theo defined in output
nurat	ratio nu/nu,theo where nu,theo defined in output
h12	bl shape factor
reh	enthalpy thickness Reynolds number

Note: The following files, useful for data plotting, were also produced during execution of TEXSTAN (because $k5>0$), but they have not been reproduced here

ftn84.txt: *x/s, yl, uinf, del2, h12, del3*
ftn85.txt: *x/s, rex, rem, cf/2, reh, st, htc*
ftn86.txt: *intg, x/s, htc, qflux, twall, tinf*
ftn87.txt: *intg, x/s, htc, uinf, st*

Variable-property modification

To change this data set to variable properties, set *kfluid*>1; for example, *kfluid*=14 models air using the Sutherland viscosity law, a constant Pr, and the ideal gas law for density, and requires two user-specified variable values for molecular weight and the ratio of specific heats, typically *amolwt*=28.97 kg/kmol and *gam/cp*=1.4; for variable-property water, set *kfluid*=4. Note: For variable properties, the automatic input profile generator is somewhat inaccurate, but this effect damps out fairly quickly.

High-velocity or high-Prandtl-number modification

For flows with Mach number > 0.3 or Pr > 10, viscous dissipation should be considered, requiring *jsor*(1)=3; and variable properties should be used.

Wall heat-flux boundary condition modification

To prescribe a variable wall heat flux, change the value of *jbc* to *jbc*(I,1)=2 and enter values for the wall bc, *fj*(I,1,m) as appropriate (units of heat flux will be W/m^2).

Variable wall boundary conditions

For this example, let the wall temperature be 295 K over the *x* distance from 0.0 m to 0.10 m; at *x*=0.10 m, the wall temperature is lowered linearly down to 290 K over the *x* distance from 0.10 m to 0.15 m; at *x*=0.15 m, the wall temperature is abruptly changed back to 295 K. Recall that TEXSTAN will linearly interpolate between boundary condition values, so for step changes, specify *x*(m) values close together. Note: To resolve the step wall temperature effect in detail, especially to compare numerical output with theory, you may elect to either reduce *deltax* or employ a more elaborate stepsize control method. For the latter, set *kdx*=1 and let *aux1*(1)=*aux1*(2)=0.2 and then let *aux1*(3)=*aux1*(4)=*aux1*(5)=0.05 (or some smaller value).

nxbc change as follows:

nxbc(I)=5
nxbc(E)=5

boundary condition table change as follows (five entries to match *nxbc* =5):

x(m)	*rw*(m)	*aux1*(m)	*aux2*(m)	*aux3*(m)
0.0000000	1.0000	0.0000	0.0000	0.0000
0.1000000	1.0000	0.0000	0.0000	0.0000
0.1500000	1.0000	0.0000	0.0000	0.0000
0.1510000	1.0000	0.0000	0.0000	0.0000
0.2000000	1.0000	0.0000	0.0000	0.0000

(and 10 entries in these tables to match *nxbc*=5)

ubI(m) *ubE*(m)	*am*(I,m) *am*(E,m)	*fj*(I,1,m) *fj*(E,1,m)	*fj*(I,2,m) *fj*(E,2,m)	*fj*(I,3,m) *fj*(E,3,m)	*fj*(I,4,m) *fj*(E,4,m)	*fj*(I,5,m) *fj*(E,5,m)
0.00	0.000	295.0				
15.00	0.0	0.0				

```
 0.00   0.000   295.0
15.00     0.0     0.0
 0.00   0.000   290.0
15.00     0.0     0.0
 0.00   0.000   295.0
15.00     0.0     0.0
 0.00   0.000   295.0
15.00     0.0     0.0
```

STARTING AND RUNNING TEXSTAN

Once the compiled TEXSTAN has been downloaded to the user's computer, it can be started by double-clicking its icon, which launches a DOS window. Within the DOS window, the user types the following command from the keyboard:

```
texstan <cr>
```

TEXSTAN immediately writes the following message to the DOS window:

```
Starting program TEXSTAN - academic version xxxx

Enter the TEXSTAN data set filename
```

Now the user types the following command from the keyboard:

```
 s10.dat.txt <cr>
```

TEXSTAN (hopefully) writes the following 20–30 lines of messages to the DOS window to help the user track the execution of TEXSTAN as the integration proceeds:

```
//////////////////
/// all input reads written to file:                 in.txt
//////////////////

///              input data check in subroutine inpt ok
///                                    file in.txt closed
//////////////////
/// output will be written to file:                 out.txt
//////////////////

s10.dat.txt lam bl, flat plate, twall(I)=c

write: sub ohtc to ftn84.txt: x/s, yl, del1, del2, h12, del3
write: sub ohtc to ftn85.txt: x/s, rex, rem, cf/2, reh, st, htc
write: sub ohtc to ftn86.txt: intg, x/s, htc, qflux, twall, tinf
write: sub ohtc to ftn87.txt: intg, x/s, htc, uinf, st

integration step = 0
intg= 1 xu= 1.04262E-03 xvo= .00000E+00 rex= 1.00149E+03
   rem= 2.10187E+01  reh= 2.58965E+01
integration step = 500
integration step = 1000
integration step = 1500
/// TEXSTAN (academic) is finished

s10.dat.txt lam bl, flat plate, twall(I)=c
```

The user will note that TEXSTAN writes numerous data files to disk. In this case TEXSTAN wrote the following files:

```
in.txt
out.txt
ftn84.txt
ftn85.txt
ftn86.txt
ftn87.txt
```

and the DOS window messages tell the user what each of these files contain. It is the file *out.txt* that the user can compare to the *s10.bm.txt* file using appropriate comparison software (the UNIX diff or Microsoft Word compare feature). Note: Some computer FORTRAN compilers create a real annoyance—they drop the leading zeros for floating point numbers, and comparison software will detect these differences between *out.txt* and the file *sxxx.bm.txt* because the leading zeros are missing.

At several points during reading the input data, TEXSTAN does limited error checking of the values assigned to the input variables. This is by no means definitive, and we add to it as we discover new "pitfalls" and "mistakes" with interpretation of the meanings of input variables. All reads of the input to TEXSTAN are free format. This makes it easy to generate an input data set, but it is potentially troublesome to the input logic. With free format, all input variables must appear in the input data set, even if they are required to be zero (0 or 0.0). If you use a blank in place of a zero, the free-format read will skip to the next nonzero entry, thus creating an input-read problem that is sometimes hard to identify.

Debugging the input is always frustrating. Every effort has been made to anticipate errors and incompatibilities. The structure of the input is to continuously read and write such that when a failure does occur, at least part of the file *in.txt* has hopefully been generated. Pay attention to whatever is written to the screen, and the same statement should exist in the file *in.txt*. One serious failure that is hard to diagnose occurs when you leave out a variable that TEXSTAN expects to read via the free format. FORTRAN will read the next line of data and try to process it, and from that point on, the data will be out of sequence and the error display that will eventually print may not be meaningful.

We wish you the best of luck with academic TEXSTAN. It and STAN5 have been in continuous use worldwide for almost three decades, and we continue to support it for the academic community of convective heat and mass transfer.

H APPENDIX

Texstan Data Sets

The website for TEXSTAN contains numerous data sets and corresponding output files to help the new user understand the variety of different geometries available for study. Listed below are representative data sets for external and internal flow geometries.

EXTERNAL-FLOW DATA SETS

Boundary layer—laminar flow over a flat plate

low-speed, constant-property air; T=const bc

s10.dat lam	
ss10.dat	(same as s10.dat, but in English units)

low-speed, constant-property air; q''=const bc

s11.dat

low-speed, variable-property, small temperature differences; T=const bc

v10_2.dat	air (*kfluid*=2)
v10_6.dat	nitrogen (*kfluid*=6)
v10_8.dat	helium (*kfluid*=8)
v10_14.dat	air (*kfluid*=14)
v10_15.dat	gas (*kfluid*=15)

low-speed, variable-property, small temperature differences; q''=const bc

v11_2.dat	air (*kfluid*=2)

low-speed, variable-property air, large temperature differences; T=const bc

v10_0.7.dat	(Ts/Tinf=0.7)
v10_1.4.dat	(Ts/Tinf=1.4)

v18_0.01_0.25.dat	M=0.01, Ts/Tinf=0.25, Tinf=217.82 K
v18_0.01_2.0.dat	M=0.01, Ts/Tinf=2.0, Tinf=217.82 K

high-speed, variable-property air, large temperature differences; T=const bc

v18_6.0_0.25.dat	M=6.0, Ts/Tinf=0.25, Tinf=217.82 K
v18_6.0_2.0.dat	M=6.0, Ts/Tinf=2.0, Tinf=217.82 K

high-speed, variable-property air, large temperature differences, adiabatic wall; q″=0 bc

v18_6.0_aw.dat	M=6.0, Tinf=217.82 K

low-speed, constant-property water; T=const bc

w10.dat	
ww10.dat	(same as w10.dat, but in British units)

low-speed, variable-property water, small temperature differences; T=const bc

w10_4.dat	
ww10_4.dat	(same as w10_4.dat, but in British units)

low-speed, constant-property Reynolds analogy fluid, Pr=1; T=const bc

s12.dat

Boundary layer—laminar flow over a flat plate with mass transfer

low-speed, constant-property binary mixture, Pr=0.707, Sc=2.50; T=const bc

m10.dat

low-speed, constant-property Reynolds analogy binary mixture, Pr=1, Sc=1; T=const bc

m12.dat

Boundary layer—laminar flow over a flat plate (user-supplied initial profile test cases)

Note: Data sets are similar to s10.dat

p10.dat tests the use of the *kstart*=0 option
file p10.pro provides a set of 107 velocity and temperature profiles
Note: The finite-difference mesh will be calculated exactly, on the basis of the $u(y)$ distribution contained in file p10.pro

pp10.dat tests the use of the *kstart*=10 option
file pp10.dat provides a set of 54 velocity and temperature profiles
Note: The finite-difference mesh will be calculated by interpolating the $u(y)$ distribution contained in file pp10.pro, based on the specified *dyi* and *rate*

t10.dat also tests the use of the *kstart*=0 option using set of 107 velocity and temperature profiles contained within the data set
Note: The finite-difference mesh will be calculated exactly, on the basis of the $u(y)$ distribution

tt10.dat tests the use of the *kstart*=10 option using a set of 54 velocity and temperature profiles contained within the data set
Note: The finite-difference mesh will be calculated by interpolating the $u(y)$ distribution contained within the data set, on the basis of the specified *dyi* and *rate*

Boundary layer—laminar stagnation-point flow (Falkner–Skan m=1)

low-speed, constant-property air; T=const bc
Note: s15 analytically generates the m=1 free-stream velocity distribution
Note: s15mod provides the m=1 free-stream velocity distribution as input data

s15.dat
s15mod.dat

Boundary layer—laminar cylinder in cross flow

low-speed, constant-property air; T=const bc
Note: s16 analytically generates the free-stream velocity distribution

s16.dat Ts/Tinf=0.997

low-speed, variable-property air, large temperature differences; T=const bc
Note: v16 analytically generates the free-stream velocity distribution

v16_0.7.dat	Ts/Tinf=0.700
v16_1.4.dat	Ts/Tinf=1.400

Boundary layer—laminar-flow-free convection over a vertical flat plate

variable-property air, small temperature differences

v90.dat

Boundary layer—turbulent flow over a flat plate

low-speed, constant-property air; T=const bc

s200_5.dat	ml turb model
s200_11.dat	1-eqn turb model
s200_21.dat	2-eqn L-S turb model
s200_22.dat	2-eqn KYC turb model
s200_23.dat	2-eqn L-B turb model
s200_24.dat	2-eqn J-L turb model

low-speed, constant-property air; q″=const bc

s210_5.dat	ml turb model

low-speed, variable-property air; T=const bc

v200_5.dat	ml turb model
v210_5.dat	ml turb model

low-speed, constant-property Reynolds analogy fluid, Pr=1, Prt=1; T=const bc

s220_5.dat	ml model

Boundary layer—turbulent accelerated flow over a flat plate

i72968.dat	Thielbahr strong acceleration

Boundary layer—turbulent flow over a curved flat plate

i70280.dat	Simon strongly curved surface
i8000.dat	Gibson mild convex surface
i8100.dat	Gibson mild concave surface

Boundary layer—turbulent flow over a rough flat plate

low-speed, constant-property air; T=const bc

s200_rek_30.dat	m-l turb model
i71374_16.dat	Pimenta fully rough surface (16 m/s)
i71374_27.dat	Pimenta fully rough surface (27 m/s)
i71374_40.dat	Pimenta fully rough surface (40 m/s)
i71374.dat	Pimenta fully rough surface (40 m/s) (*kstart*=10)
i71374_40a.dat	Pimenta fully rough surface (40 m/s) (*kstart*=3)

Boundary layer—flow in a converging–diverging nozzle

s9000.dat	m-l model

Boundary layer—transitional turbulent flow over a flat plate

low-speed, constant-property air; T=const bc

s800_5a.dat	ml turb model w/ abrupt transition model
s800_5c.dat	ml turb model w/ A-G&S transition model
s800_5d.dat	ml turb model w/ A^+ sine fn transition model
s800_5e.dat	ml turb model w/ Mayle transition model
s800_11e.dat	1-eqn turb model w/ Mayle transition model
s800_21.dat	2-eqn turb model L-S, natural transition
s800_22.dat	2-eqn KYC turb model, natural transition
s800_23.dat	2-eqn L-B turb model, natural transition
s800_23p.dat	2-eqn L-B turb model w/ controlled transition
s800_24.dat	2-eqn J-L turbulence model, natural transition

low-speed, variable-property air; T=const bc

v800_5a.dat	ml turb model w/ abrupt transition model

Boundary layer—flow over a turbine blade suction surface

Daniels & Browne turbine blade, suction side at the design blade Re; T=const bc

v700_5e.dat	ml turb model w/ Mayle transition model, no curvature effect
v700_5ec.dat	ml turb model w/ Mayle transition model, curvature effect
v700_11e.dat	1-eqn turb model w/ Mayle transition model
v700_23p.dat	2-eqn L-B turb model w/ controlled transition

INTERNAL-FLOW DATA SETS

Couette flow—laminar

Study of effects of viscous dissipation on laminar constant-property couette flow

c51 data sets use air with T=const bc (I surface), T=const bc (E surface)

c51.dat	no viscous dissipation
c51_vd.dat	viscous dissipation with V=10 m/s
c51a_vd.dat	viscous dissipation with V=350 m/s

c52 data sets use oil with T=const bc (I surface), T=const bc (E surface)

c52.dat	no viscous dissipation
c52_vd.dat	viscous dissipation with V=10 m/s
c52a_vd.dat	viscous dissipation with V=200 m/s

c53 data sets use oil with T=const bc (I surface), q″=0 bc (E surface)

c53_vd.dat	viscous dissipation with V=10 m/s
c53a_vd.dat	viscous dissipation with V=200 m/s

Pipe flow—laminar

combined entry flow, constant-property air; T=const bc

s30.dat

combined entry flow, constant-property air; q″=const bc

s31.dat

combined entry flow, variable-property air; T=const bc

v30_2.dat

combined entry flow, variable-property water; q″=const bc

v31_4.dat

thermally fully developed flow, constant-property air; T=const bc

s32.datc

thermally fully developed flow, constant-property air; q″=const bc

s33.dat

unheated starting length (usl) flow, constant-property air; T=const bc

s34.dat

unheated starting length (usl) flow, constant-property air; q″=const bc

s35.dat

Pipe flow—laminar (user-supplied initial profile test cases)

Note: Data sets are similar to s32.dat, but in British units

- p32.dat tests the use of the *kstart*=0 option
  - file p32.pro provides a set of 64 velocity and temperature profiles
  - Note: The finite-difference mesh will be calculated exactly, on the basis of the $u(y)$ distribution contained in file p32.pro
- pp32.dat tests the use of the *kstart*=10 option
  - file pp32.dat provides a set of 33 velocity and temperature profiles
  - Note: The finite-difference mesh will be calculated by interpolating the $u(y)$ distribution contained in file pp32.pro, on the basis of the specified *dyi* and *rate*

Parallel-plane flow—laminar

combined entry flow, constant-property air; T=const (symmetric) bc

s50.dat

combined entry flow, constant-property air; q″=const (symmetric) bc

s51.dat

Note: These data sets check code symmetry for s50 and s51 using *kgeom*=6

s506.dat T=const bc (I surface), T=const bc (E surface)
s516.dat q″=const bc (I surface), q″=const bc (E surface)

thermally fully developed flow, constant-property air; q″=const (symmetric) bc

s53.dat

Note: This data set checks code symmetry for s53 using *kgeom*=6

s536.dat q″=const bc (I surface), q″=const bc (E surface)

unheated starting length (usl) flow, constant-property air; T=const (symmetric) bc

s54.dat T=const bc

unheated starting length (usl) flow, constant-property air; q''=const (symmetric) bc

s55.dat	q''=const bc

Note: These data sets check code symmetry for s54 and s55 using *kgeom*=6

s546.dat	T=const bc (I surface), T=const bc (E surface)
s556.dat	T=const bc (I surface), T=const bc (E surface)

combined entry flow, asymmetric heating, constant-property air

s596.dat	q''=const bc (I surface), q''=const bc (E surface)

Annulus flow—laminar

combined entry flow at $r^*=0.5$, constant-property air

s60.dat	T=const bc (I surface), T=const bc (E surface)
s61.dat	q''=const bc (I surface), q''=const bc (E surface)

unheated starting length flow at $r^*=0.5$, constant-property air

s64.dat	T=const bc (I surface), T=const bc (E surface)
s65.dat	q''=const bc (I surface), q''=const bc (E surface)

combined entry flow at $r^*=0.9$, constant-property air

s66.dat	T=const bc (I surface), T=const bc (E surface)

combined entry flow at $r^*=0.1$, constant-property air

s67.dat	T=const bc (I surface), T=const bc (E surface)

Couette flow—turbulent

c560_6.dat	T=const bc (I surface), T=const bc (E surface), ml turb model
c560_8.dat	T=const bc (I surface), T=const bc (E surface), ml turb model + ev turb model
c560_21.dat	T=const bc (I surface), T=const bc (E surface), 2-eqn L-S turb model
c560_22.dat	T=const bc (I surface), T=const bc (E surface), 2-eqn KYC turb model
c560_23.dat	T=const bc (I surface), T=const bc (E surface), 2-eqn L-B turb model

Pipe flow—turbulent

combined entry flow, constant-property air; T=const bc

s410_6.dat	ml turb model
s410_7.dat	ml turb model + ev turb model
s410_21.dat	2-eqn L-S turb model

s410_22.dat	2-eqn KYC turb model
s410_23.dat	2-eqn L-B turb model
s410_24.dat	2-eqn J-L turb model

combined entry flow, constant-property air; q″=const bc

s420_7.dat	ml turb model + ev turb model

combined entry flow, constant-property water; T=const bc

w410_6.dat	ml turb model
w410_7.dat	ml turb model + ev turb model
w410_21.dat	2-eqn L-S turb model
w410_22.dat	2-eqn KYC turb model
w410_23.dat	2-eqn L-B turb model

thermally fully developed flow, constant-property air; T=const bc
Note: Not particularly useful because initial profiles only an estimate
better to just compute from entrance to thermally fully developed region

s450_6.dat	ml turb model
s450_7.dat	ml turb model + ev turb model
s450_22.dat	2-eqn KYC turb model

Pipe flow—turbulent (user-supplied initial profile test cases)

Note: Data sets are similar to s450_6.dat, but in British units

p450_6.dat tests the use of the *kstart*=0 option
file p450_6.pro provides a set of 91 velocity and temperature profiles
Note: The finite-difference mesh will be calculated exactly, based
on the $u(y)$ distribution contained in file p450_6.pro

pp450_6.dat tests the use of the *kstart*=10 option
file pp450_6.dat provides a set of 46 velocity and temperature profiles
Note: The finite-difference mesh will be calculated by interpolating the
$u(y)$ distribution contained in file pp450_6.pro, on the basis of the
specified *dyi* and *rate*

Parallel-plane flow—turbulent

combined entry flow, constant-property air; T=const (symmetric) bc

s510_6.dat	ml turb model
s510_7.dat	ml turb model + ev turb model
s510_21.dat	2-eqn L-S turb model
s510_22.dat	2-eqn KYC turb model
s510_23.dat	2-eqn L-B turb model
s510_24.dat	2-eqn J-L turb model

Note: These data sets check symmetry of s510 using *kgeom*=6

s516_6.dat	ml turb model
s516_22.dat	2-eqn KYC turb model

combined entry flow, constant-property air; q''=const (symmetric) bc

s520_7.dat	ml turb model + ev turb model

combined entry flow, constant-property water; T=const (symmetric) bc

w510_6.dat	ml turb model
w510_7.dat	ml turb model + ev turb model
w510_21.dat	2-eqn L-S turb model
w510_22.dat	2-eqn KYC turb model
w510_23.dat	2-eqn L-B turb model
w510_24.dat	2-eqn J-L turb model

thermally fully developed flow, constant-property air; T=const (symmetric) bc
Note: Particularly useful because initial profiles only an estimate
Better to just compute from entrance to thermally fully developed

s550_6.dat	ml turb model
s550_22.dat	2-eqn KYC turb model

Note: This data set checks symmetry for s550 using *kgeom*=6

s556_6.da	T=const bc (I surface), T=const bc (E surface), ml turb model

unheated starting length flow, variable-property air with viscous dissipation, asymmetric heating

v586_22.dat	q''=const bc (I surface), q''=const bc (E surface), 2-eqn KYC turb model

Turbulent free convection between parallel planes

body-force opposed, asymmetric heating, variable-property nitrogen

t916.dat	channel is 0.3 m wide and 18 m long

NAME INDEX

Abuaf, N., 508
Abu-Ghannam, B. J., 504
Adams, E. W., 502
Allen, R. W., 335
Andersen, Peter, 209, 496
Arpaci, V. S., 385
Arts, T., 508
Aung, W., 73, 92, 105, 298, 389

Bailey, F. J., 384–385
Baron, J. R., 12, 15
Bénard, H., 394
Birch, N. T., 503
Bird, R. B., 399
Bittus, P. W., 299
Blackwell, Ben, 235, 237, 257, 496
Blair, M. F., 273
Blasius, H., 134–135
Boelcs, A., 508
Boelter, L. M. K., 299
Boerner, C. J., 140–141
Bonhoff, B., 508
Bradshaw, P., 56, 222
Brown, S. N., 171
Brown, W. B., 339
Bunker, R. S., 508

Carlson, L. W., 287
Catton, I., 367, 391
Cebeci, T., 56, 348
Chapman, S., 12, 15
Cheesewright, R., 385
Chen, Huei, 497
Chen, T. S., 389–390
Cheng, K. C., 369
Chi, S. W., 342, 350, 425
Chien, K-Y, 503
Cho, H. H., 417
Chu, H. H. S., 386–387
Churchill, S. W., 386–387
Clauser, F. H., 208–209
Cohen, C. B., 339
Coleman, H. W., 508
Colladay, Ray, 497
Cormack, D. E., 394
Cowling, T. G., 12, 15

Crawford, Michael, 242, 266, 496–497, 508

Dawes, W. N., 503
Deissler, R. G., 333–334, 350, 362
Desmon, L. G., 335–336
Dewey, C. R., Jr., 141, 159
Dipprey, D. F., 270, 322
Donoughe, P. L., 339
Drost, U., 508
Dyadyakin, B. V., 336

Eckert, E. R. G., 167, 335, 339–340, 342, 359, 363, 370, 382–385
Ede, A. J., 367, 388
Eichhorn, R., 380
Elzy, E., 152
Emery, A. F., 391–392
Evans, H. L., 421

Falkner, V. M., 138
Fand, R. M., 388
Ferguson, J. R., 242, 508
Fishenden, M., 387
Fleming, D. P., 76
Fujii, M., 379
Fujii, T., 379, 387
Futagami, K., 390

Gartner, D., 304, 307
Gebhart, B., 367, 369, 372, 375, 389
Gnielinski, V., 298–299
Goldstein, R. J., 387, 394, 417
Graebel, W. P., 394
Gregg, J. L., 378, 382–383, 388
Gross, J. F., 140–141, 159

Hancock, P. E., 221
Harasgama, S. P., 508
Häring, M., 418
Hartnett, J. P., 287
Hassid, S., 503
Hatton, A. P., 317
Heaton, H. S., 76, 118–119
Hinze, J. O., 56
Hodge, B. K., 508

Hoffs, A., 508
Hollands, K. G. T., 387–388
Hollingsworth, D. K., 235, 273
Hornbeck, R. W., 74, 118
Humble, L. V., 335–336

Imura, H., 387
Irvine, T. F., Jr., 287

Jackson, T. W., 383–385
Jeffreys, H., 394
Jenkins, R., 239
Jischa, M., 241
Johannsen, K., 304
Johnston, J. P., 502
Jones, W. P., 207, 503
Julien, Howard, 496

Kakac, S., 73, 91, 96, 105, 287, 298–299, 308, 310
Kays, W. M., 76, 118–119, 172, 196, 266, 270, 287, 306–308, 336, 389, 496–497
Kessler, J., 390
Kim, J., 65, 238
Knuth, E. L., 14, 424
Koh, J. C. Y., 287
Kuehn, T. H., 387, 394

Langhaar, H. L., 74, 118, 119
Latzko, H., 283
Launder, B. E., 207, 503
Lee, C. P., 508
Le Fevre, E. J., 372, 377
Lel'chuk, V. D., 336
Leung, E. Y., 306–308
Lightfoot, E. N., 399
Lin, S. H., 74
Lloyd, J. R., 387, 389
Loeffler, A. L., Jr., 350, 362
London, A. L., 73–74, 76, 96, 105, 172, 287
Lowdermilk, W. H., 335–336
Lum, M., 388
Lundgren T. S., 74
Lutum, E., 508

McCarthy, J. R., 335
McCornas, S. T., 287
McEligot, D. M., 336
Mac Gregor, R. K., 391–392
Maciejewski, P. K., 274
Mansour, N. N., 65
Mayle, R. E., 504
Michelsen, M. L., 91
Miller, K. L., 508
Mills, A. F., 399
Minkowyca, W. J., 387
Miyamoto, M., 383
Moffat, R. J., 196, 266, 270, 385
Moin, P., 65, 238
Moore, F. K., 130
Moran, W. R., 387
Morgan, V. T., 171, 390
Mori, Y., 390
Morris, E. W., 388

Neelakantan, Sriram, 497, 508
Nicoll, W. B., 336
Nikuradse, J., 216, 294, 502

Ostrach, S., 367, 391, 394

Pappas, C. C., 360–361
Patankar, Suhas V., 85, 496, 503, 507
Perkins, H. C., 389
Petukhov, B. S., 335
Pietrzyk, Joe, 497
Pimenta, M. M., 270
Pohlhausen, E., 352
Poreh, M., 503
Presser, K. H., 440

Quack, H., 140–141
Quarmby, A., 317

Raithby, G. D., 387–388
Ramachandran, N., 390
Ramm, H., 304
Rayleigh, J. W. S., Lord, 394
Reshotko, E., 339
Reynolds, W. C., 76, 118–119, 308
Rieke, H. B., 241
Roganov, P. S., 236
Rogers, M. M., 238
Rohonczy, G., 335
Ross, D. C., 385, 387
Rouse, M. W., 299, 335–336
Rubesin, M. W., 360–361

Sabersky, D. H., 270, 322
Saunders, O. A., 387
Schlichting, H., 130, 216
Schmidt, R. C., 503
Schultz-Grunow, F., 194
Schwind, R. G., 385
Seibers, D. L., 385
Shah, R. K., 73–74, 76, 92, 96, 105, 298, 504
Sharma, B. I., 503
Sisson, R. M., 152
Skan, S. W., 138
Skupinski, E., 300
Slanciauskas, A., 234–235
Sleicher, C. A., 299, 303, 335–336
Smith, A. G., 167–168
Smith, A. M. O., 348
Soehngen, E. E., 370, 383

Spalding, D. B., 399, 421, 425
Sparrow, E. M., 74, 76
Stewart, A. J., 388
Stewartson, K., 171
Stretton, A. J., 388
Sutherland, W. A., 307

Tafti, D. K., 508
Tarada, F., 508
Taylor, R. P., 508
Thielbahr, W. H., 257
Tolpadi, A. K., 508
Tortel, J., 300
Tribus, M., 303

Van Driest, E. R., 357
Vautry, L., 300
Villadsen, J., 91
Vliet, G. C., 385, 387

Warner, C. Y., 385
Weigand, B., 242, 508
Wilke, C. R., 466
Williams, J. C., 171
Wolf, H., 335
Worsøe-Schmidt, P. M., 334

Yakhot, V. S. A., 239
Yang, K. T., 333, 367–378, 391, 393–394
Yavuzkurt, S., 508
Yin, S. H., 392
Yu, H. S., 159

Zukauskas, A., 172, 234–235

SUBJECT INDEX

- Adiabatic deceleration, 345
- Aerodynamics, 2
  - surface roughness and, 215–219, 268–271 (*see also* Surfaces)
- Air, 234–235, 237
  - water-vapor systems and, 430–433
- Analogies, 3
- Annulus flow, 119. *See also* Circular tubes
  - asymmetric heating and, 92–95
  - concentric, 305–309
  - eccentricity effects and, 308–309
  - Nusselt number and, 94
  - Texstan and, 528
  - thermal-entry-length and, 107–109
- Approximate solutions, 144
- Arbitrary-shape flow, 167–168, 170
- Asymmetric heating, 92–95
- Asymptotic accelerating flow, 211
- Asymptotic suction layer, 211, 215
- Axial conduction, 118
  - heat flux and, 115–118
  - surface temperature and, 109–114
  - wall shear force and, 210
- Axial curvature, 219–221, 271–273
- Axisymmetric flow, 24, 27–28
  - energy equations and, 33, 46–51
  - laminar external boundary layers and, 156, 169
  - laminar internal flow and, 69
  - momentum and, 40–43

- Bernoulli's equation, 43, 138, 499
- Beta function, 475
- Binary mixtures, 14
- Blasius equation, 355, 374
  - heat transfer and, 150
  - momentum transfer and, 134–135
  - Texstan and, 510–521
- Blowing, 140, 186, 237
  - convection and, 380–381
  - parameter, 219, 267
- Boundary conditions, 406–407
- Boundary layers
  - approximations for, 18–19, 40–51
  - asymptotic suction layer and, 211, 215
  - axial curvature and, 219–221
  - Blasius equation and, 134–135
  - body of revolution and, 143–145
  - concentration layer and, 19, 25–26, 401–406
  - concept of, 17–19
  - condensation and, 139
  - conditions for, 406–409
  - conservation principles and, 5–8
  - conserved property equation and, 409–428, 481–495
  - continuity and, 19–22, 402–403
  - control surfaces and, 5–8
  - convection and, 368–370, 374–390 (*see also* Convection)
  - cubic parabola and, 142, 160
  - differential equations for, 52–66, 401–404
  - diffusion of chemical elements and, 402
  - diffusion of component and, 402–403
  - energy equation and, 29–38, 402–403
  - equations of state and, 37
  - equilibrium and, 208–212
  - evaporation and, 139
  - Fourier's law of heat conduction and, 11–12
  - function tables for, 475–476
  - high-temperature with dissociation, 448–449
  - high velocities and, 344–366
  - incompressible, 131–141
  - integral equations for, 40–51
  - interface conditions and, 490–494
  - kinetic energy model and, 201–206
  - laminar external, 130–147 (*see also* Laminar external boundary layers)
  - laminar internal flow and, 68–129 (*see also* Laminar internal flows)
  - law of the wall and, 242–247 (*see also* Wall coordinates)
  - mass diffusion equations and, 25–29
  - mixing-length theory and, 183–186, 196–200
  - momentum and, 17–18, 22–25, 130–147, 402–403, 406–409
  - nonsimilar, 159
  - partial differential equations and, 3–4
  - primary variables of, 400–401
  - separated flow and, 171–172
  - shear thickness and, 143
  - similarity parameter and, 133
  - strongly accelerated, 259–260
  - Texstan and, 496–509 (*see also* Texstan)
  - thermal, 29–38
  - thickness and, 18, 40–49, 153, 161–162, 188–196, 373
  - transferred-substance state and, 407–409
  - transpired, 212–215
  - tubes and, 282–289 (*see also* Tubes)
  - turbulence and, 52–66, 178–228 (*see also* Turbulent external flows; Turbulent internal flows)
  - Van Driest model and, 178, 194–196, 335–336, 497, 502
  - wedge solutions and, 138–139, 143–145 (*see also* Wedge solutions)
- Boussinesq approximation, 368–370, 372, 381
- Brinkman number, 92
- Buoyancy, 56, 372, 389–391

- Cartesian coordinate system, 6, 9
  - continuity equations and, 19–21
  - Navier–Stokes equations and, 24–25
  - Nusselt number and, 303–304
  - Reynolds number and, 55–56, 303–304
  - tensor notation and, 11
  - Texstan and, 499
  - tubes and, 36–37
  - vector/scalar quantities and, 477–478

Centrifugal force, 367
Chain rule, 63
Chemical reactions, 2, 25
  boundary condition interface and, 490–494
  diffusion and, 27–29, 481–484
  energy equation simplification and, 484–489
  equal specific heats and, 486–489
  graphite ablation and, 446–448
  graphite burning and, 444–446
  heat of formation and, 486
  mass-transfer and, 402–406
  volatile fuel burning in air, 442–444
Circular tubes, 21. *See also* Turbulent internal flows
  axisymmetric flow and, 24, 27–28, 33
  concentric annuli and, 92–95, 305–309
  constant heat rate and, 84
  Couette flow and, 283
  cylindrical coordinates and, 478–479
  eccentricity effects and, 308–309
  energy differential equations and, 81–82
  enthalpy and, 81–82
  entry length and, 74–76, 97–105, 283, 312–322
  fully developed flow in, 282–287
  hydraulic diameter and, 310
  laminar internal flow and, 67–71
  liquid metals and, 299–302
  mixing length and, 293
  model correlations for, 311–312
  parallel planes and, 305–309
  peripheral flux variation and, 304–305
  Prandtl number and, 294–302
  pressure-gradient and, 36, 82
  surface roughness and, 322–323
  temperature profiles and, 82–95
  Texstan and, 524
  velocity profiles and, 82–95
Closure problem, 182
Concentration boundary layer, 19, 25–26, 401–406
Condensation, 139
Conduction, 1–3, 80, 430
  axial, 109–118, 210
  conserved property equation and, 409–428
  constant-heat-rate solution and, 86–88
  convection and, 83
  eddies and, 229–231, 238
  energy equations and, 29–38
  enthalpy thickness and, 48–49
  fluid properties and, 330–343
  Fourier's law of, 11–12
  gases and, 331–332
  high mass-transfer rates and, 418–427
  high velocities and, 344–366
  laminar external boundary layers and, 149–158 (*see also* Laminar external boundary layers)
  laminar internal flow and, 80–129 (*see also* Laminar internal flows)
  mass-transfer driving force and, 409–411
  molecular, 245
  nondimensional, 151
  Nusselt number and, 151 (*see also* Nusselt number)
  Prandtl number and, 233–242 (*see also* Prandtl number)
  Reynolds decomposition and, 56
  small mass-transfer rates and, 414–418
  Stanton number and, 51 (*see also* Stanton number)
  surface roughness and, 215–219, 268–271
Conservation principles, 33, 41
  energy and, 7–8
  instantaneous turbulence equations and, 54–55
  mass and, 5–6
  momentum theorem and, 6–7
  Reynolds-averaged equations and, 52–66
  transport equations and, 58–66
Conserved property equation, 429, 448
  boundary conditions and, 406–409
  continuity and, 482
  Couette flow and, 418–420
  defined, 405
  derivations of, 481–495
  diffusion and, 481–484
  high mass-transfer rates and, 418–427
  laminar boundary layer and, 414–416, 420–426
  l'Hospital's rule and, 420
  mass-transfer driving force and, 409–411
  momentum and, 482
  property-ratio scheme and, 424–425
  reference property and, 424
  small mass-transfer rates and, 414–418
  turbulence and, 416–418, 426–427
Constant-heat-rate solution, 84, 86–88, 118–119
Constant-property solutions, 331–332, 359, 362–363
Constant surface temperature, 85–86, 91, 118
  laminar external boundary layers and, 149–158, 166
Continuity, 32, 336, 368
  conserved property equation and, 409–428, 482
  Fick's law of diffusion and, 13–15
  Fourier's law of heat conduction and, 11–13
  mass-transfer and, 402–404
  stress and, 10–11
  transport coefficients and, 15
Control volume, 5–8
Convection, 2, 140–141, 378, 382–383, 387–389, 453–456
  air–water-vapor system and, 430–433
  approximate solutions and, 381–382
  blowing and, 380–381
  boundary layers and, 400–406 (*see also* Boundary layers)
  Boussinesq approximation and, 368–370, 372, 381
  buoyancy and, 389–391
  centrifugal forces and, 367
  conductance and, 83, 430
  conservation principles and, 5–8
  conserved property equation and, 409–429, 448
  continuity and, 368
  Coriolis forces and, 367
  cylinders and, 387–388
  diffusion and, 81
  driving force and, 429–430, 433–434, 437–440, 445–446, 448
  drying and, 437–438
  in enclosures, 390–394
  equations for, 65, 368–370
  evaporative cooling and, 438–439
  flow regimes and, 370–373
  forced, 1, 367, 389–390
  free, 367, 368–373
  gas injection and, 449–452

  general solution procedure for, 429–430
  graphite ablation and, 446–448
  graphite burning in air, 444–446
  Grashof number and, 373, 377, 379, 387, 390–391
  gravity and, 367–368
  heat-exchanger theory and, 80–81 (*see also* Heat-transfer)
  high mass-transfer rates and, 406, 418–427
  high-temperature with dissociation, 448–449
  high velocity, 344–366
  inclined surfaces and, 386–387
  inertia and, 377
  interferometers and, 370, 383
  laminar internal flow and, 81–83
  low mass-transfer rates and, 406, 409, 414–418
  Mach number and, 344
  mixed free, 389–930
  molecular weight and, 424–425, 431, 436, 440–441
  naphthalene sublimation and, 439–442
  natural, 1, 367, 390–394
  Navier–Stokes equation and, 370, 391
  Nusselt number and, 378, 380, 386–394
  other-geometry solutions and, 386–388
  plates and, 381–382, 387
  power-function laws and, 384
  Prandtl number and, 377–378, 389–390
  Rayleigh number and, 387, 391–393
  relative humidity and, 432
  Reynolds number and, 370–371
  scaling and, 370–373
  similarity solutions and, 374–381
  suction and, 380–381
  transferred-substance state and, 407–409
  transpiration cooling and, 449–452
  turbulence and, 300, 383–386 (*see also* Turbulent external flows; Turbulent internal flows)
  variable property effects and, 382–383
  volatile fuel burning in air, 442–444
  wet-bulb psychrometer and, 433–437

Cooling, 438–439, 449–452
Coriolis force, 367
Couette flow, 186, 213
  circular tubes and, 283
  conserved property equation and, 418–420
  l'Hospital's rule and, 420
  Texstan and, 526, 528
  thickness and, 188–189
  transpiration and, 260–264
  Van Driest model and, 195
  wall coordinates and, 187–191, 242–247
Creation, 5–8, 26–27
Cubic parabola, 142, 160
Curvature effects, 219–221
Cylinders, 387–388. *See also* Tubes

Damping function, 335–336, 497, 502
Density
  Boussinesq approximation and, 368–369
  conserved property equation and, 421
  continuity equations and, 19–21
  Fourier's law of heat conduction and, 11–12
  gases and, 331–332
  kinetic energy model and, 201–206
  laminar internal flow and, 69
  naphthalene sublimation and, 440
  Reynolds decomposition and, 56
  viscous stress and, 9–11
Derivative rule, 58
Destabilization, 219
Differential equations. *See* Equations
Diffusion. *See also* Heat-transfer
  axisymmetric, 27–28
  binary mixtures and, 14
  boundary condition interface and, 490–494
  chemical reactions and, 27–29, 491 (*see also* Chemical reactions)
  conserved property equation and, 481–484
  convection and, 81
  defined, 13
  eddies and, 182–183, 229–231
  energy equation simplification and, 484–489
  Fick's law of, 13–15, 25–26
  Fourier's law of heat conduction and, 11–12
  high velocities and, 344–346
  k–*ε* model and, 206–208
  kinetic energy model and, 201–206
  mass, 25–29, 264, 402–406
  mixing-length theory and, 183–186, 196–200
  molecular thermal, 82
  psychrometers and, 433–437
  Schmidt number and, 464
  Soret effect and, 14–15
  temperature and, 98–104, 194–196 (*see also* Temperature)
  thermal-entry-length and, 97–107, 117–119
  transpiration and, 264
  tubes and, 282–291 (*see also* Tubes)
  unheated starting length and, 251–254
  Van Driest model and, 194–196
  volatile fuel burning in air, 442–444
  wall coordinates and, 242–247
Diffusion-thermo effect, 12
Dimensionless groups, 15
Displacement thickness, 43–45
Dissipation, 35
  high velocities and, 347, 350, 355–356
  transport equation, 65–66
Dissociation, 448–449
Driving force, 401, 445–446, 448
  definition of, 409–411
  drying and, 437–438
  evaporative cooling and, 438–439
  general problem solution and, 429–430
  naphthalene sublimation and, 440–441
  psychrometers and, 433–437
  thermal radiation and, 494–495
Drying, 437–438
Dufour effect, 12

Eddies, 182. *See also* Turbulence
  circular tubes and, 282–287
  conductivity and, 229–231
  curvature and, 219–221
  diffusion and, 229–231
  kinetic energy model and, 201–206
  mixing-length theory and, 183–186, 196–200
  Prandtl number and, 238
  surface roughness and, 215–219, 268–271

ε equation, 66
Energy, 1. *See also* Conserved property equation
  boundary condition interface and, 492–494
  circular tubes and, 81–82
  conservation of, 7–8, 33, 54–55
  convection and, 368–370, 374 (*see also* Convection)
  differential equations for, 81–82
  dissipation function and, 35
  equations for, 8, 29–38, 46–51, 337, 402–403, 484–489
  external fields and, 33
  Fick's law of diffusion and, 13–15
  film cooling and, 265–268
  fluid properties and, 330–343
  Fourier's law of heat conduction and, 11–12
  generation of, 8
  high velocities and, 344–366
  insulation and, 346
  internal thermal, 8
  kinetic, 8, 201–206 (*see also* Kinetic energy)
  laminar external boundary layers and, 161 (*see also* Laminar external boundary layers)
  laminar internal flow and, 80–129 (*see also* Laminar internal flows)
  law of the wall and, 242–247
  mass-transfer equations and, 402–404
  peripheral variation and, 90–91
  potential, 8, 33
  Prandtl number and, 38, 233–242
  pressure-gradient and, 36–37
  psychrometers and, 433–437
  Reynolds analogy and, 231–233
  stagnation enthalpy and, 37, 47, 54, 61–62, 345–349
  Stanton number and, 51
  steady-flow and, 29–34
  stream function and, 374
  supercomputer calculations and, 236, 238
  temperature and, 231–233 (*see also* Temperature)
  thermal-entry-length and, 97–107, 117–119
  total, 346–347
  transition region and, 180–181
  transpiration cooling and, 449–452 (*see also* Thermodynamics)
  transport equations and, 62–66
  turbulence and, 52–66, 302–303
  viscous, 34–35
Enthalpy, 8, 487–489. *See also* Chemical reactions
  air–water-vapor system and, 430–433
  circular tubes and, 81–82
  conduction thickness and, 48–49
  equations for, 81–82
  flux factor, 61
  high velocities and, 344–366
  kinetic energy and, 31
  laminar external boundary layers and, 156
  mixture, 30
  partial, 31
  Prandtl number and, 238–239
  psychrometers and, 436–437
  reference, 359
  Reynolds decomposition and, 56
  stagnation, 37, 47, 54, 61–62, 345–349, 524
  strongly accelerated flow and, 259–260
  thermal boundary layer and, 29–38
  thickness and, 156, 245, 340–341
  transpiration and, 260–264
  transport equations and, 61–62
  varying free-stream velocity and, 256–259
Equations
  adiabatic deceleration, 345
  air–water-vapor system, 430–433
  Allen–Eckert, 335
  approximate turbulence solution, 192–194
  arbitrary body shape, 167–170
  arbitrary heat flux, 165–166, 255
  arbitrary temperature, 163–165, 255
  asymmetric heating, 92–96
  axial curvature, 272
  axial temperature variation, 110–114
  Bernoulli, 43, 138, 499
  beta function, 475
  Blasius, 134–135, 150, 355, 374
  blowing parameter, 267
  boundary layer, 18–19, 41–51, 138, 401–409, 490–494 (*see also* Boundary layers)
  Boussinesq approximation, 368–370, 372, 381
  Brinkman number, 92
  circular tubes, 282–287, 292–293 (*see also* Tubes)
  conduction thickness, 48–49
  conserved property, 406, 409–429, 448, 481–495
  constant heat-rate, 86–88
  constant temperature, 88–89, 149–158, 167–170, 249–250
  continuity, 19–21, 32, 336, 402–403
  convection, 65, 81–83, 368–389, 392–393
  Couette flow, 213 (*see also* Couette flow)
  cubic parabola, 142, 160
  curvature, 220–221
  Deissler, 333
  derivative rule, 58
  differential, 3–4, 52–66
  diffusion, 82, 230, 232, 401–404, 481–484
  displacement thickness, 43–45
  dissipation function, 35
  dissociation, 448
  Dittus-Boelter, 299
  drying, 437–438
  ε, 66
  eddies, 182–183, 230–231
  effective heat flux, 232
  energy, 8, 29–38, 46–51, 337, 402–403, 484–489
  enthalpy, 48–49, 81–82, 359, 443, 487–489
  entry length, 283
  equilibrium, 208–210
  error function, 476
  evaporative cooling, 439
  exponentially varying heat-flux solution, 89
  Fick's law of diffusion, 13–15
  film cooling, 266–268
  Fourier heat-flux, 53–54
  Fourier's law of heat conduction, 11–12
  free-stream turbulence, 221
  function tables, 475–476
  gamma function, 475
  Grashof number, 372
  heat-transfer coefficient, 2, 50
  heat-transfer conductance, 2, 410
  hydraulic diameter, 106, 108
  hydraulic radius, 287, 310
  instantaneous turbulence, 54–55
  $\bar{k}$, 65–66
  Kármán–Nikuradse, 286, 288–289

  - k–ε model, 207
  - kinetic energy, 201–206
  - laminar external boundary layers, 336–341
  - laminar incompressible boundary layer, 131–140
  - laminar internal flow, 68–76, 332–334
  - Latzko, 283
  - law of the wall, 189, 242–246
  - Lewis number, 15, 401 (*see also* Lewis number)
  - l'Hospital, 420
  - liquid metals, 300
  - Maciejewski, 274
  - mass concentration, 400
  - mass conservation, 5–6
  - mass-creation rate, 400
  - mass-diffusion, 25–29
  - mass-transfer conductance, 2, 3
  - mass-transfer driving force, 401, 409–411, 429, 433–434, 437–440, 445–446, 448, 495
  - mass-transfer rate/unit area, 429
  - mechanical energy, 55, 62–63
  - mixing-length, 183–186, 197
  - mixture pressure, 431
  - mixture velocity, 401
  - molar concentration, 430–431
  - molecular thermal diffusivity, 82
  - molecular weight, 424–425, 431, 436, 440–441
  - momentum, 7, 22–25, 40–46, 142–143, 192, 209–210, 336, 402–403
  - naphthalene sublimation, 441–442
  - Navier–Stokes, 17, 24–25, 34–35
  - net mass-flux, 400–401
  - Newtonian stress, 53–54
  - Nikuradse, 294
  - nondimensional temperature, 149
  - Nusselt number, 87, 90–94, 96, 100–104, 114, 171, 311 (*see also* Nusselt number)
  - parallel planes, 306
  - partial differential development, 3–4
  - peripheral flux variation, 304–305
  - Petukhov, 335
  - power law, 191
  - Prandtl number, 15, 38, 88, 233, 240–242, 311 (*see also* Prandtl number)
  - property ratio, 331
  - psychrometer, 433–436
  - Rayleigh number, 372
  - relative humidity, 432
  - Reynolds-averaged, 52–66
  - Reynolds decomposition, 56
  - Reynolds number, 179–180, 311 (*see also* Reynolds number)
  - Reynolds transport, 58–66
  - Richardson number, 220
  - Rohonczy, 335
  - Schmidt number, 15, 207, 401 (*see also* Schmidt number)
  - semi-infinite plate flow, 149–166
  - shape factor, 192, 209
  - shear stress ratio, 186
  - shear thickness, 143
  - Sherwood number, 401
  - specific heat, 401
  - stagnation enthalpy, 54, 346–349
  - Stanton number, 51, 258, 311 (*see also* Stanton number)
  - state, 37
  - statistical mean, 57
  - stream function, 374
  - substantial derivative, 24
  - surface roughness, 216–219, 269–270
  - surface temperature, 110–115, 117
  - Taylor series, 369
  - temperature profile, 82–96
  - Texstan and, 504–507 (*see also* Texstan)
  - thermal-entry-length, 97–106, 108, 118
  - thermal flux, 12
  - time averaging, 57
  - total heat flux, 242
  - transpiration, 213–215, 260–262, 449–450
  - transport, 15, 58–66
  - turbulence intensity, 221
  - turbulent external flows, 341 (*see also* Turbulent external flows)
  - turbulent internal flows, 332–334 (*see also* Turbulent internal flows)
  - unheated starting length, 252–254
  - Van Driest model, 194–196
  - velocity, 68–70, 82–96, 143–144, 345, 347–360, 362–363, 401
  - viscous fluid stress, 9–11
  - wall coordinate, 186–189, 191, 194–196
  - Yakhot, 239
  - Yang, 333
- Equilibrium
  - curvature and, 219–221
  - psychrometers and, 433–437
  - Reynolds analogy and, 231–233
  - transpiration and, 212–215, 261
  - turbulent boundary layer and, 208–212
  - varying free-stream velocity and, 256–259
  - wall coordinates and, 242–247
- Error function, 476
- Evaporation, 139, 438–439
- External fields, 33

- Fick's law of diffusion, 13–15, 25–26
- Film cooling, 265–268
- Finite volumes, 506–507
- Fixed-mass system, 5
- Flow
  - accelerated, 258–260
  - arbitrary shape and, 166–171
  - arbitrary temperature and, 170–171
  - asymptotic accelerating, 211
  - asymptotic suction layer and, 211
  - axial curvature and, 219–221
  - axial temperature variation and, 109–114
  - axisymmetric, 24, 27–28, 33, 40–43, 46–51, 69, 156, 169
  - Blasius, 510–521
  - bluff-body, 171–172
  - boundary layer and, 17–38, 41–49, 171–172 (*see also* Boundary layers)
  - conservation principles and, 5–8
  - conserved property equation and, 409–428, 448, 481–495
  - constant-property, 48
  - constant temperature, semi-infinite plate, 149–158
  - continuity equations and, 19–21
  - Couette, 186–191, 195, 213 (*see also* Couette flow)
  - creeping, 370–373
  - displacement thickness and, 43–45
  - drying and, 437–438
  - energy equations and, 29–38
  - evaporative cooling and, 438–439
  - free-stream value and, 25–26
  - high velocities and, 344–366
  - hydrodynamically fully developed, 109–114

Flow—*Cont.*
  injection and, 157–158
  kinetic energy model and, 201–206
  laminar external boundary layers and, 130–147 (*see also* Laminar external boundary layers)
  laminar internal, 67–129 (*see also* Laminar internal flows)
  laminar to turbulent, 178–180
  mass, 5–6, 25–29
  momentum thickness and, 43–45
  Navier–Stokes equations and, 24–25
  nonsimilar solutions and, 141–145
  potential flow theory and, 138
  Reynolds-averaged equations and, 52–66
  Reynolds decomposition and, 55–56
  similarity parameter and, 133
  sink, 211
  Stanton number and, 51
  steady, 20, 29–38
  suction and, 157–158
  supercomputer calculations and, 236, 238
  Texstan and, 500 (*see also* Texstan)
  time averaging and, 57–58
  tubes and, 282–291 (*see also* Tubes)
  turbulence and, 52–66, 294–299 (*see also* Turbulent external flows; Turbulent internal flows)
  unheated starting length and, 159–162
  Van Driest model and, 194–196
  wedge solutions and, 138–139, 143–145 (*see also* Wedge solutions)
  work, 8
Fluids, 1. *See also* Turbulent external flows; Turbulent internal flows
  adiabatic wall temperature and, 344–366
  air–water-vapor system, 430–433, 466
  axial conduction effects and, 91
  boundary layers and, 17–19 (*see also* Boundary layers)
  centrifugal forces and, 367
  conductance and, 2–3
  conservation principles and, 5–8
  constant-property solutions and, 331–332
  Coriolis forces and, 367
  damping function and, 335–336, 497, 502
  density and, 9–11
  energy equations and, 29–38
  Fick's law of diffusion, 13–15, 25–26
  Fourier's law of heat conduction, 11–12
  gases and, 334–342, 360–363, 449–452
  high velocities and, 344–366
  incompressible, 20
  laminar internal flow and, 80–129 (*see also* Laminar external boundary layers; Laminar internal flows)
  liquids and, 233–234, 299–302, 321, 331, 334–335, 340–341
  Mach numbers and, 341
  mass-averaged temperature and, 82–83
  mixture pressure and, 431–432
  property values for, 331, 457–470
  Reynolds analogy and, 231–233
  specific heat and, 330
  Stanton number and, 341
  temperature-dependent properties of, 330–343
  Texstan and, 501–502 (*see also* Texstan)
  transpiration cooling and, 449–452
  transport properties, 15
  tubes and, 332–334 (*see also* Tubes)
  Van Driest model and, 178, 335–336
  viscosity and, 9–11, 91–92 (*see also* Viscosity)
  vorticity and, 181
  wedge solutions and, 167
Flux, 232
  arbitrary, 165–166, 255–256
  axial, 24, 115–117, 319
  Blasius flow and, 510–521
  boundary layer thickness and, 41–49
  conservation principles and, 5–8
  conserved property equation and, 409–429, 448, 481–495
  continuity equations and, 19–21
  convection and, 379, 385–386, 401 (*see also* Convection)
  direction and, 229–230
  eddies and, 229–231
  enthalpy factor and, 61
  exponentially varying heat solution and, 89
  Fick's law of diffusion and, 13–15, 25–26
  Fourier, 11–12, 53–54
  heat-transfer coefficient and, 2
  high velocities and, 344–366
  laminar external boundary layers and, 148–177 (*see also* Laminar external boundary layers)
  laminar internal flow and, 67–129 (*see also* Laminar internal flows)
  mass conservation and, 5–6
  momentum, 42
  net-mass, 400–401
  Newtonian stress and, 53–54
  peripheral, 90–91, 304–305
  Prandtl number and, 233–242
  Riemann integrals and, 117
  Stieltjes integrals and, 117
  thermal, 12, 97–107, 117–119
  transport properties, 13–15
  turbulence and, 52–66, 229–239, 304-307 (*see also* Turbulent external flows; Turbulent internal flows)
  uniform, 104–105
  viscous fluid stresses, 9–11
  wall coordinates and, 242–247
Fourier heat-flux models, 11–12, 53–54, 304–305
Free-stream velocity, 25–26. *See also* Boundary layers; Texstan
  approximate solution for, 258–259
  arbitrary temperature and, 162–165, 254–255
  body of revolution and, 143–145
  constant temperature and, 149–158, 248–256
  energy equations and, 29–38
  heat flux and, 165–166, 255–256
  high velocities and, 344–366 (*see also* Velocity)
  kinetic energy model and, 201–206
  Mach number and, 356
  momentum integral equation and, 141–143
  nonsimilar solutions and, 141–145
  psychrometers and, 433–437
  similar solutions and, 131–141
  stagnation enthalpy and, 47
  turbulence and, 187–191, 221–222, 273–274 (*see also* Turbulent external flows; Turbulent internal flows)
  unheated starting length and, 159–162, 251–254
  varying, 143–145, 256–259

Friction. *See also* Flow; Surfaces
  curvature and, 219–221
  Deissler and, 333
  fluid properties and, 330–343
  hydrodynamic entry length and, 75–76
  kinetic energy model and, 201–206
  laminar external boundary layers and, 135–136, 140–143 (*see also* Laminar external boundary layers)
  local, 135–136
  mixing-length theory and, 183–186, 196–200
  momentum integral and, 141–143
  power law and, 191
  strongly accelerated flow and, 259–260
  surface roughness and, 196, 215–219, 268–271, 287–289, 322–323
  transition region and, 180–181
  tubes and, 282–289 (*see also* Tubes)
  turbulence and, 193 (*see also* Turbulent external flows; Turbulent internal flows)
  wall coordinates and, 186–191
Fuels. *See also* Chemical reactions
  equal specific heats and, 486–489
  graphite burning and, 444–448
  volatile burning in air, 442–444

Gamma function, 475
Gases. *See also* Fluids
  conduction and, 331–332
  high velocity, 360–363
  injection and, 449–452
  laminar external boundary layers and, 336–340
  laminar internal flow and, 334
  reference temperature and, 331
  turbulent external flows and, 341–342
  turbulent internal flows and, 335–336
  variable property, 360–363
Graphite, 444–448
Grashof number, 372–373, 377, 379, 387, 390–391
Gravity, 23, 367–368

Handbook of Single-Phase Convective Heat Transfer (Kakac), 96, 287, 310
Heat of formation, 486
Heat-transfer
  aerodynamic, 2
  analogies and, 3
  arbitrarily specified flux and, 165–166
  arbitrary shape and, 166–171
  arbitrary temperature and, 162–165, 170–171
  asymmetric, 92–95
  at high velocities, 344–366
  axial curvature and, 271–273
  axial temperature variation and, 109–117
  body forces and, 367–394
  boundary layers and, 17–38, 171–172 (*see also* Boundary layers)
  coefficient of, 2, 50, 83
  conductance and, 2–3, 410
  conservation principles and, 5–8
  constant-heat-rate solution and, 86–88
  constant temperature, 88–89, 149–158
  convection and, 80 (*see also* Convection)
  dissipation function and, 35
  energy equations and, 29–38
  exponentially varying flux solution and, 89
  Fick's law of diffusion and, 13–15, 25–26
  fluid properties and, 330–343
  Fourier heat-flux models and, 11–12, 53–54, 304–305
  heat-exchanger theory and, 80–81
  high velocities and, 344–366
  inclined surfaces and, 386–387
  laminar external boundary layers and, 148–177 (*see also* Laminar external boundary layers)
  laminar internal flow and, 80–129 (*see also* Laminar internal flows)
  laser–Doppler anemometer and, 171
  Newtonian stress and, 53–54
  psychrometers and, 433–437
  Reynolds decomposition and, 55–56
  suction and, 157–158
  surface roughness and, 268–271
  surface temperature and, 248–251, 254–255
  thermal-entry-length and, 81, 97–109, 117–119
  transition region and, 180–181
  transpiration and, 212–215
  turbulence and, 52–66, 181, 229–281, 292–327 (*see also* Turbulent external flows; Turbulent internal flows)
  unheated starting length and, 159–162, 251–254
  Van Driest model and, 194–196
  viscous dissipation and, 91–92
  wall coordinates and, 242–247 (*see also* Wall coordinates)
High mass-transfer rate convection, 406
High-velocity convection, 350
Humidity
  absolute, 432
  drying and, 437–438
  evaporative cooling and, 438–439
  psychrometer and, 433–437
  relative, 432
Hydraulic diameter, 106, 108, 307, 310
Hydraulic radius, 71–72, 287, 310
Hydrodynamic entry length, 67, 74–76, 319–321

Incompressibility, 20
Injection, 157–158
Insulation, 246
Integral equations. *See* Equations
Interferometers, 370, 383
International System of Units (SI), 457, 471–473

Kármán–Nikuradse equation, 286, 288–289
k–ε model, 206–208, 508
$\bar{k}$ equation, 65–66
Kinetic energy, 8
  dissipation of, 202
  enthalpy and, 31
  Fick's law of diffusion and, 13–15, 25–26
  Fourier's law of heat conduction and, 11–12
  production of, 202
  thermal boundary layer and, 29–38
  thermal flux and, 12
  transport equations and, 63–65
  turbulence and, 52–66, 181–182, 201–206
Kronecker delta function, 53

Laminar external boundary layers, 146–147, 159, 339–340, 359
  arbitrary flux and, 165–166
  arbitrary shape and, 166–171
  arbitrary temperature and, 162–165, 170–171
  Blasius equation and, 134–135
  blowing and, 140
  body of revolution and, 143–145
  condensation and, 139
  conserved property equations and, 414–426
  constant temperature, semi-infinite plate, 149–158
  cubic parabola and, 142, 160
  enthalpy and, 156
  evaporation and, 139
  gases and, 336–340
  heat-transfer and, 148–177
  injection and, 157–158
  liquids and, 340
  Mangler transformation and, 156–157, 169
  momentum transfer and, 130–147
  nonsimilar solutions for, 141–145, 159
  Nusselt number and, 151, 153, 155–156, 158, 162, 165, 171
  Prandtl number and, 152–158, 161–162, 167–168, 170
  Reynolds number and, 136, 154, 156, 171
  separation and, 171–172
  shear and, 143
  similarity solutions for, 131–141
  Stanton number and, 154, 157
  suction and, 140, 157–158
  superposition and, 148–149
  thickness and, 136–137, 143, 161–162
  unheated starting length and, 159–162
  wedge solutions and, 138–139, 143–145, 167–170
Laminar internal flows, 77–79, 85
  asymmetric heating and, 92–95
  axial variation effects and, 109–117
  circular tubes and, 67–71, 74–76, 81–109, 282–287
  convection and, 81–83
  energy equations and, 81–82
  flux effects and, 115–117
  friction and, 75–76
  gases and, 334
  heat-exchanger theory and, 80–81
  hydrodynamic entry length and, 74–76
  liquids and, 332–334
  Navier–Stokes equation and, 71
  noncircular tubes and, 71–76, 95–96, 105–107, 287
  problems for, 120–129
  Reynolds number and, 70–73
  surface roughness and, 287–289
  temperature profiles and, 82–97
  thermal-entry-length and, 97–109, 117–119
  velocity profiles and, 82–97
Laminarization, 211
Laser–Doppler anemometer, 171
Law of the wall, 212, 250. *See also* Wall coordinates
  thermal boundary layer and, 242–247
  turbulent internal flows and, 295
Lewis number, 15, 401
  conserved property equation and, 416
  drying and, 438
  mass-transfer and, 404–405
  simplification of, 484–485, 492–493
  transferred-substance state and, 409
l'Hospital's rule, 420
Liquids. *See also* Fluids
  laminar external boundary layers and, 340
  metals, 233–234, 299–302, 321
  reference temperature and, 331
  turbulent external flows and, 340–341
  turbulent internal flows and, 334–335
Local friction coefficient, 76
Local Stanton number, 51
Low mass transfer rate convection, 406, 409

Mach number, 341, 344, 356, 361–364
Mach–Zehnder interferometer, 383
Mangler transformation, 156–157, 169
Mass
  averaged fluid temperature and, 82–83
  conservation of, 5–6, 33, 41, 54–55
  continuity equations and, 19–21
  control volume and, 5–6
  diffusion equations and, 25–29
  energy equations and, 33–34
  transport equations and, 58–59
Mass-creation rate, 400
Mass flow, 5–6
  boundary layer thickness and, 41–49
  internal laminar, 67–79
Mass-transfer, 1, 453–456
  air–water-vapor system and, 430–433
  analogies and, 3
  boundary layers and, 17–38 (*see also* Boundary layers)
  chemical properties and, 402–406
  complexity of, 399
  conductance and, 2–3, 409–411, 430
  conserved property equation and, 406, 409–429, 448, 481–495
  convection and, 399–412 (*see also* Convection)
  diffusion and, 14–15, 402–406
  driving force and, 401, 409–411, 429–430, 433–441, 445–446, 448, 494–495
  drying and, 437–438
  evaporative cooling and, 438–439
  gas injection and, 449–452
  general solution procedure for, 429–430
  graphite ablation and, 446–448
  graphite burning in air, 444–446
  high-temperature with dissociation, 448–449
  Lewis number and, 401, 404–405
  mass concentration and, 400
  mass-creation rate and, 400
  molecular weight and, 424–425, 431, 436, 440–441
  naphthalene sublimation and, 439–442
  net-mass flux and, 400–401
  net rate of, 401
  oxidants and, 404–406
  Prandtl number and, 404
  relative humidity and, 432
  Schmidt number and, 401, 404
  Sherwood number and, 401
  specific heat and, 401
  Texstan and, 523 (*see also* Texstan)
  thermal radiation and, 494–495
  transferred-substance state and, 407–409
  transition region and, 180–181
  transpiration cooling and, 2, 449–452
  volatile fuel burning in air, 442–444
  wet-bulb psychrometer and, 433–437
Mathematics. *See also* Equations
  approximation methods and, 40–51
  boundary layer thickness and, 41–49

- chain rule, 63
- constant-property solutions, 331–332
- derivative rule, 58
- Fourier expansion, 304–305
- Grashof number, 372
- Taylor series, 369
- Texstan and, 504–507 (*see also* Texstan)
- von Kármán constant, 185

Mechanical energy equation, 55, 62–63
Method of finite differences, 506
Mixing-length theory
- description of, 183–186, 196–200
- kinetic energy model and, 201–206
- Reynolds analogy and, 231–233
- surface roughness and, 216–219
- Texstan and, 502–504
- tubes and, 282–289 (*see also* Tubes)
- turbulent internal flows and, 293, 306
- Van Driest model and, 194–196

Mixture pressure, 431–432
Mixture velocity, 401
Mixture viscosity, 466
Molar concentration, 430–431
Molecular weight, 424–425, 431, 436, 440–441
Momentum
- axial curvature and, 271–273
- boundary conditions and, 17–18, 22–25, 130–147, 402–403, 406–409
- conservation of, 41
- conserved property equation and, 409–428, 482
- convection and, 368–370
- defined, 6–7
- eddies and, 182–183
- fluid properties and, 330–343
- flux and, 42
- high velocities and, 344–366
- injection and, 157–158
- integral equations and, 40–46, 141–143, 209–210
- internal flows and, 282–291
- laminar external boundary layers and, 130–147
- laminar internal flow and, 67–79
- mass-transfer equations and, 402–404
- mechanical energy equation and, 55
- mixing–length theory and, 183–186, 196–200
- Navier–Stokes equations and, 24–25
- nonsimilar solutions and, 141–145
- Reynolds analogy and, 231–233
- similarity solutions and, 131–141
- steady-flow equations and, 22–23
- stream function and, 374
- suction and, 157–158
- Texstan and, 499 (*see also* Texstan)
- theorem of, 6–7
- thermodynamic variables and, 52–53
- thickness, 43–45, 136–137, 192, 214, 340–341, 361
- transfer and, 73, 287
- transpiration and, 212–215
- transport equations and, 59–61
- tubes and, 282–291 (*see also* Tubes)
- turbulence and, 178–228, 231–233, 298 (*see also* Turbulent external flows; Turbulent internal flows)
- unheated starting length and, 251–254
- virtual origins of, 246
- wall coordinates and, 242–247

Naphthalene sublimation, 417, 439–442
National Institute of Standards and Technology (NIST), 457
Natural convection, 1
Navier–Stokes equations, 17, 24–25, 34–35
- convection and, 370, 391
- hydrodynamic entry length and, 74
- laminar external boundary layers and, 131
- laminar internal flow and, 71
- Reynolds-averaged equations and, 52–66
- supercomputer calculations and, 236, 238

Newtonian stress, 53–54
Nusselt number, 333
- annulus and, 94
- axial conduction and, 91
- axial temperature variation and, 114, 117
- boundary layer separation and, 171
- conserved property equation and, 411, 415–417
- convection and, 378, 380, 386–394
- correlations for, 311–312
- defined, 87
- drying and, 437–438
- fluid properties and, 338, 340
- Grashof number and, 373
- high velocities and, 356
- laminar external boundary layers and, 153, 155–156, 162, 165, 171
- mean, 321
- naphthalene sublimation and, 442
- nondimensional conductance, 151
- peripheral flux variation and, 90–91
- Prandtl number and, 97
- property ratio and, 331
- Rayleigh number and, 373
- rectangular tubes and, 95–96
- temperature profiles and, 87–96
- thermal-entry-length and, 100–104, 108
- triangular tubes and, 95–96
- turbulent internal flows and, 294–304, 307–309, 311–322
- viscous dissipation and, 91–92

Oxidants. *See* Chemical reactions

Partial differential equations (PDEs), 3–4, 141
Péclet number, 91
Phase. *See* Boundary layers
Plates
- arbitrary heat flux and, 165–166, 255–256
- arbitrary temperature and, 162–165, 254–255
- constant temperature and, 149–158
- convection and, 381–382, 387
- drying and, 437–438
- heat flux and, 255–256
- injection and, 157–158
- naphthalene sublimation and, 439–442
- parallel planes and, 305–309, 317–319, 334
- suction and, 157–158
- Texstan and, 523–526 (*see also* Texstan)
- unheated starting length and, 159–162, 251–254

Potential energy, 8, 33
Power law, 191
- functions and, 382

Prandtl mixing-length theory. *See* Mixing-length theory
Prandtl number, 15, 38, 52, 88, 411, 485
- adiabatic wall temperature and, 344–366

Prandtl number—*Cont.*
  air and, 234–235, 237
  axial conduction and, 91
  conduction model for, 239–242
  conserved property equation and, 421
  constant surface temperature and, 248–251
  convection and, 377–378, 389–390
  correlations for, 311–312
  drying and, 437–438
  eddies and, 229–231, 238
  enthalpy and, 238–239
  fluid properties and, 338, 340
  gases and, 297
  Grashof number and, 377
  high velocities and, 344–366
  laminar external boundary layers and, 152–158, 161–162, 167–168, 170
  liquid metals and, 233–234
  mass-transfer and, 404
  pressure-gradient and, 241, 247–248
  Reynolds analogy, 231–233, 239–242
  Schmidt number and, 404
  sublayers and, 234–242
  surface roughness and, 269–271
  Texstan and, 497, 503
  thermal-entry-length and, 97–98, 100, 117–118
  turbulent internal flows and, 293–304, 307, 309, 311–312
  turbulent external flows and, 229–242
  unheated starting length and, 251–254
  viscous dissipation and, 92
  wake region and, 234
  wall coordinates and, 242–247, 295
  water and, 234–235
Pressure, 36–37, 42
  air–water-vapor system and, 430–434, 466
  circular tubes and, 82
  convection and, 368–370
  fluid properties and, 330–343
  high velocities and, 344–346
  hydrodynamic entry length and, 74–75
  mixture, 431–432
  naphthalene sublimation and, 440
  Prandtl number and, 241
  psychrometers and, 436
  relative humidity and, 432
  Reynolds number and, 179
  Schmidt number and, 465
  temperature profiles and, 247–248
  transpiration and, 212–215
  turbulence and, 189–193, 210, 233–239
  varying free-stream velocity and, 256–259
  wall shear force and, 210
Property-ratio scheme, 424–425
Psychrometers, 2, 433–437

Rayleigh number, 372–373, 387, 391–393
Recovery factor, 353
Rectangular tubes, 36–37, 95–96, 105–107
Reference-property scheme, 424
Reynolds analogy
  conduction model and, 239–242
  equilibrium and, 231–233
  mixing-length and, 231
Reynolds-average equations
  Fourier heat-flux and, 53–54
  instantaneous turbulence equations and, 54–55
  Newtonian stress and, 53–54
  thermodynamic variables and, 52–53
  time averaging and, 57–58
  transport, 58–66
Reynolds decomposition, 52, 55–56, 63
Reynolds number, 239, 411
  circular tubes and, 282–287
  conserved property equation and, 421
  convection and, 370–371
  correlations for, 311–312
  eddies and, 219–221
  enthalpy thickness and, 340–341
  entry-length and, 117–118, 312–317
  flat duct and, 180
  fluid properties and, 338, 340
  high velocities and, 356, 360–361
  laminar external boundary layers and, 136, 154, 156, 158, 171
  laminar internal flow and, 70–73
  momentum thickness and, 136, 214, 340–341
  naphthalene sublimation and, 441–442
  Nusselt number and, 88
  pressure-gradient and, 179
  surface roughness and, 196, 215–219, 268–271, 287–289
  Texstan and, 502, 504, 508
  transpiration and, 214, 260–264
  turbulence and, 179–182, 189–194, 296, 300–304, 309–316
  unheated starting length and, 251–254
  Van Driest model and, 194–196
  varying free-stream velocity and, 256–259
  wall coordinates and, 246–247
Richardson number, 220
Riemann integral, 117

Scaling, 370–373
Schmidt number, 15, 207, 401
  binary diffusion coefficient and, 464
  conserved property equation and, 421
  mass-transfer and, 404
  naphthalene sublimation and, 440
  Prandtl number and, 404
  pressure and, 465
  Texstan and, 497
Shear. *See* Stress
Sherwood number, 401, 415–417
Shock waves, 345
Similarity parameter, 133
Simple thermodynamic system, 5
Sink flow, 211
Sling psychrometer, 2
Software. *See* Texstan
Soret effect, 14–15
Specific heat, 401, 485–489, 493–494
Spherical coordinates, 479–480
Stabilization, 219
Stagnation enthalpy, 37, 47, 54
  equation of, 346–349
  high-velocity convection and, 345
  temperature and, 345–349
  Texstan and, 524
  transport equations and, 61–62
STANCOL. *See* Texstan
Stanton number, 51, 88, 248, 411. *See also* Heat-transfer
  axial curvature and, 271–272
  conserved property equation and, 421, 425–427
  constant-property, 359, 362–363
  correlations for, 311–312
  film cooling and, 266
  fluid properties and, 340–341
  Grashof number and, 372
  high velocities and, 357, 360, 362

  laminar external boundary layers and, 154, 157
  naphthalene sublimation and, 441
  property ratio and, 331
  surface roughness and, 269–270
  transpiration and, 260, 263, 450
  turbulence and, 273–274, 296, 311–312
  unheated starting length and, 253–254
  varying free-stream velocity and, 256–259
Steady flow. *See* Flow
Stieltjes integrals, 117
Stoichiometric ratios. *See* Chemical reactions
Stokes hypothesis, 53
Storage
  conservation principles and, 5–8
  continuity equations and, 19–21
Stress, 42
  convection and, 384
  damping function and, 335–336
  eddies and, 182–183
  high velocities and, 344–366
  laminar internal flow and, 67–79
  mixing-length theory and, 183–186, 196–200
  Newtonian, 53–54
  Reynolds, 52, 231–233
  thickness, 143
  turbulence and, 52–66, 233–239, 306
  viscous fluid, 9–11
  wall coordinates and, 186–191, 210
  wedge solutions and, 143–145
Sublimation, 417, 439–442
Substantial derivative, 24
Suction
  axial curvature and, 219
  constant temperature flow and, 157–158
  equilibrium and, 211
  mixing-length and, 186
  similarity solutions and, 140, 380–381
  transpiration and, 215
Superposition, 148–149
Surfaces, 1. *See also* Boundary layers; Tubes
  arbitrary shape and, 166–171
  arbitrary temperature and, 162–165
  axial variations and, 109–114, 319
  condensation and, 139
  conservation principles and, 5–8
  control, 5
  damping and, 335–336, 497, 502
  drying and, 437–438
  evaporation and, 139
  film cooling and, 265–268
  graphite burning and, 444–446
  heat-transfer coefficient and, 2
  high velocities and, 344–346
  isothermal horizontal, 387
  laminar external boundary layers and, 130–147 (*see also* Laminar external boundary layers)
  porous, 268
  roughness and, 196, 215–219, 268–271, 287–289, 322–323
  temperature and, 85, 110–115, 117, 248–256 (*see also* Temperature)
  Texstan and, 504–507 (*see also* Texstan)
  transferred-substance state and, 407
  turbulence and, 215–219 (*see also* Turbulent external flows; Turbulent internal flows)
  unheated starting length and, 251–254
Sutherland law, 357

Taylor series, 369
Temperature, 1
  absolute, 56, 382
  adiabatic deceleration, 345
  adiabatic wall, 346, 352–354, 359
  air–water-vapor system and, 430–433
  arbitrary, 162–165, 254–255
  arbitrary shape and, 166–171
  asymmetric heating and, 92–95
  axial variations and, 109–114, 319
  concentric annulus and, 92–95
  condensation and, 139
  conductance and, 2–3
  constant, 248–251
  constant-property solutions and, 48, 331–332
  convection and, 374–376, 384 (*see also* Convection)
  dissociation and, 448–449
  energy equations and, 29–38
  entry-length and, 97–107, 117–119, 312–321
  evaporation and, 139, 438–439
  film cooling and, 265–268
  fluid properties and, 330–343
  Fourier's law of heat conduction and, 11–12
  free-stream velocity and, 248–251
  gases and, 330
  heat-exchanger theory and, 80–81
  high velocities and, 344–366
  injection and, 157–158
  insulation and, 346
  laminar internal flow and, 80–129 (*see also* Laminar internal flows)
  l'Hospital's rule and, 420–421
  liquids and, 330
  Mach number and, 344
  mass-average fluid, 82–83
  nondimensional, 149
  power-law form, 378–379
  pressure-gradient and, 247–248
  problems for, 275–280
  profiles, 82–96
  property ratio and, 331, 424–425
  recovery factor and, 353
  reference, 331, 340, 342, 358–359, 424
  scaling and, 370–373
  semi-infinite plate velocity and, 149–158
  stagnation and, 345–349
  stream function and, 374
  strongly accelerated boundary layers and, 259–260
  suction and, 157–158
  surface, 85, 110–115, 117, 248–251, 254–255, 322–323
  transpiration and, 2, 260–264
  tubes and, 282–289 (*see also* Tubes)
  turbulent internal flows and, 294–304
  turbulent Prandtl number and, 233–239
  unequal heating and, 95
  unheated starting length and, 251–254
  viscosity and, 11
  wall coordinates and, 242–247
  wet-bulb psychrometer and, 433–437
Tensor notation, 11
  continuity equations and, 21
  Kronecker delta and, 53
  Navier–Stokes equations and, 24–25
  Newtonian stress and, 53–54
  Reynolds decomposition and, 55–56
  viscous energy equation, 35
Texstan, 496–497, 509
  annulus flow and, 528
  Blasius flow and, 510–521

Texstan—*Cont.*
  boundary conditions and, 498–500
  Couette flow and, 526, 528
  data sets for, 507–508, 510–530
  fluids properties and, 501–502
  free-stream velocity and, 503
  initial conditions and, 500–501
  laminar flow and, 522–524
  mixing length and, 502–504
  numerical method for, 504–507
  operation of, 520–521
  overview of, 496–498
  pipe flow and, 526–530
  Prandtl number and, 503
  research and, 508
  Reynolds number and, 502, 504, 508
  turbulence and, 502–504, 524–526, 528
  Van Driest model and, 497, 502
Thermal-entry-length, 67, 74–76, 81
  circular tubes and, 97–109
  hydraulic diameter and, 106, 108
  hydrodynamic length and, 117–119, 319–321
  rectangular tubes and, 105–107
Thermal flux, 12
Thermo-diffusion effect, 15
Thermodynamic equation of state, 37
Thermodynamic pressure, 11
Thermodynamics
  air–water-vapor system and, 430–433
  conservation principles and, 5–8
  continuity equations and, 19–21
  convection and, 374–376 (*see also* Convection)
  dissipation function and, 35
  dissociation and, 448–449
  drying and, 437–438
  energy equations and, 29–38
  evaporative cooling and, 438–439
  Fick's law of diffusion and, 13–15, 25–26
  First Law of, 33
  Fourier's law of heat conduction and, 11–12, 53–54, 304–305
  momentum variables and, 52–53
  naphthalene sublimation and, 439–442
  psychrometers and, 433–437
  specific heat and, 401
  thermal-entry-length and, 67, 74–76, 81, 97–109, 117–119, 312–322
  thermal radiation and, 494–495
  transpiration cooling and, 449–452
  turbulent boundary layer, 52–66
  wet-bulb psychrometer and, 433–437
Thermophysical Properties Research Center (TPRC), 457
Time
  averaging operator, 57–58
  continuity equations and, 19–21
  Newtonian stress and, 53–54
  transport equations and, 61–62
Transition region, 180–181
Transpiration
  cooling and, 2, 449–452
  enthalpy and, 260–264
  equilibrium and, 261
  Reynolds number and, 260–264
  Stanton number and, 263
  turbulent boundary layer and, 212–215, 260–264
Transport equations
  dissipation and, 65–66
  energy and, 62–66
  enthalpy and, 61
  mass conservation and, 58–59
  momentum and, 59–61
Transport mechanisms, 15
Triangular tubes, 36–37, 95–96
Tubes
  circular, 81–94, 282–287 (*see also* Circular tubes)
  constant heat rate and, 84
  cylinders and, 339
  entry-length and, 67, 74–76, 81, 97–109, 117–119, 312–322
  fluid properties and, 330–343
  gases and, 334
  high velocities and, 363
  hydraulic diameter and, 106, 287
  hydraulic radius and, 310
  laminar internal flow and, 67–129 (*see also* Laminar internal flows)
  liquids and, 332–334
  model correlations for, 311–312
  noncircular, 36–37, 95–96, 105–107, 287, 309–310
  rectangular, 36–37, 95–96, 105–107
  surface roughness and, 287–289
  temperature profiles and, 82–97
  triangular, 36–37, 95–96
  velocity profiles and, 82–97
Turbulent external flows
  approximate solution for, 191–194
  asymptotic suction layer and, 211, 215
  axial curvature and, 219–221, 271–273
  blowing and, 186, 210, 219, 267
  classification and, 208
  closure problem and, 182
  conserved property equations and, 416–417, 426–427
  convection and, 383–386
  Couette flow and, 186–191, 195, 213
  eddies and, 182–183, 201–206, 229–231
  equilibrium and, 208–212
  film cooling and, 265–268
  flat duct and, 180
  flow-direction intensity and, 206
  Fourier heat-flux and, 53–54
  free-stream, 187–191, 221–222, 273–274 (*see also* Free-stream velocity)
  gases and, 341–342
  heat flux and, 255–256
  high velocities and, 344–346, 360–363
  instantaneous equations for, 54–55
  intensity equation for, 221
  internal/external conditions and, 181
  internal flows and, 282–291
  isotropic, 221
  k–ε model and, 206–208
  kinetic energy and, 181–182, 201–206
  laminar flow and, 70, 178–180, 211
  law of the wall and, 242–247
  liquids and, 340–341
  local instability bursts and, 181, 194–196
  Mach number of, 56
  mixing-length theory and, 183–186, 196–200
  Newtonian stress and, 53–54
  power law and, 191
  Prandtl number and, 229–242
  pressure gradient and, 189–193, 210
  problems for, 223–228
  qualitative structure of, 180–182
  Reynolds analogy and, 231–233
  Reynolds decomposition and, 55–56
  Reynolds number and, 179–182, 189–194

  - Reynolds transport equations and, 58–66
  - shape factor and, 192, 209
  - Stanton number and, 273–274
  - statistics and, 57–58
  - stress tensor and, 60
  - sublayer and, 188–191
  - suction and, 186, 215, 219
  - supercomputer calculations and, 236, 238
  - surface roughness and, 215–219, 268–271
  - surface temperature and, 248–251, 254–255
  - Texstan and, 497 (*see also* Texstan)
  - thermodynamic variables and, 52–53
  - thickness and, 188–196
  - time averaging and, 57–58
  - transpired, 212–215
  - two-layer model procedure and, 206
  - unheated starting length and, 251–254
  - Van Driest model and, 194–196
  - virtual origin and, 193
  - vorticity and, 181
  - wake region and, 190
  - wall coordinates and, 186–191, 194–196, 210, 242–247
  - wedge solutions and, 208–211

Turbulent internal flows, 292
  - axial variations and, 319
  - concentric annuli and, 305–309
  - constant temperature and, 302–304
  - eccentricity effects and, 308–309
  - entry-length and, 67, 74–76, 293, 312–321
  - experimental correlations and, 311–312
  - flux and, 306–307
  - Fourier expansion and, 304–305
  - fully developed, 294–299, 302–304, 309–310
  - gases and, 335–336
  - heat-exchanger theory and, 294
  - hydraulic diameter and, 307, 310
  - law of the wall and, 295
  - liquids and, 299–302, 334–335
  - mixing-length and, 306
  - Nikuradse equation and, 294
  - Nusselt number and, 294, 296, 299–300, 303–304, 307–316, 320–322
  - parallel planes and, 305–309, 317–319
  - partially developed, 305–309
  - peripheral flux and, 304–305
  - Prandtl number and, 293–302, 307, 309, 311–312, 317–318
  - promoters and, 323
  - Reynolds number and, 296, 300, 309, 311–312, 314–316
  - Stanton number and, 296, 311–312
  - surface roughness and, 322–323
  - Texstan and, 497 (*see also* Texstan)

Van Driest model, 178, 196
  - gases and, 335–336
  - law of the wall and, 194–196
  - Texstan and, 497, 502

Vectors, 6

Velocity. *See also* Flow
  - adiabatic deceleration, 345
  - adiabatic wall temperature and, 344–366
  - arbitrarily varying, 143–145
  - Blasius flow and, 355, 510–521
  - concentric annulus and, 92–95
  - conservation principles and, 5–8
  - conserved property equation and, 409–428
  - constant temperature, 149–158
  - convection and, 344–366, 384 (*see also* Convection)
  - damping function and, 335–336
  - defect coordinates and, 208
  - dissipation and, 347, 350, 355–356
  - eddies and, 182–183
  - entry-length and, 67, 74–76, 81, 97–109, 117–119, 312–322
  - fluid properties and, 330–343
  - free stream, 25–26, 131–141, 248–256 (*see also* Free-stream velocity)
  - high mass-transfer rates and, 418–427
  - high-velocity boundary layer problem and, 346
  - kinetic energy model and, 201–206
  - laminar external boundary layers and, 130–147 (*see also* Laminar external boundary layers)
  - laminar internal flow and, 68–79
  - low mass-transfer rates and, 414–418
  - Mach number and, 341, 344, 356, 361–364
  - mean, 68
  - mixing-length theory and, 183–186, 196–200
  - mixture, 401
  - momentum integral equation and, 141–143
  - nonsimilar solutions and, 141–145
  - Prandtl number and, 349–355
  - pressure-gradient and, 36
  - profiles, 67–68, 74, 76, 82–96
  - recovery factor and, 353
  - reference properties for, 358–359, 363
  - Reynolds decomposition and, 55–56
  - shear thickness and, 143
  - shock waves and, 345
  - stagnation and, 344–345
  - Stanton number and, 357
  - stream function and, 374
  - Sutherland law and, 357
  - transpiration and, 212–215
  - tubes and, 82–95, 282–291 (*see also* Tubes)
  - turbulence and, 233–239 (*see also* Turbulent external flows; Turbulent internal flows)
  - Van Driest model and, 194–196

Viscosity
  - body of revolution and, 143–145
  - boundary layers and, 401–404 (*see also* Boundary layers)
  - Boussinesq approximation and, 368–370, 372, 381
  - constant-property solutions, 331–332
  - convection and, 368–373
  - eddies and, 182–183
  - energy equations and, 32, 34–35
  - fluid properties and, 9–11, 330–343
  - gases and, 331–332
  - heat dissipation and, 91–92
  - high velocities and, 344–366
  - insulation and, 346
  - kinematic, 97, 295
  - laminar external boundary layers and, 130–147 (*see also* Laminar external boundary layers)
  - laminar internal flow and, 67–79
  - laminar to turbulent transitions, 178–180
  - liquids and, 331–332
  - mixing-length theory and, 183–186, 196–200
  - mixture, 466
  - Newtonian stress and, 53–54

Viscosity—*Cont.*
  Prandtl number and, 38
  reference temperature and, 331
  Reynolds analogy and, 231–233
  Reynolds decomposition and, 56
  slow, 370
  Stokes hypothesis and, 53
  sublayers and, 185–191
  temperature and, 330–343
  thermal-entry-length and, 67, 74–76, 81, 97–109, 117–119, 312–322
  thickness and, 212
  transport equations and, 63–65
  tubes and, 282–291
  turbulence and, 52–66, 180–182, 294–304 (*see also* Turbulent external flows; Turbulent internal flows)
  Van Driest model and, 194–196
  varying free-stream velocity and, 259
  wall coordinates and, 186–191
Volatile fuel, 442–444
von Kármán constant, 185
von Mises stream function, 505
Vorticity, 181

Wake region, 190, 234
Wall coordinates, 178, 187–191
  blowing and, 380–381
  conserved property equation and, 417
  convection and, 380, 389 (*see also* Convection)
  mixing length and, 183–186, 196–200
  naphthalene sublimation and, 417, 439–442
  suction and, 380–381
  surface roughness and, 216–217
  Texstan and, 499 (*see also* Texstan)
  transpiration and, 212–215
  turbulent Prandtl number and, 233–239
Wall shear force, 210
Water, 234–235, 250, 334
Wedge solutions, 155
  arbitrary body shape and, 166–170
  body of revolution and, 143–144
  constant temperature and, 149–158
  incompressible boundary layer and, 131–141
  laminar external boundary layers and, 167–170
  momentum integral equation and, 141–143
  Prandtl number and, 167–168
  semi-infinite plates and, 149–158
  shear and, 143–145
  turbulence and, 179–180, 208–211
  unheated starting length and, 159–162
Wet-bulb psychrometers, 433–437
Work, 8

Convective Heat and Mass Transfer presents a strong theoretical basis for the subject, concentrating on boundary layer theory, with special emphasis on laminar and turbulent thermal boundary layers.

- *Numerous design sections show how analytical techniques are actually used to model heat exchangers, etc.*
- *Computer Problems are included in each chapter problem set.*

P9-DUT-602

HOR: KAYS
LE: CONVECTIVE HEAT AND MASS TRANSFER I
N: 978-1-259-02562-4
DOR: MCGRAW-HILL GLOBAL EDUCATION HOLDIN
2 901259 025623
USED TEXT

9 781259 025624

Mc Graw Hill Education